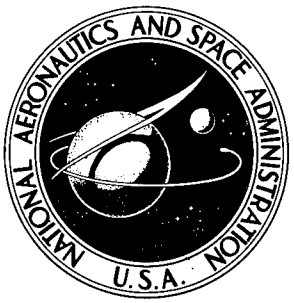
NASA CONTRACTOR REPORT



NASA CR-2315

NASA CR-2315

DISTRIBUTION STATEMENT A
Approved for public release;
Distribution Unlimited

MOTORLESS FLIGHT RESEARCH, 1972

Edited by James L. Nash-Webber

Prepared by
MASSACHUSETTS INSTITUTE OF TECHNOLOGY
Cambridge, Mass. 02139
or Langley Research Center

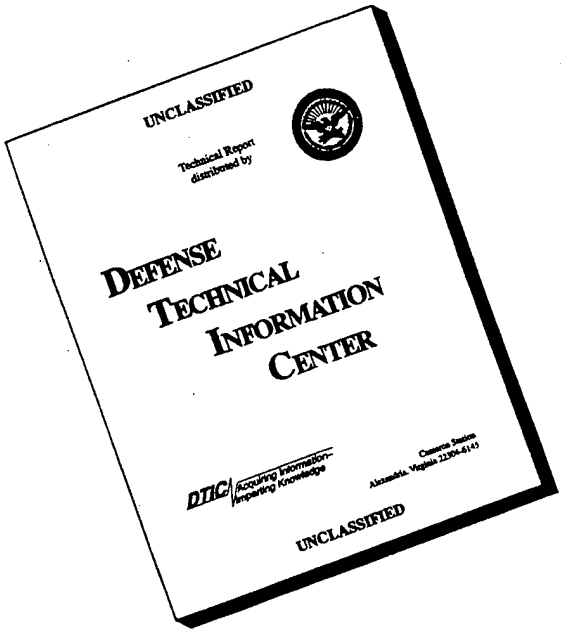
19960315 028

19980407 048

NATIONAL AERONAUTICS AND SPACE ADMINISTRATION • WASHINGTON, D. C. • NOVEMBER 1973

DTIC QUALITY INSPECTED 1

DISCLAIMER NOTICE



THIS DOCUMENT IS BEST QUALITY AVAILABLE. THE COPY FURNISHED TO DTIC CONTAINED A SIGNIFICANT NUMBER OF PAGES WHICH DO NOT REPRODUCE LEGIBLY.

1. Report No.	2. Government Accession No.	3. Recipient's Catalog No.
NASA CR-2315		

4. Title and Subtitle	5. Report Date
MOTORLESS FLIGHT RESEARCH, 1972	November 1973
	6. Performing Organization Code

7. Author(s)	8. Performing Organization Report No.
Edited by Dr. James L. Nash-Webber	
	10. Work Unit No. 760-60-99-04
9. Performing Organization Name and Address Massachusetts Institute of Technology Department of Aeronautics and Astronautics Measurement Systems Laboratory Cambridge, Massachusetts 02139	11. Contract or Grant No. NGR 22-009-731
	13. Type of Report and Period Covered Contractor Report
12. Sponsoring Agency Name and Address National Aeronautics and Space Administration Washington, D.C. 20546	14. Sponsoring Agency Code

15. Supplementary Notes

This is a final report.

16. Abstract

This document contains the recommendations of a Workshop to Identify Priorities for Motorless Flight Research, and the Proceedings of the First International Symposium on the Technology and Science of Motorless Flight, both held at the Massachusetts Institute of Technology, October 18-22, 1972. Areas discussed include Aerodynamics and Design, Instrumentation, Structural Concepts and Materials, Soaring Meteorology, Self-Launching and Ultralight Sailplanes, and Performance Testing.

17. Key Words (Suggested by Author(s))	18. Distribution Statement
Soaring Gliders Motorless Flight Sailplanes	Unclassified - Unlimited

19. Security Classif. (of this report)	20. Security Classif. (of this page)	21. No. of Pages	22. Price*
Unclassified	Unclassified	638	Domestic, $12.75 Foreign, $15.25

*For sale by the National Technical Information Service, Springfield, Virginia 22151

TABLE OF CONTENTS

PREFACE	1
INTRODUCTION	2
RESEARCH PRIORITIES, AERODYNAMICS AND DESIGN	4
Introduction	4
Circling Flight	4
Variable Geometry	6
Airfoils	9
Handling and Stability	9
Aerodynamic Tailoring	10
Systems Modelling for Design Optimization	11
Bird Flight Studies	13
Energy Gathering	15
Motorless Flight Applications	16
Coordination with Regulatory Authorities	16
RESEARCH PRIORITIES, INSTRUMENTATION	18
Introduction	18
Electric Field Measurements for Remote Thermal Detection and Turn Information	20
Turn Information Using Humidity Data	21
Variometer Systems	22
Air Markers	24
Angle of Attack Control	24
Buoyancy Indicator	25
Lightning Danger Alerting Techniques	26
Transponders and Proximity Warning Devices	27
Instrumentation Clues from Birds	28
Barographs	29
Contest Automation	29
RESEARCH PRIORITIES, STRUCTURES AND MATERIALS	30
Introduction	30
Sailplane Load Spectra	30
Flutter Analysis	30
Composite Material Data	31
Environmental Influences on Composite Structures	34

RESEARCH PRIORITIES, STRUCTURES AND MATERIALS (continued)
Non-Destructive Testing 34
Aluminum-Fiberglass Bonding for Primary Structures 34
References 40
RESEARCH PRIORITIES, SOARING METEOROLOGY 41
Introduction 41
Characteristics of Thermals 42
Thermal Waves 44
Frontal Updrafts 47
Atmospheric Boundary Layer Flux Measurements 48
Cloud Physics 50
Special Vehicles for Meteorological Research 51
Minimum Instrumentation 52
RESEARCH PRIORITIES, SELF-LAUNCHING AND ULTRALIGHT SAILPLANES 53
Introduction 53
Propellers for Powered Sailplanes and Light Aircraft 53
Ultralight Structures 53
Rough Air Hazards for Ultralight Aircraft 54
Pseudo-Ornithopter Propulsion 55
Propulsion Systems 56
Regulatory Standards 57
Low-Speed Flexible-Wing Aircraft 58
RESEARCH PRIORITIES, PERFORMANCE TESTING 60
Introduction 60
Current Activities 60
Present Techniques 60
Specific Research Proposals 64
Specialized Instrumentation Development 67
Stability and Control Research 69
Supporting Activities 69
Publication of Performance Results 70
References 72
APPENDIX I - WORKSHOP PARTICIPANTS 73
APPENDIX II - PAPERS PRESENTED AT THE SYMPOSIUM ON THE TECHNOLOGY AND SCIENCE OF MOTORLESS FLIGHT 77

The Science of Low Speed Flight (Luncheon Address) 78
Oran W. Nicks

AERODYNAMICS AND DESIGN

Sailplane Aerodynamics and Design, the State of the Art 86
A.J. Smith

Anaysis of Effect of Asymmetric Loading on Sailplane Performance in Circling Flight 89
William H. Phillips

An Introduction to Geometric Programming and its Application to Sailplane Design 119
John H. McMasters

The Search for Higher Cross-Country Speeds 147
Nicholas Goodhart

Stuttgarter Profilkatalog I -- Experimental Results from the Laminar Wind Tunnel of the Institut für Aero- und Gasdynamik der Universität Stuttgart 155
D. Althaus

Wind-Tunnel Measurements on Bodies and Wing-Body Combinations 159
D. Althaus

A Critical Review of the Physical Aspects of Airfoil Design at Low Mach Numbers 179
F.X. Wortmann

Airfoils with High Lift/Drag Ratio at a Reynolds Number of About One Million 197
F.X. Wortmann

Airfoils with a New Hinge for Ailerons and Flaps 205
D. Althaus and R. Eppler

The Development of a Two-Dimensional, High Endurance Airfoil with Given Thickness Distribution and Reynolds Number 218
George S. Pick and Douglas A. Lien

Computer Analysis of the Performance of 15m Dailplanes 249
F.G. Irving

When Sould We Use Water Ballast? 263
Richard Eppler

Cloud-Street Flying 274
F.G. Irving

INSTRUMENTATION

Instrumentation for Soaring 287
Paul B. MacCready, Jr.

Remote Detection of Thermals by Means of Horizontal Electric Field Measurements 293
Ralph Markson

Experience with a Variometer-Computer 315
John Firth

Electric Variometer Systems and Developments 322
A. Raouf Ismail

Calibration and Performance Checking of Variometer Systems 335
Wolf Elber

STRUCTURAL CONCEPTS AND MATERIALS

The State of the Art, Structures and Materials 351
Bernard Paiewonsky

Extruded Light Alloy Aircraft Structures 352
Piero Morelli

Crack-Toughened Epoxies for Room-Temperature Applications 366
K.J. Strack

Composite Systems for Aircraft Construction 376
Stephen T. Bowen

Fiberglass Reinforcement for Sailplanes 394
Barry R. Elson

SOARING METEOROLOGY

Instability Patterns at the Head of a Cold Outflow 407
John E. Simpson

The Measurement of Convection Using a Powered Glider 416
J.R. Milford, Z. Hashimi, and P. Purdie

Continuous Cloud Physics Data Obtained in Updraft Shafts of Continental Cumulus Clouds 435
J. Doyne Sartor and Wim Toutenhoofd

An Instrumented Sailplane -- A Platform for Cloud Physics Research with Continuous Rapid Response Measurements 439
Wim Toutenhoofd, Theodore W. Cannon, and J. Doyne Sartor

Some Aspects of Turbulence in the Atmosphere 442
Robert R. Long

SELF-LAUNCHING AND ULTRALIGHT SAILPLANES

State of the Art of Self-Launching Sailplanes 448
H.N. Perl

Self-Launching Sailplane D-39 452
Wilhelm Dirks

The High Performance Motor Glider and its Application in Competition Flying 461
Ian Strachan

MIT's Man-Powered Aircraft 485
Paul Hooper and Robert Peterson

Pseudo-Ornithopter Propulsion 505
Grant Smith

The Use of Stored Energy Devices in Man-Powered Self-Launching Sailplanes 521
John H. McMasters and Curtis J. Cole

Foot-Launched Gliding 548
Michael A. Markowski

PERFORMANCE TESTING

State of the Art Review -- Performance Testing 552
William M. Foley

Recent Standard Cirrus Performance Measurements 557
William M. Foley

Flight Evaluation of Aeroelastic Distortion Effects on Performance, Stability and Control of a Sailplane 565
H.A. Torode

Glider Performance Testing with an Automatic Recording System 585
G.R. Whitfield

Some Flight Tests on Self-Launching Sailplanes 598
Hans Zacher

A Comparison of Classical Drag Estimation Techniques with Sailplane Flight Test Results 614
William E. Brown

PREFACE

This volume documents the results of the Workshop to Identify Priorities for Motorless Flight Research held at the Massachusetts Institute of Technology, October 18-22, 1972. The participants in the workshop included the authors of papers presented at the First International Symposium on the Technology and Science of Motorless Flight which was held concurrently with the Workshop, as well as invited participants selected for their outstanding contributions in each of the areas surveyed. Many of the sections derive from group discussion and are, therefore, not credited to any particular person.

In order to facilitate communication, the current affiliations and contact addresses of the major participants are listed in an Appendix. These persons should be contacted directly if more information is needed on a topic with which they are identified in the text. In cases where no one person is identified with a particular topic, the chairman of the workshop section concerned may be consulted.

Edited, revised versions of the papers presented at the concurrent Symposium form another Appendix. It will be found that these, in many cases, give more background to topics raised in the Workshop reports, and also provide invaluable bibliographies. Because of space limitations, some of these papers have been considerably shortened.

We should both like to thank the many people who gave so unstintingly of their time and effort to make the Workshop and Symposium the great success that it was. We are confident that this initiative will lead to important advances in many areas touching on low-speed and unpowered flight. We look forward to further meetings in the years ahead, at which progress can be reported, ideas exchanged, and the directions set for still further advances.

James L. Nash-Webber
Editor

Rene H. Miller
Technical Supervisor

Cambridge, Massachusetts
February, 1973

INTRODUCTION

Since the pioneering days of flight in the last century, the major part of the over-all research effort in aeronautics has sought to answer questions about aircraft flying at increasing speeds and altitudes with larger and larger payloads. Since the amount of effort which could be expended on aeronautical research has always been limited, this concern with high-speed flight phenomena has led to the by-passing of several significant topics in the low-speed flight regime. The urgent need to begin to fill in some of the gaps in our knowledge has become apparent as a result of several factors. These include:

1. The rapid growth of general aviation, and of soaring in particular.
2. The emerging requirements for safe, quiet, efficient STOL aircraft of an ecologically benign nature.
3. The current need for special low-speed vehicles as tools for meteorological, geophysical, and biological research.
4. The prospects for significant reductions in bulk air-transportation costs through use of optimized unpowered vehicles and flight techniques.
5. The constant need for improvements in flight safety in an environment where an ever-larger cross-section of the public is becoming exposed to high-performance soaring and general aviation aircraft.

Given the need, the question of priorities comes at once to the fore. Consequently, the concept was evolved of trying to gather together the best available opinions and ideas from a large cross-section of the currently active workers in the several specialist fields touching on the general topics of low-speed and unpowered flight. In order to make the task of priority assessment more manageable, it was necessary to get the people involved into a situation where full and free discussion

was possible. Thus the Workshop groups whose findings are set out in the following sections of this report were set up.

Each topic discussed in this report may be assumed to be of equal priority, unless some special indication is given. The topics treated are those winnowed from a much larger list of topics initially proposed. Each one of them is well worth the research and funding efforts required to make useful progress. It is to be hoped that this will be forthcoming.

RESEARCH PRIORITIES, AERODYNAMICS AND DESIGN

Introduction

In the context of any aircraft-related research, the concepts of aerodynamics and design are inextricably linked together. This truism holds good with even more force in the case of the sailplane. Nevertheless, it is possible, in some cases, to separate out particular topics which can be investigated independently and still provide useful inputs to the over-all design problem.

We consider each of the topics treated below to be worthy of immediate effort, thus the question of their relative priorities is a difficult one to answer. We have, however, made some attempt to do this, as shown in Table 1.

Circling Flight

1. Problem Statement

Most of the existing sailplane performance measurements have been made in straight flight. The resulting characteristics in turns have been predicted, but usually without considering any corrections for curved flow effects.

The curvature of flow, and velocity differences between the various parts of the airplane require control deflections and introduce flow angle differences which become more important with increasing lift coefficient and with decreasing relative density factor $\frac{m}{\rho S b}$.

Trends in glider design may increase the maximum lift coefficient and the span, resulting in a rapid increase in importance of the effects of turning.

2. Recommendations

Thus, while turning effects may have had relatively little importance in the past, they will become more important in some future designs. For this reason, verification of the

TABLE 1

Priorities for Research in the Areas of Aerodynamics and Design

PRIORITY			TOPIC
High	Med.	Low	
x			Circling Flight
•			performance measurements
	•		extension of theory
	•		consideration of nonisotropic atmosphere
	•		piloting techniques
x			Variable Geometry
•			variable chord and camber
		•	variable incidence
	•		variable span
		•	variable sweep
		•	CG shifting
x			Airfoils
	•		test
		•	extend theory
x			Handling and Stability
	•		measurement of handling qualities
	•		handling at higher angles of attack
		•	non-steady flight dynamics
		•	stability augmentation
x			Aerodynamic Tailoring
•			fuselage
	•		wing/fuselage
	•		fuselage/tail
		•	wing planform
		•	wing tips
x			Systems Modelling for Design Optimization
	x		Bird Flight Studies
		•	collect data and evaluate
		•	instrument birds, measure
		•	applications to hardware
		x	Energy Gathering
x			Motorless Flight Applications
x			Coordination with Regulatory Authorities

effects by flight and wind tunnel tests would be very desirable. A useful program of work would be:

a. To measure the sinking speed in turns of typical gliders and compare with predictions based on straight-flight data and theory.

b. To extend the theory of induced drag in turns to take into account curvature of the wake and geometric flow angle differences.

c. To extend both theory and experiment to the case of circling in regions of non-uniform vertical air-mass speed (i.e. thermals).

d. To determine the actual techniques used by a pilot in circling flight in a sailplane so that designs are optimally tuned to the pilot's abilities and behavior.

The reader should also refer to the recommendations of the Workshop sections on Performance Measurement.

Variable Geometry

1. Introduction

In the absence of a radically new aerodynamic concept, appreciable performance gains arising from improvements in wing section design seem unlikely. In these circumstances, variable geometry seems the most promising way of achieving noticeable advances in soaring flight. Some approaches to variable-geometry sailplanes are discussed below.

2. Variable Chord and Camber

This is the Sigma system, based on a wing section designed by Wortmann. Sigma has its problems and, in particular, the design performance has not yet been achieved. However, the causes of the performance degradation are known and there is every reason to believe that the basic concept is sound. Flying Sigma is relatively straighforward and the stalling characteristics in all configurations are excellent. This arrangement offers a performance gain of perhaps 15% over comparable fixed-geometry design.

Further R&D is required on:

a. Optimization of flap extension (too small - no significant gain; too large - Reynolds number of flaps-in section too low).

b. Design of good retraction system for flaps.

c. Optimum layout of flaps and other wing-mounted control surfaces.

d. Flexible flap fairing and sealing against leaks.

e. Asymmetrical changes to optimize circling flight configuration.

f. Integration into the overall optimization process as proposed elsewhere in this report.

3. Variable Span

An examination of the optimum way to dispose a given wing area at the higher cruising speeds used in cross-country soaring shows that the best span is frequently considerably less than the span of the glider being assessed. This arises because the reduction of wing profile drag due to the increase of Reynolds number is greater than the increase of induced drag due to the span reduction. This conclusion suggests that in a variable area glider reduction of chord in order to achieve high wing loading for cruising flight will not be as effective as reduction of area by decreasing span. A brief analysis has shown, however, that unless variable span can be associated with a large camber change (as is more easily achieved using a variable chord) it may not be possible to take advantage of the benefits of variable area.

The engineering difficulties of combining variable camber with variable span appear formidable. On the basis of Goodhart's* limited analysis, the benefits of variable span appear doubtful. However, it would be relatively easy to investigate the possibilities in more detail and it is recommended that this should be done before hardware is attempted.

---

* See the paper in Appendix II of this volume.

4. Variable Wing Incidence Setting on the Fuselage

With fixed-geometry wings, there might be a small advantage in varying the wing incidence setting on the fuselage so that the fuselage is pointed along the local airstream direction at all speeds. This system becomes less important when small camber-change flaps are fitted since the sailplane then operates more nearly at a constant angle of attack.

5. Variable Sweep

It is difficult to see any useful application of symmetrical variable sweep. One could, however, imagine differential sweep being used for lateral control (as in Barnes Wallis' "Wild Goose"), particularly to avoid large aileron deflections in turning flight. However, it seems to be a very complicated way of achieving a small performance gain and is unlikely to be worthwhile.

6. Other Possibilities

There are, of course, other possibilities, such as moving the wing or the CG fore-and-aft to reduce tail loads in some conditions of flight, or laterally to reduce trim drag in circling flight.

7. Conclusions

a. First priority should be given to further investigation of variable chord and camber.

b. Theoretical examination of variable span should also be carried out.

c. Other variable geometry possibilities may be desirable but their investigation merits only a low priority.

d. These investigations should, of course, involve a survey of previous investigations, both theoretical and experimental (eg. Sigma and BJ-series flight tests).

Airfoils

1. State-of-the-Art

There now exist several techniques for the design of low-speed airfoils which are "optimum", in some sense, for a given purpose, such as maximum C_L. However, the developers of these techniques are still in some disagreement as to the most useful design methods and as to the level of performance improvements attainable. There is a lack of information needed to assess the three-dimensional behavior of the new ultra-high L/D sections.

2. Requirements

a. To resolve these differences, both experimentally and theoretically. It would be mandatory to test competing concepts in identical tunnel environments.

b. To investigate the three-dimensional problem.

c. The demonstration of the application of a selected technique to the design of a wing for a new aircraft.

d. The documentation, in detail, of this demonstration, so that a designer who is not necessarily an expert in these techniques, can use them effectively. A suitable current technique for use in items c. and d. may be Eppler's computer solution for the inverse problem.

Handling and Stability

1. Problem Statement

In general, because of their relatively slow flight speed and lack of power effects on stability, the handling qualities of most conventional sailplanes are satisfactory. Efforts to obtain higher performance, however, lead to difficulties of two types. First, the size of tailplane surfaces is reduced to an absolute minimum, leading to possible lack of control effectiveness at high angles of attack. Secondly, at high flight speeds, the period of the response and control sensitivity may approach the region of pilot-induced instability. Rough air management of the aircraft, particularly in thermally climbs is a particularly important consideration, since the climb rate

decreases occasioned by poor maneuvering in a rough thermal cannot be recovered completely, even with a configuration optimized for inter-thermal cruising.

2. Recommendations

The subject of handling qualities requires study by a combination of experimental measurements correlated with pilot opinion and analytical studies to predict trends and to provide solutions to problems. The following program is suggested to provide a basis for the advancement of knowledge in this field:

a. Measurements of handling qualities of a number of existing sailplanes. These tests should be made with instrumentation to measure control forces and positions, aircraft motions and accelerations, angle of attack, and sideslip. These tests may be conducted by methods adequately developed in the past for powered airplanes or using new inertial techniques.

b. Studies of handling qualities at higher angles of attack by means of pre-stall, stall, and post-stall tests in flight correlated with wind tunnel tests of a model at comparable Reynolds numbers.

c. Analytical or analog studies of sailplane dynamic motions, including aeroelastic deformations.

d. Studies of methods to provide additional control feel through passive devices, such as springs and dashpots, to reduce pilot-induced oscillation tendencies.

e. Analytical studies to determine possible benefits of stability augmentation devices, followed by tests if the benefits appear worthwhile.

Aerodynamic Tailoring

1. Problem Statement

We are able to calculate the optimum planform of a wing, and its profile drag, taking account of the local Reynolds number, the measured drag polar of the local airfoil, and local flap or aileron deflections. We know relatively little, however, about the influence of the wing tips and fuselage on the induced drag.

Also, when designing an aircraft, the wing has to be combined with a fuselage and the required control surfaces. At this point further gains should be possible. The combination of these parts should be specially tailored for each sailplane design, to give the greatest reduction in drag and increase in lift. However, there is little knowledge about the aerodynamic characteristics of fuselages and wing/body combinations at sailplane Reynolds numbers, in particular. The same holds for the interference of the vertical and horizontal tail surfaces with the fuselage and with each other.

2. Recommendations

a. Considerably more wind tunnel and flight testing which addresses specifically the wing tip problem at sailplane Reynolds numbers is required.

b. The scope of the existing work on wing/body and empennage interference drags should be increased, with particular emphasis on testing at sailplane Reynolds numbers.

Systems Modelling for Design Optimization

1. Short Term Objective

To create a highly general mathematical model of an unpowered vehicle operating in the real atmosphere which can be used, in the form of a computer program, to predict the performance of a vehicle of defined geometry. This model should be in the form of a very general framework ("main program") which ties together, in an analytically exact manner, the operations ("subroutines") which arise from the diverse disciplines involved in preparing an over-all model. The intent is that each of these sub-areas should be modelled initially in a simple fashion, in order that the over-all model can be operational as soon as possible. Thereafter, increasingly sophisticated treatments can replace the initial simplified models, one at a time, without disturbing the operation of the model, as a whole, in any way. A highly simplified conceptual layout of such a model is shown in Figure 1.

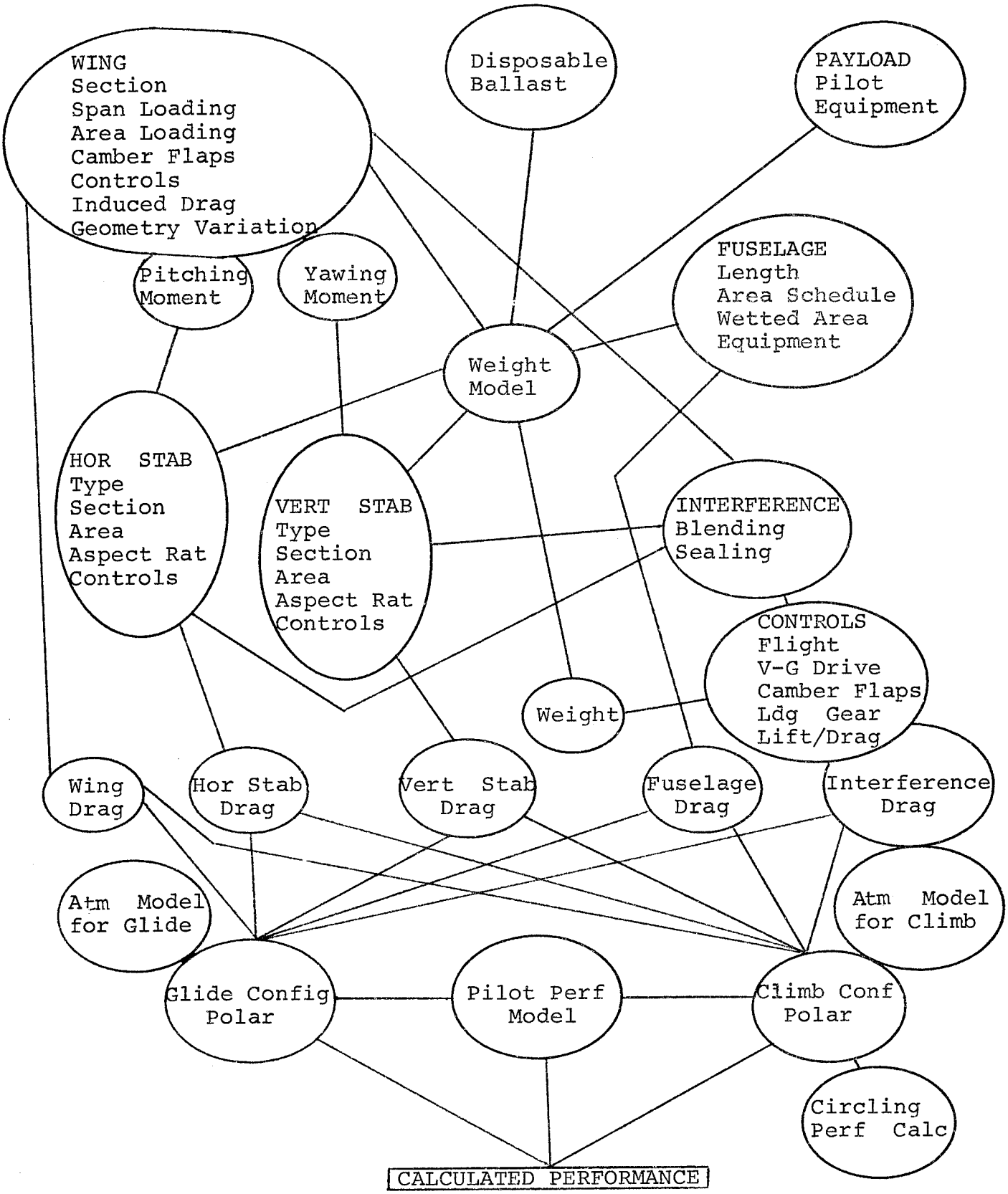


Figure 1 - Conceptual Layout of a Possible Model Structure

2. Medium Term Objective

To bring the model/computer program up to the "state-of-the-art" with respect to each of the specialized fields upon which it touches. This could best be accomplished by making the simple program of (1) widely available to workers in each field, encouraging them to replace the original calculation routines with their favored improvements in each case. This process of successive modification would require a strong central "control" agency, which would also have the job of sending out "updates" at regular intervals to each of the groups working on parts of the model. The looked-for advantages of this approach would be:

a. Wide global dissemination of the latest information and techniques.

b. Interdisciplinary cross-fertilization.

c. Availability to designers, at the earliest stage possible, of an effective performance prediction tool for a given geometry and atmospheric model.

3. Long Term Objective

In parallel with the latter stages of (2), when it seems that a "plateau" is being approached, an extension of the model/program to provide for automatic optimization of a design under specified constraints. This would be a long-term effort which would necessarily have to start simply, given the basic complexity of the over-all model, but could grow steadily in sophistication, accuracy, and utility until it becomes a standard design tool for advanced unpowered aircraft.

4. Existing Data

A start in this direction is Goodhart's Sigma program and similar programs used in Germany, as well as the aircraft design programs currently under development for NASA. For optimization there are well-established techniques such as the method of steepest descent and the geometrical programming techniques expounded by McMasters elsewhere in this report.

Bird Flight Studies

Certain features of birds are apparently used to offset disadvantages of low Reynolds number, low power loading, low

geometric aspect ratio, and other factors obviously influencing flight performance. In the hope that lessons may be learned from more diligent study of bird flight using the modern tools and knowledge of aerodynamics, it is recommended that bird aerodynamics be given at least a moderate priority for serious study. Work needs to be done in at least three areas:

a. An inventory and evaluation of existing research data should be prepared. A great deal of useful information exists in obscure sources or private files and should be made available to a wider audience. Further, much of the existing published data is either incomplete, contradictory or lacks valid empirical verification. Three areas deserve particular attention:

   (i) The why and wherefore of feathers as covering for aerodynamic surfaces. [It is believed that the Russians have done extensive work on this subject and that some of the results are available in translations prepared by the British.]

   (ii) The use of variable geometry in circling flight.

   (iii) Improvements in effective aspect ratio obtained by unusual wing tip geometries or other means.

b. Modern instrumentation and tracking techniques should be applied, in combination with visual observations, to a variety of soaring birds in a free flight environment in an effort to understand more fully the bird's use of variable span, camber, twist, CG control, etc. in circling flight. Such work should be of value in indicating ways to increase both efficiency and controllability of several types of aircraft in low-speed turning flight.

c. Studies should be undertaken of ways to translate the relevant empirical observations in (a) and (b) above, into practical hardware for sailplane, motor glider and ultra-light glider applications, in the short term, and into transportation vehicle technology in the longer term.

Energy Gathering

1. Problem Statement

In a rather indirect fashion, sailplanes use energy derived from the sun. Following a suggestion made some years ago by Raspet, it would seem logical to use the sun's energy more directly. Such a technique would not seem to be in conflict with the prevailing philosophy of motorless flight.

In a paper written many years ago, Raspet showed that with the then state-of-the-art, it would be possible to attain an effective L/D of about 100. This could be done by covering the top of the wing with solar cells and using the electrical output to drive a propeller. Since then, sailplane performance has greatly improved and solar cells have become more efficient. Level flight should now be possible - perhaps even a gentle climb under favorable conditions.

2. Recommendations

The above possibility should be examined again, bearing in mind:

a. Optimization of the aircraft (more wing area yields more energy gathering but more profile drag).

b. Achieving a suitable upper-surface contour for the wings.

c. Cost.

d. Operating techniques.

e. The use of suitably optimized airfoils.

3. Other Energy Sources

Probably the only other unexploited source of energy is associated with small-scale atmospheric motions (turbulence and wind gradients). It appears that the spectra are such that the exploitation of this form of energy by sailplane-sized vehicles is unlikely - but perhaps some further consideration is warranted, especially in the light of advances in control theory.

Motorless Flight Applications

There is a need for innovative and imaginative concepts for using unpowered vehicles in the service of mankind in ways which are not now considered. Since the sailplane is an ecologically benign vehicle, its increased use for any purpose now using powered aircraft would be beneficial. There are several concepts which deserve more study, both analytically and through hardware demonstration:

a. Advanced bulk transport gliders of highly optimized configuration and structure.

b. Very low-speed gliders and powered gliders for meteorological research, geophysical data gathering, and bird flight studies.

c. Improved low cost ultra light sailplanes capable of extending the experience of flight safely to a less-skilled and wider cross-section of the public than is currently involved in general aviation or soaring.

It must be emphasized that these do not represent the limits of possible new applications in any way.

Coordination with Regulatory Authorities

The workshop group as a whole sets a very high priority on all and any efforts to cooperate with regulatory authorities, such as the Federal Aviation Administration, in setting up legal standards for sailplane, self-launching sailplane, and ultra-light glider designs and operating techniques. These authorities must be continuously aware of the trends of research and development for advanced vehicles; this can only be accomplished by improving the degree of communication and coordination between the rule-makers and the researchers and designers. Two aspects of the problem appear to be of the greatest current urgency:

a. There is felt to be a tendency for rules to be written in such a way that they appear not to take into account

sufficiently well the particular characteristics of these aircraft and their piloting techniques. Better communication between all concerned parties should lead to achievement of the desired flexibility. It is probably the case that correction of this tendency may often be primarily a matter of education only.

b. There appears to be a tendency for rules to become more explicit than actually needed in setting up mandatory structural design practices and standards. This has the effect of inhibiting innovative progress in these areas in some cases. Every effort should be made to ensure that rules are written in terms of realistic performance standards rather than in terms of explicit mandatory practices, and that a reasonable degree of flexibility is always maintained, provided only that such flexibility is consistent with safety.

RESEARCH PRIORITIES, INSTRUMENTATION

Introduction

Instruments for soaring can be considered in two categories: Those which measure what the sailplane does (airspeed, rate of climb, altimeter, compass, gyros); and those which help to show what the atmosphere is doing. The devices in the first category are rather well-developed, inasmuch as they have been necessary since the early days of gliding. Those in the second category are in a much more primitive stage of development. The most important instrument, the rate-of-climb meter, represents a special case. It is well-developed and fits into both categories; while showing what the sailplane is doing, it can also be interpreted as showing (with corrections) what the atmosphere is doing.

The workshop did not concern itself with the normal flight instruments which tell what the sailplane does. Existing devices are satisfactory. In fact, the indicated-airspeed meters can be calibrated with sufficient accuracy for use for refined performance testing purposes. Even automatic data-loggers for efficient flight test studies are now available, and improved versions will certainly be appearing.

Increasing attention is now being focussed on considering an instrument as an element of a complete system aimed at permitting the pilot to improve his exploitation of atmospheric motions. Human factors are seen as particularly important, especially those involved in conveying the information to the pilot in a more convenient manner, and even providing automatic computations to facilitate utilization of the observations is not unreasonable. These points were treated in the workshop. Another area of the complete system was not treated explicitly,but has such importance that it deserves mention: This is the optimizing of flight maneuvers to make the best possible use of lift. This is complex, important, and at present receiving little attention. The flight strategy for locating (and continually relocating) the center of

a thermal is likewise poorly studied but all-important. It obviously relates intimately to the characteristics of various sensors, to the way their information is conveyed or displayed to the pilot, and to the characteristics of thermals. The seat-of-the pants "feel" of the pilot for gusts and acceleration is an input too. "Human factors" and their relation to instruments, sailplanes, and thermal structure represents a fertile area for improvement.

Consideration of the ordering of research priorities must consider the benefit/cost ratios for the subjects under discussion. For purposes of illustration, let us choose average thermaling climb rate improvement as the "benefit" to be sought at lowest cost. In ordinary convective conditions, inexpensive improvements in the interrelated areas of instrumentation and piloting procedures (including insight into thermal structure) are likely to give average climb increases of 0.5 - 1.0 m/sec while far more costly improvements in aerodynamics and structures may yield improvements only of the order of 0.2 m/sec. The benefit/cost ratios of these two approaches thus may turn out to be greatly in favor of the former. Aerodynamics and structures represent satisfying engineering disciplines, which are well staffed. However, we wish here to emphasize the instrumentation and piloting procedure disciplines; they offer a chance for big rewards, inexpensively, and so deserve very special attention despite the fact that they may not easily fit conventional engineering approaches and institutions.

In this review we first look at an instrument approach to locating thermals from a distance. The method is one which is very promising. We do not consider here the many other approaches to indirect probing which might work, but only at a cost and complexity which would make them impractical as aids to soaring. Then we examine methods for telling which way to turn in a thermal. Next we probe variometer systems which are the primary tool for thermal hunting and exploiting, and the use of air markers to augment that tool. Then we treat the use of an angle-of-attack sensor to simplify and improve thermaling. There is also some discussion of safety and convenience devices. The attention paid

here to hunting and using thermals comes about because so much soaring is based on thermals. Waves and slope currents are, in general, less important, and they do not appear to require any new instrumentation techniques.

Electric Field Measurements for Remote Thermal Detection and Turn Information

1. State-of-the-Art

To date the sailplane pilot has no sensor other than his eyes for deciding in what direction to fly in order to find lift; he might head for a cumulus cloud or a ridge facing the wind. Atmospheric electric field measurements may offer another means of locating thermals at a distance from the sailplane.

Space charge in the atmosphere is generally most concentrated near the earth's surface and at the top of the mixing layer. Thus a thermal chimney fed by horizontal convergence near the ground would carry anomalous space charge upward. The charge would dissipate with time (and height) as a function of the air's conductivity. Assuming a relaxation time of 15 minutes, an updraft of 3 m/sec would lose 63% of its charge in rising 2.7 km, a typical height for the top of the mixing layer. Charge would accumulate near the top of the thermal due to the air circulation pattern. Calculations assuming space charge densities of 1 to 10 elementary charges per cm^3 and a 1 km diameter sphere of space charge have indicated that these regions could be detected at a range of 1 to 4 km by measuring the horizontal electric field. When an updraft penetrates the inversion at the top of the mixing layer it will pick up additional space charge from that level which will replenish charge lost in transit from near the earth.

A lightweight, low power-consumption potential gradient measuring system has been developed and installed in a sailplane in order to explore this concept of remote thermal detection. The electric field component from the front to the rear of the sailplane has been measured initially, in order to minimize the influence of the vertical component of the earth's electric field - typically 100 times as great as the horizontal component - that would be picked up in a wing-tip-to-wing-tip measurement.

The sensitivity of the system is a few nV/m, however normal pitch variations introduce some of the vertical field and limit operational sensitivity to about 1 V/m.

In practice, the sailplane circles while the pilot watches the deflection of a zero-center needle on a meter. Maximum right deflection passing through a heading indicates that the center of positive charge - indicating the thermal - lies ahead. Maximum left deflection suggests the thermal lies directly to the rear. Limited testing under moderately strong soaring conditions tended to indicate the usefulness of the technique. Flying in the indicated direction generally resulted in good lift although sometimes strong downdrafts had to be penetrated. Areas of lift marked by clouds of about 400 m diameter and 200 m height were sensed from a distance of about 2 km. Longer range appears possible. When circling in a thermal, corrections toward the center of positive charge appeared to result in better lift.

2. Recommendations

Future research should include the left-to-right horizontal component with provisions to eliminate the vertical component. Both horizontal components presented on a cross-pointer display would indicate the direction of the positive charge from the sailplane at any time without the need for circling. However, initial tests of thermal detection using only the front-to-rear electric field component indicate that it is frequently not necessary to fly a full circle. A heading change of 30 degrees during which the maximum right deflection of the needle occurs is sufficient to determine the heading toward a region of positive charge. Measurements of the vertical electric field and conductivity may assist in learning how to use atmospheric electrical measurements for soaring purposes.

Turn Information Using Humidity Data

1. State-of-the-Art

The difference between humidity inside a thermal and outside it can be quite large, and increases with altitude. It can be measured easily across the wing from tip to tip. There is no natural large vertical gradient to confuse the measurements during banked flight. Humidity sensing with fast-response probes

is an easy instrumentation task, especially where absolute accuracy is not important. Thus a turn indicator based on humidity information offers the possibility of a very high benefit/cost ratio, and deserves a high priority for development.

One sensing approach is to employ tiny thermistors with wet wicking on them so that they sense wet-bulb temperature. Another method is to use a thermopile arrangement with wet wicking. There are also fast-response solid state sensors for relative humidity or absolute humidity.

2. Recommendations

These approaches deserve further work, including hardware demonstrations.

Variometer Systems

1. State-of-the-Art

The variometer, or sensitive rate of climb meter, is basically an altimeter with a leak in its air chamber such that the reading is quickly reset to zero. The instrument senses the leak rate or the pressure on a diaphragm. Present units are quite satisfactory, having fast response and being reasonably priced. Probably the biggest problem is zero drift elimination. Response speeds of good units are about one second; a faster response is possible, but serves no real purpose because the pilot would not absorb or use the extra information. When used to inform the pilot of the air motion, all sorts of corrections are required. An accelerometer can be phased into the unit to speed its effective response speed - but this is not done because the high frequencies provide little useful information. The major correction is the total energy device, whereby airspeed information is added to the rate of climb to remove the effect of rate of change of airspeed on the correction between vertical velocity of the sailplane and vertical velocity of the air. A special venturi or diaphragm handles the job well. Studies have established the sensitivity changes with altitude for the rate of climb and the total energy corrections. There are two other major corrections:

a. For the rate of climb: the normal equilibrium sinking speed of the sailplane can be removed by somewhat complex analog elements or displays but is usually handled by the pilot mentally making approximate corrections, and

b. For the total energy device: horizontal turbulence yields transient errors which seem very difficult to eliminate but can be minimized by filtering electronically or by flow restrictors.

The rate of climb instrument usually offers a 270° meter readout which is usually quite acceptable. In addition, the units often have an audio tone output to supplement the conventional meter reading. By the pitch of the audio tone, the pilot receives information (at least relative information) while being able to look outside the sailplane. This represents a simple but elegant example of human factors engineering.

One system growth area for variometer systems is in the subject of computerized utilization of their output information with other information such as airspeed. The simplest such computer is the speed ring which is set around the meter face to tell the pilot the optimum speed to fly between thermals. The ring position is set depending on the expected strength of the next thermal to be encountered. A more sophisiticated electronic system to do this and related tasks (such as rate of climb averaging) is the Air Data Computer. An ingenious combined rate of climb and airspeed display system is represented by the newly developed Peebles Computer. It displays best speed to fly, glide angle, and normal sinking speed correction graphically in a way which is interpreted almost instinctively by the pilot.

2. Recommendations

In summary, although variometer technology is basically in good shape, some work on zero drift, sink correction, and total energy attachments would be very useful. In order to be compatible with a MacCready ring calibration at all altitudes, an inexpensive method of correcting an electrical variometer output to be proportional to the quantity (true vertical speed) x (square root of density ratio) should be developed. Considerable effort on computerized processing and displays is justified at

this time.

Air Markers

1. State-of-the-Art

If the sailplane could draw a line in the sky which would move with the airflow and which would be visible for a minute or so, the pilot could, at a glance, qualitatively ascertain part of a thermal's flow field. Such a line can be drawn. Smoke can be made by a pyrotechnic device, and be released near a wing tip so that it gets into a tip vortex where it is relatively protected from diffusing and disappearing for some tens of seconds. The vortex wake descent speed for a sailplane will not cause appreciable error in this application. For producing many such trails throughout a flight, some other source of particles should be developed. Oil fog with 0.6 μm particles diameter has especially high visibility per unit mass of material released, but requires heat to produce. A string of bubbles can be released by an automatic dispenser. Another possibility might be a small, low-speed, smoky, non-dangerous rocket launched in the forward direction.

2. Recommendations

The value of some such air marker seems so great that development of dispensing devices and application methods should have a high priority. However, any methods chosen should not compromise unduly the ecologically benign nature of the sailplanes.

Angle of Attack Control

1. Problem Statement

Angle of attack is more valuable and fundamental for establishing the aerodynamic performance of an aircraft than is airspeed. The aircraft always stalls at approximately the same mean angle of attack, but the airspeed at stall varies with the load factor. Also, the lift to drag ratio is a direct function of angle of attack, at least to a first order approximation.

While such information is valuable, it would be desirable to have it in a manner which does not increase the pilot's workload. A display which was heads-up, audio, or external would be desirable. Even better would be simple automation which drove the elevator to provide commanded angle of attack. Advantages which would result include increased safety as well as better climbing in thermals. There would be less likelihood of stall near the ground. A decreased workload permits the pilot to spend more time on other duties. For student pilots it is easier to learn to fly using angle of attack than airspeed. For advanced pilots it would allow greater performance to be achieved from the aircraft.

2. Recommendations

Sophisticated systems for angle of attack display and control are available for large powered aircraft. Research to provide similar systems appropriate for sailplanes is desirable. Low cost, simplicity, ruggedness and non-distracting display modes are the most important characteristics to be sought after.

Buoyancy Indicator

1. Problem Statement

Variometer information tells only what a thermal is doing, not what it will do. Knowledge of the buoyancy of a thermal gives a hint as to the thermal's future. The buoyancy at a particular level in a thermal depends on the temperature and humidity relative to the temperature and humidity of the surroundings. At least in principle, the buoyancy can be measured from the sailplane. Since the sailplane is changing its altitude, an altitude correction must be made in the buoyancy device. One approach to altitude correction is to integrate the output of an electric variometer so as to have a voltage proportional to altitude change.

2. Recommendation

The development of a buoyancy indicator, for the short time (1 or 2 minutes) and low accuracy requirements of a sailplane, seems simple. Thus the benefit/cost ratio is high enough to justify a reasonable priority for future research and development efforts.

Lightning Danger Alerting Techniques

1. Problem Statement

Modern fiberglass sailplanes are particularly susceptable to damage if struck by lightning because they are poor electrical conductors. Recent investigations following the Apollo 12 incident (when it was struck twice by lightning) have confirmed earlier suggestions that an aircraft can trigger lightning in a high electric field; frequently aircraft are struck by lightning when no other lightning was observed before or afterwards in that vicinity. Being a non-conductor would not significantly inhibit the capability to trigger lightning.

2. Recommendations

Work should be continued on lightning protection for all aircraft, including plastic types. Concerning instrumentation, simple equipment carried in a sailplane could warn of potential lightning danger:

a. Electric field measuring equipment such as might be carried for thermal detection could indicate the proximity or buildup of electric fields approaching intensities characteristic of thunderstorms.

b. Thunderstorms that might be along the projected flight path beyond visual range could be detected by horizontal field intensities in that direction significantly higher than those typical of fair weather. Abrupt variations in the fair weather field signify lightning discharges. This technique has been used to detect flashes at least 100 km away.

c. Monitoring radio static can give an idea of whether or not cumulus clouds containing lightning are nearby. Various simple sensors are available including a transistor portable radio tuned off-frequency.

[It is worth mentioning that observations of cumulonibus clouds indicate that they must be at least 3 km in depth, regardless of the height of cloudbase, before they become lightning producers. Thus, as a rule-of-thumb it may be relatively safe to approach cumulus clouds that are known to be less than 3 km in vertical extent.]

Transponders and Proximity Warning Devices

1. Problem Statement

The radar beacon transponder has no intrinsic merit as part of sailplane instrumentation, yet it may become an unavoidable part of future sailplane instrumentation for flights in certain areas and into certain altitude regimes.

The first approach should be one which secures an FAA policy and operating rules wherein soaring may be done freely in VFR conditions without a radar beacon transponder on board. There is no real payoff to the VFR soaring pilot from the transponder; the whole transponder issue is fallout from a set of rules and regulations designed to accommodate traffic under so-called "instrument flight conditions". In seeking such policy any Instrumentation Working Group must lend full and active support to Government Liaison and Airspace Rules groups.

If transponders must be used in sailplanes for certain conditions, there are still some points, aside from pure technology, which will make matters easier. Because of high unit cost and infrequent use, we should plan on arrangements permitting quick removal and relocation of a transponder between different sailplanes. The FCC licensing rules do permit this for communications equipment if the license application is properly worded. A derivative of this is the "group leader" concept where only one aircraft flying amidst a group has an operating transponder. The single aircraft serves to locate the group within fairly wide bounds.

Current technology and economic pressures will continue to make transponders more affordable, but probably not less demanding of battery power. In fact, new FAA Technical Standards Orders and higher output power regulations will force the power needs, and the cost, higher than would otherwise be the case. The soaring market potential will not justisfy development of a special unit, but certain modifications to designs produced for general aviation are admissible to reduce the average power consumption. Planning for sailplane instrumentation and batteries supplying power must allow for transponder power needs, and must be more mindful of good insulation surrounding batteries to preserve their efficiency during high, cold flights.

Proximity warning has been mentioned as part of instrumentation in connection with multiple occupancy of the same cloud by sailplanes. Federal Aviation Administration policy and rules work against much cloud-flying in this country, as the recent termination of a proposed glider cloud-flying rating amply demonstrates. The mid-cloud collision at the 1972 international contest shows that at least rarely a problem can arise. Very simple alerting and warning devices such as loud audible and bright visual emissions, are worth considering. A common radio communication frequency for general in-cloud reports and altitude callouts is another helpful practice, as shown by British experience over many years.

2. Recommendations

The approaches described above should be implemented.

Instrumentation Clues from Birds

The workshop on sailplane instrumentation discussed some of the relevant aspects of bird flight. Examples of bird navigation and orientation under all kinds of weather conditions have always fascinated man and motivated some serious research in this area. Little scientific work has been done, however, in trying to explain the apparent ability of birds to sense the presence of thermals from a distance, and their undisputed ability to use those thermals. It is interesting to speculate that perhaps birds are able to sense

the most general motion of air masses relative to earth without visual contact of an earth-fixed frame of reference. Knowledge of the processes taking place in the sensory system of birds would have obvious implications for airborne instrumentation. The experimental techniques used by biologists and ornithologists, extended to include the latest developments in microelectronics, telemetry techniques and high-speed data processing might well uncover new knowledge concerning bird orientation, navigation and the sensing of small-scale air-mass motion - as well as bird aerodynamics. This knowledge may involve novel transducing principles and point the way to instruments radically different from those used today.

Barographs

The recording of altitude vs time is of value to pilots who wish to analyze the details and statistics of flights. An inexpensive barograph, with a continuous chart providing fine time resolution, is needed. If the recorder can record additional viariables, such as rate-of-climb, the value of the instrument is increased. The present altitude trace by itself is not suitable for obtaining climb rate, except by tedious post-flight analysis. It should also be noted that a true rectilinear movement is a great advantage. It would also be an advantage to record the heading in order to determine whether the aircraft is turning or flying straight.

Contest Automation

It would be possible to reduce argument and protests during competition by automating such things as starting, finish and turn points. This could be done by electronic gates or radar tracking. It would also be possible to score using a computer program with weights for starting altitudes, handicaps, etc. The computer could be fed by data obtained automatically from the ground. It would offer another form of evidence for establishing world records that would be less subject to dispute.

RESEARCH PRIORITIES, STRUCTURES AND MATERIALS

Introduction

The workshop identified six topics which require research efforts to place the design of sailplanes on a rational basis consistent with design standards in other parts of aviation. These are discussed in the subsections below. We also attempted to formulate suitable initial research projects on these topics, as set out in several formalized Description Sheets.

Sailplane Load Spectra

The sailplane's flight mission profile and ground-handling loads profile vary significantly from those of any other aircraft. Design load spectra currently used have been compiled by the FAA, or by German designers. The American data are based on estimates for rigid wing sailplanes and may not be appropriate for the generally more flexible composite structure sailplanes. Description Sheet # 1 outlines a research project to collect data for determination of improved load spectra.

Flutter Analysis

Flutter analysis for most aircraft has to be carried out using empirical estimating techniques based on past experience. These techniques are applicable to structures in which the fuselage can be considered a rigid platform. Also, they apply to metal structures with low damping properties. Many sailplanes designed today are built from fiberglass composites. All have high aspect ratios. The fuselage cannot be considered a rigid platform for flutter analysis. Flutter computation techniques are required which can be incorporated into flutter prevention design criteria. Description Sheet # 2 outlines a research project on flutter analysis.

Composite Material Data

An analysis of composite materials available and material property data available shows that for composite systems three parameters have to be considered:

- Fiber
- Matrix
- Process

At present much available material property data cannot be considered for analysis or design because often at least one of the three parameters is not applicable to the intended use. Specimens and preparation processes should be standardized to reduce the number of materials tests required. Description Sheet #3 outlines an initial research project to collect standardized data for American-produced composites and their European equivalents.

Deficiencies in Existing Data

1. The fatigue test usually is made at constant stress. For design purposes what is needed is a spectrum of loads, followed by a static test. The strength of the material found in the static test can be used as a design value, if the load spectrum corresponds to that experienced in flight, or a multiple of it. An example of such a test procedure on a full scale aircraft is given in Reference 1. However, only one test was made in that case, and the construction of the spar was found, after the static test, to be faulty at the location of the break. Nevertheless, the data from that test is being used in Germany in lieu of anything better. Note that the mean load in that test was not zero.

2. American fatigue data is normally measured using specimens which have been heat-cured. Thus the data may not be representative of room-temperature systems.

3. The fatigue specimens currently used are usually flat, but if cross-laminated constructions are tested, they must be in the form of tubes, or use special supports, if they are to be at all representative of the loading condition corresponding to shells, such as wings and fuselages [2].

4. Glass fabric styles tested are not representative of those currently used in aircraft construction.

5. Laminates consisting of many layers are usually tested, but wing shells typically use two layers only.

Recommended Tests

1.0 Spars.

1.1 Spars constructed from domestic materials, using rovings for spar caps, and woven cloth for the shear web, should undergo flexural fatigue testing, using a load spectrum such as that in Reference 1. The strains would be the most meaningful measurement to record. In GRP construction the "stress" is heavily dependent on the glass fraction of the laminate, which is not very well known in a hand-layup situation. The amount of glass, i.e. number of rovings in the cap and number of layers in the web must be included in the data output. The glass should be representative of current high-performance systems. The dimensioning of the spar should be done by the methods outlined in Reference 3. After the load spectrum has been applied, the static breaking load should be measured. The independent variable in the test would be the level of the strains, characterized by the maximum strain in the spectra. Various levels of this strain would give, for the dependent variable, the static breaking load (strain also recorded for breaking load).

1.2 The above could be done for box spars and I-beam spars, the web being made in sandwich construction in either case. Box spars should have web material wrapped completely around the spar. Tests could also be made with plywood shear webs. They are easier to construct and may not have the problem of microcracking in the shear web, but they do depend on a glue-line bond to the caps.

1.3 Room-temperature curing resins should be used: a post-cure of 12 hours at 50°C must also be observed. (Some early failures of GRP structures were due to poor understanding of the curing process, i.e. incomplete cure.)

1.4 To upgrade the fatigue life, tests could be made with a high strength resin (heat-cured) and also a high toughness resin (also heat-cured). There is evidence that in flexual loading, high strength resins can increase fatigue life by a factor of 20 [4], and the newest toughened resins developed at Goodrich can show fracture toughness 50 times that of the usual epoxy values. Amines should be used as curing agents rather than acid anhydrides, since the amines will B-stage (gel) at room temperature, and thus be more easily handled. If heat-cured systems show enough improvement over RT systems, it might be worthwhile to heat-cure only the spar.

2.0 Skins.

2.1 Specimens must be tubes, not flat specimens.

2.2 Both 45° and 70° laminates should be tested, with emphasis on the 45° laminate, since it is better in torsional stiffness. The 70° laminate is normally optimal for strength.

2.3 Unidirectional cloth, similar to the German style 92145, as well as a balanced 50/50 weave should be included.

2.4 As before, a load spectrum should be used, and then a static test made. However, torsional loading should be added to the tension-compression loading.

2.5 Only two layers of fabric should be in the laminate.

2.6 As before, the strains are far more useful than the stresses.

2.7 Hand-layup should be used.

Environmental Influences on Composite Structures

Composite airplanes, at the moment mainly fiberglass-epoxy systems, are subject to environmental influences. Of most concern amongst these are

- Freezing/thawing cycle
- Humidity, salt
- Exposure to intense insolation

No data exist on the deterioration of the fiberglass composites under these influences. Real-time structural properties in general are not fully known. Description Sheet #4 outlines a project in which it is proposed to test a full scale wing assembly in an outdoor environment, with intermittent loading, for a period of two years.

Non-Destructive Testing

An AD was recently issued against a European sailplane to guard against possible debonding between upper and lower shell sections of an elevator assembly.* This problem emphasizes the need for research laboratory and field techniques for detecting damage to composite structures. Description Sheet #5 outlines a project to assess the state-of-the-art in NDI for composites and to develop promising techniques into field-usable techniques.

Aluminum-Fiberglass Bonding for Primary Structures

For the benefit of sailplane designers it would be extremely useful to know the structural integrity of combined aluminum-fiberglass construction such as could be used in building wings. Data needed is on bonding and on mechanical fastening.

For a concrete example, the case of fixing a 7075Tg aluminum spar to top and bottom wingshells of laminated FRP sandwich construction might be considered. What bonding agents could be used for this purpose? What shear forces are encountered because of thermal expansion differences? What fatigue life could be expected of such a wing?

---

* Subsequently discovered to be a secondary failure, the primary failure being a trunnion support damaged in ground handling or ground-looping.

Description Sheet #1

Title: Load Spectra Establishment for Sailplanes

Objective: To establish load spectra for a sailplane assuming worst operation environment. To establish the severity of trailering and ground-handling loads.

Approach: Install V-g-h recorders and strain-recorders on wing (critical area), tail and landing gear of one sailplane for the duration of a 10-day competition. Further carry V-g-h recorders or g-excursion counters on three more sailplanes. Collect trailering loads data during retrieves. Construct maximum load spectrum from total accumulated test data.

Resources: 0.5 MY 3 months
[University-research project]

Description Sheet #2

Title: Flutter Prevention Criteria

Objective: To establish whether state-of-the-art flutter analysis can predict flutter in typical sailplane structures of 20 meter wing span, aspect ratio 25, total weight 500 kg built from fiberglass-foam materials. To establish parametric flutter prevention criteria for use in preliminary design.

Approach: Establish all programs and theoretical models available for flutter analysis. Carry out an analysis on a specific airframe (e.g. SB-9) to prove applicability of such analysis. Carry out a parametric study of influencing factors to arrive at design criteria for use in preliminary design.

Resources: 2 MY 1 Year
[NASA in-house or external contractor]

Description Sheet #3

Title: Composite Materials Properties Data

Objective: To establish correlation between European composites and material properties and U.S. equivalent composites and properties. . To establish standard specimens and data analysis applicable for sandwich foam construction design data. To investigate the composite construction processes to determine limitations on some processes.

Approach: Coordinate all efforts of U.S. designers and manufacturers to establish usable data banks, material equivalents, and process control methods.

Resources: 1 MY 1 Year
[NASA in-house or external contractor]

Description Sheet #4

Title: Full-scale Outdoor Fatigue-Exposure Test of Fiberglass Wing.

Objective: To establish full-scale test data on "deterioration rate" of fiberglass wings in actual operating environment under cyclic loading. To test throughout the test-life the effectiveness of NDI methods developed for fiberglass deterioration testing. To establish whether natural frequency integrity tests are meaningful.

Approach: Test a full-scale production wing under simulated symmetrical bending load in a natural outdoor environment for 2 years accumulating approximately 100 hrs. of equivalent flying per week. Test shall include all normal production splices, typical repair to shell and spar, areas not protected by gel-coat. Loading to be constant amplitude. Test shall be accomplished by companion specimens at differing stress levels.

NDI methods (ultrasonics, etc.) shall be carried out intermittantly to check effectiveness.

Resources: 2 MY 3 years

[Aircraft-manufacturers or other external contractor]

Description Sheet #5

Title: NDI for Fiberglass Composites.

Objective: To determine those NDI techniques suitable for detecting damage in fiberglass foam shells, detecting debond in epoxy-bonded shell joints and debond in metal-to-fiberglass joints.

Approach: Coordinate efforts of manufacturers, Air Force, and NASA, to determine state-of-the-art in composite NDI procedures. Develop promising techniques into field methods.

Resources: 2 MY 2 years
[NASA in-house or external contractor]

References

1. Franzmeyer, F.K.; Statische und dynamische Festigkeits-untersuchungen an einer Tragfläche des Segelflugzeuges Cirrus. Deutscher Aerokurier, Vol. 10, 1969 p. 664.

2. Grünninger, G.; Festigkeits-und Deformationsuntersuchungen an Bauteilen aus Glasfaser-Kunststoff, Kunststoffe, Vol. 54, Dec. 1964 p. 759.

3. Wurtinger, Horst; Entwurf und Vordimensionierung tragender Konstruktionen aus glasfaserverstärkten Kunststoffen. Vereinigte Deutscher Ingeniere Zeitung, Vol. 109, no. 24, August 1967, pg. 1121-1127 (Part I) and Vol. 109, no. 36, December 1967, pg. 1710-1714 (Part II).

4. Soldatos, A.C., Burnhans, A.S., Cole, L.F., and Mulvaney, W.P.; High Performance Cycloaliphatic Epoxy Resins for Reinforced Structures with Improved Dynamic Flexural Properties. 155th American Chemical Society Meeting, San Francisco, April 1968.

RESEARCH PRIORITIES, SOARING METEOROLOGY

Introduction

There are many features of the atmosphere which can be investigated most effectively and economically by aircraft flying at very low speeds and with rapid response to vertical gusting. Some of these features are of particular interest to soaring pilots and also to sailplane designers. Others are of greater interest to meteorological and environmental scientists. Some of the more immediate problems are outlined below (Section I) with the suggested approach for gathering relevant data.

In most cases, powered sailplanes have advantages over motorless ones for carrying out systematic investigations, provided that the aircraft performance with engine off is equal to that of a high performance sailplane. A specification for an ideal vehicle is given below (Section II). No vehicle fulfilling the specifications exactly is in existence at present. The development of one is recommended. The use of several identical machines would be a great advantage for the methodical investigation of some of the meteorological problems listed. However, we would stress that much useful information can still be gathered by sailplane pilots without special equipment, if they document their observations properly for use by the scientist.

A basic instrumentation and data-logging system should be designed for use in sailplanes and powered sailplanes. It need not be expensive but should be flexible. An outline specification for this is also given (Section III).

Section I - Immediate Problems

1. Characteristics of Thermals

To select the optimum design for sailplanes, it is necessary to know the characteristics of the thermal which they will use most often. Present knowledge of the three-dimensional structure of thermals, their spacing, and their development with time is incomplete.

The investigation of individual thermals is also of great theoretical interest to meteorologists: one of the subsequent applications of measurements of entrainment would be to the growth of developing hail and thunderstorms. A considerable amount of data will be needed to discriminate between different models of thermals, particularly because their characteristics vary significantly according to the time of day and according to the larger scale meteorological situation on that day. Figure 2 shows the type of variation with height which has been found.

One recommended experiment involves at least three sailplanes and one powered sailplane. On a day with apparently isolated thermals below shallow cumulus (or clear skies), the sailplanes would choose and mark one thermal. The powered sailplane would reach cloudbase and then make a number of passes diametrically through the thermal with power off. This would give an approximately instantaneous two-dimensional description of the thermal.

For this experiment the sailplanes require simple instrumentation and data-logging. All the aircraft should measure height, temperature and humidity. The powered sailplane requires a more rapid data-logger to give the detailed structure.

The site for this experiment is not critical. Measurements of winds around the thermal to show inflow to at least 1 m/sec accuracy is highly desirable but extremely difficult unless new methods, such as a short-term accurate inertial system, can be implemented.

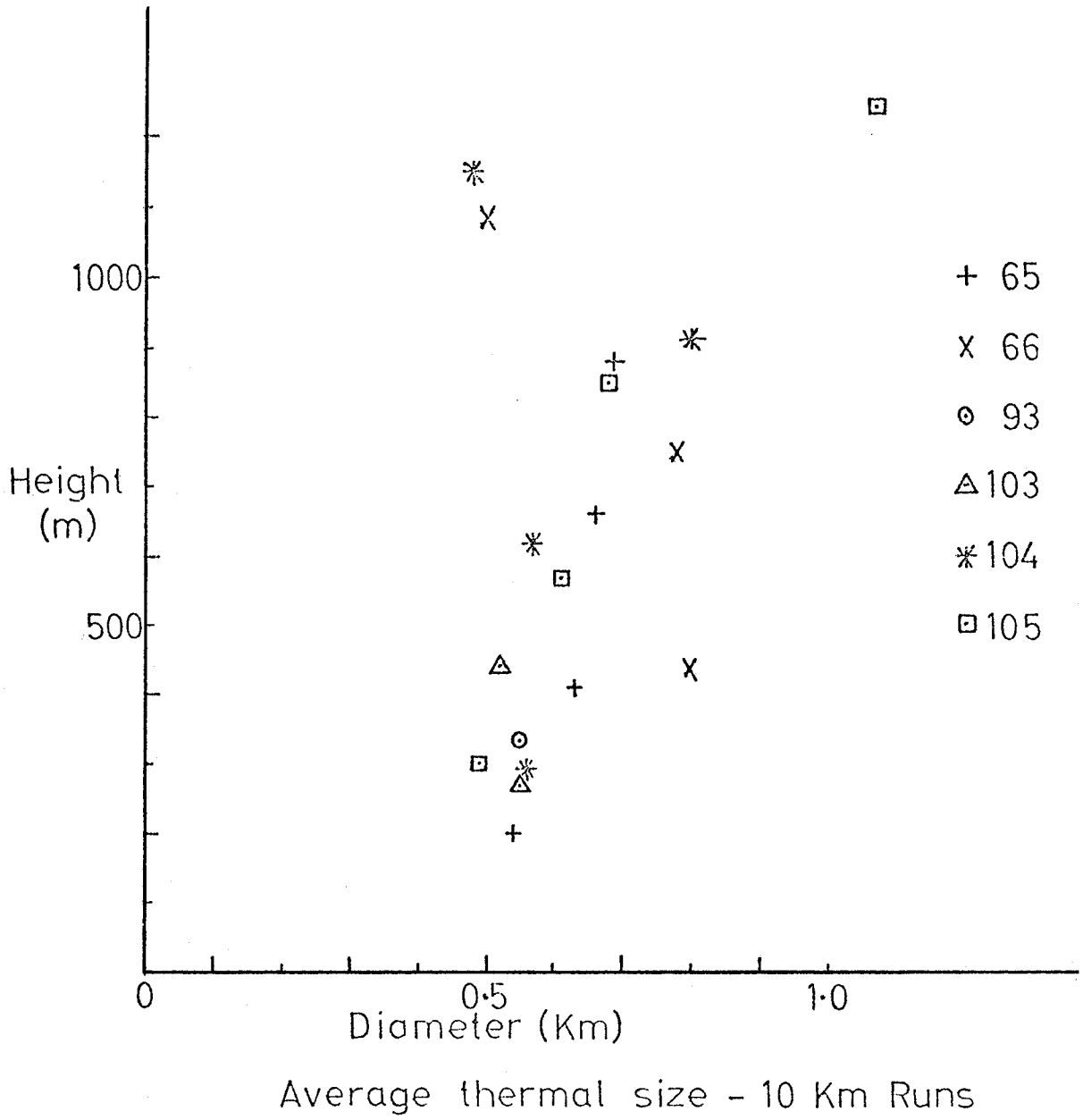


Figure 2 - Thermal growth with height. Each point represents the mean size of thermal measured over a 10 km horizontal run. 6 to 14 thermals were intersected in each run. Above 1000 m thermals have multiple cover, or are weak according to the type of day.

2. Thermal Waves

There is now good evidence that convective lift and wave lift form combined systems under conditions of vertical wind shear. These "thermal waves" allow gliders to climb on the outside and above cumulus clouds to heights far exceeding those of the cloud tops, and they are a likely source for clear air turbulence. The information presently available is primarily qualitative.

It is highly desirable from the standpoint of atmospheric sciences and the art of soaring to explore this phenomenon quantitatively. Numerical models of convection in a shearing environment should incorporate this effect.

a. The "Cumulus Wave" forms on isolated cumuli if the vertically increasing wind does not change direction with height (Figure 3). It allows the pilot to climb in clear air on the upwind side of the cloud from under the cloudbase to over the cloud top or, alternatively, to climb inside the cloud and then to continue over and upwind of the cloud top. Maximum heights reached in this way are 12 km on a cumulonimbus of 8 km cloud top height, approximately.

b. The "Cloud Street Wave" forms over convective cloud streets if the wind turns with height such that the direction of the upper flow is nearly normal to the orientation of the streets (Figure 4). The latter usually corresponds to the direction of the lower flow. Again heights of several kilometers above the cloud streets have been achieved in sailplanes.

It is recommended that this atmospheric phenomenon should be explored systematically with respect to its air flow characteristics. These include the spatial distribution of vertical and, if possible, horizontal air motions in and outside the convective clouds, as well as the temperature and humidity fields as functions of time and of the basic flow properties.

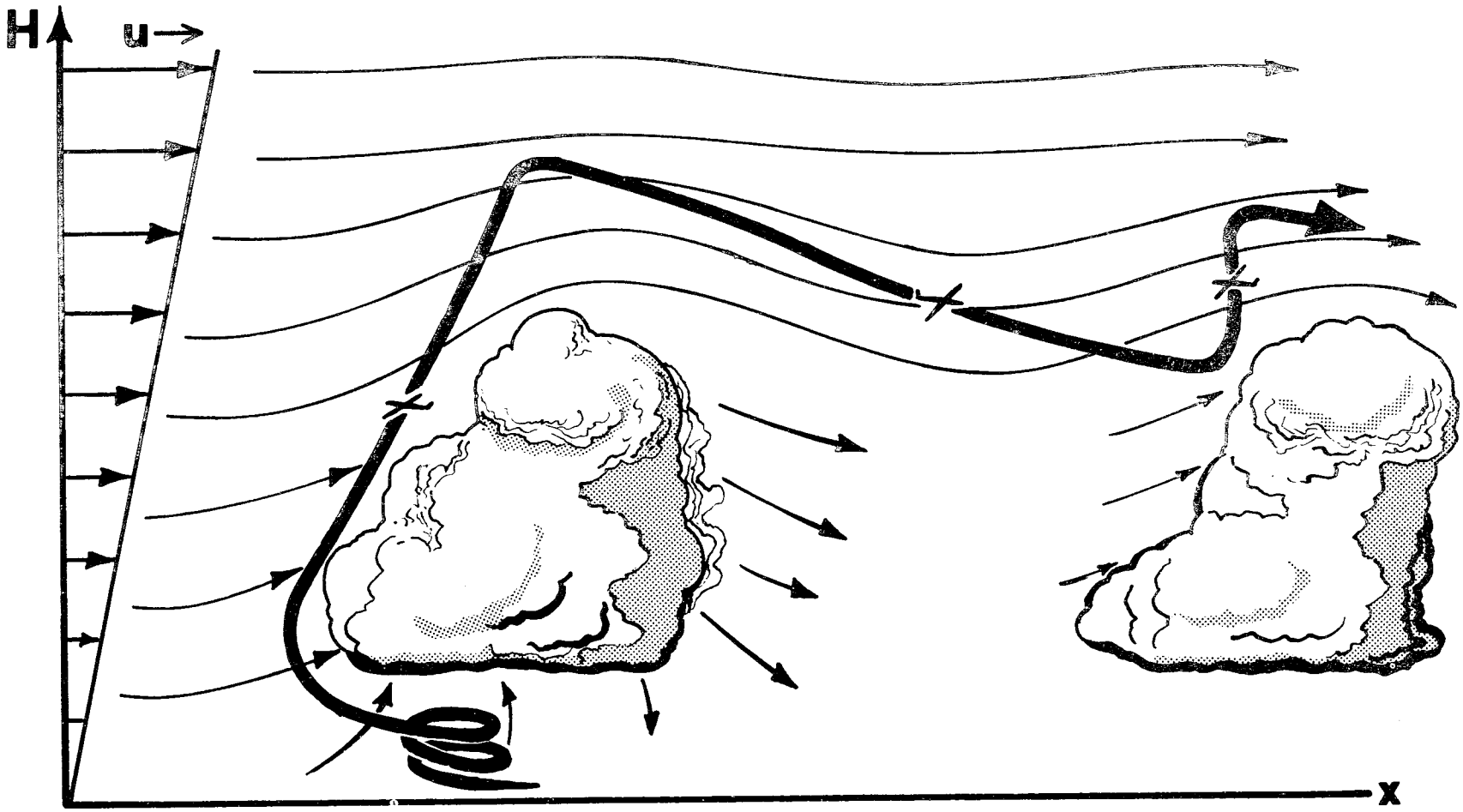
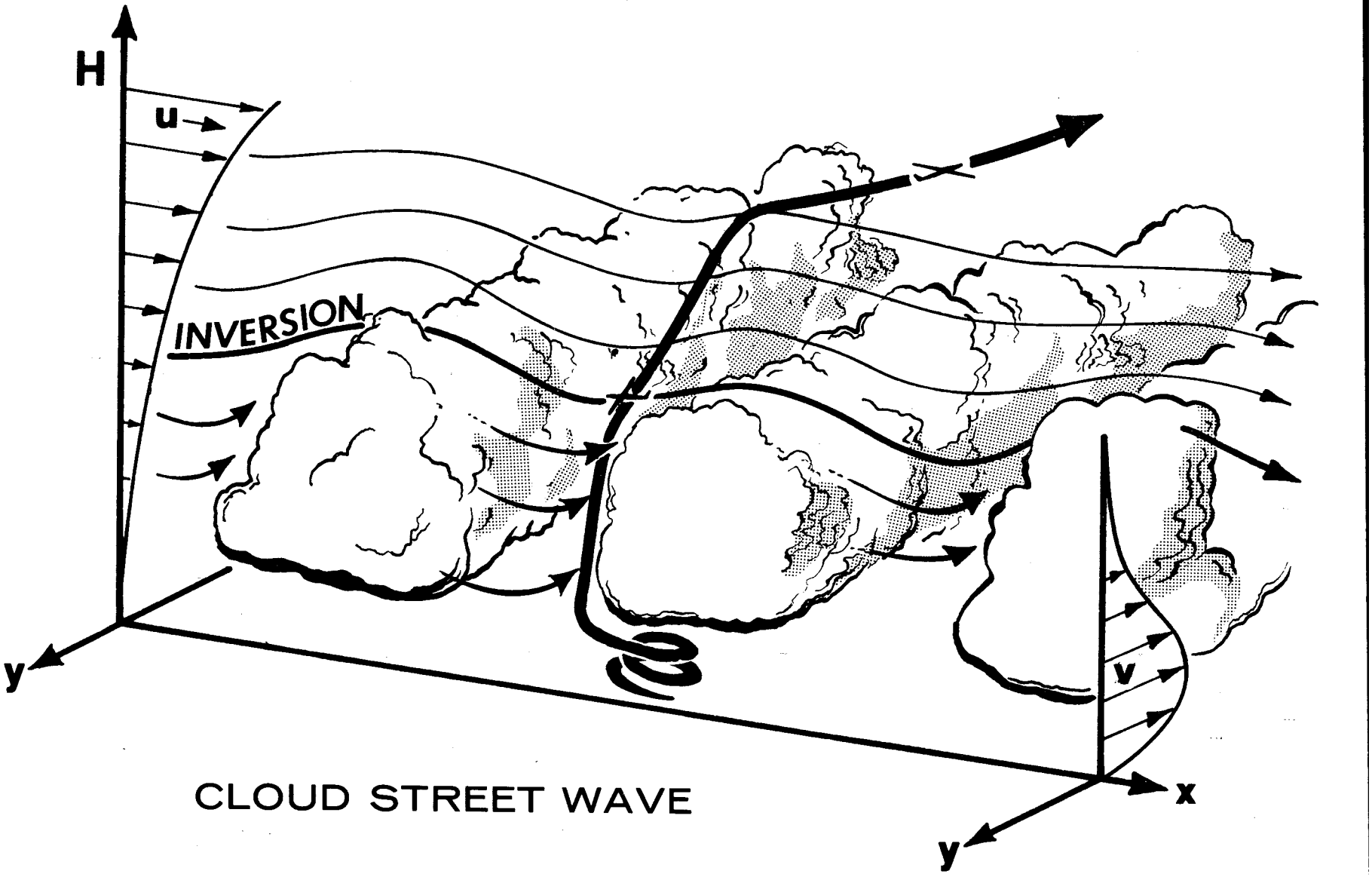


Figure 3



CLOUD STREET WAVE

Figure 4

The relative strength of updrafts in and outside the cloud should also be investigated. These experiments would require similar resources to those made in thermals. This research, which could be started immediately and in any season, must be conducted over flat ground to avoid complications from mountain waves and roll clouds. The use of time-lapse photography from the ground is recommended.

Among foreseeable difficulties will be the determination of the horizontal wind field and the measurement in a drifting system. Use of a suitable inertial measurement system might alleviate these difficulties.

3. Frontal Updrafts

In the early days of gliding the updraft along thunderstorm squall lines was used to make some of the first extended distance flights. In the 30's and 40's flights of over 300 km were made by this method, and some have been described in the literature.

Such lines of rising air may occur at all scales from quite weak sea-breeze fronts, through shearlines to violent squall lines caused by thunderstorm downdrafts which can be of serious significance for airline operation in the lower flight levels. Currently many systems of frontal updraft such as the sea-breeze convergence zones and other shearlines are being exploited, and analog experiments in laboratory tanks are in progress. Scientific investigations using sailplanes with and without motors are needed to extend our knowledge of the real phenomena.

Features of the development of sea-breeze circulation are of considerable interest in the study of atmospheric physics. Many studies have used ground observations, but very few show the complete development of the vertical velocity field as would the use of a number of powered sailplanes. One immediate application of such knowledge would be better understanding of "pollution fronts" and the distribution and concentration of airborne insect pests in the low-level air flow.

For success in this type of operation, the site must be chosen carefully. It is desirable, for example, to exclude katabatic effects which may occur in mountainous areas (though these might be explored separately). It is desirable to choose the best period of the year for such experiments as the phenomena to be studied ared usually strongly seasonal.

Pure sailplanes may be needed to mark the line of lift in "blue conditions", such as occur at some shearlines, but where clear cloud lines or haze fronts are visible these may not be essential, and all the measurements could be made using a powered sailplane.

Studies in water-tank simulation suggest the probable occurrence of Kelvin-Helmholtz type billows above the nose of these meso-fronts. The occurrence of such billows and the depth of the mixing zone at the fronts should be investigated by flights of two or more powered sailplanes flying sections perpendicular to the front, (Figure 5).

The chief difficulty to be overcome seems to be the effective measurement of horizontal velocities and hence actual values of convergence. The use of an intensive balloon network, or cooperation with large instrumented aircraft or use of a suitable inertial system might be necessary to measure a horizontal wind field.

4. Atmospheric Boundary Layer Flux Measurements

The measurement of heat and water vapor fluxes through the lowest 2 km of the atmosphere in convective conditions is a further problem of great interest to meteorologists which is amenable to approaches using powered sailplanes. Meteorologically this is part of a larger set of problems including those of natural air-mass modifications, the behavior of subsidence inversions and the dispersion of pollution.

Some previous experiments of this kind have used large aircraft with elaborate instrument systems including inertial platforms. These are very expensive in comparison with the proposed system. Other experiments have used tethered balloons, but the samples obtainable are not adequate: cross-wind spectra differ from those taken along the wind under convective conditions, and if the wind is light the sample length is small.

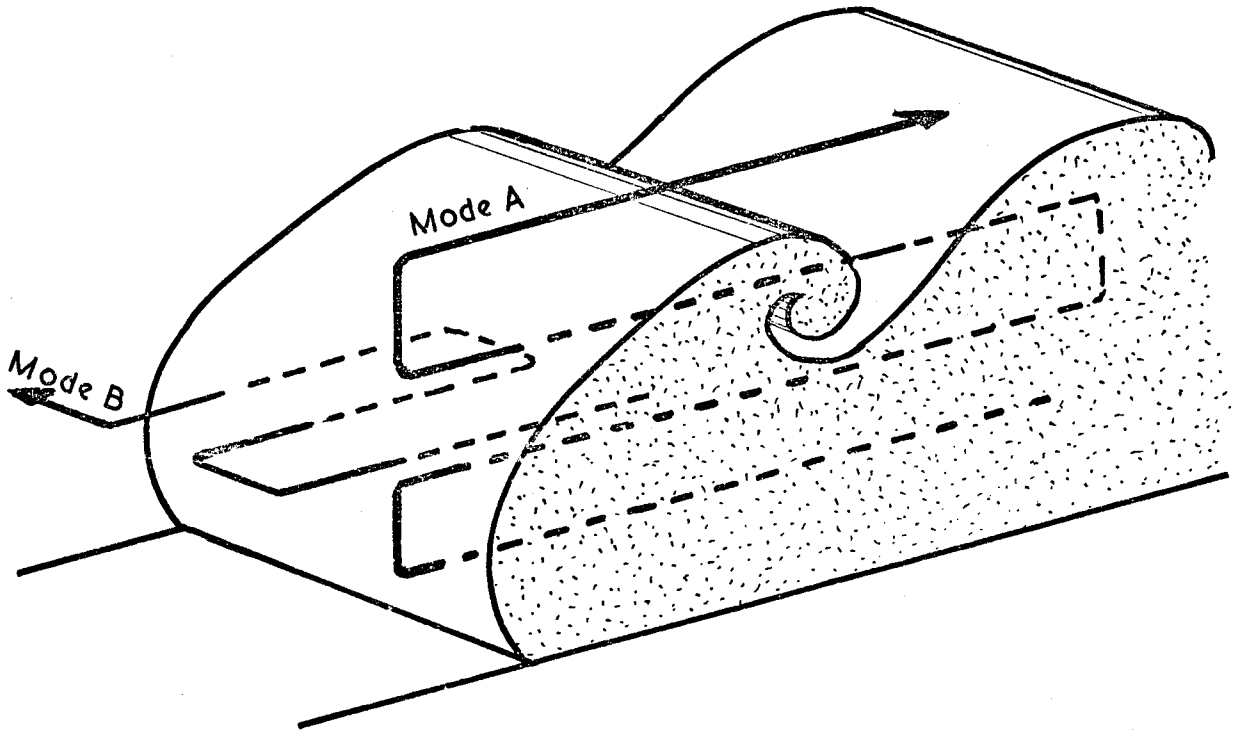


Figure 5 - Idealized sections through sea breeze front.

To measure local values of the fluxes within a period of one hour and to compare the fluxes at different levels, three or four powered sailplanes should be used. The instrumentation required is similar to that for the meteorological problems already specified, with the addition of a rapid response humidity sensor and either an accelerometer or a suitably corrected variometer.

The flights would consist of a series of horizontal runs, vertically staggered, with the engine at constant power setting. A reasonably uniform site should be used and consideration given to the uniformity of the convection on a particular day. Adequate information on horizontal winds would come from synoptic data with a few additional pilot balloons.

5. Cloud Physics

Sailplanes are also useful in cloud physics studies. The production of rain is not fully understood, and further knowledge may lead to better chances of weather modification and hail control. Within a cloud the advantages of a sailplane are that it can remain in a small region to observe the time development continuously, and that it does not introduce any exhaust gases which might modify the processes being observed.

In making measurements in a cumulus cloud, after release from the towplane at a suitable altitude, the sailplane is flown into the updraft under the base. The pilot maximizes his upward velocity, centering on the core of the updraft, and moves upward through the base of the cloud to make quasi-Lagrangian measurements of the cloud's microphysical and atmospheric state parameters. The sinking rate of the sailplane is usually small compared to the air vertical velocity during the developing stage of cumulus clouds.

In mountain wave clouds, like those over the Rockies, droplets are continuously forming and growing on the upwind side and dissipating on the downwind side. Largely because of their steady-state nature, these clouds are better suited than anything that we can produce in the laboratory for integrated cloud microphysics experiments.

Measurements have been made with a sailplane for several hours at altitudes exceeding 10 km in these clouds. Towed into the wave or other sources of lift (usually far beneath the base of the clouds), the sailplane climbs to the upwind side of the cloud and enters, making continuous measurements of the air motion and cloud microphysics. The pilot can sample atmospheric and cloud microphysics parameters with a great deal of flexibility, changing position and altitude to vary the conditions of the experiment, including measurements along the quasi-horizontal trajectories in wave clouds. In this way controlled experiments, including nucleation or other modification studies, can be performed.

Additional instrumentation is required to measure the lower range of temperatures encountered and to sample the particles.

Section II - Special Vehicles for Meteorological Research

It is considered desirable that a motorless and, if possible, a powered sailplane be developed in which a small response time to vertical gusts is combined with a very low airspeed and a very low minimum sinking speed.

A sailplane with such characteristics could be used for measuring the fine structure of convection, including vertical velocity profiles. This can be done in straight flight or by circling with a radius of 30 to 50 m allowing the sailplane to explore the cores of thermals. Wortmann has recently designed wing profiles suitable for such sailplanes, as described in his paper in Appendix II of this report.

Specification for an ideal powered sailplane for meteorological research:

Two seats
Preferred configuration: pusher propeller, or jet engine
Rate of climb, full load, sea level: 3 m/s
Altitude range (if jet propelled): >12 km
3 to 5 hr cruising duration of 500 km range
Instrument payload: 50 kg
Response to vertical gusting: <0.5 s at 20 m/s
Stall speed: <15 m/s
Best glide ratio: >30:1
Minimum sink speed: <0.5 m/s

Section III - Minimum Instrumentation

A simple on-board data-logger is required which can be installed in standard sailplanes. A more complex version would be required for powered sailplanes used primarily for meteorological research. On-board recording is preferred to transmission to a ground station on the grounds of flexibility of operation and reliability.

Decoding of recorded data should be direct into a computer with magnetic tape storage. Since speech is an essential part of the record, decoding cannot take less than real time. A useful system should not take more than twice real time.

In addition to speech, the basic parameters are pressure-height, airspeed, air temperature, humidity and time. Measurements should be taken every 1 second, and sensors must have response times less than this.

The powered sailplane will require additional data channels. The sensors would be chosen according to the particular experiment in progress, the maximum number envisaged being about ten in the case of the cloud physics program. If inertial and velocity vector instrumentation is also carried, several more channels will be needed.

RESEARCH PRIORITIES, SELF-LAUNCHING AND ULTRALIGHT SAILPLANES

Introduction

The area of self-launching sailplanes presents areas of study that range over the whole spectrum of the low-speed aeronautical sciences. Low-speed self-launching sailplanes provide a rather inexpensive method for such research. Due to the inherent character of this area of flight, human launched sailplane research provides an inexpensive area in which aeronautical engineering students can get involved. As is evidenced by the work to date, these students are eager to get involved. Thus minimal funding for this kind of research can be highly rewarding. Some of the major areas requiring study are discussed in the following subsections.

Propellers for Powered Sailplanes and Light Aircraft

To date, relatively little research has been done in the area of propellers for low engine powers. Systematic measurements of the aerodynamic characteristics of small full-scale propellers should be made and plotted as design charts similar to those in NACA Report No. 640.

The propeller diameters should be on the order of 4.5 feet and engine power setting between 5 and 150 hp for various profiles, including the ubiquitous Clark-Y.

Very little information is available on propeller profile sections at very low Reynolds numbers. Measurements are required at Reynolds numbers between 10^5 and 10^6. There is clearly a fertile field for further work on efficient, low-noise propellers for low Reynolds number operation.

Ultralight Structures

In the areas of hang-gliding and self-powered sailplanes, weight plays a primary part in performance. The state-of-the-art

presently leaves a major gap in the weights of aircraft, with man-powered aircraft at one end, having low weight and low performance, while the conventional sailplane is a relatively high weight, high performance aircraft.

If we wish to use human power to augment the performance of sailplanes we need a reduced-weight aircraft with the same or even better performance than current machines. It can be envisioned in the far future that we may have a sailplane with a 70 to 1 glide ratio with human power augmentation. With this goal in mind, work in the new composite materials is called for.

The sailplane industry has done a tremendous amount of work in the use of fiberglass, but we need to go much further to achieve a low-weight high-performance human-powered augmented sailplane. We need to look at new methods of construction using new materials to obtain a very aerodynamically clean aircraft at a very low weight in order to make the human-power augmented sailplane possible. The results of this work will, of course, be applicable to many other types of aircraft. Also, this area of study provides a relatively inexpensive route to the use of the new materials, and thus merits a high priority for further work, particularly in the university environment.

Rough Air Hazards for Ultralight Aircraft

When the speed of aircraft is reduced to levels consistent with foot launching or landing, or in order to match the limited power output of a pedaling crew, it is evident that moderately rough air poses a flight hazard whenever the tubulent velocity components of the wind become appreciable fractions of the aircraft's minimum flying speed. This hazard may take the form of a structural failure in flight or an aerodynamic upset beyond the limits of control effectiveness or recovery height. A need exists to quantify this hazard, to establish acceptable design procedures for the aircraft, to develop appropriate piloting techniques, and to devise simple methods of measuring and forecasting the micrometeorological situation at the launching and/or landing site as a guide to flight operations.

The first need is to develop a sophisticated "wind sock" - a large, inexpensive device clearly visible to all the "sky surfers" flying at a typical hang glider slope. Hopefully it would yield wind direction information and a quantitative measure of wind speed. It might take the form of high-pitch air-log/weathervane combination with a rate of rotation of about one revolution per second at "dangerous" wind speeds of about 10 meters/sec. Counting of revolutions over a period of one minute timed by wrist watch would be a good measure of the wind velocity at launch. Such a device might require about two man years for design and development. A useful auxiliary indicator is the humble smoke-pot - provided that the local environment can stand it.

Another requirement is for study of mathematical models of the structural, rotational, and translational response of "typical" man-powered aircraft, hang gliders, Rogallo kites, etc. to realistic atmospheric disturbances, and to improve design and piloting techniques. Analysis of accidents to validate mathematical models is also recommended, as well as funding of motion picture and taped television coverage (instant replay) of all "official" ultralight flying, such as that for Kremer prize trials, hang glider meets, etc.

Micro-meteorological mathematical modeling to improve forecasting of localized thermal bubble detachment and occurrence of micro-vortices like "dust devils" is quite difficult. One new approach would be to use today's highly-perfected radio control model aircraft or sailplanes to carry specially-developed meteorological research packages. These techniques would also lend themselves to atmospheric environmental analysis at minimum cost.

Pseudo-Ornithopter Propulsion

Ornithopter propulsion has been known of since very early times, yet it is the least-researched and least understood form of flight today. In the past, ornithopter research has suffered from lack of an organized research program and adequate infor-

mation reporting. Future meetings similar to the present one can do much to alleviate this problem.

Today, when most developments require elaborate facilities and financing, advancements in basic ornithopter propulsion can be made by small study groups. By developing pseudo-ornithopter propulsion we could demonstrate a full-scale practical application of flapping wing flight and thereby justify more elaborate ornithopter research. The aircraft indicated in the paper printed elsewhere in this report could be built and tested for less than $400 material cost and 1,000 man-hours labor.

Additional study projects should include:

a. A computer study of the effect of cycle variations on the performance of several aircraft designs.

b. Construction of a simulator to determine power output and cycle optimization of pseudo-ornithopter propulsion vs pedals from a human factors standpoint.

c. Additional wind tunnel research and reporting on the thrust and lift capabilities of oscillating wings, continuing the current work at Mississippi State University.

Propulsion Systems

The powered sailplane has many areas of research in common with pure sailplanes. The main thrust of research effort, therefore, comes in the area of powerplant integration. The goal of this effort should be to minimize the negative impact of the powerplant on the aircraft's soaring ability while still providing satisfactory powered performance and safety. Research areas include systems of propulsion other than propellers, superior means of retracting or otherwise reducing the drag of the stopped propulsion system, and lighter power sources, possibly of stored-energy types. Noise and the destructive effects of vibration are especially important in powered sailplanes, especially from considerations of delicate instruments and the pilot's ability to use his many senses to help him soar.

Regulatory Standards

An area of self-launching sailplane development that needs study is that of standards. While the area of performance and design standards may seem to be outside the area of research and development, it must be kept in mind by all workers.

In the field of powered sailplanes, researchers should maintain contact with the groups responsible for aircraft certification. The concept of substituting performance specifications for "hardware" specifications should be actively pursued. If standards for safety and reliability can be formulated it would free the designer from many constraints. The nature and degree of specification of these standards need investigation. As an example, having dual ignition systems does not guarantee against engine failure, it is only an attempt to make failure due to the ignition system unlikely. By contrast, a specified minimum L/D or other gliding parameter would ensure that any aircraft certified as a powered sailplane would be little endangered by engine failure for any reason.

The area of ultra-light self-launched aircraft requires even more work on performance capabilities. If the hang-glider, man-powered aircraft type of endeavor becomes widespread, some sensible standards of safety, construction and control will need to be observed. If these standards can be "enforced" as well as formulated by the ultra-light movement itself, the need for formal government control may be avoided. The home-built aircraft and sport parachuting movements have both succeeded in minimizing Federal control to maximize the flexibility of design they may enjoy. This requires close cooperation with the government and a willingness by the movement to impose reasonable restrictions on itself to avoid outside restrictions. Research is needed into the areas in which standards are required; also, work as to what constitutes a reasonable and safe standard. Proper liaison between the Federal authorities, and good standards, could avoid imposing the large additional burden on the government of regulating this area of flight activity.

A study of the background and reasoning behind the current regulations, and research into new ways of handling the regu-

lation of flight vehicles of all types is a great need. Such a study may have great benefits in general government regulation as well as for aeronautical regulation specifically. An agency whose response time is significantly shorter than that of present agencies is needed to deal with the current rapid growth of these sport activities.

Low-Speed Flexible-Wing Aircraft

To date, relatively little research has been done in the very low speed (<50 fps) region of flight; mainly because there has not been any pressing need for it. Our main concern here, however, is low speed flight research as it applies to man-prominent systems (eg. hang gliders, man-powered aircraft and man-augmented gliders). This concern is given more force by the recent revival in the sport of hang gliding with its obvious abundance of unknowns.

The Rogallo kite was studied during the early sixties as a possible spacecraft re-entry system, generating enough data for some restless enthusiasts to seize the data and design man-carrying Rogallo-kites on their own.

Having no real information on the human factors involved, they proceeded on the"leap-and-try" basis and developed what is today the most popular form of hang-glider. As it stands, however, it could most certainly benefit from research considering the man-prominent flight systems relationship. It is, therefore, proposed that additional studies be made of the concept of flexible wings with special emphasis being placed on the following areas:

a. Stability and control of flexible wings (also control means other than weight shifting).
b. Design and incorporation of integral safety devices.
c. Structural optimization from the standpoint of minimum weight and ease of ground handling.
d. Aerodynamic optimization of various structural and sail geometries.
e. Double as well as single membrane concepts (eg. the Princeton Sailwing).

f. Extension of test data to lower speeds.

g. Development of design criteria and operational standards.

In general, we are interested in developing an integration of man-flight systems, considering safety, stability, control, cost and over-all design optimization. Actual research would most likely consist of experimental type studies with wind tunnel models, free and radio controlled models, and full size, man-carrying aircraft. The theory of the flexible wing seems to have been studied sufficiently at this time.

A reasonably high priority for this proposed research program is justifiable on the basis that hang-gliding will develop into a popular new sport and consumer industry. Also, it is hoped that a collapsable ultralight will be developed to the point where it can be carried like an emergency escape device possessing superior performance and control capabilities as compared to a conventional parachute.

RESEARCH PRIORITIES, PERFORMANCE TESTING

Introduction

The workshop concerned itself principally with the measurement of the performance curve, or polar, of sailplanes. However, handling and control characteristics are so important to performance and safety that these topics were also considered briefly. After a survey of the status of current sailplane performance measurement activities, this report continues with a set of specific recommendations for future research efforts. Finally, the desirability of setting up a new Performance Measurement Group in the U.S. is discussed, as well as the necessity for the use of uniform formats for communication of data.

Current Activities

Table II lists the relatively small number of organizations and/or personnel known to be active in this field at this time. Of these, only the first two listed are performing tests on a routine basis. The other groups are working with very limited budgets, or with private funding, on a part time basis. It is perhaps significant that the list contains not a single sailplane manufacturer, nor even the Soaring Society of America, Inc.

Present Techniques

1. Performance Testing

Only three techniques of performance testing are currently in use:

a. The "partial glide" method (Refs. 1-4). The glider is towed to a convenient height and flown down in a series of straight glides at constant speed. During each of these "partial glides" the average forward speed is measured by the airspeed indicator and the rate of sink is determined, usually by means of a stop-watch and altimeter. The airspeed

TABLE II

Organizations and/or Personnel Currently Making Sailplane Flight Measurements

1. Dipl.-Ing. Hans Zacher
   DFVLR, Abt. Segelflug
   8 Muenchen 87,
   West Germany

2. SZD
   Bielsko-Biala
   Poland

3. H.A. Torode
   Department of Flight
   C.I.T.
   Cranfield, Beds.
   England

4. Dr. G.R. Whitfield
   Department of Applied Physical Sciences
   Reading University
   Whiteknights
   Reading, RG6 2AL
   England

5. Prof. George Bennett
   Mississippi State University
   State College, Mississippi 39762

6. Paul Bikle
   44926 N. Raysack
   Lancaster, California 93534

7. Dr. William M. Foley
   United Aircraft Research Laboratories
   400 Main Street
   East Hartford, Conn. 06108

8. Akademishe Fliegergruppe
   Technische Hochshule Darmstadt
   61 Darmstadt,
   West Germany

9. No. 1 Test Group
   C/O L. Welch
   14 Upper Old Park Lane
   Farhham, Surrey
   England

indicator and pitot-static system are carefully calibrated prior to these measurements so that the average speed is accurately determinable. Using standard aircraft instruments, read manually or photographed, each partial glide lasts from 2 to 5 minutes. With an automatic recording system and more sensitive transducers (Ref. 5), this can be reduced to 1 minute or less. The major source of error is vertical air movement, which can be minimized, but not eliminated, by careful choice of weather conditions. There are also several other more minor inherent error sources. Between 50 and 150 partial glides are required to establish the glider's performance with about $\pm$5% standard deviation.

b. Comparison flying (Ref. 4). If the performance of one glider is known, that of another can be found by determining their relative rates of sink when they are flown close together. The relative displacement can be determined by eye or by photography; the gliders can be flown in formation at the same speed or separately at different speeds. Excellent results can be obtained in good weather conditions with runs of 5 or 10 minutes each.

c. The "deceleration" method (Ref. 6). The glider is dived to high speed and then flown level; the change of airspeed with time is measured and used to estimate the drag at each speed and, hence, the polar. The principal problems encountered with this method are: inaccuracy in maintaining a constant height* (if the tests are well clear of the ground); correcting for ground effect (if the tests are carried out at very low altitude); hysteresis effects; and accurate data recording and interpretation (since all readings are made under transient conditions).

---

* Possible instrumentation for holding constant height is a variometer with a valve for closing off the leakage source. This method was used by the DFS in Darmstadt, Germany during 1936-1939.

The first and second methods have given good results in experienced hands. It is reported that the third method is now being used in Poland. Great care is necessary in the choice of suitable weather conditions and the avoidance of systematic errors. Casual measurements on soaring days are useless and misleading. Because of the difficulty of finding suitable weather conditions, sailplane performance testing is currently a lengthy procedure. In many parts of the world, such as in Europe, only a very few days are suitable each year. Other areas, such as the desert regions of the USA, have more extended periods of suitable weather. Thus there exists a need for the development of methods which are both less time consuming and less dependent on perfect weather.

2. Handling Qualities, Stability and Control

Flying qualities have so far been evaluated qualitatively to a greater or lesser extent by separate national airworthiness authorities. The British Authorities are particularly notable in this field, as are the independent measurements made by Zacher at the DFVLR, Munich, together with the German Akafliegs. However, these are necessarily brief assessments as they range over a variety of sailplanes. Torode, at Cranfield, England, is at present carrying out a more detailed analysis of the longitudinal handling qualities of a Cirrus. Beyond these, no other organizations are known to be performing work in this field at this time.

Although most sailplanes are essentially similar, and very simple in control layout, occasionally quite pressing problems occur due to specialized design developments; for example, the pilot-induced oscillation problems which came to light some two years ago in fiberglass sailplanes. To prepare for this sort of eventuality and also to gain a deeper understanding of sailplane flight dynamics, handling qualities and control research are still badly needed. Because of the cost and specialized nature of this work, it is not realistic to expect low-volume manufacturers to undertake it to any great extent. Thus some other ways to get it done must be found. See also the section on this topic on page 9 of this report.

3. Summary

Our specific proposals below are intended to increase the convenience and accuracy of performance testing, to establish and maintain a test facility in the U.S.A. and to take advantage of these items to obtain important scientific and engineering data through flight tests. Additionally, some recommendations are made to standardize the format of published results and thereby improve their utility.

Specific Research Proposals

1. Flight Measurements

1.1 Establishment of a Performance Test Group. Currently the most easily applicable method of performance measurement is that of comparison flying. This is facilitated in the U.S.A. by the excellent stable air mass conditions which exist in desert regions, such as near Edwards Air Force Base, California. Other countries with the appropriate technical base suffer from a relative lack of such suitable conditions. Hence it is recommended that an official flight test group be established within the U.S.A. and be suitably equipped with a calibrated reference sailplane and other appropriate equipment for performance measurement purposes. This group would serve as a focal point for sailplane performance measurements within this country. It is expected that they would establish important scientific and engineering data required for sailplane design, provide performance data for operational purposes, and provide assistance to aircraft manufactures in establishing the performance of new or modified products. It is anticipated that the initial investment for equipment could be as little as $20,000 and that annual operational expenses for maintenance, towing fees and equipment would be a similar amount. Long-term stability of this group would be important for it to perform its function. It may be desirable to have at least one permanent, full time, paid individual to head such a group.

1.2 Component Aerodynamic Performance.

Although the wind tunnel serves as a very useful tool, it is important to obtain verification of wind tunnel results in flight. This is true because of several factors - for example, the wind tunnel turbulence may not be representative of that in the atmosphere; production finishes are difficult to simulate in model scale; and particularly for fuselages, full-scale Reynolds numbers are difficult to achieve. Full-scale flight research is currently required in at least the following areas:

a. Turbulence Effects

Flight data have been obtained under the most quiescent atmospheric conditions, yet soaring is normally done in quite turbulent air. The effect of various atmospheric conditions on the degree of laminar flow over sailplanes needs to be assessed. This effect could be readily studied with a properly instrumented sailplane on which the transition points can be measured.

b. Effect of Manufacturing Tolerances

The effect of manufacturing tolerances on commonly used wing sections should be determined. Section waviness, roughness, departures from true profile shape, and trailing-edge thickness effects should all be studied. Development of a suitable device for very accurate measurement of actual wing contours, particularly near the extreme leading edge, is also required.

c. Wing Geometry Effects

The effect of wing tip geometry and wing root fairings on performance requires attention. See also the section on Aerodynamic Tailoring on page 10 of this report.

d. Leakage Effects

The effect of gaps and slots at wing roots, canopies and control surfaces requires quantitative assessment.

e. Loading Effects

The influence of center of gravity position and gross weight on performance is still debated and requires quantification. This question is allied to that of Reynolds number effects discussed below.

1.3 Over-all Aerodynamic Performance

Apart from performance in straight flight, there are two other important matters of current concern:

a. Circling Flight

Neither the theoretical performance or the measured performance of high aspect ratio aircraft operating at very high lift coefficients (C_L>1.1) in very steep turns (ϕ>45 deg) is well established, although it is known that important performance degradation can occur under these conditions. See also Refs. 13 and 14 and the section on Circling Flight on page 4 of this report.

b. Reynolds Number Effects

Without much sound backing, the discrepancies noted between performance measurements made at different altitudes have sometimes been attributed vaguely to "Reynolds number effects". Since it is clear that these exist as phenomena, it would be well to establish their magnitude by flight tests at several widely-spaced altitudes.

1.4 Reproducibility of Sailplane Performance

Performance measurements are normally performed on only one sailplane of a particular design. It is at present unclear whether

this performance is then representative of only that particular sailplane or is representative of all sailplanes of that design. Measurements are required on several sailplanes all of the same type and all prepared in like manner to determine performance variability in modern sailplane designs.

2. Specialized Instrumentation Development

2.1 Automatic Performance Data Recording System.

Present "Partial glide" performance tests involve either a large amount of ground analysis or the use of a recording system that requires highly skilled operators. It would be valuable to develop a robust and foolproof system that could record height, speed and time for computer anslysis and which did not require special care or frequent calibration. A target specification would be that given in Table III.

2.2 Angle of Glide Measuring Systems.

Even with very careful selection of weather for testing, the major surce of error in present tests is believed to be the vertical movement of the air. This error could be eliminated by the use of a system that measured directly the angle of descent of the glider relative to the air through which it is flying (Ref. 8). The range of angles is from 0 to 10 deg., and the required accuracy is on the order of $\pm$0.05 deg., depending upon the aircraft tested. We propose that such a system be developed since it would greatly enhance our ability to make performance measurements.

2.3 Inertial Measurement System

Inertial measurement systems have been developed that are small enough to be considered for glider testing and accurate enough to be useful. A strapdown system, with recording equipment and computer analysis, could be used for performance testing by the "partial glide" or "deceleration" methods. It would also be extremely valuable in some of the stability, control and handling tests.

We propose that the feasibility of adapting existing systems to perform this function be examined as a high priority and, if judged feasible, that flight evaluation be carried out.

TABLE III

Draft Specifications for an Automatic Performance Data Recording System

	Parameters		
	Height	Indicated Airspeed	Time
Range of Values	0-20000 ft	30-160 mph	1 hr
Accuracy			
Short Term	± 1 ft	± 0.2 mph	± 0.1%
Long Term	± 30 ft	± 0.2 mph	± 0.1%

Target volume	1 ft^3
Target AUW, with batteries	30 lb

NOTE: It would be an advantage if the main unit were similar in size and weight to a barograph. Such a system might be developed from that of Whitfield (Refs. 5 and 7), or independently .

3. Stability and Control Research

Either as one of the programs carried out by the Performance Test Group established under Section 1.1, or as a program under a separate group, the following tests should be conducted using a modern GRP sailplane. The topics are listed in order of priority.

a. Evaluation of both longitudinal and lateral stability.

b. Aeroelastic effects on stability and control.

c. Response to atmospheric turbulence and thermals.

d. Stalling and spinning evaluations.

e. Determination of aircraft derivatives.

This program should be laid out with due allowance for modification in the light of future problems yet to be encountered. It may be wise to consider the development of a variable-stability aircraft for this program.

4. Supporting Activities

4.1 Statistical Data Processing Techniques.

Because the entire environment, the systems being tested, and the measurement procedures can only be described, at best, using a set of uncertain (or random) parameters, it is suggested that study be directed toward viewing the performance testing problem as a nonlinear parameter identification problem, for which modern digital estimation techniques may be applied. This, potentially, would allow assessment of performance, with an established degree of accuracy, from fewer test points or with greater confidence from the same amount of testing as we now perform. The techniques in question, which are now quite widely known to control engineers, have been used with great success in larger aerospace programs such as the Apollo missions or in more modest applications in industry or even oceanography. Most of the algorithms make use of some sort of "Kalman filtering" or "smoothing" of the test data. Jazwinski (Ref. 11) has described some convincing applications.

4.2 Correlation of Performance Measurements

A significant body of performance data now exists and additional results should arise from the implementation of our earlier proposals. To make these data useful for design purposes, they should be correlated with the best available aerodynamic performance methods. Lack of correlation should be investigated by detailed flight measurements, as detailed in Section 1.2 above.

4.3 Information Transfer and Library Service

Advancement of the state of the art is presently hindered by a lack of information exchange, especially were a language barrier is involved. Such works as the non-English OSTIV papers, the Drag Estimation work by Treiber of the Akademischefliegergruppe Braunschweig, and other significant works in German, Polish and Russian are not readily available in the U.S.A. A collection of significant technical works in all languages should be undertaken, translated as required, and copies made available at modest cost to all interested parties. It is recommended that the Technical Committee of the Soaring Society of America should be consulted for recommendations of works for inclusion in such a technical library. It would be desirable to set up such a library at a site offering great permanence and continuity, such as an institute of higher learning.

5. Publication of Performance Results

5.1 Format Data for Publication

To facilitate interpretation by a large audience, it is desirable to publish performance data (e.g. glider polars) on a common basis. Thus, it is recommended that dimensional flight test data be corrected to a basic weight equal to the published manufacturers weight plus 90 kg and that metric units be used as the primary units, whether or not other units are also indicated on the graph axes. Nondimensional data in the form of C_L and C_D coefficients should also be provided over the speed range. Test weight and CG information should be provided, as well as relevant information as to the "perfection" of the configuration (eg. seals, etc.).

5.2 Accuracy

Depending upon the conditions of measurement and the number of measurements, performance results can have varying reliability. The group obtaining these measurements is in the best position to estimate the error limits of their data. It is recommended that $\pm 2\sigma$ error limits be shown for published performance results, in each case, to increase their utility.

References

1. Machin, K.E.; The Performance Testing of the Slingsby Sky, Journal of RAeS, Vol. 58, July 1954.

2. Zacher, H. and Merklein, H.J.; Leistungsmessungen an 12 Segelflugzeugen, 9th OSTIV Congress, Junin, 1962.

3. Johnson, R.; Sailplane Flight Test Performance Measurements, Soaring, April 1968.

4. Bikle, P.; Polars of Eight, Soaring, June 1970.

5. Whitfield, G.R.; Automatic Recording and Analysis for Glider Performance Testing, 12th OSTIV Congress, Marfa, 1970.

6. Pokorny, V.; Some notes on seeking new methods of sailplane lift/drag curve measurements, 7th OSTIV Congress, Leszno 1958.

7. Whitfield, G.R.; A Simple Data Recording System with Computer Analysis, Radio & Electronic Engineer, Vol. 40, No. 5, November 1970.

8. Torode, H.A ; Performance Testing of Sailplanes, College of Aeronautics Report, June 1970.

9. Zacher, H.; Flugmessungen mit Standard-Segelflugzeugen, OSTIV Congress, S. Cerney, 1965.

10. Torode, H.A.; A Flight Evaluation of Aeroelastic Distortion Effects on Performance, Stability and Control of a Sail-Plane, 1st International Symposium on Motorless Flight, M.I.T., October 1972.

11. Jazwinski, A.; Stochastic Processes and Filtering Theory, Academic Press, 1970.

12. Brown, W.E.; A Comparison of Classical Drag Estimation Techniques with Sailplane Flight Test Results, 1st International Symposium on Motorless Flight, M.I.T., October, 1972.

13. Phillips, W.H.; Analysis of Effect of Asymmetric Loading on Sailplane Performance in Circling Flight, 1st International Symposium on Motorless Flight, M.I.T., October, 1972.

14. Merklein, H.J.; Vergleich der Kreisflugleistungen einer Segelflugzeuge auf Grund vermessener Flugpolaren, OSTIV Publication VIII, 1965.

APPENDIX I

WORKSHOP PARTICIPANTS

To facilitate communication, the names and contact addresses of each of the participants in the Workshop to Identify Priorities for Motorless Flight Research are listed below, by section. It should be noted, however, that several persons participated in more than one section. In these cases they have been listed only once, in the section with which they were most closely identified. Certain FAA personnel also participated at some meetings. They are identified separately.

1. AERODYNAMICS AND DESIGN

Smith, A.J. (Chairman)
17356 Northland Park Court
Southfield, Mi. 48075

Althaus, Dipl. Ing. Dieter
Inst. fuer Aero- u. Gasdynamik
Universitaet Stuttgart
7000 Stuttgart, W. Germany

Bede, James R.
Newton Municipal Airport
Newton, Ks. 67114

duPont, Stephen
160 Long Meadow Rd.
Fairfield, Ct. 06430

Eppler, Prof. Richard
Inst. A fuer Mechanik
Universitaet Stuttgart
7000 Stuttgart, W. Germany

Francis, Samuel A.
Converse Point
Marion, Ma. 02738

Goodhart, Rear Adm. H.C.N.
Ministry of Defence
London SW1A 2HB, England

Harlan, Raymond B.
Measurement Systems Laboratory
M.I.T.
Cambridge, Ma. 02139

Irving, Frank
Dept. of Aeronautics
Imperial College of
Science & Technology
London SW7 2BY, England

Lien, Douglas A.
Naval Ship Research &
Development Center
Bethesda, Md. 20034

Miller, Prof. R.H.
Dept. of Aeronautics &
Astronautics
M.I.T.
Cambridge, Ma. 02139

Nash-Webber, Dr. James L.
Measurement Systems Laboratory
M.I.T.
Cambridge, Ma. 02139

Nicks, Oran W.
NASA/Langley Research Center
Hampton, Va. 23365

Ormsbee, Prof. A.I.
University of Illinois
Urbana, Il. 61801

Phillips, William H.
NASA/Langley Research Center
Hampton, Va. 23365

Pick, George S.
Naval Ship Research &
Development Center
Bethesda Md. 20034

Schweizer, Leslie
P.O. Box 147
Elmira NY 14902

Steinhoff, Dr. Ernst A.
P.O. Box 416
Alamogordo NM 88310

Wortmann, Prof. F.X.
Inst. Aero- u. Gasdynamik
Universitaet Stuttgart
7000 Stuttgart
West Germany

2. INSTRUMENTATION

MacCready, Dr. Paul B.
(Chairman)
AeroVironment Inc.
660 South Arroyo Parkway
Pasadena, Ca. 91105

Ball, Robert
Ball Engineering Co.
Boulder, Co.

Firth, John M.
National Research Council
100 Sussex Drive
Ottawa, Ont., Canada

Gera, Joseph
NASA/Langley Research Center
Hampton, Va. 23365

Hollister, Prof. Walter M.
Dept. of Aeronautics &
Astronautics
M.I.T.
Cambridge, Ma. 02139

Ismail,Dr. Raouf A.
Cambridge Aero Instruments
3 Jackson Rd.
Burlington, Ma. 01803

Markson, Ralph
Dept. Atmospheric Science
State Univ. of N.Y. at
Albany
Albany, N.Y. 12222

3. STRUCTURAL CONCEPTS AND MATERIALS

Paiewonsky, Dr. Bernard
(Chairman)
9309 Burning Tree Rd.
Bethesda, Md. 20034

Bowen, Stephen T.
Fiberfil
Evansville, In. 47717

Elber, Dr. Wolf
NASA/Langley Research Center
Hampton, Va. 23365

Elson, Barry R.
Owens-Corning Fiberglas Corp.
Toledo, Oh. 43659

Mar, Prof. James
Dept. of Aeronautics &
Astronautics
M.I.T.
Cambridge, Ma. 02139

Morelli, Prof. Piero
Istituto di Costruzioni
Aeronautiche
Politecnico di Torino
10100 Torino, Italy

Schreder, Richard E.
P.O. Box 488
Bryan, Oh. 43506

Stickler, Prof. David
Dept. of Aeronautics &
Astronautics
M.I.T.
Cambridge, Ma. 02139

Zimmerman, Arthur
Berkshire Mfg. Corp.
Oak Ridge, N.J.

Strack, K.J.
1976 Berkwood Dr.
Pittsburg, Pa. 15243

4. METEOROLOGY

Kuettner, Dr. Joachim P.
(Chairman)
ISMG for GATE
C/O Meteorological Office
John Scott House, Market St.
Bracknell, Berks., England

[Archimbault,C.
N.W.S. Forecast Office
Logan International Airport
Boston, Ma.]

Fitch, Robert
Dept. of Electrical
Engineering
M.I.T.
Cambridge, Ma. 02139

[Goldman, Louis
N.W.S. Forecast Office
Logan International Airport
Boston, Ma.]

Simpson, John E.
Dept. of Geophysics
University of Reading
Reading RG6 2AU, England

[Long, Prof. R.R.
Dept. of Mechanics & Materials
Science
Johns Hopkins University
Baltimore, Md. 21218]

Milford, Dr. J.R.
Dept. of Geophysics
University of Reading
Reading RG6 2AU, England

Sanders, Prof. Frederick
Dept. of Meteorology
M.I.T.
Cambridge, Ma. 02139

Sartor, Dr. J. Doyne
Lab. of Atmospheric Science
National Center for Atmospheric
Research
P.O. Box 1670
Boulder, Co. 80302

Toutenhoofd, Dr. Wim
Lab. of Atmospheric Science
National Center for Atmospheric
Research
P.O. Box 1670
Boulder, Co. 80302

5. SELF-LAUNCHING SAILPLANES

Perl, Harry N. (Chairman)
Lawrence Radiation Laboratory
Livermore, Ca. 94550

Cole, Curtis J.
401 West Ridge
Marquette, Mi. 49855

Dirks, Wilhelm
Akademische Fliegergruppe
Technische Hochschule
61 Darmstadt, W. Germany

Hooper, Paul
Dept. of Aeronautics &
Astronautics
M.I.T.
Cambridge, Ma. 02139

Larrabee, Prof. Eugene
Dept. of Aeronautics &
Astronautics
M.I.T.
Cambridge, Ma. 02139

Markowski, Michael A.
Man Flight Systems Engineering
P.O. Box 375
Marlboro, Ma. 01752

McMasters, John H.
1400 S. Farmer St.
Tempe, Az. 85281

Peterson, Robert
Dept. of Aeronautics &
Astronautics
M.I.T.
Cambridge, Ma. 02139

Smith, Grant
Williams Research Corp.
Walled Lake, Mi. 48088

6. PERFORMANCE TESTING

Foley, Dr. William M.
(Chairman)
United Aircraft Corp.
Research Labs.
E. Hartford, Ct.

Brown, William E.
Advance Product Engineering
Beech Aircraft Co.
Wichita, Ks 67201

Froidevaux, Michel R.
M.I.T. Draper Laboratory
(DL 11-240B)
Cambridge, Ma. 02139

Torode, Howard A.
Dept. of Flight
Cranfield Institute of
Technology
Bedford, England

Whitfield, Dr. G.R.
Dept. Applied Physical Sciences
University of Reading
Earley Gate No. 3
Whiteknights
Reading RG6 2AL, England

Zacher, Dipl. Ing. Hans
DFVLR, Abt. Segelflug
Postfach 870180
8 Muenchen 87, W. Germany

7. FEDERAL AVIATION ADMINISTRATION REPRESENTATIVES

Edward Maila
Chief, Airframe Section
New England Region

John Lucius
Manufacturing Specialist
New England Region

David Hmiel
Flight Test Specialist
New England Region

George Phinney
Operations Specialist
New England Region

Bernard Grochal
Airframe Specialist
Washington, D.C.

APPENDIX II

This Appendix contains the revised, edited texts of the 42 papers and other presentations given at the Symposoum on the Technology and Science of Motorless Flight held concurrently with the Workshop. Because of space limitations, some of them have been shortened considerably. Where a complete text of a presentation was not available, a summary has been provided.

THE SCIENCE OF LOW SPEED FLIGHT

by

Oran W. Nicks
Deputy Director, NASA Langley Research Center

(Luncheon Address)

After thousands of years of envying the birds and their ability to travel with apparent ease over the most dense forests or the most jagged mountain terrain, man finally was able to fly. Through a bit of good fortune, however, he was never forced to seek efficiency to the extent required in the evolution of birds. The good fortune I refer was his ability to develop lightweight power plants capable of producing a means for overcoming deficiencies in aerodynamics. While man can take pride in many accomplishments in flight which have surpassed the bird, it remains that birds regularly employ technologies which are not well understood, and many more we understand but have not been able to apply successfully.

In his book of the 1880's entitled "Bird Flight as the Basis of Aviation", Otto Lilienthal distinctly stated the challenge of his day, which I feel still before us. Quote:

"It must not remain our desire only to acquire the art of the bird, nay, it is our duty not to rest until we have attained to a perfect scientific conception of the problem of flight, even though as the result of such endeavours we arrive at the conclusion that we shall never be able to transfer our highway to the air. But it may also be that our investigations will teach us to artificially imitate what nature demonstrates to us daily in birdflight.

'Therefore let us investigate in a truly scientific spirit, without preconceived notions as to the nature of birdflight, its mechanism, and the conclusions which may be derived from it." Unquote.

From a recent review of library material, it appears that after man was able to fly with power, he paid little more attention to birds. Feathers are very mysterious, and still seem to represent a very strange material for making aerodynamic surfaces. Who has seen a really good explanation of why the Good Lord chose them for most flying creatures? The variable geometry advantages of birds are many, but we have given little thought to copying them in recent years for our own flying machines.

For example, achieving lateral control by wing warping was a feature in the Wright biplane. This was followed by a step backward from an efficiency standpoint with surfaces called ailerons, and it was many years before flaps achieved usefulness for effective camber variations. I remember great excitement when Dr. Koppen and associates succeeded with practical leading edge devices to augment lift improvements obtained by flaps, but even today, the ones in use are crude aerodynamically.

With current technologies such as those applied to the Boeing 747, the effect of variable geometry devices improves the low speed lift on the order of 2.5 to 3.0 times that of a basic wing. Thus, one might argue that some progress is being made; on the other hand, it is clear that there is plenty of room for improvement. A query to my Boeing friends confirmed this when they revealed that the B-747 in the landing configuration and operating within normal CG limits, requires a tail *down* load for trim of 40 to 60 thousand pounds opposing wing lift.

Meanwhile, all around us, birds simply sweep their wings forward near touchdown in a manner allowing every feather to be working for increased lift or deceleration. Man has managed a few designs with variable sweep wings, but we have never put it all together to use fully the promise of such variable geometry features at low speeds. Of course, the birds also have control sensors vastly superior to those we use. There have been interesting studies of how birds are able to navigate precisely, but what do we really know of their abilities to sense pressure changes or other clues for efficient use of free lift?

I have been encouraged by some of the recent scientific interest in the studies of birds and believe it is timely to reassess the fundamentals of bird flight and their applications to efficient low speed flight. Four reasons for this view are:

1. Miniature instrumentation and telemetry techniques make it possible to obtain better data than any gathered by observational scientists over the years from simply watching birds in flight.

2. Bird evolution favors efficient aerodynamics, and I believe it is timely to reemphasize efficiency of flight. Our success with powerplants has led toward the "flying barn door" approach where power overcomes all other deficiencies. This has been effective, but I believe we could make significant gains with greater aerodynamics sophistication.

3. The structures, materials, and mechanisms employed by birds have been difficult for man-made machines to duplicate. Recent strides in materials and control systems offer promising possibilities for more efficient variable geometry systems.

4. Computers, sensors, and autopilots are achieving greater capabilities which more nearly approach the most basic functions of animal control systems. Studies of animal otolith functions at the cellular level, for example, may offer insight into appropriate control advances.

Research opportunities abound for improvements in efficiency and applications of low speed flight. To stimulate your thinking, I would like to suggest a few examples - none of which are new, but which seem relevant today.

All aircraft start from a standstill and return to this condition; thus, low speed flight is unavoidable for any design. Even for supersonic aircraft, the efficiency of the low speed portion of their trajectories, if I can use that term, is a matter of some relevance. It is the low speed requirements which cause many of the headaches for fast aircraft, and unfortunately it is the low speed design factors which are most empirical. If we are to make air transportation competitive with ground systems over *short ranges*, it is efficiency at low speeds which dominates rather than cruise speed.

We are all aware of the transportation gap in the systems used to transport across the oceans. Some say that had it not been for the dramatic impact of a fateful series of dirigible accidents, that lighter than aircraft competition for the ship at speeds up to 100 miles per hour would have been significant. The gap between the 20 knot ship and the 400 knot jet remains a wide one, with a lot of room for intermediate speeds and efficiencies, especially for the transport of things - not people.

The problem of transporting oil from newly found reserves in Alaska to users in other parts of the World has recently encouraged the consideration of air transport as one means. First thoughts involved the modification or development of large jet tanker aircraft; others have suggested a combination of lighter-than-air principles, lift augmentation and subsonic aerodynamics; but as a glider ethusiast, I have pondered the question of a tractor-glider combination which might offer improvements in efficiency. I believe there are many reasons why this old idea has merit for reconsideration.

First, a lot was learned about the practical application of gliders during World War II when they became an absolute necessity. According to M.M. Postan in his "Official History of the Second World War, Design and Development of Weapons", gliders were not even considered until after Germany invaded the Low Countries in 1940. Mr. Churchill then directed that England proceed with equipping a parachute troop of 5,000 men. Postan wrote: "To provide the troops with air transport appeared an impossible task, since the only suitable aircraft was the Whitley, and the number available would carry not more than 800 men. Gliders were obviously the solution...."

Britain went on to produce a variety of troop and weapon carrying gliders, and were joined by the U.S. later on. Their largest, the Hamilcar, was built of wood but had a gross weight of some 36,000 pounds with a payload of 17,500 pounds or about 49 percent! At the time of the invasion of Western Europe, 3,500 gliders were available to the allied airborne units, and were a major factor in delivering fighting men, tanks, and equipment across the Channel.

Our largest U.S. glider came in 1950 as the Chase G-20, with a gross weight of 30,000 pounds. It carried 16,000 pounds of payload with a payload fraction of 53 percent, even though it looked very much like a powered aircraft without engines. In spite of these World War II successes, it wasn't long until gliders were retired from active use by the military in favor of faster, turbine powered transports.

Aerodynamic advances, with the help of variable geometry and new materials, have yielded spectacular gains in L/D and lift coefficient in the high performance sailplanes of the last ten years. I noted with interest the L/D of 51.1 claimed recently for the new Italian 23 meter Caproni at 95/110 km per hour. High lift technologies like those enabling high wing loading jet transports to land at reasonable speeds may also be employed to advantage on large gliders.

As to the technologies for landing large gliders, recent experiments at the NASA Flight Research Center (FRC) have been impressive. Experience with space reentry lifting body "gliders" having L/D's of 2.5 to 3.0 were followed by experiments with dead stick landings of a Convair 990 and a B-52 with very predictible and safe handling characteristics, given an initial point within gliding range of the field. Test pilots at FRC argue convincingly that the space shuttle can be safely brought back from orbit without engines, and that steep, power-off approaches could be used safely for jet transports, provided airports are equipped with appropriate instrument landing systems.

The composite materials now under development and finding use in high performance sailplanes and secondary structure applications in subsonic transports look very attractive for large, low speed aircraft. The S-glass epoxies, for example, have about the same modulus efficiency as 2024 aluminum at 100 degrees F, while giving about 7 times the tensile efficiency of aluminum at the same condition, for uniaxially aligned filament specimens. Of course, these values are based on limited data, and must be degraded for biaxial or orthotropic loading conditions. For straight wing aircraft operating at relatively low speeds, the promise of such new materials is quite great.

There is much talk these days about composites and about tremendous sums of money required to develop them for use by aircraft. I have questioned my friends, who are materials and structures researchers, about what seems to me to

be a puzzling anomaly. High performance gliders made in quantity in Europe clearly demonstrate the advantages of these new materials for aircraft use. I have been told it is the high cost of manufacture which keeps them from being competitive for American manufacture where labor rates are high. On the other hand, fiberglass boats are produced in unbelievable quantities under all sorts of manufacturing conditions with highly competitive results. What accounts for the apparent difference in practical application of these materials? I have yet to receive a satisfying answer, and continue to believe that there is significant opportunity for composite materials on a near-term basis.

A modest systems engineering look has been taken recently at Langley on the possibility of fusing several new technologies into a large glider transport system. If one assumes there is a practical size limitation for an aircraft to be built and operated in existing airport environments, then it appears that a most efficient transport system might be devised using large gliders. A simple analysis indicates that a reasonable tug aircraft can be designed to tow two large (500,000 pound) gliders. If the tug has an L/D of 15, and the gliders can operate at L/D's of 30 at speeds of 150 to 200 knots, the system efficiency of the combination would surpass that of equivalent payload carrying powered transports, and with a far greater payload per pound of thrust. A 30 percent payload fraction is very good for a transport aircraft, while 60 percent should be readily achievable with a glider. Thus, for a given gross weight limit, it would take four powered aircraft to carry the same cargo as two gliders and a tug. Several economic benefits should accrue to the glider system:

1. Initial cost. - The gliders have no engines, need only simple radios, and very modest subsystems. A preliminary examination indicates that a large glider would cost only 38 percent that of a large powered aircraft of the same size.

   The tug could be smaller and certainly cost no more than a size-limited transport. Defining a powered aircraft cost of unity, the cost factor for the powered aircraft system would be 4.0, while the cost factor for the tug and glider system would be only 1.76. Thus, the initial cost of the glider system would be only 44 percent that of the powered aircraft equivalent.

2. Operating costs. - Crew costs would be 75 percent for the glider system because of three crews as opposed to four: system L/D's for the glider-tug combination and the payload weight fraction are each 30 to 50 percent better. These factors multiply in the range equation to produce a proportionate saving in fuel, and also to reduce pollution. From a maintenance standpoint, the gliders with no powerplants and modest subsystems should be cheaper to maintain;

the tug and glider maintenance costs are estimated at about 1/2 the cost of the four airplane system.

Of course, it is the productivity of high speed aircraft tending to offset the high unit costs which allow them to compete with more efficient systems, and this tradeoff has not been taken into account in this simple analysis.

To check the technical aspects of this concept, available C-130 transport performance data were used in an analysis wherein the C-130 served as a tug for towing large gliders. By allowing the unloaded C-130 to carry some 33 percent additional fuel in its cargo compartment, allowing the takeoff run to increase to 6000 feet, and allowing the cruise speed to be lowered for optimizing L/D, it was possible to more than triple the cargo payload that could be carried the maximum range for the C-130. Thus, using the C-130 in a mode which might be practical from a commercial standpoint allows an increase in payload capability from some 40 thousand pounds when used as a cargo transport aircraft to over 120 thousand pounds if used to tow two cargo gliders.

Some research has been done of the effectiveness of formation flying to improve efficiency. Hoerner's famous drag handbook suggests a 14 percent improvement is possible for a three plane element, however, a coupling of more recent research on wing tip vortex phenomena and some additional research to better understand the gains migrant birds realize from formation flying could lead to tow positions for gliders which significantly benefit from favorable interactions.

Large gliders might be sufficiently economical to buy and maintain that a number of them could be available for loading and off-loading while allowing the tug to be continually in use, improving the productivity of the system. Another advantage of air transport over ships is the attractive possibility of delivery to the point near the place where the cargo is required, without the usual loading and unloading from ships to shore to other forms of transport.

In summary, it all sounds simple:

1. There is a significant opportunity for large cargo transports in the low to medium speed range.
2. The towing and operations technology has been thoroughly worked out.
3. Dead stick landings of gliders and large aircraft are proven, and can be routine provided initial approach conditions are within limits.
4. New aerodynamics, materials, and structures technologies exist which appear ready, and
5. The economics of tug and glider combinations for transporting cargo appear very attractive.

Another important area for research contributions to the science of low speed flight involves the study of atmospheric phenomena. A few years ago jet streams were random phenomena which occasionally resulted in fast trips or late arrivals of high flying aircraft. The Sierra Project was the beginning of a serious scientific effort which led to a better knowledge of such natural occurrences. Today, jet stream data are taken into account by the airlines on all long flights and used to advantage. With no passenger comfort considerations and with less stringent schedule requirements for cargo, more like those expected of railroads and ships, it might be possible for aerial cargo craft to benefit from planned use of frontal lift systems, cloud streets, standing waves, and even ridge lift. I have recently encouraged some of Langley's atmosphere researchers to make a study of the topographical features, recurring frontal systems cloud streets and other documented phenomena which might be charted to assist in considering their regular use for air transport. Satellite photographs showing cloud streets for hundreds of miles are not uncommon - someday I hope to have my glider at the right place at the right time.

As you can see, I am as enthusiastic as Jonathan Livingston Seagull about the opportunities for research on efficient low speed flight. Renewed interests in the mysteries of bird flight may offer discoveries of great scientific significance; I also believe birds employ principles continiously which have direct application to aircraft envisioned for the future. I see opportunities for existing technologies, suitably blended, to provide improved economic returns to relatively low speed air transportation systems of all types, but especially for cargo transports.

And finally, I believe it is time to refine our knowledge of the more localized availability of free lift energy to help others share this benefit with the birds and soaring pilots. All of these examples point up the timeliness of this symposium on Motorless Flight, which I expect someday will be regarded as a milestone in the evolution of more efficient low speed flight.

Bibliography

1. Lilienthal, Otto; Birdflight as the Basis of Aviation, translated from the Second Edition by A.W. Isenthal, A.M.I.E.E., F.R.P.S.; Longmans, Green and Co., London, New York, Bombay, and Calcutta, 1911.

2. Postan, M.M.; Weapons, Design and Development of History of Second World War. British Books in Print; Her Majesty's Stationery Office. (No date)

3. Hoerner, Sighard F.; Aerodynamic Drag - Practical Data on Aerodynamic Drag Evaluated and Presented by Sighard F. Hoerner. The Otterbein Press, 1951. (Not for Sale; published and copyright by the author.)

4. Hankin, E.H.; Animal Flight, A Record of Observation. Iliffe and Sons Ltd., London, 1913.

5. Cumming, Michael; The Powerless Ones: Gliding in Peace and War. The Tanks That Went Gliding into Normady; Chapter 5, pp. 99-119; Frederick Muller, 1966.

6. Gabrielli, G., and von Karman, Th.; What Price Speed? 1950 Thurston Lecture; Mechanical Engineering, pp. 775-781, October 1950.

7. O'Lone, Richard G.; Canada Weighs Artic Resources Airlift. Aviation Week and Space Technology, p.25, May 22, 1972.

Session Chairman's Opening Address

SAILPLANE AERODYNAMICS AND DESIGN, THE STATE OF THE ART, 1972

by

A.J. Smith

In this year of 1972, commercially available sailplanes have amazing performance relative to current theoretical aerodynamic potentials. These sailplanes clearly are more efficient at their airspeeds than are current aircraft of any other types. They have remarkably eloquent visual forms with few aerodynamic compromises for function or fabrication. They are beautiful examples of man's practical application of nearly all pertinent theory. It is exactly because they are so good that they present so great a challenge to our researchers and designers.

Current sailplanes achieve a glide ratio of approximately 45 and usable speed range of 50 to 100 knots. This performance is mostly obtained from clean smooth airfoils especially developed for sailplanes. These airfoils generally derive from the now nearly classical low drag airfoils of the late nineteen thirties and early forties. Since the performance achieved now in the field approaches laboratory results, it seems to follow that development of new airfoils is desirable for further performance advances.

The constantly increasing usable speed range is achieved just now with the help of ballast, sometimes disposable, and simple flaps. At this date there seems to be no competitive successful use of more complex flap systems and only the simplest wing and flap configurations are commercially utilized. More complex systems are still confined to one-off machines.

It is apparent that extension of the speed range, particularly at the high speed end, soon will be accomplished with development of variable geometry concepts. That these systems, quite probably expensive, can be marketed is in question. However, the development of these more complex systems is required now to determine the real performance increases which can be achieved.

Current sailplanes can achieve minimum sink rates of 2 feet per second. The low sink rates achieved across wide speed ranges encourage broader investigations of seemingly minor meteorological factors. Already there are subtle changes from the classic cross country thermal soaring techniques. These changes are exercised by individual pilots, and are

not well documented; they now require analysis and refinement in order to shape new aerodynamic research and sailplane design.

The above achievements in aerodynamics and design are results, in considerable part, from recent developments of materials and methods for sailplane construction. The development of easily formed plastics for the reproduction of complex curved structures enables sailplane manufacturers to market a product with no compromise of aerodynamic forms. Even the minor art of forming transparent plastics has been advanced in sailplanes to a level where aerodynamics need not be compromised. Interestingly, however, older classic wood and metal construction methods can survive at the current highly competitive performance level when combined with the use of a few idealized plastic fairings.

While there has recently been a remarkable basic performance increase, other important sailplane characteristics have not been compromised.

Controlability has been maintained at a high level. Recent production machines with long spans begin to suffer in roll rate and control harmony but designers continue to provide nearly satisfactory results without complicated control surfaces or systems. There has been only infrequent relaxing of landing approach controlability.

Stability has been maintained at a high level in current sailplanes. Again, there seems to be no need for compromise or use of complex systems to maintain satisfactory stability characteristics. However, it remains to sort out thoroughly the subtle relationship of stability and high performance.

Safety and pilot protection have been maintained or perhaps improved. Certainly metal structures have retained their favorable characteristics and the new reinforced plastic structures have provided surprising pilot protection in severe tests of their crash resistance.

Pilot comfort is at a new high level. With current construction materials and knowledge of physical requirements for good seating there are few compromises necessary in sailplane cockpit comfort.

The recent economic environment has been an aid to current achievements in aerodynamics and design. The current annual world market for sailplanes exceeds 1,000. A large percentage of these are the high performance machines we are considering here. With an average cost of $10,000 U.S. the annual volume of 10 million Dollars is considerable. Also, the market includes obvious pressure. Consider that a good full span flapped competition sailplane sold at the factory in Germany for $3,000 in 1957. Now, 15 years later, a competitive full span flapped machine is more likely to sell for $12,000 at the factory. This for the bare sailplane without instruments and trailer. A demand which survives such increases is strong indeed.

A strange relationship in the economics of the sailplane is found in the development of airfoils and related research in airflow. Much of our recent increase in sailplane performance is a result of airfoil design, and airflow and structural research but this most important work obviously had little funding and very little monetary return. The world soaring movement owes much to the few men who developed our current aerodynamics, construction materials and methods, and production facilities. We should find ways to reimburse them for these activities and support their continuing enthusiastic research with ample funding.

Probably the recent economics of sailplanes marketing have prevented much aerodynamic testing of complete designs prior to prototype construction. However, with the currently increasing market, this situation seems to be reversing. Now there is evidence that thorough wind tunnel testing is economically possible and is being utilized more often in the development of proposed production designs.

The anticipated increasing use of classical wind tunnel facilities and techniques is more challenged, however, in the scale and performance areas being considered here. New facilities and techniques may be required for a more systematic advance and evaluation of high performance motorless aircraft. Development of these facilities and techniques may be a difficult part of our future effort. However, solutions to this situation are possible and feasible. With constantly increasing public interest and involvement in soaring we clearly can contemplate larger sailplane markets and increasing funding for research and design. The current high level of activity in aerodynamic and design research, initiated with limited funds, can only increase with the involvement of the larger markets and increasing revenues in the future. The character of research contemplated currently and the quality of individuals and institutions involved guarantees continuing higher levels of achievement. The work presented here indicates that we need not suffer a performance plateau in the foreseeable future.

The world soaring membership can accomplish much for their own benefit by encouraging and supporting the work presented here. The world aeronautical community begins now to appreciate the solutions already existing in our soaring activities. We anticipate its increasing support and cooperation. That the general public will ultimately benefit is obvious. The advantages of knowing how to go farther faster with decreasing energy requirements are better understood by laymen now. We can anticipate their increasing support.

Our level of achievement is remarkably high for the cost paid, especially when considered in the field of historically costly general aeronautics. The immediate future includes more opportunities and challenges. The rewards for our endeavors in low speed aerodynamics are becoming more apparent to everyone. The future is bright. We welcome everyone. Let's have at it!

ANALYSIS OF EFFECT OF ASYMMETRIC LOADING ON SAILPLANE PERFORMANCE IN CIRCLING FLIGHT

by

William H. Phillips
NASA Langley Research Center
Hampton, Virginia

Notation

A_n	coefficients of Fourier series (formula 20)
b	wingspan
b_w	distance between trailing vortices
c	chord of airfoil
C_{Di}	induced-drag coefficient, $D_i/\rho/2\ V^2S$
C_ℓ	rolling moment coefficient, $\mathscr{L}/\rho/2\ V^2Sb$
C_L	lift coefficient, $L/\rho/2\ V^2S$, or section lift coefficient, $L/\rho/2\ V(y)^2c$
$C_{L\alpha o}$	two dimensional lift-curve slope of airfoil
d	distance moved by vortex system
D	drag
D_i	induced drag
K	coefficient in formula for induced drag coefficient (formula 30)
L	lift
$\mathscr{L}$	rolling moment
m	mass (w/g)
n	normal acceleration (g units)
r	yawing velocity, or radius from vortex center
R	radius of turn measured to center of gravity of glider, or aspect ratio, b^2/S
ΔR	increment in radius of turn between centerline of glider and center of gravity
s	semispan, b/2
S	wing area
t	time
v	velocity induced by vortex
V	velocity at center of gravity
$V(y)$	velocity at any spanwise station
V_o	velocity at center line of glider
V_s	sinking speed
ΔV	increment of velocity at wing tip
w	downwash velocity at wing
W	weight
y	spanwise coordinate, or spanwise displacement of center of gravity
α	angle of attack of airfoil
α_{eff}	effective angle of attack, $\alpha - w/V(y)$

Notation (cont.)

Γ	circulation, or circulation of each trailing vortex
δ_a	aileron deflection
θ	spanwise variable (formula 19)
μ	relative density factor, $m/\rho Sb$
ρ	air density
ϕ	angle of bank

Introduction

A glider in a steady turn experiences a large rolling moment tending to increase the bank angle. This rolling moment results from the difference in airspeed at the inner and outer wing tips. The moment may be offset by deflection of the ailerons. Another method to offset the rolling moment, originally suggested by W. S. Blanchard, Jr., of the NASA Langley Research Center, is to displace the center of gravity laterally toward the outer tip. A reduction in profile drag would be expected to result from the use of asymmetric loading because the relatively large aileron deflections required for trim would be avoided. The method used for trimming also affects the span load distribution and, therefore, the induced drag. A question therefore arises as to the magnitude of the effect of asymmetric loading on the total drag in a turn. The lateral position of the center of gravity which results in minimum total drag is also of interest.

In order to determine the aerodynamic effects of asymmetric loading and of aileron deflection, the lateral shift of the center of gravity required to offset the rolling moment in a turn is first estimated. Some analysis and flow visualization experiments on the effect of the glider's trailing vortex system in a steady turn are next described. Finally, the effect of asymmetric loading on the induced drag in a turn is calculated, and some experimental data are reviewed to estimate the effect of aileron deflection on profile drag.

Calculations of radius of turn and yawing velocity

Some basic formulas based on the dynamics of the turn are first presented. By equating the centripetal force in a turn to the radial component of lift, the radius of a

steady, constant-altitude turn as measured from the axis of the turn to the center of gravity of the glider is determined to be:

$$\frac{R}{b} = \frac{2\mu}{C_L \sin \phi} \tag{1}$$

The normal acceleration in g units is:

$$n = \frac{L}{W} = \frac{1}{\cos \phi} \tag{2}$$

The non-dimensional yawing velocity rb/2V is determined from the component of angular velocity along the Z body axis. The non-dimensional yawing velocity is equal to the ratio of the incremental velocity at the wing tip divided by the velocity at the centerline. Thus, if an increased forward velocity of the right wing tip is considered positive:

$$\frac{rb}{2V} = \frac{-\Delta V}{V_o} = \frac{C_L}{8\mu} \sin 2\phi \tag{3}$$

The effect of a lateral shift of the center of gravity in producing rolling moment coefficient is:

$$C_\ell = C_L \frac{y}{b} \tag{4}$$

If the center-of-gravity shift is caused by lateral motion of the wing on the fuselage, or by shifting ballast, the required lateral displacement of the wing or ballast, y_w, is

$$y_w = \frac{W_T}{W_f} (y) \tag{5}$$

where W_T is the total weight and W_f is the fuselage weight or ballast weight.

Motion of the trailing vortex system in a steady turn

The induced drag of a wing results from the tilt of the lift vectors caused by the downwash induced by the trailing vortex system. In the case of a wing in straight flight, only the vortices close behind the trailing edge have an important influence on the induced drag, because of the rapid decrease in induced velocity with increasing distance of the vortices from the wing. In the case of a glider in a turn, however, the glider, after completing one circle, may come near its trailing vortex system from the preceding

turn. This vortex system might be expected to have an effect on both the performance and trim of the glider. For this reason, calculations have been made of the motion of the trailing vortex system with respect to the glider in a steady turn.

In the subsequent analysis, the motion of the glider and vortices are both determined with respect to the surrounding air mass. The results apply whether the air mass is at rest or moving with a uniform velocity. If the motion of the air mass is non-uniform, however, as might be the case in the vicinity of a thermal, the results are only approximately correct.

A further assumption of the analysis is that the vortices from the two wingtips have equal strength. This assumption may be shown to be somewhat in error in the case of a symmetrically-loaded glider. The vortex from the inboard tip will in this case be stronger. This difference in vortex strength will affect the induced drag of the glider, but the effect on the motion of the vortex system and on the induced flow of the vortex system from a previous turn is believed to be small. Some comments on this effect are given in connection with the flow visualization experiments.

The vortex system is assumed to travel downward and outward in a direction perpendicular to the wing of the glider. The glider itself, if it is flying under steady conditions in a circle of constant diameter, is displaced directly downward from its position in the previous circle. The resulting configuration after one circle can be expected to be similar to that shown in figure 1.

The formulas for the motion of the vortex system are derived as follows. Each vortex of the pair of trailing vortices has a circulation Γ equivalent to the circulation of the bound vortex at the wing root given by the formula $\rho V \Gamma$. The motion of the vortex pair may be obtained by assuming each vortex moves with the velocity induced by the other. (See reference 1 for a more complete explanation). The velocity in the field of a single vortex is given by the formula $v = \Gamma/2\pi r$. The velocity of the system is therefore

$$v = \frac{\Gamma}{2\pi b_w} \tag{6}$$

where b_w is the distance between the vortices. It is desired to express the circulation, Γ, in terms of the wing lift coefficient, C_L, and to determine the distance between the vortices, b_w, in terms of the wing span. These relations will depend to some extent on the plan form and lift distribution of the wing. It is shown by airfoil theory that most efficient wings have a lift distribution nearly

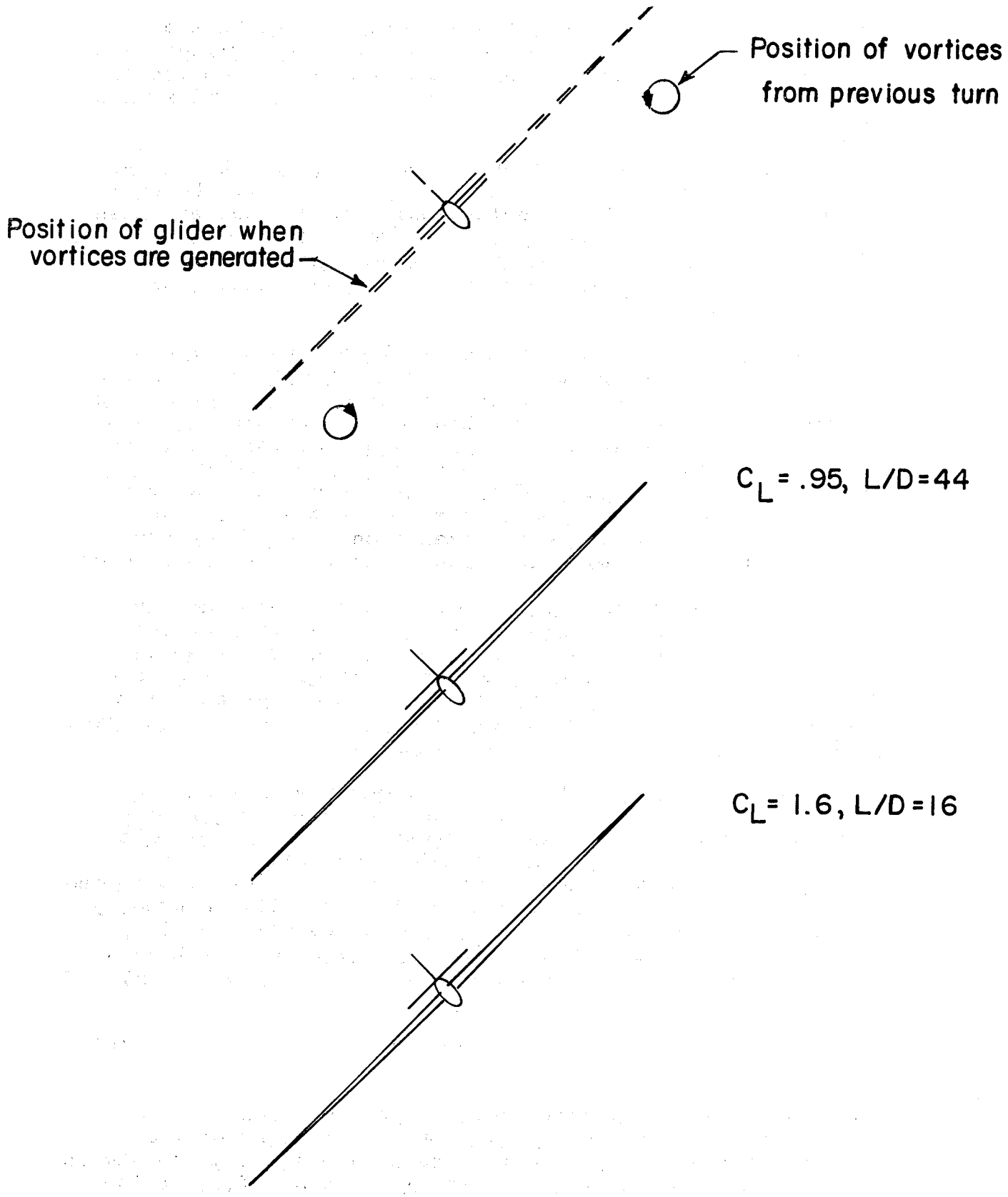


Figure 1. Position of glider with respect to vortices in a steady 45 degree banked turn at two values of lift coefficient.

elliptical. In this case, the lift per unit span at the root is $4L/\pi b$.

Making the substitution

$$L = C_L \frac{\rho}{2} V^2 S = C_L \frac{\frac{\rho}{2} V^2 b^2}{R}$$

The lift per unit span at the root is

$$\frac{2C_L \rho V^2 b}{\pi R}$$

The circulation, Γ, of each vortex is then

$$\Gamma = \frac{2C_L \rho V^2 b}{\pi R \rho V} = \frac{2C_L V b}{\pi R} \qquad (7)$$

Substituting formula (7) in formula (6):

$$v = \frac{C_L V b}{\pi^2 R b_w}$$

The distance between the vortices, again for an elliptical lift distribution, is given by airfoil theory as

$$b_w = \frac{\pi b}{4}$$

hence

$$v = \frac{4C_L V}{\pi^3 R} \qquad (8)$$

The circumference of the turn is obtained by use of formula (1).

$$\text{circumference} = 2\pi \frac{2\mu b}{C_L \sin \phi}$$

The time for the turn is the circumference divided by the velocity.

$$t = \frac{4\pi\mu b}{C_L V \sin \phi} \qquad (9)$$

Hence the distance the vortex moves in one turn is obtained by multiplying formulas (9) and (8).

$$d = \frac{4C_L V}{\pi^3 R} \cdot \frac{4\pi\mu b}{C_L V \sin\phi} = \frac{16\mu b}{\pi^2 R \sin\phi}$$

or

$$\frac{d}{b} = \frac{16\mu}{\pi^2 R \sin\phi} \tag{10}$$

The distance the glider descends in one turn is now derived. Equating the power required to the power supplied by gravity

$$WV_S = L\left(\frac{D}{L}\right)V$$

hence

$$\frac{V_S}{V} = \frac{L}{W}\left(\frac{D}{L}\right) = n\,\frac{D}{L} = \frac{D}{L\cos\phi}$$

or

$$V_S = \frac{DV}{L\cos\phi} \tag{11}$$

The distance the glider descends in a turn is obtained by multiplying formulas (9) and (11).

$$h = \frac{DV}{L\cos\phi} \cdot \frac{4\pi\mu b}{C_L V \sin\phi} = \frac{D4\pi\mu b}{LC_L \sin\phi\cos\phi} = \frac{D}{LC_L}\,\frac{8\pi\mu b}{\sin 2\phi}$$

or

$$\frac{h}{b} = \frac{D}{L}\,\frac{8\pi\mu}{C_L \sin 2\phi} \tag{12}$$

The ratio of the movement of the vortex system to the movement of the glider is

$$\frac{d}{h} = \left(\frac{16\mu}{\pi^2 R \sin\phi}\right)\left(\frac{C_L \sin 2\phi}{\frac{D}{L}\cdot 8\pi\mu}\right) = \frac{4C_L\cos\phi}{\pi^3 R\,\frac{D}{L}} \tag{13}$$

In the section on Results and Discussion, it is shown that the trailing vortices from a previous turn do not have a strong influence on the induced drag of a glider in a steady turn. For this reason, the subsequent analysis of induced drag is made without considering the effect of these vortices.

Analysis of effect of turning and of asymmetric loading in induced drag

The equation for the velocity variation along the span is

$$V(y) = V_o\left(1 + \frac{\Delta V}{V_o}\frac{y}{s}\right) \tag{14}$$

where $\Delta V/V_o$ may be obtained from formula (3).

As will be shown subsequently, the ratio $\Delta V/V_o$ is quite small, usually less than 0.15 on actual gliders even in tight turns. Theories for the induced drag of a wing with varying velocity across the span have been given in references 2 and 3. These theories, which consider large velocity variations across the span, required some terms to be added to those in the usual analysis of induced drag. In case of a small velocity variation, however, these added terms are very small. The usual method of induced-drag analysis can therefore be applied to this case with reasonable accuracy.

A brief review of the method of calculating lift and induced drag, based on the use of lifting line theory, follows. In this method, the trailing vortex sheet is assumed to induce a downwash at each point on the airfoil. This downwash tilts the lift vector at each spanwise station rearward, producing components of drag which, when they are integrated across the span, form the induced drag. A sketch of the wing showing the notation is given in figure 2. The induced downwash at each spanwise station is obtained by integrating the contributions of the trailing-vortex sheet across the span in accordance with the following formula.

$$w(y_1) = \int_{-s}^{s} \frac{-\frac{d\Gamma(y)}{dy}\,dy}{4\pi(y - y_1)} = \frac{1}{4\pi}\int_{-s}^{s} \frac{\frac{d\Gamma(y)}{dy}}{y_1 - y} \tag{15}$$

This formula is based on the assumption that the vortex sheet extends back from the wing in a straight line, whereas in a turn it forms a descending spiral. The neglect of curvature of the vortex sheet is a further approximation of the present analysis.

In formula (15), $\Gamma(y)$ and $w(y)$ are initially unknown. A second relation between w and Γ is obtained from the basic relation between circulation and lift at any spanwise station.

$$L(y) = \rho V(y)\,\Gamma(y) \tag{16}$$

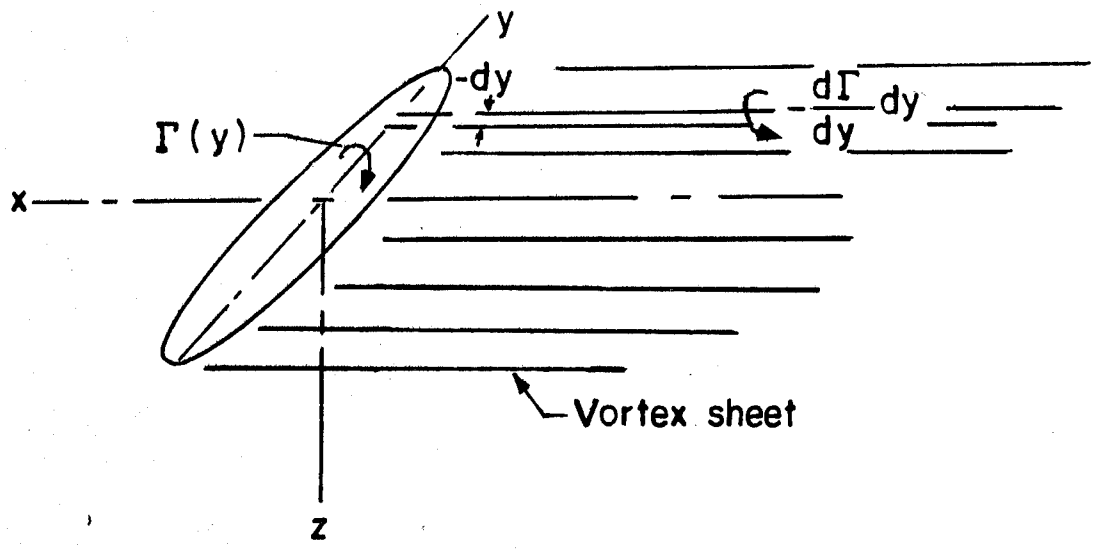


Figure 2. Sketch of wing showing vortex sheet and axes used in calculation of induced downwash.

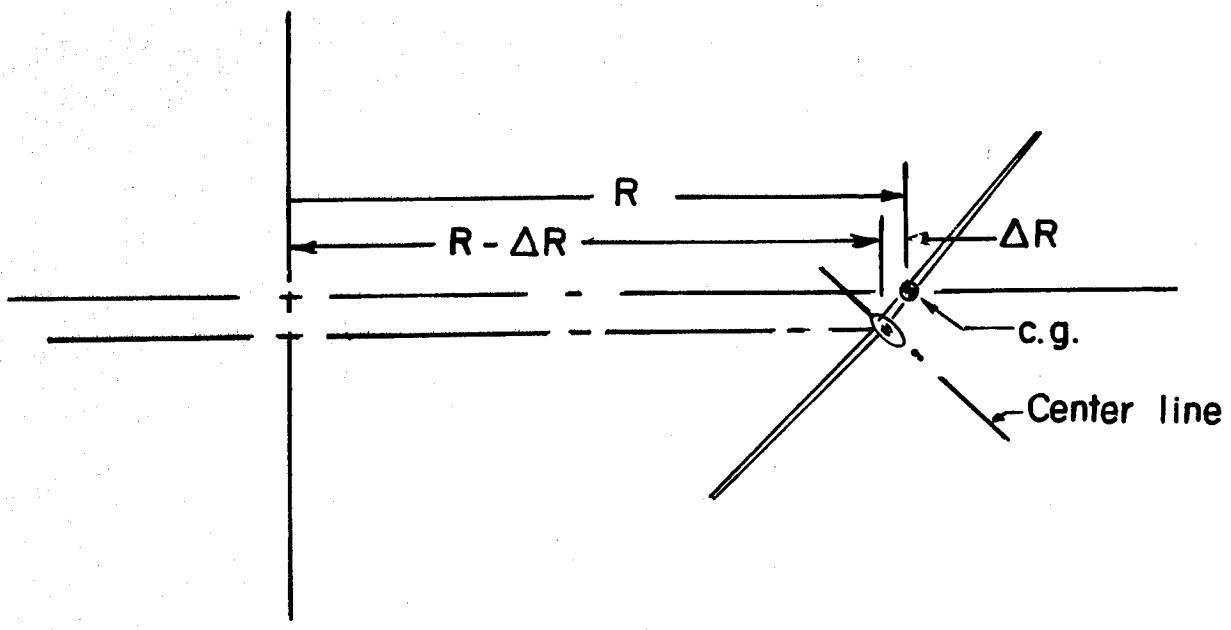


Figure 3. Sketch showing relation between velocity at centerline and velocity at center of gravity.

This equation is known as the Kutta-Jowkowski theorem. Expressing the lift in terms of the section-lift coefficient and solving for Γ:

$$\Gamma(y) = \frac{C_L \ \rho/2 \ V(y)^2 c}{\rho V(y)} = \frac{1}{2} C_L c \ V(y) \tag{17}$$

but

$$C_L = \alpha_{eff} \ C_{L_{\alpha_o}} = \left(\alpha - \frac{W}{V(y)}\right) C_{L_{\alpha_o}}$$

hence

$$\Gamma(y) = \frac{1}{2} C_{L_{\alpha_o}} \ c(V(y)\alpha - W) \tag{18}$$

By solving equations (15) and (18) simultaneously, the circulation and downwash may be obtained when c, α, and V are given as functions of y. In general, numerical solution of the equations is required, but analytical results may be obtained for certain useful special cases.

In previous analyses of induced drag, such as that given in reference 4, the variation of circulation across the span has been expressed as a Fourier series in a spanwise variable θ, related to y by the formula:

$$y = - s \cos \theta \tag{19}$$

The circulation is assumed to be given by the formula:

$$\Gamma = 4s \ V_o (A_1 \sin \theta + A_2 \sin 2\theta + \text{----} + A_n \sin n\theta)$$

or

$$\Gamma = 4s \ V_o \sum_{n=1}^{n} A_n \sin n\theta \tag{20}$$

In this series, the odd coefficients may be shown to represent symmetrical distributions of circulation, and in straight flight only these coefficients need to be considered. In turning flight, however, the circulation is usually unsymmetrical and the effects of the even coefficients must be included also. If cases with an offset position of the center of gravity are considered, the wing must develop both lift and rolling moment about the center line to maintain a steady turn. For this reason, it is desired to solve for the lift and rolling moment as a function of the coefficients A_n in turning flight.

The lift may be related to the values of the coefficients A_n as follows:

$$L = \int_{-s}^{s} L(y)\, dy = \int_{-s}^{s} \rho V(y)\, \Gamma(y)\, dy$$

Making the substitutions of expressions (14), (19) and (20):

$$V(y) = V_o\left(1 + \frac{\Delta V}{V_o}\frac{y}{s}\right),$$

$$y = -s \cos\theta,\ dy = s \sin\theta\, d\theta$$

and

$$\Gamma = 4s\, V_o \left(\sum_{n=1}^{n} A_n \sin n\theta\right)$$

The expression for the lift becomes

$$L = \int_o^{\pi} \rho V_o \left(1 - \frac{\Delta V}{V_o}\cos\theta\right)\left(4s\, V_o \sum_{n=1}^{n} A_n \sin n\theta\right) s \sin\theta\, d\theta$$

or

$$\frac{L}{4\rho V_o^2 s^2} = \int_o^{\pi} \sum_{n=1}^{n} A_n \sin n\theta \sin\theta\, d\theta - \frac{\Delta V}{V_o}\int_o^{\pi} \frac{\sin 2\theta}{2} \sum_{n=1}^{n} A_n$$

$$\sin n\theta\, d\theta$$

The values of these integrals are, respectively

$$\int_o^{\pi} \sum_{n=1}^{n} A_n \sin n\theta \sin\theta\, d\theta = \frac{\pi}{2} A_1, \quad \text{for} \quad n = 1$$

$$= 0 \quad \text{for} \quad n \neq 1$$

$$-\frac{\Delta V}{V_o}\int_o^{\pi} \frac{\sin 2\theta}{2} \sum_{n=1}^{n} A_n \sin n\theta\, d\theta = \frac{-\Delta V}{V_o}\frac{\pi}{4} A_2, \quad \text{for} \quad n = 2$$

$$= 0 \quad \text{for} \quad n \neq 2$$

Thus only the coefficients A_1 and A_2 contribute to the lift. The lift is therefore

$$L = 2\pi\ \rho V_o^2\ s^2 \left(A_1 - \frac{A_2}{2}\frac{\Delta V}{V_o}\right) \tag{21}$$

Similarly, the rolling moment may be related to the values of the coefficient as follows:

$$\mathcal{L} = \int_{-s}^{s} -L(y)y\ dy = \int_{-s}^{s} -\rho V(y)\Gamma(y)y\ dy$$

Again make the substitutions of expressions (14), (19), and (20).

The expression for the rolling moment becomes

$$\mathcal{L} = 4\rho V_o^2 s^3 \int_o^{\pi} \left(\sum_{n-1}^{n} A_n \sin n\theta\right)\left(1 - \frac{\Delta V}{V_o}\cos\theta\right)\sin\theta\cos\theta\ d\theta$$

$$\frac{\mathcal{L}}{4\rho V_o^2 s^3} = \int_o^{\pi} \sum_{n=1}^{n} A_n \sin n\theta \sin\theta\cos\theta\ d\theta$$

$$- \frac{\Delta V}{V_o}\int_o^{\pi} \sum_{n=1}^{n} A_n \sin n\theta \sin\theta\cos^2\theta\ d\theta$$

To determine the value of the first integral, the following relation may be used:

$$\int_o^{\pi} \frac{An}{2} \sin n\theta \sin 2\theta\ d\theta = \frac{\pi}{4} A_2 \quad \text{for} \quad n = 2$$

$$= 0 \quad \text{for} \quad n \neq 2$$

The value of the second integral is derived in the appendix. The result is:

$$- \frac{\Delta V}{V_o}\int_o^{\pi} A_n \sin n\theta \sin\theta\cos^2\theta\ d\theta = - \frac{\pi}{8}\frac{\Delta V}{V_o} A_1 \quad \text{for} \quad n = 1$$

$$= - \frac{\pi}{8}\frac{\Delta V}{V_o} A_3 \quad \text{for} \quad n = 3$$

$$= 0 \quad \text{for} \quad n \neq 1 \quad \text{and} \quad 3$$

The value of the rolling moment is therefore:

$$\mathcal{L} = \pi\rho V_o^2 s^3 \left(-\frac{A_1}{2}\frac{\Delta V}{V_o} + A_2 - \frac{A_3}{2}\frac{\Delta V}{V_o} \right) \qquad (22)$$

The values of the lift and rolling moment, (21) and (22) may be expressed in coefficient form as follows:

$$C_L = \frac{L}{\frac{\rho}{2} V^2 S} = \pi R \frac{V_o^2}{V^2} \left(A_1 - \frac{A_2}{2}\frac{\Delta V}{V_o} \right) \qquad (23)$$

and

$$C_\ell = \frac{\mathcal{L}}{\frac{\rho}{2} V^2 Sb} = \frac{\pi}{4} R \frac{V_o^2}{V^2} \left(-\frac{A_1}{2}\frac{\Delta V}{V_o} + A_2 - \frac{A_3}{2}\frac{\Delta V}{V_o} \right) \qquad (24)$$

For a wing with a known lift distribution in straight flight, the ratio A_3/A_1 may be estimated. For any known values of C_L and C_ℓ, the values of A_1 and A_2 may then be determined by solving equations (23) and (24) simultaneously. In the work which follows, the value of A_3 will be assumed to equal zero, corresponding to a wing with elliptical lift distribution in straight flight.

The induced drag may be realted to the coefficients as follows:

$$D_i = \int_{-s}^{s} \rho V \Gamma \frac{w}{V}\, dy = \int_{-s}^{s} \rho \Gamma w\, dy$$

$$= 4sV_o \int_o^{\pi} \rho \left(\sum_{n=1}^{n} A_n \sin n\theta \right) w(\theta) s \sin\theta\, d\theta$$

In reference 4, the value of $w(\theta)$ is obtained by inserting the Fourier series expression for Γ, formula (20), in formula (15) and evaluating the integral. The result is:

$$w(\theta) = V_o \sum_{n=1}^{n} n \frac{A_n \sin n\theta}{\sin\theta}$$

The induced drag is therefore

$$D_i = 4\rho s^2 V_o^2 \int_o^{\pi} \left(\sum_{n_1=1}^{n_1} A_{n_1} \sin n_1 \theta \right) \left(\sum_{n_2=1}^{n_2} A_{n_2} \sin n_2 \theta \right) d\theta$$

When $n_1 \neq n_2$, the integral is zero
When $n_1 = n_2$, the integral is $\pi/2/nA_n^2$
Therefore:

$$D_i = 2\pi\rho s^2 V_o^2 \sum_{n=1}^{n} n A_n^2$$

or

$$C_{D_i} = \pi R \frac{V_o^2}{V^2} \sum_{n=1}^{n} n A_n^2 \qquad (25)$$

This formula shows that the induced drag depends on all the coefficients, A_n, whereas the lift and rolling moment, in turning flight, depend only on A_1 and A_2. A well-known result of lifting-line theory as applied to straight flight is that the lift depends only on the value of A_1. If all the higher-order coefficients are zero, this distribution of circulation corresponds to an elliptical loading and the induced drag is a minimum. Since high-performance soaring gliders are designed for very low drag, this condition is closely approached in actual designs. Moderate changes in plan form do not change the loading very much from elliptical, indicating that the higher-order coefficients decrease rapidly with increasing values of n. As a result, the major part of the induced drag may be obtained by considering only the contribution of the coefficient A_1.

Similar reasoning may be used to estimate the induced drag in turning flight. In this condition, the lift and rolling-moment coefficients are related to the coefficients A_1 and A_2. The coefficient A_2 adds to the induced drag in accordance with formula (25). The unsymmetrical circulation distribution associated with the coefficient A_2 is the one which produces a rolling moment with the minimum induced drag. Higher-order even coefficients, A_4, A_6, etc., add to the induced drag without increasing the rolling moment. For efficiently designed ailerons, the higher-order coefficients are expected to decrease rapidly with increasing values of n. In this case, the major part of the induced drag may be obtained by considering only the

contributions of the coefficients A_1 and A_2.*

In order to determine the induced drag of a glider under conditions of turning flight and asymmetric loading, the values of A_1 and A_2 may be obtained by solving simultaneously equations (23) and (24). These values may then be substituted in equation (25) to determine the drag. The rolling moment coefficient with asymmetric loading is given by the expression

$$C_\ell = C_L\left(\frac{-y}{b}\right)$$

If this value is substituted in equations (23) and (24) and these equations are solved simultaneously for the coefficients A_1 and A_2, the result is:

$$A_1 = \frac{C_L\left(1 - 2\,\frac{y}{b}\,\frac{\Delta V}{V_o}\right)}{\pi R\,\frac{V_o^2}{V^2}\left[1 - \frac{1}{4}\left(\frac{\Delta V}{V_o}\right)^2\right]} \tag{26}$$

$$A_2 = \frac{C_L\left(-4\,\frac{y}{b} + \frac{1}{2}\,\frac{\Delta V}{V_o}\right)}{\pi R\,\frac{V_o^2}{V^2}\left[1 - \frac{1}{4}\left(\frac{\Delta V}{V_o}\right)^2\right]} \tag{27}$$

From equation (25)

$$C_{D_i} = \pi R\,\frac{V_o^2}{V^2}\left(A_1^2 + 2A_2^2\right)$$

Substituting equations (26) and (27) and omitting small terms involving $(\Delta V/V_o)^4$ gives the expression

$$C_{D_i} = \frac{C_L^2\,\frac{V^2}{V_o^2}}{\pi R}\left(\frac{1 + \frac{1}{2}\left(\frac{\Delta V}{V_o}\right)^2 + 32\left(\frac{y}{b}\right)^2 - 12\,\frac{y}{b}\,\frac{\Delta V}{V_o}}{1 - \frac{1}{2}\left(\frac{\Delta V}{V_o}\right)^2}\right) \tag{28}$$

---

*The unsymmetrical loading corresponding to the coefficient A_2, which produces minimum induced drag in straight flight for a given rolling moment, may be shown to result from linear spanwise twist of an elliptical wing.

The induced drag is influenced by asymmetric loading not only because of the effect of this loading on the coefficients A_1 and A_2 but also because of the term (V^2/V_o^2) which occurs outside the brackets. This term results from the fact that the radius of turn was defined as the distance from the axis of rotation to the center of gravity of the glider. If the center of gravity is outboard of the centerline of the glider, the velocity V_o measured at the centerline is less than V measured at the center of gravity. The term V^2/V_o^2 reflects the direct geometric effect of this slower velocity at the centerline. This slower velocity requires the glider to fly at a higher angle of attack and, therefore, to have a higher drag coefficient than it would if the center of gravity were on the centerline. The term $(V/V_o)^2$ may be expressed as a function of y/b and $\Delta V/V_o$.

As shown by figure 3 :

$$\frac{V}{V_o} = \frac{R}{R - \Delta R} \cong 1 + \frac{\Delta R}{R}$$

but from formulas (1) and (3)

$$\frac{\Delta R}{R} = \frac{\frac{y}{b} \cos \phi \, C_L \sin \phi}{2\mu} = \frac{2 \frac{y}{b} C_L \sin 2\phi}{8\mu} = 2 \frac{y}{b} \frac{\Delta V}{V_o}$$

Hence

$$\frac{V}{V_o} = 1 + 2 \frac{y}{b} \frac{\Delta V}{V_o}$$

$$\left(\frac{V}{V_o}\right)^2 = 1 + 4 \frac{y}{b} \frac{V}{V_o} + 4\left(\frac{y}{b} \frac{\Delta V}{V_o}\right)^2$$

In this expression, the term $(y/b \; \Delta V/V_o)^2$ may be dropped because both y/b and $\Delta V/V_o$ are small quantities.

Substituting the expression for $(V/V_o)^2$ in formula (28) gives

$$C_{D_i} = \frac{C_L^2}{\pi R} \left(1 + 4 \frac{y}{b} \frac{\Delta V}{V_o}\right) \left(\frac{1 + \frac{1}{2}\left(\frac{\Delta V}{V_o}\right)^2 + 32\left(\frac{y}{b}\right)^2 - 12 \frac{y}{b} \frac{\Delta V}{V_o}}{1 - \frac{1}{2}\left(\frac{\Delta V}{V_o}\right)^2} \right)$$

Carrying out the multiplications and divisions and omitting terms higher than second order in $\Delta V/V_o$ or y/b gives:

$$C_{D_i} = \frac{C_L^2}{\pi R}\left(1 + \left(\frac{\Delta V}{V_o}\right)^2 + 32\left(\frac{y}{b}\right)^2 - 8\,\frac{y}{b}\,\frac{\Delta V}{V_o}\right) \qquad (29)$$

The first term of this formula is the familiar expression for the induced drag of a symmetrically loaded elliptical wing in straight flight. The additional terms give the induced drag increments due to asymmetric loading and turning.

While the asymmetric loading and turning are, in general, independent quantities, an optimum condition may be sought in which the asymmetric loading is related to the turning in order to produce the minimum induced drag. Consider first the case with symmetrical loading ($y/b = 0$). The expression for the induced drag, formula (29), may be reduced to:

$$C_{D_i} = \frac{C_L^2}{\pi R}\left[1 + \left(\frac{\Delta V}{V_o}\right)^2\right]$$

In this case, the distribution of circulation is not symmetrical, as shown by the fact that the term A_2 is not zero (formula (27)). The value of A_2 is:

$$A_2 = \frac{A_1}{2}\,\frac{\Delta V}{V_o}$$

The fact that A_2 is positive shows that the circulation is greater on the inboard wing.

The coefficient A_2 is about equal in magnitude, but opposite in sign, when the center of gravity is moved outboard to the point at which zero aileron deflection is required to trim in a turn. This result may be derived by means of lifting-line theory through use of formulas (15) and (18) or by use of the known result that, for an untwisted elliptical wing of high aspect ratio, $C_{\ell_r} = .25\ C_L$ [reference 5].

The value of y/b for zero aileron deflection, as obtained from formula (15), is therefore

$$\frac{y}{b} = \frac{1}{4}\,\frac{\Delta V}{V_o}$$

The value of C_{D_i} is again

$$C_{D_i} = \frac{C_L^2}{\pi R}\left[1 + \left(\frac{\Delta V}{V_o}\right)^2\right]$$

At the center-of-gravity position halfway between the centerline and that for zero aileron deflection, the coefficient A_2 is zero. The corresponding value of y/b is:

$$\frac{y}{b} = \frac{1}{8} \frac{\Delta V}{V_o}$$

If this formula is substituted in the formula for the induced drag (formula (29)) the result is obtained:

$$C_{D_i} = \frac{C_L^2}{\pi R} \left[1 + \frac{1}{2} \left(\frac{\Delta V}{V_o} \right)^2 \right]$$

In general, as the formula for induced drag in a turn may be written in the form

$$C_{D_i} = \frac{C_L^2}{\pi} \left[1 + K \left(\frac{\Delta V}{V_o} \right)^2 \right] \qquad (30)$$

The value of K varies with the distance that the center of gravity is moved outboard as shown in figure 4. The minimum induced drag in a turn occurs when the center of gravity is halfway between the centerline and the point for zero aileron deflection to trim.

Determination of profile drag

The increment of profile drag coefficient due to aileron deflection must be evaluated in order to evaluate the magnitude of the effect of asymmetric loading on the total drag in a turn. Unfortunately, very little information exists on typical glider airfoils at the low Reynolds numbers of the narrow-chord tip sections. For a glider having the characteristics given in table I, the Reynolds No. of an airfoil with a chord of .4572 m (1.5 feet), a typical value in the aileron region, at the speed required in a 45° banked turn, would vary from $.79 \times 10^6$ at a lift coefficient of 1.0 to $.625 \times 10^6$ at a lift coefficient of 1.6. One set of test data at a Reynolds number of $.7 \times 10^6$ is given for an FX 60-126 airfoil with 35 percent chord flap in reference 6. These data have been used to estimate the magnitude of the profile drag increments.

The aileron deflection required as a function of lift coefficient, with the center of gravity on the centerline, may be obtained from the formula

$$\delta_a C_{\ell_{\delta_a}} = C_{\ell_r} \frac{rb}{2V}$$

TABLE I

Characteristics Used in Calculations

b	18.29 m	(60 ft)
ρ	1.226 kg/m^3	(.00238 slugs/ft^3)
S	12.99 m^2	(140 ft^2)
W	4057 N	(912 lb)
Aspect Ratio	25.8	
m	413.7 kg	(28.3 sl)
μ	1.41	

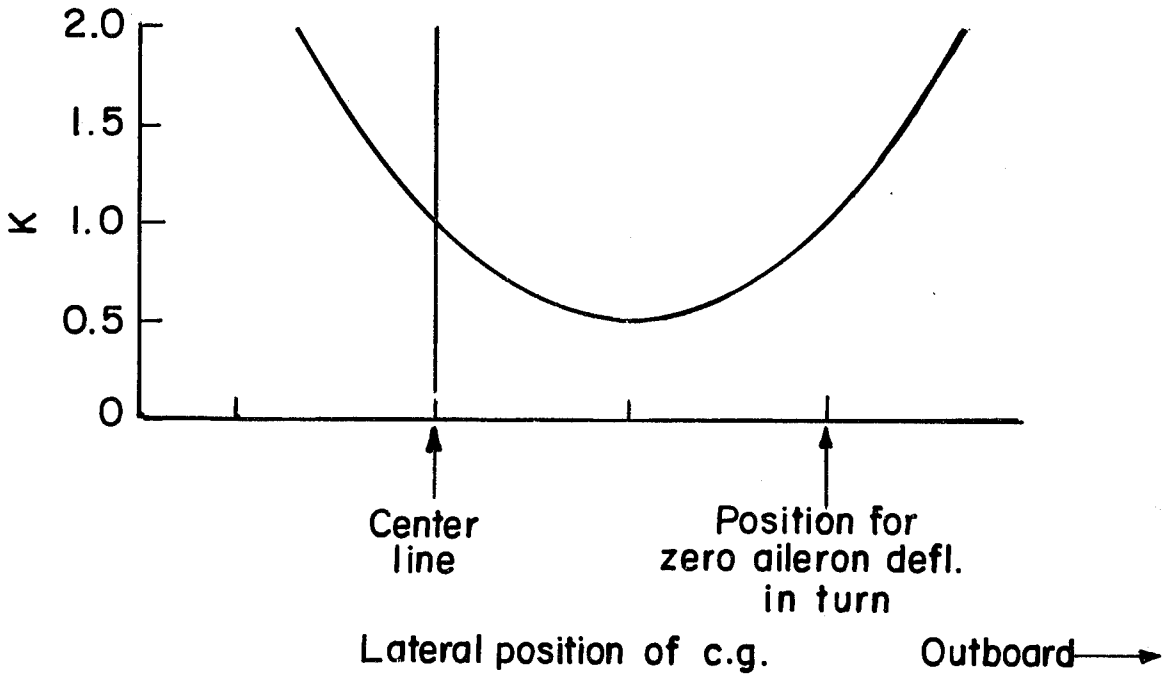


Figure 4. Value of K in the formula $C_{D_i} = \frac{C_L^2}{\pi R}\left[1 + K\left(\frac{\Delta V}{V_o}\right)^2\right]$ as a function of lateral position of the center of gravity.

The value of rb/2V, formula (3), may be substituted to give:

$$\delta_a C_{\ell_{\delta_a}} = C_{\ell_r} \frac{C_L}{8\mu} \sin 2\phi$$

or

$$\delta_a = \frac{C_{\ell_r}}{C_{\ell_{\delta_a}}} \frac{C_L}{8\mu} \sin 2\phi \qquad (31)$$

Values of C_{ℓ_r} and $C_{\ell\delta a}$ may be estimated from the data given in reference 7.

Results and discussion

The results presented herein have been calculated for a typical soaring glider having the characteristics given in table 1.

Aileron deflection or lateral shift of the center of gravity for trim

Plots of the radius of turn, normal acceleration, and non-dimensional yawing velocity obtained from formulas (1), (2), and (3) are given in figure 5 as a function of bank angle. These values were calculated for a lift coefficient of 0.95, which is the lift coefficient for minimum sink rate on the example glider, and for $C_L = 1.6$, which is close to the maximum lift coefficient. Thermal soaring would probably be done in the range between these two values. In a wide region of rising air, the lower value should be used, but in a small-diameter thermal, the tightest possible turn would probably be required to gain maximum benefit from the thermal.

As shown by formula (3), the yawing velocity is greatest at a bank angle of 45°, and at the lowest altitude (sea level), inasmuch as the relative density factor, μ, is smallest at this condition. The rolling moment coefficient due to yawing velocity, $C_{\ell r}$, was obtained from reference 7 by extrapolating the values given for values of aspect ratio of 6, 10, and 16 to a value of 25.8.

Values are given in the following table for the rolling-moment coefficient and aileron deflection for trim at 45° bank and for the lateral shift of the center of gravity at values of lift coefficient of 0.95 and 1.6. The lateral

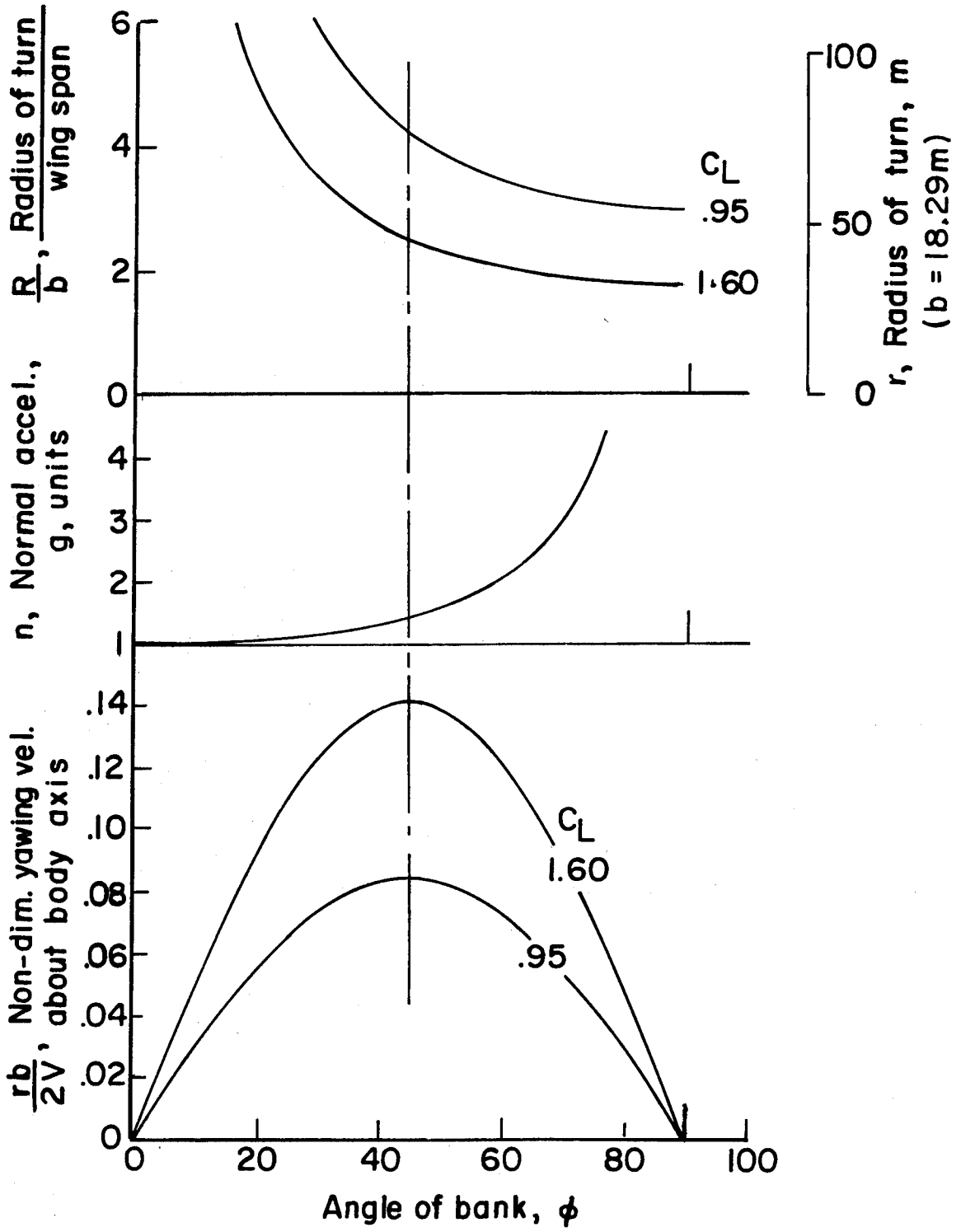


Figure 5. Radius of turn, normal acceleration, and non-dimensional yawing velocity as a function of angle of bank for a soaring glider having b=18.29 m (60 ft), S=12.99 m^2 (140 ft^2), W=4057 N (912 lb), C_L=0.95 and 1.60, sea level.

shift of the fuselage required has been calculated under the assumption that the fuselage weight is 2722 N (612 lb) and the total weight 4057 N (912 lb). As an alternative, the lateral shift of 889 N (200 lb) of ballast has been calculated with the same total weight.

Lift coefficient, C_L	0.95	1.6
Rolling-moment coefficient, C_ℓ	0.0188	0.0533
Aileron deflection for trim, deg	4.36	12.35
Lateral shift of c.g.	.3597 m (1.18 ft)	0.6096 m (2.00 ft)
Lateral shift of fuselage	0.5395 m (1.77 ft)	0.9053 m (2.97 ft)
Lateral shift of ballast	1.645 m (5.40 ft)	2.776 m (9.11 ft)

These results show that the required lateral shift of the center of gravity varies directly with the lift coefficient, whereas the aileron deflection for trim varies as the square of the lift coefficient. The shifting of water ballast, if it is carried in the glider for reasons of performance, is probably the simplest way to accomplish the lateral center-of-gravity shift. The water ballast could be shifted by sideslipping the glider provided the tanks in the two wings were connected with suitable pipes and valves. In view of the rather large shift required, however, a study is required of effects of asymmetric loading on induced and profile drag to determine whether the full amount of the shift is necessary.

As was mentioned previously, a glider in a steady turn may be influenced by its own trailing vortices shed on a previous turn. If this effect were important, the calculation of induced drag would have to take these effects into account. Before proceeding with the calculation of induced drag, therefore, results of some studies to investigate the effects of the trailing vortices are presented.

Relative positions of the glider and vortex system:

The relative positions of the glider and the vortex system after one turn in a 45° bank have been calculated for the example glider using the same flight conditions as those assumed previously. The conditions and results are as follows:

C_L	$\frac{L}{D}$	μ	$\frac{d}{b}$	$\frac{h}{b}$	$\frac{d}{h}$
.95	44	1.41	.125	.846	.148
1.6	16	1.41	.125	1.383	.090

These results, sketched in figure 1, show that the vortex system moves only slightly, in the course of one turn, from

the position of the wing at which vortices were initially generated. Surprisingly, the distance the vortices move, when expressed as a fraction of the span, is independent of the lift coefficient for a given bank angle. In a steady turn, however, the glider itself moves down a distance ranging from 0.8 to 1.4 times the span, depending on the lift coefficient. In actual flight, the glider may not be in a steady turn, and if it is entering a turn from a high-speed flight condition it may either lose or gain altitude with respect to the vortex system. The velocity induced by the vortices at various positions is therefore of interest.

An estimate of the component of velocity normal to the line joining the vortices at various distances below the vortex system is shown in figure 6. The velocity has been converted to an equivalent flow angle in degrees and is given for a value of $C_L = 1.0$. The angles for other values of lift coefficient would be proportional to the lift coefficient. These calculations were made assuming two-dimensional flow; that is, the vortices were assumed to extend in straight lines perpendicular to the plane of the paper rather than in a descending spiral as would be the actual case. The downwash region of the actual vortices would therefore probably be shifted somewhat toward the center of the circle.

In a steady turn, as indicated in figure 6, the downwash induced by the vortex system has its greatest effect on the outboard wing of the glider. This induced velocity would produce a rolling moment tending to roll the glider out of the turn, and would therefore reduce the aileron deflection held against the turn to offset the rolling moment due to yawing velocity. The magnitude of the effect appears to be quite small when the glider is displaced downward the amount corresponding to a steady turn. For example, with the glider displaced downward one wing span, the effect would reduce the aileron deflection required on each wing by less than 1 degree. The effect on the induced drag of the glider also appears to be very small.

If the glider were in a non-steady maneuver and flew closer to the vortex system, the effect could be quite large, but such a condition would be only temporary. Also, the induced downwash near the vortex system is large enough to have an appreciable effect on the performance of the glider if the glider flies within about 20 percent of the wingspan above or below the vortex system. For example, at a distance of 10 percent of the span above or below the vortex system and at a lift coefficient of 1.0, the average velocity normal to the wingspan would be about .3962 m per second (1.3 ft per second). If possible, therefore, flying directly into the wake from a previous turn should be avoided. Some slight gain in efficiency could be obtained by flying just outboard of the vortex system, thereby taking

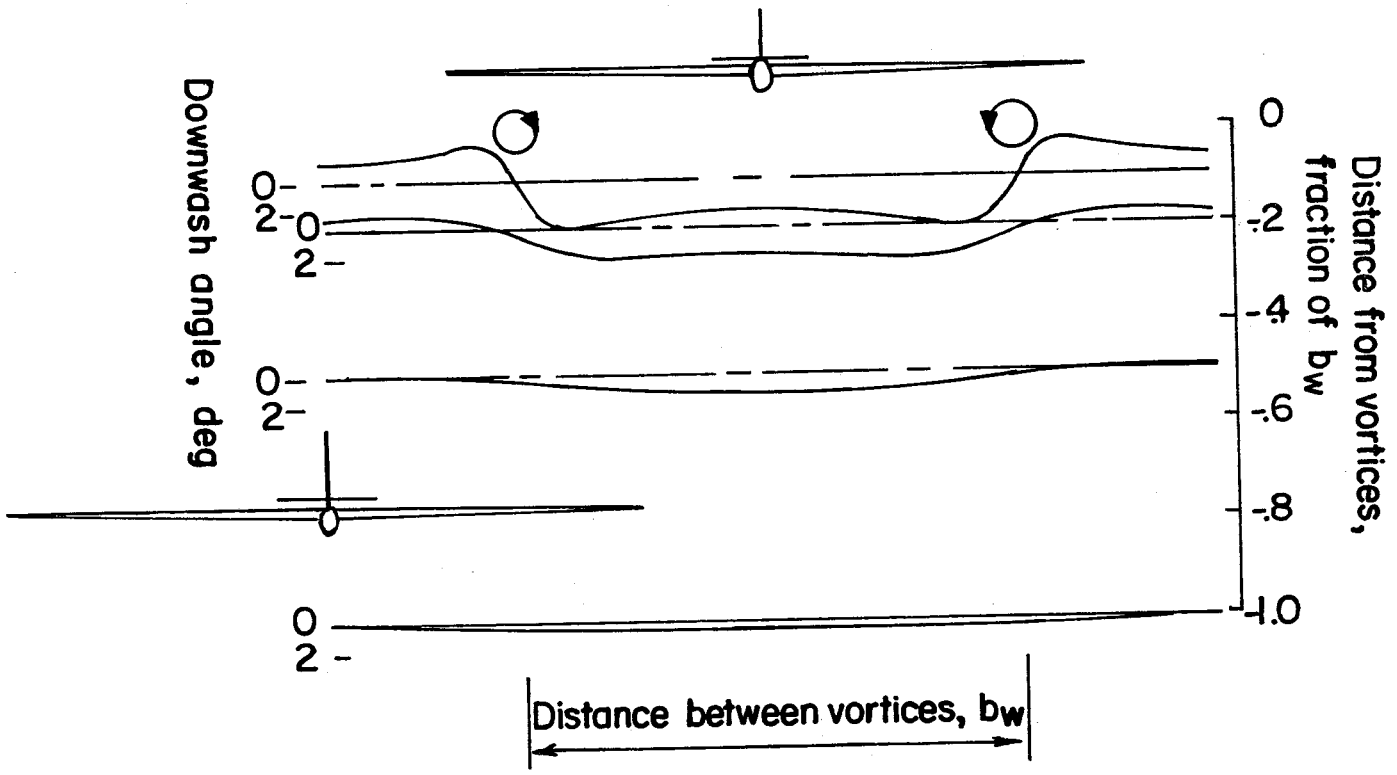


Figure 6. Induced downwash angle normal to line joining vortices in vicinity of vortex system with $C_L = 1.0$

advantage of the upwash to reduce the sinking speed and to reduce aileron deflection for trim.

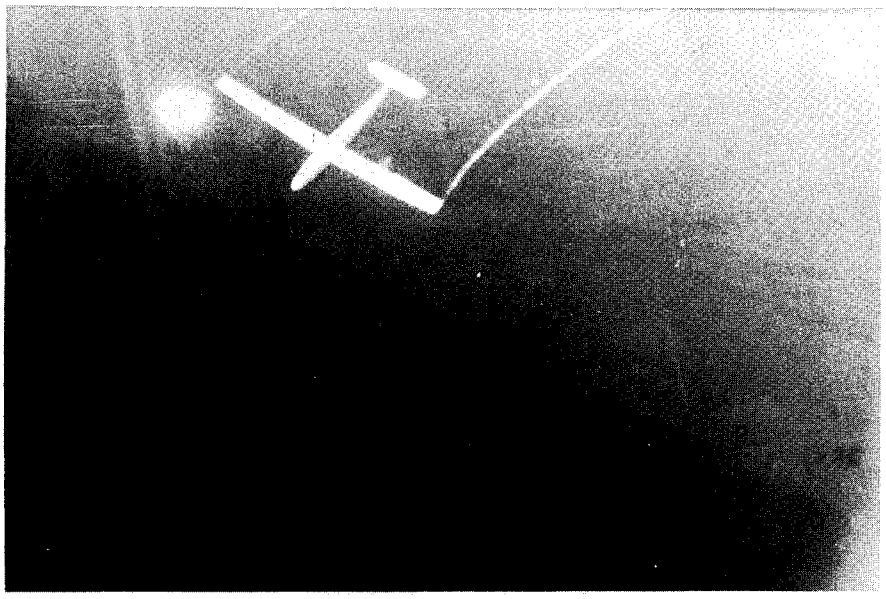
Flow visualization experiments

Some tests have been made of a heavy model of 40-inch span gliding in circles in a large water tank. Dye was emitted from tubes in the wingtips to mark the trailing vortices. These tests confirm the analytical results in that the vortex system moves down very slowly and that the glider descends more rapidly. The vortices dissipate very slowly and are still evident after the glider has completed several circles. With the model loaded symmetrically, the outer vortex moves down slightly faster than the inner one, indicating that the inner vortex is stronger. This result would be expected from an analysis of the lift coefficient and speed of the two wings. This effect has been neglected in the preceding analysis. The difference in the rate of motion of the two vortices is so small, however, that their relative position after the glider has completed one turn is affected only a small amount. Some photographs of the vortices produced by the model gliding in the tank are shown in figure 7.

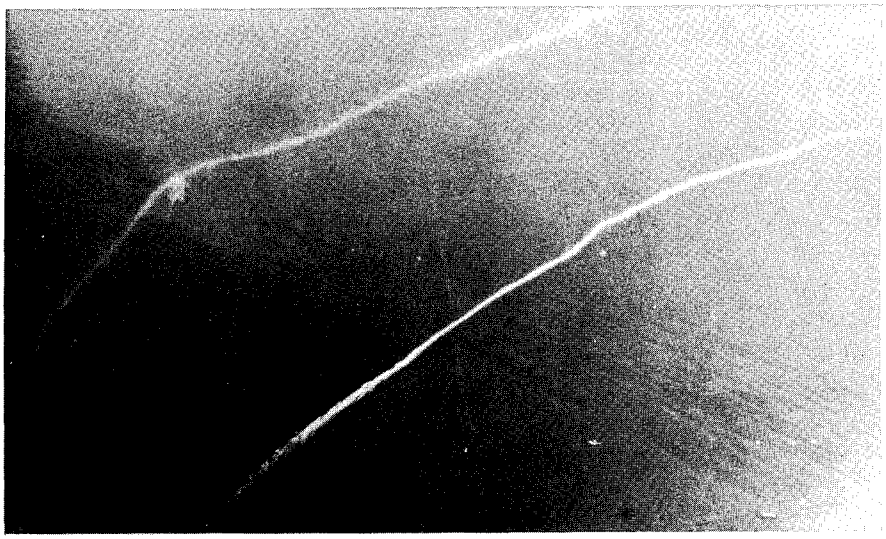
Induced and profile drag in a turn

The preceding discussion shows that the conventional lifting-line theory may be used with good accuracy to estimate the effects of turning and of asymmetric loading on the induced drag in a steady turn. The value of induced drag is given by formula 30 and figure 4. In this formula, the term $C_L^2/\pi R$ is the familiar expression for induced drag of a symmetrical wing in straight flight. This term is multiplied by the factor $1 + K\,\Delta V/V_o{}^2$. The value of $\Delta V/V_o$, equivalent to $rb/2V$, may be read from figure 5. The maximum value of $\Delta V/V_o$ for the example considered is 0.14, and the value of K remains between 0.5 to 1 in the range of center-of-gravity positions for zero aileron deflection. The formula shows that the induced drag coefficient in a turn is always slightly greater than that in straight flight at a given value of lift coefficient, and that the drag increment is a minimum when the center of gravity is halfway between the centerline and the location requiring zero aileron deflection for trim. In any case, however, the induced drag increment is very small. In the case used as an example, the increase of induced drag under the most unfavorable combination of conditions (center of gravity on centerline, $\phi = 45^o$, $C_L = 1.6$) is less than 2 percent.

The increments of induced and profile drag coefficient for the center of gravity on the centerline are shown in figure 8. These values are each based on total wing area.



(a) Model glider circling in water tank



(b) Vortices some time after passage of glider

Figure 7. Photographs of vortices produced by model gliding in circles in water tank.

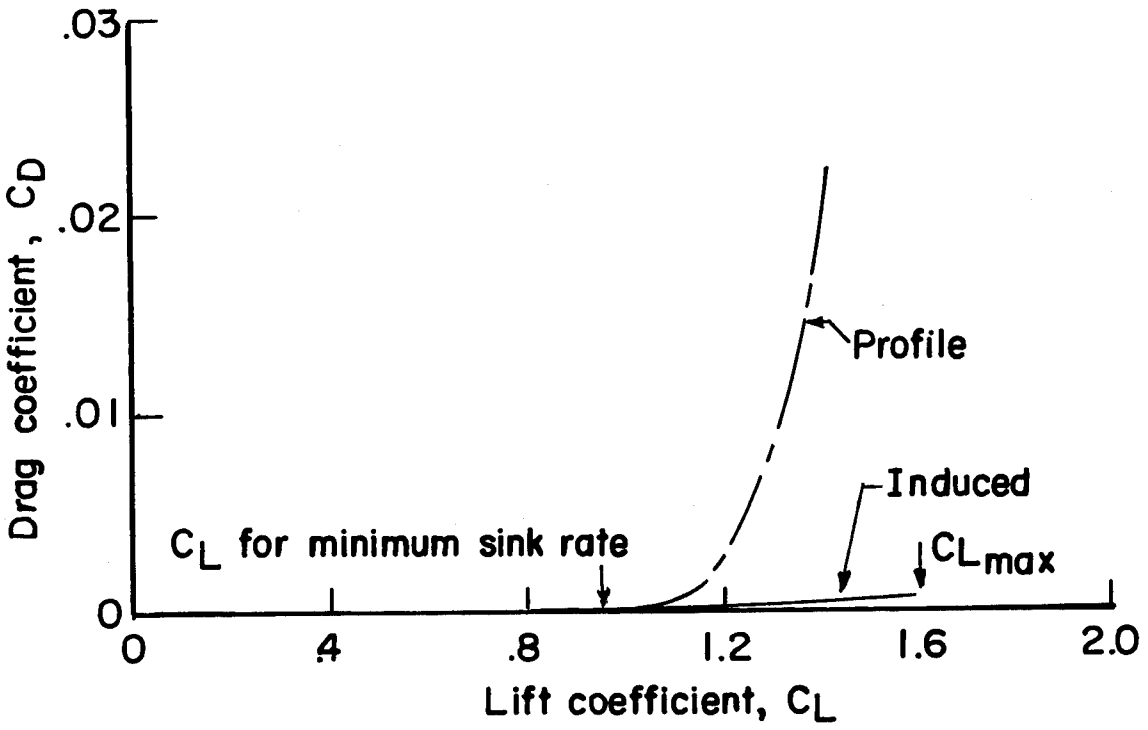


Figure 8. Increments of induced and profile drag as a function of lift coefficient in a steady turn for center of gravity on the centerline.

This figure shows that the induced and profile drag increments are both small for lift coefficients below about 1.0. The increment of induced drag remains negligible throughout the lift coefficient range. The profile drag increment rapidly becomes larger at lift coefficients between 1.0 and the maximum lift coefficient of 1.6. This large increment of profile drag is entirely due to the downward-deflected aileron on the inboard wing. The upward-deflected aileron on the outboard wing produces a slight reduction in profile-drag coefficient. Evidently the flow is separating from the upper surface of the downward-deflected aileron under the conditions of low Reynolds number experienced by the tip sections.

The small value of induced drag coefficient which exists throughout the range of lateral center-of-gravity positions of interest imposes no constraint on the use of lateral shift of the center of gravity to reduce the aileron deflection for trim and therefore the profile-drag increments associated with aileron deflection. The lift coefficient or aileron deflection at which flow separation becomes serious will depend on the particular airfoil section used on a glider. At the low Reynolds numbers typical of the tip regions of a glider wing, however, flow separation on the upper surface of the downward-deflected aileron is likely to occur at high angles of attack for most airfoil sections.

Concluding remarks

In the tight turns used in thermal soaring, large aileron deflections are required to offset the rolling moment associated with the velocity gradient along the span. This velocity gradient is a maximum in turns at low altitude, near the maximum lift coefficient, and at a bank angle of 45°. Formulas are presented for estimating the lateral shift in center of gravity required to trim the glider laterally with the ailerons in neutral.

The reduction in profile drag resulting from reduced aileron deflection may be estimated from suitable wind-tunnel airfoil data. The use of asymmetric loading, however, may be expected to affect the induced drag. A question therefore arises as to the effect of asymmetric loading on the total drag in a turn.

Calculation of the induced drag of a glider in a tight turn introduces certain possible problems not ordinarily considered in the classical determination of induced drag from lifting-line theory. The glider, after completing one circle, may be in the proximity of its own trailing vortex system. The behavior of this vortex system has been studied by means of flow visualization tests with a heavy, freely-

gliding model in a water tank. Calculations of the possible influence of the vortex system on the performance and trim of the glider have been made. This effect was found to be small provided the glider is descending at the rate corresponding to a steady turn.

Some calculations, based on lifting-line theory, have been made to determine the effect of turning and asymmetric loading on the induced drag. The induced drag in a turn was found to be always greater than that in straight flight at the same lift coefficient. For a given turn radius, the induced drag increment is a minimum when the center of gravity is halfway between the centerline and the location requiring zero aileron deflection for trim. In any case, however, the increment of induced drag is very small, usually less than two percent of the induced drag in straight flight at the same lift coefficient.

For the conditions investigated, which are typical of those of a high-performance soaring glider, the induced drag increments associated with turning are negligible compared with the profile-drag increment caused by flow separation on the downward-deflected aileron. For minimum drag, therefore, the center of gravity should be moved outboard to the point required to reduce the aileron deflection for trim to a value below that at which flow separation occurs.

References

1. Lamb, Horace: Hydrodynamics. Sixth Edition, pp. 221-222, Dover Publications, N.Y.

2. Morita, Kuninobu: Lifting Line Theory of a Wing in Uniform Shear Flow. JSME Bulletin, vol. 14, June 1971, pp. 550-558.

3. Von Kármán, Th.; and Tsien, H. S.: Lifting-Line Theory for a Wing in Non-Uniform Flow. Quarterly Applied Mathematics, vol. 3, no. 1 (1945), p. 1.

4. Glauert, H.: The Elements of Aerofoil and Airscrew Theory. Cambridge University Press, Second Edition, 1948, Chapter XI, pp. 137-155.

5. Durand, W. F.: Aerodynamic Theory. vol. V, div. N III, sect. 18, p. 70.

6. Althaus, D.: Windkanalmessungen an Profilen mit Klappen bei mittleren Reynoldszahlen. Aero-Revue, November 19, 1970, pp. 669-670.

7. Pearson, H. A.; and Jones, R. T.: Theoretical Stability and Control Characteristics of Wings with Various Amounts of Taper and Twist. NACA Report No. 635, 1938.

APPENDIX

Evaluation of the integral

$$\int_o^{\pi} A_n \sin n\theta \sin \theta \cos^2\theta \, d\theta$$

$$= \int_o^{\pi} A_n \sin n\theta \sin \theta \left(\frac{1 + \cos 2\theta}{2}\right) d\theta$$

$$= \int_o^{\pi} \frac{A_n}{2} \sin n \sin \theta \, d\theta + \int_o^{\pi} \frac{A_n}{2} \sin n\theta \sin \theta \cos 2\theta \, d\theta$$

make the substitution

$$\sin \theta \cos 2\theta = \frac{\sin 3\theta}{2} - \frac{\sin \theta}{2}$$

The integrals become

$$\int_o^{\pi} \frac{A_n}{2} \sin n\theta \sin \theta \, d\theta + \int_o^{\pi} \frac{A_n}{4} \sin n\theta \sin 3\theta \, d\theta$$

$$- \int_o^{\pi} \frac{A_n}{4} \sin n\theta \sin \theta \, d\theta$$

$$= \frac{A_1}{2} \int_o^{\pi} \sin^2\theta \, d\theta + \frac{A_3}{4} \int_o^{\pi} \sin^2 3\theta \, d\theta - \frac{A_1}{4} \int_o^{\pi} \sin^2\theta \, d\theta$$

$$= \pi\left(\frac{A_1}{4} + \frac{A_3}{8} - \frac{A_1}{8}\right) = \pi\left(\frac{A_1}{8} + \frac{A_3}{8}\right)$$

AN INTRODUCTION TO GEOMETRIC PROGRAMMING AND ITS APPLICATION TO SAILPLANE DESIGN

by

John H. McMasters
Tempe, Arizona

Notation

AR	Geometric Aspect Ratio = b^2/S
b	Wing Span
BHP	Brake Horsepower
$\bar{c}$	Wing Mean Chord = S/b
C_D	Total Drag Coefficient $C_D = C_{D_\pi} + C_{D_p} + C_{D_i} + C_{D_t}$
C_{D_π}	Parasite Drag Coefficient of the Aircraft Components Excluding the Wing
C_{D_p}	Profile Drag (Parasite Drag of the Wing Alone)
C_{D_i}	Induced Drag $C_{D_i} = K_W C_L^2/\pi AR$
C_{D_t}	Trim Drag Coefficient
C_{D_o}	"Zero Lift" Drag Coefficient
C_L	Lift Coefficient
$d(\underline{w})$	Dual Objective Function
D	Drag Force $D = C_D qS$
K_W	Span Efficiency Factor (Wing Alone)
K	"Oswald" or "Airplane" Efficiency Factor
L	Lift Force $L = C_L qS$
q	Dynamic Pressure $q = \frac{1}{2}\rho V^2$
R	Turn Radius
$\bar{R}_n$	Mean Reynolds Number $\bar{R}_n = \frac{V\bar{c}}{\nu}$
S	Wing Area
S_π	Parasite Drag Reference Area
T	Thrust Force
V	Speed (Measured Along the Flight Path)
W	Vehicle Weight
$\underline{w}$	Dual Variables in the Geometric Program
$\underline{x}$	Design Variables
$\dot{h}$	Vertical Velocity (climb or sink rate)

Greek Letters

η	Propulsive Efficiency
θ	Climb (Glide) Angle
ν	Kinematic Viscosity
ρ	Air Density
σ	Signum Muliplier $\sigma = \pm 1$
$\Phi(\underline{x})$	Objective Function
ϕ	Bank Angle

Notation (cont.)

Additional Symbols

$( )^*$	Denotes an optimum value
$( )^o$	Denotes a stationary points (points at which all $\partial\Phi/\partial X_i = 0$)
$(\underline{\ })$	Denotes a vector, e.g., $\underline{X} = (X_1, X_2, \ldots, X_n)$
$\prod$	Product
$\sum_{n}^{n}$	Summation

PART I: AN INTRODUCTION TO GEOMETRIC PROGRAMMING

Features

Geometric programming is a relatively new non-linear optimization technique initially derived from certain inequalities rather than classical calculus. Important features of the method are:

1. The method is often computationally convenient. A problem may be reduced from one of solving (when classical techniques are used) $\underline{m}$ non-linear equations for $\underline{m}$ unknowns (the optimum design variables), to solving $m + 1$ linear equations in $m + 1$ new variables which may have important physical significance in their own right. Once the optimum values of these new (dual) variables are determined, the optimum design variables can be easily determined by routine calculations. In many cases it is unnecessary to resort to the use of a computer.

2. In a problem with constraints (which may be non-linear), the constraints are reduced to linear form and inequality constraints are handled quite naturally.

3. The optimal solutions obtained by the method often reveal important invariance properties which are independent of economic or technological state-of-the-art factors in the problem. This is a unique and important feature of the method and can give the designer substantially greater insight into a given problem than is possible when it is simply "fed into a computer".

4. The major restriction on the method is that the objective function and any constraints must be in the specific form of polynomials, the terms of which are made up of products of the design variables raised to arbitrary real exponents. In addition, the total number of terms in the objective function and the constraints must exceed the number of design variables by *at least* one.

5. It is the nature of the method that it attempts to establish the *minimum* value of the objective function. In the restricted case where all the terms in the objective function and constraints are positive, and the constraint inequalities

are of the correct sense (i.e., ≤ 1), the method guarantees the establishment of a global minimum.

The simplest way to present the method and to illustrate the features described above, is to chronicle its relatively brief history. The general method will then be summarized. Application of the method to several classical sailplane design problems will be demonstrated in Part II of the paper.

Historical development

Geometric programming was discovered in 1961 by Clarence Zener at Westinghouse. Zener [1] noted that the sum of the component "costs" of a process can sometimes be minimized almost by inspection, provided each "cost" is a function of the product of the "design" variables each raised to arbitrary (but known) real exponents. The *exponents* are not restricted to positive integers, and may be any real number, either positive or negative. At this stage in development of the method it was necessary that the *coefficient* of each term in the summation by positive. Zener and his colleagues [2] coined the word *posynomial* to describe these "positive polynomial" functions. For example:

$$\Phi(\underline{X}) = 2X_1^2X_2^{-1} + 4X_2^3X_3^{1/2} + X_1^{-2}X_2X_3^{-1/2} + 2X_2^{-3} \text{ is a posynomial.} \quad (1)$$

$$\Phi(\underline{X}) = X_1^2X_2^{-1} - 28X_1^{-1}X_2^2 + 6X_2^{-3} \text{ is } \textit{not} \text{ a posynomial.} \quad (2)$$

One's immediate instinct when confronted with an objective function like eqn. (1) is to regard the X_i as the independent variables, the optimum values of which may be established by the solution of the set on N non-linear equations $\partial\Phi/\partial X_i = 0$, $i = 1...N$. Zener, however, pointed out that one could with equal justification regard each *term* in the objective function as an independent variable and seek instead to establish the optimal contribution of each term to the total minimum sum. Once the minimum value of the objective function was established in this way, and if the value was acceptably low, *then* the optimum values of the X_i could be determined. This latter operation requires relatively uncomplicated calculations.

Zener's procedure involved forming a *dual* function of the original *primal* objective function. This dual function was constructed by dividing each term in the primal function by a weight (the dual variables) and then raising each of these modified terms to the power given by its weight. Each of these new terms multiplied together formed the dual function. As an example, the dual † of eqn. (1) is

†In the terminology of the method, eqn. (3) is actually the *pre-dual* of eqn. (1) because it contains the X_i explicity.

$$d(\underline{w}) = \left[\frac{2\chi_1^2\chi_2^{-1}}{w_1}\right]^{w1} \cdot \left[\frac{4\chi_2^3\chi_3^{\frac{1}{2}}}{w_2}\right]^{w2} \cdot \left[\frac{\chi_1^{-2}\chi_2\chi_3^{-\frac{1}{2}}}{w_3}\right]^{w3} \cdot \left[\frac{2\chi_2^{-3}}{w_4}\right]^{w4} \qquad (3)$$

$\underline{w} = w_i = w_1, \ldots, w_4$ = dual variables (weights)

The weights were chosen such that: (1) the dual function was "non-dimensionalized" with respect to the χ_i (primal design variables) and (2) the sum of the w_i equaled unity. This latter is the *normality condition* and the former requirements yield, formally, a set of *orthogonality conditions*.

When the values of the weights which satisfy the normality and orthogonality conditions were substituted into the dual equation, a pure number resulted (because of the non-dimensionalizing process). Zener noted the apparently remarkable fact that this number was the *minimum* value of the primal objective function. To clarify the procedure, consider the primal function given by eqn. (1) and its dual function, eqn. (3). To eliminate that χ_i from eqn. (3), values of the w_i must be found which satisfy:

$$\left.\begin{aligned} 2w_1 - 2w_3 &= 0 \\ -w_1 + 3w_2 + w_3 - 3w_4 &= 0 \\ \tfrac{1}{2}w_2 - \tfrac{1}{2}w_3 &= 0 \end{aligned}\right\} \quad \text{orthogonality conditions} \qquad (4)$$

$$w_1 + w_2 + w_3 + w_4 = 1 \qquad \text{normality condition.} \qquad (5)$$

Simple inspection of this system of linear algebraic equations shows that the solution is:

$$w_1^* = w_2^* = w_3^* = w_4^* = \tfrac{1}{4} \qquad (6)$$

When these values are substituted into eqn. (3), the result is:

$$d^* = \Phi^* = \left(\frac{2}{\frac{1}{4}}\right)^{\frac{1}{4}} \cdot \left(\frac{4}{\frac{1}{4}}\right)^{\frac{1}{4}} \cdot \left(\frac{1}{\frac{1}{4}}\right)^{\frac{1}{4}} \cdot \left(\frac{2}{\frac{1}{4}}\right)^{\frac{1}{4}} = 8 \qquad (7)$$

Now, if the value of Φ^* obtained in eqn. (7) is acceptable, the optimum values of the primal variables can be extracted from the following relations:

$$\begin{aligned} 2\chi_1^2\chi_2^{-1} &= w_1^*\Phi^* & \qquad \chi_1^{-2}\chi_2\chi_3^{-\frac{1}{2}} &= w_3^*\Phi^* \\ 4\chi_2^3\chi_3^{\frac{1}{2}} &= w_2^*\Phi^* & \qquad 2\chi_2^{-3} &= w_4^*\Phi^* \end{aligned} \qquad (8)$$

These formulas (with w_i^* and Φ^* known) give:

$$\chi_1^* = 1 \qquad \chi_2^* = 1 \qquad \chi_3^* = \frac{1}{4} \tag{9}$$

Two factors in the above procedure are important:

1. The dual variables w_i, in addition to being computationally convenient, have considerable physical significance in their own right. The values of the w_i^* obtained from eqns. (4) and (5) measure the relative importance (or weight) of each term in Φ^*. Thus, in this example, at the optimum value of Φ each term in eqn. (1) is exactly $\frac{1}{4}$ of the total. In addition, regardless of the values of the numerical coefficients of the terms in eqn. (1), if the values of the exponents do not change, the optimum weight of each term does not change-only the value of Φ^* would be altered, according to eqn. (3).

2. In the initial work by Zener, only objective functions with exactly one more term (T) than the number (N) of primal design variables could be handled (i.e., T = N + 1). Under these circumstances there are always N + 1 dual variables w_i, and exactly N orthogonality conditions plus the normality condition which result in N + 1 linear algebraic equations for the N + 1 w_i^*. Thus, in this case, the w_i^* values can be uniquely determined. Such a geometric program is said to have *zero degrees of difficulty*. The case where T > N + 1 is of great computational significance and will be discussed later.

Contemporaneously with Zener, Richard Duffin at Carnegie Tech. had been developing a duality theory with applications to non-linear programming and when he learned of Zener's work, was immediately able to make two important contributions. Duffin observed that if the primal objective function (in posynomial form) was considered a *weighted arithmetic mean*, and the dual function a corresponding *weighted geometric mean*, then Cauchy's inequality [3] stated that the geometric mean is always less than or equal to the arithmetic mean. The simplest example of this relation is:

$$\overline{U}_{arith} = \frac{1}{2} U_1 + \frac{1}{2} U_2 \geq U_1^{\frac{1}{2}} \cdot U_2^{\frac{1}{2}} = \overline{U}_{geo} \tag{10}$$

where, U_1 and U_2 are *positive* numbers or functions.

The equality in eqn. (10) holds if and only if $U_1 = U_2$. In general, it can be shown [Ref. 2] that: Given the set of *positive* numbers or functions U_n and a set of *positive* weights w_n, then:

$$\overline{U}_a = w_1 U_1 + \ldots + w_n U_n \quad \text{weighted arithmetic mean.}$$

$$\overline{U}_g = U_1^{w_1} \cdot U_2^{w_2} \ldots\ldots U_n^{w_n} \quad \text{weighted geometric mean.} \tag{11}$$

$$\overline{U}_a \geq \overline{U}_g \quad \text{where the equality holds if all the } U_n \text{ are equal.}$$

Defining a set of new quantities $u_n = w_n u_n$, eqn. (11) becomes:

$$u_1 + u_2 + \ldots + u_n \geq \left(\frac{u_1}{w_1}\right)^{w_1} \cdot \left(\frac{u_2}{w_2}\right)^{w_2} \ldots \left(\frac{u_n}{w_n}\right)^{w_n} \qquad (12)$$

It is readily seen that equations (1) and (3) are in exactly the same form as the left and right hand sides of the inequality (12).†

Duffin's recognition of the connection between Zener's procedure and the geometric inequality allowed him to show formally that the problem of *minimizing* a posynomial primal objective function $\Phi(\underline{X})$ could be transformed to one of *maximizing* its *dual* function $d(\underline{w})$ with respect to its weights (the dual variables). Duffin could further show that, in fact, the maximum of the dual was exactly equal to minimum of the primal function (if a minimum existed), and that the normality and orthogonality conditions were necessary and sufficient conditions to establish the maximizing values of the w_i. The formal proof of these ascertions can be found in Ref. 2. A simpler proof, based on classical differential techniques and establishing only the necessity of the conditions, can be found in Ref. 4.

Duffin's second contribution to Zener's basic procedure was to show how to extend the method to objective functions where the number of terms in the primal function exceeded the number of design variable by more than one (i.e., problems with one or more degrees of difficulty). This procedure will be demonstrated by example later.

Although, as a consequence of Duffin's initial work, the basic method now rested on firm theoretical ground, it remained for Charnes and Cooper [5] and Duffin and his student Peterson [6] to raise the method to the status of viable optimization technique by showing how to handle *inequality constraints* in the form of posynomials less than, or equal to, unity. All of this work, together with rigorous proofs and many examples and transformations for expressing practical optimization problems in proper posynomial form can be found in the book by Duffin, Peterson and Zener [2].

In order to extend the applicability of the geometric programming technique to more general problems, two difficulties arising as consequence of reliance on Cauchy's inequality had to be circumvented:

†Duffin, et al. [2] call the inequalities (11) and (12) *geometric inequalities* for brevity. The use of the geometric inequality and vector concepts like orthogonality and normality led Duffin to name the overall procedure *geometric programming*.

1. the restriction to positive coefficients in the objective function and constraints (i.e., they must be posynomials) and
2. the inability of the basic method to handle *arbitrary* inequality constraints.

Wilde and Passy [7,8] were able to divorce the method from the restrictions imposed by Cauchy's inequality by appealing to classical optimization theory; specifically, by the substitution of Lagrange multipliers for the weights and employment of "Signum multipliers" ($\sigma = \pm 1$) to deal with the problem of negative coefficients. A full discussion of these extensions can be found in the book by Wilde and Beightler [9].

Generalized (or extended) geometric programming is now applicable to any well posed optimization problem (i.e., one in which a minimum value of the objective function exists) *provided*:

1. the primal objective function and any constraints are in the form of *polynomials* (negative coefficients allowed),
2. the constraints are in the form of *arbitrary* inequalities ($\gtrless 1$), and
3. the total number of terms in the objective function and constraint inequalities exceeds the number of primal design variables ($\underline{X}$) by at least one (i.e., $T \geq N + 1$).

Unfortunately, the generalization of the basic technique is not obtained without a penalty. Any deviation from the full, *posynomial* situation (in either the objective function or the constraints) invalidates the geometric inequality and one is no longer guaranteed that the "optimal" weights obtained from the orthogonality and normality conditions correspond to even a *local* minimum of the objective function. All that can be said is that the "optimal" weights occur at a *stationary* point, which may be a minimum, a saddle point or even a maximum. Thus in a problem with mixed signs and/or arbitrary inequality constraints the solution must be carefully checked by appropriate tests (9, 10) to assure that the values obtained represent what is sought. Despite these problems, the general procedure preserves many of the advantageous features of the restricted method, and if proper care is taken, has the potential of providing a very powerful tool in engineering design.

Generalized geometric programming

Given a set of generalized polynomials of the form:

$$\Phi_m(\underline{X}) = \sum_{t=1}^{T_m} \sigma_{mt} C_{mt} \prod_{n=1}^{N} X_n^{a_{mtn}} \qquad (13)$$

where $m = 0, 1, \ldots M$ eqn. number

$t = 1, \ldots\ldots, T_m$ term number

$$T = \sum_{m=0}^{M} T_m$$

such that

$$\sigma_{mt} = \pm 1 \quad \text{(signum multipliers)} \tag{14}$$

$$C_{mt} > 0 \tag{15}$$

$$X_n > 0 \quad \text{(design variables)} \tag{16}$$

$$n = 1, \ldots, N$$

The basic optimization problem is to *minimize* the *primal* objective function $\Phi_o(\underline{X})$ subject to the M constraints:

$$\Phi_m(\underline{X}) \leq \sigma_m \ (= \pm 1) \qquad m = 1, \ldots, M \tag{17}$$

Note: The sense of the inequality (17) is important. $\Phi_m \leq +1$ means $\sigma_m = +1$ and $\Phi_m \leq -1$ means $\sigma_m = -1$.

The corresponding dual problem is to *maximize* the *dual objective function* $d(\underline{w})$ in terms of the T *dual variables* $\underline{w}$. The dual objective function is:

$$d(\underline{w}) = \sigma \left[\prod_{m=0}^{M} \prod_{t=1}^{T_m} \left(\frac{C_{mt}\, w_{mo}}{w_{mt}} \right)^{\sigma_{mt} w_{mt}} \right]^{\sigma} \tag{18}$$

where $\max d(\underline{w}) = d(\underline{w}^o) = \Phi_o(\underline{X}^o) =$ a stationary point.

and $d(\underline{w}^*) = \Phi_o(X^*) =$ a minimum, if it exists.

The dual variables (weights) $\underline{w}^o$ must satisfy:

normality condition:
$$\sum_{t=1}^{T_o} \sigma_{ot} w_{ot} = \sigma \ (= \pm 1) \tag{19}$$

N *orthogonality conditions:*
$$\sum_{m=o}^{M} \sum_{t=1}^{T_m} \sigma_{mt}\, a_{mtn}\, w_{mt} = 0 \tag{20}$$

T *non-negativity conditions:* $w_{mt} \geq 0$ (21)

M *inequality constraints:*
$$w_{mo} = \sigma_m \sum_{t=1}^{T_m} \sigma_{mt}\, w_{mt} \tag{22}$$

$$m = 1, \ldots, M$$

By convention, we formally select:

$$w_{oo} = 1 \tag{23}$$

and define:

$$\lim_{w_{mt} \to o} \left[\frac{C_{mt}\, w_{om}}{w_{mt}} \right]^{\sigma_{mt}\, w_{mt}} \equiv 1 \tag{24}$$

By definition:

$$\sigma \doteq \pm 1 \tag{25}$$

(the value to be determined by eqns. (18) and (21)

When the dual variables $\underline{w}$ and the corresponding $\underline{\sigma}$ are found from eqns. (19)-(25), and the value of $d(\underline{w}^o) = \Phi_o(\underline{\chi}^o)$ established from eqn. (18), the optimum values of the primal (design) variables $\underline{\chi}^o$ can be determined from the relations:

$$C_{ot} \prod_{n=1}^{N} x_n^{a_{mtn}} = w_{ot}\, \sigma \Phi_o(\underline{\chi}^o) \qquad m = 0,\ t = 1, \ldots, T_o \tag{26}$$

$$C_{mt} \prod_{n=1}^{N} x_m^{a_{mtn}} = w_{mt}/w_{mo} \qquad \begin{matrix} t = 1, \ldots, T_m \\ m = 1, \ldots, M \end{matrix} \tag{27}$$

Comment: The value of the quantity T - (N+1) is the number of *degrees of difficulty* of the program. If the problem has *zero* degrees of difficulty (i.e., T = N+1) then eqns. (19)-(25) are necessary and sufficient to uniquely define the required $\underline{w}^o$ and $\underline{\sigma}$. If T > N+1, the additional conditions must be generated from the condition that max $d(\underline{w}) = \Phi_o(\underline{\chi}^o)$ in order to completely define the $\underline{w}^o$ and $\underline{\sigma}$ values.

Concluding comments

Geometric programming, when it works, yields elegant and often insightful solutions to optimization problems which would be difficult and/or laborious to solve by classical techniques. However, when the *generalized* method is applied to problems with objective functions/constraints with mixed signs, great care must be taken to assure that the solution obtained is actually a minimum. This factor plus the degree of difficulty problem, and the fact that only objective functions and constraints in the form of polynomials can be handled, would tend to indicate that geometric programming is of very limited value and applicability.

It should be noted, however, that most existing non-linear programming techniques suffer from the same problems of eratic behavior demonstrated by generalized geometric programming. This is simply a fact to be forewarned against and requires that any solution obtained must be carefully analyzed before relying on it. The degree of difficulty

problem can be partially circumvented if care and ingenuity are exercised in formulating the mathematical model to which the technique is to be applied. It is frequently possible by judicious choice of design variables and simplifying assumptions, to formulate a complex physical problem into a model with no more than one or two degrees of difficulty. A sort of rule of thumb has it that: If the number of degrees of difficulty is equal to or exceeds the number of design variables, it is usually wiser to resort to some other method of solution (e.g., multi-variable search techniques).

Finally, regarding the limitations on applicability imposed by the requirement that the objective function and constraints be in the form of polynomials, one need only reflect on the number of engineering problems involving

1. a summation of forces,
2. the use of linear super-position in the expression of quantities like total drag coefficients, and
3. the very wide-spread use of logarithmic graphs and curve fits to deal with statistical data on complex phenomena and systems.

Geometric programming is a potentially powerful tool in the hands of an intelligent designer, but unfortunately much of his potential has yet to be realized. This is due in part to the fact that the method is new and not yet well known to many engineers. The majority of applications to date have been in the fields of electrical [2,11] and chemical [12,13] engineering. Two interesting applications to tool design have also been published [14,15], but so far the author knows of no applications to aeronautical design problems.

PART II. THE APPLICATION OF GEOMETRIC PROGRAMMING TO SAILPLANE DESIGN

Introduction

Modern high-performance sailplanes have reached an extraordinary state of development, particularly during the last decade. To increase sailplane performance beyond present limits will require ever increasingly sophisticated and complex designs (e.g., the Sigma). As a consequence it appears that the days when a designer, armed only with imagination and a slide-rule, could produce a viable competition machine by ingenious cut-and-try techniques are past. Fortunately, the same period which has seen the rapid increase in sailplane performance has also witnessed spectacular advances in computer technology which could, in principle, give the designer the increased analytical capability required to produce even more advanced vehicles. Computers are, however, soulless devices and, at least at present, clumsy and expensive to use. If the designer is not working on a well-funded project and does not have ready access to the equipment, his use of computer facilities must often be severely limited.

Geometric programming has the potential of providing the designer with a powerful tool for the solution of optimalization problems in which the objective function and constraints are in the form of generalized polynomials. Solutions of this sort can often be obtained without recourse to a computer. The purpose of this part of the paper is to show how geometric programming can be applied to aeronautical engineering design problems, at least for purposes of making preliminary design and performance estimates.

Mathematical models

Application of a paricular programming technique is only the final third of any optimization problem. Before one can "optimize" anything, appropriate indices of system cost and/or performance must be selected. As a second step, these performance indices must be expressed in quantitative form, together with any constraints, as functions of the desired design variables. When this has been done, one has an objective function/constraint system or *mathematical model* to which a particular optimization technique can be applied.

Index of performance

In the design of sailplanes and related types of aircraft (e.g., motor-gliders, man-powered aircraft) there are several obvious performance indices which could be used as the basis for optimizing a given design. Among these are:

1. maximize the lift-to-drag ratio (minimize the glide angle),
2. minimize the sink rate in rectilinear or circling flight,
3. maximize the cross-country speed.

In the powered sailplane or man-powered aircraft design problem one may also wish to:

1. minimize the power required for level flight,
2. maximize the rate of climb for a given installed power,
3. minimize the take-off distance.

Several other less obvious performance indices could be constructed or several of those listed could be combined into a single model. For example, the designer might decide to maximize the glide angle subject to the constraint that the corresponding sink rate be less than or equal to some specified minimum. The particular problem formulation will depend on the intended purpose of the machine and the bias of the designer.

Basic equations

For reference purposes, the forces (in somewhat simplified form) acting on an aircraft executing a steady, constant radius, climing (or gliding) turn are shown in Figure 1. Summation of these forces in the vertical, horizontal and radial directions yield, respectively:

$$L \equiv \frac{1}{2} \rho V^2 C_L S = \frac{W \cos \theta}{\cos \phi} \tag{28}$$

$$T - D = W \sin \theta \quad \text{where } \theta \text{ is positive for a climb.} \tag{29}$$

$$R = \frac{V^2}{g \tan \phi \cos \theta} \tag{30}$$

In addition we can write:

$$\frac{\dot{z}}{V} = \sin \theta \quad \text{where } \dot{z} \text{ is positive for climb.} \tag{31}$$

and (in the English system of units):

$$BHP \equiv \frac{TV}{550\ \eta} = \frac{WV \cos \theta}{550\ \eta (L/D) \cos \phi} \cdot \left[1 + \left(\frac{L}{D}\right) \cos \phi \tan \theta\right] \tag{32}$$

In the restricted case where the flight path is a straight line, $\phi = 0$. In addition, if we assume that θ is a sufficiently small angle (implying in the case of a glider

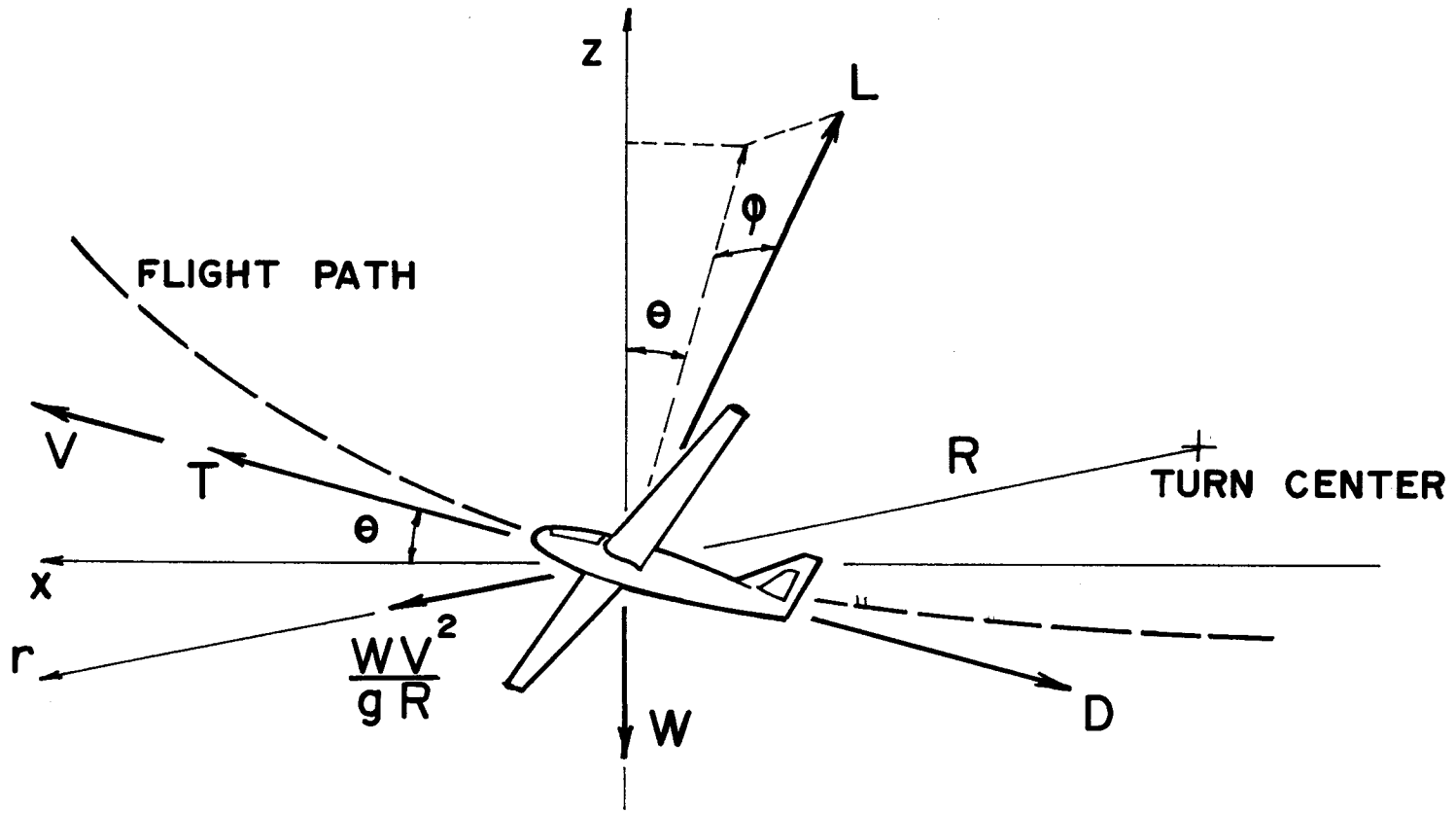


FIGURE 1. FORCES ON AN AIRCRAFT IN A CLIMBING TURN

that L/D is large), then sin θ = tan $\theta \simeq \theta$ and cos $\simeq 1$. Eqns. (28)-(32) then become:

$$L \simeq W \tag{33}$$

$$\dot{\gamma} \simeq V\theta \qquad \text{and} \quad |\dot{\gamma}| \simeq \frac{V}{L/D} \text{ when } T = 0 \tag{34}$$

$$BHP \simeq \frac{WV}{550\ \eta(L/D)} \cdot \left[1 + \frac{L}{D}\,\theta\right] \tag{35}$$

Objective function formulation

Considerable care must be taken in the formulation of the optimization problems to be discussed here, to distinguish between *performance* problems and *design* problems. In a performance problem, it is assumed that the main physical characteristics of the aircraft (e.g., weight, size, shape) are known. The only "configuration" variables in the problem are items such as throttle setting, control surface deflections and flap setting. The problem in this case is to find the values of any of these configuration variables and the performance variables (e.g., speed, altitude, bank angle) which optimize the selected performance index, subject to any constraints on the system.

In the *design* problem, the physical characteristics (e.g., size, shape factors) which optimize a given performance index subject to a set of constraints on desired performance, are sought. This class of problems can be viewed as the inverse of the performance problem.

The distinction between design and performance problems is important (as will be demonstrated later), but may in many cases be rather subtle. Many textbooks on applied aerodynamics and airplane design tend to obscure the difference by treating design by a parametric approach. In this method, the physical characteristics of the proposed aircraft are estimated (and thus become fixed) and the appropriate performance calculations are carried out. By an iteration process which may come perilously close to "exhaustive enumeration", one attempts to find the values of the physical parameters which best satisfy the mission specification. This process may be adequate in many cases (particularly if the designer has access to a computer) but, at best it is inefficient and success depends to a large extent on the experience and judgement of the particular designer.

With the advent of modern computers and the concomitant development of sophisticated methods of numerical analysis, (e.g., gradient search techniques) it has become possible to solve directly for the optimum values of the variables in a complex design problem, provided the mathematical model is carefully formulated. The distinction between design and performance problems, and the necessity for careful formulation of the mathematical model may become clearer if one

considers the required expressions for total aircraft drag coefficient.

It has become customary in first order aerodynamic theory to specify the drag coefficient of a complete aircraft in the simple parabolic form:

$$C_D = C_{D_o} + \frac{KC_L^2}{\pi AR} \qquad \text{where } D = C_D qS \tag{36}$$

The simple form of eqn. (36) is justified by computational expedience, and its analogy to the theoretically justifiable expression for the drag coefficient of a wing alone:

$$C_D = C_{D_p} + \frac{K_w C_L^2}{\pi AR} \tag{37}$$

The use of eqn. (36) may be quite adequate for may preliminary design purposes, but the novice designer frequently fails to realize that it is really only a simple curve fit, valid over a limited range of lift coefficient (C_L) values. To extend the range of applicability of this sort of expression, a more general polynomial would be required which includes both first and higher (than quadratic) order functions of C_L.

A second difficulty with the use of eqn. (36) is the problem of accurately estimating the curve fitting parameter K for a new design, and more importantly, differentiating between the factor K and the theoretically derivable span efficiency factor for a wing alone, K_w. Goodhart [16] has clearly shown the difference between K and K_w, and proposed the following relationship between the two:

$$K = K_o AR + K_w \tag{38}$$

where K_o accounts for variations in parasite and profile drag coefficients with lift coefficient, which are independent of aspect ratio.

A final "error" often committed when using eqn. (36) is to assume a constant value of C_{D_o}. It is well known that quantities like airfoil profile drag may vary radically over certain ranges of a number of scale factors (e.g., Reynolds number, Mach number). The assumption of constant C_{D_o} may be legitimate in some cases, but care must be taken in the Reynolds number range in which many sailplanes operate. This factor is well demonstrated in several articles by Wortmann [17,18]. The crux of Wortmann's demonstration is that: if one has an aircraft of fixed (and known) weight and geometry operating in a low Reynolds number range in steady (V = = constant), level flight, the lift must equal the weight for any particular value of lift coefficient. Now, since the weight, altitude and wing area are all fixed, according to eqn. (28), each value of C_L must correspond to a different (constant) value of speed. If one has curves showing the variations in drag with both C_L and R_n, a composite drag

polar diagram can be constructed for the aircraft over its operating C_L range, by employing the relations:

$$\bar{R}_n = \frac{V\bar{c}}{\nu} = \left(\frac{\bar{c}}{\nu}\right)\left[\frac{2W}{\rho S}\right]^{\frac{1}{2}} \cdot C_L^{-1} = C/C_L \qquad (39)$$

where C is a "constant" function of vehicle weight and flight altitude. Thus one can, in general, construct an envelope of polar curves (with different values of C_{D_o}) covering the anticipated range of operating weights and altitude. Such a set of polars would be appropriate for the *performance* problem discussed above. It can also be seen (Fig. 2) that a parabolic fit of these polars would imply that the factor K in eqn. (36) is also an indirect function of Reynolds number.

Matters become more complicated when one tries to construct "correct"polars for a *design* problem. In this case, none of the geometric characteristics of the aircraft are known beforehand. The general expression for the drag polar should, therefore, include at least the following terms:

$$C_D = \frac{C_{D_\pi} S_\pi}{S} + C_{D_p}(\bar{R}_n, C_L) + \frac{K_w C_L^2}{\pi AR} + C_{D_t} \qquad (40)$$

where $C_{D_\pi} S_\pi = \sum_i C_{D_{\pi_i}} S_{\pi_i}$ + interference effects

is the sum of the parasite drag contributions of each of the aircraft components excluding the wing [See Ref. 19]. Because, in the general design problem, the angle of incidence is free, C_{D_π} is assumed independent of C_L. For simplicity C_{D_π} is also assumed independent of R_n. C_{D_t} is the trim drag coefficient which is made up of both parasite and induced drag contributions [See Ref. 20]. For preliminary design purposes, it is customary to estimate an average constant value for C_{D_t} and add this into the parasite drag term. With this approximation and using eqn. (38), a set of preliminary design polars can be constructed on the basis of:

$$C_D = \frac{C_{D_\pi} S_\pi}{S} + C_{D_p}(\bar{R}_n) + (K_o AR + K_w)\frac{C_L^2}{\pi AR} \qquad (41)$$

It can be seen that in the case where $\bar{R}_n$, S and AR are known, eqn. (41) can be reduced to the form of eqn. (36).

To complete the objective function formulations for the design problem, it remains to express the vehicle weight as a function of the size variables. Many such functions have been proposed for sailplane weight estimation based on statical data for existing machines. Among the more credible of these are the analyses by Wilkinson [21], Cone [22], Morelli [23] and Stender [24]. All of these analyses result in expressions in the form of polynomials made up of terms involving the geometric size variables (e.g., S, b, AR) raised to various exponents. For purposes of this paper, a simple weight statement based on formulas used by Stender [24] is proposed. For aircraft like sailplanes, which have

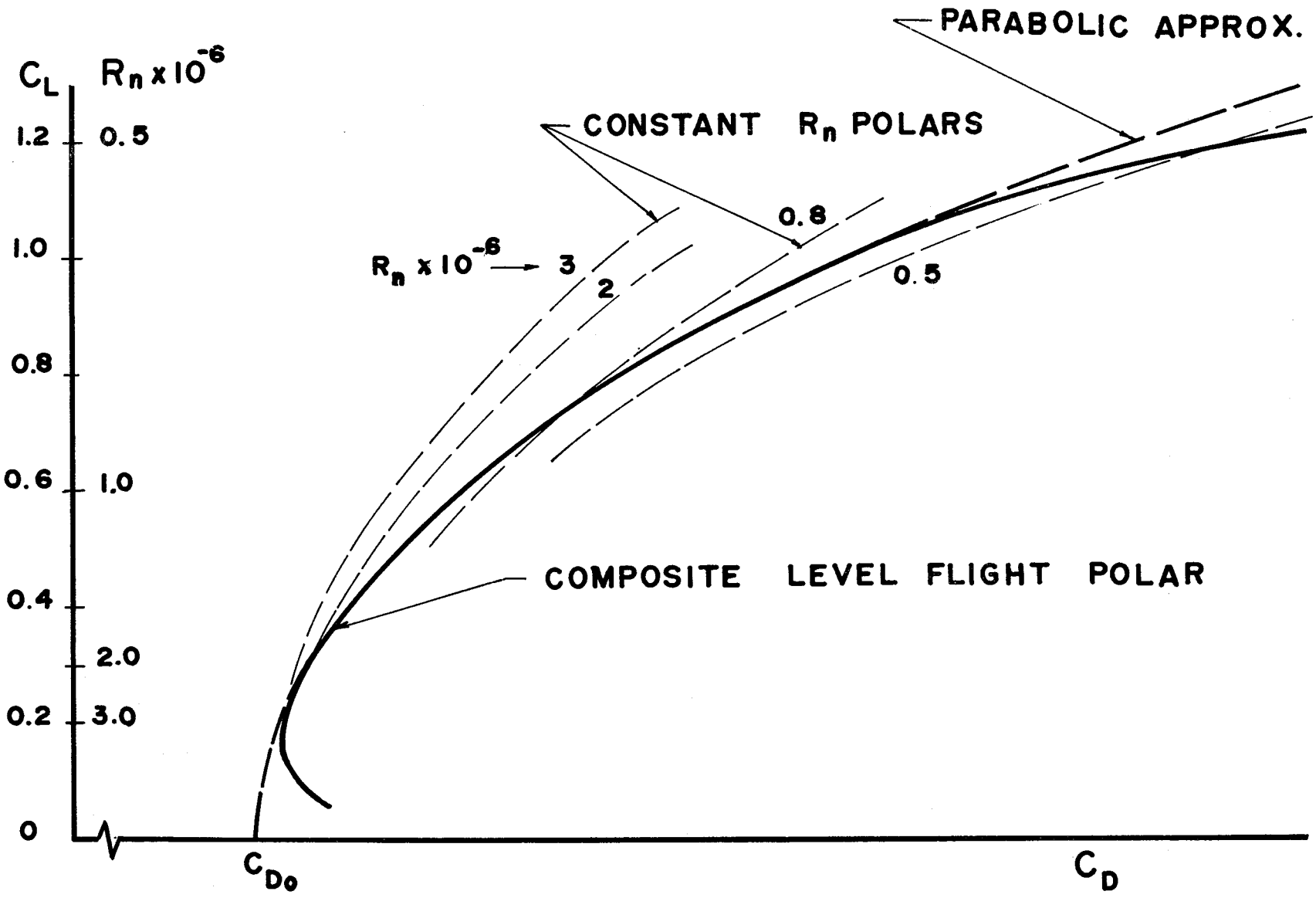


FIGURE 2. TYPICAL TOTAL DRAG POLAR

a fixed weight, assume:

$$W = U + W_E = U + W_o + C_E\, b^p\, S^q \tag{42}$$

where W is the total weight of machine, U is the disposal load (i.e., pilot, ballast, etc.) and W_E is the empty weight. C_E, p and q are constants to be determined by proper fitting of appropriate statistical data.

Some simple examples

Example I

The simplest possible *performance* problem may be formulated as follows: Given a sailplane of known geometry and weight, flying at a specified altitude. At what speed should the aircraft fly in order to *minimize* the glide angle?

From eqn. (29), with the substitution of eqn. (28) and eqn. (36), the mathematical statement of the problem is:

$$\text{Minimize} \quad \Phi(V) = \theta \simeq D/L = C_1 V^2 + C_2 V^{-2} \tag{43}$$

$$\text{where:} \quad C_1 = \frac{\rho}{2W} C_{D_o} S$$

$$C_2 = \frac{2W}{\pi \rho b^2} K \quad \text{where } K = K_o \frac{b^2}{S} + K_w$$

If no constraints are placed on eqn. (43), we have a simple *posynomial* with two terms and only one design variable, thus the problem has *zero degrees of difficulty*. This problem can be solved by inspection by employing Zener's original technique [1]. To show this, construct the *pre-dual* function of eqn. (43).

$$d(\underline{w},V) = \left(\frac{C_1 V^2}{w_1}\right)^{w_1} \cdot \left(\frac{C_2 V^{-2}}{w_2}\right)^{w_2} \tag{44}$$

According to Zener, eqn. (44) is stationary with respect to $\underline{w}$, when it has been non-dimensionalized with respect to V. Further the value of $d(\underline{w}^*)$ is equal to the minimum value of $\Phi(V)$. It can be seen that the unique values of w_1 and w_2 (subject to the normality condition that $w_1 + w_2 = 1$) which remove V from eqn. (44) are:

$$w_1^* = w_2^* = \frac{1}{2} \tag{45}$$

and, following Zener:

$$d(\underline{w}^*) = \Phi(V^*) = \theta_{min} = \left(\frac{C_1}{\frac{1}{2}}\right)^{\frac{1}{2}} \cdot \left(\frac{C_2}{\frac{1}{2}}\right)^{\frac{1}{2}} = 2\left[\frac{C_{D_o} KS}{\pi b^2}\right]^{\frac{1}{2}} \tag{46}$$

Eqn. (45) is simply a statement of the classical result that at the condition of maximum L/D (or minimum glide angle),

the "parasite" drag must equal the "induced" drag. Further since the values of w_1 and w_2 can be uniquely determined from eqn. (44) and the normality condition, the optimal relationship between the two terms in eqn. (43) (i.e., at $\Phi^*(V)$, $C_1V^2 = C_2V^{-2}$) is invariant with respect to the "state-of-the-art" values of C_1 and C_2.

If the value of θ_{min} obtained from eqn. (46) for a particular choice of C_1 and C_2 is acceptable, the corresponding value of V* can then be found from:

$$C_t \sum_n \chi_n^{a_{tn}} = w_t \Phi(\underline{\chi}^*) \rightarrow \begin{cases} C_1V^2 = \frac{1}{2}\theta_{min} \\ C_2V^{-2} = \frac{1}{2}\theta_{min} \end{cases} \tag{47}$$

which, when combined with eqn. (33) gives:

$$V^* = \left(\frac{2W}{\rho b}\right)^{\frac{1}{2}} \cdot \left(\frac{K}{\pi C_{D_o} S}\right)^{\frac{1}{4}} \tag{48}$$

$$C_L^* = 2W/\rho S V^{*2} = \left(\frac{\pi C_{D_o} b^2}{KS}\right)^{\frac{1}{2}} \tag{49}$$

This example is of course easily solved by simple differentiation. It does, however, clearly demonstrate the salient features and ease of solving a well posed problem by geometric programming.

Example II

A slightly more interesting performance problem can be formulated as follows: Given a sailplane of known geometry and weight; flying at a specified altitude. At what value of lift coefficient must the aircraft fly in order to minimize the sink rate?

From eqn. (34), again substituting eqn. (28) and eqn. (36), the basic problem is:

$$\text{Minimize} \quad \Phi(C_L) = |\dot{h}| = \left(\frac{2W}{\rho S}\right)^{\frac{1}{2}} \left[C_{D_o} C_L^{-3/2} + \frac{K C_L^{\frac{1}{2}}}{\pi AR}\right] \tag{50}$$

where $K = K_o AR + K_w$.

As pointed out earlier, eqn. (36) is only valid (for given values of C_{D_o} and K) over a limited range of C_L values. For this, and perhaps other (e.g., safety) reasons, it may be necessary to constrain the possible C_L range. Define a value of C_{L_m} beyond which eqn. (36) is no longer valid. The problem statement, in a form suitable for application of geometric programming, now becomes:

$$\text{Minimize: } \Phi_o(C_L) = |\dot{h}| = C_o \left[C_{01} C_L^{-3/2} + C_{02} C_L^{1/2}\right] \tag{51}$$

$$\text{subject to: } \Phi_1 = C_{11} C_L \leq 1$$

where: $C_o = (2W/\rho S)^{1/2}$ $\qquad C_{02} = K/\pi AR$

$C_{01} = C_{D_o}$ $\qquad C_{11} = 1/C_{L_m}$

In this problem there are a total of three terms in the objective function/constraint system, and only one design variable. Therefore the problem has *one degree of difficulty*. The solution to the problem statement in eqn. (51) proceeds formally as follows:

The *dual* function of eqn. (51) is:

$$d(\underline{w}^*) = \Phi_o(C_L^*) = C_o \left(\frac{C_{01}}{w_{01}^*}\right)^{w_{01}^*} \cdot \left(\frac{C_{02}}{w_{02}^*}\right)^{w_{02}^*} \cdot \left(\frac{C_{11} w_{10}}{w_{11}^*}\right)^{w_{11}^*} \tag{52}$$

where the $\underline{w}^*$ satisfy:

normality $\qquad w_{01}^* + w_{02}^* = 1 \tag{53}$

orthogonality $\qquad -\frac{3}{2} w_{01}^* + \frac{1}{2} w_{02}^* + w_{11}^* = 0 \tag{54}$

non-negativity $\qquad w_{01}^*, w_{02}^*, w_{11}^* \geq 0 \tag{55}$

constraint $\qquad w_{10} = w_{11}^* \qquad w_{oo} = 1 \tag{56}$

Unfortunately, eqns. (53) and (54) give only two equations for the three unknown w_{mt}^*. Thus we can write only:

$$\begin{aligned} w_{01}^* &= \tfrac{1}{4}(1 + 2w_{11}^*) & w_{oo} &= 1 \\ w_{02}^* &= \tfrac{1}{4}(3 - 2w_{11}^*) & w_{10} &= w_{11}^* \end{aligned} \tag{57}$$

To find the optimal weights (w_{mt}^*), we make use of the fact that the maximum of $d(\underline{w})$ is equal to the *minimum* of $\Phi_o(\underline{X})$. Therefore, construct the *substituted dual function* by combining eqns. (52) and (57).

$$d(w_{11}^*) = \left[\frac{C_{01}}{\frac{1}{4}(1+2w_{11})}\right]^{\frac{1}{4}(1+2w_{11})} \cdot \left[\frac{C_{02}}{\frac{1}{4}(3-2w_{11})}\right]^{\frac{1}{4}(3-2w_{11})} \left[\frac{C_{11} w_{10}}{w_{11}}\right]^{w_{11}} \tag{58}$$

Taking the derivative of eqn. (58) with respect to w_{11}^* and setting it equal to zero, we obtain a formula for the value of w_{11}^* which maximizes eqn. (58). Thus:

$$w_{11}^* = \frac{1}{2}\left[\frac{3 - C_{02}/C_{01}C_{11}^2}{1 + C_{02}/C_{01}C_{11}^2}\right] = \frac{1}{2}\left[\frac{3 - \varepsilon}{1 + \varepsilon}\right] \qquad (59)$$

where $\varepsilon = KC_{L_m}^2/\pi ARC_{D_o}$

We observe, in eqn. (59), that if $\varepsilon > 3$ then w_{11}^* becomes negative, which violates eqn. (55). Therefore, whenever $\varepsilon \geq 3$, we must specify that $w_{11}^* = 0$ which implies that under this condition the constraint on C_L is inactive. Substituting eqn. (59) into eqn. (57) we obtain:

$$\underline{\varepsilon < 3}: \quad w_{01}^* = 1/1+\varepsilon \qquad w_{02}^* = \varepsilon/1+\varepsilon \qquad w_{11}^* = \frac{1}{2}\left[\frac{3-\varepsilon}{1+\varepsilon}\right] \qquad (60a)$$

$$\underline{\varepsilon \geq 3}: \quad w_{01}^* = \frac{1}{4} \qquad w_{02}^* = \frac{3}{4} \qquad w_{11}^* = 0 \qquad (60b)$$

where $\varepsilon = KC_{L_m}^2/\pi AR\ C_{D_o}$

Note the eqn. (60b) is a simple statement of the classical result that in the unconstrained case, at the condition of minimum sink, the "induced drag" should be three times the "parasite drag" or that the "induced drag" should be (optimally) 3/4 of the total drag. The remainder of the solution goes through as before and will not be shown here. It should also be noted that had the corresponding problem for the establishment of the condition of minimum power in level flight been solved, exactly the same results would have been obtained (i.e., when solving *performance* problems, the conditions for minimum sink rate are also the conditions for minimum required power).

Example III

One may conclude from the previous examples that performance problems are not very interesting. Consider now the following *design* problem: Given a sailplane of known configuration, but of undetermined size. Assume that detailed calculations have been carried out to establish the variation in wing profile drag with lift coefficient and Reynolds number for the general planform selected. The problem is to determine the optimum wing which, when fitted to a given fuselage/tail combination, will result in a sailplane with a low sink rate at a specified altitude. The mathematical model for this problem (in very simplified form) might be written from eqns. (34) and (41):

$$|\dot{\underline{z}}| = \left(\frac{2W}{\rho}\right)^{1/2}\left[\frac{C_{D_\pi} S_\pi}{C_L^{3/2} S^{3/2}} + \frac{C_{D_p}(\bar{R}_n, C_L)}{C_L^{3/2} S^{1/2}} + \frac{K_w C_L^{1/2} S^{1/2}}{\pi b^2}\right] \tag{61a}$$

$$C_{D_p}(\bar{R}_n, C_L) = C_{D_{p_o}} \left(\frac{2}{\rho\nu^2}\right)^{m/2} \cdot \left(\frac{WS}{C_L b}\right)^{m/2} C_L^{\ell} \tag{61b}$$

$$W = (U + W_o) + C_E b^p S^q \tag{42}$$

Suppose that a statistical survey of comparable machines shows that the weight of this new design should scale according to eqn. (42) if values of p = 3 and q = $\frac{1}{4}$ are selected. Also, assume m = -1/5 and ℓ = 1. Now eqns. (61b) and (42) could be substituted into eqn. (61a), but this would result in posynomial with six terms and, in this formulation, we have a maximum of three independent variables (i.e., b, S and C_L). The resulting geometric program would thus have two degrees of difficulty. This is extremely undesirable, and can be avoided by letting W also enter as a design variable and introducing eqn. (42) into the problem as a constraint. Proceeding in this fashion, the appropriate geometric programming problem becomes:

$$\text{Minimize } \Phi_o(W,b,S,C_L) = |\dot{\underline{z}}| = C_o\left[C_{01} W^{1/2} C_L^{-3/2} S^{-3/2} + C_{02} W^{2/5} b^{1/5} S^{-3/5} C_L^{-2/5} + C_{03} W^{1/2} C_L^{1/2} S^{1/2} b^{-2}\right] \tag{62}$$

$$\text{subject to: } \Phi_1 = C_{11} W^{-1} + C_{12} W^{-1} b^3 S^{1/4} \leq 1$$

where
$$C_o = (2/\rho)^{1/2} \qquad C_{03} = K_w/\pi$$
$$C_{01} = C_{D_\pi} S_\pi \qquad C_{11} = U + W_o$$
$$C_{02} = C_{D_{p_o}} \left(\frac{\rho\nu^2}{2}\right)^{1/10} \qquad C_{12} = C_E$$

The model given by eqn. (62) is a zero degree of difficulty geometric programming problem with four design variables.

The optimal dual variables $\underline{w}^*$ can be uniquely determined in this problem, independent of the coefficients C_{mt}, from the relations (eqn. 19-22):†

$$\text{normality} \qquad w_{01} + w_{02} + w_{03} = 1 \tag{63}$$

† In all the problems in this section, all σ = +1.

orthogonality

$$1/2\ w_{01} + 2/5\ w_{02} + 1/2\ w_{03} - w_{11} - w_{12} = 0$$
$$1/5\ w_{02} - 2\ w_{03} + 3w_{12} = 0 \qquad (64)$$

$$-3/2\ w_{01} - 3/5\ w_{02} + 1/2\ w_{03} + 1/4\ w_{12} = 0$$
$$-3/2\ w_{01} - 2/5\ w_{02} + 1/2\ w_{03} = 0$$

non-negativity

$$w_{mt} \geq 0 \qquad m = 0,1 \qquad (65)$$

constraints

$$w_{10} = w_{11} + w_{12} \qquad (66)$$

The unique solution to the set of eqns. (63-66) is:

$$w_{01}^* = 0.068 \qquad w_{11}^* = 0.135$$
$$w_{02}^* = 0.405 \qquad w_{12}^* = 0.325 \qquad (67)$$
$$w_{03}^* = 0.527 \qquad w_{10} = 0.460$$

These results mean that, regardless of the values of quantities like $C_{D_\pi} S_\pi$ and K_W (the C_{mt}), at the condition of minimum sink, the parasite drag term should be 7% of the total, the wing profile drag should be 40% and the induced drag is 53% of the total drag. These results are only correct if:

(1) the weight and drag scale according to the rules assumed in eqn. (61) with $\ell = 1$, $m = -1/5$, $p = 3$ and $q = 1/4$, and

(2) the resulting design variables (C_L, W, etc.) fall within the range where eqn. (61) are applicable.

If the w_i^* appear reasonable, the value of minimum sink rate can be found from eqn. (18):

$$\Phi_o(\underline{X}^*) = |\dot{z}|_{min} = \left(\frac{C_{01}}{w_{01}^*}\right)^{w_{01}^*} \cdot \left(\frac{C_{02}}{w_{02}^*}\right)^{w_{02}^*} \cdot \left(\frac{C_{03}}{w_{03}^*}\right)^{w_{03}^*} \cdot \left(\frac{C_{11} w_{10}}{w_{11}^*}\right)^{w_{11}^*} \cdot \left(\frac{C_{12} w_{10}}{w_{12}^*}\right)^{w_{12}^*} \qquad (68)$$

where the C_{mt} are given by eqn. (62) and the w_{mt}^* by eqn. (67). If the value of $\dot{z}_{min}$ from eqn. (68) is acceptable for a given set of numerical values of C_{mt}, then the design variables which yield it can be found from eqn. (26,27) and eqn. (68):

$$C_{01} W^{1/2} C_L^{-3/2} S^{-3/2} = 0.068 \Phi_o^* \quad (69a)$$

$$C_{02} W^{2/5} b^{1/5} S^{-3/5} C_L^{-2/5} = 0.405 \Phi_o^* \quad (69b)$$

$$C_{03} W^{1/2} b^{-2} S^{1/2} C_L^{1/2} = 0.527 \Phi_o^* \quad (69c)$$

$$C_{11} W^{-1} = 0.135/0.460 \quad (69d)$$

$$C_{12} W^{-1} b^3 S^{1/4} = 0.325/0.460 \quad (69e)$$

Eqn. (69) may appear difficult to solve until one observes that, in each equation, the design variables are grouped into a single term. Therefore, it is possible to expand eqn.(69) into a set of simultaneous equations which are *linear* in the *logarithms* of the design variables. These equations are then easily solved by standard techniques. In this problem a further simplification is possible. Note that in eqn. (69d) the only design variable present is the total vehicle weight W. We find that, regardless of the other C_{mt} coefficients, the optimal weight here is always:

$$W^* = C_{11} \frac{W_{01}}{W_{11}^*} = 3.4 \ (U + W_o) \quad (70)$$

Therefore, it is only necessary to solve three of the remaining eqns. (69a-c, e) to find S*, C_L* and b*.

Example IV

As a final example, consider the minimum power *design* problem corresponding to the previous minimum sink rate problem. We have indicated above that when treated as a *performance* problem, the conditions which yield minimum sink rate are also the conditions for minimum power required. This can be seen easily from the formula:

$$BHP_{reg} = \frac{W|\dot{z}|}{550\eta} \quad \text{(level flight)} \quad (71)$$

Obviously, *if* W is a fixed quantity, minimum sink rate implies minimum power required. In the *design* problem W is not a fixed quantity initially, and there is no reason to expect that a design optimized for minimum sink rate will also be optimum if minimum power required is the main performance index.

Combining eqn. (71) and (61) with $\ell = 1$, $m = -1/5$, $p = 3$ and $q = 1/4$ we can construct the following geometric programming problem:

$$\text{Minimize } \Phi_o(W,b,S,C_L) = BHP = C_o\left[C_{01}W^{3/2}\, S^{-3/2}\, C_L^{-3/2} + \right.$$

$$\left. + C_{02}W^{7/5}\, b^{1/5}\, S^{-3/5}\, C_L^{-2/5} + C_{03}\, W^{3/2}\, C_L^{1/2}\, S^{1/2}\, b^{-2}\right] \quad (72)$$

$$\text{subject to: } \Phi_1 = C_{11}W^{-1} + C_{12}W^{-1}\, b^3\, S^{1/4} \leq 1$$

$$\text{where } C_0 = \frac{(2/\rho)^{1/2}}{550\,\eta} \qquad C_{02} = C_{D_{p_o}}\left(\frac{\rho v^2}{2}\right)^{1/10} \qquad C_{11} = U + W_o$$

$$C_{01} = C_{D_\pi} S_\pi \qquad C_{03} = K_w/\pi \qquad C_{12} = C_E$$

Inspection of eqn. (72) shows that the conditions for the optimal dual variables in this problem are exactly the same as the conditions given by eqns. (63-66) *with the exception* that the orthogonality condition associated with W in eqn. (64) must, in this problem, be replaced with:

$$3/2\; w_{01} + 7/5\; w_{02} + 3/2\; w_{03} - w_{11} - w_{12} = 0 \qquad (73)$$

With this substitution, we find that the new optimal dual variables for the minimum power problem are:

$$\begin{aligned} w_{01}^* &= 0.068 & w_{11}^* &= 1.135 \\ w_{02}^* &= 0.405 & w_{12}^* &= 0.325 \\ w_{03}^* &= 0.527 & w_{10} &= 1.460 \end{aligned} \qquad (74)$$

Comparison of these results with eqn. (67) shows that the optimal drag distributions in the minimum power and minimum sink cases are the same, but that the dual variables associated with the weight equation constraint are substantially altered. Proceeding from eqn. (69d) as before, we obtain in this case:

$$W^* = C_{11}\,\frac{w_{10}}{w_{11}^*} = 1.29\;(U + W_o) \qquad (75)$$

If one views the term $C_E\, b^p\, S^q$ in the weight equation (eqn.42) as representing the wing weight, then comparison of eqns.(75) and (70) shows the quantitative difference in optimal wing weights for the two examples. The apparently much larger (and consequently heavier) wing in the minimum sink rate problem reflects the fact that low *wing loading* (low W and/or large S) is the dominant wing sizing criterian. In the minimum power problem, low *weight* is the dominant factor. These are of course, classical results, but geometric programming shows them in a particular elegant manner.

Further examination of eqns. (67) and (73) shows what appears to be an unrealistic value of the contribution of parasite drag to the optimal total drag. In this problem,

where no bounds have been placed on allowable wing area, the equations simply specify that to minimize both power and sink rate, a wing of very large area is desirable - thus, even if the parasite area ($C_D S_w$) is substantial, the parasite drag coefficient based on *wing area* is small compared to the wing profile and induced drag coefficients. Again, one must carefully check to assure that the optimal design variables obtained from equations like (69) are within the range of applicability of the particular curve fits like eqns. (42) and (61b) used in the model. If not, the model must be modified, either by alteration of the coefficients or by the addition of suitable constraints.

Conclusions

It has been shown that the recently-developed non-linear optimization technique of geometric programming can be used to solve problems which commonly arise in sailplane performance estimation and design. The major restriction on the method is that the objective function and constraints must be in the form of polynomials. It has been demonstrated that due to the common practice of specifying quantities, such as drag coefficients by a linear superposition of terms, and the fitting of statistical data on factors such as weight and drag by polynomial curves, that several fundamental problems in aircraft design can be cast in the form required for application of geometric programming.

The sailplane design examples presented here have been kept simple and only hint at the ultimate power of the basic technique. An extremely important feature of the general geometric programming technique is that the difficulty of obtaining a solution to a particular problem is *not* directly proportional to the number of design variables, but rather to the relationship between the total number of terms in the polynomials in the model and the number of design variables. Thus, in principle, it is no more difficult to solve a geometric program with twenty design variables and twenty-one terms than one with one variable and two terms. The prior case is only more laborious. It turns out in practice that one of the major problems in formulating a model is that of finding enough design variables to cover the number of terms one might like to include in the objective function/constraint system. With this factor in mind, it appears possible to expand the models used in the examples shown here, to include the effects of wing twist and taper, thickness/chord ratio, tail volume coefficient, etc. to arrive at a very general and complete model for a chosen performance index. These extensions only await the designer eager enough to attempt them.

References

1. Zener, C.; A Mathematical Aid in Optimizing Engineering Designs, Proc. Natl. Acad. Sci., Vol. 47, No. 4, April 1961, pp. 537-539.

2. Duffin, R.J., Peterson, E.L. and Zener, C.; Geometric Programming, Wiley, New York, 1967.

3. Hardy, G.H., Littlewood, J.E. and Polya, G.; Inequalities, Cambridge University Press, England, 1959.

4. Wilde, D.L.; A Review of Optimization Theory, Ind. and Eng. Chem., Vol. 57, No. 8, August 1965, pp. 18-31.

5. Charnes, A., and Cooper, W.W.; Optimizing Engineering Designs Under Inequality Constraints , Northwestern University ONR Research Memo 64, August 1962.

6. Duffin, R.J. and Peterson, E.L.; Constrained Minima Treated by Geometric Means, Westinghouse Scientific Paper 64-158-129-p3, March 1964.

7. Passy, U. and Wilde, D.J.; Generalized Polynomial Optimization, SIAM App. Math., Vol. 15, September 1967.

8. Passy, U., and Wilde, D.J.; Geometric Programming Algorithm for Solving Chemical Equilibrium Problems, SIAM App. Math., Vol. 16, March 1968, pp. 363-373.

9. Wilde, D.J. and Beightler, C.S.; Foundations of Optimization, Prentice-Hall, New Jersey, 1967.

10. Citron, S.J.; Elements of Optimal Control, Holt, Rinehart and Winston, New York, 1969.

11. Peterson, E.L. and Zener, C.; The Rectangularity Law of Transformers, Proc. Natl. Acad. Sci., June 1964.

12. Sherwood, T.K.; A Course in Process Design, MIT Press, Cambridge, MA., 1963.

13. Auriel, M, and Wilde, D.J.; Optimal Condenser Design by Geometric Programming, I and CE Process Design and Development, Vol. 6, No. 2, April 1967, pp. 256-263.

14. Beightler, C.S., Lo, Ta-Chen and Rylander, H.G.; Optimal Design by Geometric Programming, Journ. of Eng. for Industry, Vol. 92, February 1970, pp. 191-196.

15. Phillips, D.T. and Beightler, C.S.; Optimization in Tool Engineering Using Geometric Programming, AIIE Transactions, Vol. II, No. 4, December 1970, pp. 355-360.

16. Goodhart, H.C.N.; A Note on the Measurement of the Induced Drag Factor (K) of a Glider, Technical Soaring, Vol. I, No. 4, April 1972, pp. 7-9.

17. Wortmann, F.X.; Some Laminar Profiles for Sailplanes, Soaring, Vol. 28, No. 1, January 1964.

18. Wortmann, F.X.; Drag Reduction in Sailplanes, Soaring, Vol. 30, No. 6 and 7, June and July 1966.

19. Hoerner, S.F.; Fluid-Dynamic Drag, Published by the author, 1965.

20. Bauman, J.T.; Effect of Stabilizer Lift on Sailplane Performance, Technical Soaring, Vol. I, No. 4,

21. Wilkinson, K.G.; The Design of Sailplanes for High Performance, Aircraft Engineering, September 1951, pp. 263-271.

22. Cone, C.D., Jr.; The Design of Sailplanes for Optimum Soaring Performance, NASA TN D-2052, January 1964.

23. Morelli, P.; On the Weight of Sailplanes as a Function of Their Main Geometric Parameters, OSTIV Publication V, 1958.

24. Stender, W.; Sailplane Weight Estimation, OSTIV Publication, June 1969.

THE SEARCH FOR HIGHER CROSS-COUNTRY SPEEDS

by

Nicholas Goodhart
Project Sigma, Ltd.

PART I. THE RATIONALE FOR VARIABLE GEOMETRY

Introduction

For the last 20 years we have seen a progressive development of glider cross-country performance which has probably outstripped even the wildest dreams of most of those active in the business at the beginning of the period.

The development has come partly from a change in philosophy, i.e., we now trade some thermalling performance for speed and glide ratio in the cruising mode; but mainly from the fantastic development of aerofoil sections. Who, before World War II, would have believed that section L/D's of over 200 would be obtainable from practical aerofoils?

Aerofoil development

The development of glider aerofoils, which owes so much to the work of Wortmann and Eppler, has stemmed from a deep understanding of the boundary layer and how it may be made to stay laminar over a greater and greater proportion of the total aerofoil surface. Whereas, on the old pre-war sections, transition was probably 5-10% on the upper surface and 10-20% on the lower surface, the position now is that the lower surface can be made almost entirely laminar and the upper surface can be laminar to the extent of 60% or even a little more.

The other important aspect of a glider aerofoil is the C_L max obtainable with reasonable drag figures and it is in this area that the latest aerofoils show as significant an improvement as in their L/D's. C_L max as high as 1.4 is now obtainable on the same aerofoil as an L/D of over 200.

However, this fantastic progress seems to be reaching a plateau. There is little more to come in L/D since almost the full theoretical benefit of laminarisation is already being achieved and C_L max seems unlikely to increase much as long as the aerofoil is of fixed shape over the major part of the chord.

In simple theory performance can always be increased by making the glider larger, but we have probably already taken up most of the gain available by going up to spans of 22 meters plus. Beyond this sort of figure, handling difficulties as well as sheer cost begin to negate the benefit.

Where then can future major performance increases come from, or have we really reached a plateau from which only minor improvements are possible?

The basic compromise in the design of a cross-country racing glider lies in the need to provide both a good thermalling performance and a good cruising performance. (There are some optimists who would argue that the so-called "dolphin" soaring technique alters all this, but a little realistic calculation would show them that the ordinary soaring day does not provide anywhere near adequate conditions; if it did, performances in current gliders would be far higher.)

For good climbing characteristics, the glider needs low wing loading, good C_L max and large span, while for cruising flight it needs high wing loading and moderate span. In both configurations, low drag is required, but while this is advantageous in circling flight, it is paramount in cruising flight.

Reynolds number effects

The statement that moderate span is required in cruising flight is not immediately obvious, but becomes clear if one takes an example of the drag at 100 knots of two wings having the same area and wing loading but with one having two-thirds the span of the other. Assume a wing loading of 33 kg/m^2 and an all-up weight of 430 kg. Thus wing area is 13 m^2 and C_L is 0.31.

Consider a 20 m wing and a 13.3 m wing both having FX61-184 wing section.

Span (m)	Mean chord (m)	Re	Profile drag coeff.	Profile drag (kg)	Induced drag (kg)	Total drag (kg)
20	0.65	2.25×10^6	0.0063	13.75	0.9	14.65
13.3	0.98	3.4×10^6	0.0053	11.56	2.02	13.58

From this it will be seen that the reduced profile drag due to higher Reynolds number more than offsets the increased induced drag and the low aspect ratio (13.6) wing has 8% less total drag than the high aspect ratio (30.8) wing.

Wing loading

However, by far the most important variable is wing loading. Basically, one wants the wing loading as low as possible in circling flight and as high as possible in cruising flight. Barring repeated weight change in flight, and this is impractical, the only possible way to vary wing loading is by varying wing area, and it seems fairly clear that this must be from where the next step in performance will come.

Wing area can be changed either by varying the wing chord or by varying the span - or, of course, by doing both. Obviously, either of these raises formidable engineering problems but these will be ignored for the time being.

The relative merits of various configurations can best be examined by considering some possible designs and estimating their performance. The author has information on the theoretical performance of Sigma which will be used as an example of the variable chord approach. Two imaginary variable span gliders will be considered, one of which uses a "fixed" wing section (FX-61-163) and the other uses a flapped section (FX-67-K-170), both will be assumed to have the same area change as Sigma (cruising wing area is 0.74 of climbing wing area). Finally, an imaginary fixed wing area glider will be considered for comparison purposes; this will also be assumed to have the FX-67-K-170 wing section. All four will be given the same span in the climb configuration. Aspect ratio for the two variable span gliders and the fixed wing area machine is arbitrarily set at 28 in the climb configuration. The weight for each machine is then adjusted so that the stalling speed (climb configuration) is the same in each case, and even though it is not immediately obvious, it will be shown later that this results in substantially equal thermalling performance for all four machines.

The four gliders are designated A, B, C, D and their leading characteristics are outlined in Table I.

In studying this table, one of the main points to note is that the span change in the variable span machines is greater than the factor of 0.74 area change. This arises because the wing has been assumed to have a straight taper (0.6 tip/chord ratio) thus decrease of span by retracting the tips removes area less rapidly than span. To achieve 0.74 area factor the span factor is 0.686.

It must also be mentioned that no study has been done to optimize the variable span machines whereas Sigma is an optimized design. The leading characteristics given for the variable span machines are arbitrarily selected though it is believed they are not too far off optimum.

The first aspect of these four gliders to analyse is their climing performance. The weights of all four machines

TABLE I

Leading Characteristics of possible Glider Configurations

		A	B	C	D
Type		Variable chord variable camber	Variable span no flaps	Variable span with flaps	Conventional with flaps
All up weight(kg)		682	540	540	540
Wing section		Sigma	FX-61-163	FX-67-K-170	FX-67-K-170
CLIMB	Wing span (m)	21.0	21.0	21.0	21.0
	Mean chord(m)	0.78	0.75	0.75	0.75
	Aspect ratio	26.8	28.0	28.0	28.0
	Wing area (m^2)	16.38	15.75	15.75	15.75
	Wing loading (kg/m^2)	41.6	34.3	34.3	34.3
CRUISE	Wing span (m)	21.0	14.4	14.4	21.0
	Mean chord(m)	0.58	0.81	0.81	0.75
	Aspect ratio	36.2	17.8	17.8	28.0
	Wing area (m^2)	12.18	11.66	11.66	15.75
	Wing loading (kg/m^2)	55.9	46.3	46.3	34.3

have been chosen so that all have the same stalling speed; however, circling in thermals is not done at C_L max but at some lower C_L which leaves a margin for handling. The value arbitrarily chosen is 0.9 C_L max (which gives them all a straight flight speed of 40.2 knots) and it is sufficient for comparison purposes to examine the straight flight performance of each machine when flown at this C_L.

Table II lists the results of the calculations for all four machines, This is based on the assumption that only the wing profile and induced drags vary between them and that miscellaneous + fuselage + tail drag is the same in each case.

TABLE II

Climb configuration

Performance in straight flight at 0.9 C_L max

Glider	A	B	C	D
Wing Reynolds no. ($\times 10^{-6}$)	1.11	1.07	1.07	1.07
C_L	1.53	1.26	1.26	1.26
Wing profile drag coeff.	0.0109	0.012	0.0122	0.0122
Wing profile drag (kg)	4.8	5.1	5.2	5.2
Induced drag (kg)	13.1	8.2	8.2	8.2
Other drag (kg)	1.6	1.6	1.6	1.6
Total drag (kg)	19.5	14.9	15.0	15.0
Glide ratio	35.0	36.2	36.0	36.0
Sink speed (m/sec)	0.59	0.57	0.575	0.575

These results show, perhaps surprisingly, that all four machines have substantially equal sinking speeds at 40.2 knots. This fortunate situation makes it unnecessary to tie the comparison of their cross-country performance to any particular shape or size of thermal. For all practical purposes, they will all achieve the same rate of climb whatever thermal is selected. Thus a direct comparison of cross-country speed is given by simply selecting some arbitrary but reasonable cruising speed, and comparing the sinking speeds. Bearing in mind that it is the variable area aspect that we are examining a fairly high speed will be normal in cruising flight and a speed of 99.5 knots has been selected. This is of course rather hard on glider D (conventional) which will not normally fly as fast as this.

The results in Table III show at once that Glider A has a significantly lower sink than any of the other three. Even Glider C, the best variable span glider, is 20% worse than A. Thus there would not appear to be any point in even considering facing up to the considerable engineering problems of variable span with flaps.

TABLE III

Cruise configuration

Performance in cruising flight at 99.5 knots

Glider	A	B	C	D
Wing Reynolds no. ($\times 10^{-6}$)	2.03	2.83	2.83	2.62
C_L	0.34	0.28	0.28	0.21
Wing profile drag coeff.	0.0055	0.0056	0.0048	0.0049
Wing profile drag (kg)	11.0	10.8	9.2	12.7
Induced drag (kg)	2.1	2.8	2.8	1.3
Other drag (kg)	6.0	6.0	6.0	6.0
Total drag (kg)	19.1	19.6	18.0	20.0
Glide ratio	35.7	27.5	30.0	27.0
Sink speed (m/sec)	1.43	1.86	1.71	1.90

It is worth noting from Table III that the reason Glider A (the Sigma type) is so much better than the others is that it can be operated at much higher weight, and this in turn stems entirely from the variable camber capability (together with the variable area) which produces a much higher C_L max in the climb configuration and hence, allows the extra weight to be carried while still keeping a reasonable circling speed.

Conclusion

The conclusion is therefore reached that a step jump in cross-country performance can be reached by going to the variable area/variable camber wing; achieving variable area by varying span appears unattractive even if simple flaps are fitted; since no other way of making the next major advance in performance has emerged, the author concludes that this is most likely to come from variable area/variable camber along the general lines of Sigma.

PART II. ENGINEERING OF VARIABLE AREA/VARIABLE CAMBER

Many people active in glider development will be aware that for some years various attempts have been made to achieve variable area/variable camber. However, none has yet succeeded in demonstrating the full performance benefit to be expected.

The best known, and at least partly successful, efforts are those of Pat Beatty in South Africa with his BJ series of machines. Using a part span flap, only a limited gain can be expected; furthermore, he did not have the benefit of a

specially tailored wing section capable of a substantial degree of laminar flow both flap in and flap out. Within these limitations, the BJ machines have demonstrated the principle but not achieved the step jump in performance.

In Europe three other attempts at the formula are known to exist. The AN 66C built by Albert Neukom in Switzerland is believed to have been brought to the test-flying stage, but work has now stopped on it; no results have been published. Sigma has been built in UK and has done some 70 hours flying but has not yet demonstrated more than a small part of its theoretical performance envelope; the reasons for this stem from the engineering difficulties. Very little is known of the third attempt which is being built by a group in Hamburg and is believed to be aiming for first flight in the Spring of 1973. It is understood that this machine is similar in concept to Sigma.

The common thread running through all these machines is long development times and considerable engineering difficulty. It is worth examining the reasons for this.

Looking first at the variable chord principle, the prime factor is that the wing will inevitably have a very high aspect ratio with the flap in. Parametric studies indicate that, depending on the span selected, an aspect ratio of well over 30 is required. The parametric studies also indicate that the flap needs to be about 35% of the flap-in chord.

A full span flap is essential, thus, if convential ailerons are to be used, they must be fitted to the flap: the same applies to variable camber flaps which are required to maintain the section in the laminar bucket throughout the cruising speed range. The ailerons are unlikely to be less than 12.5% chord, thus the flap plus the ailerons will amount to 47.5% of chord. This puts the shear web at 50% chord and the flap operating mechanism will have to protrude through it probably for a further 35% chord.

Due to the extent of the space within the wing which is swept by the moving flap, great difficulty is inevitably experienced in accommodating within the section:

1. sufficient wing structure - particularly where a transport joint is fitted;
2. flap operating mechanism;
3. control runs.

The major difficulties can therefore be listed as follows:

1. Engineering a high aspect ratio wing including transport joints which is sufficiently free of internal structure to accommodate-

2. A full span flap and drive mechanism, noting that the flap must move chordwise as well as changing its angle.
3. The flap must carry either camber flaps or ailerons along the entire extent of its trailing edge and must accommodate separate camber and aileron drive mechanisms.
4. The trailing edge of the upper and lower wing surfaces must be so arranged as to make a good seal with the flap in both positions.

Turning now to variable span, there appear to be even more severe problems than with variable chord. The outer one-third (approx.) of the wing must move inwards to be housed in the inner wing. At least a half of this inner wing is therefore swept by the outer wing as it retracts and it is hard to visualize how any satisfactory structure can be accommodated within this section. Add to this the problem of including simple flaps and ailerons and the mind (the author's at least) boggles at the structural problems involved.

It is fortunate that the apparent benefits from variable span are lower than from variable camber, since the engineering problems appear significantly more difficult.

STUTTGARTER PROFILKATALOG I

EXPERIMENTAL RESULTS FROM THE LAMINAR WIND TUNNEL OF THE INSTITUT FÜR AERO- UND GASDYNAMIK DER UNIVERSITÄT STUTTGART

by

D. Althaus
Institut für Aerodynamik und Gasdynamik
der Universität Stuttgart

Introduction

When this wind tunnel began operation in 1962, the development of improved laminar airfoils was initiated, among other activities. Through the work of F.X. Wortmann, these airfoils have become widely known as FX-airfoils. Recently the instrumentation of the wind tunnel has been modernized appreciably. In order to get a consistent set of data, most of the earlier measurements have been repeated with the new instrumentation, some of them with new and more carefully built models. All data on FX-airfoils are summarized in an airfoil catalog called "Stuttgarter Profilkatalog I"*. The following text provides a short abstract of its contents:

The laminar wind tunnel

The tunnel, built between 1958 and 1962, is an open tunnel of the Eiffel design. It works practically independently of the weather through use of a wind guard in front of the tunnel intake and a sheltered position in a forest. Fig. 1 illustrates the general arrangement. The wind guard is on the left hand side of the picture, followed by the intake with the contraction section. The working section is within the building. The fan is in the middle of the long diffuser. Through use of an extremely high contraction ratio of 90:1 (based on the surface of the wind guard) and the use of many air filter screens with graded resistance, the turbulence level can be maintained as low as 2×10^{-4}.

The tunnel speed is adjusted with the aid of hydraulic power transmission. The blades of the fan are adjustable at rest. The dynamic head can be varied between 25 and 500 mm water gauge. Airfoil sections with a span of 0.73 m are fitted flush between two turntables in the tunnel walls. The chord of the models may be changed between 0.2 and 1.2 m, giving Reynolds numbers between 0.2×10^6 and 6×10^6.

* Copies of this catalog must be ordered directly from the Universität Stuttgart.

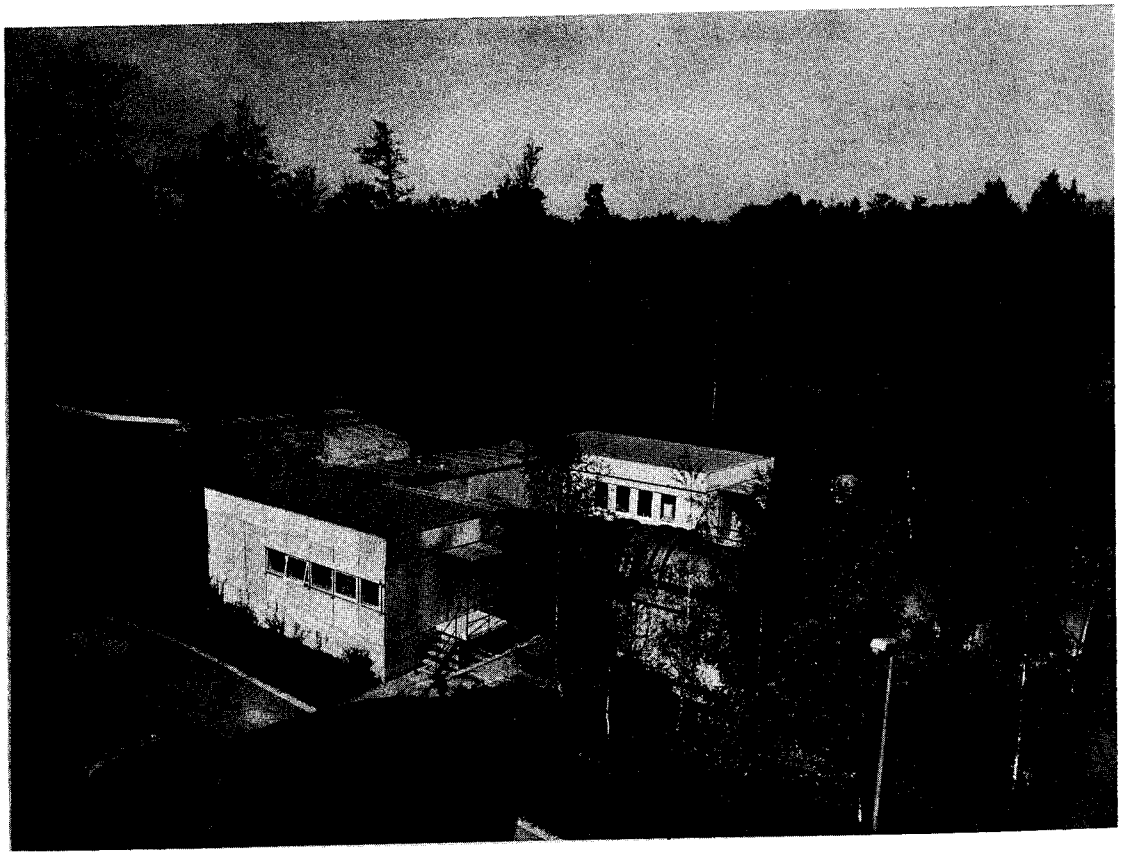


Fig. 1. Laminar Wind Tunnel

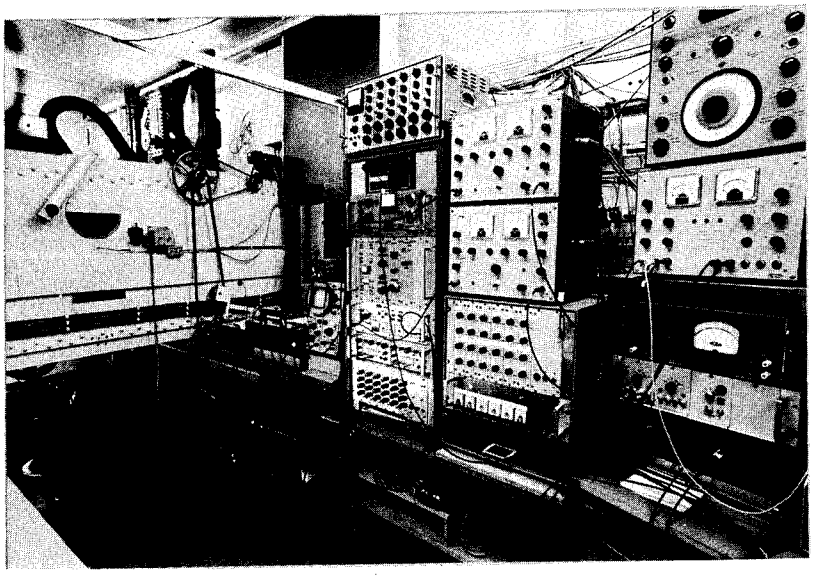


Fig. 2. Wind Tunnel Working Section
with Instrumentation

Instrumentation

The lift and drag of two-dimensional airfoil sections are ascertained from the pressure distributions on the tunnel wall and in the wake of the model. The mean values of the pressure distributions are produced experimentally. The lift and drag coefficients can also be obtained if the undisturbed dynamic head, the static pressure and the maximum total pressure in the wake are measured as well. The width of the wake traverse rake and its distance from the trailing edge are selected depending on the model thickness and chord. The rake automatically travels in the middle of the wake and turns parallel to the local flow direction. The newer type of pressure transducers, which work without mechanical friction, allow for accurate measurement down to very small pressure differences.

Additionally, an external force balance for the measurement of lift, drag and pitching moment, and an internal balance for measurements on bodies are available. The hinge moment of flaps is also measured by an external force balance. For measurements in boundary layers, a hot wire device and sophisticated probe traverses are used. Transition of the boundary layer is detected by a stethoscope or by hot wires. For visualization the oil film method is preferred.

Data processing

The tedious test and plotting work is greatly reduced through use of a data processing installation (Fig. 2). All pressures and forces are available as electrical voltages at the outputs of the transducers. These signals are processed in an analog computer applying all wind tunnel corrections and finally are plotted as $C_L(\alpha)$ and $C_L(C_D)$ on two x-y plotting tables. The installation is calibrated before and after each run using absolute calibration pressures.

When measuring the complete polars of an airfoil, only the angle of attack of the model has to be set by use of an electric drive; the aerodynamic coefficients of the model are produced simultaneously on the plotters. In this way the polar of a model for one Reynolds number can be produced in about three minutes, and the reproducability of data can be checked easily.

Test data content

The "Stuttgarter Profilkatalog I" is a summary of the data for 36 airfoils which are divided in groups:

cambered airfoils;
airfoils with flaps;
symmetrical airfoils with flaps and special airfoils (airfoils with variable chord).

For each airfoil the coordinates, the shape, the theoretical velocity distribution and the experimental data for several Reynolds numbers are given.

Some special measurements are also provided:

measurements on an airfoil with modified flap and high flap deflection;
measurements on two airfoils with various arrangements of airbrakes;
measurements on airfoils with brake-flaps.

For comparison with NACA results, measurements on some NACA airfoils are listed too.

The text of the catalog is written in German, but a short introduction in English is included.

WIND-TUNNEL MEASUREMENTS ON BODIES AND WING-BODY COMBINATIONS

by

D. Althaus
Institut für Aerodynamik und Gasdynamik
der Universität Stuttgart

Introduction

In recent times the wing drag of airplanes has been substantially reduced through use of modern laminar airfoils. A further gain can be achieved by reducing the drag of the fuselage and the interference drag. Experimental investigations have been made in order to show the possible reduction in drag of fuselages and, moreover, to get some idea of the interaction of the fuselage with a wing and the influence of various wing positions. The measurements were made in the Laminar Wind Tunnel of the Institut für Aerodynamik und Gasdynamik der Universität Stuttgart.

Measurement of drag

The drag of the bodies and of wing-body combinations was measured by a pitot rake rotating in steps of 15^{o} around the axis at the end of the body. The rake was 150 mm high. The static pressure in the boundary layer was measured by three static tubes. The total pressure of the 48 rake tubes was measured by one pressure transducer via a scanivalve. The data were punched on cards and evaluated on a digital computer.

The fuselage models were mounted on a sting fixed to the wind tunnel turn-tables. The models of wing-body combinations were mounted with their wing tips attached to the turn-tables. Measurement of the drag of wing-body combinations with an external balance proved to be unreliable, owing to the interference of the wing tips with the tunnel boundary layer.

Measurement of lift

The lift of the wing-body combinations was measured by integrating the pressure along the tunnel walls and by an external balance. Both methods gave the same results.

Measurements on fuselages

A fuselage should offer enough volume for the pilot and should have a drag as small as possible. For a given frontal area this can be achieved in two ways:

1. Similar to laminar airfoils, the front part of the body should produce favorable pressure gradients in all meridians even at incidences of about $\pm 10^{\circ}$. At the same time the whole surface should be smooth and leak-free in order to avoid any disturbances to the laminar flow.
2. Behind the transition front it is favorable to contract the cross section. On one hand this reduces the wetted surface, on the other hand it shifts the unavoidable pressure rise to the thinner parts of the turbulent boundary layer, which is a well-known principle of favorable boundary layer control.

In order to investigate different degrees of contraction, measurements were made on a body of revolution with various modifications. In all cases the thickness-to-length ratio was 0.1 at $x/L = 0.25$. The Reynolds number based on body length was $Re = 7.1 \times 10^6$ for all measurements reported, unless otherwise specified. The shape of the base model (shape 1), its pressure distributions, and transition line are illustrated in Fig. 1. At incidence the transition line is only slightly shifted from its position $x/L = 0.33$ at $\alpha = 0$. The rear part of the fuselage is formed by a conical cylinder tangent to the front part at maximum cross section.

Modifications to base shape 1

Shape 1 was modified in the following ways: Three different contraction parts were inserted between the front part and a cone with small diameter, yielding shapes 2, 3 and 4 (Fig. 2). Shape 3 was further modified to shapes 3a and 4 with a blunter nose. The velocity distributions of shapes 1, 2 and 4 are given in the upper part of Fig. 2. Obviously the position, the maximum value of the velocity peaks, and the total pressure rise correspond to the local surface curvature of the contraction part. The transition lines are influenced in the same way. Fig. 3 shows the variation of velocity distribution and transition lines due to angle of attack, for shape 2.

The left side of Fig. 4 presents the drag coefficients (based on frontal area) versus angle of attack for shapes 1 and 2. There is only a gradual increase of drag with incidence. The transition lines are nearly unchanged, as shown in Fig. 3, but there is a considerable drag reduction from shape 1 to shape 2. The drag of all shapes is lowered further by increase in Reynolds number.

Table 1.

Coordinates of bodies of revolution.

R = radius.

shape	2	3	3a	4
x/L	R/L	R/L	R/L	R/L
0.0125	0.01075	0.01075		
0.0195			0	0
0.0250	0.01725	0.01725	0.0115	0.0115
0.0350			0.0180	0.0180
0.0500	0.02395	0.02395	0.0240	0.0240
0.0650			0.0275	0.0275
0.0750	0.03000	0.03000	0.03000	0.03000
0.1000	0.03520	0.03520	0.03520	0.03520
0.1250	0.03880	0.03880	0.03880	0.03880
0.1500	0.04230	0.04230	0.04230	0.04230
0.1750	0.04525	0.04525	0.04525	0.04525
0.2000	0.04760	0.04760	0.04760	0.04760
0.2250	0.04925	0.04925	0.04925	0.04925
0.2500	0.05000	0.05000	0.05000	0.05000
0.2750	0.04970	0.04950	0.04950	0.04950
0.3000	0.04820	0.04650	0.04650	0.04400
0.3250	0.04565	0.04100	0.04100	0.03300
0.3500	0.04200	0.03300	0.03300	0.02450
0.3750	0.03675	0.02600	0.02600	0.02150
0.4000	0.03075	0.02250	0.02250	0.02100
0.4250	0.02600	0.02000	0.02000	0.02000
0.4500	0.02250	0.01970	0.01970	0.01970
0.4750	0.02075	0.01975	0.01975	0.01975
0.5000	0.01975	0.01975	0.01975	0.01975
0.5250	0.01925	0.01925	0.01925	0.01925
1.0000	0.01000	0.01000	0.01000	0.01000

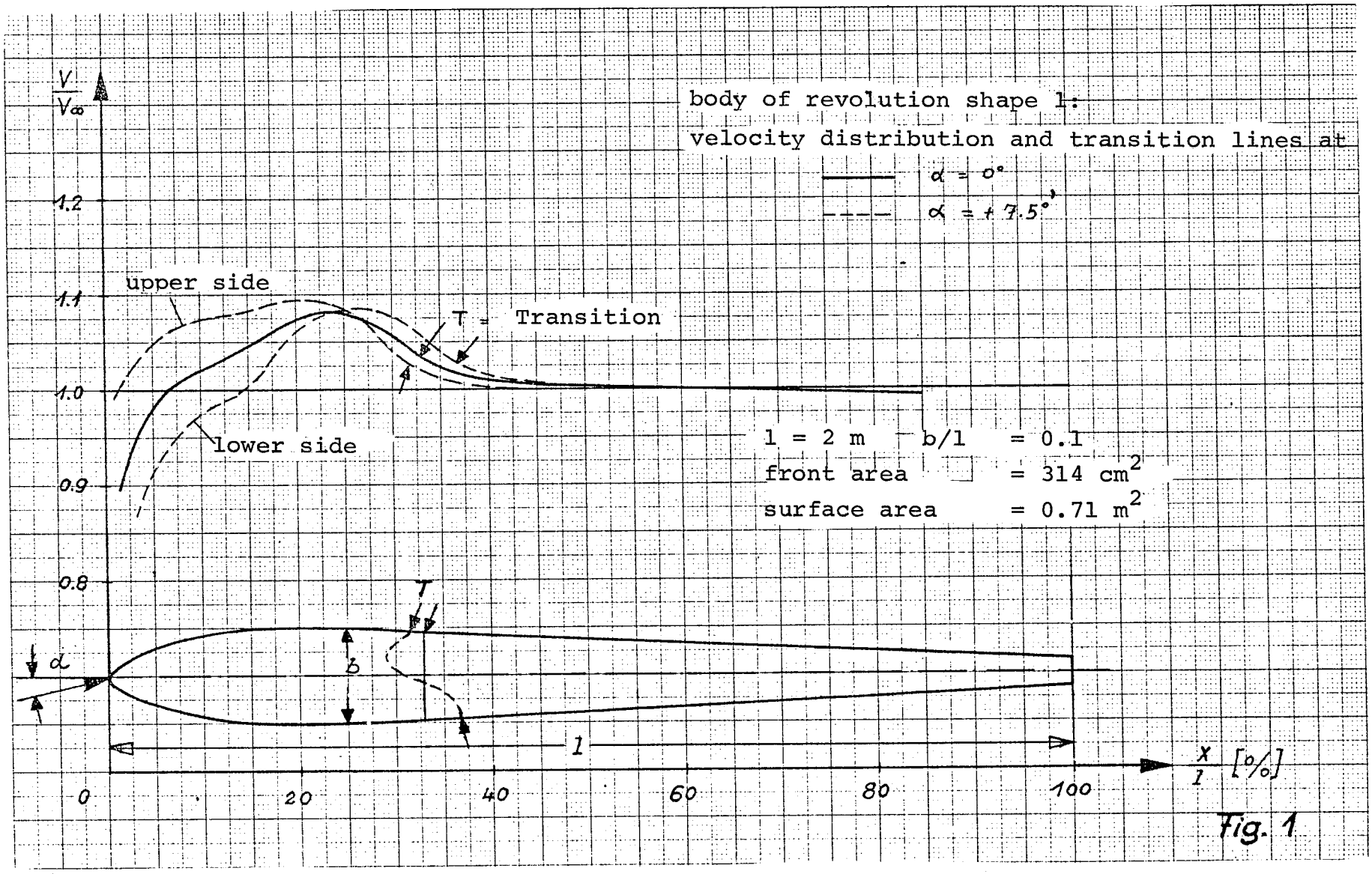

body of revolution shape 1:
velocity distribution and transition lines at
α = 0°
α = ± 7.5°
V/V∞
1.2
1.1
1.0
0.9
0.8
upper side
lower side
T = Transition
l = 2 m
b/l = 0.1
front area = 314 cm²
surface area = 0.71 m²
T
α
b
l
x/l [%]
0
20
40
60
80
100

Fig. 1

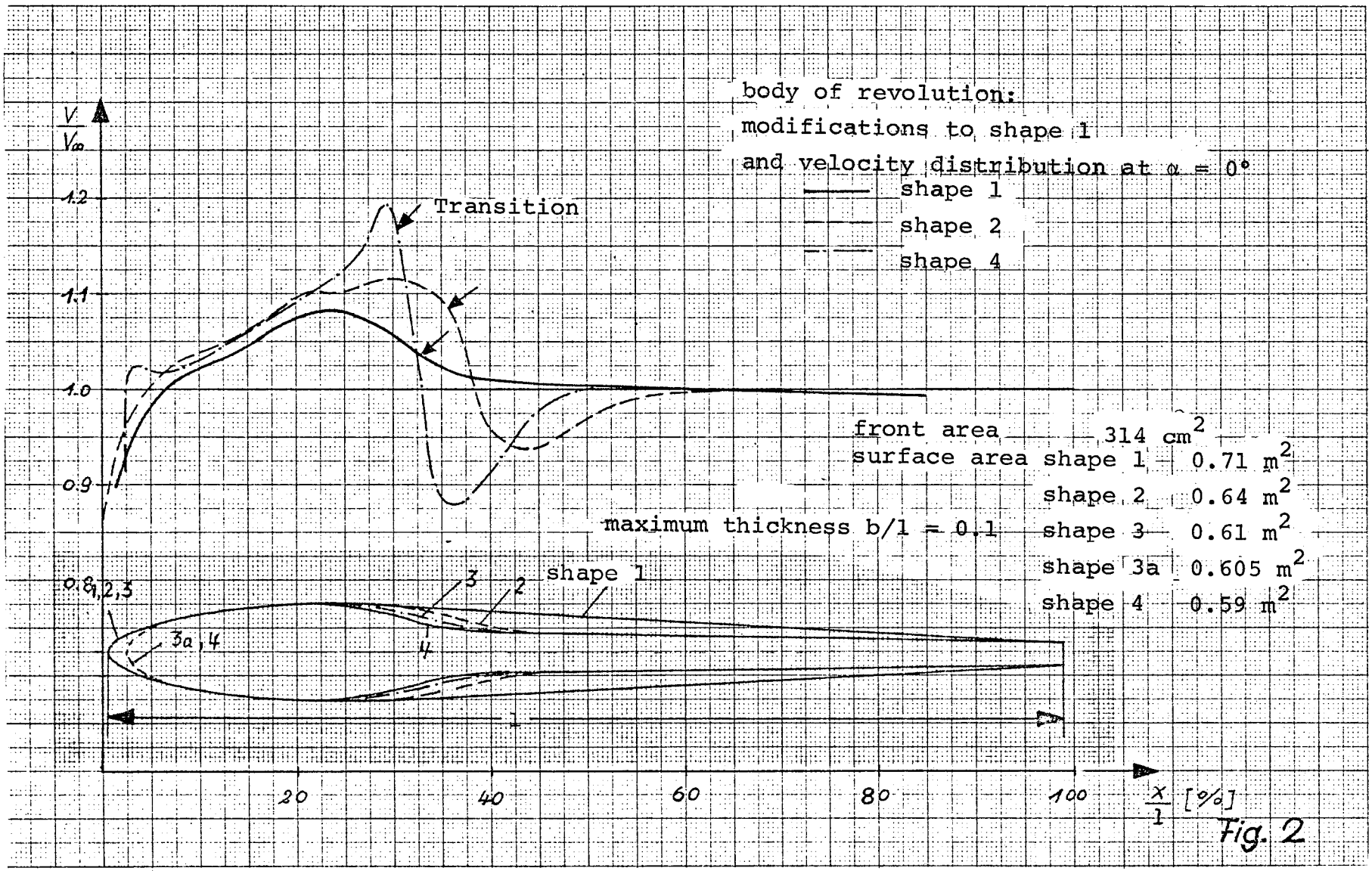

body of revolution:
modifications to shape 1
and velocity distribution at α = 0°
shape 1
shape 2
shape 4
V/V∞
1.2
1.1
1.0
0.9
Transition
front area 314 cm²
surface area shape 1 0.71 m²
shape 2 0.64 m²
shape 3 0.61 m²
shape 3a 0.605 m²
shape 4 0.59 m²
maximum thickness b/l = 0.1
shape 1
0.8
1,2,3
3
2
3a, 4
4
20
40
60
80
100
x/l [%]

Fig. 2

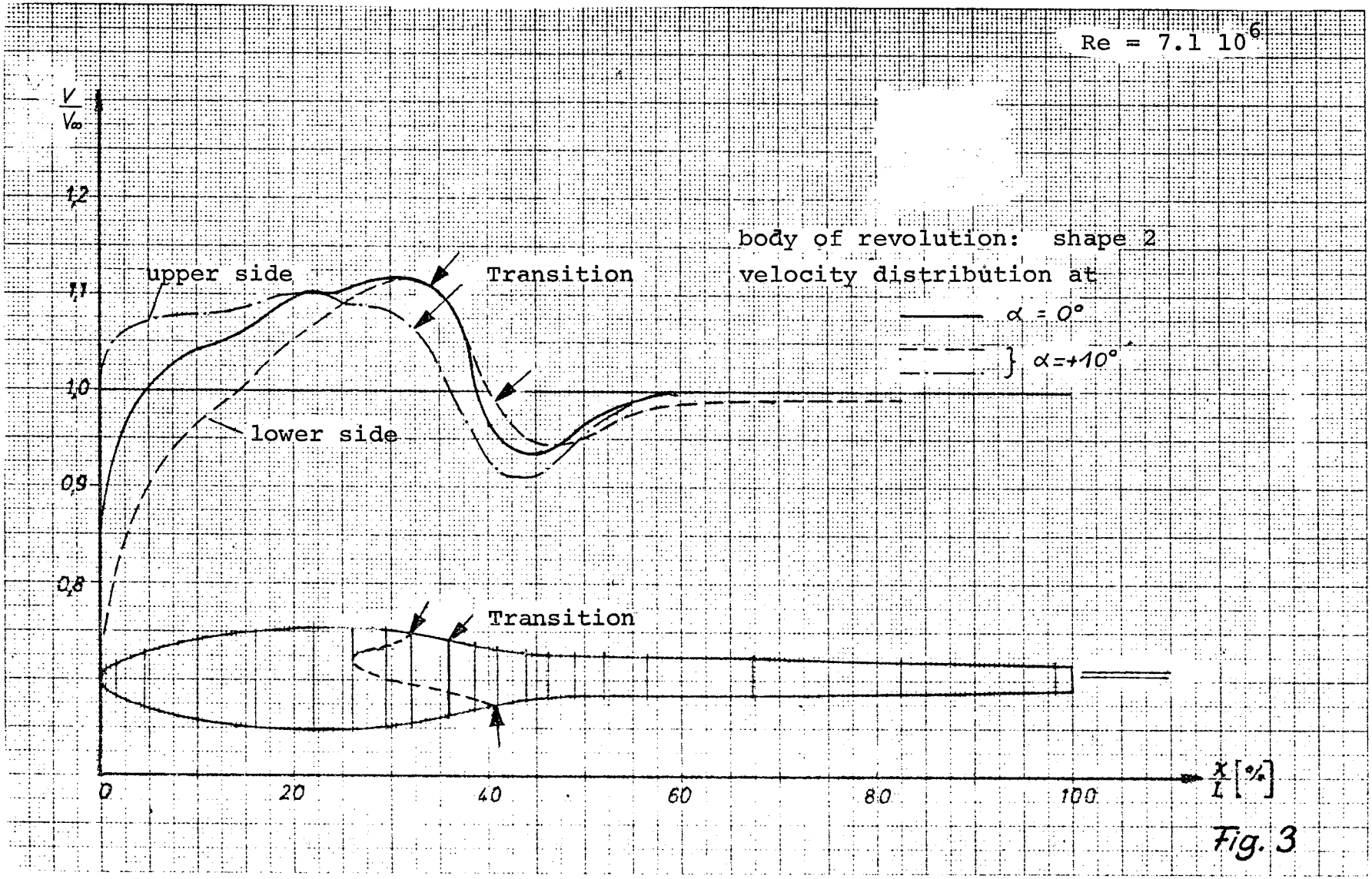

Re = 7.1 10^6
V/V∞
1,2
1,1
1,0
0,9
0,8
upper side
Transition
lower side
Transition
body of revolution: shape 2
velocity distribution at
α = 0°
α = +10°
0
20
40
60
80
100
x/L [%]

Fig. 3

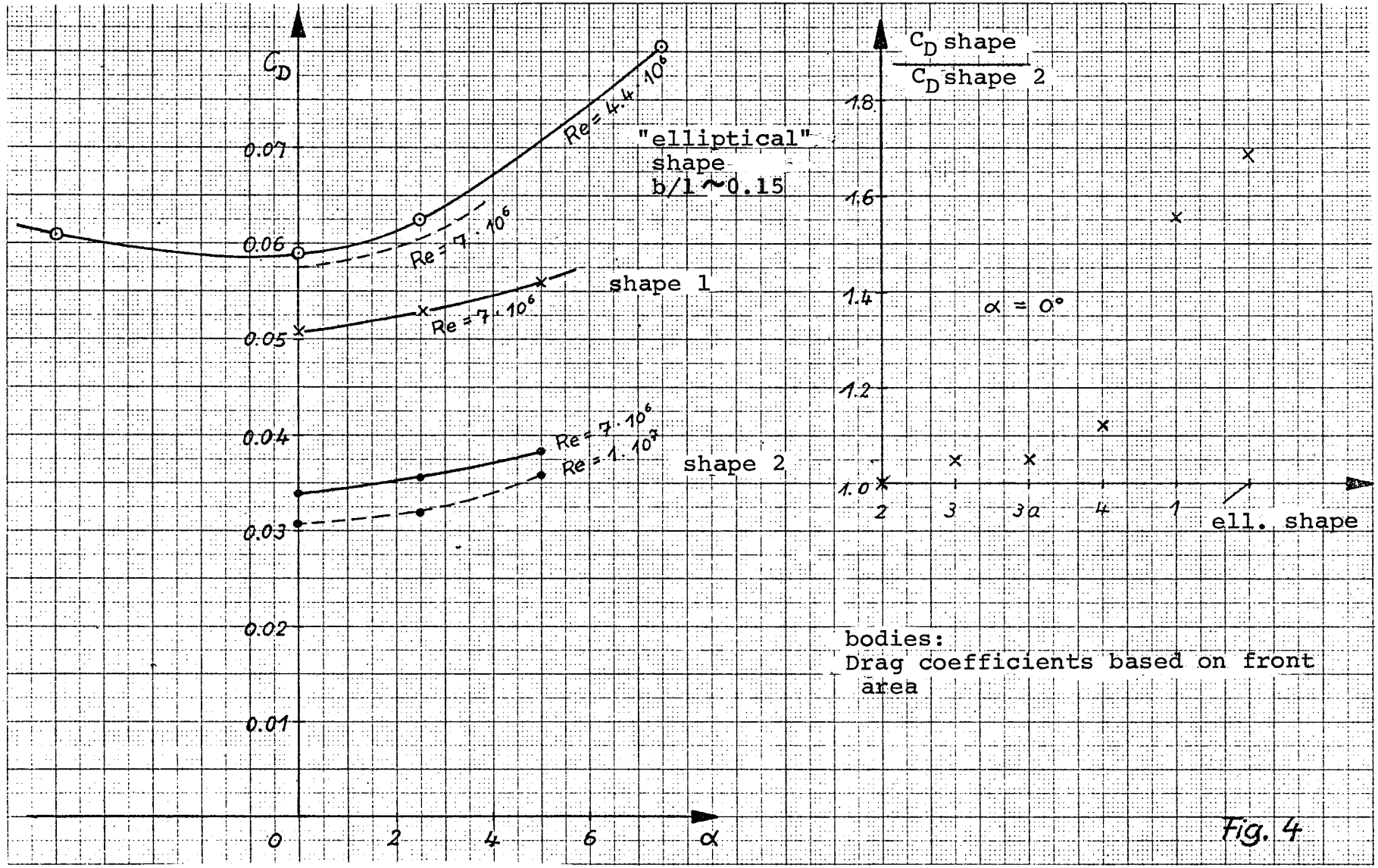

C_D
0.07
0.06
0.05
0.04
0.03
0.02
0.01
0
2
4
6
α
Re = 4.4 · 10^6
Re = 7 · 10^6
"elliptical" shape
b/l ~ 0.15
shape 1
Re = 7 · 10^6
Re = 7 · 10^6
Re = 1 · 10^7
shape 2
C_D shape / C_D shape 2
1.8
1.6
1.4
1.2
1.0
α = 0°
2
3
3a
4
1
ell. shape
bodies:
Drag coefficients based on front area

Fig. 4

The drag polar labelled as "elliptical shape" in Fig. 4 corresponds to a body which is built up of an ellipsoid in the front part, with a linear continuation to a circular cross section at its end (idealized body of the saiplane Ka 6). This body is used for examining the influence of various vertical wing positions, as described below.

As the influence of incidence is nearly the same for all shapes of the bodies of revolution, the drag coefficients of the other shapes tested are only plotted in relation to the drag coefficients of shape 2 (see right side of Fig. 4, $\alpha = 0^{o}$ and $Re = 7 \times 10^{6}$). The drag coefficients of shapes 3, 3a and 4 with the stronger contractions are higher than those of shape 2 due to the steeper pressure rises in the contraction part and correspondingly earlier transition as demonstrated in Fig. 2. There is no difference in drag between shapes 3 and 3a (up to incidences of $\alpha = \pm 7^{o}$), which differ only in having a sharp or blunt nose. A sharp nose results in only a slight increase of the wetted surface. Shape 2 has the lowest drag of all the shapes tested.

Measurements on wing-body combinations

Wing-body combinations not only produce complicated pressure distributions at their junction but also lead to a strong interference with the boundary layers of the wing and the body. To get some experimental results, the body with shape 2 was fitted with a wing as shown in Fig. 5. The wing is in "middle-wing position" just above the mean-line of the body. The wing airfoil has a thickness/chord ratio of 0.18 and spans the tunnel width (0.73 m). The maximum diameter of the body is 0.2 m. The lift and drag coefficients of this wing-body combination, based on wing area, are plotted in Fig. 6. The lift coefficients of the isolated wing are reduced by the interference of the body; the angle of attack corresponding to maximum lift is reduced by about one degree. In the lift-drag polar, the drag of the isolated parts and their arithmetic sum, together with the drag of the wing-body combination, give an indication of the interference drag which increases with increasing lift.

In Figs. 7, 8, 9 and 10 some details of the flow are shown:

Fig. 7 is a photograph of the upper side with an oil-film at $\alpha = 0^{o}$ incidence, showing the wall streamlines. In Fig. 8 the incidence is increased to 5^{o}, that is, almost to the maximum lift condition. Flow separation appears near the rear part of the wing-body junction with a vortex on each wing, and a distinct divergence and convergence of streamlines on the body above the wing. The fairing on the upper side of the wing-body junction (see Fig. 7) has no influence on the lift characteristics but increases the drag at low incidence approximately 5 percent.

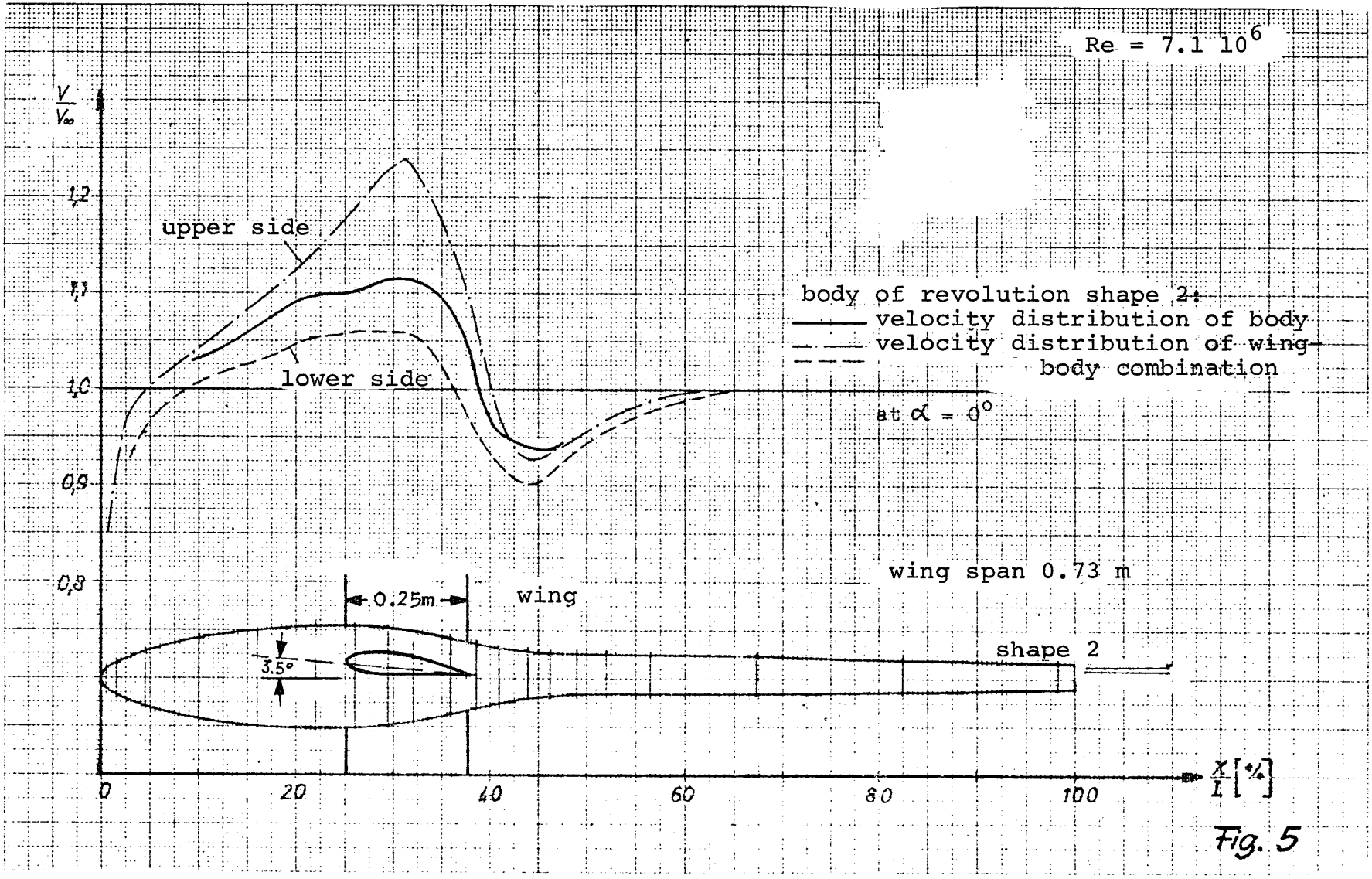

Re = 7.1 10^6
V/V∞
1,2
1,1
1,0
0,9
0,8
upper side
lower side
body of revolution shape 2:
velocity distribution of body
velocity distribution of wing-body combination
at α = 0°
wing span 0.73 m
0.25m
wing
shape 2
3.5°
0
20
40
60
80
100
x/l [%]

Fig. 5

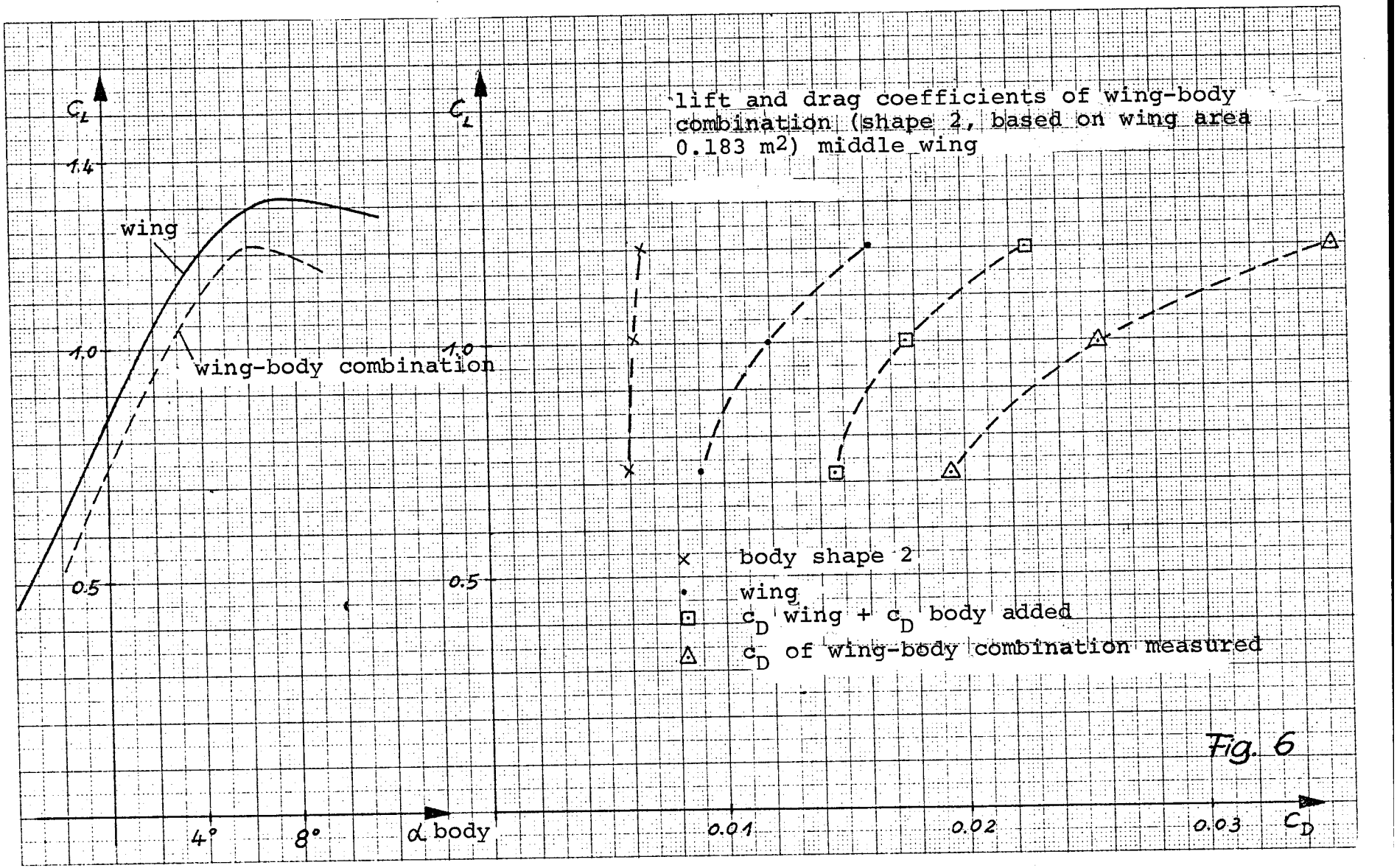

lift and drag coefficients of wing-body combination (shape 2, based on wing area 0.183 m2) middle wing
C_L
1.4
1.0
0.5
wing
wing-body combination
4°
8°
α body
× body shape 2
• wing
⊡ c_D wing + c_D body added
△ c_D of wing-body combination measured
0.01
0.02
0.03
C_D

Fig. 6

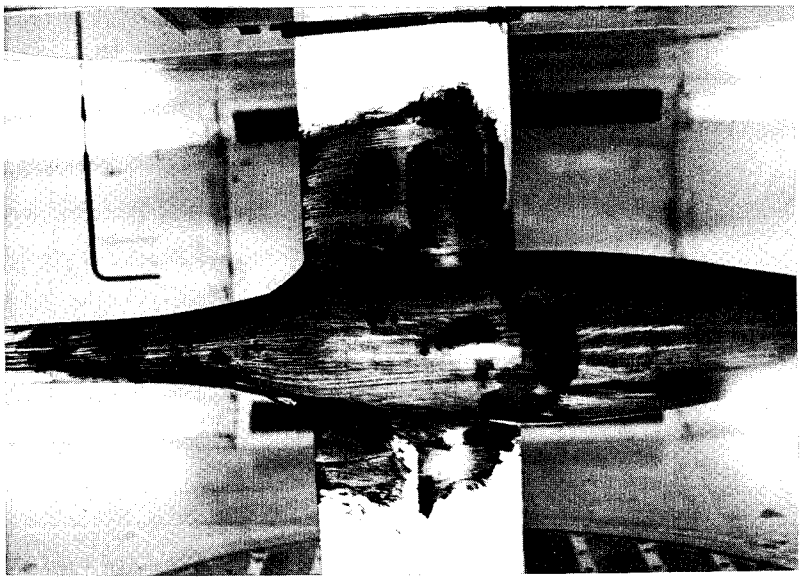


Fig. 7: Upper side of model with oil-film at $\alpha=0°$

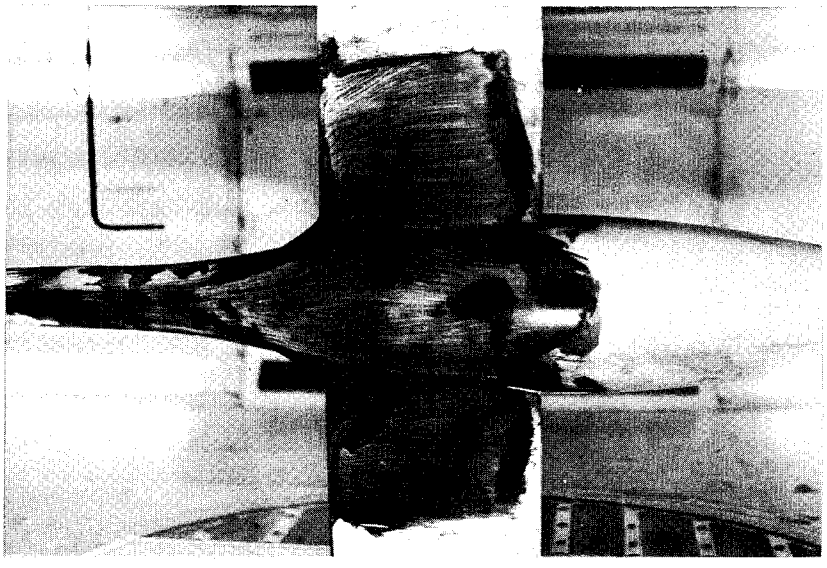


Fig. 8: Upper side of model with oil-film at $\alpha=+5°$

In Fig. 9 lines of constant velocity $V/V_1 = 1.0$ at the end cross section of the body are plotted for the isolated body and the wing-body combination. The wake of the wing is raised near the body and seems to continue above the body. The angle of downwash has the same distribution, yielding a decrease in spanwise lift and, accordingly, additional induced drag. On the lower side of the body the thickness of the boundary layer is diminished.

In Fig. 10 the momentum thickness δ_2 is plotted around the circumference of the body end for $\alpha = +5°$ incidence. The left side holds for the isolated body and the right side for the combination.

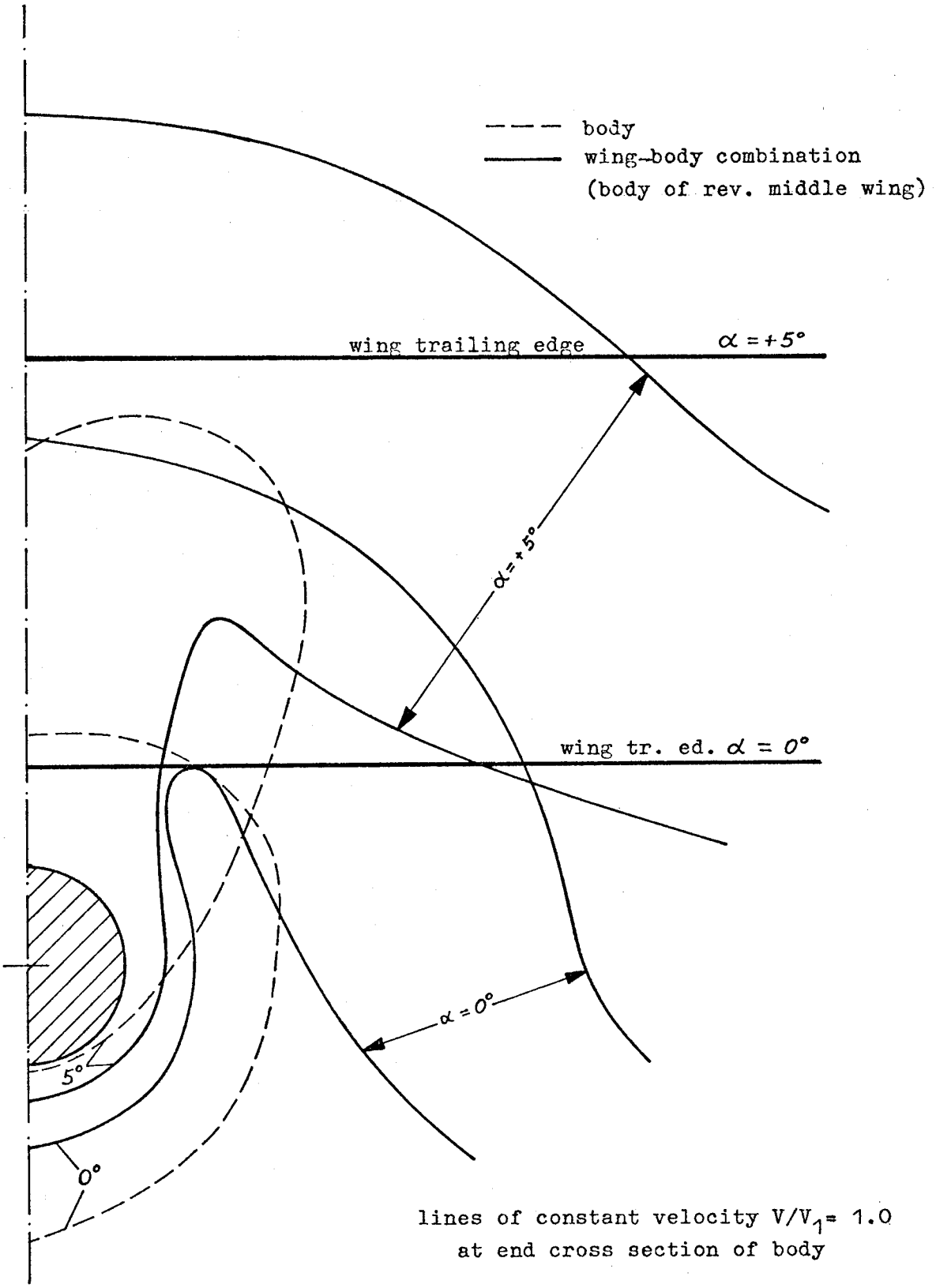
The influence of wing position

To investigate the influence of the vertical position of the wing the "elliptical" body already mentioned, and a wing with a chord of 0.35 m (airfoil t/c = 0.184) were used. The two different versions of the model are shown in Figs. 11 and 12. For the high-wing version a fairing was used at the intersection of the lower wing surface with the body. In this way separation at negative incidences could be delayed by one degree. With the mid-wing version (Fig. 12) no change in lift characteristics could be observed by fairing the upper wing-body intersection, but the drag at low incidence was increased by some 5%.

The lift and drag coefficients (based on wing area) of the two versions and of the isolated parts are plotted in Fig. 13 in the same manner as for the wing-body combination of Fig. 6. There is a distinct difference in lift characteristics: The lift polar of the high-wing version is similar to the polar of the isolated wing (maximum lift at same incidence). On the mid-wing version separation occurs earlier and the maximum lift is smaller. The drag coefficients of the mid-wing are about 13% higher than those of the high-wing version, the difference increasing with higher lift coefficients. The difference between the drag coefficients measured on the wing-body combinations and the drag coefficients composed of the sum of the drag coefficients of the isolated parts is a measure of the interference drag. This difference has a minimum at $\alpha = 0°$ incidence of the body.

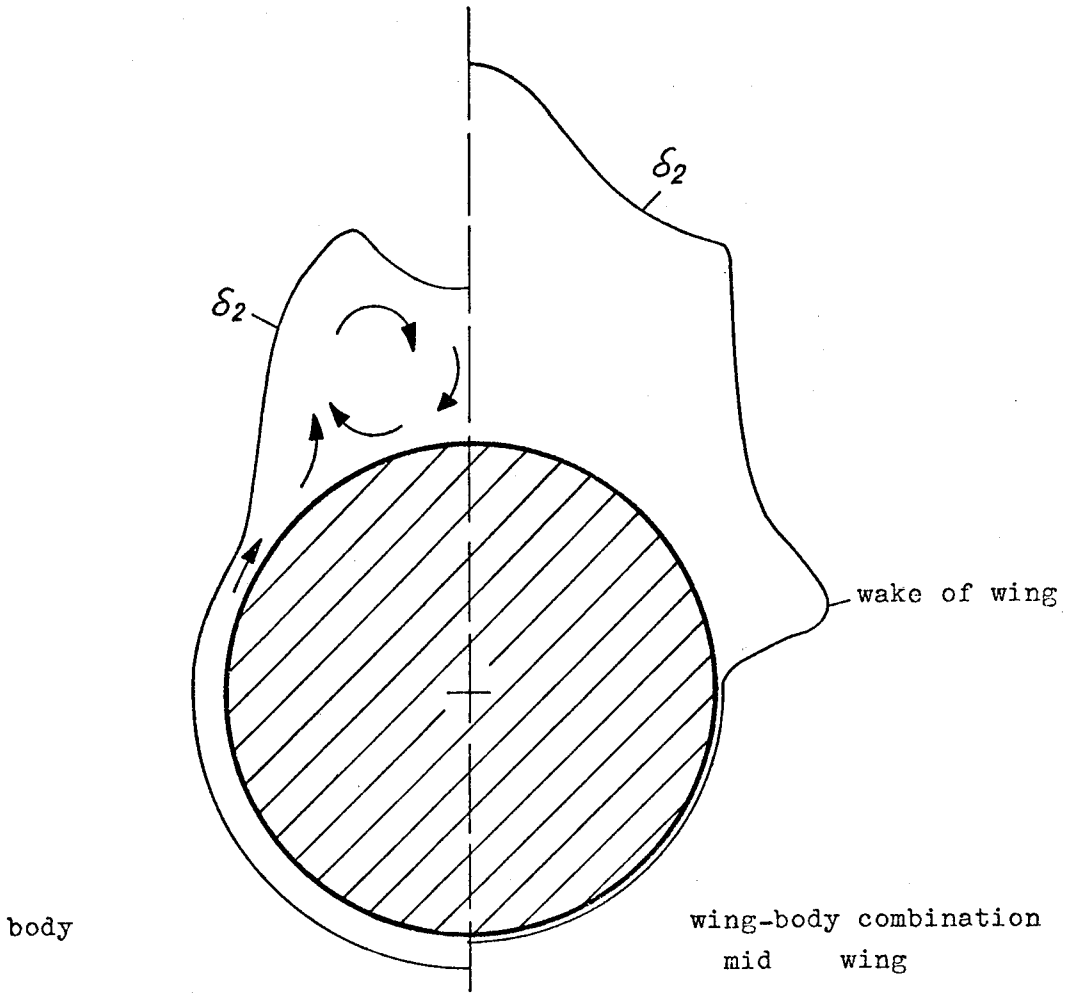
Photographs of the different models with an oil-film helps to reveal some details of the flow mechanisms:

Fig. 14 shows the upper side of the high-wing model at $\alpha = +6°$ incidence ($C_L = 1.3$). Fig. 15 shows the mid-wing model at $\alpha = +5.5°$ ($C_L = 1.25$). Both configurations exhibit a region of separated flow containing two vortices on each wing near the body. On the high-wing model the separation begins further downstream, and the vortices are rather separated from each other, while on the mid-wing model sepa-



lines of constant velocity $V/V_1 = 1.0$
at end cross section of body

Fig. 9



momentum thickness δ_2
at end cross section of body of revolution

Fig. 10

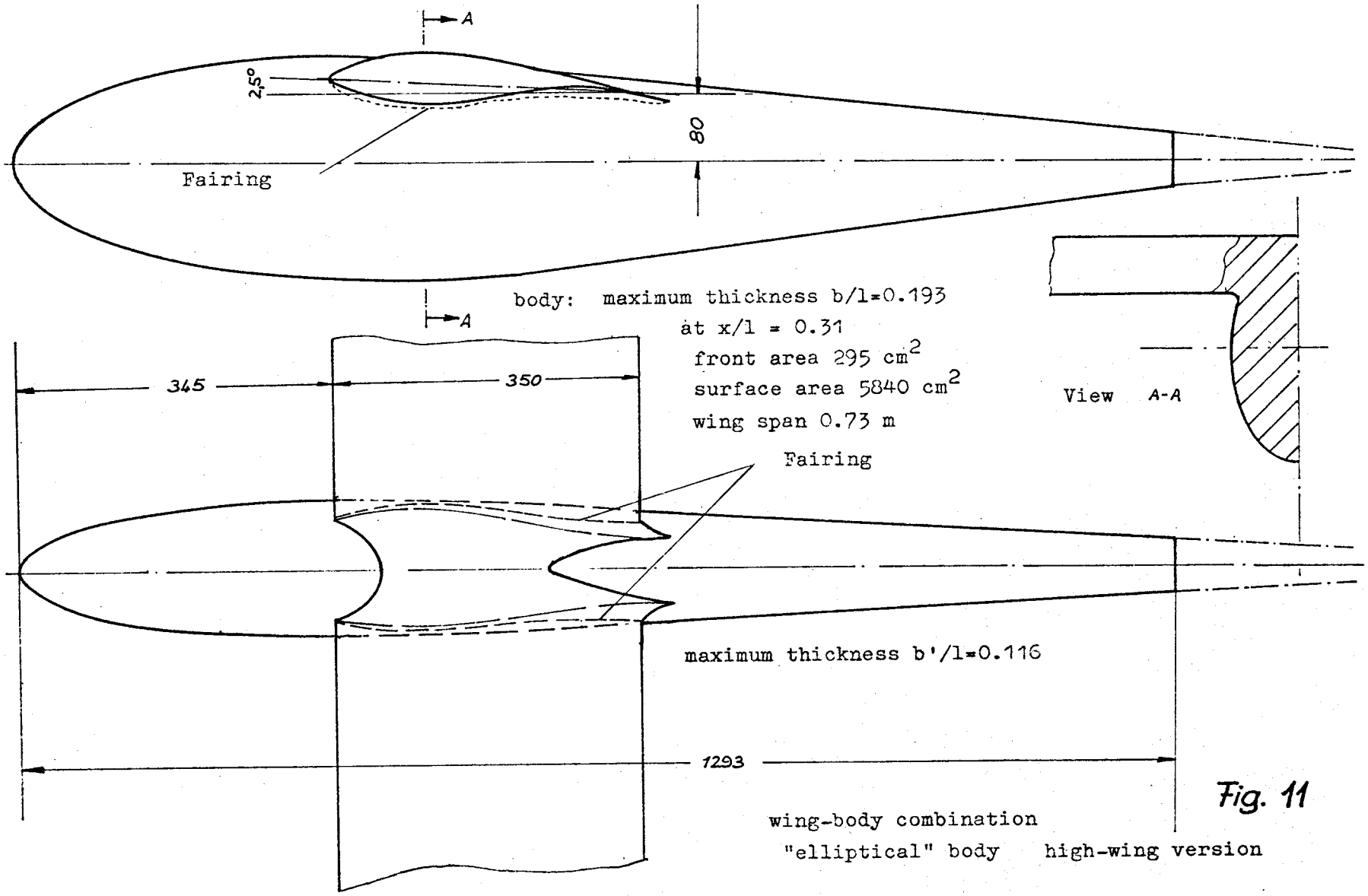
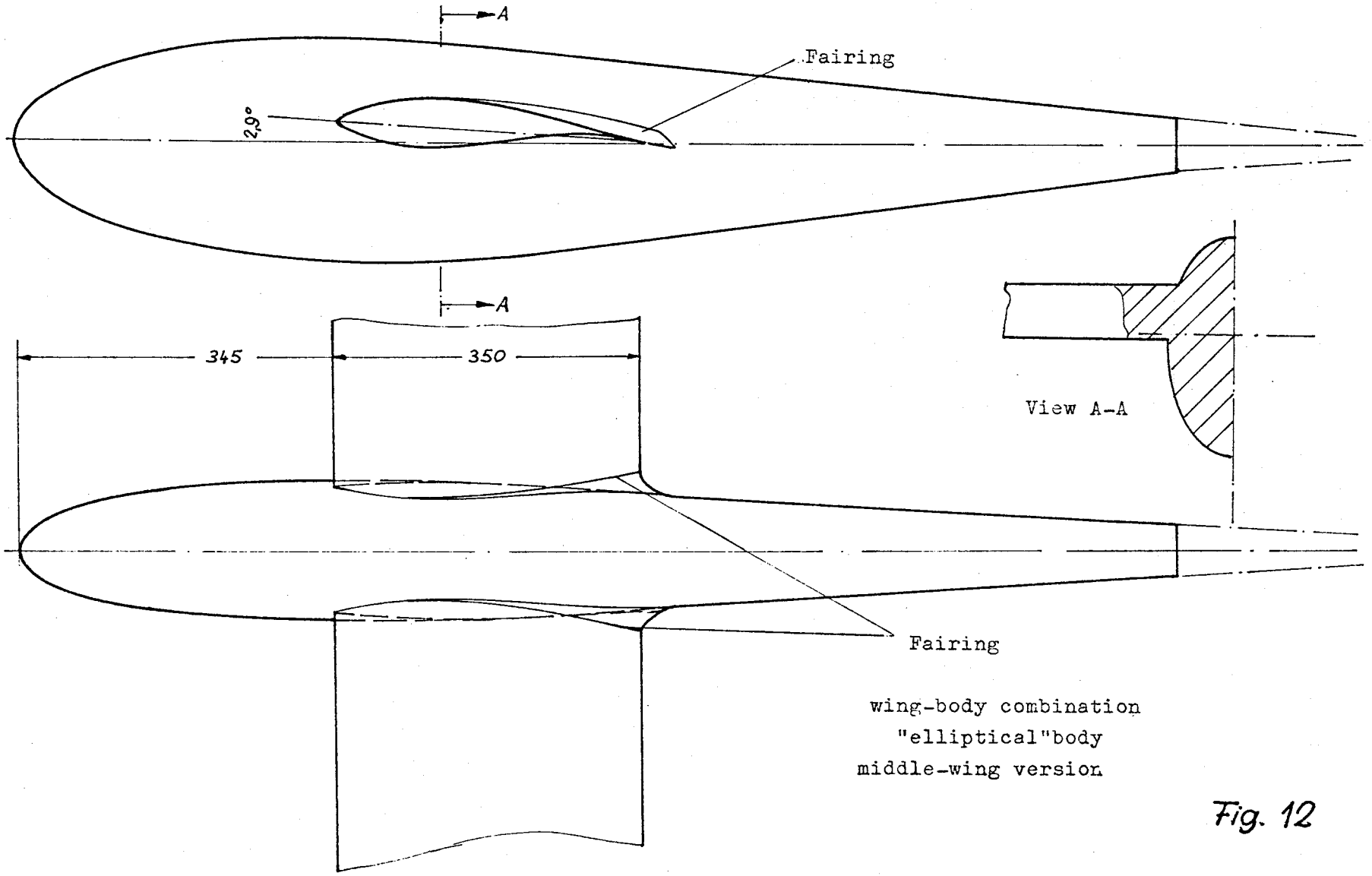


Fig. 11

wing-body combination
"elliptical" body high-wing version



wing-body combination
"elliptical"body
middle-wing version

Fig. 12

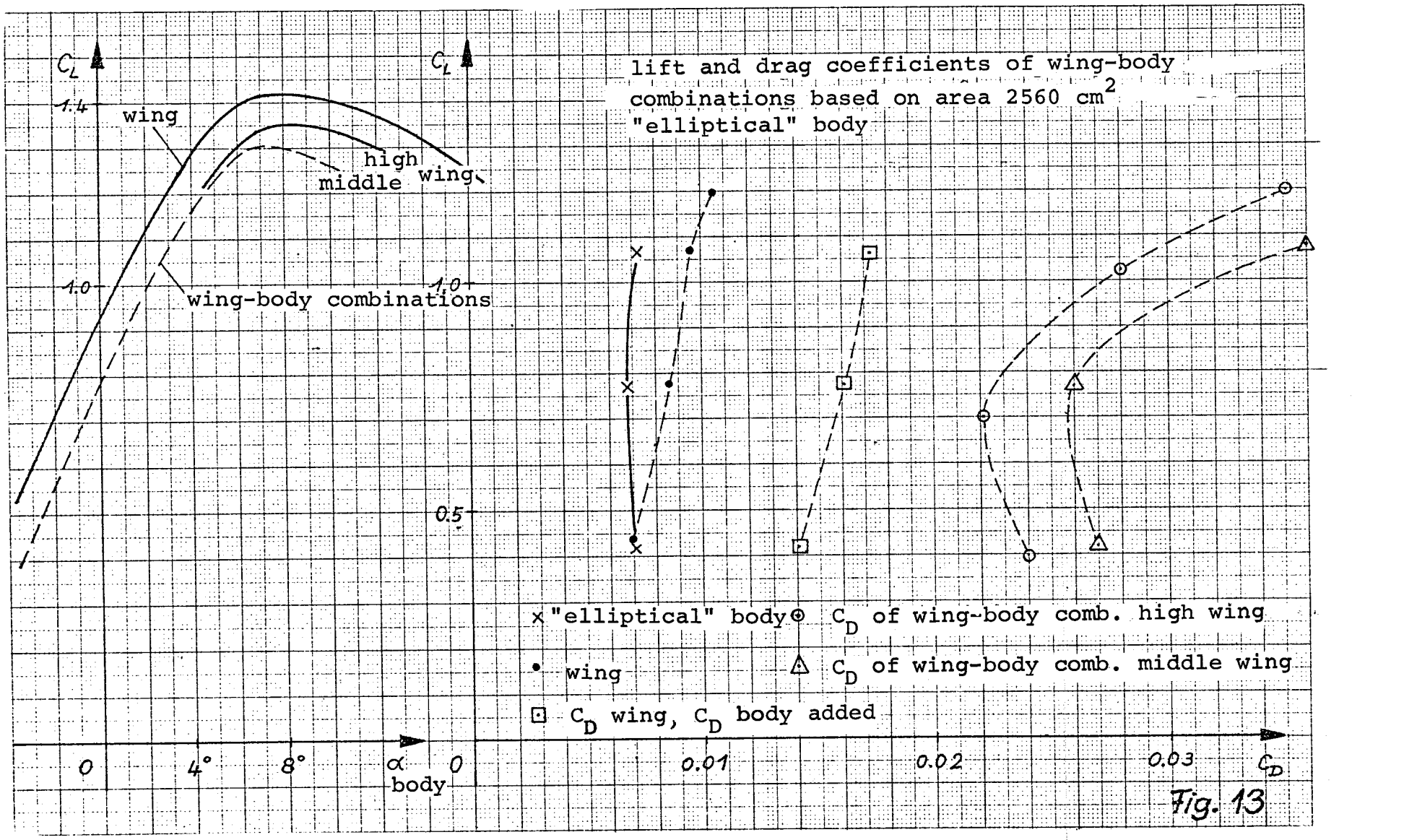

lift and drag coefficients of wing-body combinations based on area 2560 cm²
"elliptical" body
C_L
1.4
1.0
0.5
wing
high wing
middle wing
wing-body combinations
× "elliptical" body
⊙ C_D of wing-body comb. high wing
• wing
△ C_D of wing-body comb. middle wing
⊡ C_D wing, C_D body added
0
4°
8°
α body
0
0.01
0.02
0.03
C_D

Fig. 13

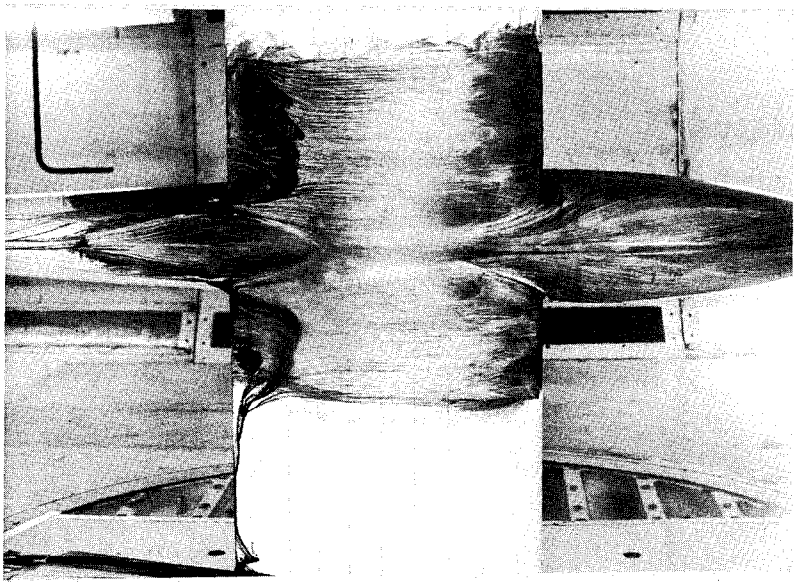


Fig. 14: Upper side of model with high wing position at $\alpha = +6°$ ($C_L = 1.3$)

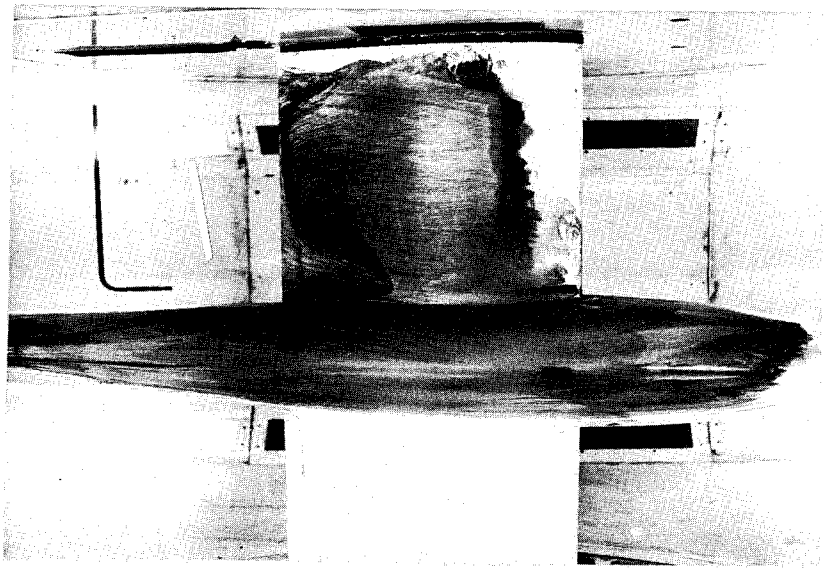


Fig. 15: Upper side of model with middle wing position at $\alpha = +5.5°$ ($C_L = 1.25$)

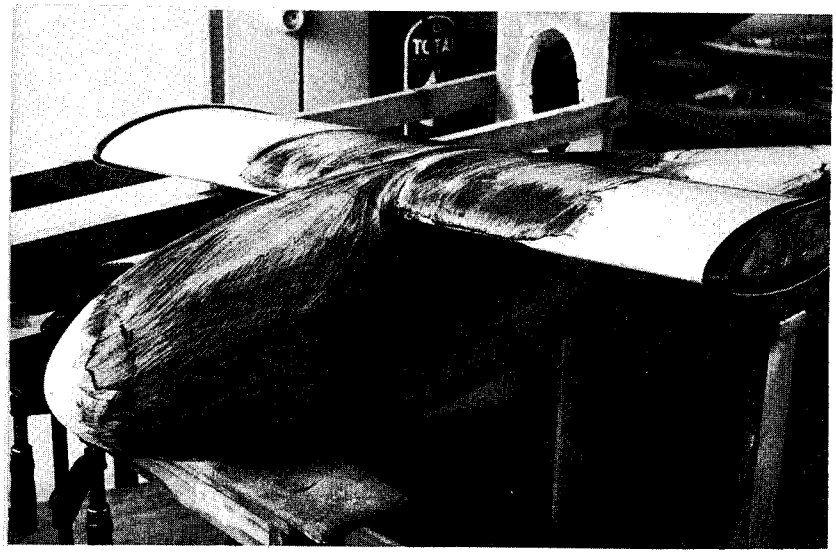


Fig. 16: Side view of model with high wing position at $\alpha = +6°$ ($C_L = 1.3$)

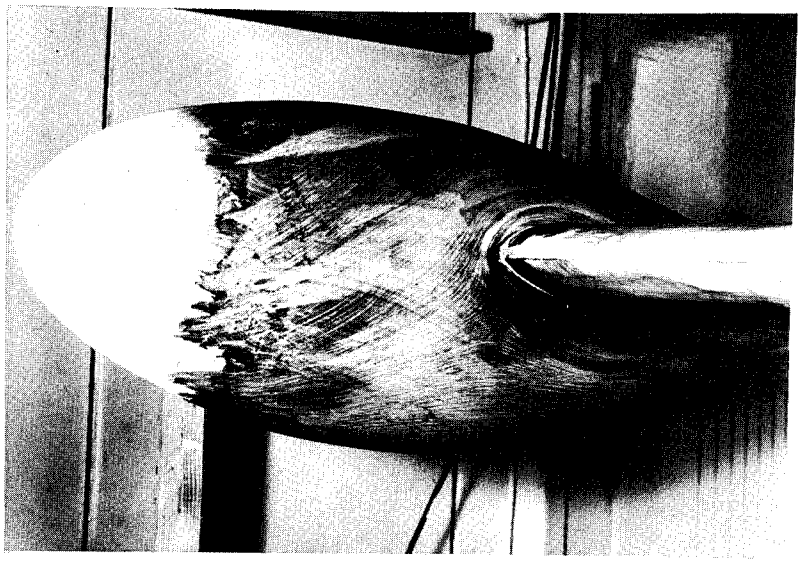


Fig. 17: Side view of model with middle wing position at $\alpha = + 5.5°$ ($C_L = 1.25$)

ration begins at nearly half chord of the wing and spreads in a wedgeshape over the wing. There is only a small distance between the two vortices and they seem to be more intense.

Figs. 16 and 17 show the corresponding side views of the two model configurations, demonstrating the streamline patterns on the front portions. The position of the stagnation points in relation to the wing leading edge is nearly the same on both models. The dividing streamline on the mid-wing model, however, originates much lower than with the high-wing version. In consequence, substantially more boundary-layer material of the forebody is swept over the endangered upper side of the wing-body junction than in the high-wing case. This is undoubtedly one reason for the better performance of the high-wing combination.

The measurements reported here give some rough ideas about the flow mechanism on bodies and wing-body combinations. Since the wing spans completely from wall to wall, the wing flow is mostly two-dimensional. For a better understanding of the complex flows, more, and more detailed measurements are required in this area.

I am indepted to Eberhard Schott and Klaus Fischer who built the models, assisted with the experiments, and did most of the evaluation work.

A CRITICAL REVIEW OF THE PHYSICAL ASPECTS OF AIRFOIL DESIGN AT LOW MACH NUMBERS

by

F.X. Wortmann
Institut für Aerodynamik u. Gasdynamik
der Universität Stuttgart

Introduction

In the first two decades of aviation, airfoils were simply copies of the patterns which Nature demonstrates in the variety of birds. Later on, with the advent of monoplanes, thicker airfoils were needed, and at this time man started a long and rarely interrupted quest after better airfoils for a large variety of purposes. This led to large and expensive experimental research activities in the third and fourth decades of our century. The accumulated experience resulted in airfoil catalogs from which users such as aircraft designers could make their choice. Today the state of the art is different: At the beginning a more or less well-defined set of desired airfoil performance parameters and the conditions under which these parameters should be attained are gathered. The airfoil designer must then find out what type of airfoil would meet these conditions best. Very often there are conflicting requirements, and it is not easy to ascertain the benefits of different compromises. Even the type of wing construction is one important part of the boundary conditions. Aircraft designers are sometimes not aware of the strong interactions between airfoil design and wing construction. It might be useful, therefore, to sketch some guidelines which enable the airfoil designer as well as the user to find better airfoils.

Friction drag

At low angles of attack and Mach numbers below the critical Mach number, the friction drag is the overriding factor in the profile drag. It is primarily the Reynolds number which characterizes the flow environment. In this paper the Reynolds number may vary between 0.4 and 40 million. At lower Reynolds numbers the airfoil flow is complicated by the increasing danger of separation and the higher Reynolds numbers are usually combined with critical Mach numbers.

Basic considerations

1. The first and most effective way to reduce friction is to avoid a turbulent boundary layer as long as possible. This is best illustrated by comparing the laminar and the turbulent boundary skin friction for a flat plate with different positions of transition. It can be seen from Fig. 1 that the drag is more influenced, relatively, when the Reynolds number is larger and/or when the transition point moves backwards. This picture can be translated into approximate airfoil drag by multiplying the flat-plate values by $1 + 2\delta$, where δ is the relative airfoil thickness.

The all-important position of transition is governed by two parameters: the stability of the laminar boundary layer and the perturbations introduced into the laminar boundary layer. The stability, in turn, depends on one hand on the Reynolds number, and on the other hand on the pressure gradient in the flow direction. At the upper end of the Reynolds number range mentioned above, the stability seems to fade out, whereas at the lower end it becomes difficult to overcome the stability and to provoke turbulence at just the right moment.

Perturbations are fed into the boundary layer by surface waviness and roughness. The latter may be caused by connecting skin steps, access openings, leakage, insects, erosion, or the turbulence of the free stream.

2. There is always an adverse pressure gradient on the aft part of airfoils, and since our present state of technology yields no hope for a complete laminarization by suction, we have to live with turbulent boundary layers. The second principle of drag reduction, therefore, takes care that the turbulent boundary layer develops in a favorable manner. Today it is very well known that a "concave" pressure or velocity distribution has advantages, and this has been applied to airfoils, very often successfully. Fig. 2 shows an early and typical example of how different velocity distributions influence the boundary layer thickness at the trailing edge [1]. The gain in drag reduction is of the same order of magnitude as the airfoil thickness and becomes more pronounced with increasing Reynolds number. However, some caution is necessary, because most airfoils have to work also under off-design conditions.

3. Between the laminar and the turbulent part of the boundary layer lies the transition region. Very often it is quite important to control this region carefully, and to avoid, if possible, laminar separation bubbles, which may spoil the initial conditions of the turbulent boundary layer. This is especially true when a concave pressure distribution follows the transition region [2]. The solution for the transition region lies in using a small region with a slightly adverse pressure gradient which destabilizes the laminar boundary layer without causing separation. This may be called the instability region.

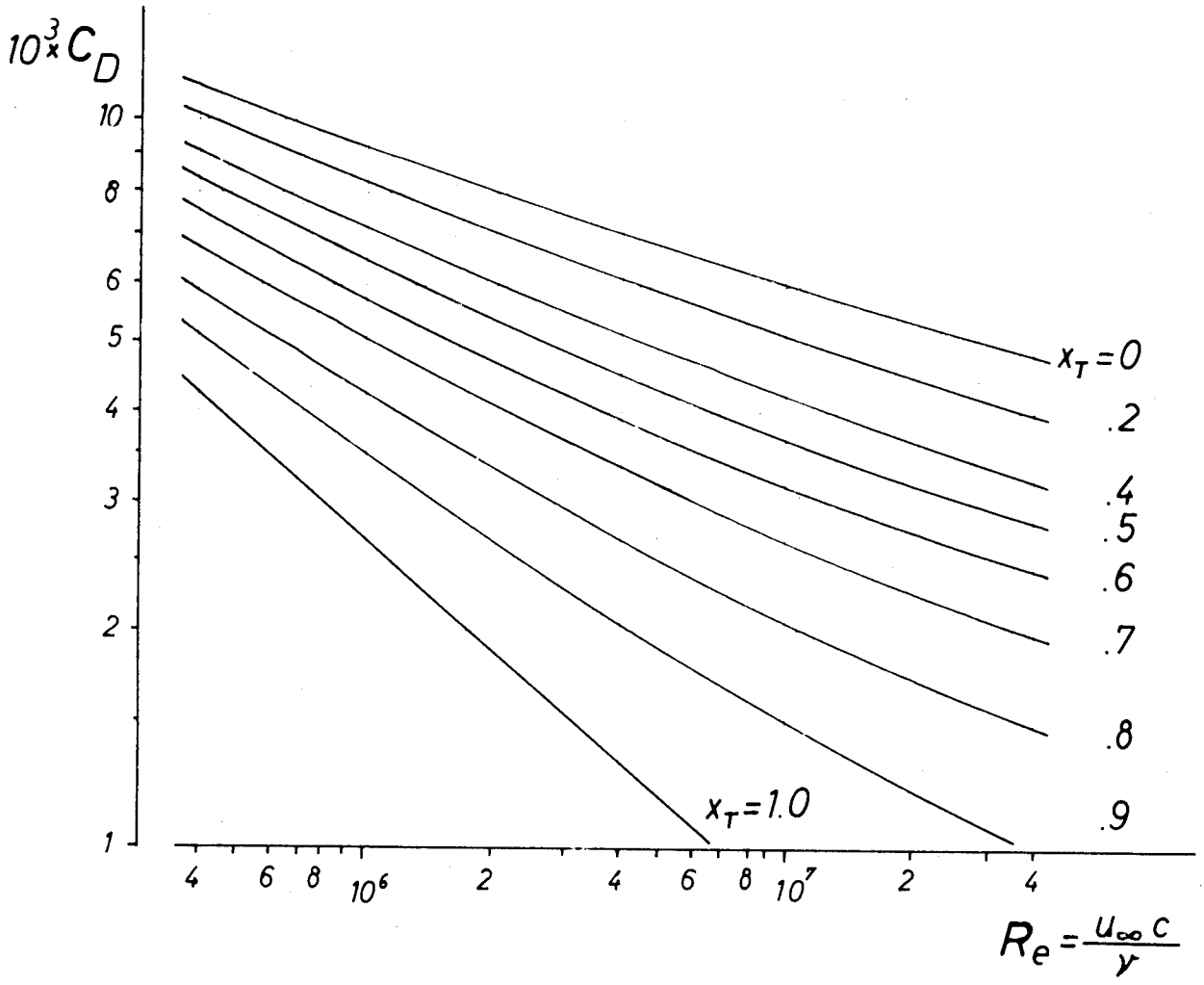


Fig. 1 Drag of a flat plate with different positions of transition

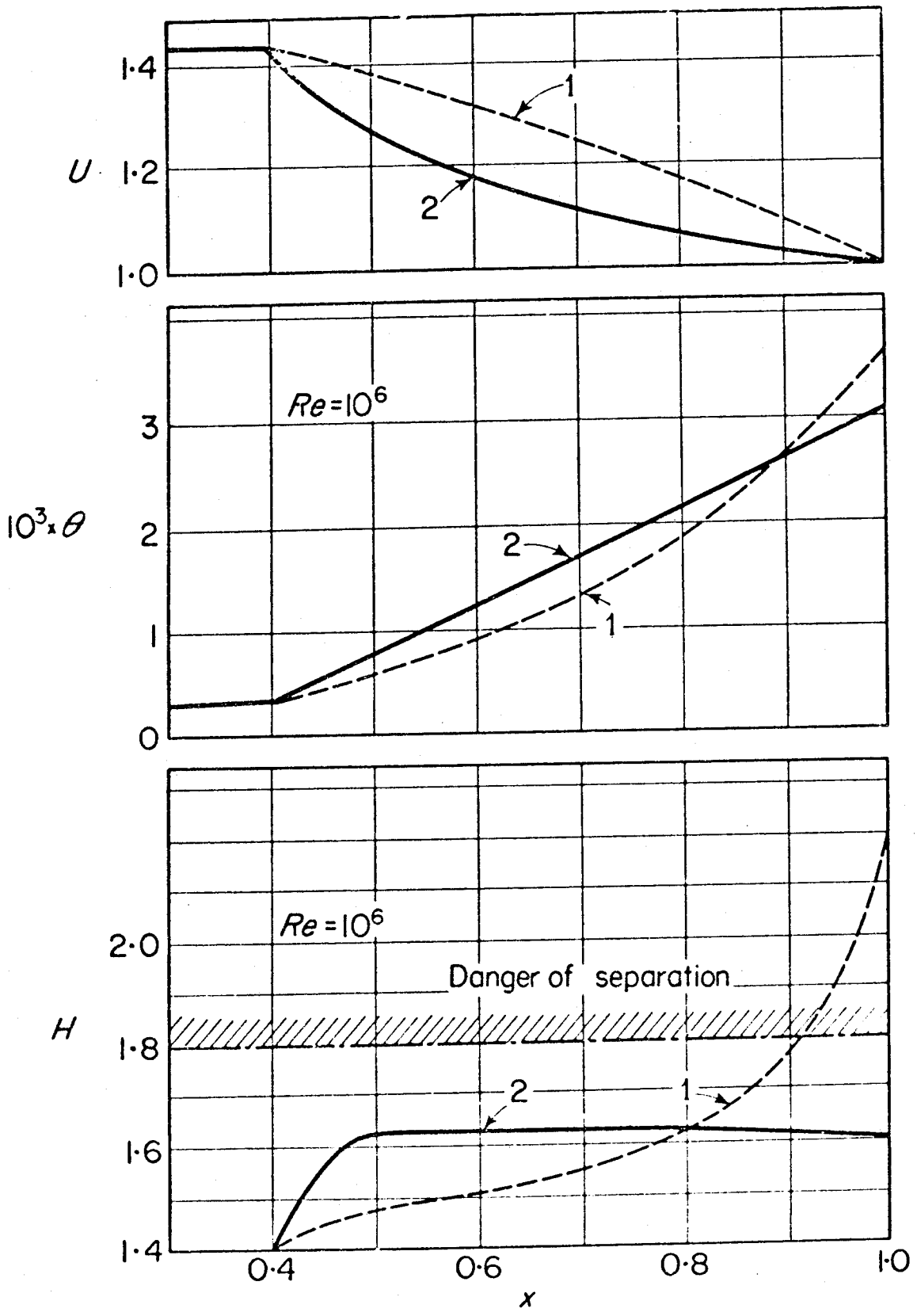


Fig. 2 Development of the turbulent boundary layer for two different velocity profiles.
θ = momentum thickness; H=shape parameter

With these three basic principles of boundary layer control in mind, let us take as an example the following simple design task: to find a symmetrical airfoil with the lowest drag at zero angle of attack for a certain given airfoil thickness and Reynolds number.

The symmetrical airfoil with zero angle of attack

As long as the surface curvature is small in proportion to the boundary layer thickness, the geometry of an airfoil has only a minor influence on the boundary layer development. This is then determined only by the pressure or velocity distribution. In such cases the form of the airfoil can be considered purely as the means for producing a certain velocity distribution. For symmetrical airfoils at small angles of attack this is very nearly true. Thus it is reasonable to start the quest with an educated guess for a velocity distribution. This, however, produces another problem since not every velocity distribution can be realized by a real airfoil. Obviously it is not possible to solve even this simple task directly. One has to rely on iterative steps.

Fig. 3 shows an example: let the Reynolds number be 4×10^6. The stability of the laminar boundary layer is just sufficient to guarantee a laminar state by using a constant velocity up to 50-60% of the chord. Behind this point an instability range of 5 to 10% chord length may be necessary to provoke transition and to develop a fully turbulent boundary layer. Downstream of the transition region the velocity has to decrease with stronger gradients in order to close the airfoil with reasonable trailing edge angles. This type of velocity distribution may be modified by shifting the transition region; say backwards. Under the constraint of a constant airfoil thickness, the supervelocity of the laminar part decreases slightly, and the velocity gradients in the turbulent part increases strongly. The longer laminar part reduces the friction drag, but this gain is very soon overbalanced by the pressure drag due to the faster growing turbulent boundary layer thickness. There exists for a certain Reynolds number a rather flat optimum for the position of the transition. This, in turn, depends on the prescribed airfoil thickness.

In Fig. 4 two velocity distributions for the same goal, minimum drag at zero angle of attack, are shown, but the design Reynolds number is ten times higher and lower than in Fig. 3. The differences are due mainly to different stability characteristics in the laminar part. At lower Reynolds number even a negative velocity gradient and an expanded transition region are necessary, whereas the opposite is true for the higher Reynolds number.

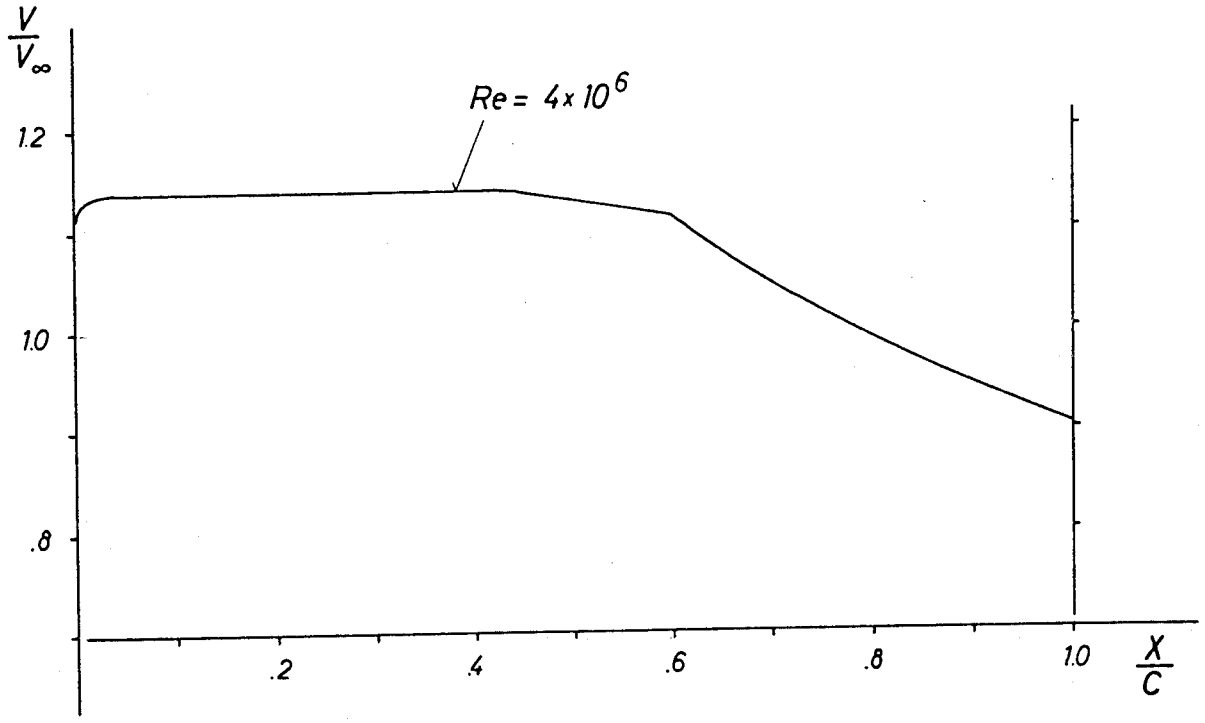


Fig. 3 Typical velocity distribution of a symmetrical airfoil optimized for minimum drag at Re = 4.10^6

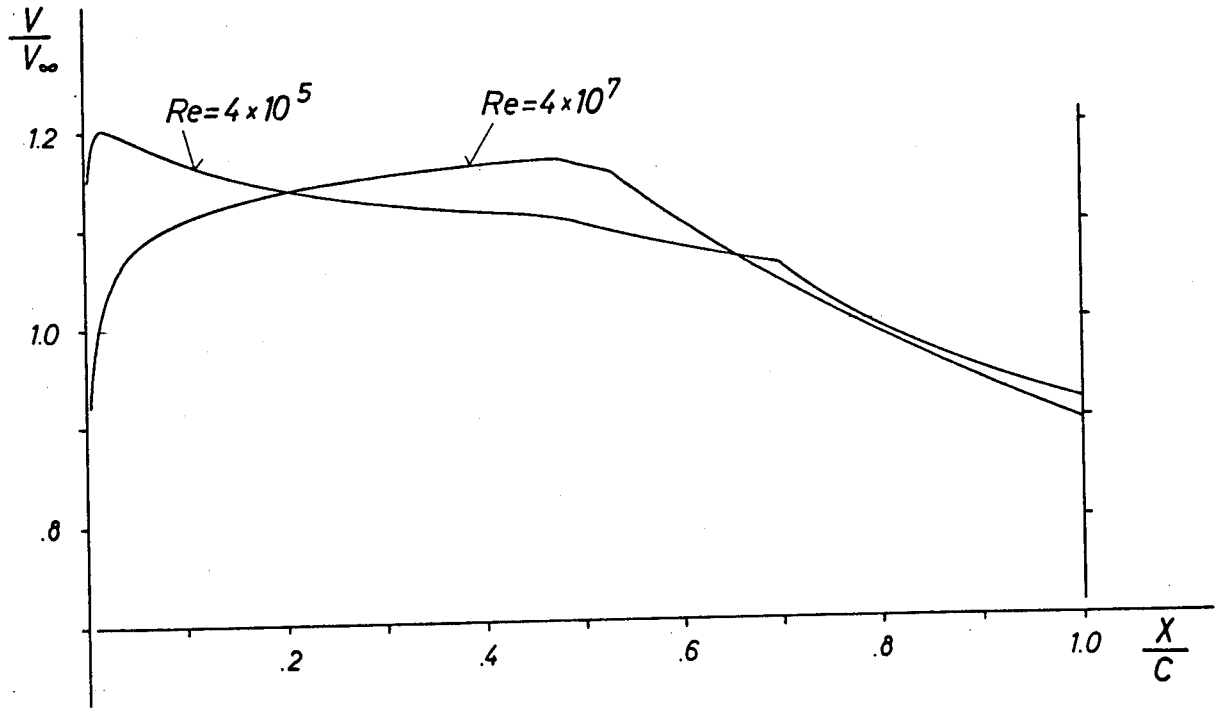


Fig. 4 Typical velocity distribution of two symmetrical airfoils optimized for minimum drag at Re = 4.10^5 and 4.10^7

Symmetrical airfoil with low drag bucket

For the airfoil of Fig. 3, any angle of attack induces in the nose region on one side a velocity peak with negative, and, on the other side, with positive velocity gradient. The latter stabilizes the laminar boundary layer more than necessary. On the other side transition jumps forward, causing a sharply increased drag. At that Reynolds number this airfoil has only a very small lift range with low drag. In order to produce more practical airfoils with low drag over a wider lift range, we have to superimpose a positive velocity gradient upon the distributions in Figs. 3 and 4, to counterbalance the effect of incidence. It follows that for a constant airfoil thickness, the maximum velocity goes up, as well as the velocity gradients in the turbulent part. A certain drag increase is unavoidable. The ability of the airfoil thickness to counteract the effects of incidence is restricted, and for larger low-drag ranges it is necessary to shift the transition region forward in order to produce stronger velocity gradients at zero angle of attack. This, in turn, increases the drag further. Fig. 5 gives an example of this relationship for airfoils with different drag buckets. The envelope in Fig. 5 is, to some extent, not even restricted to a certain airfoil thickness. It has a more general significance: Suppose that the velocity distributions are all carefully selected to meet the boundary layer principles given above as basic considerations; then for a single-element airfoil with rigid surfaces there seems to exist no further possibility of crossing the envelope in Fig. 5 to the left. In other words, this envelope seems to be an absolute boundary which cannot be improved.

Sometimes the lowest drag at one single Reynolds number is not the primary goal, but a low drag in a certain range of Reynolds numbers. Usually a reduced sensitivity to the Reynolds number influence can be achieved by a more extended instability range. Now the position of the transition can easily move fore and aft, and compensate partly for the adverse effects of Reynolds number on the friction coefficients.

Symmetrical airfoils with flaps

If an airfoil can be equipped with flaps, it has a variable camber, and this fact can be used to improve upon the lift-drag envelope of Fig. 5. Let us assume an airfoil with practically no low-drag range, as in Fig. 3. Basically, the deflected flap causes an aft loading, or higher and lower velocities in the region of the flap. For a particular incidence, similar velocity splits can be produced on the front part of the airfoil. Both the flap deflection and the incidence can act together in producing lift, without changing the type of velocity distribution and, therefore, the drag. In order to exploit the full benefits of this idea we have to remember that a flat plate with a kink at the flap hinge produces, at constant angle of attack, a velocity peak at

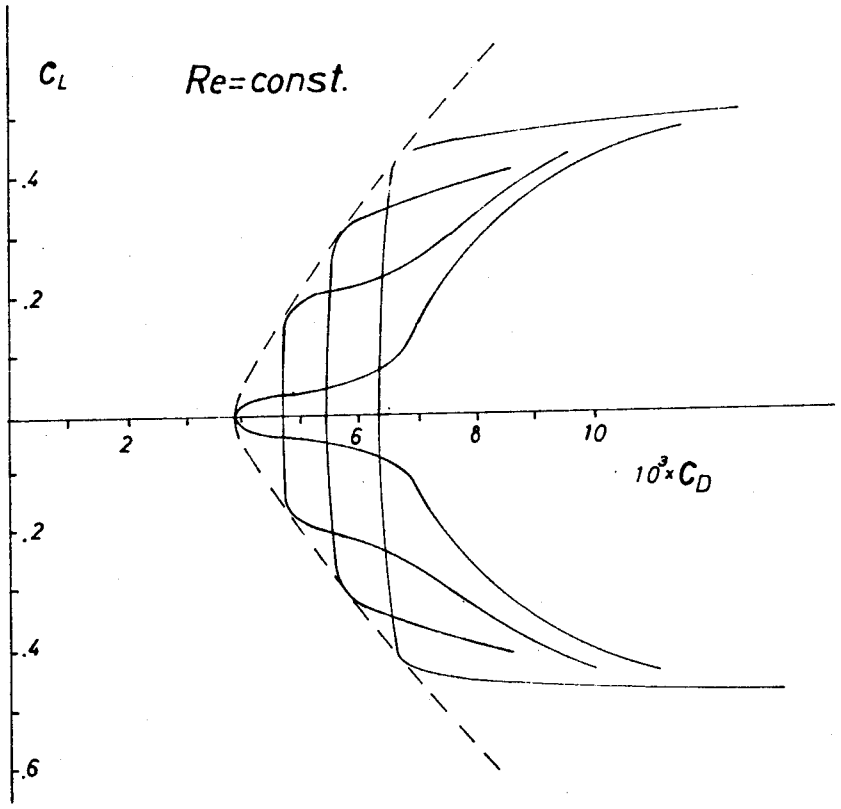


Fig. 5 Tyical lift-drag polars for different low drag ranges

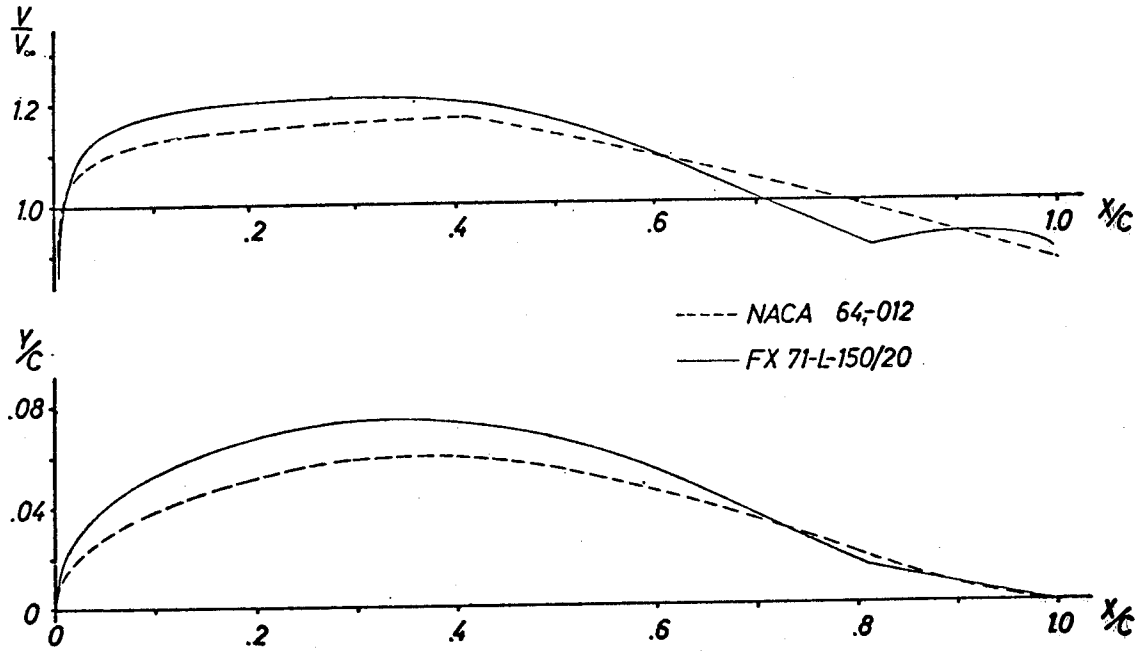


Fig. 6 Velocity and thickness distributions for two symmetrical airfoils

the leading edge and at the kink. To eliminate these unfavorable peaks we can use the thickness distribution. In terms of airfoil design this poses a mixed problem in which the flap deflection, i.e., a part of the airfoil geometry, is prescribed, and both the thickness distribution in front of the airfoil and the angle of attack are modified to produce the desired velocity distribution. Some experience with airfoils of 12-15% thickness shows that this problem has reasonable solutions for flap chords of 20 to 30% and prescribed flap angles of 8-12 degrees, yielding an additional low-drag C_L range of about $\pm$ 0.4. Fig. 6 shows an airfoil which was optimized, in this way for a flap deflection of 10 degrees. Fig. 7 illustrates the benefits of such advanced airfoils [3].

Airfoils with small camber and low-drag bucket

All considerations of symmetrical airfoils with and without flaps can be transferred to lifting airfoils as long as the average position of transition is similar. The simplest way to do this uses a constant velocity difference between lower and upper side which yields the well known NACA meanline with a = 1.0. However, this type of camber is not always the right solution. Small pitching moments require reduced aft loading and imply higher velocities on the upper side on the front part of the airfoil. The contrary is true when the critical Mach number is to be increased. Fig. 8 shows a systematic variation of lift distribution [2].

With increasing camber, especially when thicker airfoils are cambered, the assumption of a boundary layer which is only controlled by the velocity distribution no longer holds. The geometry of the airfoil becomes equally important. For the turbulent boundary layer, the surface curvature influences the development more and more. In other words, now both the geometry *and* the velocity distribution must be coupled when considering the boundary layer development. The physical reason is quite clear: in a curved potential flow, pressure and centrifugal forces perpendicular to the streamlines are in perfect equilibrium. In the boundary layer flow, the centrifugal forces fade out towards the wall, and the flow becomes dynamically stratified, stable on a convex wall and unstable on a concave wall. On the upper side of a cambered airfoil, the turbulence has to work against the stable stratification, the momentum exchange is reduced and the separation moves forward. Unfortunately, there seems to be no boundary layer calculation method which takes these well-known effects into account adequately, and no generally valid statements on favorable combinations of velocity and airfoil form can be made at this time.

Hence, in contrast to the low-cambered airfoils, there is some freedom to speculate as to how the highest lift at low drag may be realized. Some experience seems to indicate

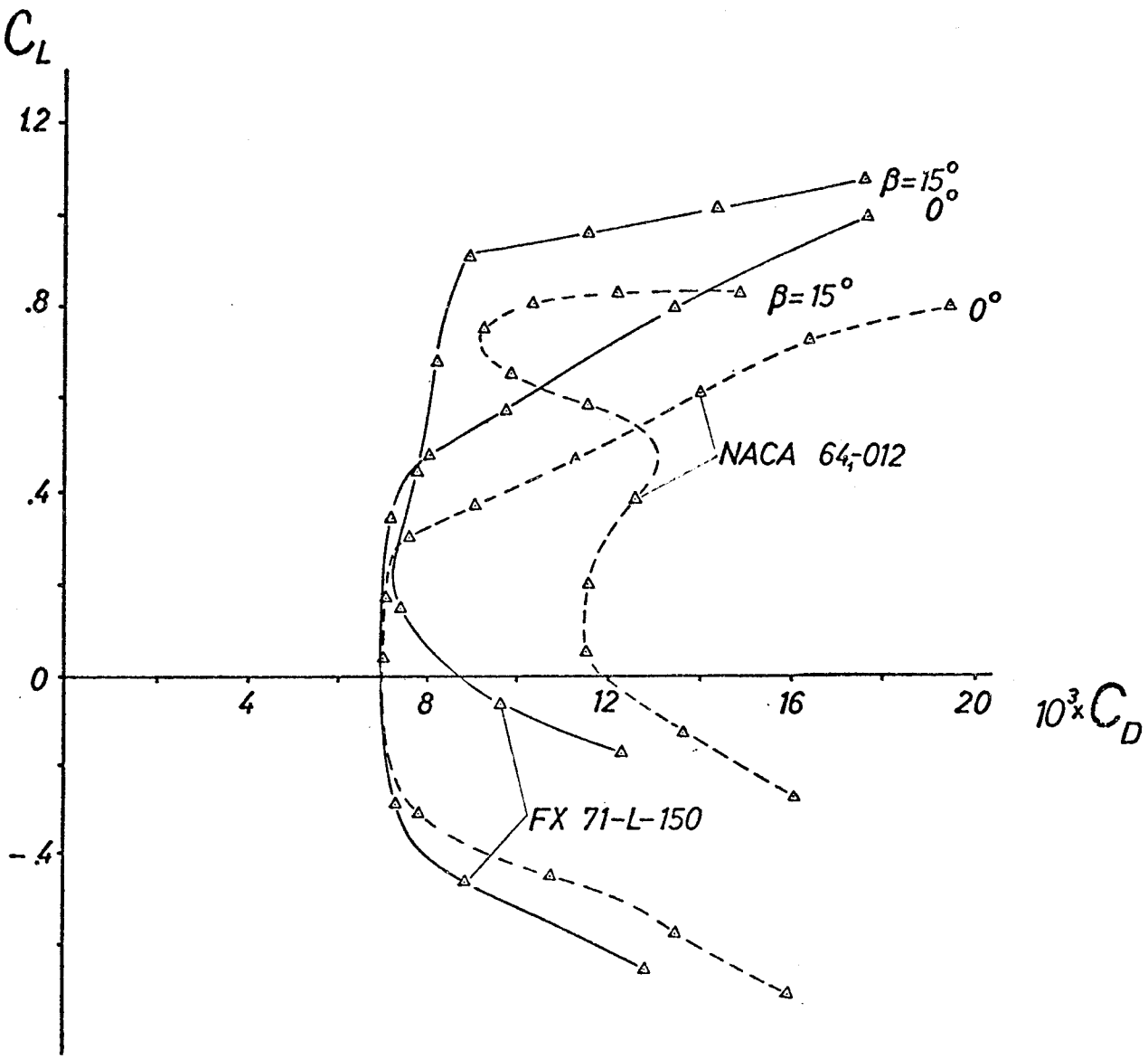


Fig. 7 Comparison of an NACA and an optimized airfoil for two flap settings Re = 1.10^6

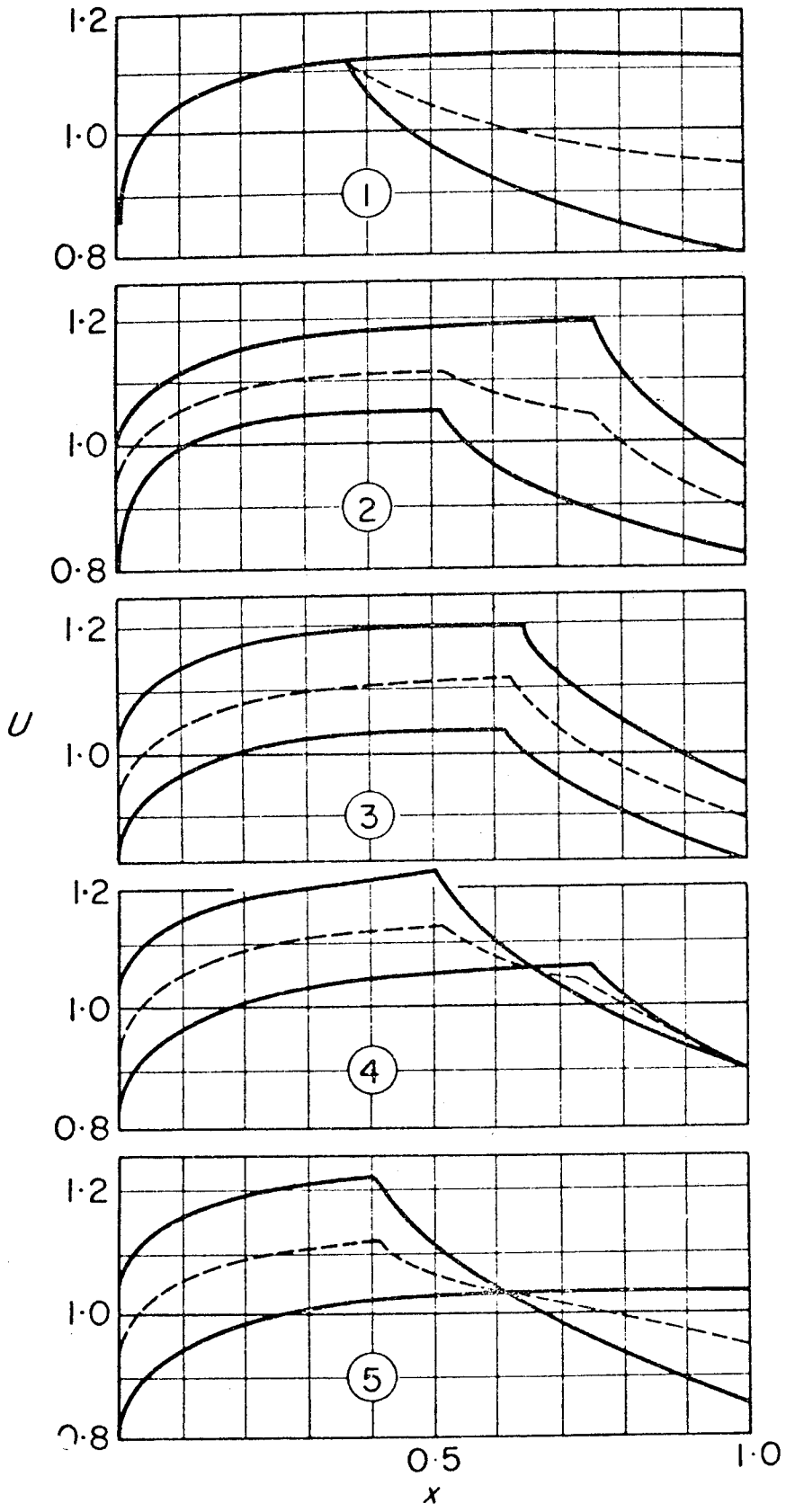


Fig. 8 Systematic variation of the lift distribution for five sample designs

that an unseparated flow is not possible when the camber of the upper airfoil surface itself exceeds 15-17%. If this rough guess is accepted it is clear that a thinner airfoil can produce more lift than a thicker one with the same upper surface.

A good example for a highly cambered airfoil with low-drag is shown in Fig. 9. This airfoil is the extended version of the variable geometry airfoil designed for the British project "Sigma" [4]. The maximum glide ratio goes to 160 at $C_L = 1.7$ and $Re = 1.5 \times 10^6$. On the upper side, the transition occurs between 40-50%. Behind the transition region the curvature soon disappears as the thickness of the turbulent boundary layer increases. The design technique for such an airfoil is quite similar to the case of an airfoil with a prescribed deflected flap mentioned above [5]. However, in this case and even more in the following sections, the feed-back of the thick boundary layer on the pressure distribution has to be included in the iterative design process.

In the context of higher cambered airfoils, there exists another interesting feature: in potential flow a camberline can easily produce a lift loading up to the trailing edge, shifting the necessary pressure recovery into the free stream behind the trailing edge. However, in reality the boundary layer changes the "fluid" camberline, and the adverse pressure gradients are shifted forward of the trailing edge. This may cause a separation which in turn modifies the fluid camberline even more. This is another example where the feed-back of the boundary layer on the pressure distribution has to be considered seriously.

For fixed wing aircraft different C_L values of the wing are coupled with different Reynolds numbers. Therefore the design of the lower and upper airfoil surface should take into account the different curvature as well as the different Reynolds number.

Maximum lift

For low drag airfoils which are optimized so as to yield the widest possible low-drag bucket, the maximum lift is clearly an "off design" condition. However, when the low-drag range requirement is relieved, some freedom is gained to include in the design considerations some high lift control also.

For low-cambered airfoils at higher angles of attack, the nose form plays an important rôle in the development of the upper side boundary layer. Usually the situation in the first few percent of the noselength is characterized by high velocity peaks followed by a deep slope which separates the laminar flow and spoils the initial conditions of the turbulent boundary layer by the laminar separation bubble. Now ideas similar to those in the low-drag case can be applied at high angles of attack: due to the low local

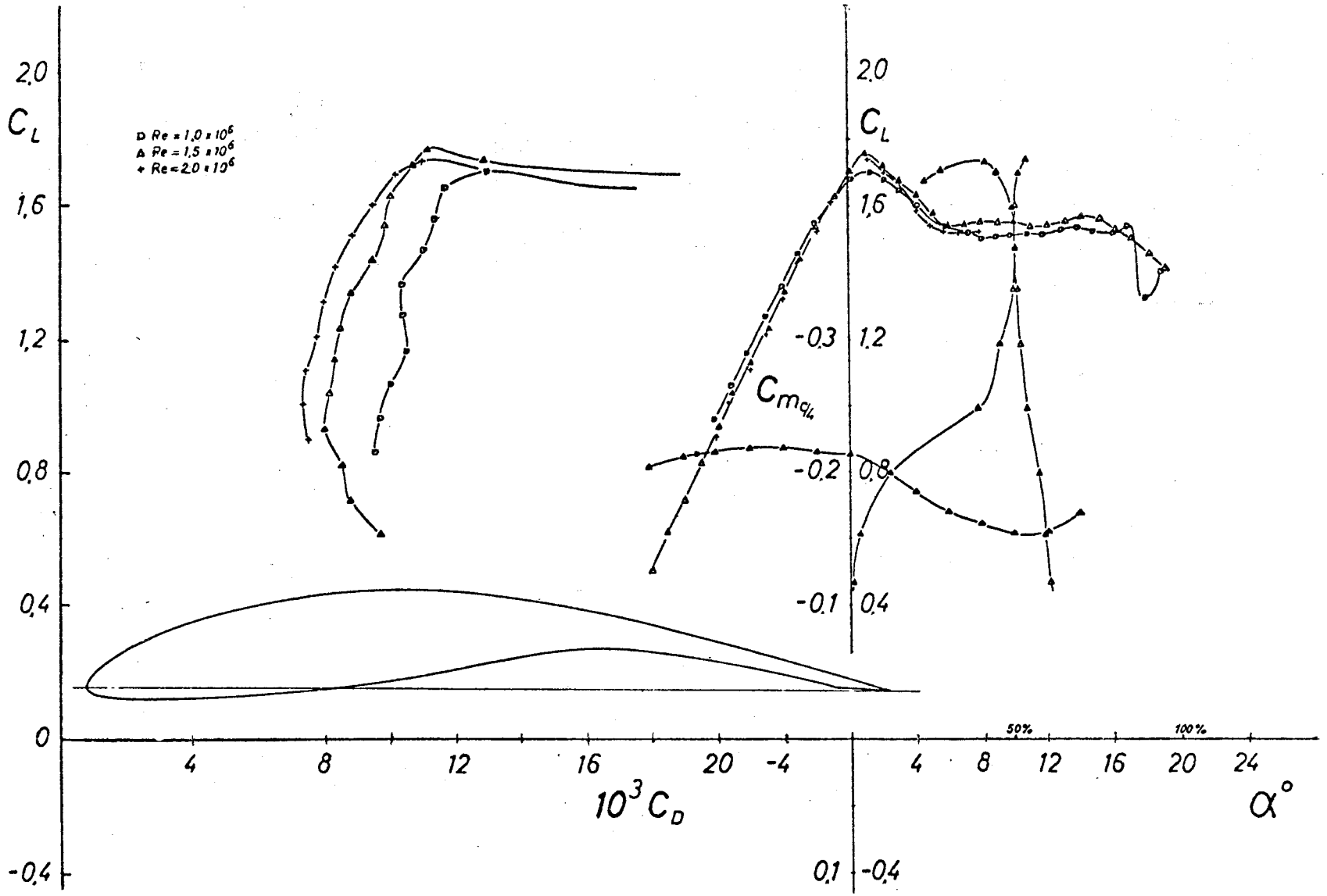


Fig. 9 Lift-drag polars, $C_L(\alpha)$, $C_m(\alpha)$ and $\frac{x_t}{c}$ of the extended version of the FX 67-VG-170/136 airfoil

Reynolds numbers, the thin laminar boundary layer is quite stable and needs a pronounced instability range to provoke turbulence, ideally without any separation bubble. There is, however, some experimental evidence that it is not necessary to suppress the separation bubble completely. The effect is nearly the same when the bubble stays very thin. The velocity distribution downstream of the transition region is clearly a concave one, and it is well-known that the associated turbulent boundary layer reacts very favorably to improved initial conditions.

Such a boundary layer control which is restricted to the first 5-10% of the chord length can help to increase the maximum lift. Figs. 10 and 11 provide an extreme example, where these ideas have been applied to a symmetrical airfoil regardless of low-drag considerations at low angles of attack [6].

Stall

Very often it is not the maximum lift which is of primary interest but the behavior of the airfoil at and beyond the maximum lift, i.e., in the partly or completely stalled region. A properly designed airfoil should at least avoid the dangerous "leading edge stall". This is not too difficult, and even a mild form of boundary layer control as shown in Fig. 10 will change the type of stall into a "trailing edge stall".

Sometimes airfoil users want a $C_L(\alpha)$ curve which reaches a maximum and stays there. We can understand the trailing edge stall as the result of two counteracting effects: the increasing angle of attack should raise, and the growing separation will lower, the circulation. If both effects cancel each other, a constant C_{Lmax} will occur. Obviously there are three important parameters: the change of position of transition, and of separation, and the size of the separated region or the separation angle. For an airfoil whose upper side is configured so as to give a maximum low-drag range, the transition point jumps forward too fast and the C_L beyond the C_{Lmax} decreases. If the upper edge of the low-drag range is allowed to round off, the movement of velocity peaks and hence the transition can be slowed down. This is also approximately true for the separation of the turbulent boundary layer. Thus C_L may be unchanged during the stall.

The advantage of such an arrangement is that not only is the lift curve smoother, but also the drag increase is far less severe than with the "squeezed-out" type of airfoil. A typical example of such behavior is given in Fig. 12 [7].

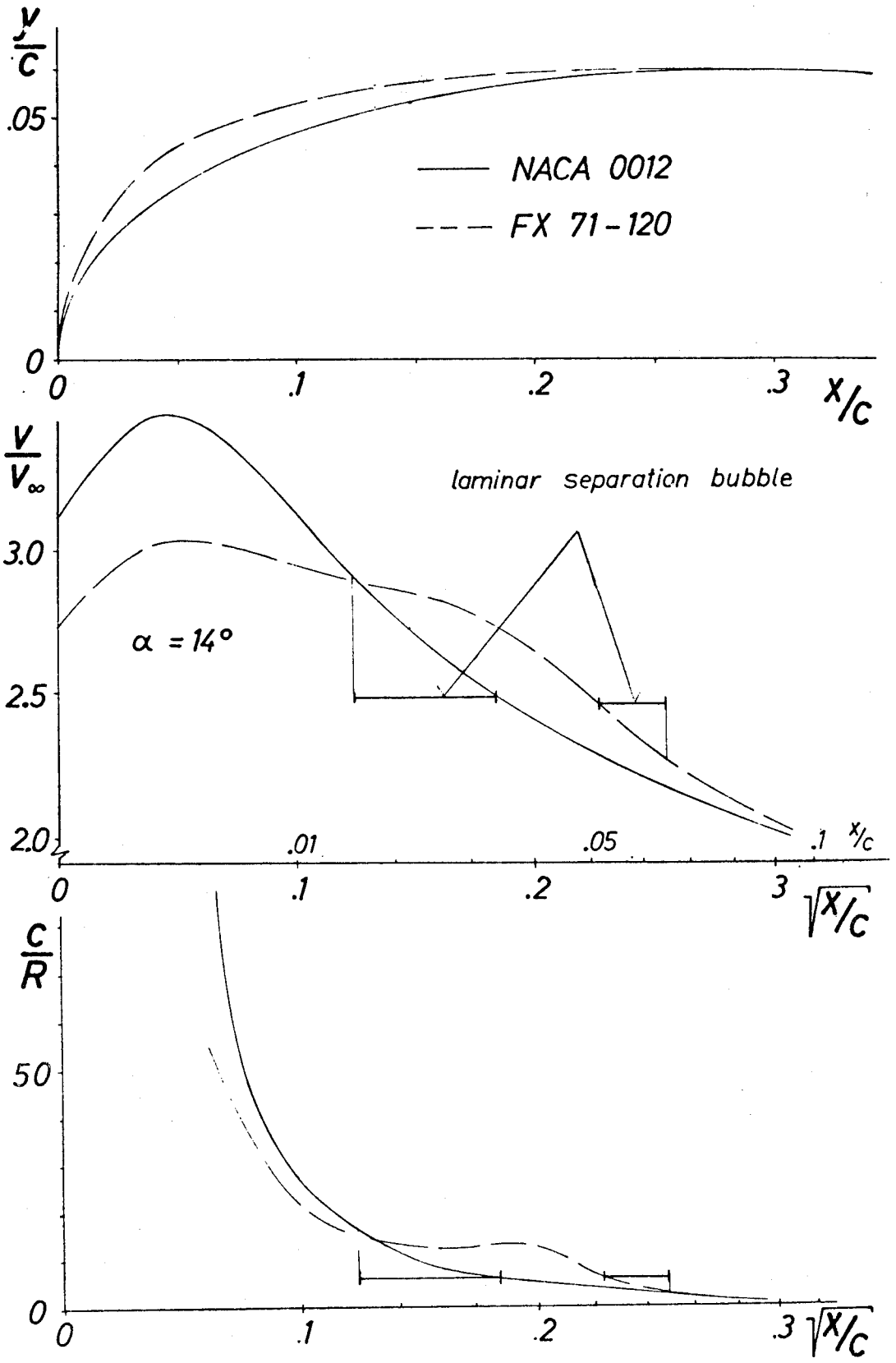


Fig. 10 Characteristics of the FX 71-120 airfoil compared with the NACA 0012 airfoil near maximum lift

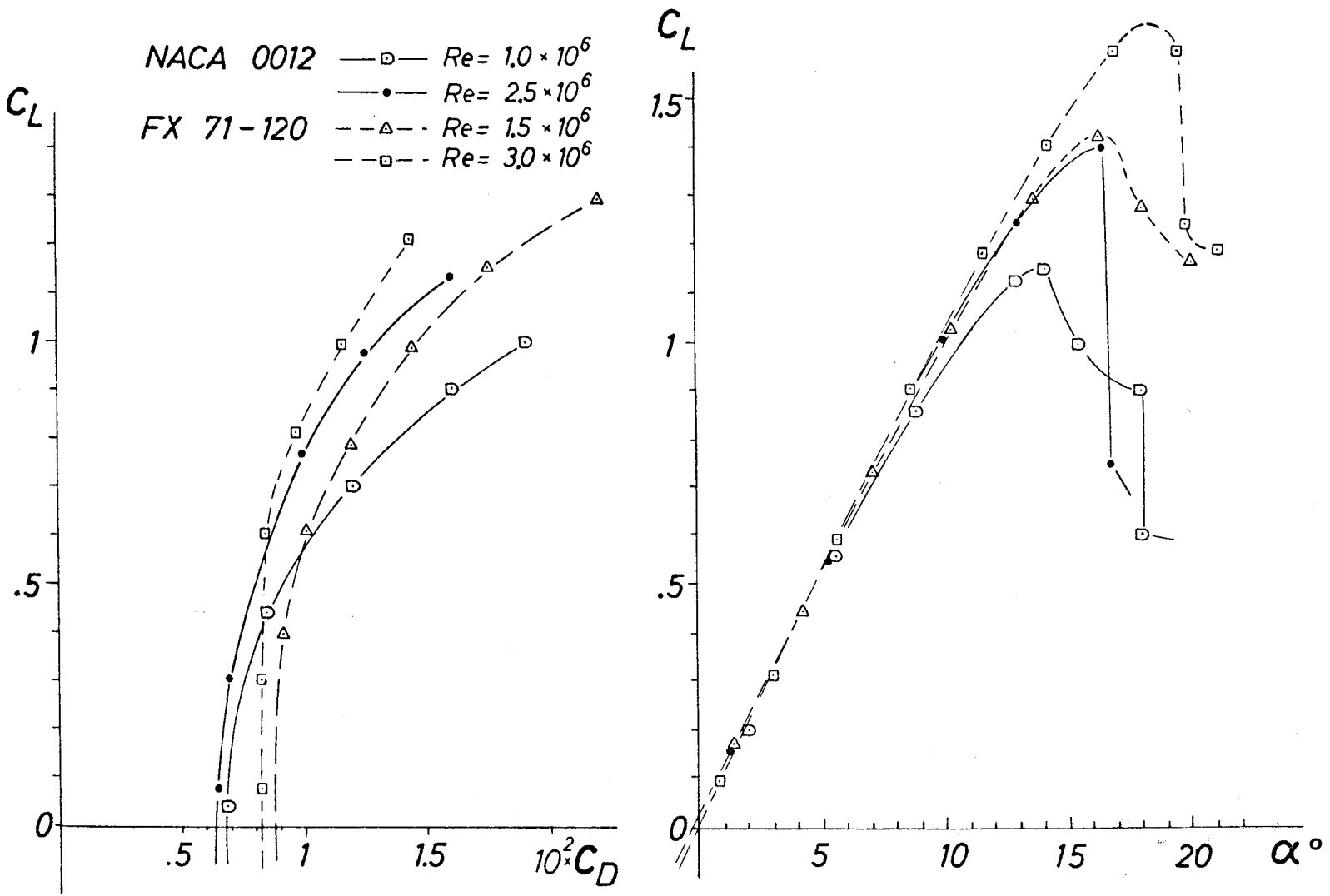


Fig. 11 Lift-drag polars of the NACA 0012 and the FX 71-120 for Reynolds numbers between 1.10^6 and 3.10^6

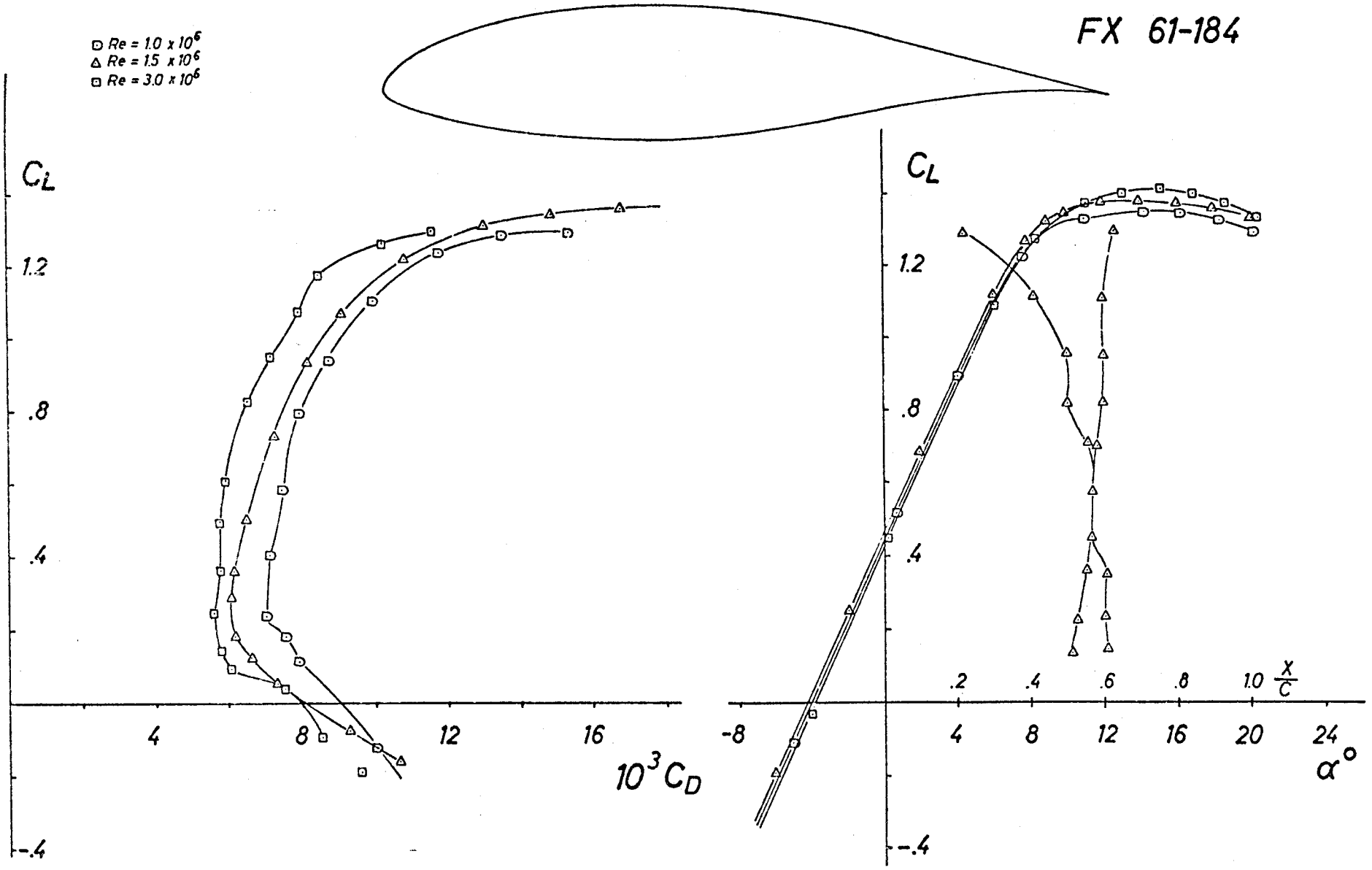


Fig. 12 An airfoil with constant C_L at stall

Conclusion

Airfoil design is always a matter of more or less direct boundary layer control. To accomplish this goal we obviously need airfoil and boundary layer theory, the availability of computers and programs, and, finally, a suitable wind tunnel, as tools.

It has been the purpose of this paper to show that another quality is equally indispensable: imagination which enables one to carve out of the physical aspects of the problem an advanced airfoil. However, the physical aspects are transparent enough to state that we cannot expect a breakthrough. This is especially true for the low-cambered, low angle of attack airfoil. Any advances are slow and hard to achieve as one approaches the physical limits. There exist, however, numerous details in the "airfoil and boundary layer" field where our present knowledge is open to further refinements, and this raises the hope that further advanced airfoil design may also be possible in the future.

References

1. Wortmann,F.X.; Ein Beitrag zum Entwurf von Laminarprofilen für Segelflugzeuge und Hubschrauber, Zeitschrift f. Flugwiss. 3 , pp. 333-345, 1955.

2. Wortmann, F.X.; Progress in the Design of Low-Drag Airfoils, G.V. Lachmann, Boundary Layer and Flow Control, London 1961, pp. 748-770.

3. Wortmann, F.X.; Symmetrical Airfoils Optimized for Small Flap Deflection, OSTIV-Congress 1972, Vrsac/ Yugoslavia .

4. Wortmann, F.X.; Airfoils for the Variable Geometry Concept, OSTIV-Congres 1970, Alpine/Texas. Schweizer Aero-Revue 46 , pp.303-305, 1971.

5. Wortmann, F.X.; Zur Optimierung von Klappenprofilen, Schweizer Aero-Revue 44, 1969 , pp. 89-92 or OSTIV-Publ. IX, or Soaring 34, 1970.

6. Wortmann, F.X.; Design of Airfoils With High Lift at Low and Medium Subsonic Mach Numbers, AGARD CL 102 1972, Lisbon.

7. Althaus, D.; Stuttgarter Profilkatalog I, Publ. by Inst. für Aero-u Gasdynamik, der U. Stuttgart, 1972.

AIRFOILS WITH HIGH LIFT/DRAG RATIO AT A REYNOLDS NUMBER OF ABOUT ONE MILLION

by

F.X. Wortmann
Institut für Aerodynamik u. Gasdynamik
der Universität Stuttgart

Introduction

There seems to be a growing interest in a special type of aircraft which can stay in the air with the lowest expenditure of energy, i.e., at the lowest possible sinking speed. Obviously such aircraft need airfoils with high lift to drag ratios. To be more exact, it is the ratio $C_L^{1.5}/C_D$ which should attain the highest possible value. In the following, two airfoils are described which, as a first approach, fill the gap of suitable airfoil data.

Design considerations

Before designing such airfoils some brief remarks may be necessary. In the ratio $C_L^{1.5}/C_D$ the lift has more weight than the drag. Therefore the desired airfoil will have in all cases an unusually high degree of camber. On the other hand, when the aircraft has to "float" only on straight courses or wide circles, the optimum aspect ratio will also be high and structural strength and stiffness call for a thick airfoil. In an earlier paper [1] it was mentioned that the combination "thick *and* cambered" poses a serious difficulty for the boundary layer on the upper side. The situation is aggravated by the low Reynolds numbers anticipated for such a slow and/or high-flying machine.

In order to reduce the risk, two airfoils with a medium thickness of 15% were designed which differ only in the degree of camber. Fig. 1 shows the geometry of the two airfoils, A with 8.3% and B with 9.7% camber. See also Table 1.

Test data

The experimental results are shown in Figs. 2 and 3*. It can be seen that both airfoils have maximum L/D ratios of about 160 at high C_L values. The sinking speed ratio

* These measurements were performed by D. Althaus.

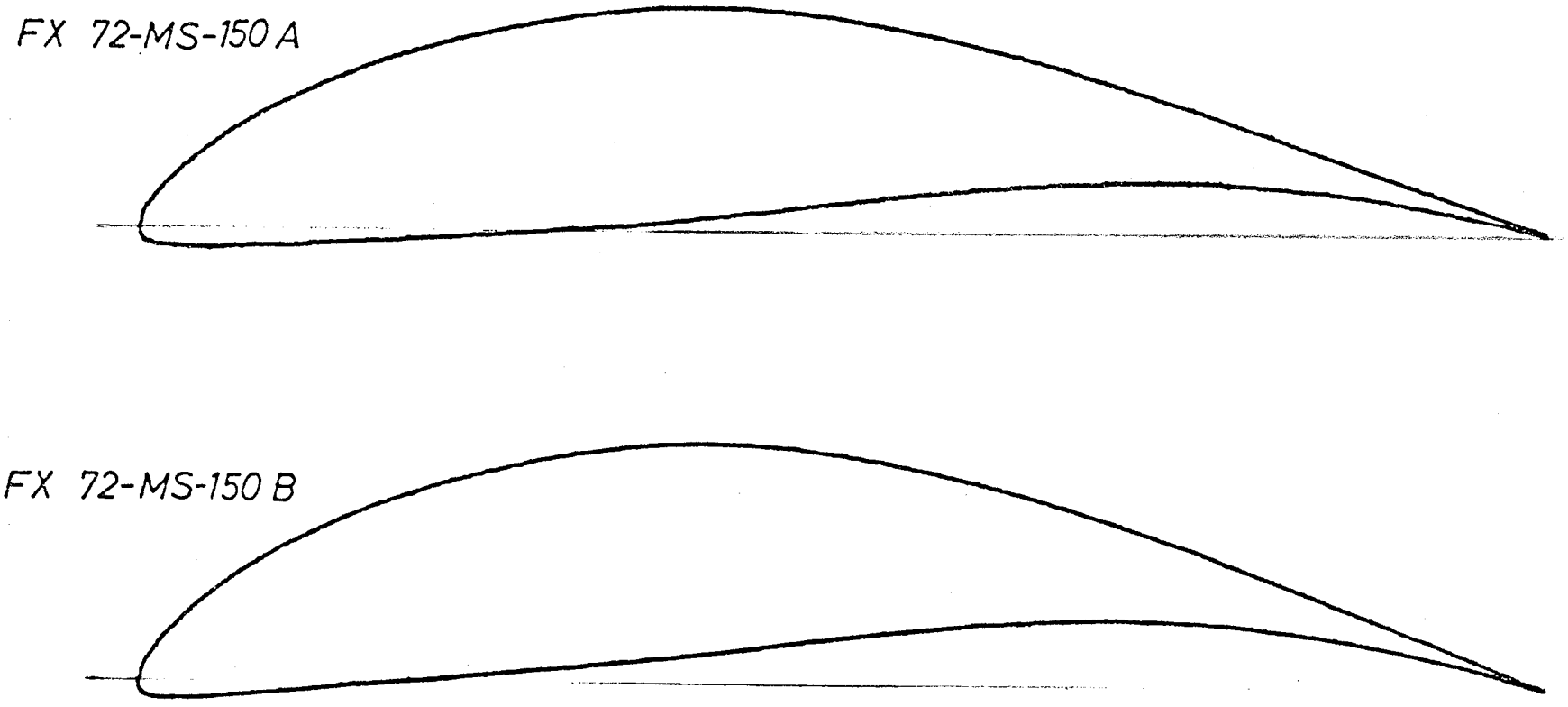


Fig. 1 Two airfoils for low sinking speeds

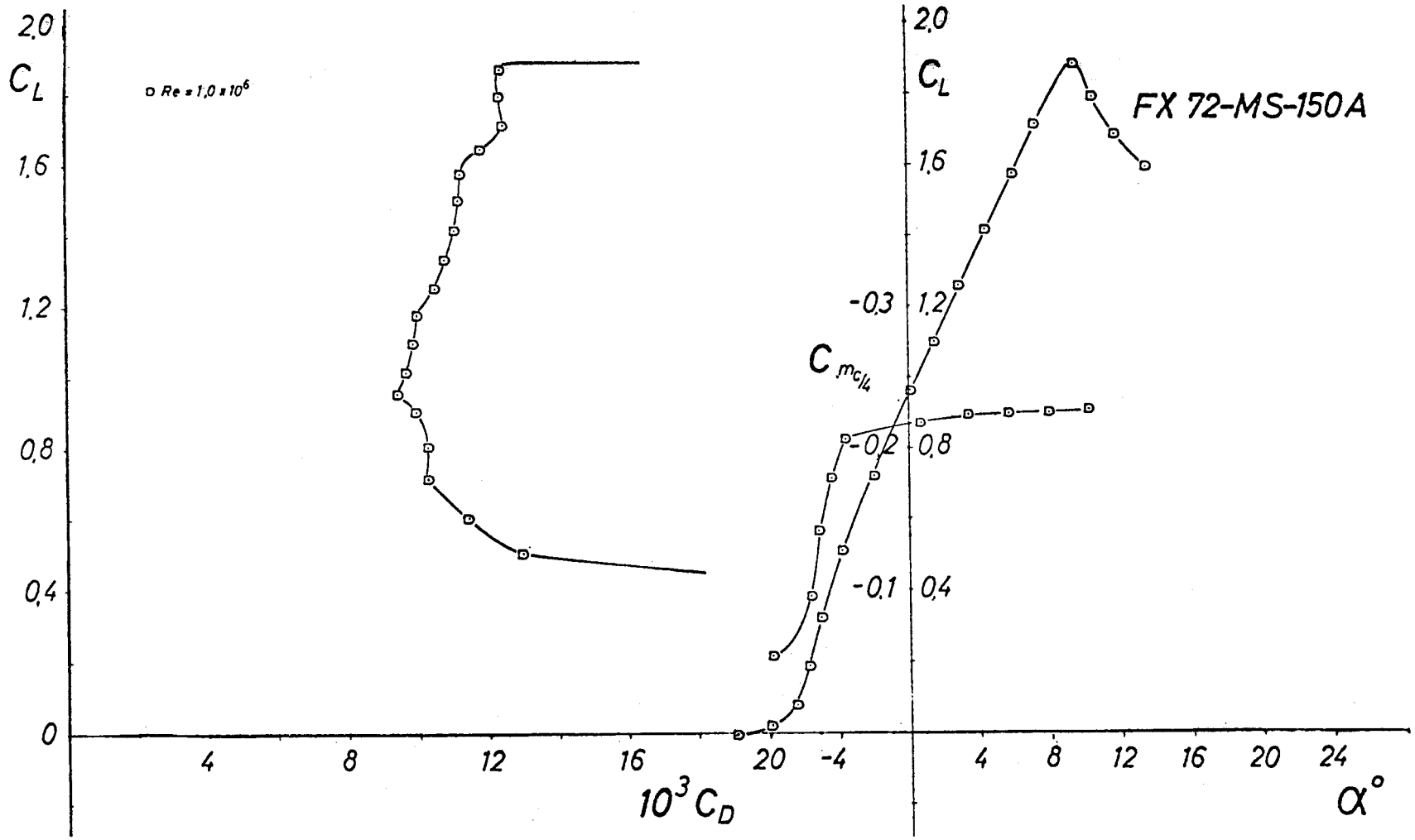


Fig. 2 Lift drag polars and pitching moments at Re = 10^6 for the FX 72-MS-150A

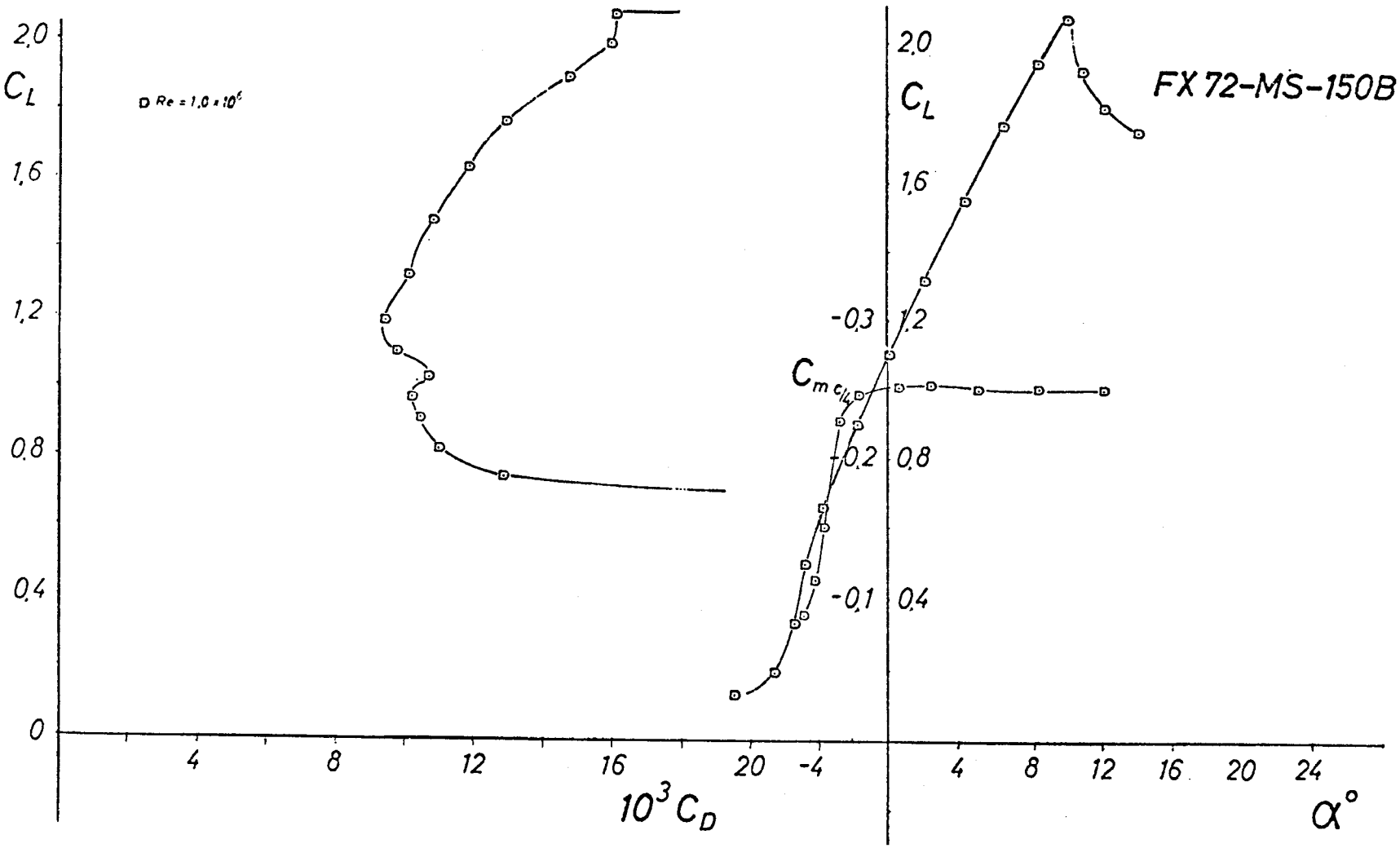


Fig. 3 Lift drag polars and pitching moments at Re = 10^6 for the FX 72-MS-150B

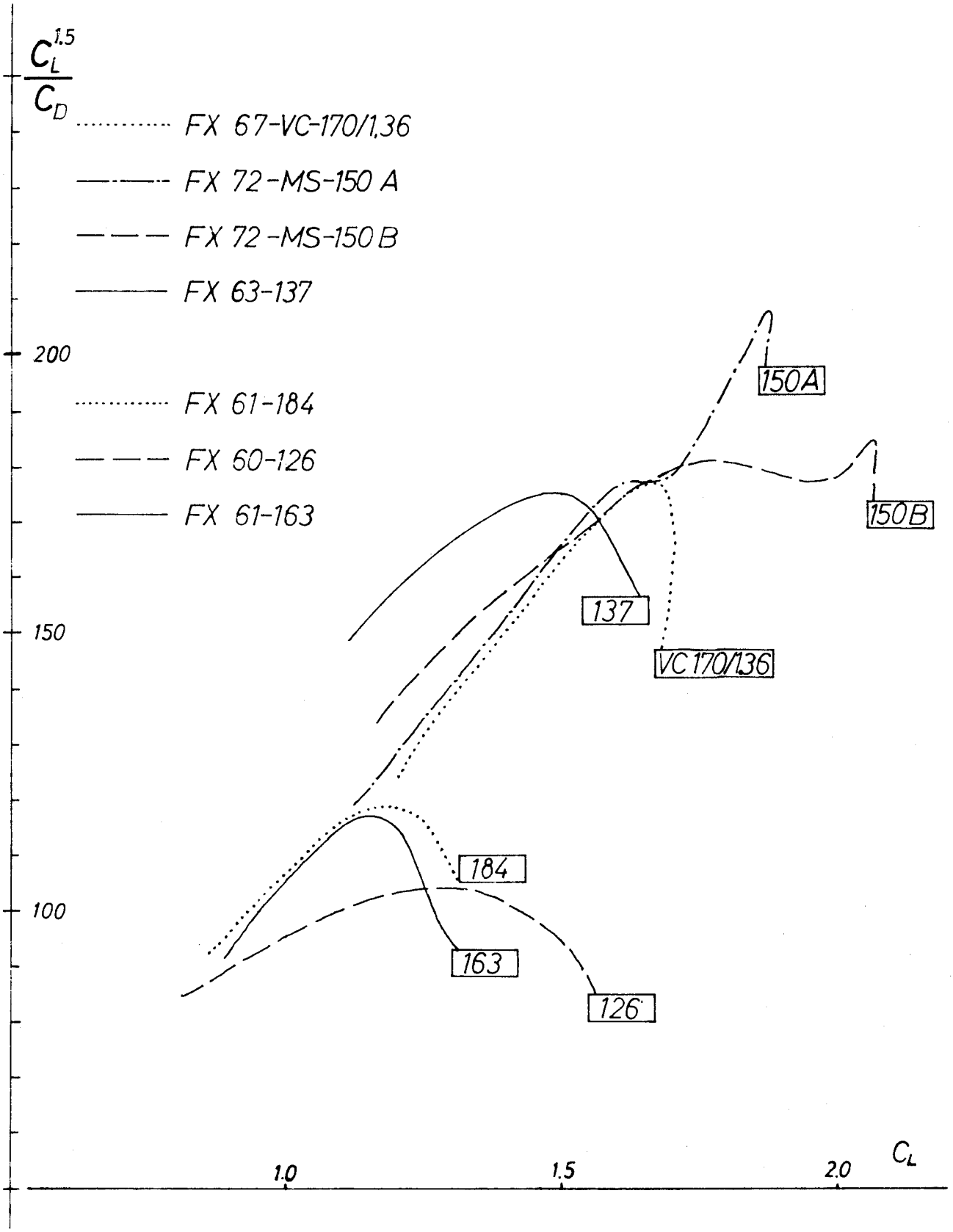


Fig. 4 The value $C_L^{1.5}/C_D$ for different airfoils at Re = 10^6

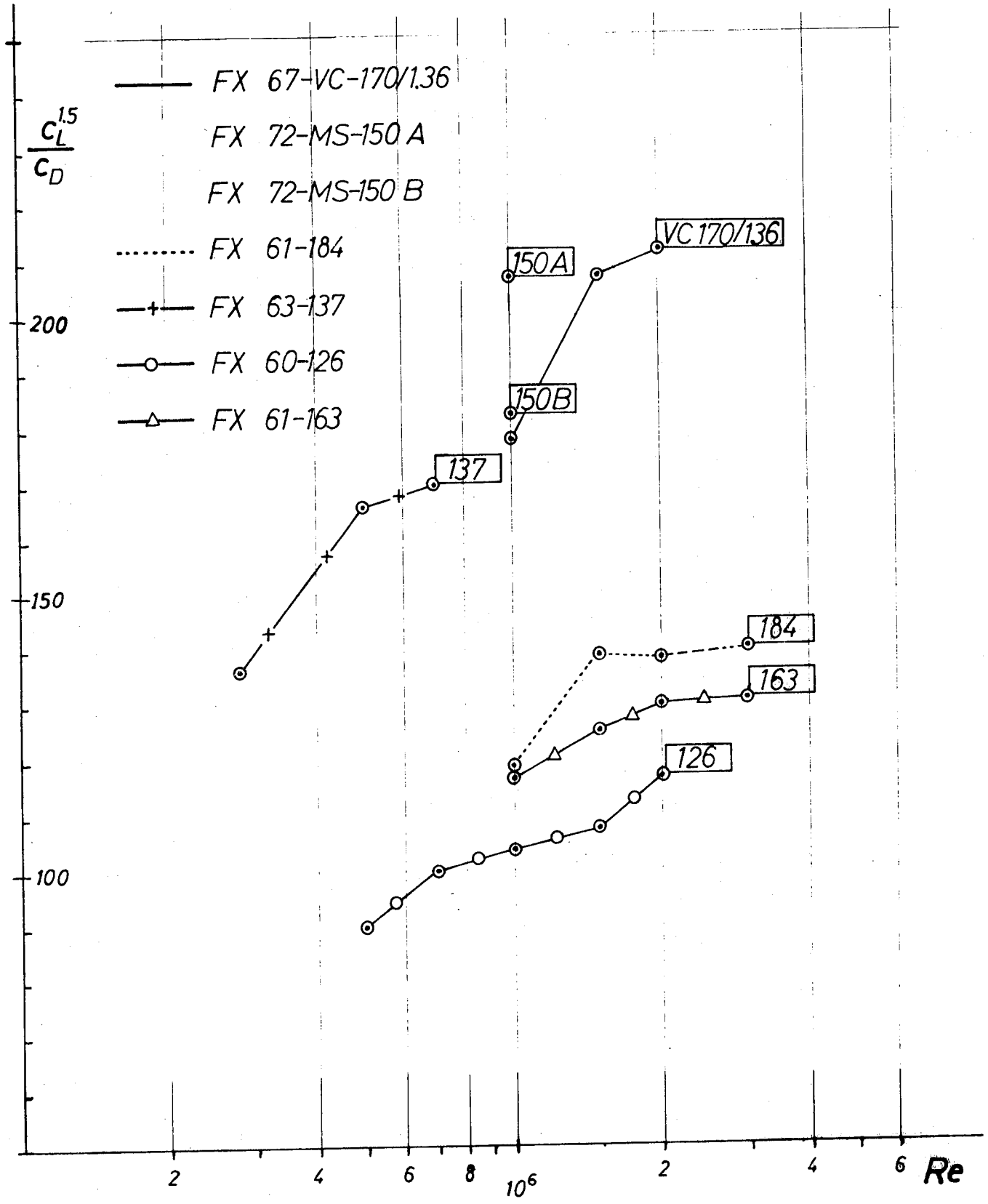


Fig. 5 The influence of Reynolds number on the sinking speed parameter $C_L^{1.5}/C_D$

Table 1.

		FX 72-MS-150A		FX 72-MS-150B	
No.	$\frac{x}{c}$	$(\frac{y}{c})_u$	$(\frac{y}{c})_l$	$(\frac{y}{c})_u$	$(\frac{y}{c})_l$
2	.99893	.00037	.00034	.00041	.00042
4	.99039	.00331	.00236	.00368	.00296
6	.97347	.00914	.00617	.01017	.00767
8	.94844	.01775	.01160	.01977	.01430
10	.91573	.02901	.01793	.03230	.02210
12	.87592	.04272	.02437	.04756	.03022
13	.85355	.05042	.02735	.05614	.03408
14	.82967	.05864	.03005	.06529	.03768
15	.80438	.06735	.03223	.07498	.04074
16	.77779	.07651	.03391	.08518	.04330
17	.75000	.08607	.03487	.09583	.04507
18	.72114	.09517	.03522	.10572	.04619
19	.69134	.10425	.03473	.11554	.04639
20	.66072	.11294	.03363	.12487	.04591
21	.62941	.12137	.03170	.13387	.04449
22	.59755	.12916	.02924	.14213	.04245
23	.56526	.13631	.02609	.14964	.03962
24	.53270	.14247	.02266	.15605	.03640
25	.50000	.14781	.01881	.16155	.03266
26	.46730	.15175	.01506	.16553	.02892
27	.43474	.15444	.01090	.16813	.02463
28	.40245	.15510	.00741	.16858	.02092
29	.37059	.15434	.00423	.16753	.01742
30	.33928	.15171	.00171	.16449	.01449
31	.30866	.14813	-.00072	.16046	.01158
32	.27886	.14325	-.00277	.15503	.00897
33	.25000	.13753	-.00480	.14872	.00626
34	.22221	.13084	-.00659	.14137	.00377
35	.19562	.12339	-.00826	.13321	.00132
36	.17033	.11528	-.00975	.12433	-.00098
37	.14645	.10657	-.01113	.11484	-.00324
38	.12408	.09733	-.01231	.10474	-.00527
39	.10332	.08773	-.01328	.09430	-.00716
40	.08427	.07785	-.01407	.08352	-.00886
41	.06699	.06777	-.01461	.07256	-.01030
42	.05156	.05767	-.01485	.06154	-.01138
43	.03806	.04769	-.01486	.05072	-.01227
44	.02653	.03791	-.01432	.04007	-.01243
45	.01704	.02867	-.01380	.03050	-.01234
46	.00961	.01985	-.01246	.02150	-.01150
47	.00428	.01252	-.01056	.01330	-.00950
48	.00107	.00679	-.00596	.00650	-.00560

$C_L^{1.5}/C_D$ of these two and some other airfoils [2] is evaluated for a Reynolds number of 1.0×10^6 in Fig. 4. Fig. 5 shows the influence of different Reynolds numbers. The less cambered airfoil 150 A has a single peak of $C_L^{1.5}/C_D$ over 200, whereas the 150 B reaches the value 180 over a much more extended range of C_L. Both new airfoils are better than the VC-170/136 airfoil which has only 11.4% thickness, as well as the FX 63-137 which was designed for man-powered aircraft. The fact that the new airfoils attain the maximum values of $C_L^{1.5}/C_D$ at higher lift values than any previous airfoils seems to be especially attractive when the flight mechanics of an aircraft are taken into account: unusually high aspect ratios, which might be attainable with future fiber technology, call for high C_L values and this is even more true when the sinking speed in circling flight is to be minimized.

References

1. Wortmann, F.X.; A critical Review of the Physical Aspects of Airfoil Design at Low Mach Numbers, Proceedings of the First International Symposium on the Technology and Science of Motorless Flight, M.I.T., Cambridge Mass., 1972.

2. Althaus, D.; Stuttgarter Profilkatalog I, Publ. by Inst. für Aero-u Gasdynamik, der U. Stuttgart, 1972.

AIRFOILS WITH A NEW HINGE FOR AILERONS AND FLAPS

by

D. Althaus and R. Eppler
Universität Stuttgart

Introduction

Every sailplane designer knows that the air blowing through the slot of an aileron or flap causes considerable parasitic drag. For example, the well-known RJ5 had its best performance with fixed flaps and a filled slot [1]. For the same reason modern sailplanes have less aileron span than earlier types.

A certain improvement can be made by sticking a tape over the slots, but this tape has to form corners and wrinkles while moving the aileron or flap, and one can still find considerable parasitic drag.

The best aerodynamic solution presented so far has been the use of an elastic upper surface, for example in the well-known HKS sailplanes developed in the early fifties by Haase, Kensche and Schmetz. However, as a consequence of this, they had very high stick forces. The elastic slot cover had to carry all the forces between wing and flap and had to be rather strong.

In this paper a new design of a hinge is presented which allows for a very thin elastic cover for the slot between wing and flaps or ailerons, thus combining the advantages of the low stick forces of normal sailplanes with the favorable aerodynamics of the HKS sailplanes. Moreover, since the best solution for automatic correspondence between flap position and airspeed is a simple mechanical connection of the elevator and flap, causing additional elevator stick forces, we present a new airfoil having a good drag polar with minimum flap deflection.

The hinge mechanism

A particular ideal motion of the aileron or flap is sketched in Fig. 1 for the special case of an airfoil with a flat upper surface. For the case without deflection we imagine that the slot of length a is covered by a flat, thin elastic sheet. With deflection, this cover is assumed to be a circular arc of the same length a. Obviously it is not possible to approximate this ideal motion by a single hinge, as different

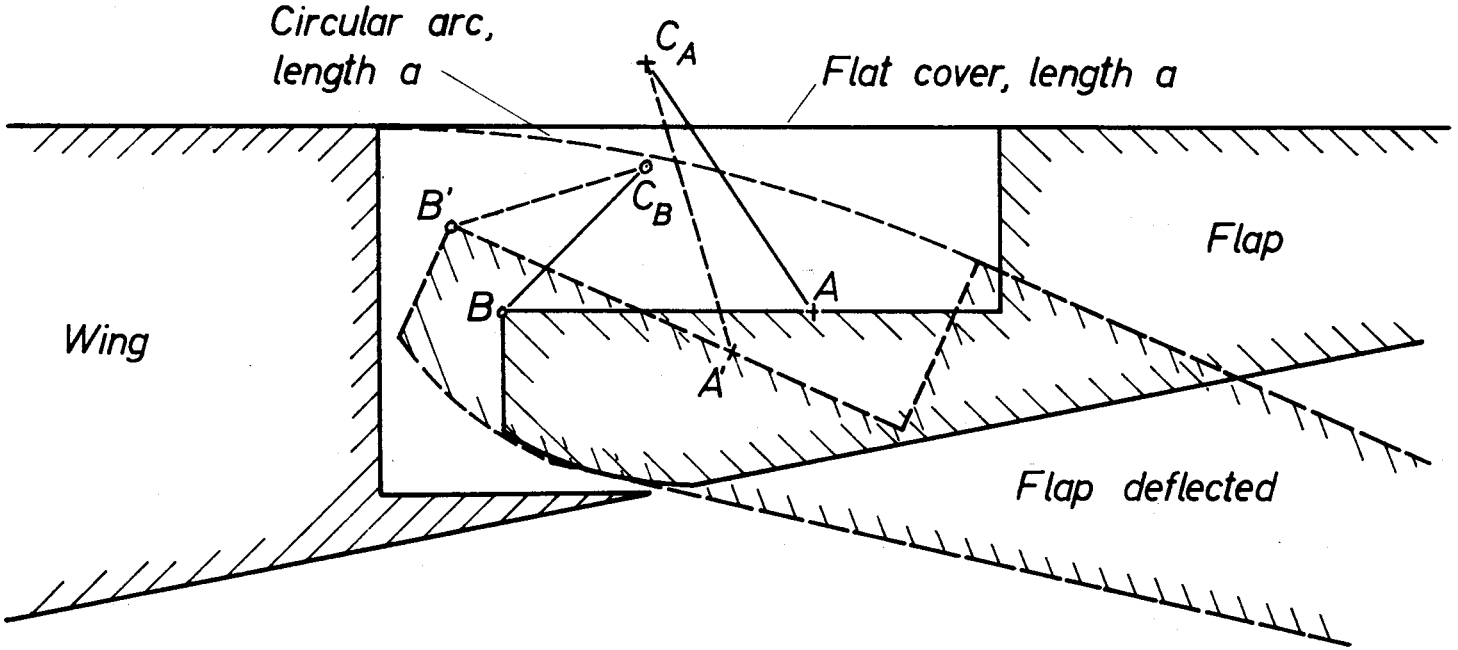


Figure 1. Ideal motion of a flap.

points of the flap A, A' or B, B' have different centers of motion C_A or C_B, but a very good approximation of the ideal motion is possible by connecting two different points of the flap, by single bars, with their centers of motion. Of course, it is no problem to find for any point of the flap the center of motion for the prescribed ideal motion of the flap. The only problem is to find two points in the flap so that the two centers of motion have enough distance for arranging the bearings and the bars and so that the entire hinge has as few parts as possible above the upper side of the airfoil. The hinges can be covered by a little rubber hat, and the parts between the hinges by a thin elastic sheet, which forms approximately a circular arc during the deflection of the flap. In Fig. 2 a typical solution in three flap positions is shown.

In the case of an airfoil with a cambered upper surface we have the flat slot cover not as it is sketched in Figures 1 and 2 for the undeflected flap, but with some small flap deflection.

Obviously the double hinge can be produced for a certain length a of the slot cover. Thus the designer may use a prefabricated double hinge instead of a (normally also prefabricated) single hinge, and has to prepare a slot of given width a.

A kinematic model and a production prototype of the double hinge have been constructed.

The airfoil

As mentioned previously, a mechanical connection between elevator and flap is a simple solution for automatic optimal flap position. Such a connection causes additional elevator stick forces, although there exists a certain effect of the airloads on the flap, which allows one to decrease these forces considerably by using a spring. Thus it is desirable to have maximum flap effect with only a small flap chord and deflection. Even without flap-elevator connection, one can show, and see in many experimental data that really good L/D ratios are always reached with a small flap deflection only.

The fundamental problem of flapped airfoils is sketched in Fig. 3. A conventional laminar airfoil at an angle-of-attack near the upper edge of the laminar bucket has a more-or-less constant velocity over the laminar section of the upper surface. Flap deflection down causes a suction peak near the flap hinge. Additional angle-of-attack causes a suction peak near the leading edge. Thus the velocity distribution becomes a very unfavorable shape for laminar effects. While in the rear part of the airfoil the pressure gradient is still favorable, no laminar flow exists due to the adverse pressure gradient near the leading edge. The adverse pressure

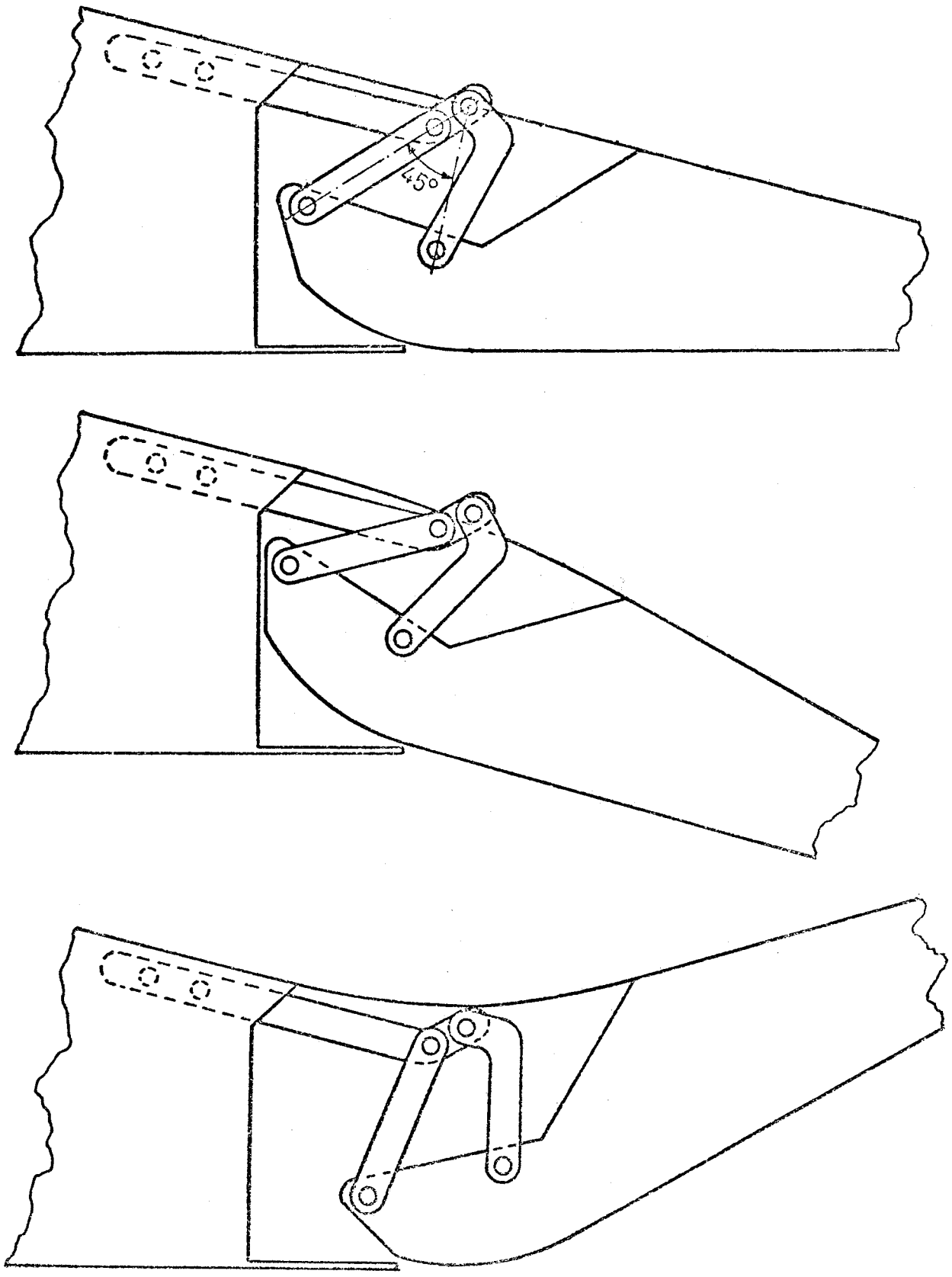


Figure 2. Double-hinge flap in 3 positions.

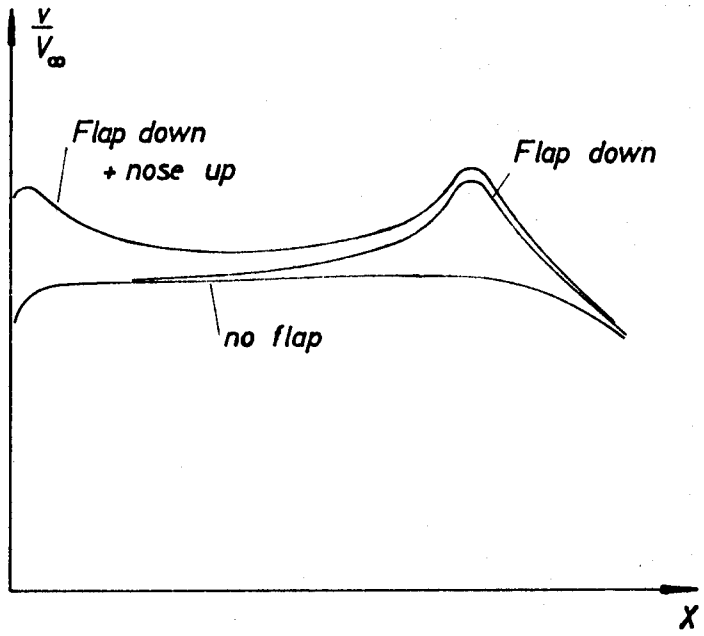


Figure 3. Influence of flaps on the velocity distribution of a laminar airfoil, upper surface.

gradient near the trailing edge causes separation of the turbulent boundary layer arriving there with considerable thickness.

Prevention of this cow-belly like velocity distribution promises improvements. However, until now airfoil shape computation starting from a given pressure distribution [2,3] has only been possible for one airfoil configuration. Now the problem is different. We need for the flapped airfoil a given pressure distribution on the upper surface, while for the unflapped airfoil the lower surface is most important, since it determines the lower end of the laminar bucket.

To solve this problem, the usual method for direct computation of an airfoil shape from the pressure distribution [2,3] has been extended. The fundamental idea was to give, in some region, fixed parameters for the properties of the pressure distribution, while the parameters in other parts of the airfoil are used for a least-squares fit to a given shape.

It is not possible to present the details of this method here. The method developed uses an iteration process of the following kind:

1. Firstly, an airfoil $A^{(o)}$ for the high-speed case is computed, which has low drag at low C_L and high Reynolds number. We assumed about 75% laminar flow on the lower surface and 55% on the upper surface. As an example, for a velocity distribution meeting these conditions for an angle-of-attack of 1° or a C_L of 0.11 we can use Fig. 4. The adverse pressure gradient, or the decrease of velocity in the region of the trailing edge is chosen such that the airfoil has a thickness of about 15%. On both sides, at $Re = 3 \cdot 10^6$ only short destabilization areas are needed to prevent laminar separation bubbles. The over-all pressure rise on the upper surface is less than it would be without turbulent separation, thus a certain reserve for the suction peak of the flap exists. It should be noticed that the velocity distribution of the lower surface shows a little adverse pressure gradient near the leading edge and a very little favorable pressure gradient behind x = 50%. This is the optimal distribution near transition. The methods giving this result are described in [4]. For the upper surface it is required only that transition lies behind 55% chord. The details of the pressure distribution before this point are free for airfoil A^o and are chosen arbitrarily.
2. Secondly, an airfoil $B^{(o)}$ for the high-lift case and smaller Re is computed, which has given properties of the pressure distribution over the first 50% of the upper side and approximates airfoil $A^{(o)}$ for the

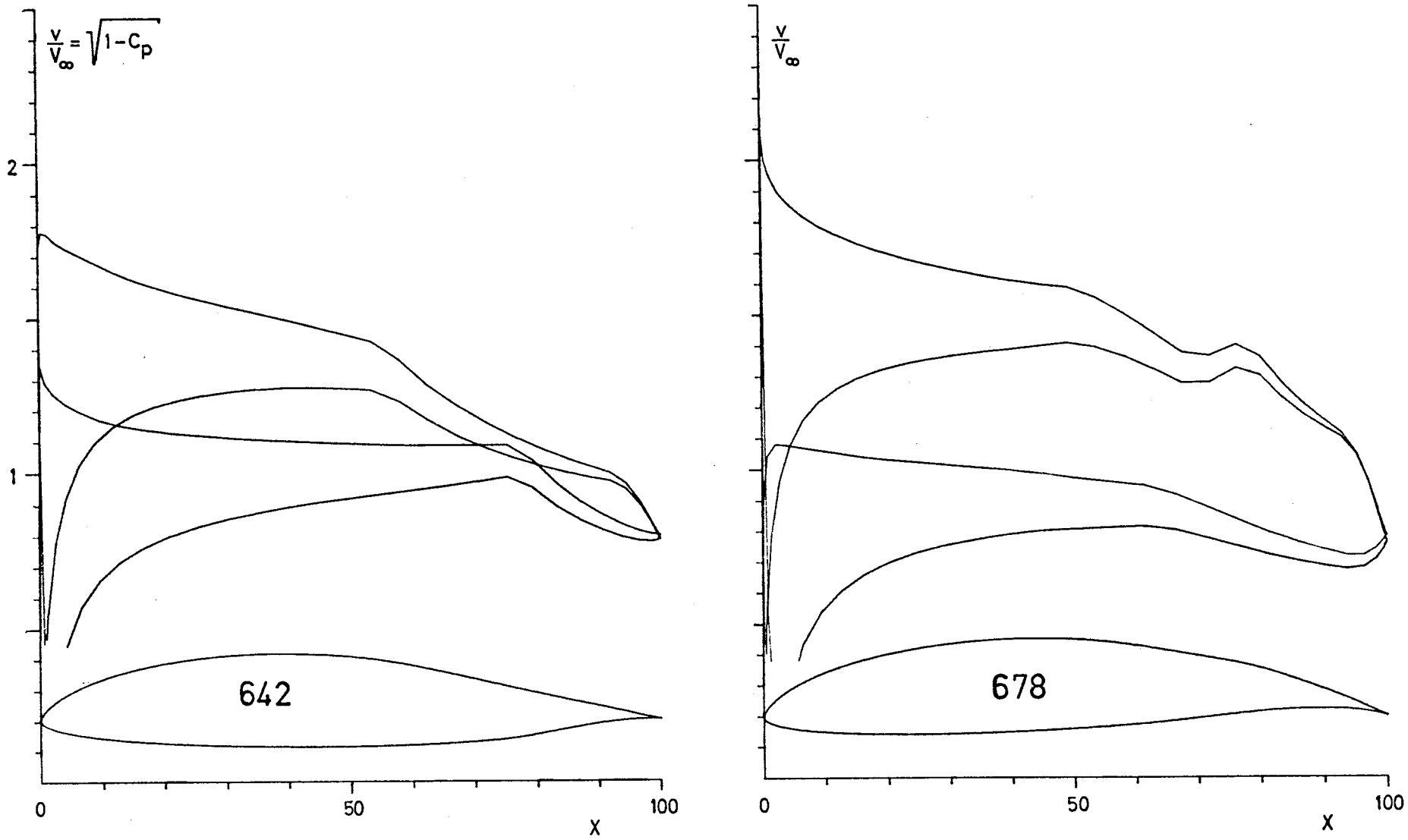


Figure 4. Airfoils 642 and 678 and their theoretical velocity distributions

upper side between 50% and 70% and for the lower side between 0 and 70%.

3. Airfoil $A^{(i+1)}$ keeps the areas of given pressure distributions of airfoil $A^{(o)}$ and approximates airfoil $B^{(i)}$ in the area originally having an arbitrary pressure distribution. This approximation also influences somewhat the shape of the airfoil in the part in which the pressure distribution does not change.
4. Airfoil $B^{(i+1)}$ keeps the area of given pressure distribution of airfoil $B^{(o)}$ and approximates airfoil $A^{(i+1)}$ in the same areas where airfoil $B^{(o)}$ approximated airfoil $A^{(o)}$. This approximation again influences the shape of the airfoil very slightly in the part with unchanging pressure distribution.
5. If the difference between airfoil $B^{(i+1)}$ and airfoil $B^{(i)}$ is small enough, the iteration process is terminated. Otherwise it continues with step 3.

The approximation process used in each step of the iteration process is not very fully automated and still needs some effort. However, the convergence of the iteration process is very rapid, and only 1 or 2 iterations are usually needed.

A typical result is shown in Fig. 4. The two airfoils coincide over the first 70% of the chord, and can be considered as unflapped (No. 642) and flapped (No. 678) airfoils, having for the front portions, as exactly as possible, the desired pressure distribution features. Airfoil 678 has the typical suction peak of a flap just behind the end of the portion over which it coincides with airfoil 642.

On both sides, when the flap is deflected down, longer destabilization areas develop. These are necessary, at lower Reynolds numbers, to prevent laminar separation bubbles. A wind-tunnel model of airfoil 642 has been built, with a double hinge flap at 75% chord. The 10° flap-down position approximated airfoil 678 very well. The measurements are shown in Figs. 5 and 6.

The results are disappointing in two respects. The minimum drag of 642 is higher than expected from the boundary layer computations. This is probably due to an inexact fit of the flap at the lower surface. The slope of the C_D-polar for $Re = 3 \cdot 10^6$ agreed very well with the theoretical results, however.

Also, the maximum lift measured was not as high as the theoretical value. We therefore looked for laminar separation bubbles, but found none. The turbulent separation was found to occur a little too early. This is probably due to a too-long instability area. The turbulent boundary layers are already too thick when reaching the adverse pressure gradient

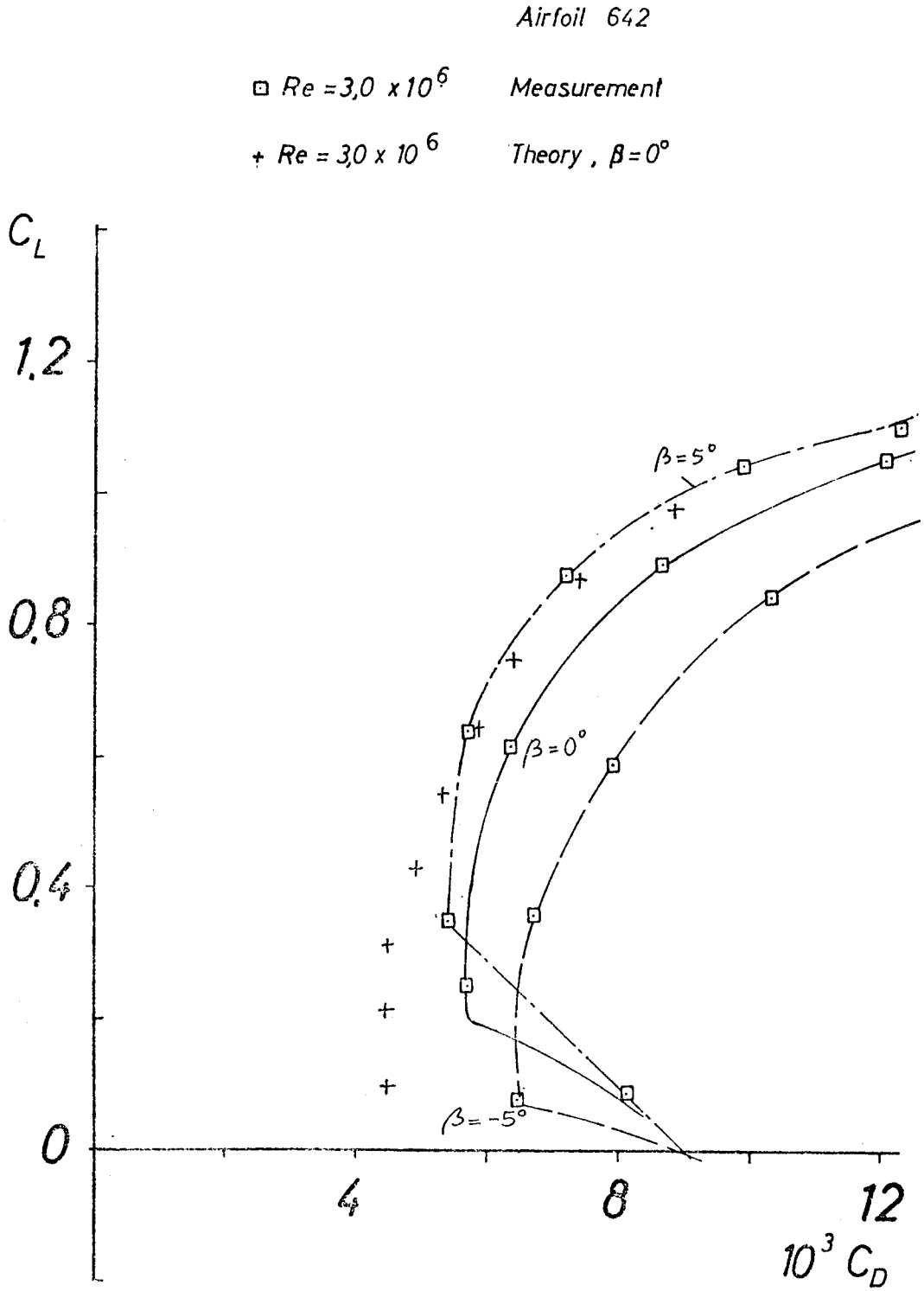


Figure 5. Theoretical and experimental drag polar of airfoil 642.

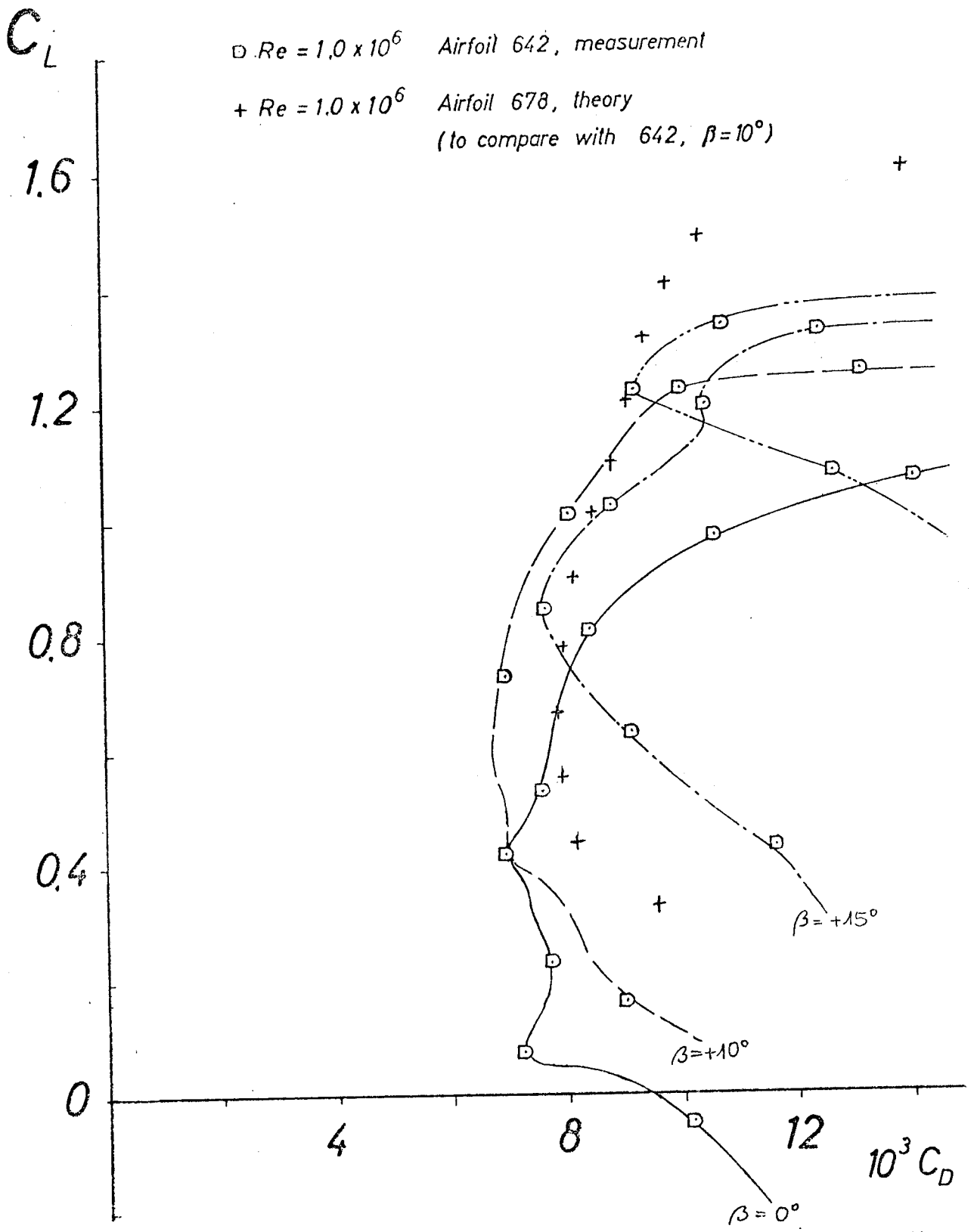


Figure 6. Theoretical drag polar of airfoil 678, experimental drag polar of flapped airfoil 642.

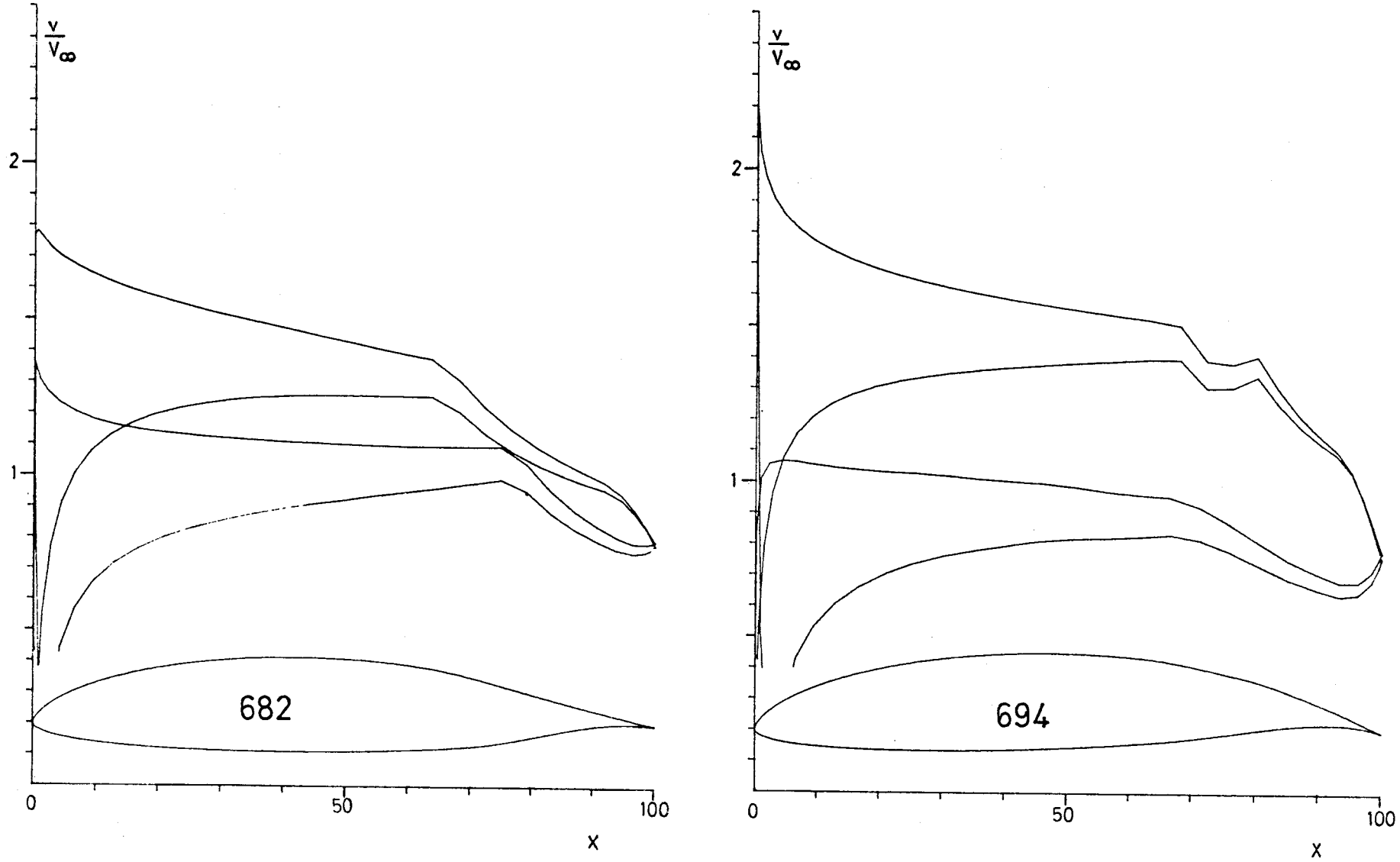


Figure 7. Airfoils 682 and 694 and their theoretical velocity distributions

Table 1

PROFIL 642		PROFIL 678		PROFIL 682		PROFIL 694	
X	Y	X	Y	X	Y	X	Y
100.000	0.000	100.000	0.000	100.000	0.000	100.000	0.000
99.624	0.059	99.642	0.136	99.623	0.065	99.640	0.142
98.541	0.268	98.640	0.567	98.534	0.288	98.632	0.588
96.849	0.651	97.130	1.277	96.823	0.697	97.110	1.325
94.630	1.170	95.207	2.172	94.572	1.265	95.172	2.263
91.917	1.770	92.880	3.159	91.825	1.953	92.835	3.313
88.712	2.441	90.140	4.216	88.608	2.751	90.100	4.450
85.055	3.206	87.031	5.349	84.978	3.671	87.023	5.674
81.019	4.071	83.638	6.529	81.020	4.707	83.699	6.943
76.683	5.025	80.043	7.663	76.825	5.828	80.202	8.112
72.129	6.048	76.219	8.613	72.490	6.990	76.399	9.069
67.445	7.103	72.033	9.395	68.113	8.095	72.246	9.999
62.717	8.143	67.527	10.178	63.704	9.002	67.996	10.909
58.027	9.082	62.908	10.983	59.178	9.665	63.668	11.587
53.386	9.807	58.280	11.688	54.523	10.146	59.165	12.054
48.735	10.285	53.659	12.219	49.799	10.473	54.541	12.360
44.073	10.561	49.047	12.528	45.059	10.649	49.844	12.506
39.447	10.660	44.427	12.613	40.352	10.676	45.125	12.502
34.904	10.588	39.817	12.514	35.726	10.555	40.431	12.347
30.483	10.355	35.275	12.256	31.224	10.288	35.810	12.049
26.227	9.972	30.849	11.848	26.889	9.884	31.310	11.612
22.178	9.451	26.585	11.298	22.764	9.350	26.975	11.043
18.377	8.803	22.526	10.617	18.889	8.696	22.848	10.352
14.860	8.041	18.710	9.816	15.299	7.931	18.968	9.548
11.660	7.180	15.174	8.908	12.027	7.071	15.373	8.646
8.807	6.233	11.950	7.910	9.103	6.133	12.095	7.658
6.326	5.218	9.069	6.838	6.554	5.132	9.166	6.603
4.231	4.156	6.554	5.711	4.397	4.091	6.608	5.499
2.536	3.080	4.425	4.553	2.649	3.038	4.445	4.369
1.259	2.025	2.695	3.392	1.328	2.006	2.692	3.239
0.414	1.027	1.379	2.261	0.446	1.031	1.365	2.141
0.012	0.147	0.488	1.200	0.017	0.171	0.469	1.113
0.176	-0.536	0.032	0.269	0.166	-0.501	0.029	0.218
0.980	-1.102	0.117	-0.437	0.961	-1.071	0.146	-0.466
2.366	-1.649	0.827	-0.991	2.333	-1.627	0.908	-1.022
4.292	-2.152	2.123	-1.491	4.246	-2.143	2.249	-1.539
6.734	-2.602	3.973	-1.914	6.674	-2.611	4.135	-1.989
9.669	-2.998	6.351	-2.264	9.595	-3.029	6.544	-2.367
13.064	-3.346	9.229	-2.538	12.974	-3.401	9.455	-2.673
16.874	-3.648	12.574	-2.737	16.768	-3.728	12.854	-2.915
21.053	-3.902	16.352	-2.865	20.929	-4.008	16.640	-3.096
25.551	-4.108	20.517	-2.929	25.409	-4.239	20.823	-3.222
30.313	-4.265	25.017	-2.931	30.152	-4.420	25.325	-3.289
35.289	-4.370	29.798	-2.869	35.105	-4.549	30.099	-3.286
40.408	-4.425	34.810	-2.744	40.207	-4.623	35.099	-3.217
45.622	-4.426	39.992	-2.560	45.401	-4.641	40.268	-3.093
50.865	-4.374	45.287	-2.311	50.625	-4.602	45.534	-2.912
56.078	-4.266	50.649	-2.000	55.817	-4.502	50.840	-2.661
61.195	-4.103	56.014	-1.644	60.919	-4.342	56.148	-2.343
66.152	-3.877	61.306	-1.230	65.853	-4.112	61.389	-1.982
70.885	-3.576	66.499	-0.723	70.567	-3.800	66.472	-1.556
75.331	-3.154	71.611	-0.147	74.994	-3.356	71.384	-1.000
79.522	-2.539	76.619	0.410	79.167	-2.699	76.177	-0.334
83.562	-1.798	81.446	0.859	83.209	-1.895	80.862	0.336
87.424	-1.108	85.979	1.129	87.103	-1.132	85.382	0.875
90.970	-0.568	90.078	1.192	90.715	-0.531	89.596	1.161
94.070	-0.207	93.612	1.050	93.901	-0.137	93.310	1.141
96.604	-0.020	96.441	0.741	96.520	0.045	96.309	0.849
98.475	0.034	98.449	0.377	98.447	0.069	98.414	0.432
99.617	0.017	99.619	0.101	99.612	0.026	99.615	0.114
100.000	0.000	100.000	0.000	100.000	0.000	100.000	0.000

C_{M0} = 0.0551 β = 2.88° C_{M0} = 0.2062 β = 7.76° C_{M0} = 0.0701 β = 3.25° C_{M0} = 0.2115 β = 7.85°

behind the flap hinge. Wortmann [5] has remarked that in such a situation the boundary layer theory may sometimes fail.

An improvement should be possible by taking a longer area of laminar boundary layer on the upper surface, as calculated for the airfoil combination 682/694. The shapes and velocity distributions are shown in Fig. 7. The wind-tunnel experiments have been prepared but still await execution.

The coordinates, angles of zero lift and moment coefficients of all the airfoils discussed are given in Table 1.

References

1. Raspet, A.; Systematic Improvements of the Drag Polar of the Sailplane RJ5, Soaring 1951, Nr. 5.

2. Eppler, R.; Direkte Berechnung von Tragflügelprofilen aus der Druckverteilung. Ing.-Arch. 25 (1957), S. 32-57.

3. Eppler, R.; Über die Entwicklung moderner Tragflügelprofile. De Ingenieur 77 (1965), S. L17-L22.

4. Eppler, R.; Laminarprofile für Reynolds-Zahlen grösser als $4 \cdot 10^6$. Ing.-Arch. 38 (1969), S. 232-240.

5. Wortmann, F.X.; A Critical Review on the Physical Aspects of Airfoil Design at Low Mach Numbers, Proceedings of the First International Symposium on the Technology and Science of Motorless Flight, M.I.T., Cambridge, Mass., October 1972, pp 179-196.

THE DEVELOPMENT OF A TWO-DIMENSIONAL, HIGH-ENDURANCE AIRFOIL WITH GIVEN THICKNESS DISTRIBUTION AND REYNOLDS NUMBER

by

George S. Pick and Douglas A. Lien
Naval Ship Research and Development Center
Bethesda, Maryland

Notation

c	Chord length
C_D	Drag coefficient
C_ℓ	Lift coefficient
C_m	Moment coefficient
C_p	Pressure coefficient
H	Form factor
L/D	Lift/Drag ratio
Re_c	Reynolds number
V	Velocity
x/c	Chord station
x_o/c	Point joining the rooftop and Stratford velocity distributions
y_c	Mean camber line
y_t	Airfoil thickness
α	Angle of attack
γ_{corr}	Corrected vortex distribution
ΔV	Velocity difference between upper and lower surface
δ^*	Boundary layer displacement thickness
δ	Boundary layer thickness (in)

Subscripts

c	Chord length
i	Ideal condition
l	Lower surface
TE	Trailing edge
u	Upper surface
∞	Free-stream conditions

Introduction

Liebeck and Ormsbee [1] have developed airfoils which attain maximum total lift in incompressible flow. The pressure distribution on the upper surface employs the Stratford separation theory which recovers a pressure difference in the shortest possible distance. Incipient

separation is thus present on the aft portion of the upper surface. The lift coefficients on both upper and lower surfaces are maximized. This criterion results in airfoils with high lift coefficients and high L/D ratios. The shapes of the airfoils thus obtained have unconventional thickness distributions and leading edge radii.

In the present development, restricted thickness distributions were specified to reduce the lower surface lift coefficient and produce more conventional-looking airfoils. Such airfoils might be used on aircraft which require high L/D ratios and high cruise lift coefficients.

An airfoil shape was selected and the theoretical results were verified experimentally for a range of wind speeds and angles of incidence. The complete performance envelope of this airfoil was computed prior to testing.

This paper describes the process and associated experimental verification of an airfoil section designed to have a high lift coefficient and a high ratio of lift over drag (L/D). Several studies provided the theoretical basis for the design process. The experimental program was conducted in the Boeing two-dimensional, low-speed research wind tunnel.

Theoretical development

Use of linear theory to determine the initial airfoil profile

Liebeck and Ormsbee [1] showed that in order to maximize lift on the upper surface of the airfoil, a rooftop velocity distribution must be specified in a region that extends from the leading edge to a designated point x_o. According to Strand [2] x_o/c must lie between 0.3 and 0.45 in order to attain maximum upper surface lift. The Stratford velocity distribution for zero skin friction and incipient separation was specified from x_o to the trailing edge.

A generalized parametric study of the upper surface velocity, lift, and drag characteristics for various flow conditions resulted in a series of preliminary design curves. These curves, in conjuction with a survey by Abbot and Von Doenhoff [3] of existing symmetrical NACA airfoil thickness distributions, were used to select appropriate design lift coefficients and L/D ratios for further study. A tradeoff analysis between desirable high performance characteristics and practical thickness distribution showed that the NACA 63A006 thickness distribution came closest to an overall optimum condition.

Strand [2] shows that for a given Reynolds number and pressure coefficient at the trailing edge, maximum upper surface lift occurs at $x_o/c = 0.3$. This is illustrated in Fig. 1. A plot of total lift coefficient and L/D ratio

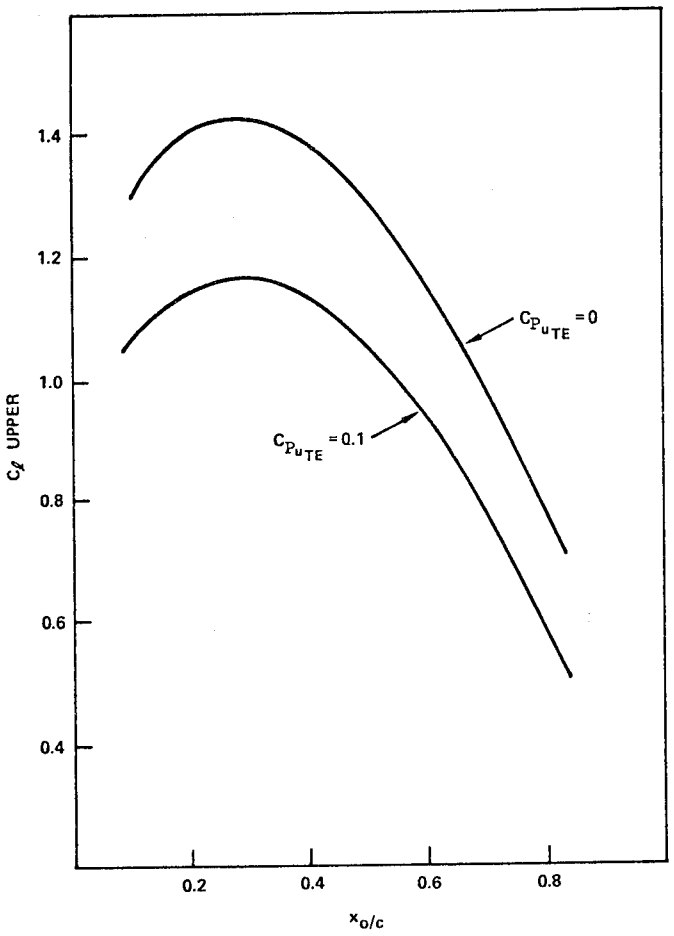


Figure 1. Upper surface lift coefficient versus x_o/c.

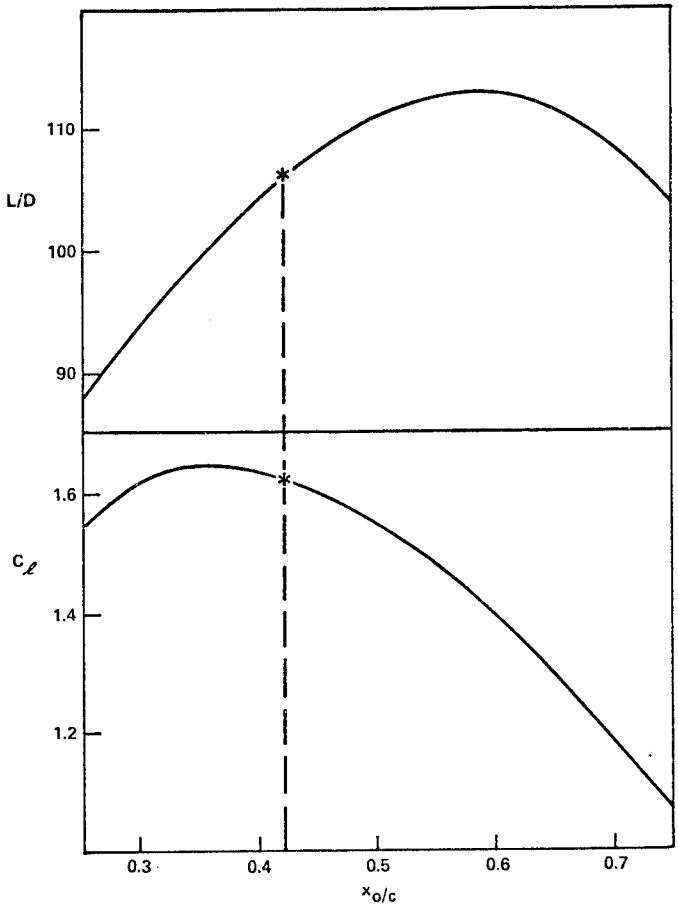


Figure 2. L/D and C_ℓ versus x_o/c for a NACA 63A006 thickness distribution.

versus x_o/c is given in Fig. 2. The point $x_o/c = 42$ was chosen from Fig. 2 because of practical considerations, e.g., a smaller x_o/c would compromise the L/D ratio and a larger x_o/c would sacrifice total lift.

In addition to the specified rooftop and Stratford velocity distribution on the upper surface, other parameters are needed to compute the lower surface velocity distribution and the final airfoil coordinates, namely, the thickness distribution of a symmetrical airfoil and the local velocity on the airfoil due to this thickness distribution. If the total velocity or velocity due to thickness is designated as V_t, then the lower surface velocity is defined as

$$V_l = 2V_t - V_u \tag{1}$$

The velocity distribution thus determined is shown in Fig. 3. The final airfoil coordinates can be determined for a known velocity distribution and a given thickness distribution. With

$$\Delta V = V_u - V_t \tag{2}$$

the vortex distribution corrected for the airfoil thickness is

$$\gamma_{corr} = 2\Delta V \left[1 + \left(\frac{dy_t}{dx}\right)^2\right] \tag{3}$$

where y_t is the airfoil thickness at a point. The equation for the mean camber line is given by thin airfoil theory as

$$\frac{dy_c(\bar{x})}{dx} - \alpha_i = \frac{1}{2\pi}\int_o^x \frac{(\gamma/V_\infty)_{corr}}{x-\bar{x}}\, dx \tag{4}$$

where y_c is the mean camber line and α_i is the ideal angle of attack. The final airfoil coordinates can be determined from the mean camber line and the thickness distribution.

The lift coefficient is calculated according to the equation

$$C_\ell = -\int_o^1 (C_{Pu} - C_{Pl})\, d\left(\frac{x}{c}\right), \tag{5}$$

where $C_p = 1 - \left(\frac{V}{V_\infty}\right)^2$.

The drag coefficient is computed according to Thwaites [5] as

$$C_d = \sum\left[\frac{0.02429}{Re_\infty^{1/5}}\int_o^1 \left(\frac{V}{V_\infty}\right)^4 d\,\frac{x}{c}\right]^{5/6} \tag{6}$$

where the summation refers to both upper and lower surfaces.

The velocity distribution, pressure distribution, airfoil coordinates, and boundary layer are calculated by means of computer program MAXLIFT. Documentation, program listings, and input-output example have been reported informally by Lien in NSRDC Tech Note (to be published).

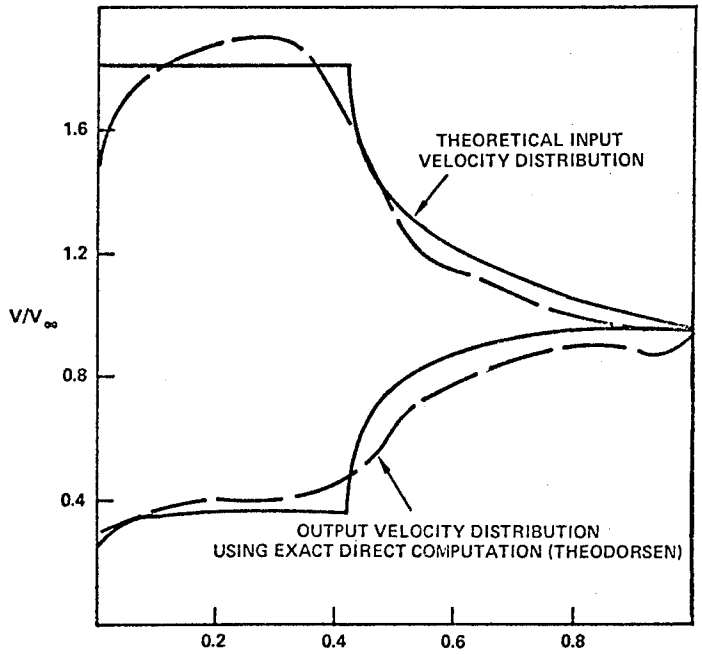


Figure 3. Comparison of velocity distributions using linear inverse theory and exact direct computation.

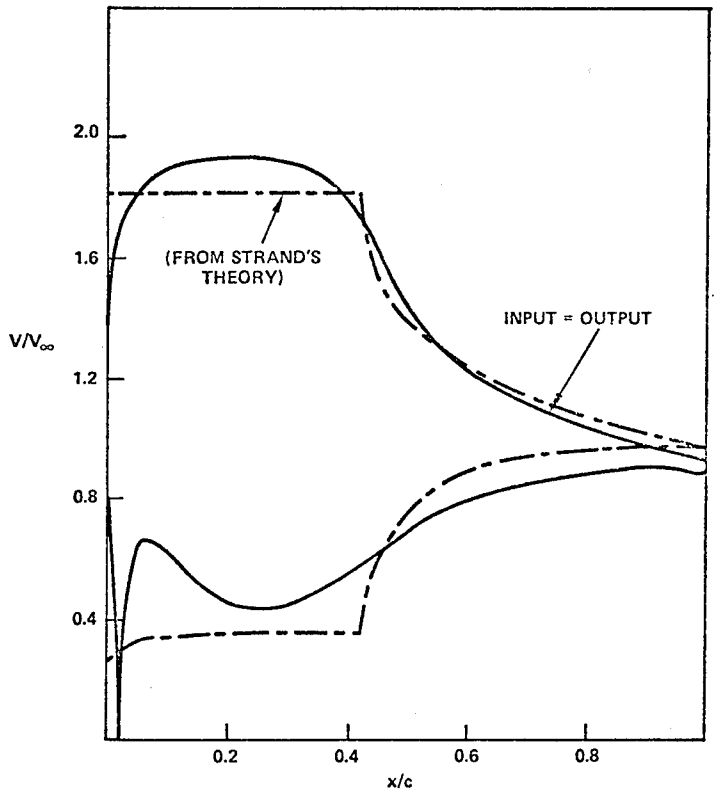


Figure 4. Final velocity distribution for airfoil using James method.

Use of nonlinear theory to determine the final airfoil profile

In order to check the validity of the linear inverse theory, the exact direct method of Theodorsen [6] was used to compute the velocity distribution around the airfoil shape obtained from this theory. This velocity distribution is also shown in Fig. 3. The discrepancy between the two velocity distributions indicates that linear inverse theory cannot be used to determine the final airfoil shape because the velocity gradients on the upper surface are too large.

The initial airfoil shape obtained from the linear theory describes the camber of the airfoil and can be used as a first approximation in a more sophisticated nonlinear inverse airfoil program such as the James [7] airfoil design method developed at McDonnell-Douglas. This method uses a conformal mapping procedure and is very accurate and extremely flexible with regard to the input velocity distribution.

The input velocity distribution is expressed as a function of the airfoil arc length. The steps which follow the input are:

1. Calculate the potential by quadrature.
2. Interpolate through this potential and the known potential for a circle to obtain the velocity in the circle plane.
3. Fit the circle plane velocity with a Fourier series.
4. Conjugate the series in 3 to obtain surface angle.
5. Obtain airfoil coordinates by quadrature, again as a function of velocity and angle in the circle plane, i.e., parametrically.

This system has several advantages. For one thing, it gives the designer some immediate control over the reality of shapes because the trailing-edge angle is a necessary input parameter. For another, it applies an automatic closure condition. Moreover, the output from the program provides the nearest pressure distribution which will give a closed airfoil (not every demanded pressure or velocity distribution will "design" such an airfoil). Finally, the magnitude of the Fourier terms can be used as a measure of input suitability since according to the theory, certain of these terms should vanish for a proper input velocity.

By using the input velocity distribution of Fig. 3, the airfoil shape was determined according to James design method. However, the output velocity distribution corresponding to the resulting airfoil shape had higher velocities in the rooftop region and failed to match velocities at the trailing edge. Accordingly, the input velocity distribution had to be modified. In the next attempt, an adverse pressure gradient was added to the lower surface near the leading edge. This change in

the velocity distribution lowered the rooftop velocity without sacrificing important performance characteristics. Further modifications were made for the final velocity distribution shown in Fig. 4. The input velocity distribution closely agreed with the output of the James method.

Since the James method was based on inviscid theory, boundary layer corrections had to be made in order to compensate for the extra thickness from boundary layer buildup in turbulent flow. The characteristic boundary layer thickness displacement of Fig. 5 was used for boundary layer corrections. The prime consideration in airfoil correction was to preserve the flow properties on the upper surface to meet the Stratford criterion aft of $x_o/c = 0.42$. Flow properties on the lower surface were of secondary importance. For this reason, both the upper and lower surfaces of the airfoil were corrected by an amount equal to the thickness of the upper surface boundary layer displacement (i.e., the thickness of local boundary layer displacement on the upper surface was subtracted from the inviscid airfoil profile ordinate and an equal amount was added to the local lower surface profile ordinate at each chord station). This process resulted in a slight change of camber distribution but not thickness distribution. The final airfoil shape shown in Fig. 6 incorporates the boundary layer correction. The airfoil coordinates are given in Table 1.

Predicted performance characteristics of the final airfoil

The prescribed performance characteristics are given in Fig. 7 as a function of angle of attack. The L/D ratio has a value of 95 and is essentially constant in the vicinity of the design angle of attack (10 deg). Velocity distributions for the off-design conditions are plotted in Fig. 8. It is evident from this graph that there are adverse pressure gradients on the lower surface near the leading edge at all angles of attack. This pressure gradient becomes less adverse when the angle of attack is increased.

In order to determine at which angle of attack separation would occur on the lower surface, a calculation of the boundary layer behavior was performed in accordance with Von Doenhoff and Tetervin [8]. Figure 9 shows the form factor H at the final point of the adverse pressure gradient as a function of angle attack. Separation occurs when the form factor is greater than 2.6. By this criterion, separation does not occur on the lower surface above an angle of attack of 5.5 deg. This was satisfactory for all design flow conditions.

Figure 10 delineates the general flow diagram of the design procedure outlined above.

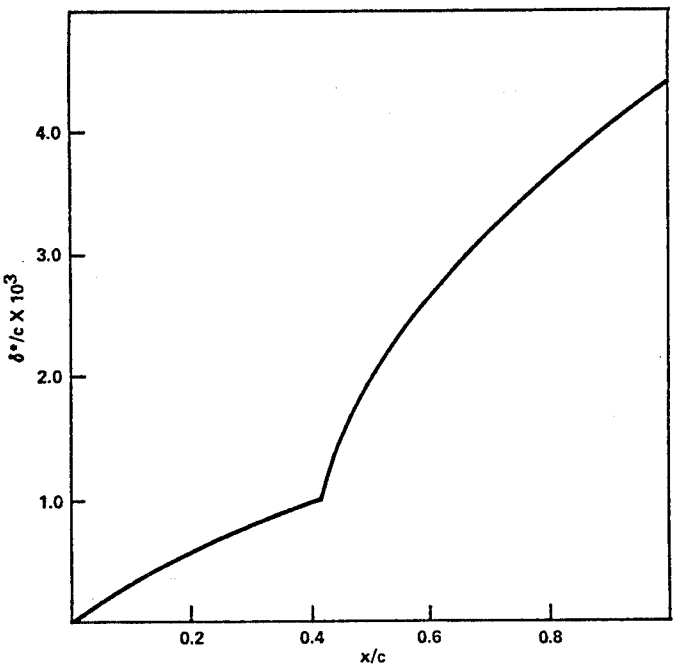


Figure 5. Characteristic boundary layer displacement thickness on airfoil.

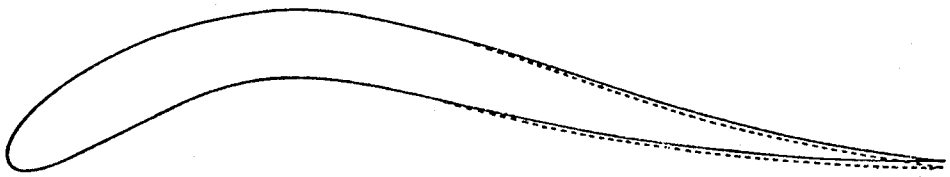


Figure 6. Final airfoil shape.

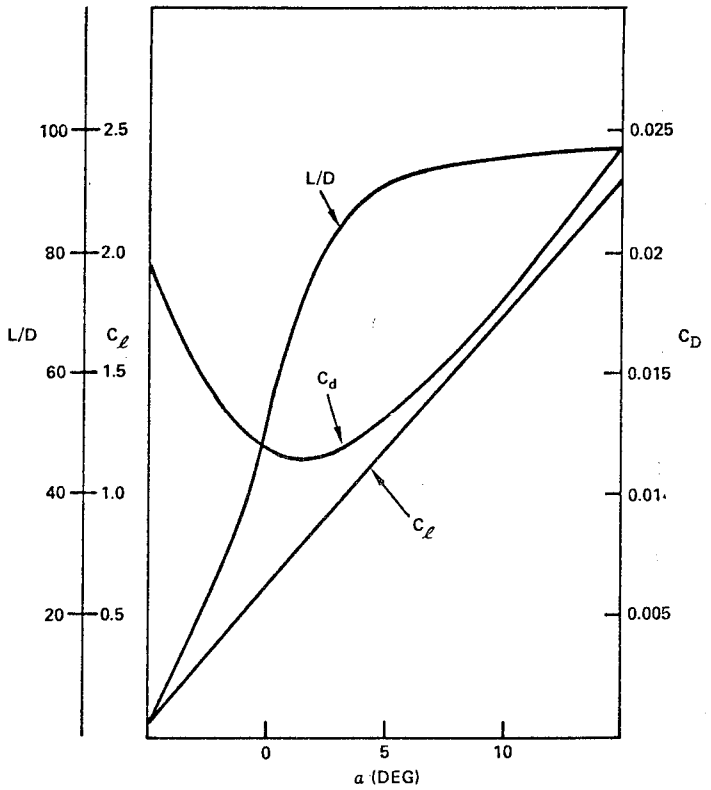


Figure 7. Performance characteristics for all angles of attack.

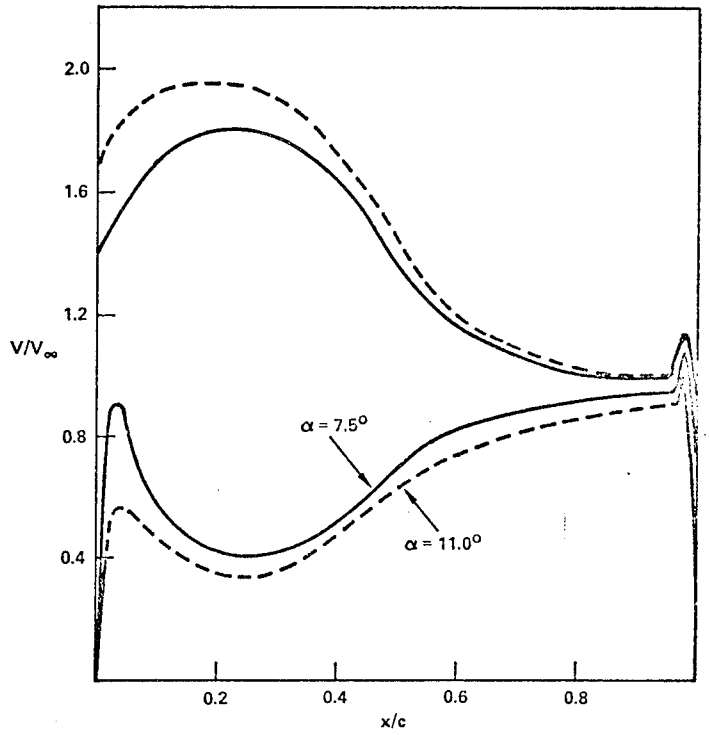


Figure 8. Off-design velocity distributions.

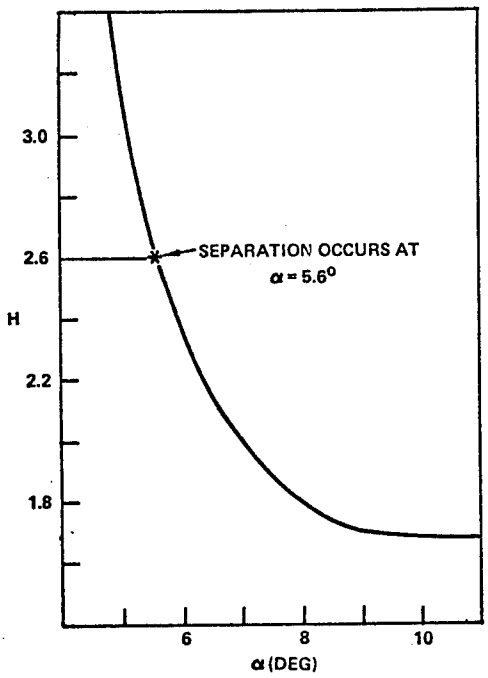


Figure 9. Form factor, H versus α.

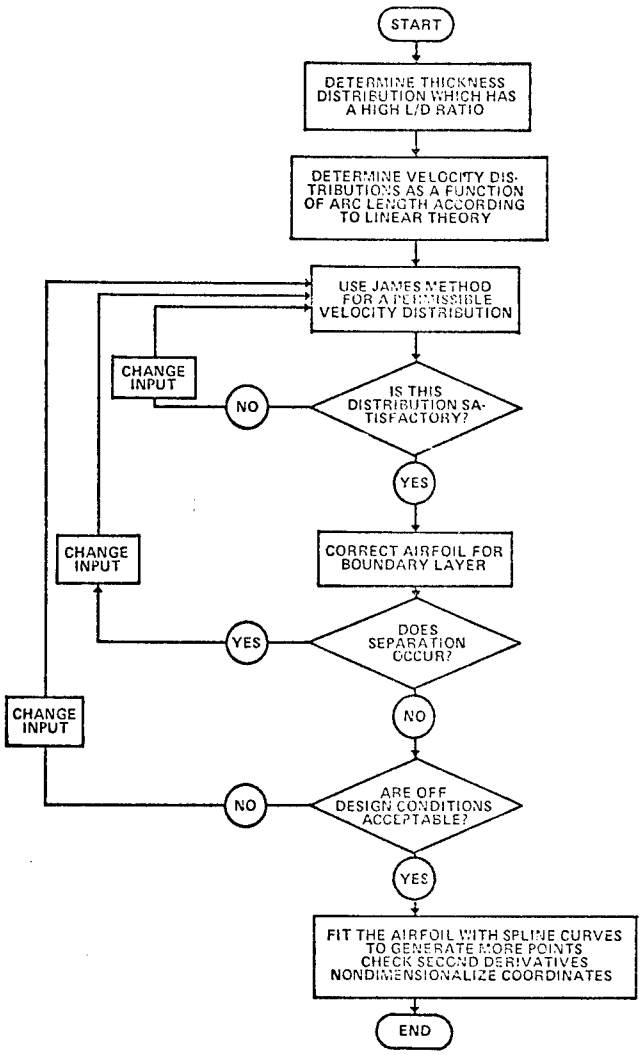


Figure 10. Design flow diagram.

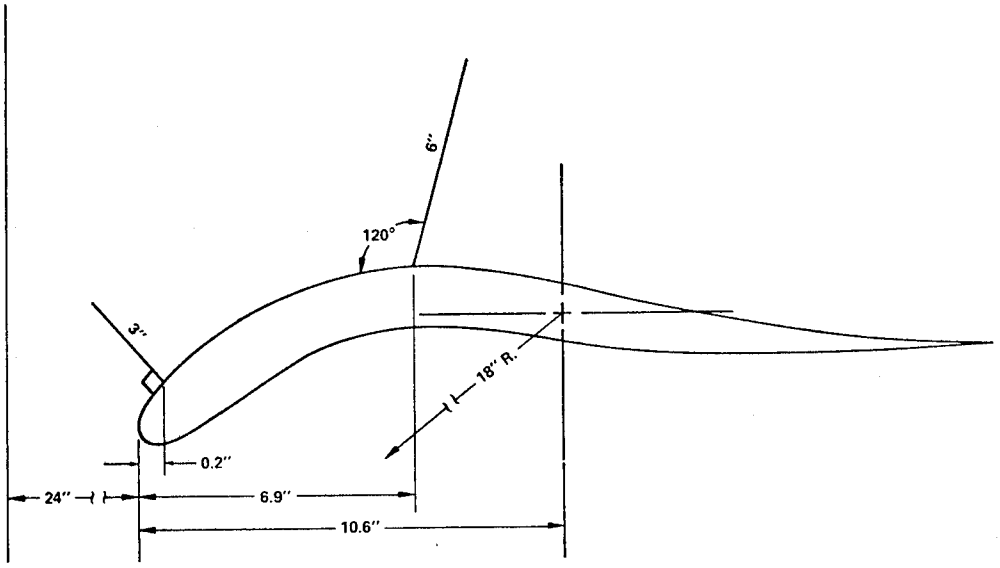


Figure 11. Slot arrangement for wall blowing.

x/c	y/c Upper Surface	y/c Lower Surface
0.0000	0.0000	0.0000
0.0050	0.0172	-0.0140
0.0075	0.0216	-0.0167
0.0100	0.0254	-0.0188
0.0125	0.0289	-0.0202
0.0150	0.0322	-0.0210
0.0175	0.0353	-0.0214
0.0200	0.0382	-0.0215
0.0250	0.0437	-0.0210
0.0275	0.0463	-0.0206
0.0300	0.0488	-0.0199
0.0350	0.0536	-0.0183
0.0400	0.0583	-0.0162
0.0450	0.0626	-0.0140
0.0500	0.0668	-0.0116
0.0550	0.0707	-0.0091
0.0600	0.0745	-0.0066
0.0650	0.0781	-0.0041
0.0700	0.0815	-0.0015
0.0750	0.0848	0.0011
0.0850	0.0909	0.0064
0.0950	0.0966	0.0012
0.1000	0.0993	0.0146
0.1300	0.1134	0.0311
0.1600	0.1248	0.0471
0.1900	0.1340	0.0607
0.2000	0.1367	0.0645
0.2300	0.1432	0.0732
0.2600	0.1479	0.0786
0.2900	0.1508	0.0813
0.3000	0.1514	0.0816
0.3500	0.1508	0.0794
0.4000	0.1444	0.0718
0.4300	0.1375	0.0654
0.4600	0.1290	0.0584
0.4900	0.1196	0.0513
0.5000	0.1163	0.0489
0.5300	0.1065	0.0420
0.5600	0.0968	0.0357
0.5900	0.0874	0.0299
0.6000	0.0843	0.0282
0.6300	0.0751	0.0233
0.6600	0.0662	0.0192
0.6900	0.0578	0.0156
0.7000	0.0552	0.0146
0.7300	0.0474	0.0116
0.7600	0.0401	0.0088
0.7900	0.0331	0.0062
0.8000	0.0309	0.0054
0.8300	0.0243	0.0032
0.8600	0.0181	0.0012
0.8900	0.0123	-0.0004
0.9000	0.0105	-0.0009
0.9200	0.0071	-0.0017
0.9400	0.0040	-0.0025
0.9600	0.0011	-0.0032
0.9800	-0.0016	-0.0037
0.9900	-0.0030	-0.0040
1.0000	-0.0044	-0.0044

Table 1. Airfoil profile coordinates.

Experimental verification

Description of model

The model had a nominal chord length of 24 in , a span of 36 in , and overall dimensional tolerances of $\pm$ 0.002 in. The airfoil was constructed of aluminium and had a highly polished surface finish.

The important objective of the model design was to keep the upper surface free of discontinuities and to minimize the possibility of downstream contamination and boundary layer tripping. To this end, extreme care was exercised in sizing and locating pressure orifices. Coordinates for the 81 pressure orifices on the surface of the model are given in Table 2. Surface pressure orifices at or near midspan provided good definition of the pressure distribution, and orifices at several spanwise stations and at the trailing edge provided information about the two-dimensionality of the flow over the airfoil. All pressure tubings were installed through lower surface plates to ensure an aerodynamically clean upper surface. After final assembly, every office was examined and tested for burrs, blockage, and leakage.

Careful dimensional inspection showed that the model was well within the prescribed tolerances for profile coordinates (see Table 1) and spanwise waviness.

Description of wind tunnel

The model was tested in the Boeing two-dimensional research wind tunnel. This is a closed-circuit, single-return, continuous-flow, atmospheric tunnel. The test section is 8 ft high, 3 ft wide, and 20 ft long and has a contraction ratio of 12:1. The speed range is between 20 and 230 mph ($M \simeq 0.3$), with maximum unit Reynolds number of about 2×10^6/ft.

The wind tunnel is intended primarily for two-dimensional testing of high lift systems. Two-dimensionality of flow at all lift levels was ensured by application of wall blowing (up to a mass flow of 20 lb/sec at 1000 psia) that matched boundary layer control with the local pressure levels on the airfoil. Flow in the test section was uniform and parallel; turbulence levels were less than 0.08 percent of free-stream velocity. The tunnel dynamic pressure was regulated within $\pm$ 0.2 percent by a unique automatic control system that involved flaps far downstream of the model at the entrance of the diffuser. This control system was interlocked with the data acquisition system in such a way that no data were recorded if the tunnel speed deviated from the present values by more than the regulated tolerance level ($\pm$ 0.2 percent).

The model spanned the width of the tunnel and was mounted on two 3-ft-diameter turntables that were flush with the

Orifice No.	x/c Chord	y/c Height	z/c Span	Orifice Diam In.
1	0.0000	0.0000	0.750	0.015
2	0.0047	0.0168	0.708	0.010
3	0.0098	0.0251	0.791	
4	0.0148	0.0320	0.783	
5	0.0199	0.0381	0.716	
6	0.0299	0.0487	0.774	
7	0.0498	0.0667	0.724	0.010
8	0.0702	0.0817	0.766	0.020
9	0.1002	0.0994	0.732	
10	0.1201	0.1091	0.756	
11	0.1500	0.1213	0.741	
12	0.2003	0.1368	0.750	
13	0.2502	0.1466	0.787	0.020
14	0.2697	0.1491	0.712	0.025
15	0.2995	0.1514	0.779	
16	0.3197	0.1518	0.720	
17	0.3500	0.1508	0.770	
18	0.4001	0.1444	0.729	
19	0 4201	0.1400	0.762	
20	0.4503	0.1319	0.737	
21	0.5000	0.1164	0.754	
22	0.5489	0.1004	0.744	
23	0.5999	0.0843	0.749	
24	0.6502	0.0690	0.784	
25	0.7000	0.0552	0.713	
26	0.7501	0.0425	0.776	
27	0.8003	0.0308	0.722	
28	0.8503	0.0201	0.768	
29	0.9004	0.0105	0.730	
30	0.9500	0.0025	0.760	0.025
31	0.9916	-0.0036	0.750	0.010
32	0.0049	-0.1389	0.750	0.010
33	0.0097	-0.0186	0.707	
34	0.0150	-0.0210	0.783	
35	0.0198	-0.0215	0.716	
36	0.0299	-0.0199	0.724	
37	0.0499	-0.0116	0.774	0.010
38	0.0698	-0.0016	0.733	0.020
39	0.0998	0.0145	0.766	
40	0.1497	0.0418	0.758	
41	0.2000	0.0645	0.746	
42	0.2502	0.0772	0.713	0.020
43	0.3002	0.0816	0.721	0.025
44	0.3502	0.0793	0.730	
45	0.4000	0.0718	0.771	
46	0.5002	0.0488	0.746	
47	0.6001	0.0282	0.754	
48	0.7003	0.0145	0.785	
49	0.8001	0.0054	0.777	
50	0.9000	-0.0009	0.769	0.025
51	0.0500	0.0172	0.357	0.010
52	0.4002	0.1443	0.354	0.025
53	0.6003	0.0843	0.374	0.025
54	0.0498	0.0667	1.141	0.010
55	0.4000	0.1444	1.146	0.025
56	0.6002	0.0843	1.125	0.025
57	0.0498	0.0667	0.041	0.010
58	0.2005	0.1368	0.049	0.025
59	0.4002	0.1443	0.041	
60	0.6002	0.0843	0.050	
61	0.8001	0.0308	0.041	0.025
62	0.0495	0.0667	1.458	0.010
63	0.1999	0.1368	1.450	0.025
64	0.3999	0.1444	1.458	0.025

Table 2. Pressure orifice locations.

Orifice No.	x/c Chord	y/c Height	z/c Span	Orifice Diam In.
65	0.6000	0.0843	1.449	0.025
66	0.3002	0.1514	1.458	0.025
67	0.9916	-0.0036	0.375	0.010
68	0.9916	-0.0036	1.125	0.010
69	0.9916	-0.0036	0.042	0.010
70	0.4003	0.1443	0.937	0.025
71	0.4002	0.1443	0.187	↓
72	0.4002	0.1443	1.312	↓
73	0.2000	0.0645	1.466	↓
74	0.4003	0.0718	1.450	↓
75	0.1998	0.0644	0.033	↓
76	0.3996	0.0719	0.050	↓
77	0.6000	0.0282	0.354	↓
78	0.3999	0.0718	0.375	↓
79	0.6003	0.0282	1.146	▽
80	0.4002	0.0718	1.125	0.025
81	0.9916	-0.0036	1.458	0.010

Table 2. Continued.

Instrument	Range	Accuracy
Balance		
Lift	0 to 4000 lb	±3 lb
Drag	0 to 600 lb	±1 lb
Pitching Moment	0 to 20,000 in lb	±20 in lb
Pressure		
Transducers	0 to 2.5 psid	±0.25 percent full scale
	0 to 5.0 psid	↓
	0 to 7.5 psid	↓
	0 to 100 psia	±0.25 percent full scale
Boundary Layer Probe		
Traversing Mechanism	0 to 1.5 in	±0.001 in.
Angle of Attack		
Mechanism	-10 to 24 deg	±0.05 deg

Table 3. Range and accuracy of instrumentation.

tunnel walls. A remotely controlled hydraulic servosystem was used to rotate the turntables for changes in angle of attack. Two tangential blowing slots on each turntable provided boundary layer control on the tunnel wall (Fig. 11 for slot arrangement) together with long vertical slots upstream of the turntables. The blowing rates were matched for each tunnel test condition. The flow in the tunnel test section was found to be free of angularity.

Test conditions and techniques

The wing model was tested at seven speed levels ranging from 95 to 290 fps (full-scale equivalent of 45 to 200 mph) and at angles of attack from $\alpha \simeq -3.5$ deg ($C_\ell \simeq 0$) to stall angle ($C_\ell \simeq$ maximum, up to $\alpha = +16$ deg). Both free and fixed transition configurations were investigated. Each test run consisted of approximately 17 points at fixed pitch angles. Balance and pressure data were taken at each of the test points. Five pitch angles were chosen (close to the minimum drag value and stall), and horizontal integrated wake rake and vertical wake traverse measurements were also performed for each test run. The integrated value (area under curve) of the vertical wake survey served as the most reliable measure of the true drag levels. These drag values were then compared with the integrating wake rake measurements at each point. The average discrepancy between these two measurements was usually less than $\pm$ 5 percent. The direct drag force measurements were unreliable and did not represent the true two-dimensional section coefficients; therefore they are not used in the present paper.

At design conditions ($q \simeq 78$, $Re_c = 3 \times 10^6$), boundary layer measurements were taken at three chord stations for five angles of attack with clean wing configuration. Table 4 summarizes the test conditions.

Considerable care had been exercised at the beginning of the test program to ensure the two dimensionality of the tunnel flow by the use of wall blowing. The proper wall slot blowing pressures were determined for each tunnel speed at maximum lift conditions by using tuft flow visualization on the surface of the wing and by monitoring the lift as a function of the blowing rate. Once the blowing rate was high enough to control the boundary layer, steady uniform two-dimensional flow was obtained, and a further increase in the blowing rate did not affect the flow over the model. Two-dimensional flow was verified during the entire test by several means: model surface flow visualization (tufts and oil flow techniques), spanwise static pressure distributions, and spanwise traverse of the integrating wake rate. All these methods indicated that the two-dimensional flow was extremely uniform at all test conditions prior to upper or lower surface flow separation. For example, spanwise static pressure distributions for the entire test envelope deviated less than $\pm$ 2 percent along the entire span at 5-, 20-, 40-, 60-,

Configuration	q psf	$Re_c \times 10^6$	α deg	Type of Data: Balance lb	Pressure psid	Wake Rake psid	Boundary Layer psid; in	Flow Visualization
Wing-Natural Transition	10.1	1.06	-4 to stall	x	x	x	-	Tuft
↓	20.1	1.48	↓	x	x	x	-	Tuft
	38.9	2.13		x	x	x	-	Tuft;Oil
	59.6	2.59		x	x	x	-	Tuft
	78.3	2.99		x	x	x	x	Tuft;Oil
	86.8	3.13		x	x	x	-	Tuft
▽	97.6	3.28	▽	x	x	x	-	Tuft
Wing-Fixed Transition (a)	78.3	2.99	+5 to stall	-	-	-	-	Oil
	38.9	2.13	-4 to stall	x	x	x	-	Oil
Wing-Fixed Transition (b)	38.9	2.13	-4 to stall	x	x	x	-	-
↓	78.3	2.99	↓	x	x	x	-	-
Wing-Fixed Transition (c)	38.9	2.13	▽	x	x	x	-	-
▽	78.3	2.99	-4 to stall	x	x	x	-	-

Notes: 1. Angle of Attack Schedule:
Force and Pressure Data: α = -4° to +2° by 2°
+3° to α_{stall} -2° by 1°
α_{stall} -2° to α_{stall} by 0.5°

Wake Survey Data: α = +2; 4; 6; 7; α_{stall} - 2° and α_{stall} -1°

2. Boundary Layer Probe Location:
Spanwise Location: 9.6 in from left wall
Chordwise locations: 40, 60, 90 percent chord from leading edge.
Probe mounted from support bracket bolted to the underside of the wing.

3. Boundary Layer Trip
(a) No. 80 grit, 0.10 in width, 21.7 percent chord
(b) No. 100 grit, 0.10 in width, 21.7 percent chord
(c) No. 100 grit, 0.10 in width, 16.7 percent chord

Table 4. Test conditions.

Tunnel Dynamic Speed psf	Forward Slot psia	Left Forward Slot psia	Left Aft Slot psia	Right Forward Slot psia	Right Aft Slot psia
10.1	15.7	19.1	24.1	19.1	26.5
20.1	15.7	21.2	28.5	21.2	32.5
38.9	off	22.0	30.1	22.0	33.8
59.6	off	23.2	32.2	23.3	36.4
78.3	off	25.2	35.6	25.2	40.2
86.8	off	29.6	42.5	29.9	47.8
97.6	off	33.6	48.0	33.9	54.7

Table 5. Schedule for turntable and forward slot blowing.

and 80-percent chord as well as at the trailing edge on both surfaces when attached flow was present. Table 5 summarizes the blowing slot pressure at various tunnel speeds.

The grit sizes used to fix boundary layer transition were computed according to Braslow [9]. These were placed in the rooftop pressure region ahead of the pressure recovery zone to ensure turbulent rooftop pressure distribution.

Instrumentation and accuracy

Lift, drag and pitching moment data were obtained with a three component straingange balance mounted under the tunnel floor. Model surface pressures, tunnel static and total pressures, as well as wall blowing were measured with pressure transducers through nine multiposition scanivalves using 2.5-, 5.0-, and 7.5-psid transducers and one 100-psia transducer. A pneumatically integrating wake rate, which included separate total and static pressure probes, permitted rapid definition of the wake profile and drag. Its accuracy had been substantiated by comparing with actual integration of wake profiles. The same rake also incorporated a shielded total pressure probe and a Prandtl-tube static pressure probe for wake traversers.

Surveys of boundary layers were made with a miniature traversing mechanism that used a very high fineness ratio rectangular total pressure probe and a 2.5-psid transducer. Table 3 indicates the range and approximate accuracy of the instrumentation.

Data acquisition, display, and reduction

Data acquisition was fully automated with simultaneous on-line data display of x-y plotters. The data system consisted of a 19-channel digital analyzer and magnetic tape recorder. Angle of attack, dynamic pressure, and balance data were recorded together with information on model surface pressure, wake rate, boundary layer, and tunnel pressure and then processed through a data reduction program. This program converted the raw data counts into engineering units (i.e., pounds per square inch, pounds, inches, etc.), subtracted balance tares, and applied solid and wake blockage, incidence, streamline curvature, and compressibility corrections to the data. In the printout, both corrected and uncorrected data appeared in engineering units and coefficient form. The applied corrections were about $\pm$ 1.5 percent of the measured quantities (i.e., lift, drag, pitching moment, C_p, α, etc.).

During the test run, uncorrected real time signals were plotted on four x-y Moseley recorders. Continuously monitored quantities were plotted for C_ℓ versus α, C_ℓ versus C_D, C_D

along the span (the integrating wake rate data), and C_D along the vertical distance (the single total pressure probe that measured the wake profile at midspan.

Blockage, incidence, streamline curvature, and compressibility corrections were applied to all the data presented in the paper.

Results and discussions

Figure 12 shows the lift coefficient as a function of angle of attack for the wing with natural transition. The angle of attack at zero lift coefficient (-3.5 deg) was very clearly independent of the Reynolds number or speed. Except for q = 38.9 psf, the lift curves in the entire speed range were linear almost up to $C_{\ell_{max}}$ and stall. However, there were changes in the lift curve slopes at around α = 4 to 5 deg for each speed. The angle of attack value of α = 5 deg was closely related to flow attachment on the lower surface; below α = 4 deg, part of the lower surface flow separated at around 5 percent chord and reattached at around 35 percent chord length. Beyond α = 5 deg, the entire lower surface flow was attached. When this happened, the lift slope changed. Table 6 gives the initial and final slopes for the lift curves. The initial slopes were nearly independent of the tunnel speed* in the test range. On the other hand where the flow was attached on both surfaces, the final slopes had a maximum value at q = 38.9 psf (M = 0.165).

It is interesting to note that at M = 0.165, the lift line became highly nonlinear and maximum lift was maintained up to a rather high angle of attack without the typical sharp brake in the lift curve.

Both the maximum lift coefficient and the stall angle varied with wind speed. At the lowest speeds (q = 10.1 and 20.1 psf) $C_{\ell_{max}}$ reached above 2.0; however, at q = 38.9 to 78 psf (M = 0.165 to 0.232, $C_{\ell_{max}}$ = 1.75. Likewise, the stall angle dropped from about 14 to around 10 deg in the speed range studied.

Flow visualization and integrated wake measurements showed that stall occurred first around midspan close to the trailing edge and propagated toward the tunnel walls when the angle of attack was further increased. Flow separation also was propagated toward the leading edge, and strong trailing edge vortices were present at the later stages of stall. This phenomenon started at decreasing angles of attack as wind speed was increased. Flow visualization also showed the presence of a small laminar separation bubble, about 0.5 in in length, at around 35 percent chord, followed by

*Note: The test setup with an atmospheric wind tunnel made it difficult to separate Reynolds number and compressibility effects. However, in general, loss of $C_{\ell_{max}}$ is ascribed to the adverse effects of incompressibility.

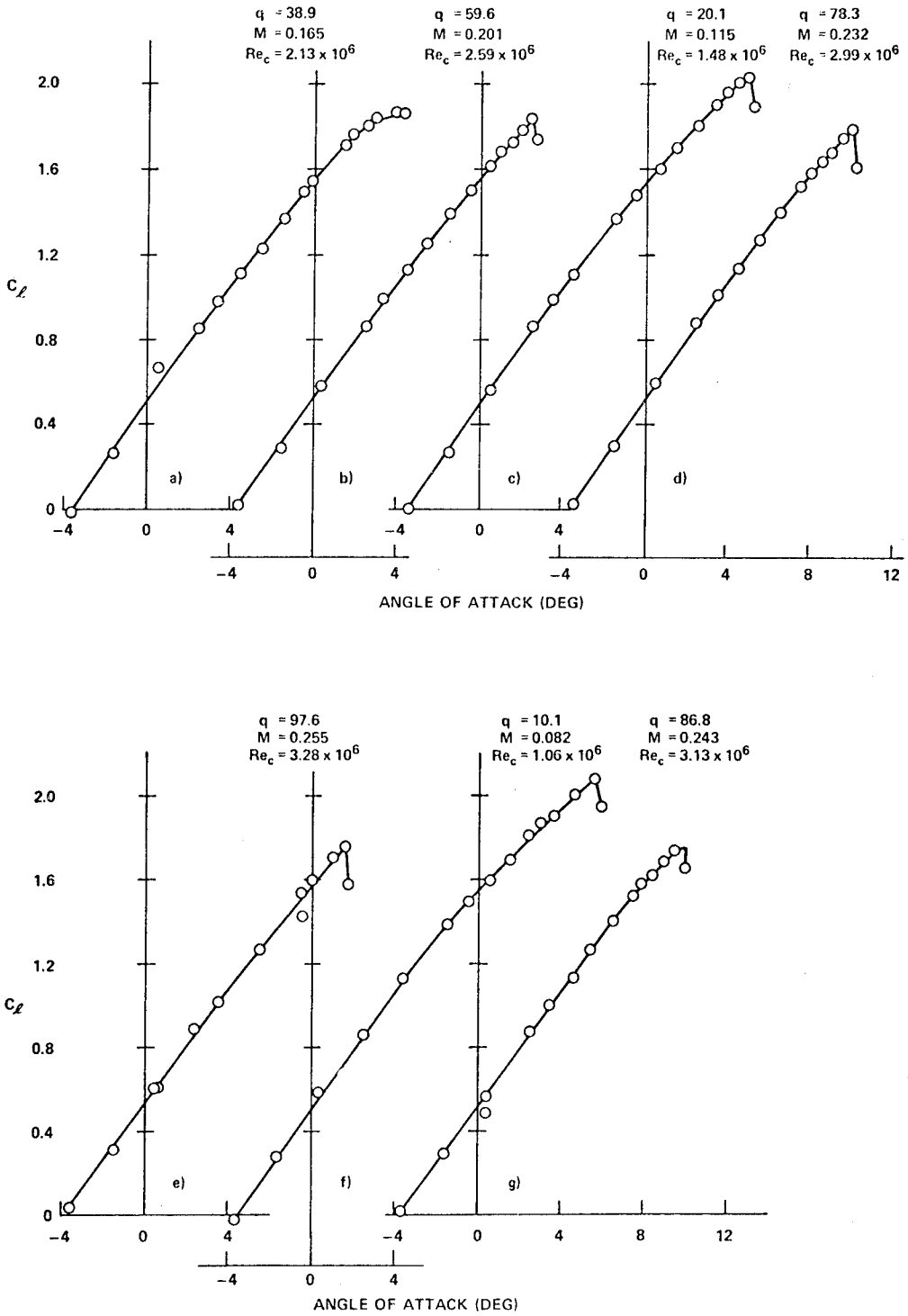


Figure 12. Lift coefficient as a function of angle of attack.

reattachment for the wing with free transition. When a boundary layer trip was present, this bubble was absent. As expected, however, $C_{\ell_{max}}$ occurred at lower angle of attack and reached values that were generally 10 percent below the $C_{\ell_{max}}$ values obtained at natural transition because of the artificial thickening of the upper surface boundary layer.

Figure 13 shows the section drag coefficient as a function of angle of attack for the wing natural transition. The drag levels stayed relatively constant and close to the minimum value at around α = 6 to 10 deg. Minimum drag coefficient level decreased slightly with increasing Reynolds number. Drag rise occurred at rather high angles of attack at high C_ℓ values. This is further substantiated by Fig. 14 which shows the drag polar in each test speed. Except for q = 38.9 psf, where an abrupt rise in drag occurred at around C_ℓ = 1.82, the drag polars showed very gradual changes in the aerodynamic character of the model. This was despite the continual increase in lift that occurred due to high suction over the forward portion of the upper surface where pressure levels were almost constant.

The presence of boundary layer trips on the wing upper surface increased the minimum drag levels by as much as 40 percent above the comparable values obtained at natural transition. Figure 15 shows the lift to drag ratios for all test conditions at free transition. As the angle of attack exceeded 5 deg, the L/D ratios increased rapidly over the entire speed range. In the low speed range (at M = 0.082 and 0.115), the high lift/drag ratio was maintained for large changes in angle of attack and variations of C_ℓ. As the speed increased, there were decreases in both the level of $(L/D)_{max}$ and the α range within which the L/D was nearly constant. However, since L/D ratios of well over 110 were achieved at all speeds within C_ℓ = 1.20 to 1.90 (these characteristics are well above the aerodynamic performance of currently used airfoils) the tested airfoil section must be considered superior to present day profiles.

When boundary layer trips were present, the L/D was 50 percent less than for the clean wing configuration (q = 38.9 and 78.3 psf) because of increased skin friction and decreased peak suction at around 25-percent chord length. Figure 16 indicates the variation of the quarter-chord pitching-moment coefficient with angle of attack for various air speeds. As the angle of attack increased from α = -3.5 deg, the pitching-moment coefficients rapidly grew more negative up to the point where fully attached flow was present on both surfaces of the airfoil (at around α = 4 to 5 deg). Thereafter, the increase became practically linear and less rapid up to stall angle. Throughout the speed and angle of attack ranges, the airfoil remained aerodynamically stable (negative pitching-moment coefficient). There was little variation with speed at any given angle of incidence and on the average, $C_m \simeq -0.095$ at maximum lift coefficients. In fact, beyond C_ℓ = 1.0, a further rise of the lift coef-

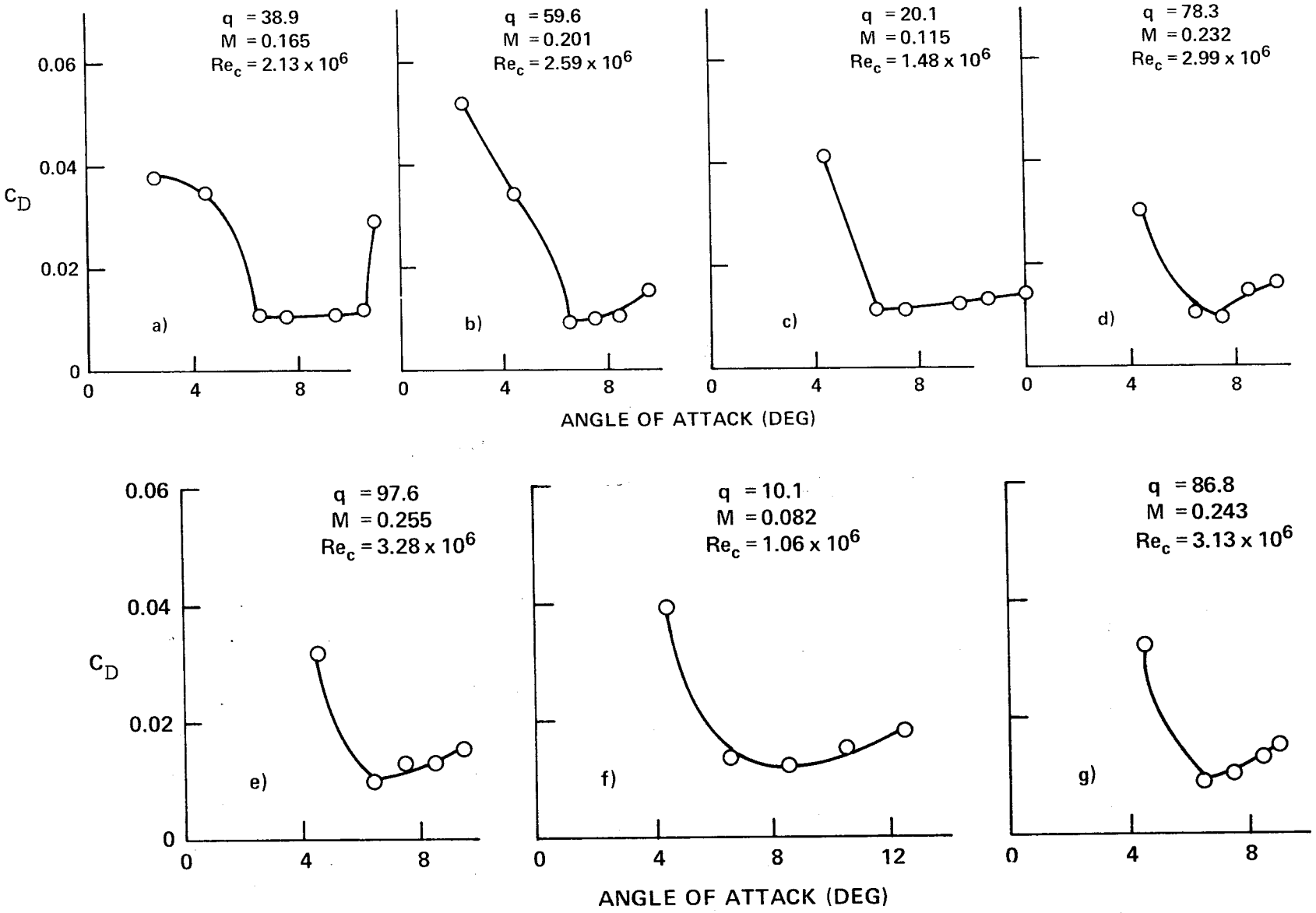


Figure 13 - Drag Coefficient as a Function of Angle of Attack

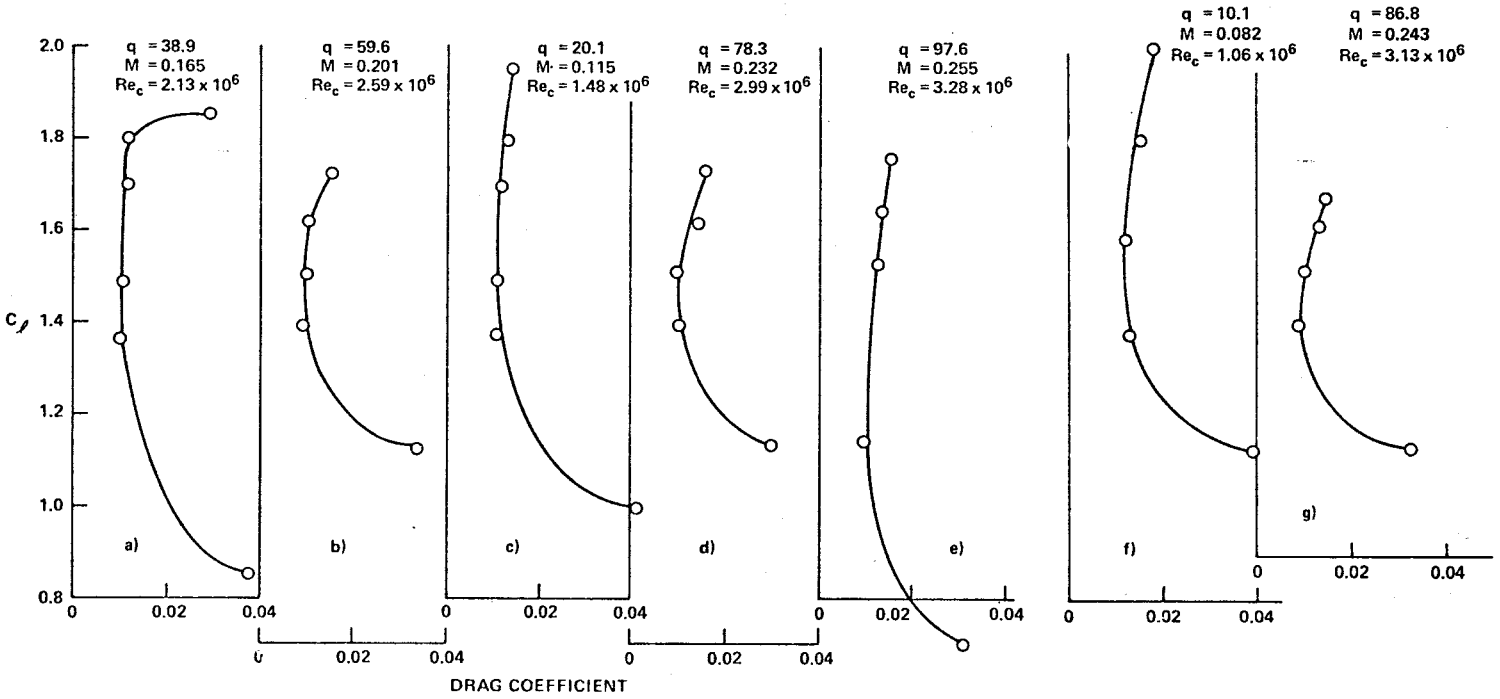


Figure 14. Drag polar.

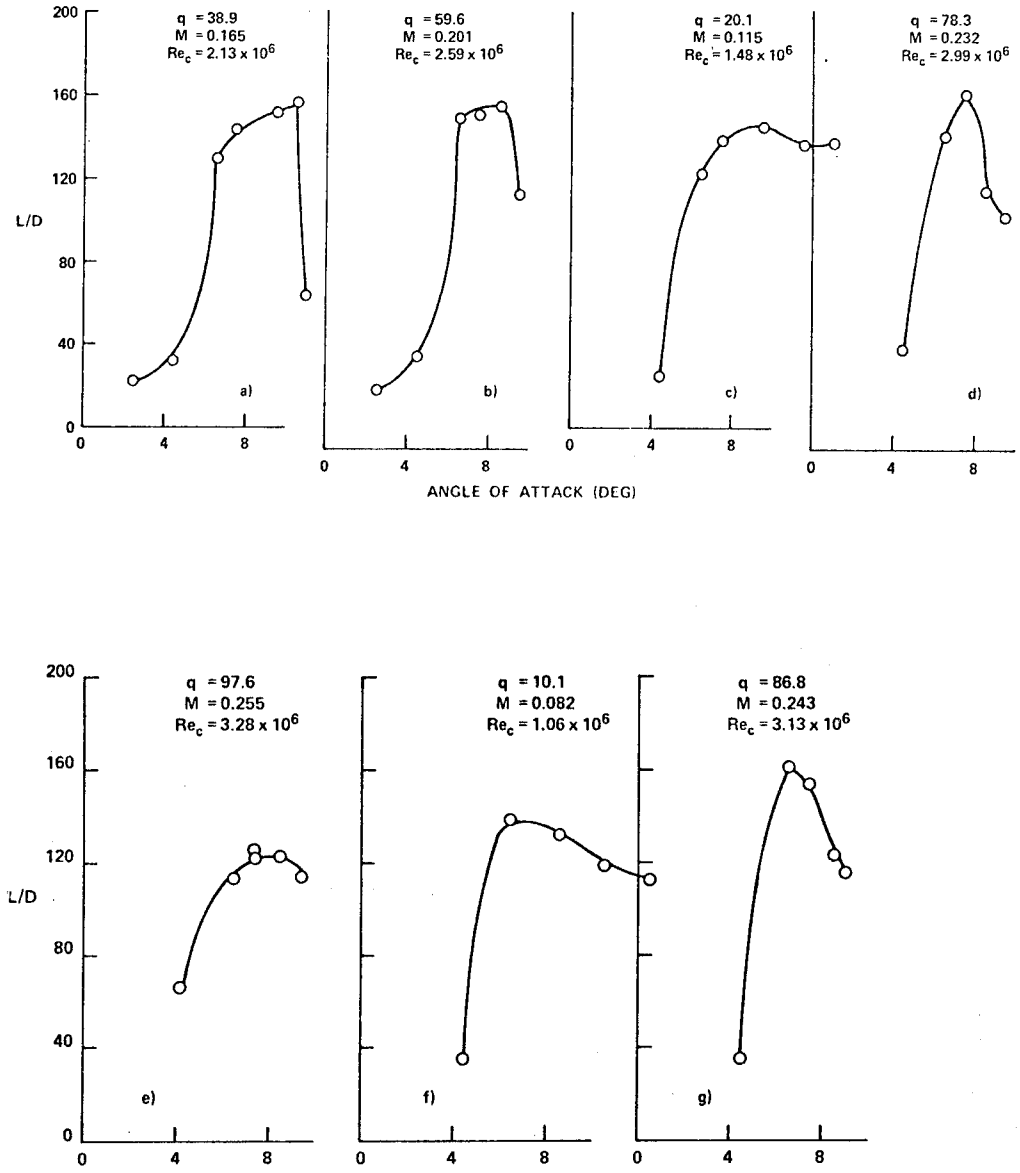


Figure 15. Lift to drag ratio as a function of angle of attack.

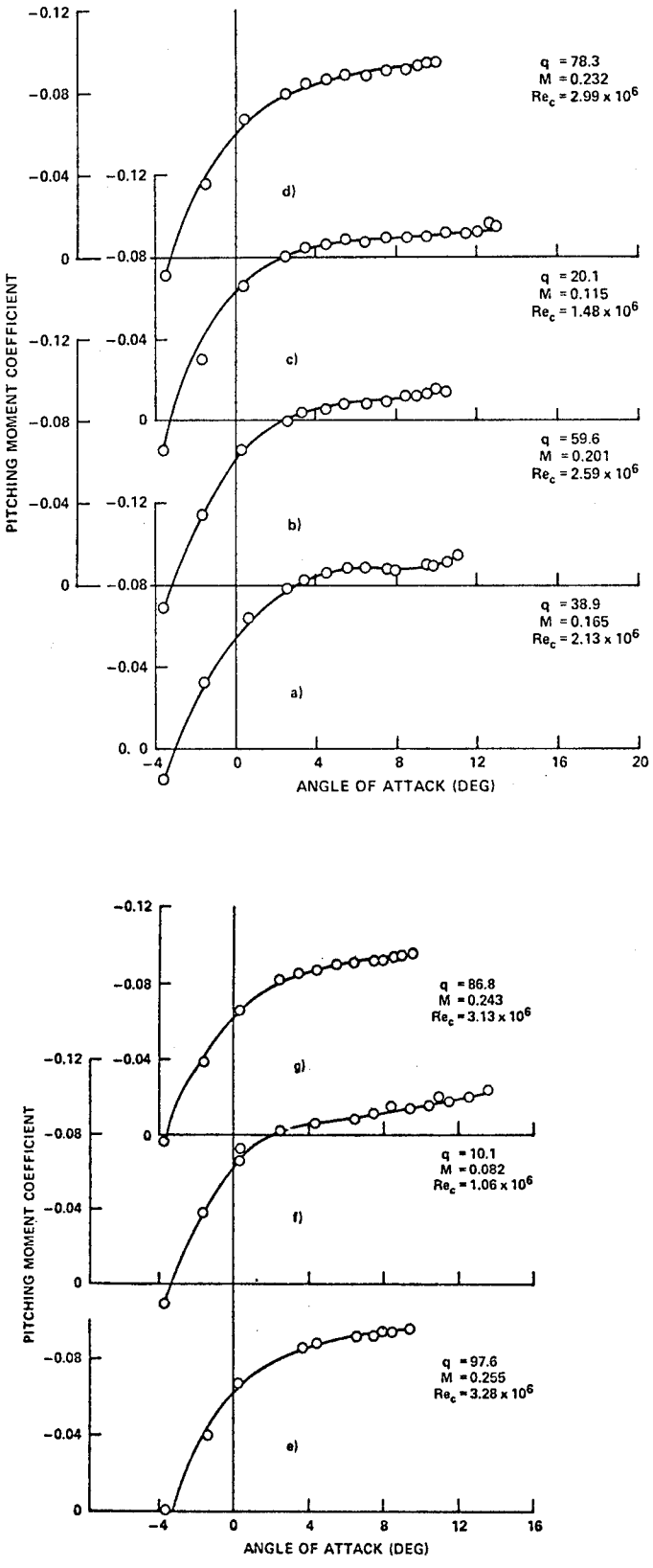


Figure 16. Pitching moment coefficient as a function of angle of attack.

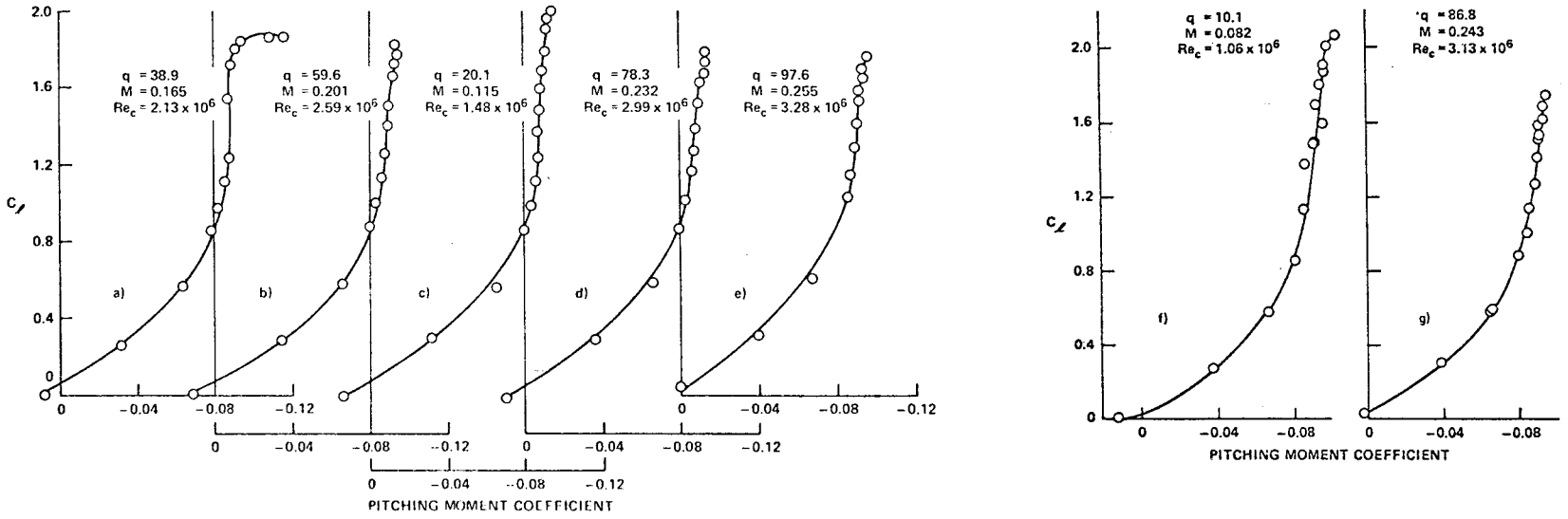


Figure 17. Lift coefficient as a function of pitching moment.

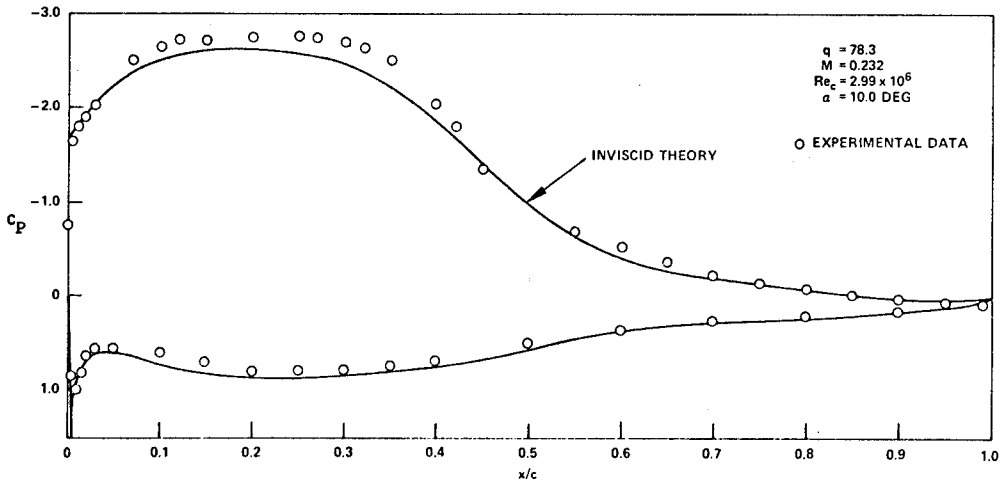


Figure 18. Pressure coefficient distribution at design condition

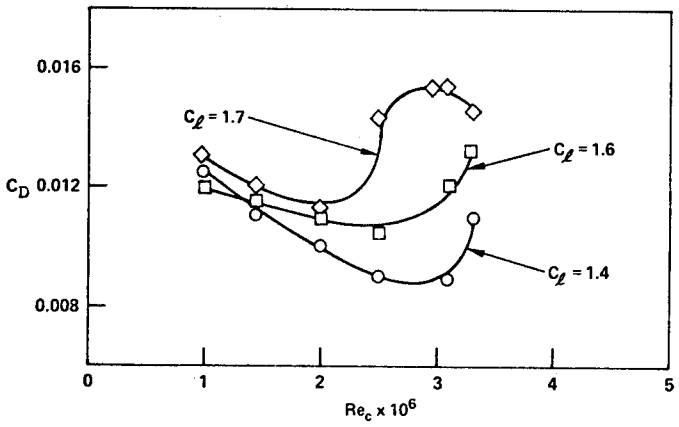


Figure 19. Effect of Reynolds number on the drag coefficient.

ficient did not cause appreciable increase in C_m. This shows up rather well in the C_ℓ - C_m curves presented in Fig. 17.

Figure 18 indicates the experimental pressure coefficient distribution along the chord; the theoretical distribution is included for purposes of comparison. It is evident that the experimental value of the pressure coefficient was within 5 percent of the theoretical value. The largest deviation occurred at the minimum pressure area between 10- and 35-percent chord length on the upper surface. This was caused by the occurrence of laminar flow in that area despite design predictions that the flow there would be turbulent. The presence of laminar flow caused higher suction levels and hence lower local C_p values. In the adverse pressure region (beyond the 40-percent chord point), the agreement between theory and measurements was quite good, confirming the validity of the Stratford theory. Boundary layer measurements also showed that the velocity profile closely agreed with the Stratford incipient separation criterion at 60 and 90-percent chord lengths.

It is evident from Table 7, which presents the boundary layer thickness distribution at design speed (q = 78.3 psf), that the boundary layer was turbulent at 60 and 90-percent chord lengths and that it increased in thickness as the angle of attack increased. At 40-percent chord length on the other hand, the value for boundary layer thickness indicated laminar conditions throughout the angle of attack range even though the thickness increased considerably at higher α.

Figure 19 shows the effect of Reynolds number on the drag coefficient at various high lift coefficient levels. At $C_\ell = 1.4$, the drag coefficient decreased with increasing Re_c and reached a minimum value of $C_D = 0.0088$ at $Re_c \simeq 3.1 \times 10^6$, the drag coefficient rapidly increased to a value of $C_D \simeq 0.015$. As the lift coefficient increased, the minimum drag coefficient increased in absolute value and occurred at progressively lower Reynolds numbers as well. Accordingly, drag divergence was encountered at the lower Reynolds numbers. Since drag divergence is dependent on Mach number and compressibility effects at high lift are quite severe even at M = 0.15 - 0.20 (according to Van den Berg [10]), Fig. 19 may also represent a combination of the influence of Reynolds and Mach numbers

The effects of compressibility on the maximum L/D ratio and stall angle are shown in Fig. 20. Below M = 0.12, $(L/D)_{max}$ was nearly independent of Mach number; however, even at this low speed, α_{stall} decreased with increasing M. There was a 30 percent decrease in $(L/D)_{max}$ level between M = 0.14 and 0.23. Beyond M = 0.23, $(L/D)_{max}$ seemed to level off at $\sim$ 120. The stall angle decreased about 23 percent between M = 0.12 and 0.20; beyond that speed range, it leveled off at stall $\alpha \simeq 10.5$ deg. The rather significant compressibility effects showed that the present form of the theory used in the design of the airfoil is applicable only to low speed airfoil sections.

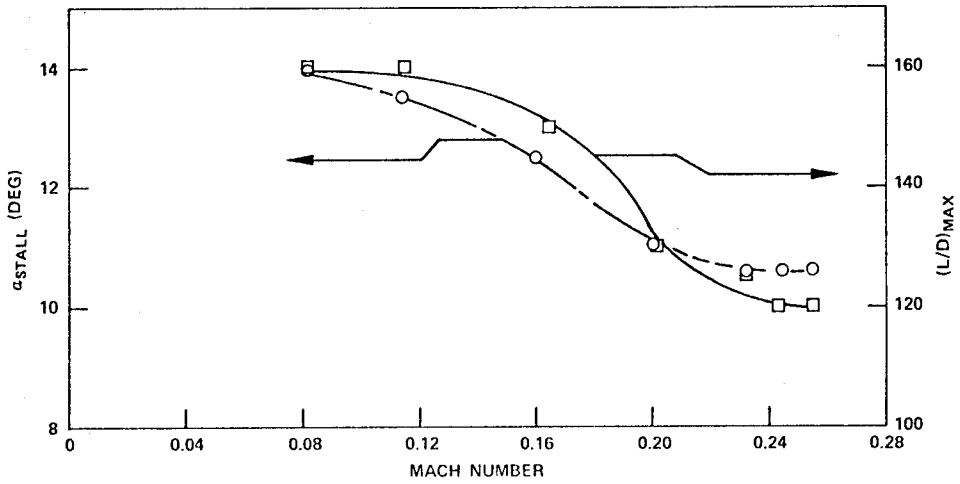


Figure 20. Mach number effect on $(L/D)_{max}$ and α_{stall}.

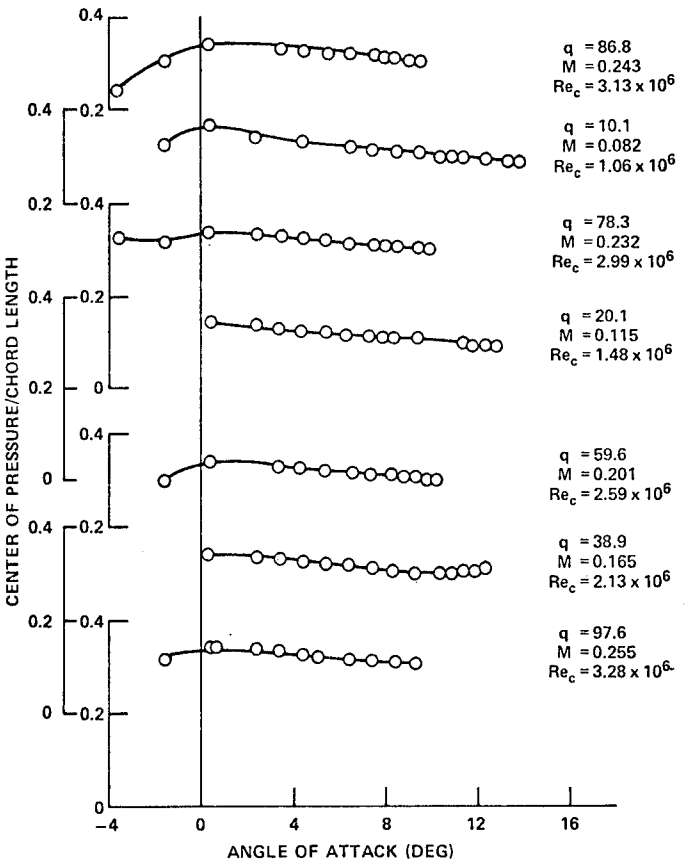


Figure 21. Center of pressure as a function of angle of attack.

M	Reynolds Number	(dC_ℓ/d_α) Initial	Final
0.082	1.06×10^6	0.140	0.095
0.115	1.48×10^6	0.140	0.100
0.165	2.13×10^6	0.142	0.125
0.201	2.59×10^6	0.137	0.115
0.232	2.99×10^6	0.140	0.100
0.243	3.13×10^6	0.133	0.110
0.255	3.28×10^6	0.140	0.110

Table 6. Lift curve slopes. (Angle of attack is in degrees.)

α	Chord Length		
	40 Percent	60 Percent	90 Percent
5.5	0.075	0.334	0.608
6.5	0.083	0.337	0.623
7.5	0.091	0.341	0.639
8.5	0.099	0.344	0.662
9.5	0.115	0.348	0.705

Table 7. Boundary layer thickness distribution at q = 78.3 PSF.

Figure 21 presents the variation of chordwise position of the center of pressure for various Reynolds numbers. Air speed or Reynolds number did not seem to affect the center of pressure, but there was a small variation with angle of attack. At around $\alpha = 0$ deg, the center of pressure was located about 33 percent from the leading edge; as the angle of incidence increased, the center of pressure moved forward toward the 30-percent chord location where it remained up to stall angle.

Conclusions

An analytical procedure developed for the design of two-dimensional, high-endurance airfoils permits the desired performance point to be determined prior to the existence of an airfoil profile (inverse problem). Once the airfoil profile is determined, the off-design characteristics can be obtained by applying existing direct inviscid methods in combination with boundary layer theory. Experimental verification showed good agreement but indicated that the analytical design tends to be conservative, i.e., underpredicts performance.

It was demonstrated that proper use of the analytical method can yield monoelement airfoils with performance characteristics that are superior to those of any existing section. Hence, this development adds a valuable tool to the growing body of knowledge for airfoil design.

However, the analytical method has its limitations. In its present form, it is most successfully applied in the low speed range where compressibility effects are small. It is possible, however, to extend the theory to include compressibility. A second limitation stems from the fact that the theory does not address three-dimensional effects, and these are always present on a real aircraft wing. This is perhaps the most fruitful area for further research, namely, the extension of the present two-dimensional theory to a more realistic three-dimensional wing design method.

References

1. Liebeck, R.H. and Ormsbee, A.I.; Optimization of Airfoils for Maximum Lift, Journal of Aircraft, Vol. 7, No. 5, pp. 409-415.

2. Strand, T.; Wing Sections Designed for Maximum Upper Surface Lift and Low Drag, with a Given Thickness Distribution at a Given Reynolds Number, Air Vehicle Corporation Report 375, Oct 1971.

3. Abbot, I.H. and Von Doenhoff, A.E.; Theory of Wing Sections, Dover Publications, 1959.

4. Stratford, B.S.; The Prediction of Separation of the Turbulent Boundary Layer, Journal of Fluid Mechanics, Vol. 5, 1959.

5. Thwaites, B.; Incompressible Aerodynamics, Oxford University Press, 1960.

6. Theodorsen, T. and Garrick, I.E.; General Potential Theory of Arbitrary Wing Sections, NACA Report 452, 1933.

7. James, R.M.; A New Look at Two-Dimensional Incompressible Airfoil Theory, McDonnell Douglas Report DC-J0918/01, May 1971.

8. Von Doenhoff, A.E. and Tetervin, N.; Determination of General Relations for the Behavior of Turbulent Boundary Layers, NACA Report 772, 1943.

9. Braslow, A.L.; Use of Grit-Type Boundary-Layer-Transition Trips on Wind-Tunnel Models, NASA TN D-3579, 1966.

10. Van den Berg, B.; Reynolds Number and Mach Number Effects on the Maximum Lift and the Stalling Characteristics of Wings at Low Speeds, NLR TR 69025U, 1969.

COMPUTER ANALYSIS OF THE PERFORMANCE OF 15m SAILPLANES

by

F.G. Irving
Senior Lecturer
Department of Aeronautics
Imperial College of Science and Technology
London, England

Notation

A	Aspect ratio
r	Radial distance from the axis of the thermal
R	Value of r at which $v_t = 0$
v_t	Local vertical velocity of air in thermal at radius r
V_t	Vertical velocity at r = 0
V_{cc}	Cross-country speed
W	All-up weight of sailplane
W_{opt}	Optimum value of W giving max V_{cc}.

Introduction

The object of the analysis is to find the optimum characteristics of a fixed-geometry 15m sailplane so as to give the maximum cross-country speed when using thermals with a given vertical velocity profile.

A previous paper [Ref. 1] considered thermals with a parabolic velocity profile and concluded that, under most conditions of thermal core strength and radius, a sailplane with an aspect ratio of about 16 would provide the best compromise, so long as provision were made for the carriage of a large amount of ballast. It was noted that, under most conditions, the achieved cross-country speed was very insensitive to aspect ratio, provided that the weight of the sailplane was optimised for the prevailing thermal conditions.

The present paper reconsiders the above results in the light of an updated estimate of practical sailplane weights and concludes that the revised weight figures do not have a great influence. A slightly higher aspect ratio (say 18) might be more suitable.

The calculations have also been extended to consider thermals with a fourth-power-law velocity distribution. Whilst the optimum aspect ratio tends to be lower than in parabolic thermals, values of 16 or 18 still provide an excellent compromise, although low aspect ratios are desirable if the thermals are strong. Again, provision should be made for a large amount of ballast.

Computations for parabolic thermals

A computer program has been devised by Goodhart which will calculate the performance of a sailplane of given characteristics in straight and circling flight. The program takes into account the effects of Reynolds number on the characteristics of the wing section, using wind-tunnel figures and extrapolating if necessary. An approximate allowance for the effects of Reynolds number on tail profile drag is also included. The results are very realistic, as shown by Fig. 1, which compares a measured polar for the Schleicher ASW-15 with the computed figures for a sailplane of roughly similar geometry. The program will also compute the maximum rate of climb attainable when circling in a thermal which has a given core strength and a given shape of vertical velocity distribution and will then find the corresponding maximum cross-country speed.

In Ref. 1, this program was applied to considering the performance of a family of Standard Class fixed-geometry sailplanes operating in thermals having a parabolic distribution of vertical velocity [i.e., $v_t/V_t = 1 - (r/R)^2$]. Results were presented for sailplanes having aspect ratios between 12 and 28, each with a suitable range of all-up weights, in thermals having values of V_t between 4 and 12 knots and values of R of 300, 500 and 700 ft. Some representative results are shown in Figs. 2 and 3. A remarkable feature of these curves is the insensitivity of the achieved speed to aspect ratio, provided that the sailplane is flown at its optimum weight at each aspect ratio.

However, the weight of a sailplane of given geometry is not entirely open to choice. In Fig. 3, the optimum aspect ratio in 4-knot thermals is about 26, but the corresponding optimum all-up weight is impracticably low, at 380 lb. We must therefore consider the effect of realistic weights. We can assume that the weight can always be increased by the use of ballast, but cannot be reduced below some minimum figure. Hence, in Fig. 2, optima to the left of the W_{min} line are not attainable, but those to the right can be achieved if ballast is carried. However, if for the moment, we ignore such considerations, Fig. 4 shows that it is more important to optimise the weight at a given aspect ratio than to optimise both the aspect ratio and the weight.

The minimum weight figures used in Ref. 1 were taken from an expression derived by Morelli [Ref. 2]. When these calculations were discussed at Euromech Symposium 26 (Oberwolfach, July 1971), it was pointed out to the author that Morelli's figures were based mainly on sailplanes of wood/fabric construction. Glass-fiber were likely to be heavier, with an increasing penalty at lower aspect ratios due to the inherently higher weight per unit area of the skins. Accordingly, the "practical weight" figures have been revised using data given by Stender [Ref. 3], with the results shown in Fig. 5. It is, in fact, remarkably difficult to obtain firm and representative figures from the statistical data of Stender's paper, so Fig. 5 should be taken as indicating a reasonable trend, not necessarily showing the lightest possible sailplanes.

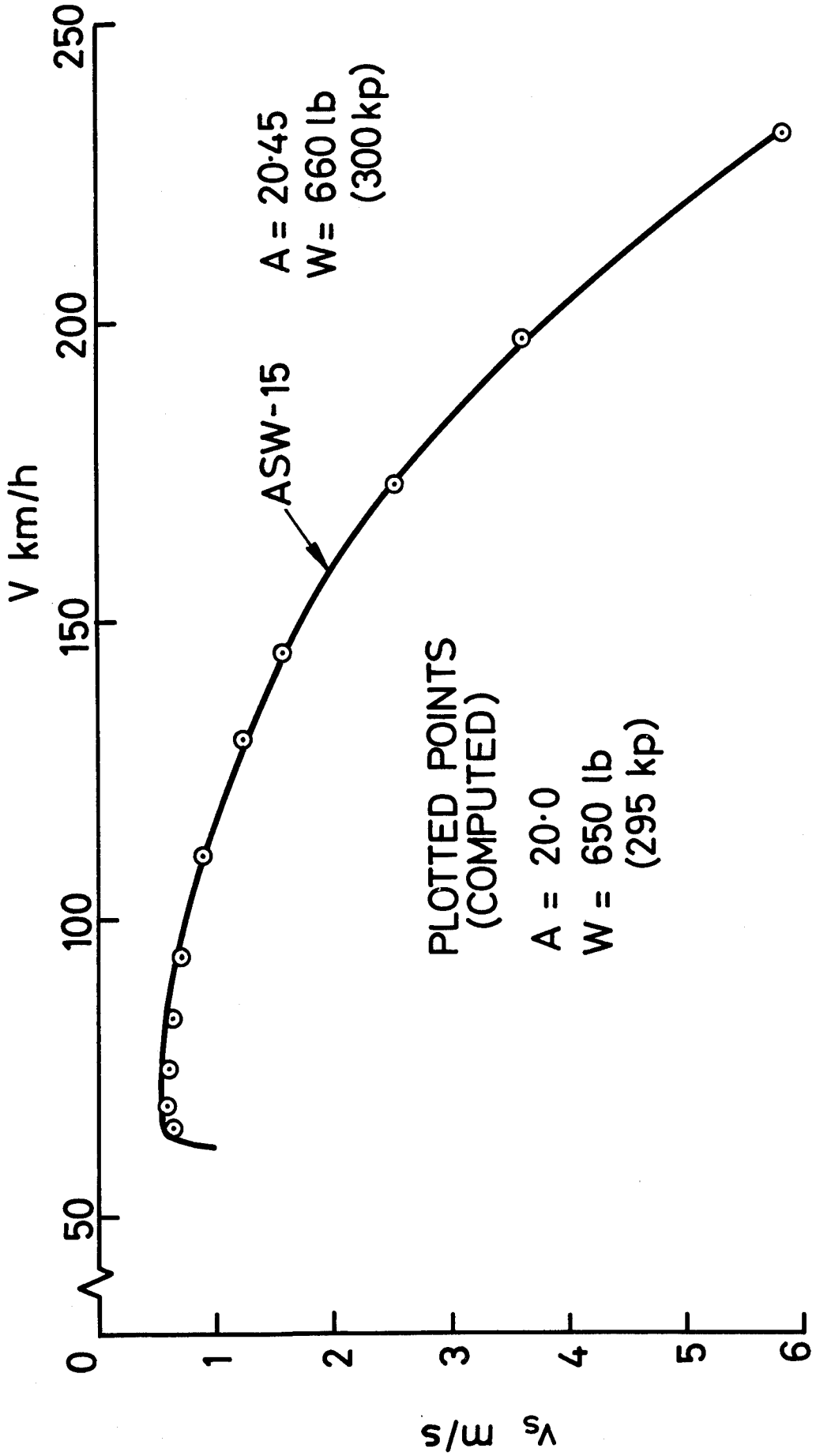

V km/h
0
50
100
150
200
250
1
2
3
4
5
6
v_s m/s
ASW-15
A = 20·45
W = 660 lb
(300 kp)
PLOTTED POINTS
(COMPUTED)
A = 20·0
W = 650 lb
(295 kp)

FIG. 1

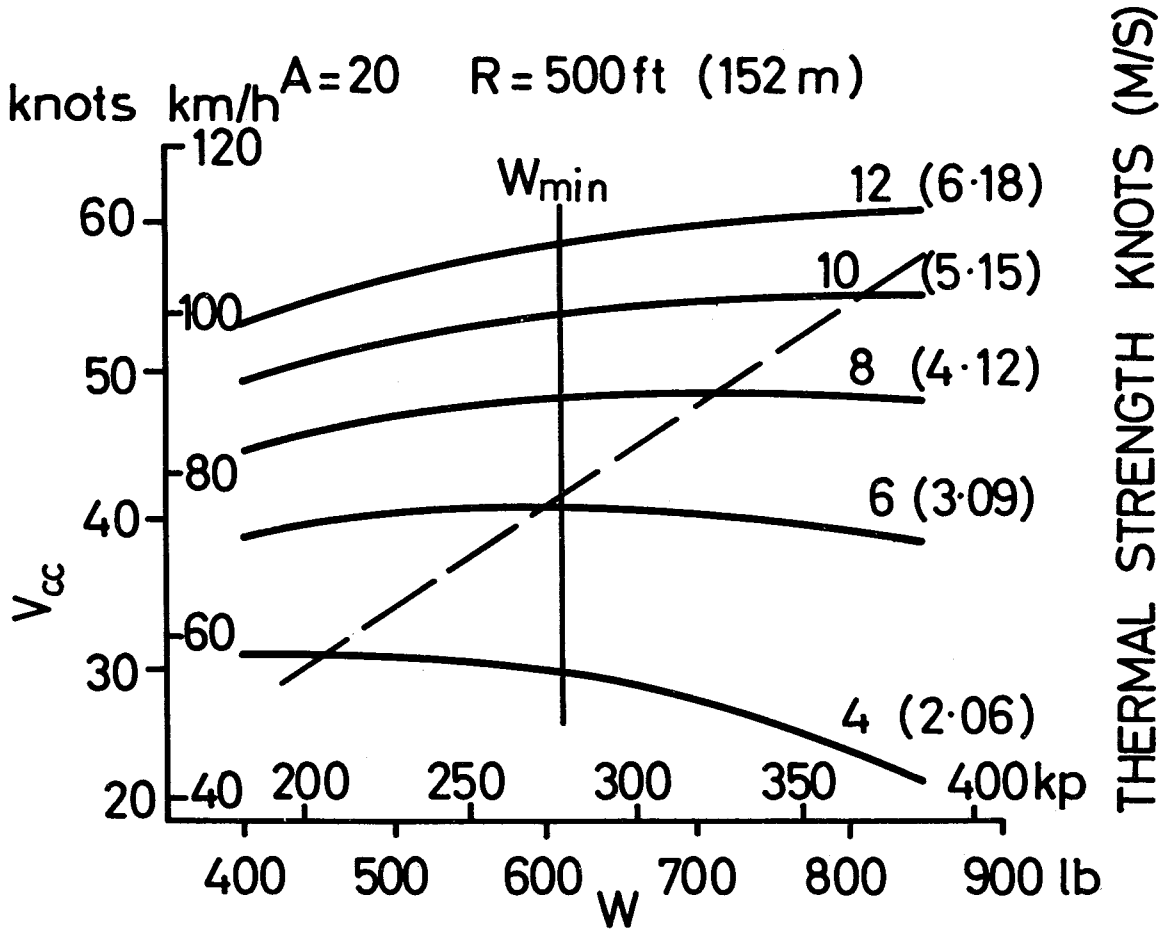

knots km/h
A=20 R=500ft (152m)
120
100
80
60
40
20
60
50
40
30
V_{cc}
W_{min}
12 (6·18)
10 (5·15)
8 (4·12)
6 (3·09)
4 (2·06)
40 200 250 300 350 400kp
400 500 600 700 800 900 lb
W
THERMAL STRENGTH KNOTS (M/S)

FIG. 2

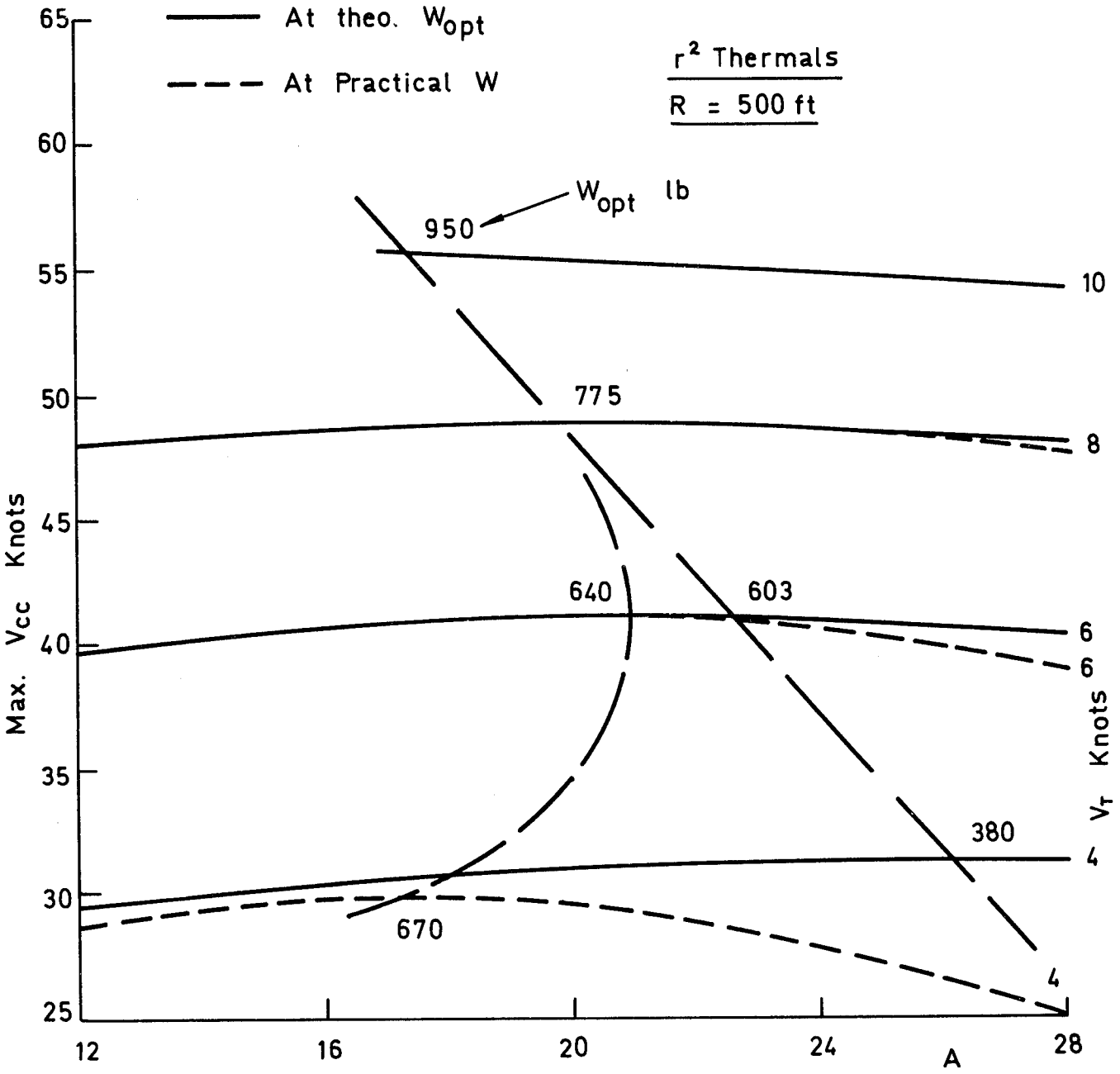
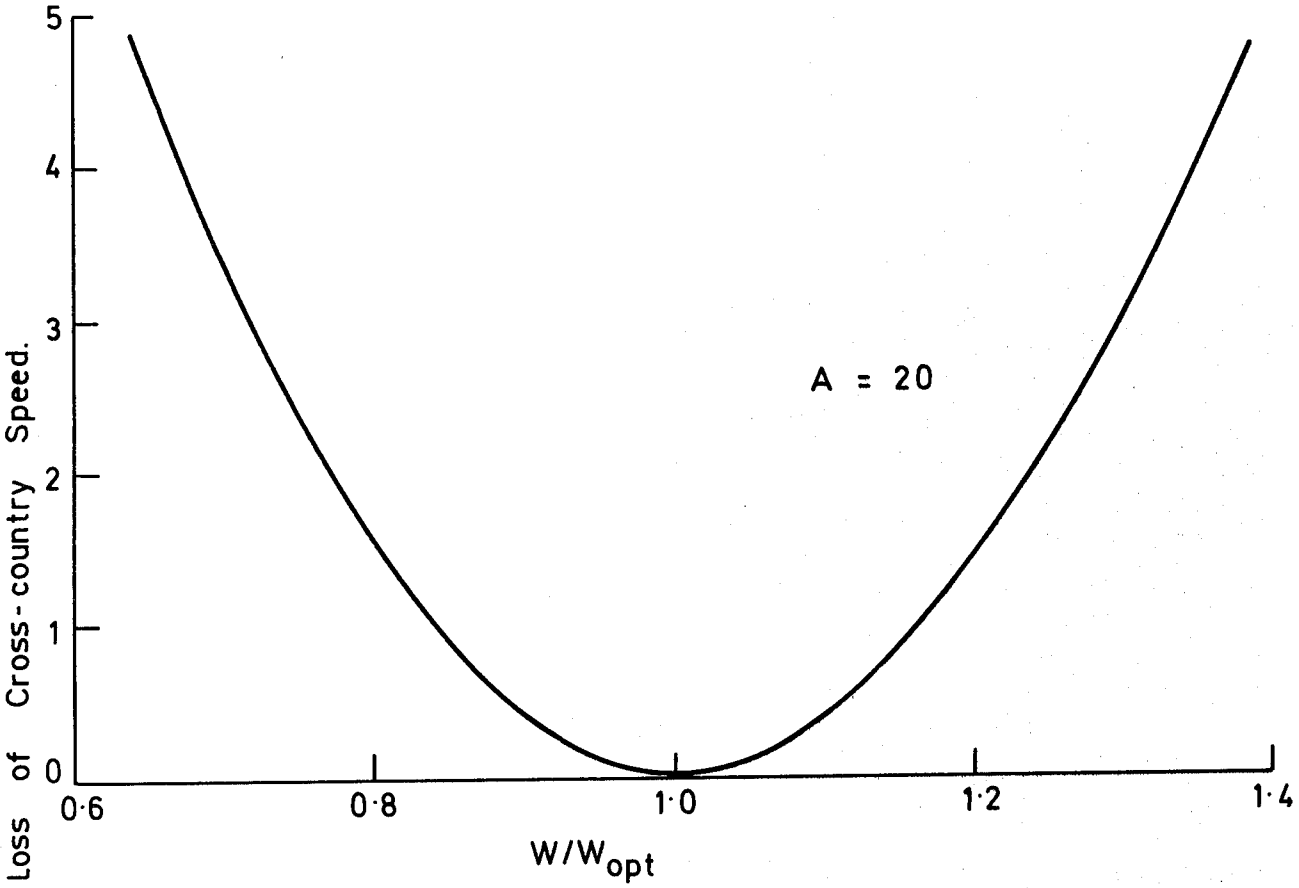
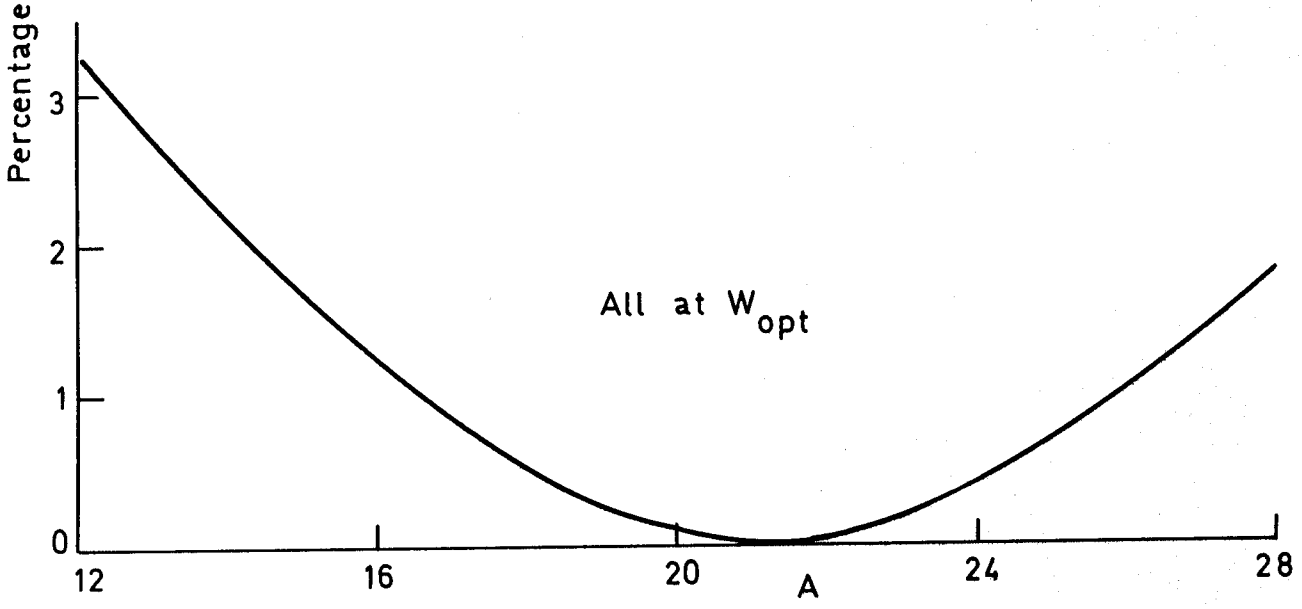

At theo. W_{opt}
At Practical W
r^2 Thermals
R = 500 ft
W_{opt} lb
950
775
640
603
670
380
10
8
6
6
4
4
65
60
55
50
45
40
35
30
25
12
16
20
24
28
A
Max. V_{cc} Knots
V_T Knots

FIG. 3





r^2 Thermal V_t = 6 Knots R = 500 ft

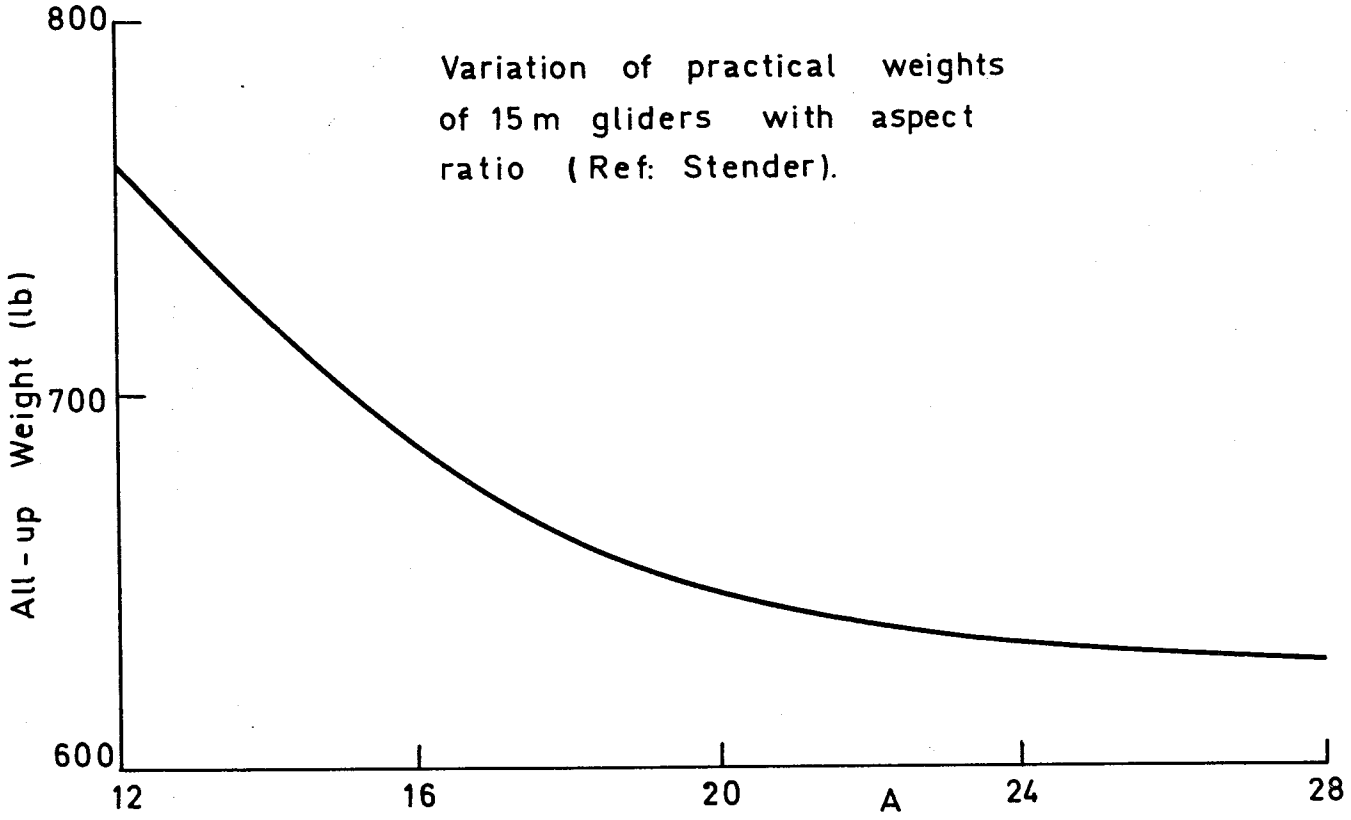

Variation of practical weights of 15 m gliders with aspect ratio (Ref: Stender).
All-up Weight (lb)
800
700
600
12
16
20
A
24
28

FIG. 5

Reverting to Fig. 3, we can now show the effect of considering practical weights. At the lower thermal strengths, the optimum aspect ratios are reduced: in 4-knot thermals, the optimum is now about 17, corresponding to a weight of about 670 lb.

From curves such as those of Fig. 3, we can derive the optimum aspect ratio and corresponding optimum weight for various values of thermal strength for a given radius of thermal. The results for parabolic (r^2) thermals are presented in Fig. 6. (This is an updated version of Fig. 12 of Ref. 1).

It is important to stress that Fig. 6 is by no means an accurate plot. The curves of Fig. 2 (and the corresponding curves for other thermal radii) are so flat that it is difficult to locate the maxima within about $\pm$ 2 units of aspect ratio. Rather than drawing sharp lines, one should really show vague areas. Similarly, the results for R = 500 ft and R = 700 ft are not really the same but they are sufficiently close for the same curve to indicate the trends.

Ref. 1 concluded that the most satisfactory all-round glider would have an aspect ratio of about 16. It is near-optimum in weak thermals and, when ballasted, in strong thermals. In thermals of intermediate strength (6-7 knots), the loss in performance compared with the theoretical optimum (A = 20-21) would be very small indeed. The revised weight figures do not greatly alter this conclusion so far as 500 ft and 700 ft thermals are concerned, save that A = 18 might be more suitable. It is also apparent that the current generation of sailplanes with aspect ratios of about 20 are also close to optimum provided that one only uses ballast in thermals stronger than about 7 knots core velocity. (It cannot be stressed too strongly that achieved rates of climb are far less than the thermal core strengths.) It is, however, clear that if sailplanes are required to use weak narrow thermals, much lower aspect ratios are required.

Thermal velocity profiles

A parabolic law was selected for the thermal velocity profiles in this study on the grounds of mathematical convenience: it gave the simplest smooth curve which might be thought somewhat realistic. At Euromech 26, it was suggested that, whilst the results seemed plausible, real thermals would not normally provide such an engagingly simple velocity profile and other velocity profiles might lead to different conclusions. Also, assorted real thermals might well have various velocity profiles.

It is hoped that the work of Whitfield at Reading University will clarify the characteristics of real thermals but, in the meantime, it seemed profitable to consider whether other shapes of velocity profile had a significant effect on the previous conclusions.

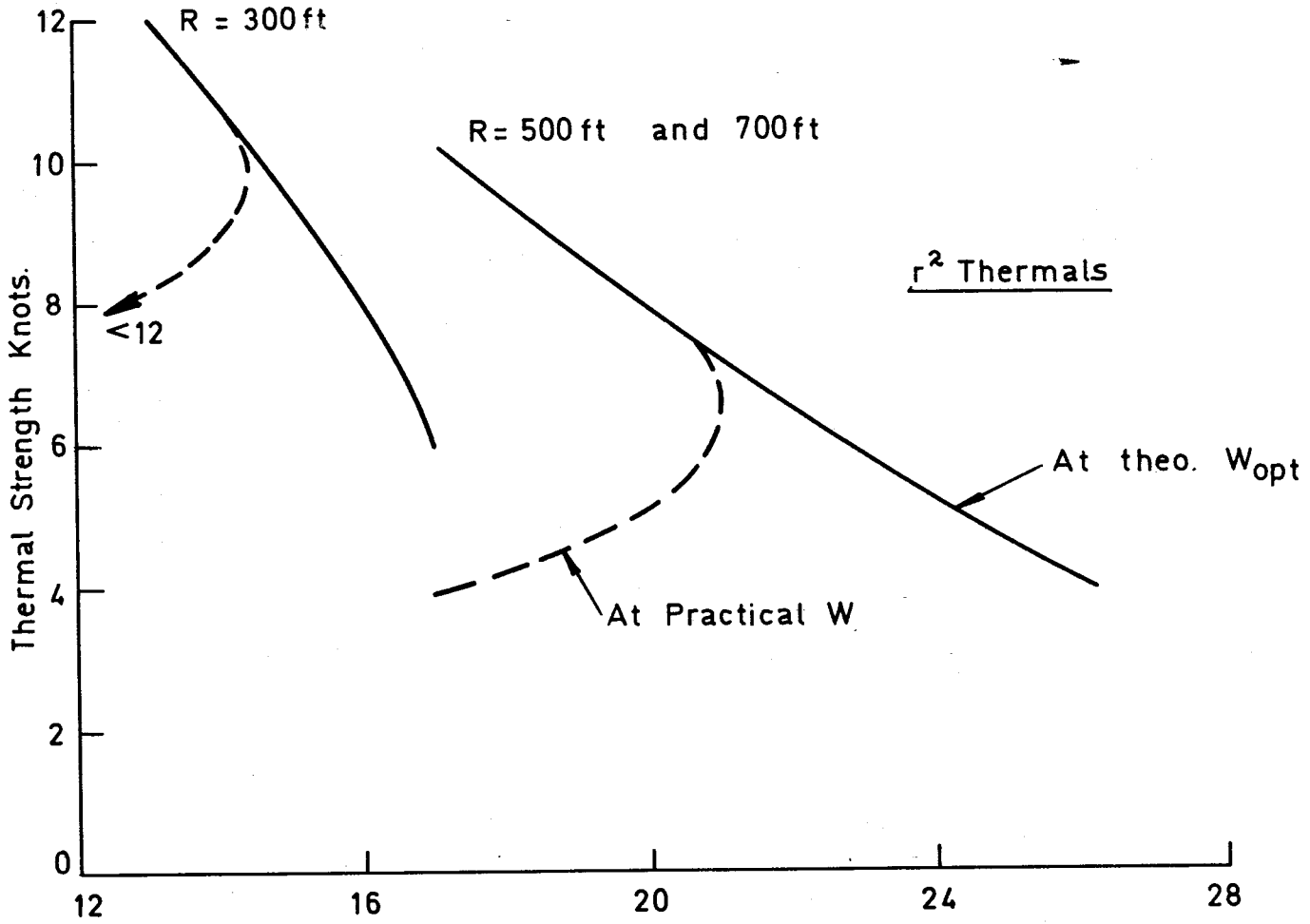

R = 300 ft
R = 500 ft and 700 ft
r² Thermals
<12
At theo. Wopt
At Practical W
Thermal Strength Knots.
12
10
8
6
4
2
0
12
16
20
24
28

FIG. 6

In general, one can consider velocity profiles given by a simple power-law expression

$$v_t/V_t = 1 - (r/R)^n$$

n = 1 would give a triangular profile, which seems rather unlikely in reality, whilst n = 2 gives the parabolic profile of Ref. 1. Larger values of n give more nearly rectangular profiles. All of these shapes obviously become unrealistic at large values of the radius, but the radius of the circles performed by the sailplanes (also given by the computer) was generally sufficiently less than R for this effect to be ignored.

To take a fairly extreme case, the calculations of Ref. 1 were repeated for the case n = 4, hereafter called "r^4 thermals".

Computations for r^4 thermals

Fig. 7 shows the results for 500 ft radius thermals. As one would expect, the cross-country speeds are all appreciably higher than in the corresponding r^2 thermals and the effects of practical weights only become significant in a small part of the diagram. Again, the curves are very flat indeed.

Regrettably, the chosen ranges of weight and aspects ratio did not always encompass the optimum conditions, so the summary presented in Fig. 8 does not show the effects of strong thermals and low aspect ratios. However, the trends are apparent: optimum aspect ratios are lower than for the r^2 thermals and very low aspect ratios are desirable for narrow thermals. Again, curves such as those of Fig. 7 are so flat that Fig. 8 should be taken to indicate a vague trend rather than exact optima and an aspect ratio of 16 to 18 will give a cross-country speed close to the maximum attainable under most conditions.

Overall, one concludes that if real thermals have a vertical velocity profile which is parabolic or "flatter", fixed-geometry Standard-Class sailplanes with aspect ratios of about 16 to 18 will give near-optimum cross-country performance over a wide range of conditions, provided that provision is made for the carriage of a large amount of ballast. Fig. 9, although it relates to A = 20, indicates the desirable ranges of all-up weight. Many current sailplanes have aspect ratios of about 20: they would tend to be more suited to thermals having sharper-than-parabolic profiles, provided the weight can be optimised, but are unlikely to be significantly worse than the theoretical best under the conditions considered above.

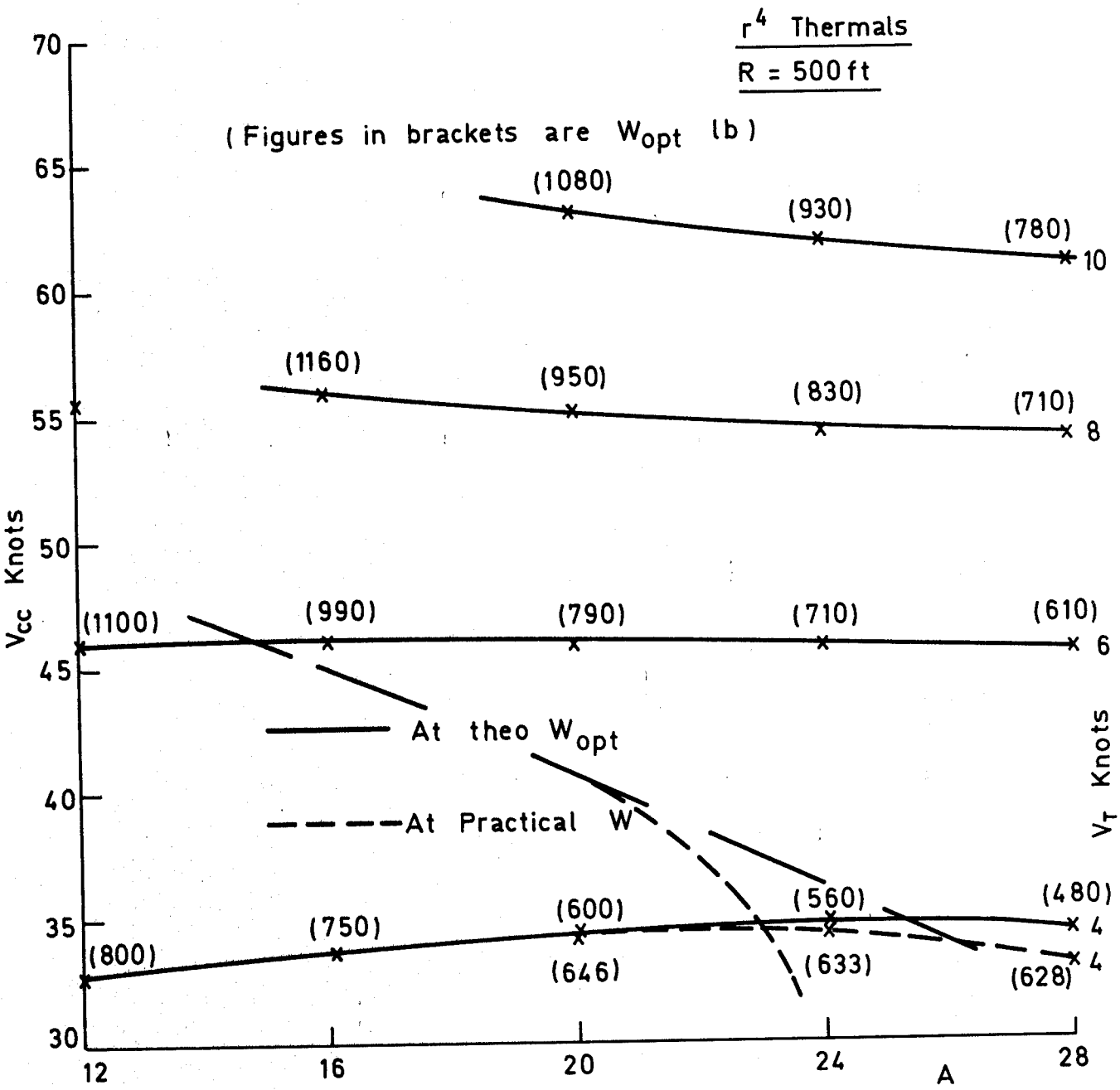

r⁴ Thermals
R = 500 ft
(Figures in brackets are Wopt lb)
(1080)
(930)
(780)
10
(1160)
(950)
(830)
(710)
8
(1100)
(990)
(790)
(710)
(610)
6
At theo Wopt
At Practical W
(800)
(750)
(600)
(646)
(560)
(633)
(480)
(628)
4
4
70
65
60
55
50
45
40
35
30
12
16
20
24
28
A
Vcc Knots
VT Knots

FIG. 7

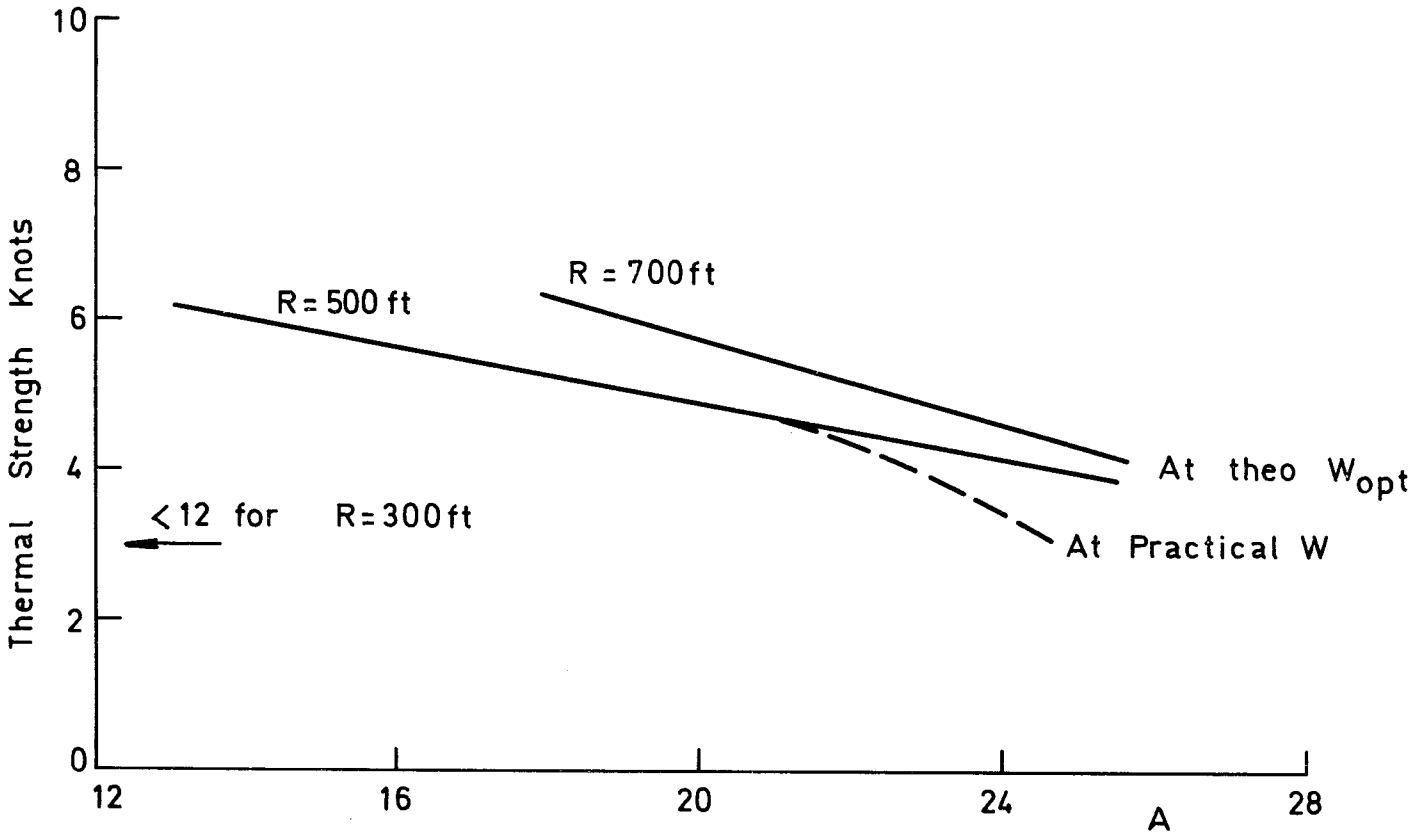

Thermal Strength Knots
10
8
6
4
2
0
12
16
20
24
28
A
R = 700 ft
R = 500 ft
At theo W_{opt}
At Practical W
< 12 for R = 300 ft

FIG. 8

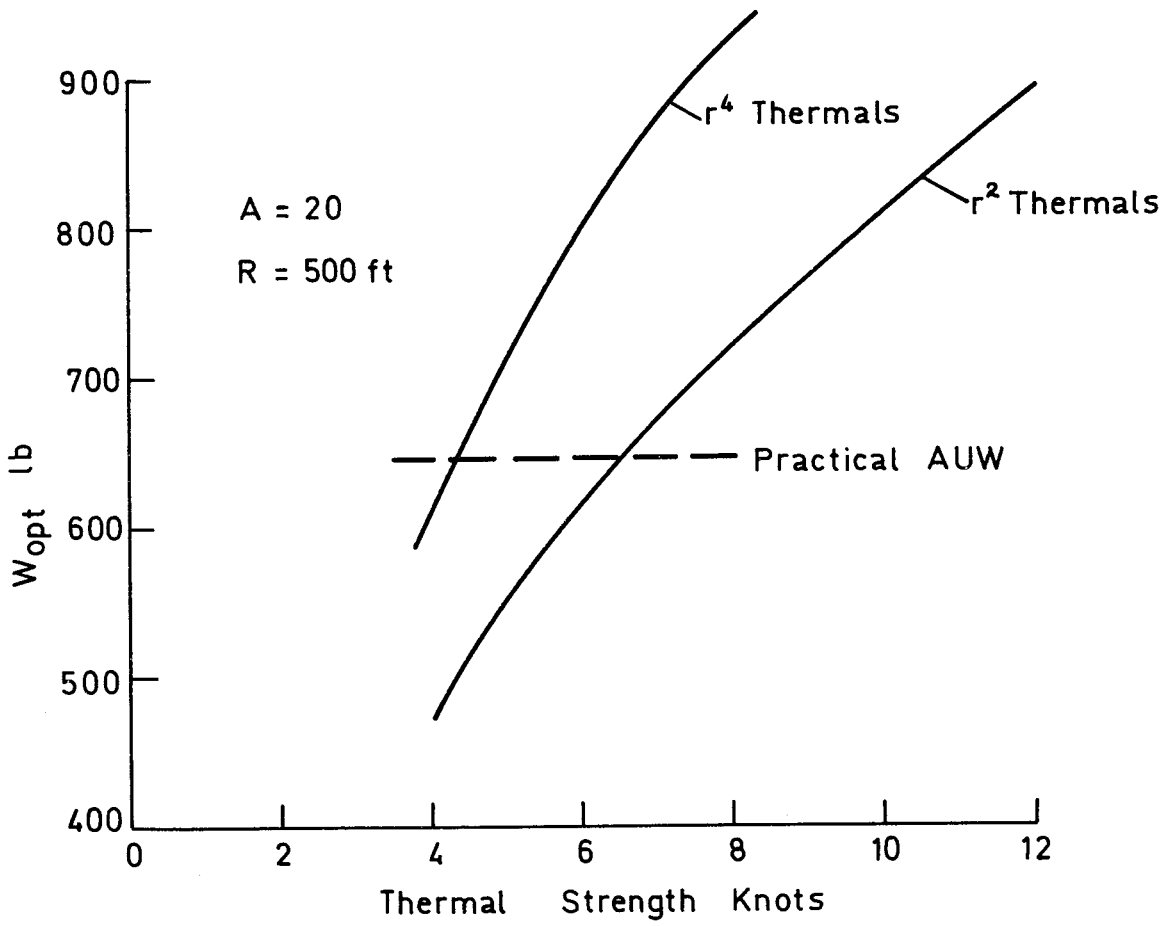

900
800
700
600
500
400
W_{opt} lb
A = 20
R = 500 ft
r^4 Thermals
r^2 Thermals
Practical AUW
0
2
4
6
8
10
12
Thermal Strength Knots

FIG. 9

Conclusions

On the basis of these calculations - and it must be remembered that they are not necessarily representative of how real pilots perform in real conditions - it seems that aspect ratio is of surprisingly little consequence provided that it is not too high. There is some suggestion that values somewhat lower than the current 20 would often be slightly beneficial, but the effect is small unless one is concerned with very strong or very narrow thermals.

Given a sailplane with a certain aspect ratio, it is fairly important to ballast it to suit the prevailing conditions. These calculations suggest that, for strong conditions, provision should be made for much more ballast than is currently provided. For example, the present max. AUW of the Glasflügel Libelle with water ballast is 772 lb: there would seem to be a case for increasing this by about another 100 lb for use in strong conditions. This increased figure is appropriate to r^2 thermals of 12 knots core strength. The optimum rate of climb would then be about $7\frac{1}{2}$ knots, which is by no means outrageous in some countries.

References

1. Irving, F.G. Computer Analysis of the Performance of 15m Sailplanes using Thermals with Parabolic Velocity Distributions. Aero Revue, May and June 1972.

2. Morelli, P. On the Weight of Sailplanes as a Function of their Main Geometric Parameters. OSTIV Publication V.

3. Stender, W. Sailplane Weight Estimation. OSTIV Publication, June 1969.

WHEN SHOULD WE USE WATER BALLAST?

by

Richard Eppler
Inst. A für Mechanik
Universität Stuttgart

Introduction

Heavier sailplanes have better penetration in glide, but climb worse in a thermal. We know from experience that in wide and strong thermals the advantages outweigh the disadvantages. Thus open class sailplanes have been using water ballast for many years. For the standard class also, it has been common practice to keep the weight as high as possible. Henceforward, water ballast is also permitted in the standard class. Thus it is of interest to analyse in a more rigorous manner in order to elucidate the conditions in which ballast is indeed useful. For this purpose a numerical method suitable for digital computation has been developed and will be described. Results for various aircraft with 15 m wingspan will be presented.

Basic considerations and method

Aircraft with the same lift coefficient C_L but different weights have different speeds and thus different Reynolds numbers Re. It is difficult, however, to consider this influence on the drag coefficient C_D and thus on the glide ratio, if for a given weight we start out from a measured or calculated speed polar $V(V_S)$, for which we only know the sinking speed V_S as a function of the forward speed V. It is necessary instead to return to the relationship $C_D = C_D(C_L, Re)$ for the wing. In the following section aircraft of different layout will be considered. Thus, to facilitate comparison, an identical profile (No. 571), which has been thoroughly investigated theoretically as well as experimentally, will be used for all calculations. The relation $C_D(C_L, Re)$ for this profile is shown in Fig. 1.

For the calculations, a larger number of points will be given for each Re value in the form of a table. Then for each value V we can calculate C_L and Re and then C_D by linear interpolation with respect to C_L and Re. Variation of the parasitic drag C_{D_P} and of the induced drag C_{D_i} due to varying Re will not be considered. For all variants we assumed $C_{D_i} = 1.03\ C_L^2/\pi\Lambda$ and $C_{D_P} \cdot A_P = 0.045$, with A_P being the area related to C_{D_P}, and the wing aspect ratio Λ.

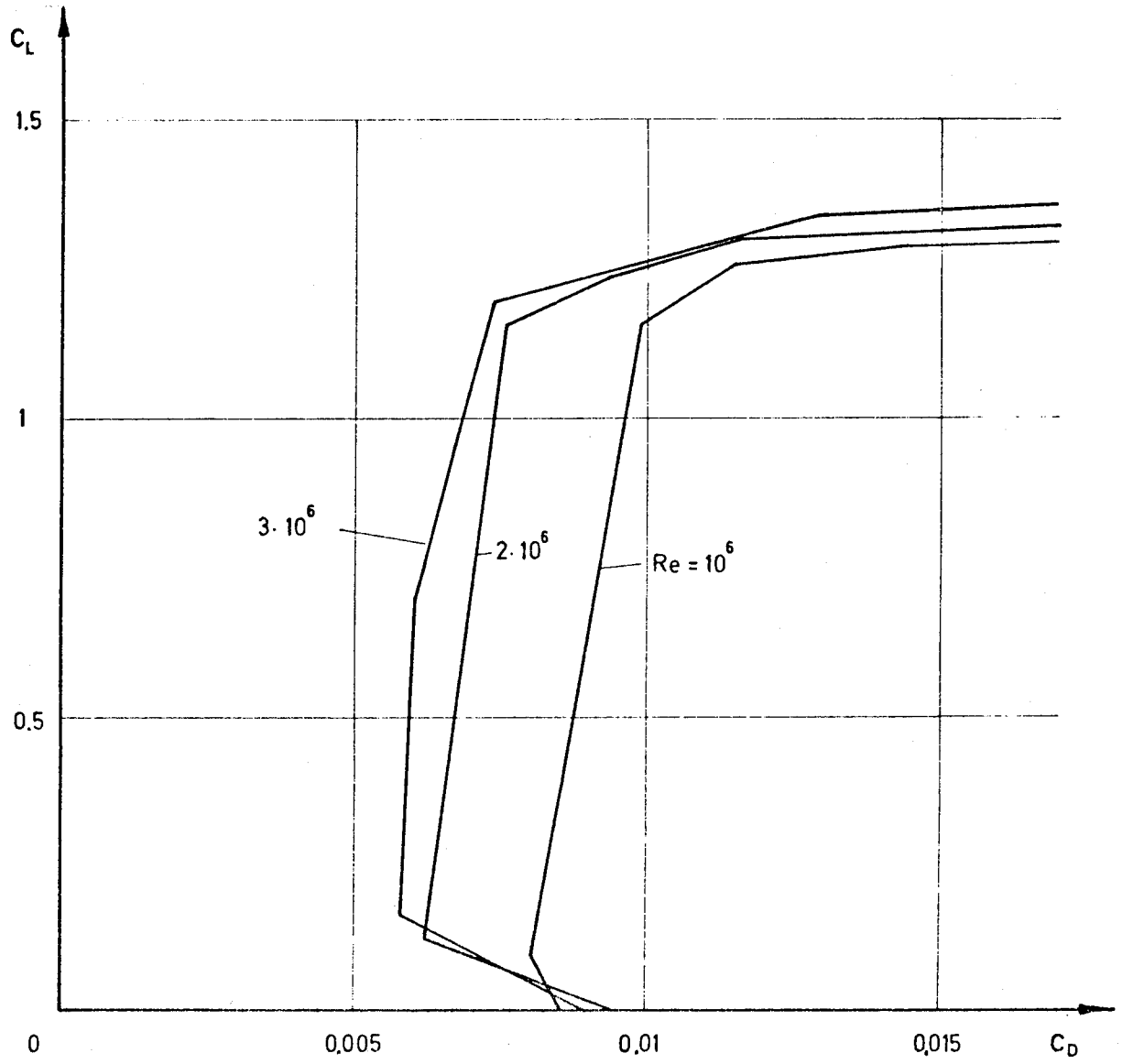


Figure 1.

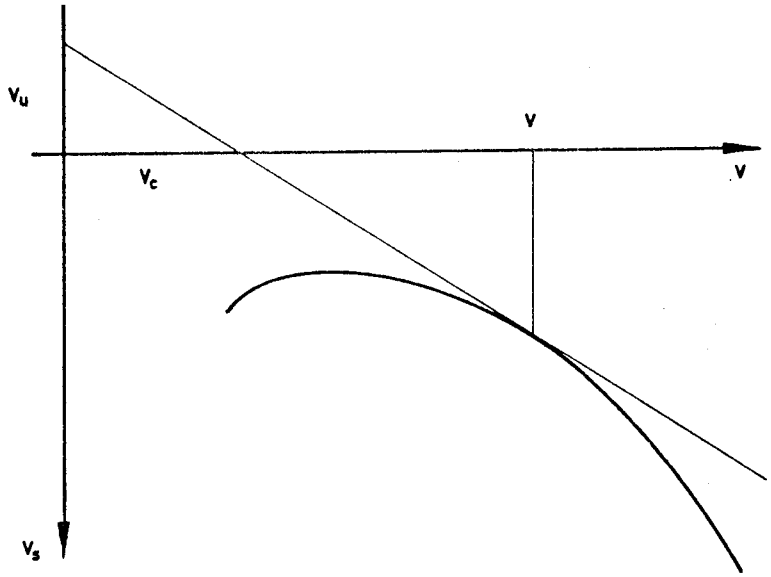


Figure 2.

With this, for a sailplane of weight W, wing area A and wing span b(= 15 m), it is possible to calculate the sinking speed V_S for any velocity V. Thus an arbitrary number of points of the speed polar can be determined. However, as preveously mentioned, the relation $V_S(V)$ delivers very little information about the performance. It is necessary to work with the cross-country polar $V_C(V_u)$ and the climbing speed V_u of the airplane in the thermal. The best possible average cross-country speed V_C for a climbing speed V_u in the thermal can be obtained in the usual way, namely by constructing the tangent to the curve $V_S(V)$ according to Fig. 2.

In practice, however, it is common not to stick to this rule unconditionally, because only the lowest part of the climbing phase has an influence on the optimal penetration speed, and it is possible to increase greatly the probability of reaching the goal by paying some small penalty in V_C.

Let us now compare different sailplanes and weights using MacCready tactics and assuming constant average climbing speed V_u: The process of constructing the tangent to the curve $V_S(V)$ using a digital computer is not trivial. Approximating this curve, which is given by a number of discrete points, by a function, it happens frequently that the approximating function exhibits a slightly wavy character; therefore the tangent may become very inaccurate.

We have found the approximating relationship

$$V_S = \sum_{\nu=1}^{N} A_\nu (V - 0.9\ V_{min})^{4-\nu} \qquad (1)$$

to be most satisfactory, however.

It is recommended that one choose the degree of the approximating function $N \simeq 8$ and determine the A_ν such that the previously calculated values $V_S(V)$ are approximated by a least squares method. In this way small irregularities of the speed polar, such as the end of the laminar bucket are represented well without the tangent becoming too inaccurate. The largest exponent of relationship (1) is 3. It can be shown easily that this is reasonable. Larger exponents would require a singularity of the function $C_D(C_L)$ at $C_L = 0$. Also, larger exponents lead to inaccuracies of the tangent for high speeds.

For a value V of the speed polar, the corresponding tangent and thus, per Fig. 2, values V_u and V_C can be calculated using the A_ν and equation (1). V, V_u and V_C are related to each other in the following manner: If we have the climbing speed V_u in a thermal then we require the velocity V in glide penetration, and will have V_C for our average cross-country speed. With this, as many points as we wish of the cross-country polar $V_C(V_u)$ can be determined and plotted. For two extreme sailplanes, one with A = 9 m^2 and the other having A = 15 m^2, the curves for various weights and wing

loadings are shown in Figs. 3 and 4.

As we all know, sailplanes with higher wing loadings and with equal V_u reach higher cross-country speeds V_C. Here, we will also have to find the value V_C for a given value V_u. Therefore, for every curve of the relationship

$$V_C(V_u) = B_1(V_u + 2V_{S_{min}})^{1/3} + \sum_{\mu=2}^{M} B_\mu(V_u + 2V_{S_{min}})^{2-\mu} \qquad (2)$$

a number of values B_μ were determined which approximate the calculated points $V_C(V_u)$ by a least squares fit. This approximation proved sufficient with M = 4. The cross-country polar $V_C(V_u)$ alone, however, is still not a sufficient criterion for judging the performance of sailplanes. The different climbing speeds of various sailplanes in the same thermal have to be taken into consideration also. Doing this, we have the difficulty that the climbing speed is influenced by both the strength and the form of the thermal. For this reason, Irving [1] assumed the thermal to be of parabolic form and suggested the relationship

$$V_{th}(r) = V_{th_o}\left(1 - \frac{r^2}{R^2}\right) \qquad (3)$$

with V_{th_o} being the thermal velocity in the center, r the distance from the center, and R being the distance for which we have $V_{th} = 0$. Of course real thermals do not have precisely this distribution, and a sailplane does not circle constantly in such a mannner that the center of the circle is identical with the center of the thermal. But when climbing, flying in smaller circles has a certain advantage, and it can be assumed that this advantage is expressed by relationship (3). The curves described by Equation (3) are, in any event, only used in the vicinity of the center; varying the value of R, it is possible to describe approximately a narrow core(R = 100 m), a medium width (R = 150 m), and a wide thermal (R = 200 m). With V_{th_o} = 2,3,4 and 5 m/sec 4 different thermal strengths or, all in all, 12 different thermals, are considered. They are plotted in Fig. 5. Note that throughout this paper the curves corresponding to wide, medium and narrow thermals are drawn in the same manner as in Fig. 5.

In order to determine the climbing speed of a sailplane in a thermal, the sinking speed in circular flight has to be known. The lowest sinking speed on a circle of radius r can be calculated by using a slightly modified version of the method described in [2].

For this, the tangents to the curve $V_S(V)$ have to be drawn again, now, however, in the area below the speed corresponding to the minimum sinking speed. With this we can calculate certain radii r and the corresponding minimum sinking speed $V_S(r)$ which are possible on these radii. In Fig. 5 the resulting curves $V_S(r)$ for b = 15 m, A = 15 m^2 and different wing loadings W/A are plotted also.

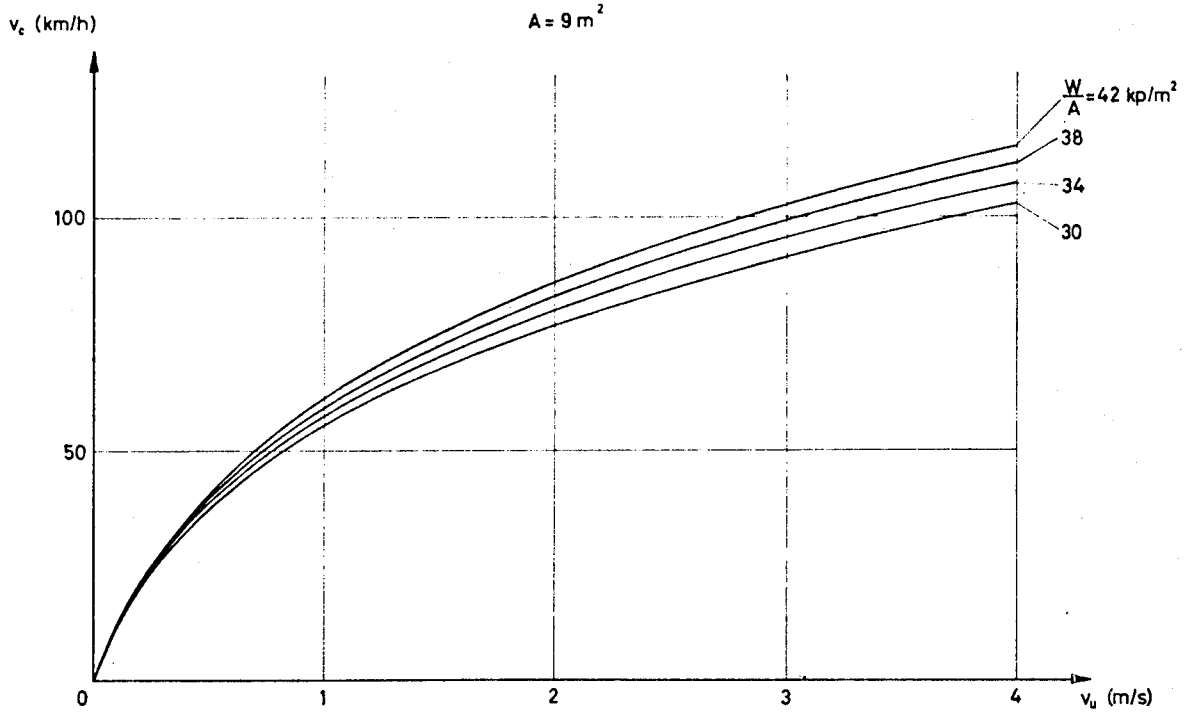


Figure 3.

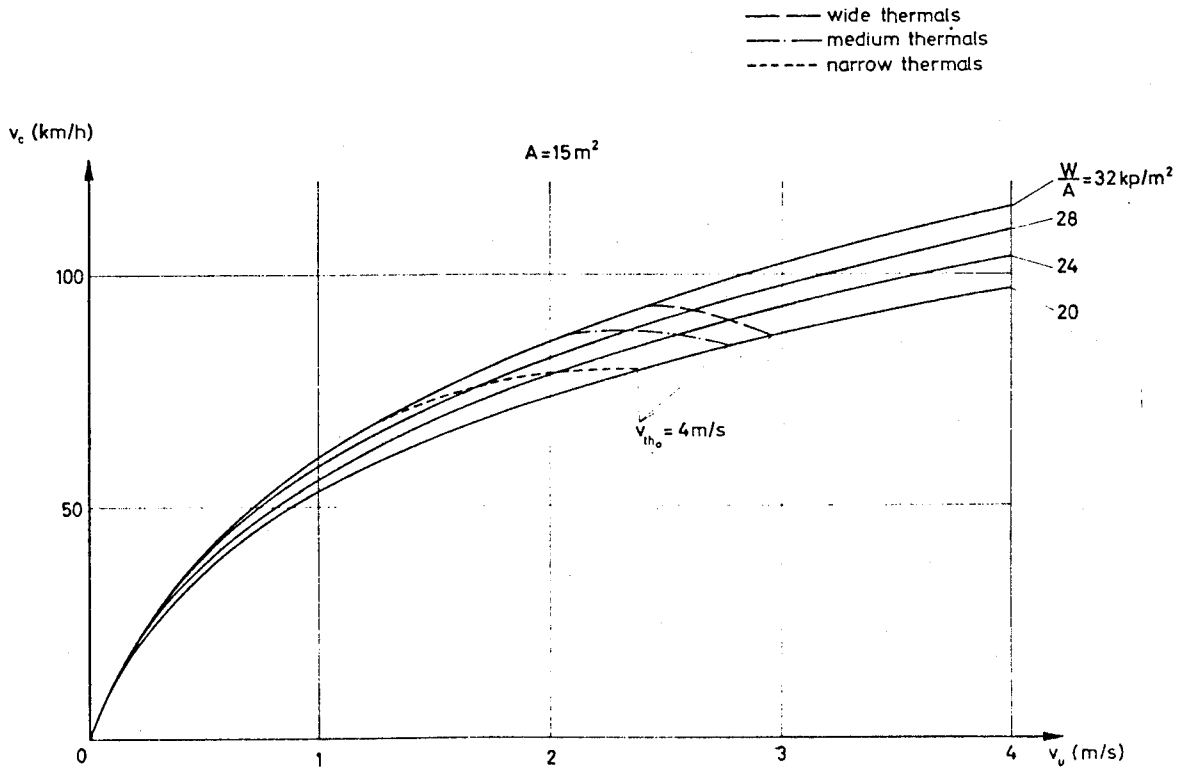


Figure 4.

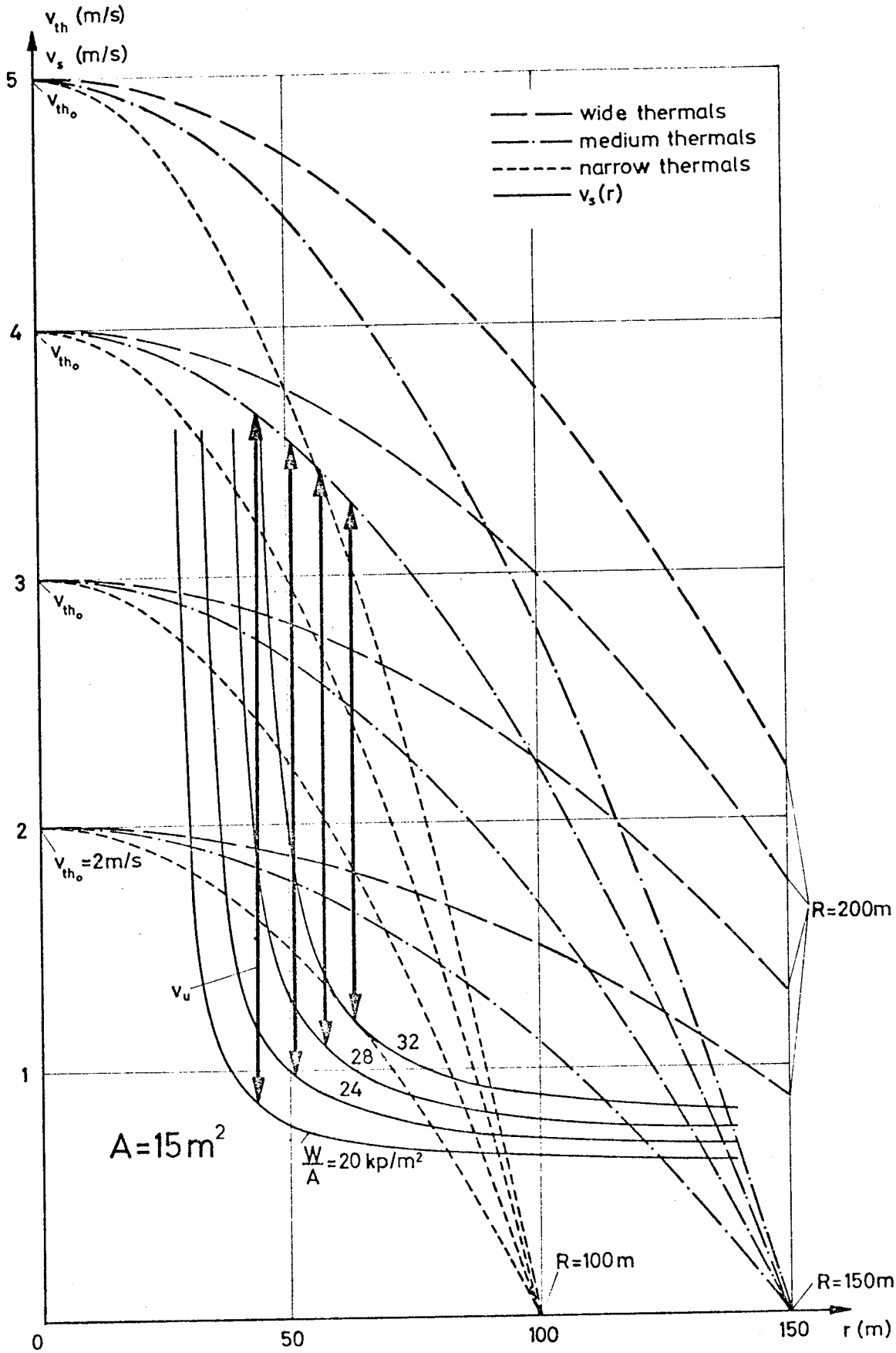

v_{th} (m/s)
v_s (m/s)
5
4
3
2
1
0
50
100
150
r (m)
v_{th_o}
v_{th_o}
v_{th_o}
v_{th_o} =2m/s
wide thermals
medium thermals
narrow thermals
$v_s(r)$
v_u
32
28
24
A=15 m²
$\frac{W}{A}$ =20 kp/m²
R=200m
R=100m
R=150m

Figure 5.

These lines are also approximated by a function, for which the expression

$$V_S(r) = C_1\left(1 - \frac{r_{min}^2}{v^2}\right)^{-3/4} + \sum_{\lambda=2}^{L} C_\lambda r^{4-2\lambda} \qquad (4)$$

with

$$r_{min} = \frac{2W}{\rho g A C_{L_{max}}} \qquad (5)$$

has shown good results. For this degree of approximation L = 4 has turned out to be sufficient.

Knowing $V_S(r)$, the best possible climbing speed V_u in a thermal can be determined as the greatest distance between the curves $V_{th}(r)$ and $V_S(r)$. In Fig. 5 this is shown for a thermal of V_{th_o} = 4 m/sec, R = 150 m and the 4 given circling flight polars. The determination of V_u follows again from (4) and (3). Given V_u, the average cross-country speed V_C is then given by (2).

Naturally a pilot seldom flies exactly in the most favorable circle with the correct bank, but this is true to the same degree of approximation for any sailplane. Thus the best possible climbing speed can be used for comparison purposes.

The computer program is organized in the following way: The values $C_D(C_L,Re)$ for the profile must be available. Then, for the particular aircraft, values of b,W,A and $C_{D_P}\cdot Ap$ are read in. For this aircraft the speed polar, cross-country polar, the circling flight polar, and the corresponding approximation functions are determined, and then, for each thermal, V_u and V_C. The required computing time is negligible. Now we have the tool to compare many cases.

The influence of weight

In Fig. 4 the cross-country polars for 4 sailplanes are shown, all having b = 15 m, A = 15 m^2, but different wing loadings of W/A = 20, 24, 28 and 32 kp/m^2. This can be interpreted as a sailplane with a minimum weight W = 300 kp, which can take up to 180 kp ballast. With that assumption probably all the possible weight limits have been covered. Performing the calculations of the previous section for all weights, we obtain the climbing speed V_u and the average cross-country speed V_C for all thermals and all versions and can compare them easily. Higher weight always results in higher sinking rate and greater circling radius, that is, slower climbing. In Fig. 4 we can clearly observe the consequences for some typical thermals. At a higher weight we indeed get to a higher line $V_C(V_u)$, at a smaller value of V_u, however; and this does not mean that this necessarily gives a gain in V_C. For a strong thermal with V_{th_o} = 4 m/sec we obtain, for example, the best V_C at the maximum wing

loading, as long as the thermal is wide. For the same V_{th_o} and the medium diameter we have the optimum at a wing loading of only 28 kp/m^2. For a narrow thermal of the same strength the lightest sailplane is the best.

In the same way one can determine the optimal W/A and the associated V_C for each thermal. For this the climbing rate V_u is not relevant; it shows only the origin of the eventually decreased V_C. We can find the optimal wing loading in a simpler way by plotting V_C directly versus W/A. This has been done for all thermals and all wing areas. The results are shown in Figs. 6-9 for 4 sailplanes with different wing areas A. For each thermal diameter the optimal V_C and the corresponding wing loading W/A is shown versus thermal strength. From this some important conclusions can be drawn: At a wing area of 9 m^2 (Fig. 9) and for wide thermals, ballast *begins* to have an advantageous effect, only if the thermal strength is above 2.6 m/sec and the speed V_C is above 66 km/h. For a medium thermal diameter, which is probably closer to reality, ballast begins to increase V_C from V_{th_o} = 3.5 m/sec with V_C = 77 km/h; for a narrow thermal, ballast should not be used at all for the weights and thermal strengths considered here.

For a wing area of 15 m^2 (Fig. 6) ballast can be recommended for much weaker conditions. In wide-thermal weather, no ballast should be used below V_{th_o} = 2.1 m/sec and V_C = 58 km/h. In medium thermals the corresponding values are V_{th_o} = 2.4 m/sec and V_C = 61 km/h. In narrow thermals we need V_{th_o} = 3.7 m/sec and V_C = 77 km/h, before ballast can be advantageous.

The results for A = 11 m^2 and A = 13 m^2 lie between those of the extreme cases, as shown in Figs. 7 and 8.

If the exact flight conditions upon which the results presented have been based are not met, then a stronger thermal is necessary for the same climbing speed. The influence of the wing loading in this case should not be too different. Therefore, it makes sense to approximate the general limits for the use of ballast by using the limit values of V_C computed for the exact conditions. These values are plotted in Fig. 10 as a function of the wing area. Below the lowest curves there is no advantage even in wide thermals. These curves can be interpreted as absolute limits for the use of ballast.

If you do not reach at least these limits, in any flight with ballast, for any considerable period, you should immediately produce artificial rain. However, if you reach higher values of V_C, you should examine the diameter of the thermals. If you are finding medium or narrow thermals, you should orient your ballast-keeping decisions to the higher values of V_C shown in Fig. 10.

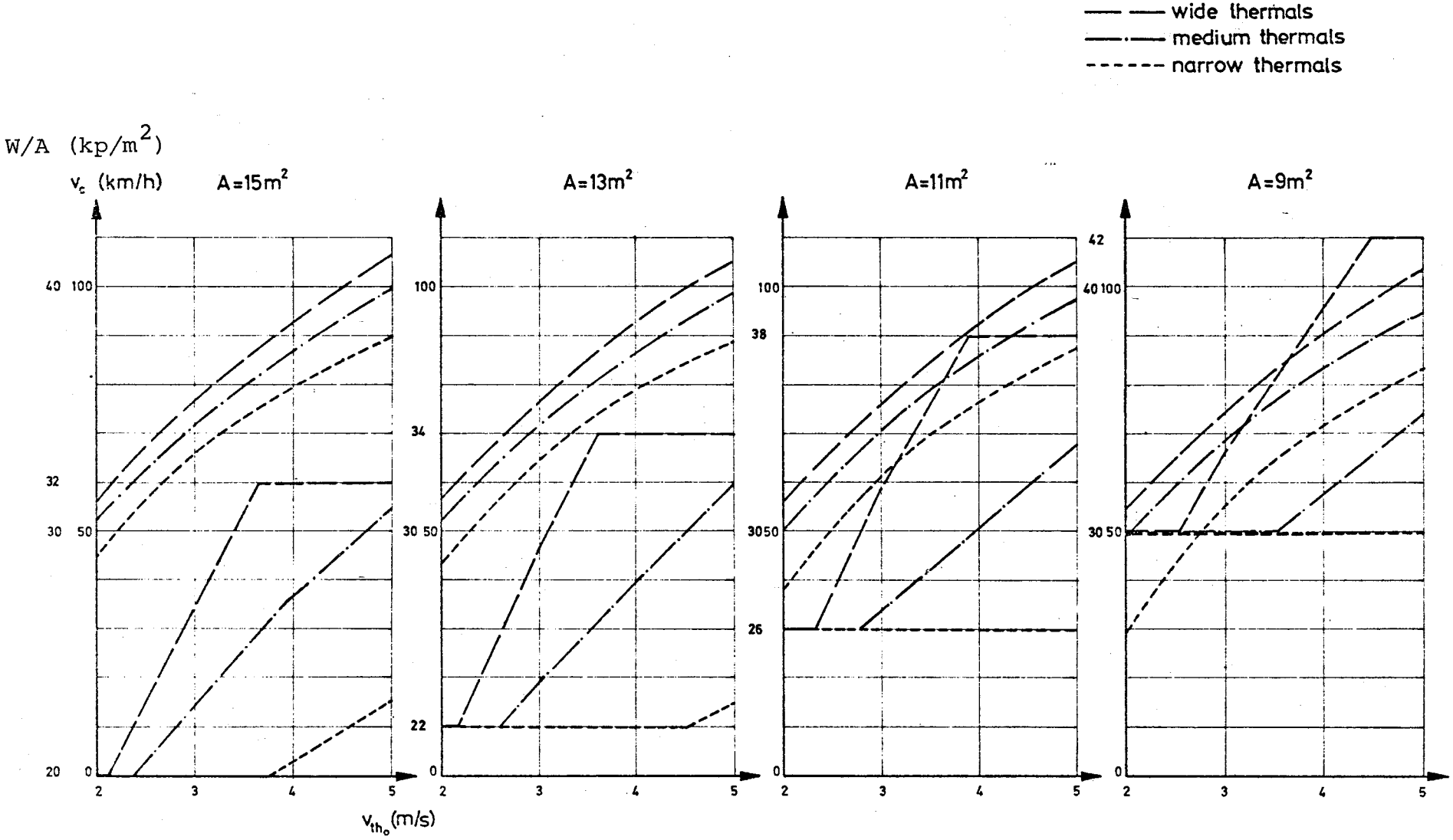


Fig. 6 Fig. 7 Fig. 8 Fig. 9

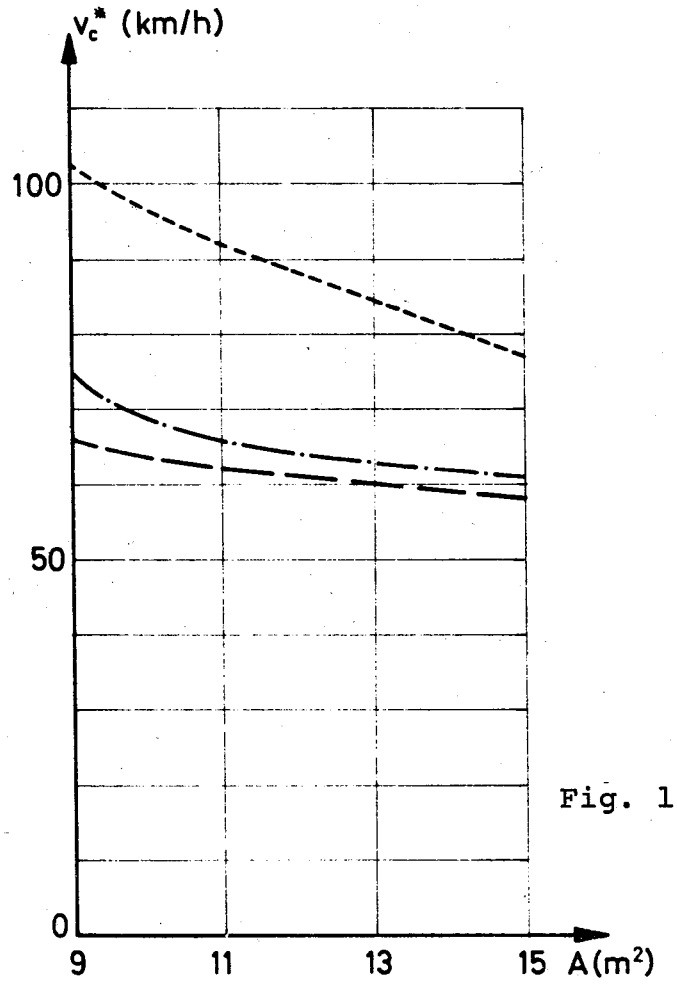

v_c^* (km/h)
100
50
0
9
11
13
15
A(m²)

Fig. 10

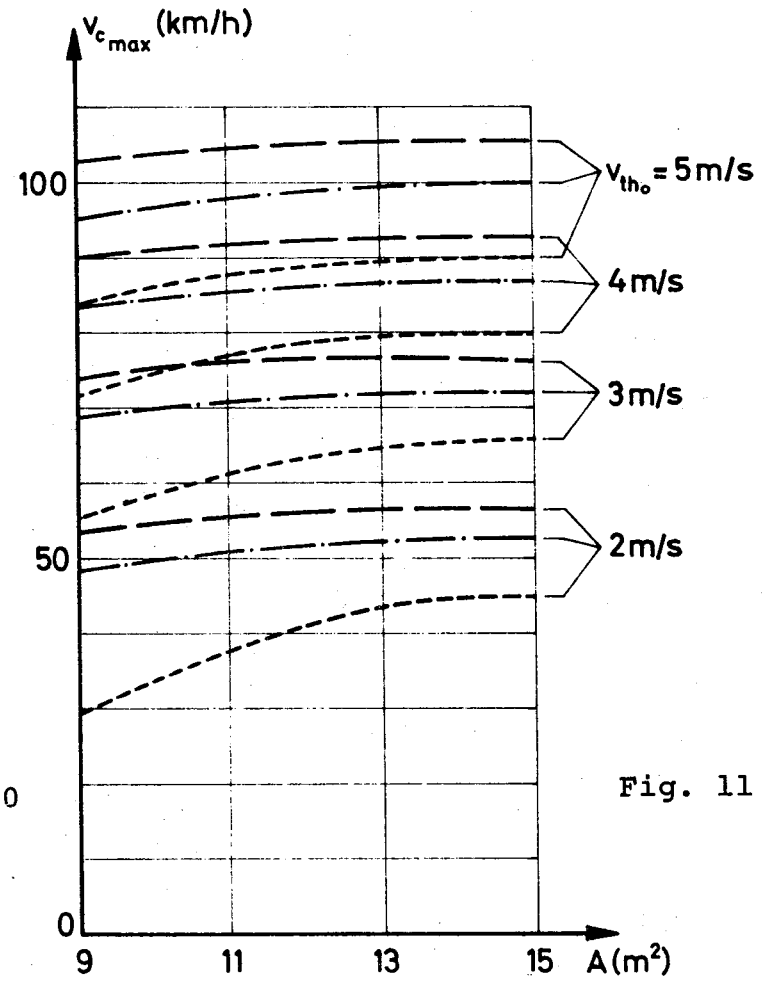

wide thermals
medium thermals
narrow thermals
$v_{c\,max}$ (km/h)
100
50
0
9
11
13
15
A(m²)
v_{th_o} = 5 m/s
4 m/s
3 m/s
2 m/s

Fig. 11

The optimal wing area

The computational results can also be used to reach some other conclusions. Permitting ballast in the standard class, we again face the problem of determining the optimal wing area.

To answer this question we assume that for different thermals each sailplane, characterized by its wing area A, flies at its optimal weight.

In Fig. 11, for a variety of thermals, the optimal cross-country speed is shown versus the wing area A. In all cases the smaller wing areas (below 12 m^2) show a considerable disadvantage; in narrow thermals even A = 15 m^2 is less than optimum.

Assuming that small thermals do not occur very often, one might select a wing area of 12.5 - 13.5 m^2 (i.e., aspect ratios of 18 - 16.7). Should it turn out, however, that some parts of the flights will take place in small thermals, then it may be beneficial to have even larger wing areas and to put up with the disadvantages in respect of transport and assembly.

References

1. Irving, F.G.; Computer Analysis of the Performance of 15 m Sailplanes Using Thermals with Parabolic Velocity Distributions, Aero Revue 1972, No. 5, pp. 262-265.

2. Eppler, R.; Der günstigste Kreisflug von Segelflugzeugen, Z.f. Flugwiss. 2 (1954), pp. 15-16.

CLOUD-STREET FLYING

by

F.G. Irving
Department of Aeronautics
Imperial College of Science and Technology
London, England

Notation

C_D	Drag coefficient
C_L	Lift coefficient
D	Drag, assumed to be D(U) in a constant-density atmosphere
F(U)	A function such that $T = \int F(U)dx$
$F^* = F + \lambda G$	
G(U,x)	A function such that $H_e = \int G(U,x)dx$
g	Acceleration due to gravity
h	True height
h_e	Energy height
H_e	Total change of energy height
L	Lift
t	Time
T	Total flight time
U	Forward speed
U_o	Speed corresponding to $(L/D)_{max}$
$\bar{U} = U/U_o$	
U_{cc}	Average cross-country speed
$\bar{U}_{cc} = U_{cc}/U_o$	
v_s	Rate of sink
v_{so}	Rate of sink at U_o
$\bar{v}_s = v_s/v_{so}$	
v_c	Rate of climb
$\bar{v}_c = v_c/v_{so}$	
w	Strength of up-current
$\bar{w} = w/v_{so}$	
$w^* = 1/\lambda$	
$\bar{w}^* = w^*/v_{so}$	
W	Weight
x	Distance along flight path
λ	A Lagrange multiplier, constant for an optimum flight profile
θ	Flight path slope (positive nose-up)

Suffices are explained in the text.

Introduction

The criterion for the optimum inter-thermal speed was first published in its simplest form by Barringer in 1940 and has since been elaborated to deal with more realistic situations, notably by McCready. All of these analyses assume a "normal" cross-country flight in which the sailplane generally gains height by circling in thermals.

Kronfeld's "Austria" was designed in the hope that it would be possible to carry out cross-country flights without circling in the thermals but simply flying straight through them at a low forward speed. At that time, the performance available from even the most refined machines was inadequate for sustained flight in such a fashion and it is only recently that the performance of sailplanes has become so good that significant portions of flights may be carried out without circling. Of course, it has been possible almost since the beginnings of thermal soaring to take advantage of cloud streets, where one finds an almost continuous line of lift or a well-defined closely-spaced succession of thermals.

Whilst the title of this paper refers specifically to cloud streets, its analysis is applicable to any cross-country flight carried out without circling. A criterion for optimising such flights has not been previously proposed, to the best knowledge to the author, doubtless because even a simplified analysis can involve several independent variables. Moreover, as is formally the case in any flight, the forward speed is not necessarily constant and hence the equation of motion involves an acceleration term. Consequently, various integrands similar to those derived in the analysis below are functions (inter alia) of the derivative of forward speed with respect to some other quantity such as time, distance or height, as may be convenient. The analysis then becomes an exercise in the Calculus of Variations, similar to that of the Reference. However, the introduction of the energy height concept serves to eliminate acceleration terms and the problem effectively becomes one in ordinary calculus.

This leads to a result of such a nature that its practical application is difficult. However, it does enable one to assess the conditions under which such flights are possible and indicates the maximum attainable performance.

The analysis below is only concerned with those parts of the flight path having a small inclination to the horizontal. It can also be shown by the methods of the Reference that, if the sailplane's speed at any instant does not correspond with the optimum speed appropriate to the prevailing conditions, it should be adjusted by performing a vertical climb or dive. In reality, such maneuvers are both impracticable and unnecessary but this result does suggest that it is advantageous, when adjusting the speed to the prevailing optimum, to do so as rapidly as is practicable. The analysis neglects the effects of transitions between different conditions of flight, in that it implicitly as-

sumes that the load factor is always unity. Other things being equal, push-over and pull-up maneuvers will produce decreases and increases in induced drag, respectively, so to some extent the effects of a series of such maneuvers will be self-cancelling so far as the overall dissipation of energy is concerned.

Analysis

Consider a sailplane flying on a constant heading. Let x denote distance along the flight path and w (positive upwards) the local vertical velocity of the air. To an external observer, w will in general be a function of both x and time t but, from the point of view of the pilot, it may be regarded as a function of x only. Suppose that the instantaneous forward speed of the sailplane is U. Assume also that the air density is substantially the same as the standard sea-level value.

The time to travel from x_1 to x_2 will be

$$T = \int_{x_1}^{x_2} \frac{dx}{U} \tag{1}$$

The equation of motion of the sailplane along its flight path will be, in still air,

$$D + W \sin \theta + \frac{W}{g} \frac{dU}{dt} = 0, \tag{2}$$

where θ is positive nose-up (See Fig. 1).

If the energy height is h_e, where

$$h_e = h + U^2/2g,$$

and h = true height, then

$$\frac{dh_e}{dt} = \frac{dh}{dt} + \frac{U}{g} \frac{dU}{dt}$$

$$= U \sin \theta + \frac{U}{g} \frac{dU}{dt},$$

and from (2)

$$\frac{dh_e}{dt} = - \frac{DU}{W} \tag{3}$$

But $\frac{DU}{W}$ is the rate of sink of the sailplane, v_s, when flying steadily at speed U.

In the presence of the upcurrent w, the total rate of change of energy height will be

$$\left(\frac{dh_e}{dt}\right)_{tot} = w - v_s. \tag{4}$$

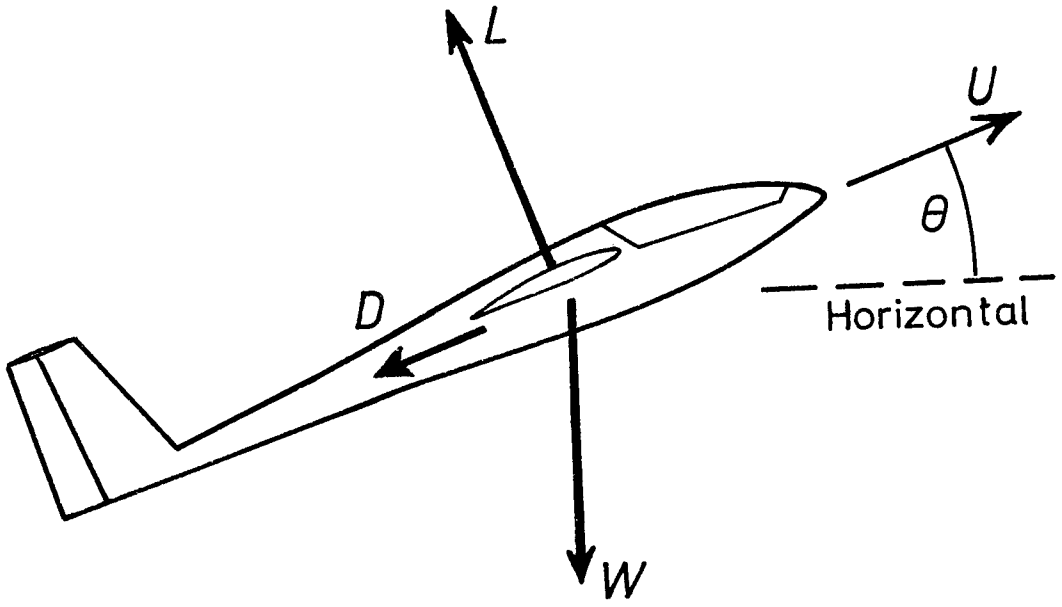


Fig.1

The total change of energy height between x_1 and x_2 will be:

$$H_e = \int_{x_1}^{x_2} \left(\frac{dh_e}{dt}\right)_{tot} \frac{dt}{dx}\, dx$$

$$= \int_{x_1}^{x_2} (w - v_s)\, \frac{1}{U}\, dx. \qquad (5)$$

Let us suppose that we wish to fly in such a fashion that, for a given $(x_2 - x_1)$, T is a minimum and $H_e = 0$. This is not the only criterion which could be applied but it represents a simple case analogous to the usual criterion for analysing cross-country flying.

T is of the form $\int F(U)dx$ and

H_e is of the form $\int G(U,x)dx$.

It therefore follows that the criterion to be satisfied is

$$\frac{\partial F^*}{\partial U} = 0,$$

where

$$F^* = F + \lambda G$$

$$= \frac{1}{U} + \frac{\lambda}{U}(w - v_s), \qquad (6)$$

and λ is a constant Lagrange multiplier.

So the criterion is:

$$-\frac{1}{U^2} - \frac{\lambda}{U^2}(w - v_s) - \frac{\lambda}{U}\frac{\partial v_s}{\partial U} = 0,$$

since v_s is a function of U only.

This can be re-arranged to give

$$\frac{\partial v_s}{\partial U} = \frac{v_s - w - \frac{1}{\lambda}}{U},$$

or, since $\frac{1}{\lambda}$ must clearly have the dimension of velocity,

$$\frac{\partial v_s}{\partial U} = \frac{v_s - w - w^*}{U}. \qquad (7)$$

The criterion expressed by eqn. (7) is shown graphically in Fig. 2.

This is the standard "MacCready" situation. (Indeed any optimum flight path for a sailplane gives a similar result, leaving w* to be interpreted according to the circumstances.) w* is, in effect, the zero-setting of the MacCready ring and, whilst the diagram is drawn for a positive value (equivalent

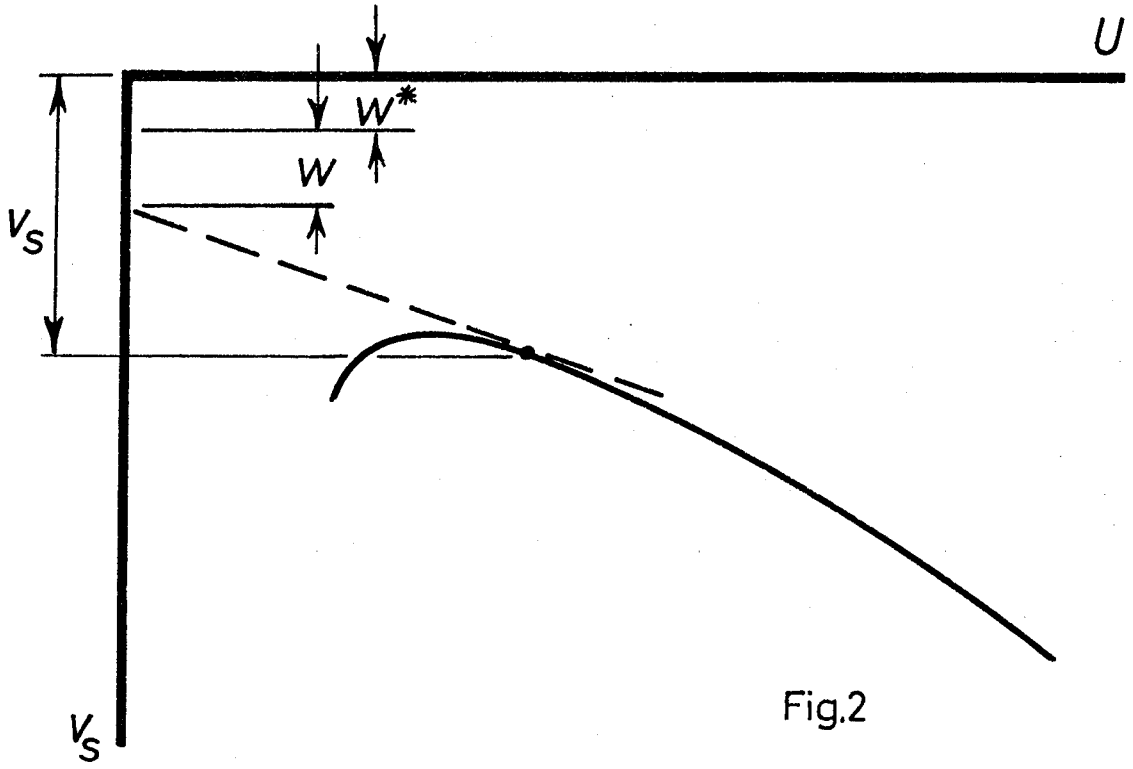


Fig.2

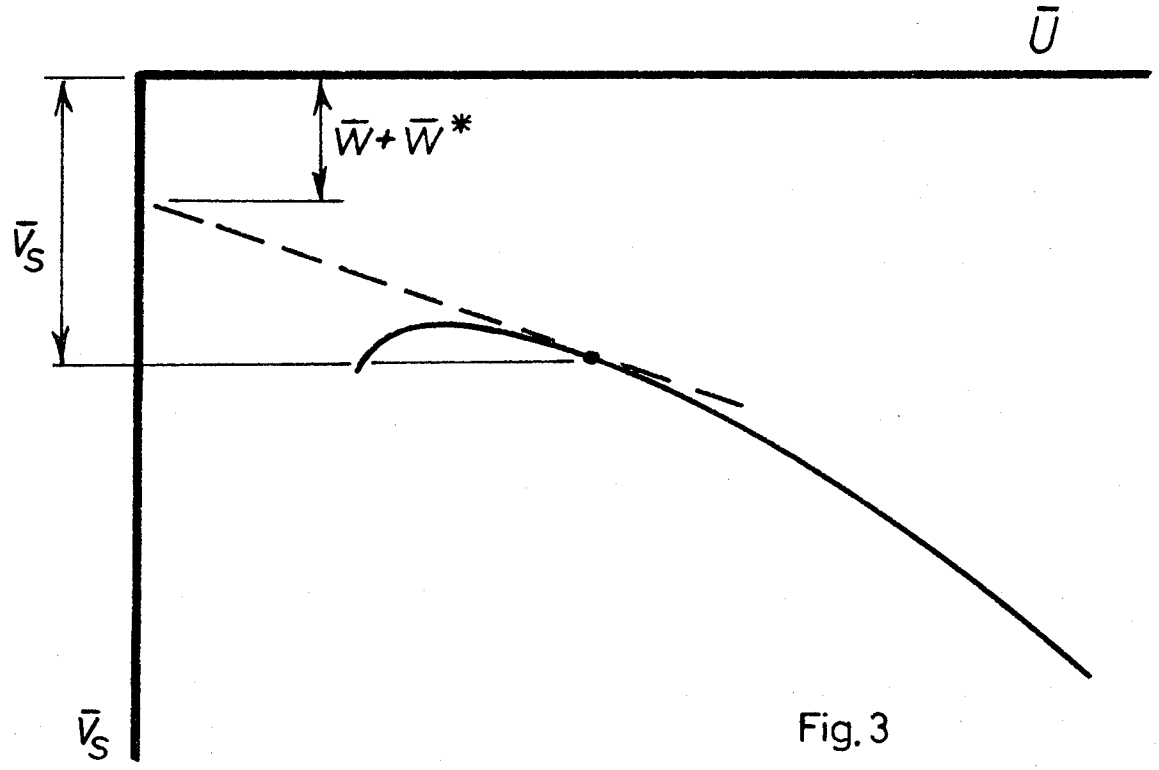


Fig. 3

to setting the datum opposite some rate of sink figure), the sign of w* remains to be determined. In practice, it will often be negative. It should be noted that circumstances can arise in which one should fly at less than the speed for minimum rate of sink: in other words it may be advantageous to spend a long time in the upcurrent at the expense of some increase in rate of sink.

From the pilot's point of view, this analysis contains a severe difficulty: w* is ultimately determined by the condition that $H_e = 0$ and hence requires a knowledge of w as a function of x over the distance $x_2 - x_1$. Unfortunately the pilot has no powers of prophecy. When flying under a cloud-street, the pilot may initially wish to gain height (on the average) until he is reasonably close to cloud-base and then adjust the MacCready ring by a process of successive approximation so that, overall, there is no net change of height. In real life, there tends to be insufficient time to make the adjustments other than very approximately.

Illustrative calculations for a fixed-geometry sailplane

For a sailplane with a parabolic $C_D - C_L$ curve, the performance polar may be described by

$$\frac{v_s}{v_{so}} = \bar{v}_s = \frac{1}{2}\left(\bar{U}^3 + \frac{1}{\bar{U}}\right), \tag{8}$$

where $\bar{U} = U/U_o$ and both v_{so} and U_o relate to the $(L/D)_{max}$ condition.
Let $\bar{w} = w/v_{so}$ and $\bar{w}^*/v_{so}$. Then, in dimensionless terms, the criterion of eqn. (7) becomes

$$\frac{\partial \bar{v}_s}{\partial \bar{U}} = \frac{\bar{v}_s - \bar{w} - \bar{w}^*}{\bar{U}} . \tag{9}$$

This is illustrated in Fig. 3.
From (8) and (9)

$$\frac{1}{2}\left(3\bar{U} - \frac{1}{\bar{U}^2}\right) = \frac{1}{2}\left(\bar{U}^2 + \frac{1}{\bar{U}^2}\right)\frac{\bar{w} + \bar{w}^*}{\bar{U}}$$

whence $\bar{w} + \bar{w}^* = \frac{1}{\bar{U}} - \bar{U}^3$. (10)

Suppose for the sake of simplicity, that a distance X_1, in which the upwards velocity of the air has the constant value w, is covered at an optimum speed U_1 and a distance X_2, in which $w = 0$, is covered at the corresponding optimum speed U_2 .

Then from (10)

$$\bar{w} + \bar{w}^* = \frac{1}{\bar{U}_1} - \bar{U}_1^3,$$

and $$\bar{w}^* = \frac{1}{\bar{U}_2} - \bar{U}_2^3 ,$$

whence $$\bar{w} = \frac{1}{\bar{U}_1} - \bar{U}_1^3 - \frac{1}{\bar{U}_2} + \bar{U}_2^3. \qquad (11)$$

Also, the rate of climb over distance X_1 will be $v_c = w - v_{s1}$. For zero overall height change:

$$\frac{X_1 \bar{v}_c}{\bar{U}_1} = \frac{X_2 \bar{v}_{s2}}{\bar{U}_2} . \qquad (12)$$

(Strictly, since the previous theory dealt with energy heights rather than true heights, this expression should include a kinetic energy correction.)

So $$\frac{X_1}{W_2} = \frac{\bar{v}_{s2}}{\bar{U}_2} \cdot \frac{\bar{U}_1}{(w - v_{s1})} . \qquad (13)$$

Since $\bar{v}_{s1}$ and $\bar{v}_{s2}$ are functions of $\bar{U}_1$ and $\bar{U}_2$ respectively, (11) and (13) can in principle be solved simultaneously to give $\bar{U}_1$ and $\bar{U}_2$ if $\bar{w}$ and X_1/X_2 are known.

It is interesting to consider what combinations of thermal strength ($\bar{w}$, in effect) and distance ratio X_1/X_2 are required to maintain continuous flight. One obvious particular case occurs when $\bar{U}_2/\bar{v}_{s2}$ is a maximum (i.e., when the sailplane is flown at $(L/D)_{max}$ over the distance X_2). This will correspond to $\bar{U}_2 = 1$, $\bar{v}_{s2} = 1$.

Under these conditions

$$\bar{w}^* = 0,$$

$$\bar{w} = \frac{1}{\bar{U}_1} - \bar{U}_1^3 , \qquad (14)$$

$$\frac{X_1}{X_2} = \frac{2\bar{U}_1^2}{1 - 3\bar{U}_1^4} . \qquad (15)$$

Eliminating U_1 from (14) and (15) gives a relationship between $\bar{w}$ and the least value of X_1/X_2 which will just permit continuous flight. It is apparent that $\bar{U}_1^4 < 1/3$, from (15). Now, from (8), $\bar{U}_1^4 = 1/3$ corresponds to $\bar{v}_{smin}$ so, as is apparent on physical grounds, the limiting case corresponds to flying at minimum sink in a continuous up-current of the same strength (i.e., $X_1/X_2 = \infty$, $\bar{w} = 2/3^{0.75}$, $\bar{v}_{s1} = 2/3^{0.75}$).

The choice of values of $\bar{U}_1$ is therefore very limited: the maximum value is $3^{-1/4}$ and the minimum value is that corresponding to the stall.

A few results are given in Table 1.

$\bar{U}_1 = \dfrac{\text{Speed}}{\text{Speed at best L/D}}$

$\bar{U}_1$	X_1/X_2	w
0.759	∞	0.877
0.75	20.4	0.91
0.70	3.50	1.09
0.65	1.87	1.27

$\bar{w} = \dfrac{\text{Thermal strength}}{\text{Rate of sink of glider at best L/D}}$

TABLE 1

These results are not realistic: because we have imposed the condition that the average speed shall be a max., even very weak thermals require the glider to be flown at unrealistically low speeds. The expression we have used for the performance (8), has no implied lower limit to $\bar{U}$. It would be better to assume that the sailplane is never flown at a speed less than its speed for min. sink, in which case, in examining the limiting conditions for continuous flight, we abandon the maximum average concept. The sailplane is flown at min. sink in the rising air and at its best gliding angle in the still air.

Inserting $\bar{U}_2 = \bar{v}_{s2} = 1$, $\bar{U}_1 = 3^{-1/4}$ and $\bar{v}_{s1} = 2/3^{0.75}$ in (13), this becomes approximately:

$$\frac{X_1}{X_2} = \frac{0.759}{\bar{w} - 0.878} \,. \qquad (16)$$

Figures obtained from eqn. (16) are given in Table 2.

$\bar{w} = \dfrac{\text{Thermal strength}}{\text{Rate of sink of sailplane at best L/D}}$

$\bar{w}$	X_1/X_2	$\dfrac{X_1}{X_1 + X_2}$
0.878	∞	1
1.0	6.22	0.86
1.5	1.22	0.55
2.0	0.675	0.403
3.0	0.375	0.272
4.0	0.243	0.196
5.0	0.184	0.155
6.0	0.148	0.129
7.0	0.124	0.110
8.0	0.1065	0.096

X_1 = distance in rising air

X_2 = distance in still air

TABLE 2

If we now consider in general terms the case of achieving maximum average speed, we can assign some likely constant value to $\bar{U}_1$ and then consider a series of values of $\bar{U}_2$. From (11), we can obtain the value of $\bar{w}$. Since $\bar{v}_{s1}$ and $\bar{v}_{s2}$ are simply related to $\bar{U}_1$ and $\bar{U}_2$ respectively, X_1/X_2 can be found from (13). A more useful quantity is $(X_1 + X_2)/X_1$, i.e., the ratio of the total distance to the distance traversed in lift. It is then possible to derive the non-dimensional average cross-country speed, $\bar{U}_{cc}$, since

$$\bar{U}_{cc} = \frac{\frac{X_1}{X_2}\bar{U}_1 + \bar{U}_2}{1 + X_1/X_2} . \qquad (17)$$

For the present purposes, the assumed values of $\bar{U}_1$ were 0.7 (for the sake of illustration; slightly less than the speed for minimum rate of sink), 0.759 (speed for minimum rate of sink), 1.0 (speed for best gliding angle) and 1.2. Values of $\bar{U}_2$ up to 2.0 were taken.

The results are presented in Table 3 and in Fig. 4 on $(X_1 + X_2)/X_1$, $\bar{w}$, axes. Lines of constant $\bar{U}_1$, $\bar{U}_2$ and $\bar{U}_{cc}$ are drawn.

Numerical example

Consider a sailplane whose $(L/D)_{max}$ is 42 at 42 knots EAS.

If $\bar{w}$ = 4 over 25% of the flight path, the upcurrent strength would be 4 knots. Flown at $\bar{U}_1$ = 0.759, the rate of climb would be 4 - 0.878 = 3.122 knots. $\bar{U}_{cc}$ would be about 1.34, corresponding to an average speed of 56.2 knots. The appropriate $\bar{U}_2$ would be 1.55, or 65 knots.

For the same glider with the same vertical air velocity extending over one-third of the distance the results become:

Speed to fly in lift:	42 knots
Rate of climb:	3 knots
Speed to fly between lift:	70 knots
Average speed:	60 knots

	$\bar{U}_2$	$\bar{w}$	$\frac{X_1 + X_2}{X_1}$	$\bar{U}_{cc}$
$\bar{U}_1 = 0.70$ $\bar{v}_{s1} = 0.886$	1.0	1.086	1.287	0.765
	1.1	1.508	1.8-9	0.886
	1.2	1.981	2.469	0.995
	1.4	3.116	3.584	1.207
	1.6	4.557	4.545	1.398
	1.8	6.363	5.405	1.600
	2.0	8.586	6.173	1.785
$\bar{U}_1 = 0.759$ $\bar{v}_{s1} = 0.878$	1.0	0.878	1.0	0.759
	1.1	1.300	1.543	0.878
	1.2	1.773	2.114	0.988
	1.4	2.908	3.164	1.197
	1.6	4.349	4.115	1.392
	1.8	6.155	4.926	1.590
	2.0	8.378	5.649	1.783
$\bar{U}_1 = 1.0$ $\bar{v}_{s1} = 1.0$	1.22	1.0	1.0	1.0
	1.4	2.030	1.838	1.182
	1.6	3.471	2.710	1.378
	1.8	5.277	3.401	1.564
	2.0	7.500	4.048	1.750
$\bar{U}_1 = 1.2$ $\bar{v}_{s1} = 1.120$	1.395	1.120	1.0	1.2
	1.4	1.135	1.010	1.2
	1.6	2.576	1.825	1.382
	1.8	4.382	2.545	1.565
	2.0	6.605	3.145	1.745

TABLE 3

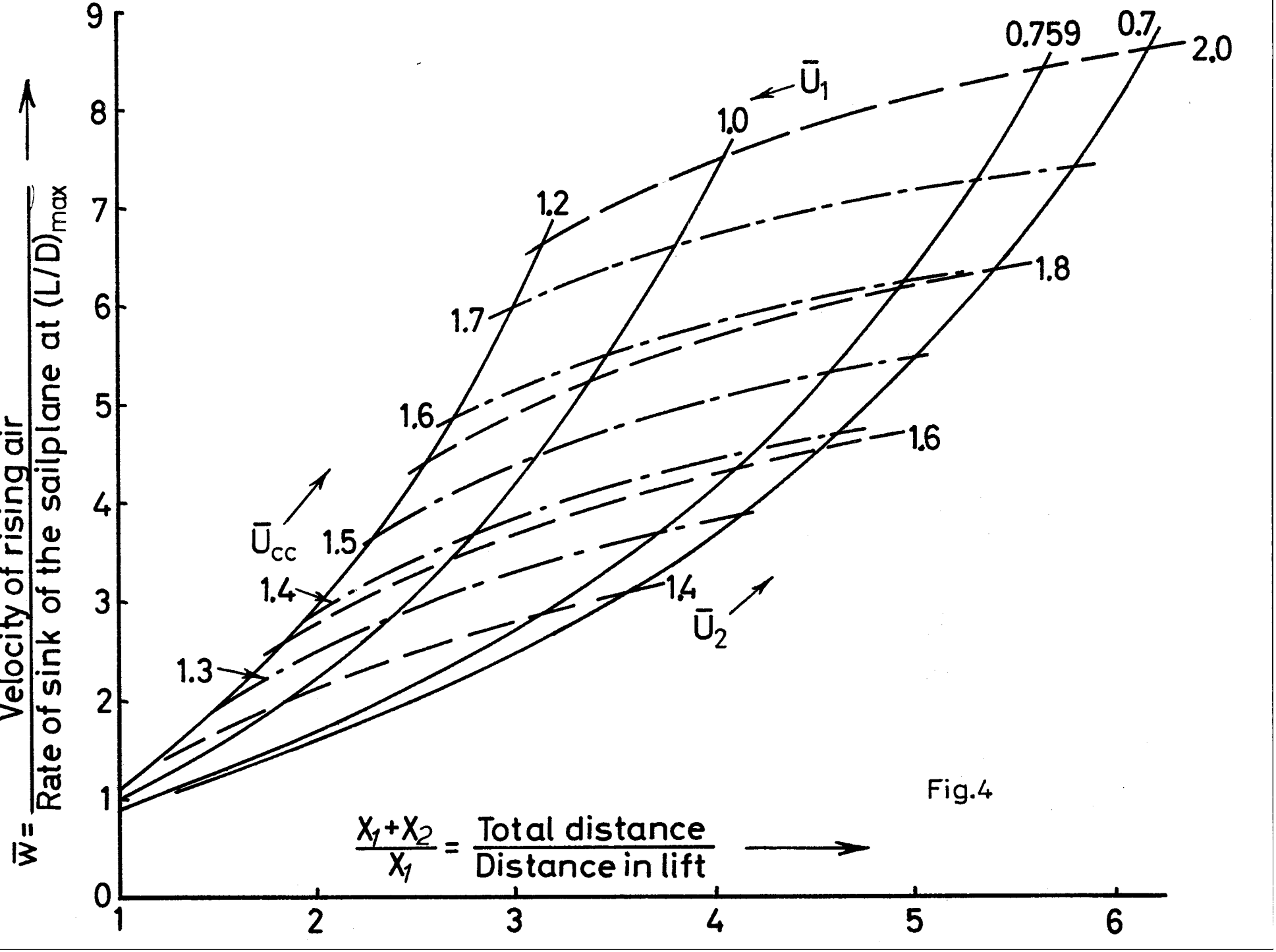

$\bar{w} = \frac{\text{Velocity of rising air}}{\text{Rate of sink of the sailplane at } (L/D)_{max}}$
$\frac{X_1+X_2}{X_1} = \frac{\text{Total distance}}{\text{Distance in lift}}$
$\bar{U}_1$
$\bar{U}_{cc}$
$\bar{U}_2$
0.759
0.7
2.0
1.0
1.2
1.7
1.8
1.6
1.5
1.4
1.3
1.6
1.4
0
1
2
3
4
5
6
7
8
9

Fig.4

Conclusions

If a cross-country flight is carried out in conditions which permit it to be made without circling, the criterion which must be applied in order to achieve maximum average speed is similar to the MacCready criterion for determining optimum speed between thermals in a normal cross-country flight. However, the datum vertical velocity (denoted by w* in the analysis, and corresponding to the datum setting of a MacCready variometer ring) is determined by the overall distribution of vertical air velocity along the flight path together with some overall condition such as zero change of energy height between the beginning and the end of the flight. In practice, a pilot would have to proceed by a process of successive approximation.

Some calculations have been made for fixed-geometry sailplanes flying through air which has a constant vertical velocity over part of the flight path and is at rest elsewhere.

Reference

Miele, A. and Cappellari, J.O.; Approximate Solutions to Optimum Flight Trajectories for a Turbojet-Powered Aircraft, NASA Tech. Note D-152, Sept. 1959.

Session Chairman's Opening Address

INSTRUMENTATION FOR SOARING

by

Paul B. MacCready, Jr.
AeroVironment, Inc.
Pasadena, California

Introduction

Instruments for soaring can be considered in two categories: (1) those which measure what the sailplane does (airspeed, rate of climb, altimeter, compass, gyros), and (2) those which help show what the atmosphere is doing. The devices of the first category are rather well developed inasmuch as they have been necessary since the early days of gliding. Those of the second category are in a much more primitive stage of development. The most important instrument, the rate of climb meter, represents a special case. It is well developed and fits into both categories; while showing what the sailplane is doing, it can also be interpreted as showing (with corrections) what the atmosphere is doing.

In the past several decades there has also been more attention paid to considering each instrument as part of a whole flight system. There has arisen an appreciation for human factors; in particular, methods of conveying the information to the pilot in a more convenient manner, and even providing automatic computations to facilitate utilization of the observation.

This paper comments only briefly on the utilization of instrumentation methods which are already in wide use, and then focuses on those which may deserve new emphasis. The paper is not a review with extensive references, but rather an updating of prior articles by MacCready [1961, 1971] which examined some ways of improving methods for locating thermals remotely and utilizing them effectively.

Measurements of what the sailplane does

The existing normal flight instruments are satisfactory for all normal soaring flight purposes. In fact, the indicated airspeed meters can be calibrated with such great accuracy, they can be used for refined performance testing

purposes. The common instruments are well described in Volume 7 of the American Soaring Handbook, "Equipment 1, Instruments and Oxygen". The latest versions appear in ads. in *Soaring* magazine.

The special case: rate of climb

The rate of climb meter (R/C) is basically an altimeter with a leak in its air chamber such that the reading is quickly reset to zero. The instrument senses the leak rate or the pressure on a diaphragm. Response speeds of good units are about one second; faster response serves no real purpose because the pilot would not absorb or utilize the extra information. When used to inform the pilot of the air motion, all sorts of corrections are required. An accelerometer can be phased into the R/C to speed its effective response speed -- but this is not done because the high frequencies provide little useful information. The major correction is the total energy device, whereby airspeed information is added to the R/C to remove the effect of rate of change of airspeed on the correction between vertical velocity of the sailplane and vertical velocity of the air. A special venturi or diaphragm handles the job well. Studies have established the sensitivity changes with altitude for the R/C and the total energy corrections. There are two other major corrections: (1), for the R/C: the normal equilibrium sinking speed of the sailplane, which can be removed by somewhat complex analog elements or displays but is usually handled by the pilot mentally making approximate corrections, and (2) for the total energy device: horizontal turbulence yields transient errors which seem impossible to eliminate but can be minimized by filtering electronically or by flow restrictors.

The R/C commonly has an audio tone output to supplement the conventional meter reading. By the pitch of the audio tone, the pilot receives information (at least relative information) while being able to look outside the sailplane. This represents a simple but elegant example of human factors engineering. The other R/C system growth area is in the subject of computerized utilization of R/C information with other information such as airspeed. The simplest such computer is the speed ring which is set around the R/C meter face to tell the pilot the optimum speed to fly between thermals. The ring position is set depending on the expected strength of the next thermal to be encountered. A more sophisticated electronic system to do this and related tasks is the Skye Mark II Air Data Computer, described in *Soaring*, December, 1971. An ingenious combined R/C and airspeed display system has been developed by Peebles (see MacCready, Peebles, and Moretti, 1972). It displays best speed to fly, glide angle, and normal sinking speed correction graphically in a way which is interpreted almost instinctively by the pilot.

Locating and using thermals

The main points of the two prior articles by MacCready will be reviewed here. In looking at the whole thermal-instrument-vehicle-pilot system, one first takes into consideration how the thermal differs from the surrounding air. Characteristics cited were:

Buoyancy Factors - Temperature; water vapor
Flow Factors - Vertical velocity; lateral velocity; turbulence
Rooc Symptom Factors - Dust; foreign bodies, smells; ions and space charge; conductivity; condensation nuclei.

For locating thermals from a distance there are various techniques for active or passive examination of electromagnetic radiation which can be shown to sense things related to thermals. The eye, looking at clouds in visual light, is the best and simplest method -- if cumulus clouds exist. The complexity of most or all of the other radiation techniques makes them completely inappropriate for consideration as a practical tool for soaring. Radar and its laser equivalent, lidar, can work to some extent, but are ruled out by the complexity problem. Extremely sensitive radar can sense the water vapor fluctuations which are strongest in growing thermals, while lidar can pick up scattering from particulates. Both can be used in the doppler mode to yield velocity along the line of sight, but this velocity component is not the vertical one which is desired. Passive radiometers can detect temperature and moisture effects remotely, but in an "averaged" way, which is difficult to interpret. To avoid confusion from the strong vertical temperature gradient, the radiometer beam must be held accurately horizontal. Existing infrared radiometers can be used to measure, approximately, ground temperatures remotely; these temperature data may help show the pilot where a thermal is likely. One thermal-locating method which may be useful is observing atmospheric potential gradients from the sailplane. A thermal, by virtue of its particular conductivity and space charge, may produce some measurable horizontal gradient at several miles distance. Fairly simple equipment can readily make the measurement; however, making the measurement meaningful in the presence of the strong natural vertical field requires considerable sophistication. Experiments to date suggest the method may work, but will require a lot of development.

Once the thermal is located, an important question is which way to turn to move toward its center. One likely candidate method here is the measurement of the water vapor gradient across the tips, most easily done with tiny wet bulb thermistor thermometers. The often discussed concept of measuring temperature variations across the wing span has never proved fruitful, presumably because the strong vertical temperature gradient makes sensitive measurements difficult, and good thermal cores are not necessarily warmer than the surrounding air. Another good candidate method is the poten-

tial gradient measurement technique. If it works for remote detection, it probably helps with turn information. Another approach is to interpret the thermal configuration from the data available from the R/C. The problem here is to use effective core-search flight patterns, and to remember the prior records -- position and upcurrent strength.

The 1961 article also went into buoyancy measurement, whereby the observations during a thermal penetration would show thermal buoyancy and hence suggest the thermal's subsequent behavior.

Observations on the ground

Various techniques are available for ground information to suggest the location of a thermal. This information can be used to tell when and where soaring can begin for the day; it can also be telemetered to the sailplane or even be visually observed by the pilot.

The simplest method is for the pilot to see horizontal convergence at ground level by noting smoke or dust blowing at several points. Convergence must be associated with updrafts. A group of windsocks can serve the same function. Free flight model fliers commonly use this sort of approach, with adaptations suitable to hunting the small thermals close to the ground which are useful for models. Several 20 ft poles are placed around the model field, each with a long, light streamer at the top. The streamer shows wind direction and, when it blows upward, even directly shows a thermal. Temperature sensors are also sometimes used.

In the past several years, remote probing by acoustic waves has made rapid strides, to where now relatively simple equipment is often able to detect atmospheric variations at ranges of a kilometer or so. The device emits a brief sound pulse, usually at a frequency in the 500-2000 Hz range, and then listens to the echo scattered back from the atmospheric variations. For a monostatic system, one where the transmitter and receiver are located at the same spot, the variations sensed are primarily temperature fluctuations. The results are continuously plotted on a time-height chart, just as is normally done with acoustic depth recorders used on boats. On land, the sounder readily shows the presence of inversions and of convective cells. If a bi-static system is employed, wherein the receiver and transmitter are separated so the scattered echo comes back at, say, 135° instead of 180°, the scattering is stronger since it is due to velocity perturbations in addition to temperature (density) fluctuations. The bistatic system operates at only one range, and needs to vary antenna orientation to vary range. It can be operated continuously rather than being pulsed. The return signal from any acoustic sounder can be analyzed for its doppler shift, which shows a function of the velocity of scatterers and the geometry of the transmitter-receiver orientation.

At a soaring site, a monostatic system can be quite helpful. The time-height display of echo intensity shows inversions and convective cells. Since the cells are thermally driven, temperature anomalies are always associated with them. The height to which convective cells are seen with a simple system is likely 500 m or less, according to Hall*. He notes the signal intensity falls off as $(\text{height})^{2/3}$, which is in agreement with convective theory. This falloff, coupled with the z^2 attenuation associated with range, quickly puts an upper limit on the maximum height for useable signals. Doppler information can also be obtained wherever there is any return detected, meaning you are directly able to read the vertical velocity in a thermal.

Conceptually, at least, the monostatic doppler acoustic sounder can be pointed in various directions and so, from a single ground location, build up velocity component information from which low level convergence can be estimated. Such convergence correlates well with an upcurrent within the area of measurements. Also, conceptually, an acoustic sounder can be installed in a sailplane to probe ahead or to measure relative vertical velocities above and below the flight path. However, basic factors related to wavelength tradeoffs between antenna size, beam width, atmospheric attenuation, and scattered signal strength, as well as spurious noise pickup problems, probably render the apparatus impractical for mounting on the sailplane.

Areas for emphasis

Some subjects offering the sailplane enthusiast a high potential for gain per "unit of development effort" are:

1. Continued experiments with horizontal potential gradient measurements for thermal locating from a distance and turn information when once in a thermal.
2. Using wet bulb thermistor sensors on wing tips to sense humidity gradients for turn information.
3. Making a thermal buoyancy sensor to tell whether the thermal should be strengthening or weakening.
4. Developing memory and visualization aids for R/C information during upcurrent core searches. Couple this with optimized trajectories for maximizing both climb and information. Releasing flow visualizers (bubbles, smoke) can be very useful.
5. Developing instrument readout devices so that instrument information is conveyed in the most effective (simplest) possible form to the pilot, as with the Peebles computer. A knob or lever on the stick which

---

*Dr. Freeman Hall, NOAA, Wave Propagation Lab, Boulder, Colo. Private Cummunication.

moves as a function of angle of attack can give airspeed information to the pilot through his fingers and leave his eyes free for other tasks. Alternatively, the finger-sensed indicator can be set to give speed-to-fly information between thermals. The audio R/C instruments can be switched to speed-to-fly audio when between thermals.

Around the airport, an acoustic sounder can be useful to tell exactly when soaring should begin. A network of windsocks rather than just one or two can give hints to those on the ground or flying as to where a thermal's roots might be.

If soaring enthusiasts put together many of the best thermal-hunting methods, they may be able to rival the skill of soaring birds in locating and using thermals. Perhaps the most useful recommendation is to discover how birds do it.

References

1. MacCready, P.B., Jr.; Improving Thermal Soaring Flight Techniques, Swiss Aero-Review, July 1961.

2. MacCready, P.B., Jr.; Instruments and Techniques for Locating and Exploiting Thermals, Aero Revue. February and March 1971.

3. MacCready, P.B., Jr., Peebles, P. and Moretti, F.; The Peebles Computer. Aero Revue, March an April 1972.

REMOTE DETECTION OF THERMALS BY MEANS OF HORIZONTAL ELECTRIC FIELD MEASUREMENTS

by

Ralph Markson
Atmospheric Sciences Research Center
State University of New York
Albany, New York.

Introduction

In the past, sailplane pilots have had no sensor for determining the location of regions of lift other than their eyes. They might have headed for a cumulus cloud or a convenient ridge oriented perpendicular to the wind when searching for rising air. Atmospheric electric field measurements from a sailplane may offer another means of locating thermals and using them more effectively by indicating the regions of maximum lift. This technique has been suggested in the past by MacCready [1954, 1971].

The basic principle is dependent on the vertical gradient of space charge density in the atmosphere. In general an excess of positive ions (compared to negative ions) exists in the atmosphere, and the concentration decreases with altitude. A particularly dense region exists in the planetary boundary layer within a few tens of meters from the earth's surface. This charge can be fed into convective updrafts through horizontal convergence near the ground and be carried aloft by the thermal. Thus pockets or columns of positive charge can accumulate in thermals, particularly near the top, where they will set up electric fields. Measurements of the horizontal component will indicate the direction of the charge center (marking the thermal) from a sailplane. This paper will discuss use of such measurements to increase soaring efficiency.

Review of fair-weather atmospheric electrical conditions

In order to understand the mechanism it is necessary to understand some aspects of fair-weather electricity. The subject is gone into more completely in texts by Chalmers [1967] and Israël [1971]. "Fair-weather" in atmospheric electricity essentially implies regions distant from thunderstorms, dust storms (or other electrical generators), precipitation or extensive cloud layers. Thunderstorms generally are considered the main electrical generator maintaining the

earth's electric field. Potential gradient, the term used in making electric field measurements, is the negative of the electric field, i.e., it is a vector of equal magnitude but in the opposite direction. While the mechanism by which thunderstorms make electricity is still not agreed upon (and probably several exist), most investigators concur that the upper portion of a thundercloud contains excess positive charge and the bottom contains negative charge excess. Thus a dipole model can be assumed in explaining how thunderclouds maintain the earth's electric field.

The atmosphere contains ions of both signs mostly caused by cosmic radiation ionizing air molecules. Because of the variation of conductivity with height a small excess in ions of one sign will occur. Since the earth is charged negatively and the upper atmosphere positively due to the polarity of thunderclouds, this excess charge in the atmosphere is positive. Typically, near the earth's surface 1000 ion pairs (an ion of each sign) per cm^3 will be present. However, the net positive charge is only a few ions per cm^3 generally. There appears to be great variation from one location to another, and this is a function of air mixing, pollution, radioactive gases and other factors. While 1 to 10 elementary charges per cm^3 may be typical over land with convection present, measurements on a mountain in New Mexico indicate 200 elementary charges per cm^3 were typical and at times space charge densities of over 1000 elementary charges per cm^3 were recorded (Vonnegut and Moore, [1958]).

A thunderstorm acts as a generator by causing the positive space charge above it to move upward into the highly conductive upper layers of the atmosphere. Similarly negative ions move downward. Because of high conductivity in the upper atmosphere the charge moves sideways redistributing itself homogeneously around the earth in much less than a second at a height of 60 km. For purposes of atmospheric electricity this height is called the "equalizing layer". It is at a potential that is fairly constant at any given time all over the world. This potential is about +300,000 volts relative to the earth. The "equalizing layer" can be considered the outer conductor of a spherical capacitor, the inner conductor of which is the earth. Between them the atmosphere acts as a leaky dielectric through which charge drifts. Under a thunderstorm large electric fields exist; these can be sufficient to cause point discharge from sharp objects on the earth's surface. When most pronounced this is recognized as Saint Elmo's fire. Because the bottom of a thunderstorm is charged negatively, positive charge enters the atmosphere in the point discharge leaving negative charge on the earth. This is the primary factor accounting for the earth's charge. Cloud to ground lightning provides an additional 10%. Because the earth is a good conductor the negative charge distributes itself uniformly over the surface, and a vertical electric field is established in the atmosphere all over the world. The fair-weather electric field intensity is about 120 volts per meter in all fair-weather regions near the earth's sur-

face. It decreases exponentially with altitude due to the exponential increase in atmospheric conductivity.

In fair-weather regions positive ions in the atmosphere drift downward toward the negative charge on the earth, and negative ions drift upward. Two-thirds of the atmospheric charge would be lost in about 20 minutes in the lower atmosphere due to conductivity allowing the charge to leak away if the electrical generator maintaining the field, thunderstorms, were turned off. However, thunderstorms are always occurring at various places on earth, particularly near longitudes where it is afternoon. The fair-weather field intensity varies simultaneously all over the world as a function of the sum of worldwide thunderstorm activity. The minimum occurs at about 0400 GMT and the maximum (about 30% higher) about 1900 GMT.

The distribution of space charge density with altitude varies greatly as a function of atmospheric mixing. When there is strong mixing beneath the inversion the density gradient will be small, and the average space charge through the mixing layer may be only 1 elementary charge per cm^3 although there still may be a layer of space charge close to the earth depending on the details of low level mixing and terrain. With weak or widely-spaced convection a relatively dense layer of space charge can exist near the earth, and 10 to 100 elementary charges per cm^3 may occur in the lowest 100 meters of the atmosphere. The particular high values measured on a mountain in New Mexico were probably confined to a layer less than 50 meters thick.

Another region where high space charge densities will occur is at the interface of two horizontal layers of different conductivity such as at the inversion when thick haze exists below that level. Here through a depth of 50 meters a positive space charge density of 50 elementary charges per cm^3 may exist. Thermals acquire excess positive charge densities compared to their surroundings from these two regions of relatively high positive space charge densities. The technique to be described operates by sensing the direction from a sailplane to the regions of relatively high density positive space charge in thermals.

Mechanism for electrical thermal detection

Figure 1 illustrates how space charge should be redistributed in the atmosphere by a thermal and the resulting electric field equipotential lines. Whether a thermal is continuous (as a column extending up from the earth), a bubble, a plume or a vortex ring, essentially the same electric field configuration will exist. Near the earth's surface air carrying positive charge converges toward the thermal and is entrained in the rising air. Near the top of the column, where a cloud may form if the air is sufficiently moist, the air

will decelerate; the space charge concentration will be greater in this volume than in the surrounding air. Similarly, a buoyant bubble formed near the earth will contain higher density space charge than its surroundings. The diagram shows these volumes as positive charge centers. Because the earth is a good conductor, an image of the electrical charges in the atmosphere but of opposite sign can be considered to exist in the earth in mapping the electric field. To a first approximation the two charge centers can be considered as a dipole that would have an electric field configuration resembling that of Figure 1. It is seen that an aircraft measuring the horizontal field component would have the largest signal to work with near the altitude of the top of a thermal column or near the height of a bubble. However, excess positive charge also exists within the column, and the horizontal components at altitudes between the top of the thermal and the earth will be greater than suggested by the diagram. Another factor not depicted is that horizontal components near the earth will be larger than further up because the charged air entering the base of the column will mix with entrained surrounding air through the sides of the thermal during its ascent and be diluted. The decrease in charge concentration with altitude in the thermal will be enhanced because of the increase in conductivity with altitude which will increase the rate of change dissipation. On the other hand, the entrainment of surrounding air into the thermal as it passes through an inversion could supply a fresh supply of positive charge to the upper portion of the thermal.

In Figure 2 a columnar thermal is envisioned in more detail. The semi-circular dome near the top depicts a cloud which may or may not be present depending on the moisture of the air. Air trajectories are depicted by arrows. At the top of the thermal a vortex-ring type of circulation is shown. The air rises above the neutral buoyancy level -- which might be in the lower portion of the cloud -- and falls back to the sides as in a fountain. Some of the air recirculates back into the central portion where there is rising air, some may continue downward with appreciable velocity, and some may spread out sideways. Positive charge from near the earth is shown being carried aloft in the thermal. A diffuse pocket accumulates at the top of the thermal. This charge would generate an electrical force on the ions of the atmosphere such that positive ones would move away and negative ones would move toward the cloud of positive charge at the top of a thermal. If a liquid water cloud exists, the negative ions become attached to cloud droplets near the cloud surface, forming a layer of negative charge that is probably less than 10 meters thick. This has been called a "screening layer" because it can prevent the diffuse positive charge within the cloud from being seen electrically. Even without a cloud of water drops, a similar effect may take place if sufficient haze or pollution particles are present for the negative ions to become attached. The negative ion sheath covering the top and sides of the cloud of water droplets or haze particles would move along with the air unfolding at the top of the thermal and descending down the sides as depicted in

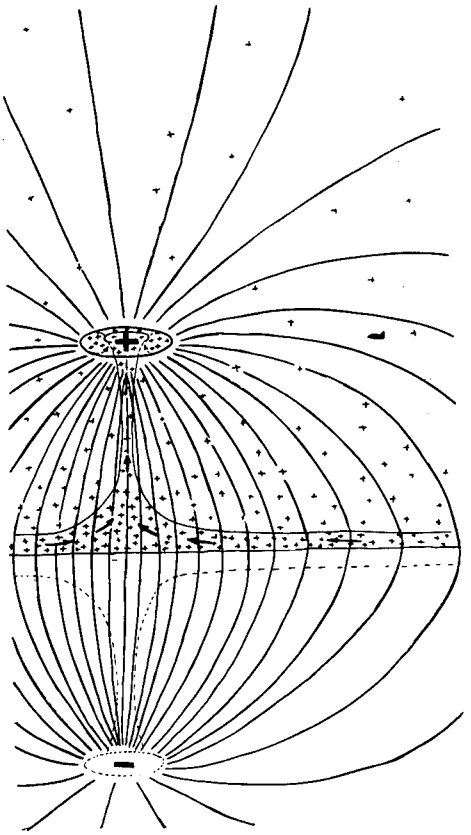


Figure 1. Dipole model of electric field created by an accumulation of positive space charge at the top of a thermal.

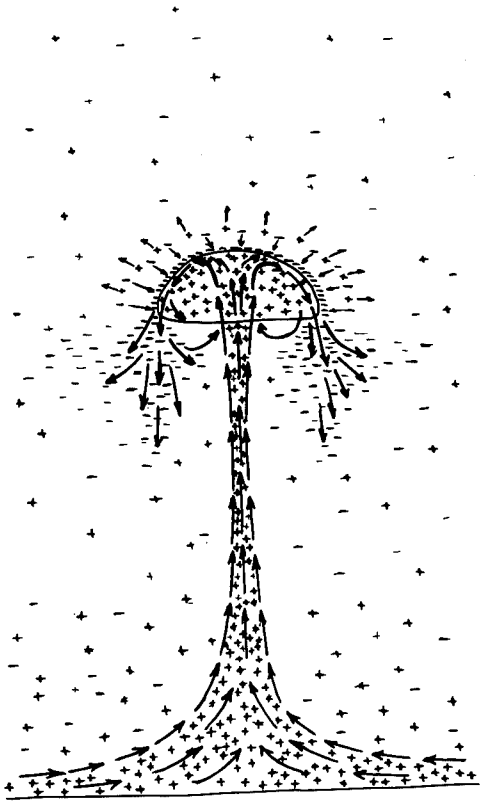


Figure 2. Air motions and distribution of space charge in and around a thermal.

Figure 2. Pockets of negative charge could accumulate to the sides of thermals near the neutral buoyancy level and in the downdraft regions. Unless these factors were understood, electric field detection of thermals might be quite confusing and the patterns seem chaotic. If a sailplane came near a local pocket of negative charge while flying toward a thermal marked by positive charge there might be a reversal of the potential gradient. The author apparently encountered such conditions as will be described subsequently. The suggested model is supported by measurements of Vonnegut, et al., [1962] in which the vertical potential gradient was recorded from an airplane passing under cumulus clouds charged from the ground by space charge generating apparatus. The charge was carried aloft into the clouds by the mechanism suggested in Figures 1 and 2. Their data showed positive charge overhead when the airplane was passing under the central portion of the cloud and positive charge was being released on the ground. Negative charge was encountered near the lower edges of the cloud as suggested in Figure 2.

Previous electrical measurements of convection

Before the electric field measurements from a sailplane were begun, several years experience in making such measurements had been acquired during a program in which a powered aircraft was used. This aircraft, a Starfire one-of-a-kind home-built, is equipped to measure the vertical component of the atmospheric electric field using polonium (radioactive) probes seen at the left wing tip in Figure 3. During the course of this work, measurements made when flying at constant altitude have suggested that convective patterns were being recorded. A brief look at some of these data will illustrate the potential for airborne electric field detection of convection and how space charge may be accumulated by convection in the atmosphere.

Figure 4 was made during constant level runs at heights of 5, 50 and 160 meters over the ocean in the Bahamas. Atmospheric conditions favored organized convection. Just above an ocean surface is a region particularly rich in positive space charge produced by the breaking of bubbles and the "electrode effect" (see Chalmers [1967]). Measurements indicated a space charge density of 72 elementary charges per cm^3 in the 5 to 50 meter height layer. Sharp increases in the vertical potential gradient when flying at 5 meters suggest the presence of positive charge above the plane at the time these anomalies were recorded. They were probably caused by organized convection -- perhaps in the form of horizontal roll vortices (Kuettner [1971])-- with a spacing of about 2 km between rolls. The updrafts were weak and periodicity in the potential gradient record was no longer present at a height of 160 meters probably because the space charge had dissipated through conduction and air mixing.



Figure 3. Starfire aircraft used in atmospheric electrical research.

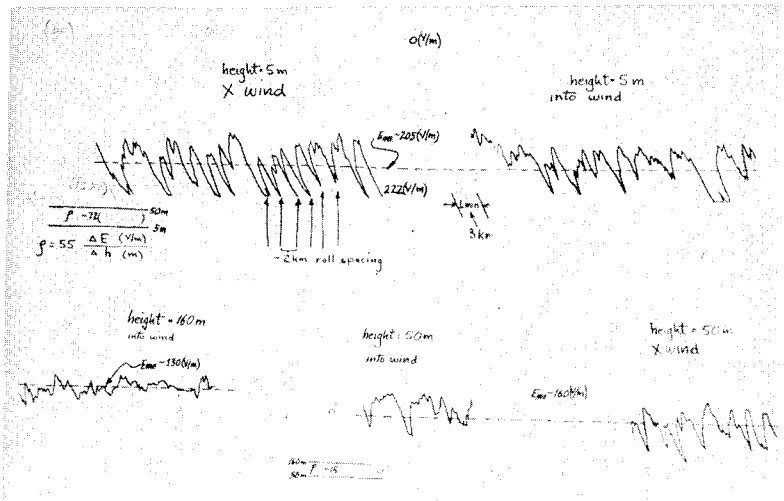


Figure 4. Graphic recordings of vertical potential gradient illustrating organized convection over the ocean.

Figure 5, showing data taken at another time and location, illustrates sharp decreases in the vertical potential gradient flying at 3.4 km crossing the Gulf Stream east of Miami. Here the spacing of the anomalous changes in potential gradient is about 5 km. These were presumed to be caused by pockets (or lines) of positive space charge accumulating at the inversion beneath the aircraft due to organized convection in the mixing layer. The air mass over the Gulf Stream when this flight was made in December would favor instability with cool air over warmer water.

Figure 6, depicting air flow patterns and the relative space charge distribution during organized convection over the ocean, is a schematic attempt to explain Figures 4 and 5. In the case of the airplane flying near the sea, positive charge density is increased in the air column above the airplane when its is passing through a rising plume; thus the potential gradient increases at these locations. When the airplane is flying above the inversion it passes over pockets (or lines) of positive charge which are at the inversion over the thermal plumes. The potential gradient decreases when the airplane is over these regions. Details concerning these measurements will be published separately.

These data suggested that the horizontal electric field measurement might be useful in locating updrafts and the airplane was instrumented to measure the potential gradient between wingtip probes. Normally, clear of clouds and over flat land, there should be little or no horizontal component of the atmospheric electric field. However, initial measurements indicated that frequently during convective conditions in both clear and cloudy skies appreciable horizontal fields were present. Typical values were 1 to 2 V/m (volts per meter). Sometimes as much as 5 V/m was observed. These values were at a height of 3 km where typical vertical field intensities are 15 to 20 V/m.

The airplane proved to be a poor platform for electric field measurements relative to thermals because of its relatively fast speed and large turning radius. Even more important was the problem of the vertical field component introduced into the wingtip-to-wingtip measurement in a bank. It quickly became apparent that it would be necessary to measure the potential gradient longitudinally. Large vertical separation occurs between wingtips when a plane is banked compared to the longitudinal axis which remains essentially horizontal in a turn. Even if the vertical component were compensated for by flying at a constant bank angle and introducing a bias voltage, it is inherently more difficult to maintain a constant bank angle than a constant pitch angle. Also when flying a sailplane it is necessary to frequently vary the bank angle while searching for lift and thermaling.

A single engine airplane does not provide good sites for locating antennas at the nose and tail which would have been required to measure the longitudinal horizontal component. Thus a sailplane was acquired and instrumented to con-

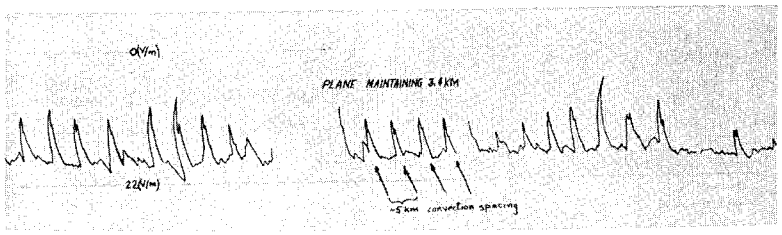


Figure 5. Graphic recording of vertical potential gradient made above the inversion illustrating organized convection within the mixing layer.

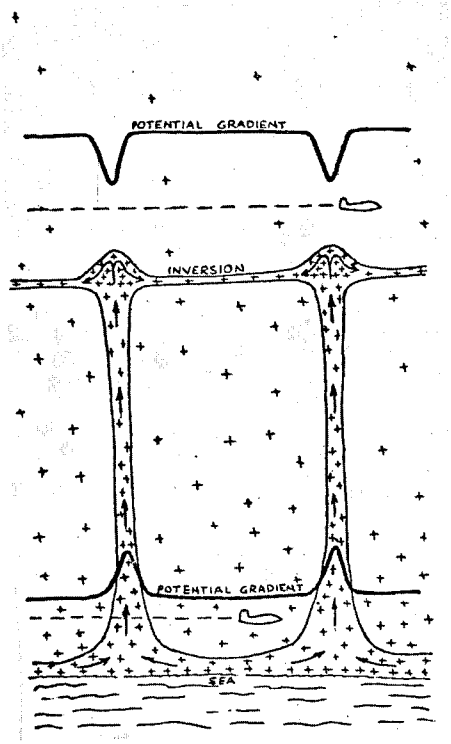


Figure 6. Schematic explanation of Figures 4 and 5.

tinue the investigation. Besides flying slowly it offers suitable mounting locations at the nose and tail for the necessary antennas.

Estimates of horizontal electric field associated with thermals

Two simple charge geometries have been assumed -- a sphere and a cylinder -- in order to estimate field strength as a function of distance from a charged thermal. For simplicity, mirror image charge which will decrease the horizontal field somewhat, particularly near the earth's surface, has been neglected. On the other hand, charge in the rising thermal column which will increase the horizontal field to the sides of the thermal column has been omitted. Figure 7 is a set of tables listing potential gradient at distances from 0.1 to 30 km from a charge center for space charge densities of from 0.1 to 1000 elementary charges per cm^3. For simplicity, all the charge is considered to be at the center of the spheres or along the axis of the cylinder. The three top tables are for spherical clouds of charge while the bottom one is for an infinately long cylindrical column of charge. The latter would approximate conditions half way up and to the side of a column of charge, without the charge concentration at the top of the thermal that would add to the horizontal component of the column itself.

For example, it is seen that in the case of a 100 meter diameter sphere of charge with a density of 10 elementary charges per cm^3 the electric field would be 0.2 V/m at a distance of 0.3 km from the center. This is about the detection threshold of the measuring system indicated by the diagonal dashed lines (to be discussed). It is estimated that field intensities to the left of the line can be detected. These tables suggest that thermals of typical sizes might be detected from a sailplane several km away, particularly if the sailplane were at an altitude about the same as the top of the thermal. This would be near cloud base, an altitude where sailplanes frequently fly. A particularly suitable region for electrostatic thermal detection should be above the inversion since the vertical electric field, the major source of noise, is typically reduced by a factor of two to ten passing up through the inversion because of the corresponding increase in conductivity.

Instrumentation

Potential gradient has been measured from aircraft by electric field mills (Clark [1956]) and electrometers with radioactive probe antennas (Vonnegut and Moor [1961]). Field mills suffer from inherent noise problems due to contact potentials and rotating components. They are relatively heavy,

FOR 100 m SPHERE

ρ = 0.1 (e/cm³)	D=0.1(km)	0.3	1	3	10	30
1	.02 (V/m)	.002	–	–	–	–
10	0.2	.02	.002	–	–	–
100	2.0	0.2	.02	.002		
1000	20	2.0	0.2	.02	.002	
	200	20	2.0	0.2	.02	.002

FOR 300 m SPHERE

0.1	.5	.05	.005	–	–	–
1.0	5	.5	.05	.005	–	–
10	50	5	.5	.05	.005	–
100	500	50	5	.5	.05	.005
1000	5000	500	50	5	.5	.05

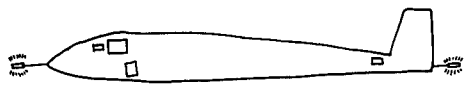
FOR 1 km SPHERE

0.1	20	2	.2	.02	.002	–
1.0	200	20	2	.2	.02	.002
10	2000	200	20	2	.2	.02
100	2×10^4	2000	200	20	2	.2
1000	2×10^5	2×10^4	2000	200	20	2

FOR 100m DIAM. CYLINDER

0.1	.03	.01	.003	.001	–	–
1.0	.3	.03	.01	.003	.001	–
10	3	.3	.03	.01	.003	.001
100	30	3	.3	.03	.01	.003
1000	300	30	3	.3	.03	.01

Figure 7. Potential gradient as a function of distance and space charge density for charged spheres of different diameter and a long charged cylinder.



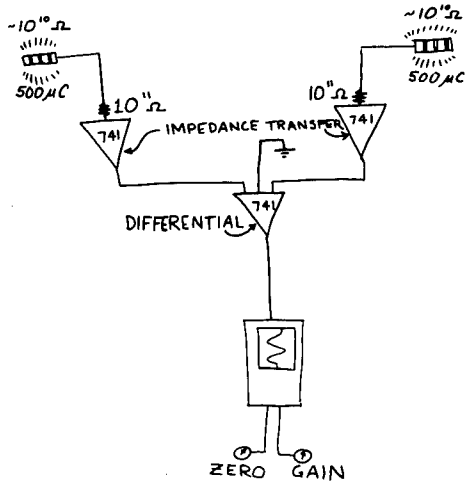


Figure 8. Block diagram in electric field measuring system.

bulky and require large amounts of power to drive the rotating parts. Mounting them on an aircraft requires structural modification of the airframe. For these reasons they are not attractive for use in a sailplane.

Modern miniature solid state electrometers offer light weight, low noise, low power requirement devices capable of measuring the picoamp currents required. Their high input resistance, 10^{14} ohms when field-effect transistors are used, makes them suitable for electric field measurements using radioactive probes as antennas. Radioactive probes are well suited for aircraft measurements because of adequate ventilation which removes space charge from the vicinity of the probes which otherwise could distort the measurement. The electrometer/radioactive probe technique seems clearly preferable to field mills for potential gradient measurements from a sailplane.

The main problem in making airborne potential gradient measurements is eliminating fields created by charge on the aircraft from the measurement. This is difficult with a powered aircraft because the engine charges the airframe and considerable precaution and experience is required. With a sailplane the problem is considerably easier but still the system must be able to handle charging that can occur when the craft strikes particles in the air or by movements in the cockpit; rubbing a plexiglas canopy can give it a high charge.

Figure 8 is a block diagram of the major components in the sailplane electric field measuring system. An antenna with a radioactive probe is in front of the nose; another is behind the rudder. An input buffer amplifier is near each antenna. Their signals go to a differential amplifier in the cockpit. Readout is on a Rustrak recorder on the cabin floor. This diagram illustrates how charge on the aircraft is eliminated from the measurement. A more detailed description of the instrumentation and its development will be published separately. The potential difference is measured between two radioactive probes on highly insulated antennas. Since the effective resistance of the ion cloud created by the radioactive material which couples the antenna to the atmosphere is about 10^{10} ohms, higher input resistance is required for the measuring system. In the sailplane 10^{11} ohms is used to minimize the time constant. For thermal detection only qualitative data is needed. Quantitative measurements require at least 10^{12} ohms input resistance. Field effect transistors at the inputs to the 741 operational amplifiers unload the signal source. Charge on the aircraft is eliminated from the measurement through differential function of another operational amplifier with its common connection grounded. In a differential measurement the potential of the common point can vary since this potential does not effect the potential difference between both inputs; i.e., if one input voltage is A, the other input voltage is C and the common voltage is B, then AB - CB = AB + BC = AC. The output of the differential

amplifier goes to a recorder that serves as a meter as well as a device for letting the pilot remember the field intensity as a function of headings flown. Gain and zero controls are provided.

Figure 9 is a side view of the Tern sailplane used in this research. The front to back potential difference is measured between antennas at the nose and tail.

A close up of the front antenna is seen in Figure 10. The radioactive element is mounted on an antenna which is a metal tube extension of the pitot tube. This arrangement does not effect the function of the airspeed indicator and allows the antenna to be positioned at a point of electrical symmetry in front of the nose to reduce problems associated with aircraft charge. The antenna is insulated from the pitot by a teflon sleeve and is connected to the input amplifier by a wire routed through the air duct.

In Figure 11 the rear antenna is shown. It is a flexible rod mounted on the bottom of the rudder by teflon insulators and bent upward so as to be level with the front antenna when the sailplane is in its normal flight attitude. This is to minimize the effect of the vertical electric field in the measurement. The rear antenna is connected to its input amplifier by a wire running through a rudder cable hole in the fuselage.

Figure 12 is a picture of the differential amplifier (large box) and front antenna input amplifier (small box) mounted in front of the instrument panel. Each input amplifier is located as close to its antenna as possible to minimize the time constant. The differential amplifier box can be considerably smaller than the one pictured which had been used in the airplane and contains a power supply.

The output of the differential amplifier is displayed on a strip chart recorder mounted on the cabin floor where it can be read along with the rest of the flight instruments (see Figure 13).

Rapid response time is desirable in the system so that field strength can be associated with variations in heading when the sailplane is circling. Flying a tight circle in which it takes 20 seconds to complete 360 degrees, the heading variation is 18 degrees per second. The time constant of the system described is approximately one-third of a second.

It was decided to measure the horizontal potential gradient from front to rear since the longitudinal axis remains relatively horizontal during turns; if the measurements were made between wingtips, a large signal would be introduced in a bank. Wingtip probes on a 15 meter wingspan sailplane in a 30 degree bank would sense a potential difference of 150 volts in a vertical field of 20 V/m. This is ten times the horizontal potential difference available if the

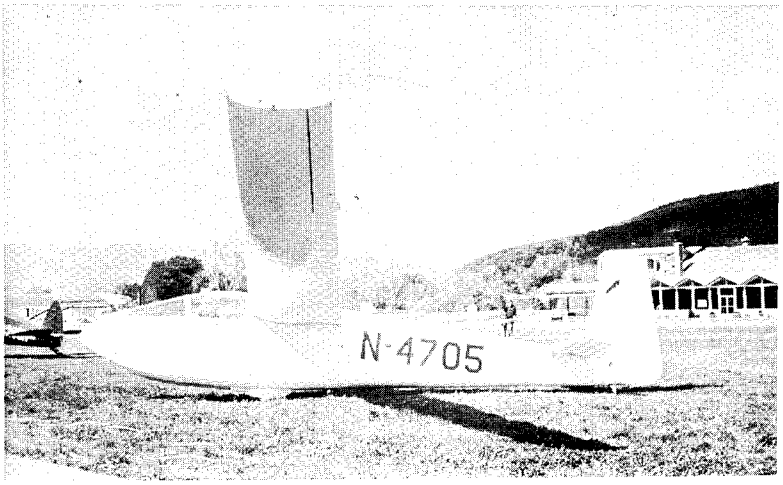


Figure 9.
Side view of Tern sailplane showing location of front and rear antennas.

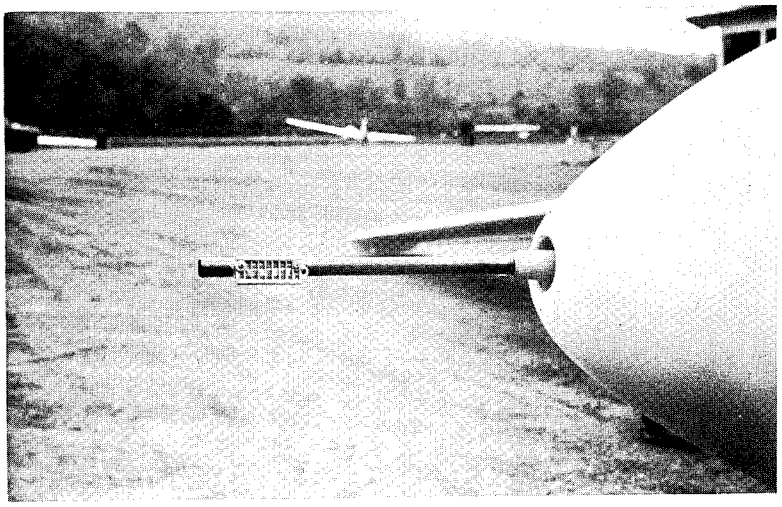


Figure 10.
Close up of front antenna showing radioactive element.

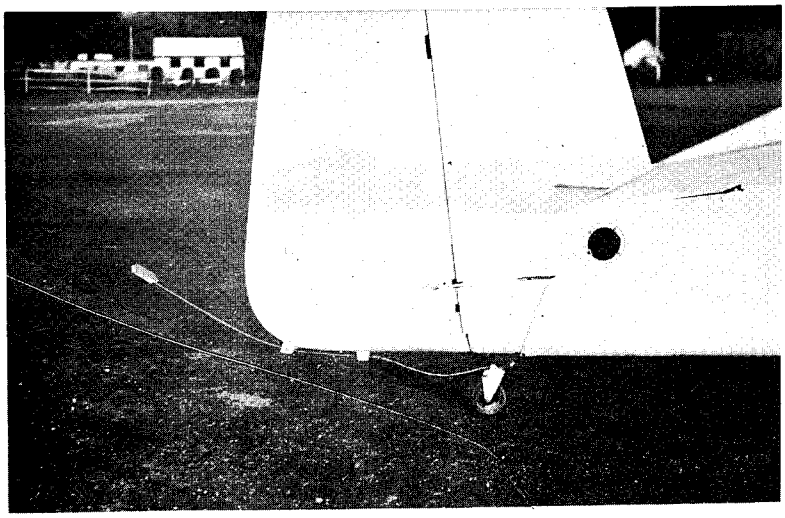


Figure 11.
Close up of rear antenna.

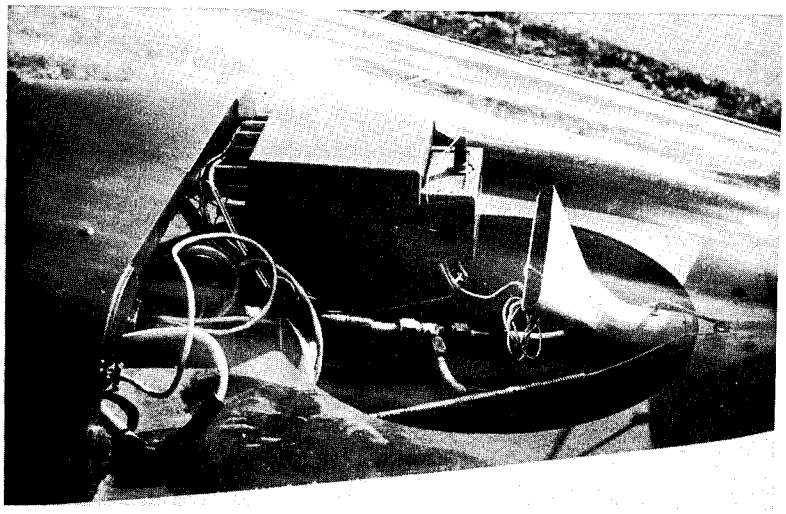


Figure 12. Front input amplifier and differential amplifier. Units located in front of instruments in cabin.

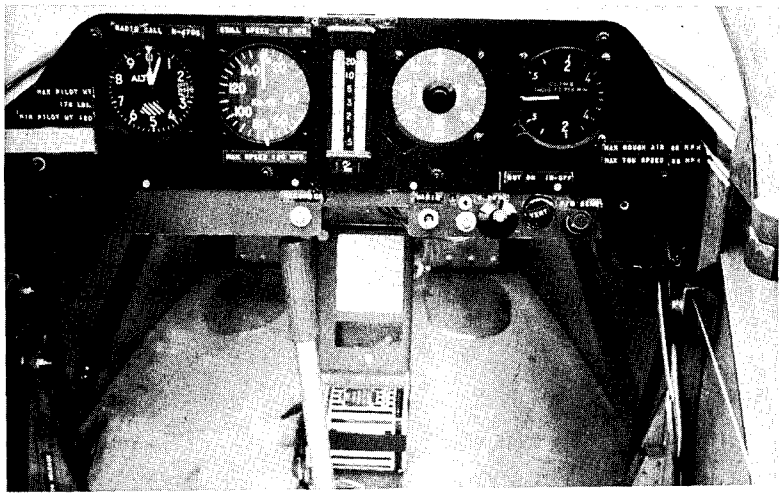


Figure 13. Pilot's eye view of instruments. Recorder mounted on the floor displays electric field data. Electric field sensitivity and zeroing controls shown.

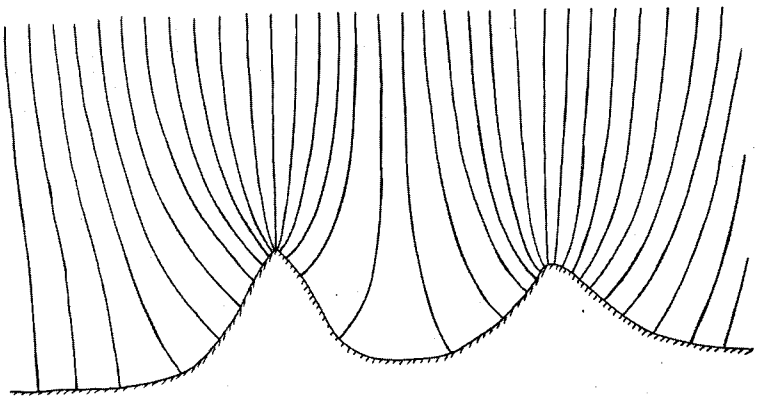


Figure 14. Distortion of the vertical electric field lines due to uneven terrain.

horizontal potential gradient is 1 V/m, i.e., the noise would be ten times the signal. The limiting factor in determining the sensitivity of the system is the vertical component of the electric field. With front to back probes, it is important to minimize variations in the pitch axis. If the distance between front and rear probes is 7 meters, a pitch variation of 1 degree causes a 12.5 cm vertical separation between the probes. In a vertical field of 20 V/m, this is 2.5 volts. A horizontal field of 1 V/m would produce a signal of 7 volts between the probes. In practice, small variations in pitch will be occuring, but they can be somewhat averaged out -- especially with the graphic recorder-- so that a mean value can be estimated. This will be a function of angle of attack, i.e., air speed. The mean needle position can be shifted to the center of the recorder scale with the zero control. When the sailplane can be flown smoothly with little variation in pitch angle, it is estimated that a field as small as 0.2 V/m can be detected. The diagonal dashed lines in Figure 7 were thus placed at this sensitivity limit. The ultimate sensitivity of the system is a few mV/m obtainable only in a static situation. Piloting skill in maintaining constant pitch angles will be an important factor in maximizing the sensitivity of the instrument. In rough air near thermals larger pitch variations will occur, but stronger field strengths will produce a compensating effect.

Operational procedure

How is this instrumentation used? Before takeoff the zero is adjusted so the needle is in the center of the meter and sensitivity is low. The system is set up so that a deflection of the needle to the right indicates positive charge is ahead of the glider and deflection to the left means positive charge is to the rear. On tow the needle should move to the right as the glider's nose is up and the vertical field is sensed. If the needle does not move the sensitivity should be increased; if it goes off scale, sensitivity should be reduced or the needle can be brought back on scale with the zero control. Rocking the nose up and down should cause corresponding needle movements to the right and left. This is a test that the system is operating properly. The sensitivity is adjusted so typical pitch variations of a few degrees correspond to about $\pm$ 15% of full scale deflection. The device may not work on tow because of charge on a nonconducting tow rope. This can be recognized by the needle deflecting to full scale on either side and the zero control being unable to bring it back on scale. After release from the tow plane, the apparatus should work normally. The needle will come back on scale and be adjustable with the controls. Readjustment of the zero center position is necessary whenever airspeed is changed because of the pitch angle variation. It is important to maintain as constant an airspeed as possible to allow the most sensitive setting when searching for

thermals. Pitch variation is the critical noise source, limiting the gain at which the instrument may be set. When regions of space charge are approached, the gain will have to be greatly reduced.

To locate lift, the sailplane is flown in a circle, and generally there will be enough horizontal field present so that the needle will have a maximum right deflection on one side of the circle and a maximum left deflection on the other side. Flying in continuous circles with the chart paper moving in the recorder, a sine wave will be produced on the chart. The heading at maximum right needle deflection will be toward positive charge; for maximum left deflection the reciprocal heading can be flown toward the positive charge. Zero and sensitivity controls are adjusted so the maximum and minimum of the sine wave occur near the edges of the chart. The zero position can be set by centering the sine wave on the chart. Another zeroing procedure that can be used when not flying in a circle is to rock the longitudinal axis of the plane through the horizon. The needle should be near center scale when the plane is horizontal and move back and forth through this position as the sailplane's nose passes up and down through the horizon.

Gain can be increased if the glider gains height since the vertical field decreases with altitude and this noise source will be less. In practice it is frequently necessary to readjust gain depending on field strengths over a range of as much as 100 to 1. The needle centering zero control may also have to be readjusted if gain is increased because some of the vertical electric field is probably being sensed and nulled out by the zeroing voltage. Centering a thermal requires the same technique as locating one from a distance. It is interesting that, when spiraling in what appeared to be the center of a thermal or under the middle of a cloud base, sine waves generally appeared on the recorder indicating the precise center of charge was still to one side.

The recorder display helps show the direction to fly for lift. In addition it provides a reminder of the relative field strength. Flying toward charged regions field strength should increase. However, the situation may be confused by coming near pockets of space charge of the opposite sign. As previously described, the meter movements frequently do not present a coherent picture.

While the operational procedure may sound confusing at first, in practice one rapidly learns to use the equipment. The challenge lies in integrating the continual variations of field strength and direction with other factors such as the locations and configurations of clouds and mountains, wind flow, type of terrain, haze, turbulence and variometer readings. It is believed most soaring pilots will find the challenge enjoyable and rewarding.

Initial results

During the summer of 1972 flights were conducted from the North Adams, Massachusetts, airport to test the electric field detecting system. In general, it was necessary to fly in ridge lift or in thermals close to the mountains which surround the airport. It was apparent that, while the system operated satisfactorily, it was mostly measuring horizontal components of the fair-weather electric field created by the mountains. Figure 14 illustrates how the vertical fair-weather electric field lines of force would bend toward mountains and create horizontal components. These in effect are noise and made it difficult to separate horizontal fields due to thermals from those caused by the terrain. Although there were suggestions of thermals sensed against the background noise, it was necessary to get higher or farther away from the mountains in order to properly evaluate the system. Since mountains and ridges are particularly favorable soaring locations, the above illustrated a limitation that electric field thermal detection will have to live with. In addition, standing waves may carry space charge aloft and confuse the picture in mountainous terrain while possibly offering a new way to locate waves.

On October 15 1972 a strong NW flow brought excellent soaring conditions with cloudstreets to the North Adams area. On this day, when it was possible to get high and away from the mountains, the electric field thermal detection system appeared capable of locating regions of lift. It seemed particularly effective when flying near cloud-base at about 2 km and appeared capable of locating thermals from distances of 1 to 2 km. The clouds appeared to be about 200 to 400 meters in diameter and 100 to 200 meters high.

Of particular interest were reversals in the sign of the potential gradient and strong downdrafts encountered when flying toward a region of positive charge. These are interpreted as possibly due to negative charge pockets associated with downdrafts at the periphery of thermals as suggested in Figure 2. By continuing on course, regions of good lift were generally encountered. In one case, away from clouds while flying toward positive charge, very strong descending air was flown into with no warning on the electric field meter. Pushing through the strong downdraft while holding course, a thermal was eventually reached. This downdraft with no negative charge may have been in agreement with Figure 2 but, since there was no cloud or haze, a screening layer did not form. Large fluctuations of the needle were frequently observed when lift was nearby.

On this day like others, anytime a circle was flown a sine wave was generated on the chart. Thus information suggesting preferential headings to locate lift regions was always available. Although flying toward positive charge when clear of mountains usually resulted in good lift, on this strongly convective day it is possible that thermals might have been encountered eventually on any random course

if flown long enough. However, it was not necessary to fly the electrically suggested courses for very long before finding lift, and it is the author's impression that thermals were being located through the electric field measurements. When flying at cloud base along a cloud street, positive charge areas could be associated with the location of clouds. Once lift was encountered and the sailplane started spiraling, a maximum positive needle deflection was usually observed at one side of the circle during each turn. It appeared that correcting the circle in the direction indicated resulted in better lift.

It is emphasized that so far very little experience has been acquired with this technique. However, in good soaring weather, there have been encouraging indications that thermals can be located and centered using the system. Sufficient electrical signals certainly are available. The problem is to make sense out of them because they can be quite variable. The picture is not as clear as the idealized model suggested in the figures of this article. Undoubtably the structure of thermals and space charge distributions can be complex. Potential gradient measuring instruments will sense a field that is the resultant of components contributed by all sources of charge. With several charged regions close to the point of measurement, the electrical picture is ambiguous. This is why it is still impossible to locate precisely the numerous charge centers in a thundercloud. When two or more charge centers are close to each other, and each has about the same charge, it will be necessary for the sailplane to be closer to one of them in order to define its direction. This is because electric field intensity is inversely proportional to the square of the distance from the measuring location to the center of charge. If charged regions contain unequal charge, field intensity is directly proportional to the quantity of charge so the measurement will be influenced more by the larger charged region of equidistant sources. These considerations tend to illustrate that electric field measurements from one location can only give information suggesting the direction of charge centers but not their distance since the amount of charge is unknown.

Future plans and possibilities

The research described above will be continued to explore the practical possibilities of electric field thermal detection. It would be important to try the system in various parts of the country where different space charge concentrations and convective patterns exist. The system might be particularly useful over flat country and where thermals are large and widely separated such as in desert regions. Also, high space charge concentrations, such as apparently exist over some mountains in the Southwest United States, should produce relatively large horizontal electric fields when convection is present and may make possible thermal detection

at greater distances than elsewhere.

It is planned to experiment with other techniques that may improve soaring efficiency. One will be to measure conductivity with a Gerdien capacitor. The conductivity of air near the ground is increased by radioactive gases and radioactive emanations from the earth. This air carried aloft in a thermal can be much more conductive (two to ten times) than the surrounding air. Glider flights by Rossmann [Israel, 1971] have been conducted in which such measurements were made.

Another approach will be to measure wet-bulb temperature gradients between the wingtips as well as possibly from nose to tail. Wet-bulb measurements indicate humidity, and thermals are significantly moister than their surroundings. Both components cen be displayed simultaneously on a dual-channel graphic recorder or with cross-pointers on a single meter. The instrumentation is being designed initially so that a temperature difference of 0.1°C will give full-scale deflection on the meter at maximum sensitivity. MacCready [1971] suggested this technique to provide information that would indicate which direction to turn to position the sailplane in the region of maximum lift once a thermal is located. It will be interesting to compare the wet-bulb, conductivity and electric field measuring techniques. While the first two can not be used for remote thermal detection, all three should be useful in obtaining information on the thermal structure. Centering thermals may also be enhanced through measurements of the vertical electric field as suggested by Figure 6.

In the future, variometer readings will be graphically recorded. With simultaneous records of the electric field, conductivity, moisture and lift, it may be possible to gain a better understanding of the structure and growth patterns of thermals. A tape recorder would be useful for verbally recording additional data such as air-speed, proximity to clouds, the location of smoke and haze, temperature and terrain. A limited amount of this information can be written on the charts.

An attempt may be made to measure the lateral (left-to-right) horizontal electric field component in addition to the front-to-back component. Eliminating the vertical component would be the big problem in this measurement. It might be done by electrically biasing the signal with a voltage proportional to the sine of the bank angle sensed by a gyro horizon. The vertical field magnitude would also have to be known and could be measured with vertical probes when the wings were level. Continuous recording of the vertical component should be valuable in centering lift as suggested in Figure 6.

A simpler approach to measuring the left-to-right horizontal component would be to position the radioactive elements

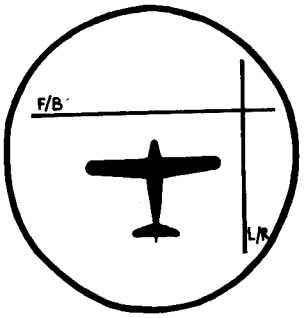


Figure 15. Cross pointer display of two components of the horizontal electric field.

at the ends of the horizontal member of a tee shaped antenna. The vertical member of the antenna would be the mast. It would be mounted on a longitudinal pin in the top of the canopy so it could be pivoted left or right. The bottom of the antenna mast would come down in the cockpit in front of the pilot. When circling, the pilot could move the mast by hand to keep it perpendicular to the horizon; thus the top of the tee with the radioactive elements could be kept parallel to the horizon at any bank angle and the vertical component eliminated. Having both horizontal field components, the resultant total horizontal electric field would be known at all times, and it would not be necessary to circle in order to find the direction of the positive charge. Figure 15 illustrates how both electric field components could be displayed on a meter with cross pointers -- an ILS indicator with glide slope could be used. In Figure 15, F/B indicates the front to back component and L/R is for the left to right component. The system would be arranged so that the direction from the center of the meter to the point where the needles cross would be the direction toward the positive charge from the aircraft. While it would be nice to have both horizontal components, this is not necessary for thermal detection since the circling technique utilizing the front to back component alone seems sufficient. In fact, it is generally not necessary to fly complete circles; the nose can be swung back and forth horizontally through a heading corresponding to maximum right deflection of the needle in order to define the direction to fly for lift.

Besides directly improving soaring efficiency, electric field measurements from sailplanes may benefit soaring indirectly by providing a new tool for learning more about convection. MacCready [1971] has suggested that instrumentation techniques should provide a considerably more efficient path toward improved soaring performance than further developments in sailplanes themselves. Preliminary results in the present program indicate that electric field thermal detection is possible. The potential of this technique seems considerable.

References

Chalmers, J.A.; Atmospheric Electricity, 2nd Edition, London, Pergamon Press, 515 pp, 1967.

Clark, J.F.; The Fair Weather Atmospheric Electrical Potential and its Gradient, doctoral thesis, University of Maryland, 151 pp., 1956.

Israël, H.; Atmospheric Electricity, Vol. 1, Published for the National Science Foundation, Washington, D.C., by the Israel Program for Scientific Translations, Clearinghouse for Scientific and Technical Information, Arlington, Va. 22151, 1971.

Kuettner, J.P.; Cloud Bands in the Earth's Atmosphere, Tellus XXIII, 404-425, 1971.

MacCready, P.B.; Improving Thermal Soaring Flight Techniques, Soaring, Dec. 1961, 6-11.

MacCready, P.B.; Instruments and Techniques for Locating and Exploiting Thermals, Technical Soaring, July 1971, 14-18.

Vonnegut, B. and Moore, C.B.; A Study of Techniques for Measuring the Concentration of Space Charge in the Lower Atmosphere; final report to Geophysics Research Directorate, Air Force Cambridge Research Center, Air Research and Development Command (Contract No. AF 19(604)1920), 163 pp, 1958.

Vonnegut, B. and Moore, C.B.; Apparatus Using Radioactive Probes for Measuring the Vertical Component of Atmospheric Potential Gradient from an Airplane, Bull. Am. Meteo. Soc. 42, 773-777, 1961.

Vonnegut, B., Moore, C.B., Semonin, R.G., Bullock, J.W., Staggs, D.W., and Bradley, W.E.; Effect of Atmospheric Space Charge on Initial Electrification of Cumulus Clouds, J. Geophys. Res. 67, 3909-3922, 1962.

EXPERIENCE WITH A VARIOMETER-COMPUTER

by

John Firth
Ottawa, Canada

Introduction

An electric variometer using a diaphragm climb transducer has been built, and coupled to a simple analog computer; besides the normal variometer functions, fully electronic total energy compensation is used; average rate of climb is obtained from the integrated variometer output, and used in a difference circuit with other inputs to give an indication of the correct speed to fly. The instrument has been in use for three years and has been used in two World Contests. The main features of the instrument are discussed below and the mathematical basis of the speed computation is given. This is followed by the author's personal evaluation of the usefulness of the instrument for contest flying.

Features of the instrument

The basic ideas for this instrument were conceived in 1969; after several years of using a mechanical variometer backed up by a rather poor thermistor type, I decided I needed something better for the 1970 World Contest. The principal aim was a fast variometer with good total energy compensation at all altitudes, good zero stability and accuracy, and an averager. Variable damping and sensitivity, and audio output were added. After suggestions by Raouf Ismail, a speed-to-fly pitch indicator was incorporated also.

For fully electronic T.E. compensation, the climb transducer must be linear to the high climb rates produced in a high-speed pull-up - that is, to about 40 kts. If the error during pull-up is not to exceed one kt, the linearity must be better than 3%. A diaphragm sensor was chosen for both the climb and the airspeed transducers; the diaphragm is 0.0005 in stainless steel with this material used for the case structure also. Equal coefficients of expansion throughout the sensor minimize zero-drift and maintain the diaphragm tension constant. Similar construction is used for the airspeed sensor; both were found to meet the linearity and stability requirements. Figure 1 shows the internal layout of the instrument, while Figure 2 shows its physical realization.

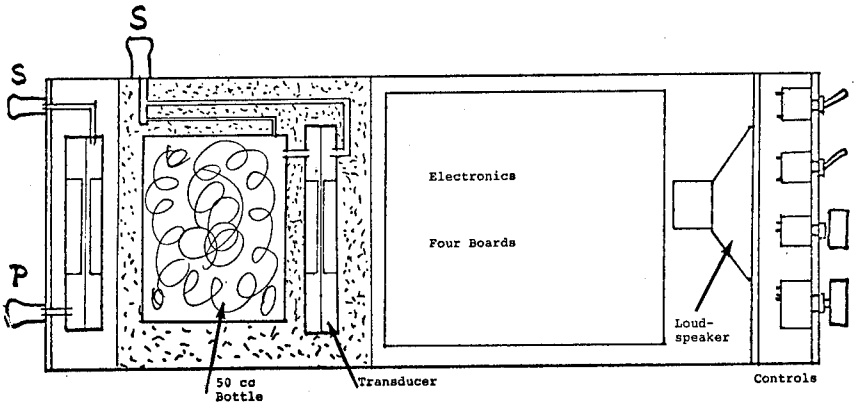


Figure 1. Internal arrangement

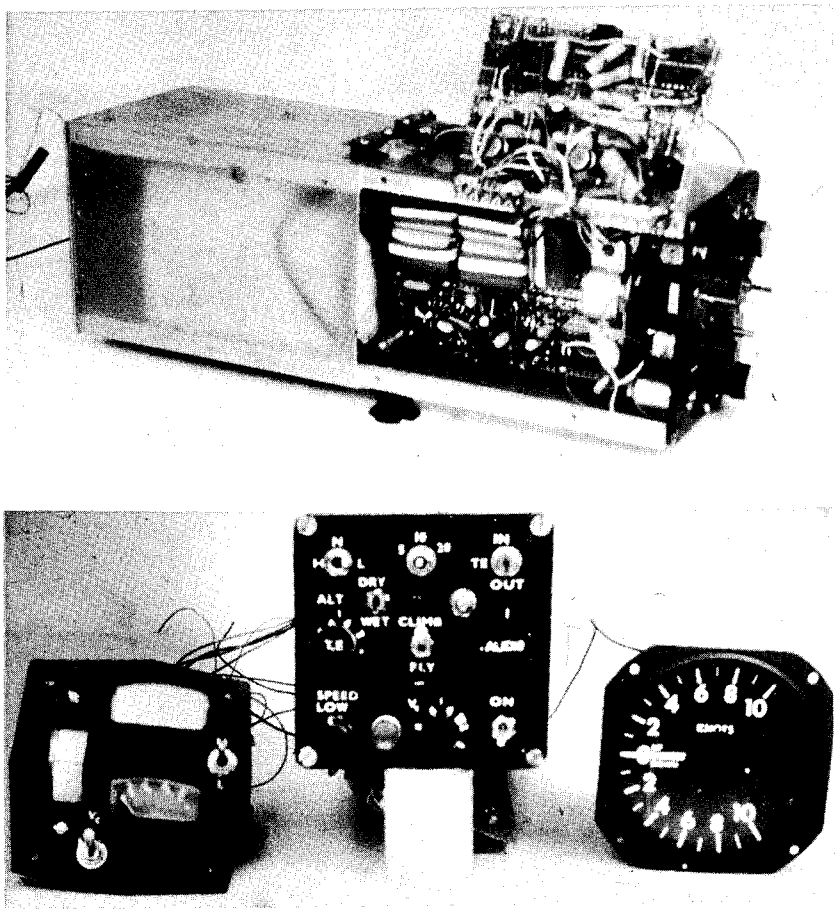


Figure 2. Integrated sensor and signal processing package, and associated readout instruments.

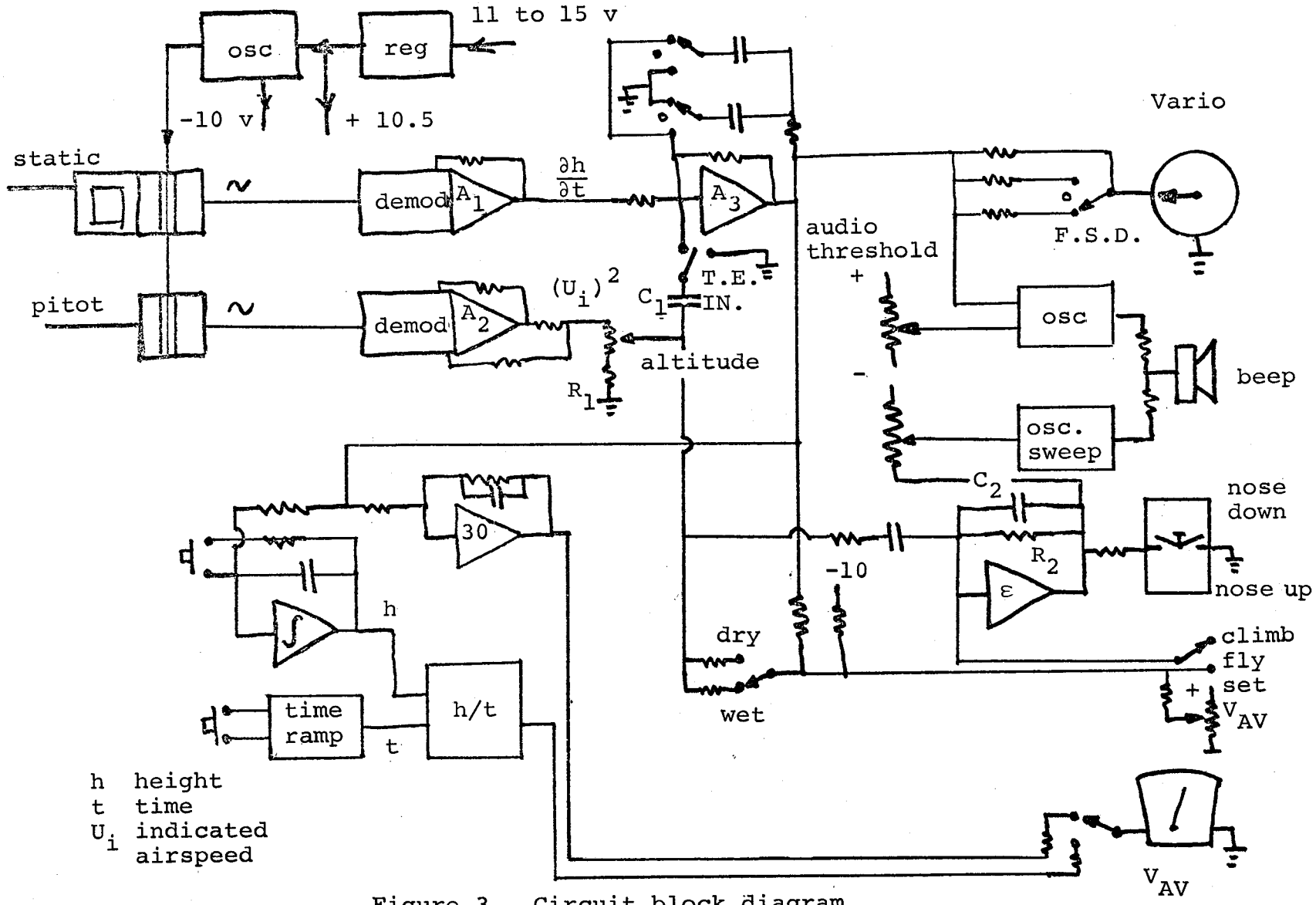


Figure 3. Circuit block diagram.

Figure 3 shows a blockdiagram of the electronics. Extensive use is made of integrated circuits; fifteen are used in all, including twelve operational amplifiers. Power required is 11 to 15v at 80 ma; this is regulated to 10.5v, and a converter provides a -10v rail needed for the op. amps. The converter also provides an A.C. voltage for the transducers, which use capacitive position pick-off.

After demodulation and amplification we have two signals representing rate of climb and airspeed squared; the airspeed signal is taken through a capacitor to the summing amplifier A3; the capacitor performs the function of differentiation on the airspeed signal, and this, summed with the rate of climb signal, gives T.E. compensation. Gene Moore has pointed out the desirability of equalizing the time constants associated with these two signals, in order to give good second-order compensation. The climb transducer has a time constant of about 1 second; R_1 and C_1 in series give a 1 second time constant also. Though the climb transducer gives true rate of climb at all altitudes (if we neglect small temperature effects) the time constant increases, and the airspeed signal falls, with density decrease. Both these effects are compensated by varying R_1, which is calibrated in altitude. Note that A_2 is connected for high output impedance so that R_1 is the effective source impedance for C_1. T.E. compensation can be switched in or out. Three response times are available; the fastest is the basic transducer time constant, but damping can be added to amplifier A_3 to give either two or four seconds. The variometer display is conventional and the full scale deflection can be selected as 5, 10, or 20 kts.

At the bottom left are the averager circuits; long time-constant integrators produce signals representing h and t, starting from the last time the reset was pressed. An analog division circuit incorporating a four-quadrant multiplier calculates the climb or sink rate. Up to 30 minutes of time ramp and 10,000 feet of climb can be used. An over-range light is provided. After two minutes of averaging, the result is accurate to better than 5%. The vario output is smoothed with a 30 second time constant; both the average and this smoothed result can be displayed on a small meter (Figure 2).

The variometer also has a standard audio output fed to an internal speaker, together with a SPEED LOW warning from the pitch director.

Figure 4 shows the basis for the simple computation required to derive the pitch director signal. The top graph shows the standard construction for best speed to fly. The sum of the three vertical components divided by the airspeed U_i gives the slope of the polar at the correct operating point. The quantity ($U_i \tan \theta$) is plotted against $(U_i)^2$ for two different wing loadings, or operating altitudes. For several polars tried, a linear approximation turns out to be quite good. A signal proportional to $(U_i)^2$ is readily available from the airspeed sensor. At any non-optimum airspeed,

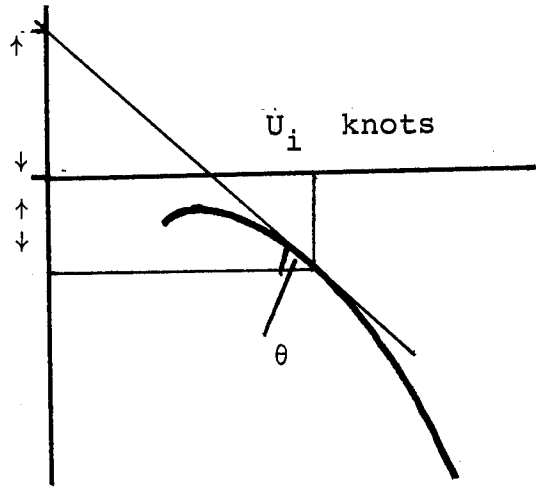
$$\text{Tan } \theta = \frac{V_{AV} + V_{AIR} + V_P}{U_i}$$

Let $\beta = U_i \tan \theta$

When U_i is correct

$$V_{AV} + V_{AR} + V_P - \beta = 0 \quad (1)$$

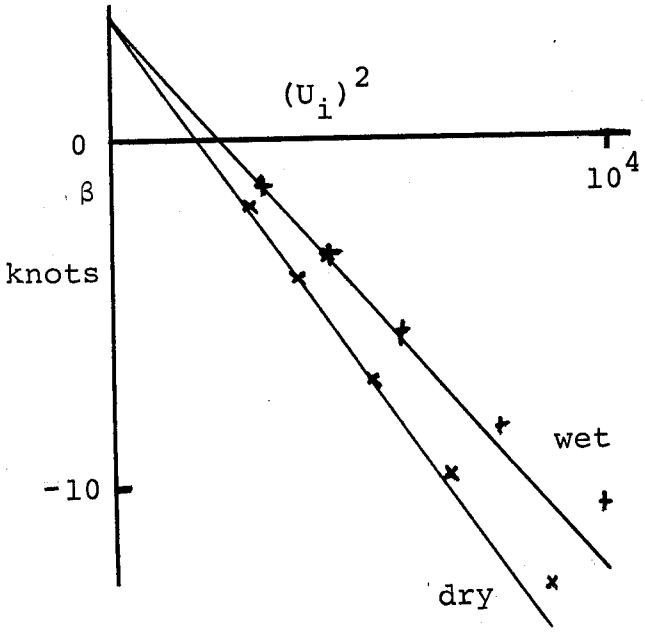
Now $V_{AR} + V_P$ = vario output and V_{AV} is known.



Plot β against $(U_i)^2$ good approximation to β given by

$$\beta = A - B(U_i)^2 \quad (2)$$

which is obtained easily from the transducer.



From (1) and (2) for non-optimum airspeed vario +

$$V_{AV} - A + B(U_i)^2 = \varepsilon$$

ε is now used as a nose up/down signal.

$V_{AT} + V_{AV}$	U_{opt}	U_ε
0	50	50
2	61	61
4	75	74
6	90	88
8	98	94

Figure 4

we have a quantity ε remaining; this is used as a nose up/down signal.

The bottom table shows the results of the linear approximation used, compared with the optimum speeds taken from tangents to the polar. The differences are insignificant and in any case are arranged to direct one to fly slower than the theoretical optimum; as we have all read recently, this is probably a good strategy.

The computation described is performed by amplifier Σ (see Figure 3). It takes suitably scaled signals from the airspeed (including some phase advance), the variometer, and a front panel control on which has been set the estimated average climb rate for the next thermal. The output speed error signal is smoothed with a 4 sec time constant and fed to a small edge-reading center-zero meter, on which the pointer is imagined to represent the glider (see Fig. 2). If the pointer is high, one pushes the stick forward. A warning for flying too slowly in sink is provided by a siren type signal generated by a swept oscillator. The DRY/WET switch gives a facility for an instantaneous change of wing loading.

Flying experience with the variometer computer

Naturally this is going to be a subjective assessment of the instrument. After using it for over two years, I have a good idea of what is useful to me. Other pilots may find different priorities.

The variometer section is excellent, and to my surprise, I discovered that to get maximum advantage from the T.E., one must reset the HEIGHT control every 2000 ft or so. The compensation is as good as a venturi, while the response is faster than a mechanical variometer. In thermals with strong horizontal gusts, it is often helpful to switch out the T.E.

The variable damping is very useful; for normal use the 2 sec position is preferred, when it is somewhat faster than a PZL, and without that annoying reluctance to return to zero usually shown by variable leak instruments. In smooth thermals and wave one can use the fastest response.

If one has not been in the habit of timing climbs, honest evaluation (that is, pressing the reset, immediately on turning) of average climb rates is quite revealing. When one uses this result in the speed-to-fly computer, the pitch demand display is a much easier way of responding to changes in sink than the normal MacCready ring. The SPEED LOW warning has also turned out to be perhaps even more valuable than expected. It quickly nudges you into responding to sink, when you were map reading or looking around at the weather, which, as A.J. Smith has pointed out, is probably the most useful thing you can be doing most of the time.

In the FLY mode the original design incorporated subtraction of glider sink; air mass movement is then displayed, which can also be averaged; this is sometimes useful. However, I found that the visual and subconscious conflict between the two variometers was disturbing; I had a tendency to keep reducing speed as I saw zero on the variometer. A pilot with less ingrained responses may adapt better to the situation.

Comparison of the 30 sec weighted average with the averager reading is very helpful in showing when the rate of climb at the top of the thermal is falling below the overall achieved rate.

Selectable full scale deflection is occasionally useful, and is so easy to incorporate that it should be available in every electric variometer. One changes scale for very weak conditions, or for those rare occasions when the needle hits the stops.

The instrument has been very reliable. Only two failures have occurred in three years; one was due to a leak, and the other a failed capacitor installed with polarity reversed.

At the last World Championships in Vrsac (Yugoslavia), the instrument was used very little; the average climb rates were immaterial, as the next climb was usually uncertain, both as to strength and availability. Inter-thermal speeds tended to be conservative. One became more concerned with conserving battery power for gyros, and the all-important radio, than with achieving optimum cruise speeds, and time was better spent surveying the rapidly varying weather, looking for other gliders, or searching for features which actually corresponded with the map. All in all, the whole exercise has been very instructive, but there may be better ways the serious pilot can spend his time.

ELECTRIC VARIOMETER SYSTEMS AND DEVELOPMENTS

by

A. Raouf Ismail
Cambridge Aero Instruments
Burlington, Mass.

Introduction

Much has been written and said on the subject of cross-country soaring by eminent practitioners of the art. Thus it is difficult to find anything that has not been said before in some form or other. This paper, however, is intended to focus the attention of electric variometer users on factors which may be of use to them in better understanding of their instruments, and their interpretation. Special emphasis has been placed on the understanding of total-energy tuning, which seems to cause more problems than practically everything else combined. (As manufacturers of variometers, we can attest to this.)

A chapter is also devoted to future developments, more specifically to Averagers and Air-Data Computers. These have already appeared on the market in limited quantities, and with relatively unknown characteristics. We will try to describe how such instruments do their job, and we will define some of the problems inherent in them.

Variometers and cross-country speeds

General analysis

In a typical cross-country flight, a pilot has a number of fixed factors over which he has little or no control. (For the duration of that flight anyway.) He has a particular sailplane, thus his performance options are fixed. He is in a given set of meteorological conditions, over which he has only limited control. (Through choice of track, he may be able to select weather conditions to a degree.)

However, two factors which are, to a great extent, under his direct control are the rate-of-climb he achieves in a thermal, and the cruising speed adopted between thermals. (Clearly there are also structural, aerodynamic and meteorological limits to his control over these factors.)

These two factors, rate-of-climb and speed are intimately associated with cross-country speed, but their effects on it differ greatly. For the purposes of this paper, we will be disregarding the effects of pilot judgement as to course selection, thermal selection etc. These are important too, but they do not negate the factors of climb and speed.

Effect of inter-thermal speeds on cross-country speeds

It is a well-established theorem that the rate-of-climb, the performance polar, the best speed to fly and the achieved cross-country speed are geometrically related. (See for example Ref. 1) Using this theorem, and Bikle's [2] performance testing figures for a Libelle, Figure 1. was derived.

This figure represents the reduction in cross-country speed (expressed as a percentage of the theoretical maximum) caused if the pilot deviates from his theoretical optimum cruising speed (expressed as a percentage deviation from optimum). Three curves are shown for achieved climbs of 1, 3, and 5 knots.

The surprising result is that even with variations in speed up to $\pm$ 15%, a mere 2 or 3% change in achieved cross-country speed occurs. This is surely a negligible factor, when weighed against other variables such as sailplane condition, pilot condition, sheer luck, and so on.

Effect of rates of climb on cross-country speeds

Figure 2. was derived using the same data and methods as for Figure 1. This plots the theoretical cross-country speed against achieved rate-of-climb, assuming optimum cruising speeds. Examination shows that a 15% increase in rate-of-climb increases speed by around 10%. This result is very different from that given by Figure 1.

Conclusions

The primary conclusion which may be drawn from the above results is that a pilot's primary goal, given a particular sailplane, task and weather, is to seek out the best thermals and get the best out of them. Of equal importance to him is to be able to extricate himself efficiently from difficult situations, since this greatly affects the outcome of the flight.

What then should be the characteristics most valued in an electric variometer? We rate them in the following order:

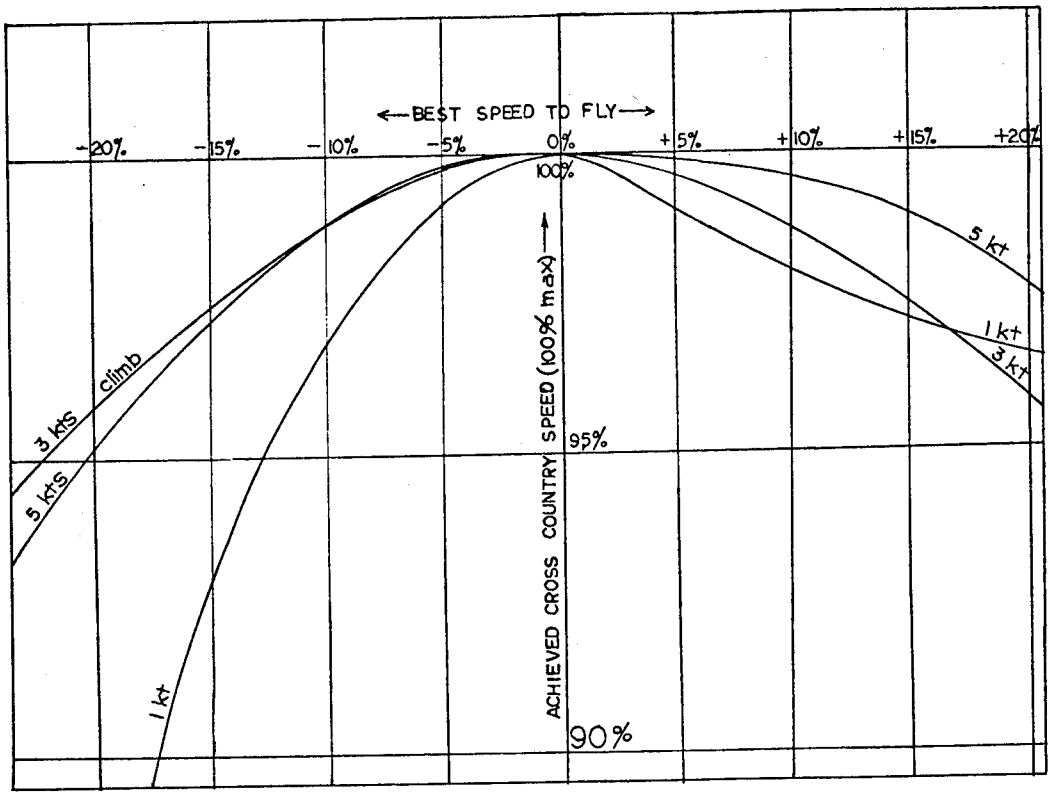


Figure 1.

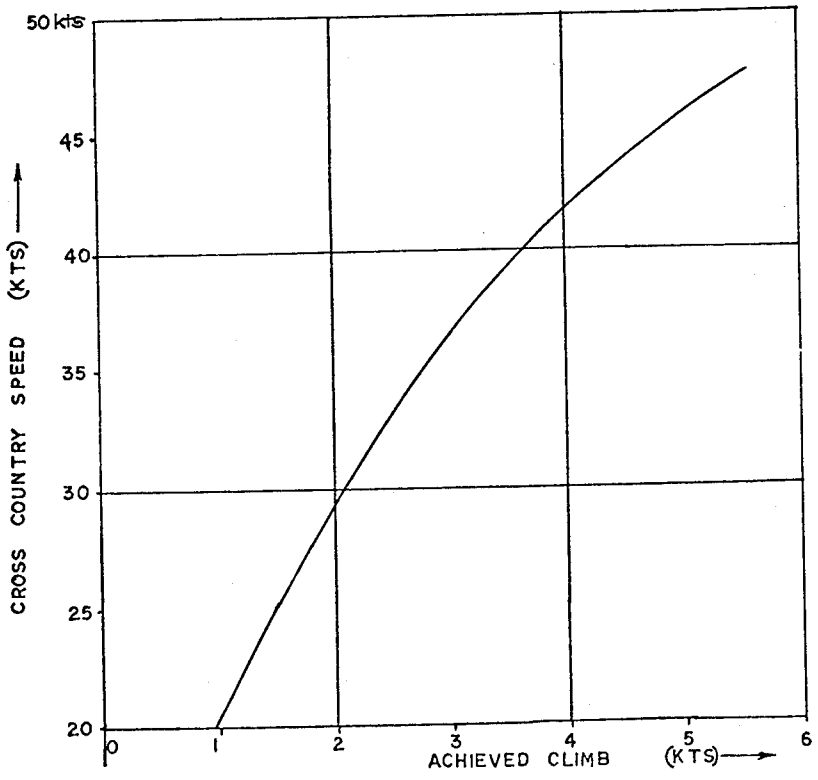


Figure 2.

1. Reliability. We need not expand on this.
2. A good total-energy compensation scheme. This is of great value when searching out and centering in thermals.
3. Low zero-drift. We consider this of the utmost importance, particularly in marginal situations, such as low scrapes. There is a tremendous advantage in knowing that 1/2 or 1 knot UP is UP, not 1/2 knot down, and so on.
4. Smooth, well damped, but fast response.
5. Accuracy and Linearity. These factors are desirable, but if the above analysis is valid, it is less important to know the exact value of rate-of-climb, since the subsequent choice of cruising speed is not critical.
6. Size and general packaging considerations.

Survey of types of electric variometer in general use

Most electric variometers cause air to flow into or out of a reference capacity, when outside pressure changes occur due to vertical displacement of the aircraft. This reference capacity may be located either internally or externally with respect to the instrument.

Heated element types

In this type, the bi-directional flow is used to cool a heated element, such as a thermistor or a hot wire. The change in electrical characteristics is measured and is a function of the rate of change of altitude. In practice more than one such heated element is used (normally two or even three) to enable the instrument to differentiate between climb and sink.

In this country, the best-known types using this technique are the Crossfell, Moore and Cambridge. This type of instrument has been very adequately described by Moore [3]. The principal advantages of this type are its simplicity and its lack of moving parts, apart from the meter indicator.

Leaky capsule types

This method causes the flow to and from a reference capacity to develop a pressure drop across a pneumatic restrictor, the drop being a function of the rate of climb. The pressure drop is measured, usually by detecting the displacement of a diaphragm. The best known type is the Ball, which is well described in the promotional literature for

this instrument. The principal advantage of this type is its good altitude characteristic.

Total energy compensation

A good total energy system is of the utmost importance to better thermal soaring. Until recently, the diaphragm type (Burton, Winter et al.) was the only kind widely available. However, the venturi (Althaus) is now here to stay. (For further description of the venturi see Ref. 1.)

Another method which has occasionally been used is that of electronic compensation. We have done development work on this, and a completely electronic total-energy variometer is described elsewhere in this paper.

Diaphragm type

This type has been very widely used to date. Its primary advantages are its simplicity and the absence of any part which protrudes externally from the glider. It has been very adequately described at various times (See, e.g., Ref. 3), so we will not repeat the description here.

The major difficulty with the diaphragm type is the fact that the accuracy of compensation provided is dependent on the altitude of the aircraft. This is a major snag, and one not capable of easy resolution. More recently, the diaphragm type has largely been superseded by the venturi systems. The diaphragm compensator can be tuned to the system in a way similar to that in which an electronic compensator is tuned to the system, as described below.

Venturi type

In principle, a venturi is a protuberance in the airstream which develops a suction equal to $(p_s - 1/2\rho v^2)$.

where p_s = static pressure
ρ = density of air
v = airspeed.

It can be seen that the value of this suction is proportional to the total energy of the sailplane, and no change in this suction is therefore recorded if, as in diving or zooming, a potential/kinetic energy exchange occurs.

The major advantage of the venturi is that its compensation is inherently correct at all altitudes. Its major disadvantages are that it is vulnerable to damage as well as prone to icing and gathering water in the tubing.

Electronic compensation

Electronic compensation is a third method of total-energy compensation which has gained some popularity in Europe. It is inherently free from altitude errors, and does not require any external protruding parts which may be damaged or blocked by ice. This type of compensation is also inherently less yaw sensitive than a venturi. Its yaw sensitivity is about the same as that of the airspeed system, since it derives its airspeed information from the pitot. It is also relatively easy to tune this instrument to the aircraft electronically.

A description of this method of compensation may be found in Reference 4. We have been flying developmental prototypes for some time now. The results have been very encouraging.

Figure 3 shows the functional arrangement of such an electronically compensated variometer. In general terms, a sensor is connected on one side to a capacity C, and the other side is connected to the static source. A second identical sensor is connected between a capacity 1/2C and the pitot. The first sensor measures the rate of change of static pressure, while the second senses the rate of change of pitot pressure.

Thus, in normal steady flight, the climb sensor would be indicating climb or sink as the case might be, while the speed-change sensor would indicate zero, since the speed is not changing at this time. In the event of the sailplane being dived or zoomed, opposite and equal (assuming exact matching of the sensors) changes occur at each sensor, and a summing network cancels them out. Subsequent circuitry takes care of small differences resulting from imperfect matching.

The climb sensor and the speed-change sensor are connected to separate amplifiers A1 and A2. In addition, there is a small restrictor in the pneumatic circuit of the climb sensor, to make it slightly slower than the speed-change sensor. It is, however, still fast enough for practical use.

The speed-change amplifier A2 has two "adjust and forget" controls, one for damping (or time constant), the other for gain. The final adjustment of these controls is done in the aircraft during flight, one flight only being usually required. This adjustment is described later in this section.

The outputs of the amplifiers A1 and A2 are summed in amplifier A3, and this sum is read out on a meter indicator. A control for adjustable damping of A3 is provided for the pilot's use, to enable him to change the time constant of the whole instrument. This is very useful in gusty conditions.

Adjustment of this type of variometer is relatively simple, but can be confusing if not properly understood. The first task is to match the time constants. The second is to match the gains of the climb and speed-change sensor

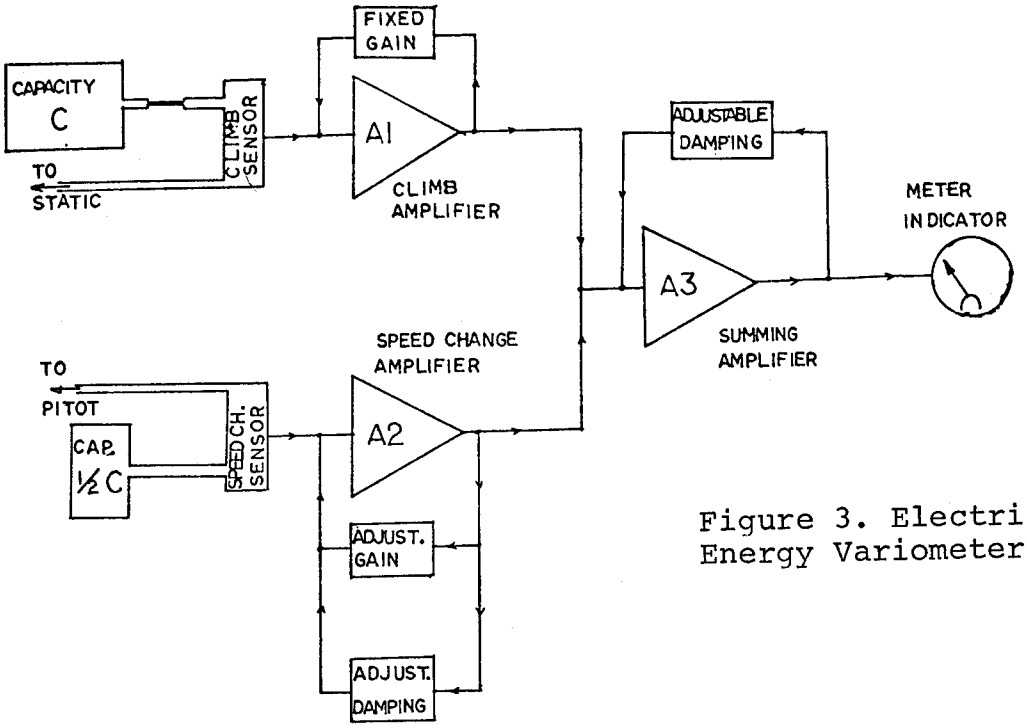


Figure 3. Electric Total Energy Variometer.

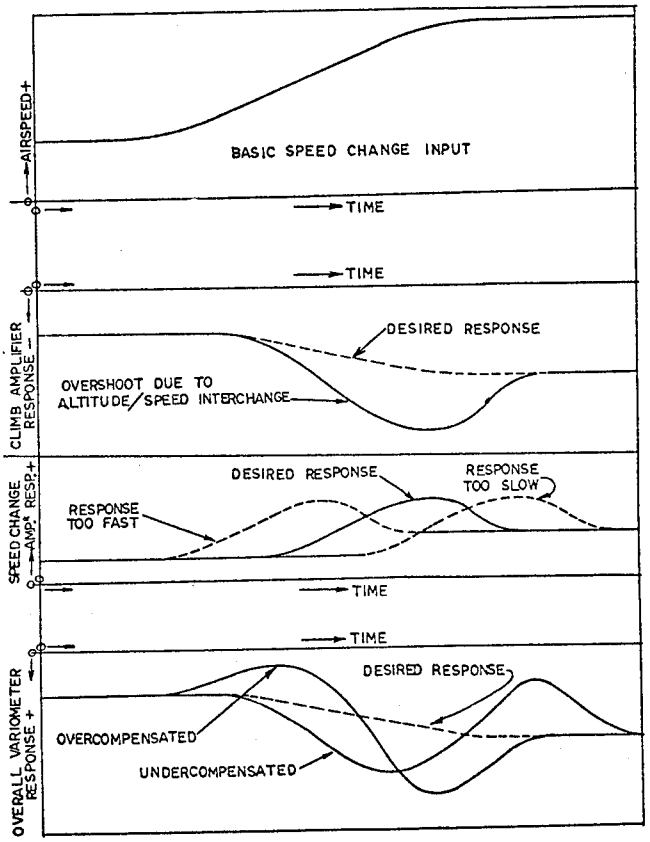


Figure 4. Matching of T.E. Response (Speed).

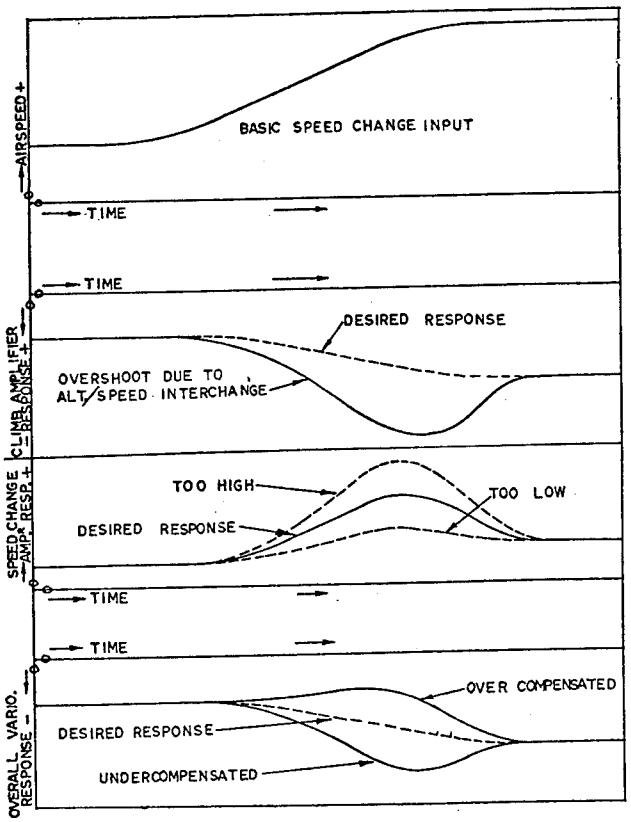


Figure 5. Matching of T.E. Response (Gain).

systems. Figure 4 shows the result of a speed-change input to this variometer. The climb amplifier system response shows the characteristic "dip" common to all uncompensated variometers, due to altitude/speed interchange. The speed-change amplifier response shows a corresponding and opposite "bulge".

If the speed change response is too fast, this bulge occurs before it is desired, and a wavy response of the over-all system takes place, as shown in the lowest set of curves in Fig. 4. If the speed-change response is too slow, this "bulge" comes too late, and a wavy response, similar but opposite to the "too fast" curve takes place, as is also shown in the lowest set of curves in Fig. 4. By adjustment of the damping control on A2 (Figure 3) the compensating "bulge" can be brought to the correct position, resulting in the desired response. This is, however, also subject to the adjustment described in the following paragraphs.

Figure 5 shows the result of a speed-change input to this variometer, assuming that the time constants have already been correctly matched in the preceding paragraphs. Again, the climb sensor system will show the characteristic "dip", and the speed-change sensor the corresponding "bulge". The lowest set of curves in Fig. 5 shows the effect on the over-all system of over and under-compensation. This can be adjusted to the correct curve by use of the gain control on A2.

In practice, it can be a problem to sort out the two adjustments, because of mixed gain and time constant effects. In fact, the lowest curves in Fig. 4 and Fig. 5 are fundamentally different. The system response curves in Fig. 4 show a distinct double-change, while the system response curves in Fig. 5 show a single change. Recognition of this single and double change is fundamental to correct total energy tuning.

This situation is directly analogous to tuning a diaphragm compensator system. The gain has already been predetermined by compensator/capacity matching. The addition of restrictors between the compensator and the pitot line effectively simulates the adjustable damping of A2.

Future developments

The developments described so far lend themselves logically to the next step, the averager. It would be of benefit to the pilot to know his achieved rate-of-climb, for then he would have a basis (amongst other factors) for his speed-to-fly decision. To obtain such a reading, he would require an averager.

An averager logically leads into the next, perhaps ultimate step towards "automatic" flying: the Air-Data-Computer (hereinafter referred to as the ADC). Such a device would use the measured average rate-of-climb, and would also use an airspeed transducer to provide a zero-reader output.

It has to be pointed out that technically an averager is a tricky instrument to produce in this application. The reasons are examined in the following section. By comparison, the ADC is relatively straightforward technically (though not cheap). We have been doing development work in the laboratory on these problems, but it is too early to draw any conclusions.

Averagers

An averager requires that the pilot hit a reset switch which starts the averaging process from that point on. It then provides him with a continuous reading of the average to date. When he breaks from his climb to fly on, the final reading on his averager would give him the input he needs for choosing the setting on his speed-to-fly ring, if he uses one.

Electrically this can be achieved with an integrator as follows;

$$\text{Vario Reading} = dH/dt, \quad \text{where } H = \text{Altitude}, \; t = \text{Time}$$

$$\text{Thus, } \int_{t=o}^{t=t_1} (\text{Vario Reading}) \qquad H = \Delta H$$

In other words, if the vario reading was applied to a freshly-zeroed integrator, this integrator would provide a readout of the altitude gained.

If a second integrator were also to be zeroed at the same time, and be allowed to accumulate at a fixed rate from zeroing, its output would be a measure of the time elapsed.

In that case, a divider circuit which divided the climb integrator reading by the time integrator reading, would provide the average (or achieved) rate-of-climb. Figure 6 shows such an arrangement.

The primary difficulties with this type of instrument occur in the integrators themselves, which are required to integrate over anything up to 10 or 20 minutes. For those readers familiar with capacitive integrators, the problem needs no further definition. For others, the following calculation may be of interest.

Capacitor charge is governed by the following equation:

$I = C.dV/dt$ where I = charge current
C = capacitor value
V = voltage across C
t = time

Given the very wide operating ambient temperature range, it is not possible to use high capacitance electrolytic capacitors, even tantalums. Their leakage current and value change over the ambient range is simply too great to be of any use. Thus, we are forced to use the lower capacity (typically 2 microfarads or so) high-stability types. A few simple calculations will show that charge currents are of the order of nanoamps (10^{-9}) for realistic integrator outputs. This requires very high performance amplifiers. Furthermore, the integrators need to be encapsulated to eliminate humidity-induced leakages. All in all, this is not a very encouraging situation.

An alternative method of integration would be to use a digital integrator, where a variometer-controlled clock would increment an up-down counter, the outputs of which would be passed through and A/D converter. This arrangement is also shown in Figure 6. Digital integration is clearly free of many of the problems mentioned above. Time of integration is not a difficulty. However, it does use many components, and can have a heavy power consumption.

A further assumption in this design is that the input variometer reading is representative of the true rate of climb. Most variometers will do this to within a few percent at least over a restricted altitude range. Linearity is also of importance, as is zero drift.

The air-data-computer

In one version of an ADC, the output is a zero-reader indicator, and all the pilot is required to do is to follow the needle. If this indicates high, he should go faster, and vice versa.

Such a device requires the following inputs:

Achieved rate-of-climb
Airspeed (from a transducer)
Variometer reading
Altitude possibly (from a transducer).

Information on the sailplane's polar is stored in the computer. Figure 7 shows the derivation of an expression for the theoretical variometer reading at a certain airspeed, given an achieved average of climb input.

This expression is compared electrically with the actual variometer reading, and an indication is provided which tells

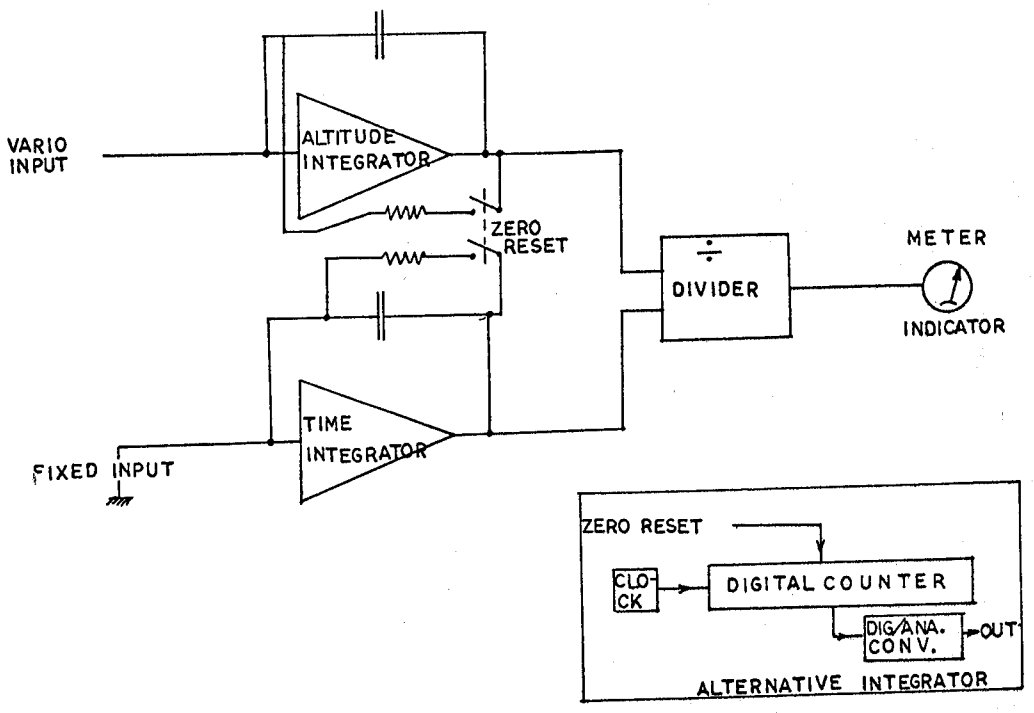


Figure 6. Averager System Diagram

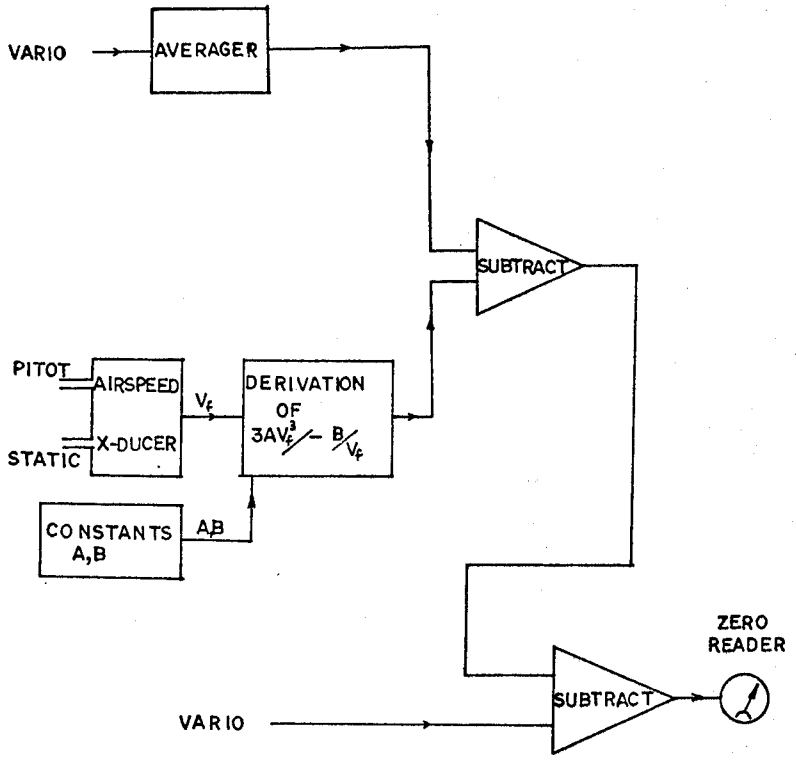


Figure 8. Air Data Computer

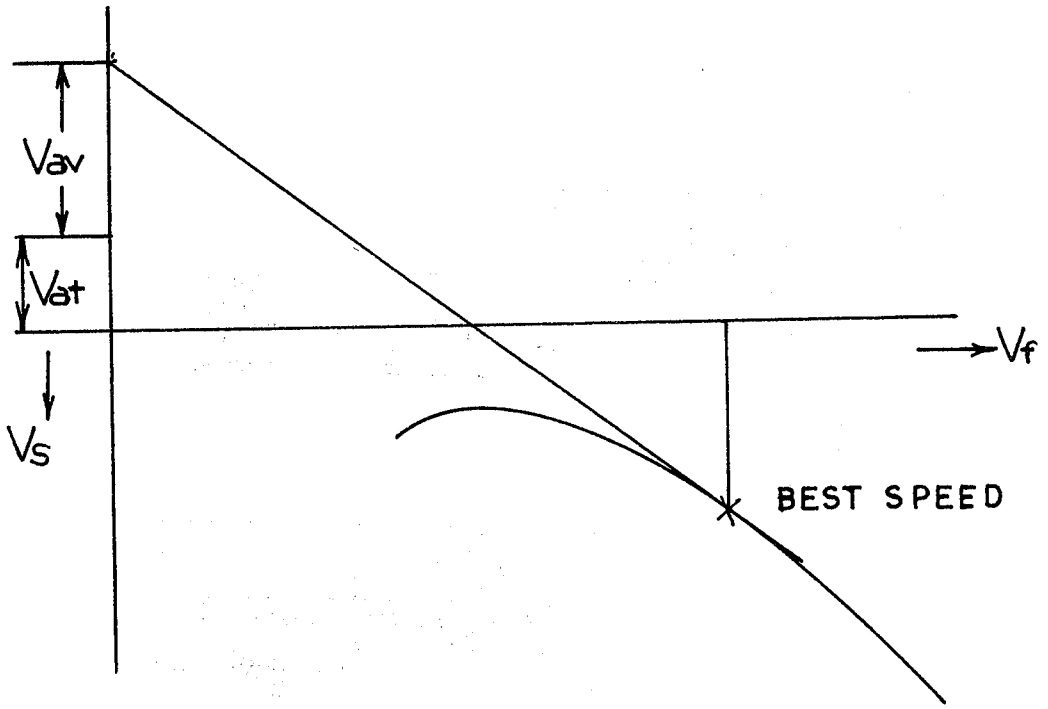


Fig. 7 A.D.C. Analysis

The above represents a Polar of the form :

$V_s = AV_f^3 + B/V_f$ where V_s = Sinking speed of glider through air.

V_f = Airspeed of glider

For a given achieved climb V_{av}

And a given air-mass vertical speed of V_{at}

A Tangent drawn as shown would provide the best speed to fly.

A Tangent to the Polar has slope $3AV_f^2 - B/V_f^2$ (1)

But the ideal tangent has slope $\frac{(V_{av} + V_{at} + V_s)}{V_f}$ (2)

Equating (1) and (2)

$$V_{at} + V_s = 3AV_f^3 - B/V_f - V_{av} \quad (3)$$

But $V_{at} + V_s$ = Vario Reading.
Hence RHS of (3) is compared to Vario Reading.
Difference, if any, is presented of a zero-reader.
Co-incidence, or a zero read will occur at the correct speed to fly.

the pilot to fly faster or slower as the case may be. The current air-mass vertical speed is an inherent factor in the comparison. Figure 8 shows one general arrangement of an ADC with which we have experimented at CAI. The expression $3AV_f^3 - B/V_f$ is derived in a calculation circuit, and the output is applied to a center-zero indicator.

In this brief description of an ADC, we have not mentioned the effect of altitude on both the airspeed and the variometer readings. The airspeed output from the transducer is in fact the equivalent airspeed. The effect of altitude on variometers varies with the type, but is not generally great in the usual glider height band. Ideally, an altitude transducer could be used to compensate, and a true airspeed output produced. The variometer reading could also be compensated in this way. In fact, this transducer could eliminate the need for integrators altogether.

Finally it must be pointed out that any ADC must perform at least as well as the pilot's own judgement to become a valid instrument. This criterion alone makes it a very difficult instrument to produce. This must remain the ultimate criterion for any such devices, if they are to be more than technical curiosities.

References

1. Welch & Irving; The New Soaring Pilot, John Murray, London, 1968.

2. Bikle, Paul; Polars of Eight, Soaring, 1970, 1971.

3. Moore, A. Gene; The Electric Variometer System, Soaring Symposia, Cumberland, Md., 1970.

4. Burton, George; Two-Bottle Total-Energy, Sailplane & Gliding, April/May 1972.

CALIBRATION AND PERFORMANCE CHECKING OF VARIOMETER SYSTEMS

by

Wolf Elber
NASA Langley Research Center
Hampton, Virginia

Introduction

The variometer is the most important instrument of the soaring pilot. Several good basic papers on the theory and operation of sailplane variometers have been written. Among these are the papers by Moore [1] and Byars and Holbrook [2]. However, little information is available on the maintenance, calibration, and general performance checking of variometers. The soaring pilot's most important instrument is, in fact, often the most neglected and misunderstood instrument. This opinion was confirmed in this study where a calibration and performance check was carried out on the variometer systems of several club and private competition sailplanes.

The purpose of this paper is to present the methods and equipment required for checking variometer systems. The necessary equipment was developed and built for this investigation. It can be home-made and is cheap enough to encourage pilots to copy the checking procedures outlined here.

The paper is intended to help the soaring pilot to make the best possible use of his equipment.

Equipment and method

A vacuum chamber is required to test or calibrate an instrument such as a variometer. The chamber used in this investigation was made from a five gallon oil container. A portion of the bottom (9 inches diameter) was removed, and a half-inch Plexiglass cover (10-1/2 inches diameter) installed for a viewing window and access port. A Neoprene rubber gasket sealed the window against the chamber bottom. The connecting lines were made using quarter-inch Neoprene tubing, quarter-inch copper fittings and a quarter-inch needle valve. A diagram of the system is shown in Figure 1. The manifold vacuum of an automobile was found to be a suitable vacuum source. The available vacuum is 20 in Hg below atmosphere. The chamber in this investigation was first "proof tested" to 12 in Hg below atmosphere, and was never operated afterwards to more than 8 in Hg below atmosphere.

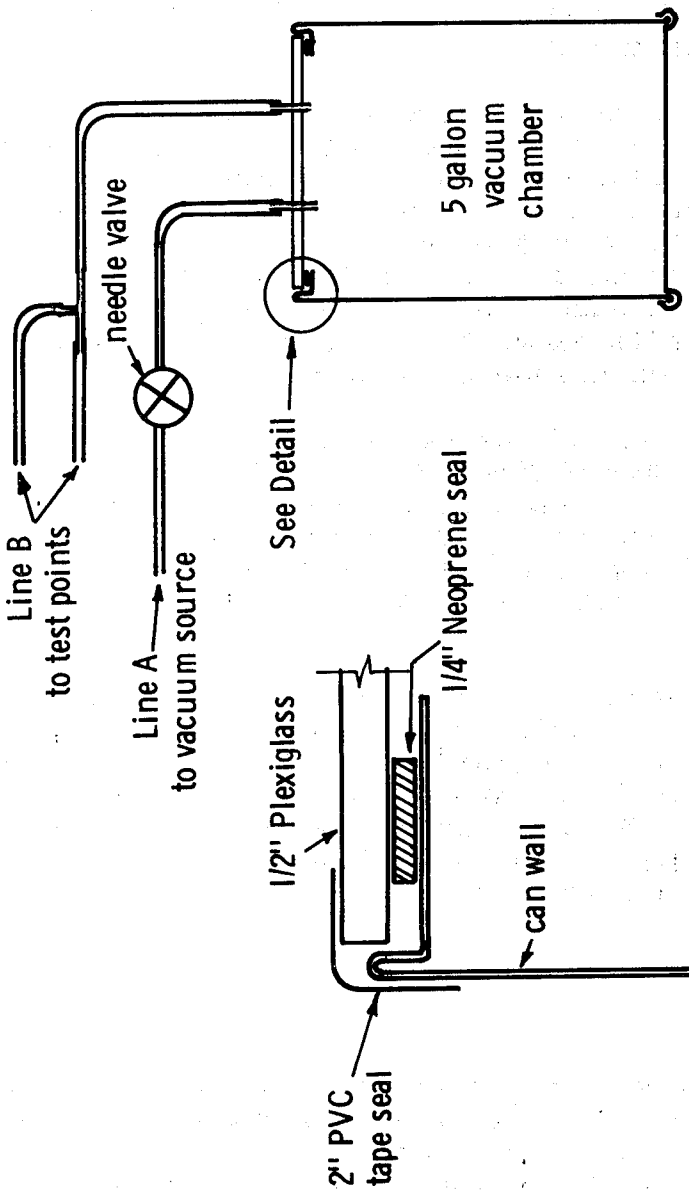


Figure 1. Vacuum Chamber System

Figure 1 shows two vacuum lines. Line A is the vacuum source from the automobile intake manifold. The needle valve in this line throttles the flow to control the vacuum in the drum. For this line configuration the motor must be running to increase the vacuum and must be stopped to decrease the vacuum. Line B is the vacuum test line with one or more vacuum ports. Instruments can be tested "immersed" in vacuum if they are placed inside the chamber with line B clamped, or they can be tested in atmosphere connected to line B. In the latter test a pressure differential exists across the casing of the instrument. This test is used to detect leaks and in field calibrations where the instruments are not removed from the aircraft.

The chamber's main purpose is to hold instruments in a vacuum environment. Its second purpose is to improve the control over the rate of change of vacuum to the instruments. The volume of air in a variometer system is so small that a cheap needle valve cannot be used to control the airflow through the instruments. Since the large volume of the five gallon chamber increases the air volume by a factor of 40 a gasoline-line needle valve has sufficient sensitivity to control the rate of change of vacuum.

For calibration of variometers an altimeter and a stopwatch were used. The altimeter and variometer were connected to the two ports of line B of the chamber or were sealed into the chamber and observed through the chamber window. The time rate of change of altimeter indication was taken as the calibration standard and is here referred to as actual climb or sink.

During the test the vacuum should be changed cautiously while calibrating a variometer, otherwise the instrument might be damaged by "pegging". During calibration operations it was found helpful to have two operators, each working from a checklist. The main point on the checklist was to ensure that the needle valve was closed before starting or stopping the vacuum pump (automobile motor).

Leak checks

Leak checks can be carried out on the individual instruments or on the total "plumbing" system. The latter test involves the pitot line, the static line and the total-energy venturi line, if such a venturi is used. For the leak test on a Schweizer 1-26D, which is the author's club sailplane, line B of the test apparatus had three branches. One branch was attached to the pitot tube, one branch was equipped with a suction cup and was taped to one static port, the third line was attached to the total energy venturi. The remaining static port was sealed with tape. The vacuum chamber was sealed and line A was attached to the vacuum source. In this configuration sailplane altimeter and variometers act as test instrumentation and test object.

By opening the needle valve the system was evacuated to 2000 ft altitude monitored on the altimeter. The valve was then closed, and the rate of sink observed on the variometer. Locations of leaks could be isolated by successively clamping off various sections of the connecting lines. A list of possible leak locations is given below:

1. Static port fittings.
2. Tee junctions.
3. Split or hardened tubing.
4. Membrane compensators.
5. Instrument glass 0-ring seals.
6. Vacuum flask stoppers.

In the case described all these leaks were repaired until no sink was indicated from 2000 ft altitude. A more sensitive check was obtained by clamping line B to eliminate the chamber volume from the test system. A 10 ft/min indication of sink will then appear as about 400 ft/min sink. The clamp on line B must then be released slowly to avoid pegging the variometer while the system pressure equalizes.

A second leak check must be carried out to determine leaks from the pitot line to the static line. A leak can occur through the airspeed indicator or a membrane compensator. For this check the pitot line is opened to atmospheric pressure and a vacuum is applied to the static port. The maximum vacuum allowable is determined by the full-scale indication of the airspeed indicator. Again leaks can be isolated by clamping the connecting lines involved in the system. A leak in the compensator will indicate as lift on the variometer while the altitude is dropping.

Because of the small pressure differential between static pressure and cabin pressure in actual sailplane operation, leaks in the static line are of relatively little importance. The important leak locations are those involving pitot pressure leaks into the variometer system, and cabin pressure leaks into the total energy venturi line between the variometer and the variometer bottle.

Variometer calibration

The types of errors which are easily determined in the vacuum chamber calibration are the zero error, full-scale error and the non-linearity. For most competition pilots $\pm$ 5 percent full-scale error and non-linearity are acceptable limits. In a series of tests it was found that most new instruments perform within these limits. Full-scale errors and non-linearities exceeding these limits may develop during the life of an instrument.

In each test of the series each variometer system was tested at five indicated values of climb, from zero altitude to 10,000 ft altitude. The same procedure was used for five indicated values of sink. Altitude was recorded every minute using a stopwatch. Three types of variometers were tested:

1. Enclosed can rate-of-climb; Type A
2. Mechanical variometer with external 1 pint bottle; Type B (Two instruments were tested)
3. Electric double-range variometer; Type C

The calibration plots are shown in Figures 2, 3, 4 and 5.

Instrument A has a logarithmic scale to $\pm$ 2000 ft/min. The results are plotted in the form of indicated climb/sink against real climb/sink in Figure 2. Full-scale error is of the order of 5%

$$\left[\text{error} = \left(\frac{\text{Indicated climb/sink}}{\text{Actual climb/sink}} - 1\right) \times 100\%\right]$$

for both climb and sink. No zero error is recorded as the zero indication is adjustable. Non-linearity of the response is small.

Instrument B1 is a new instrument designed to operate with a 0.47 liter bottle. The calibration plot in Figure 3 shows that scale error, zero error and linearity are all better than $\pm$ 5%.

Instrument B2 was an instrument of the same type as instrument B1 with several years of use. Inspection of the calibration plot in Figure 4 shows surprisingly large errors; 100% overindication at full scale climb, underindication at 400 ft/min sink and overindication at full scale sink.

Similar but not as severe errors have been found on another instrument of the same type. The cause of the errors in these cases are suspected to be mechanical distortion of the mechanism. The reason for this assumption comes from the number of inflexion points in the calibration plot.

In both instruments where such errors occurred the instrument panels were mounted rigidly in the sailplane, and the owner of instrument B2 believed that a change in the instrument may have occurred during an extensive trailer trip. This leads to the assumption that the instrument may be shock sensitive.

Instrument C was a dual range (x1, x3,) electric variometer. Unlike instruments of type A and B this system shows a pronounced non-linearity in the calibration plot as shown in Figure 5. The calibration is shown not as a line but as a band. The width of the band covers indication differences between 0 and 10,000 ft. The zero indication is adjustable so no zero error exists. The amplification between ranges is fixed.

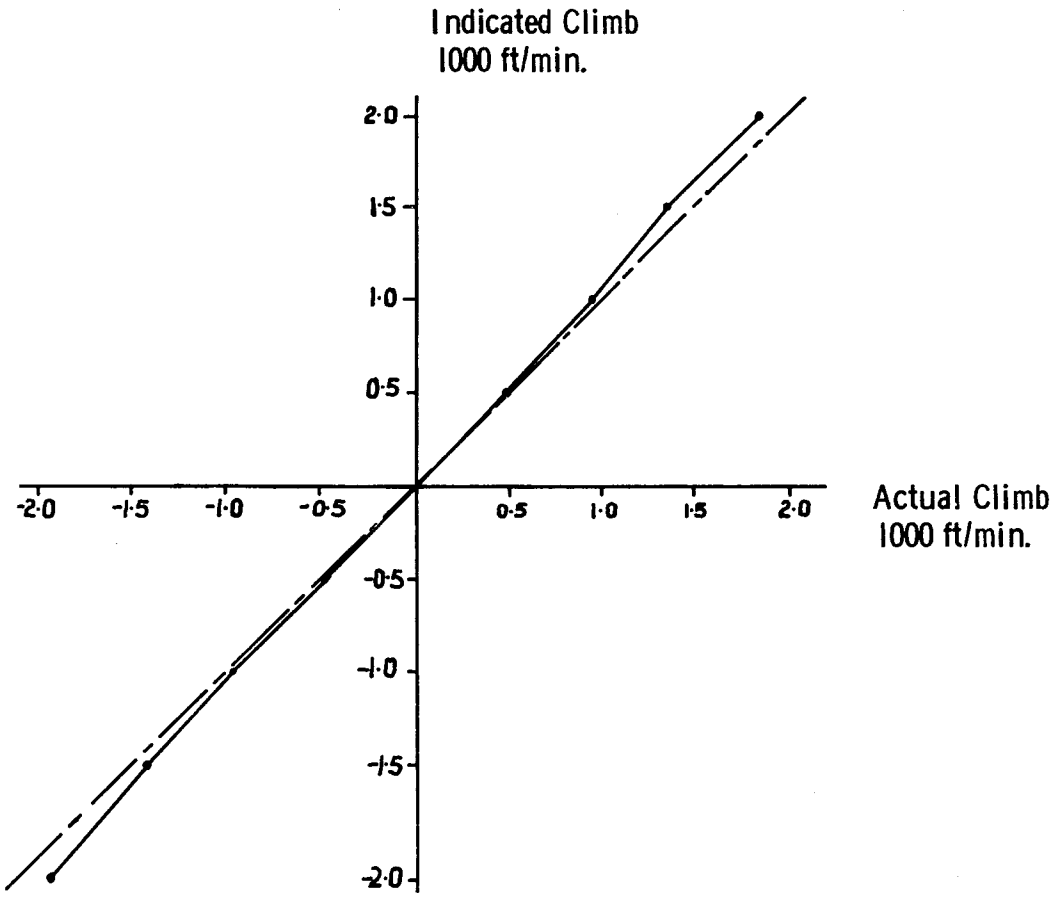


Figure 2. Calibration Plot for Instrument A

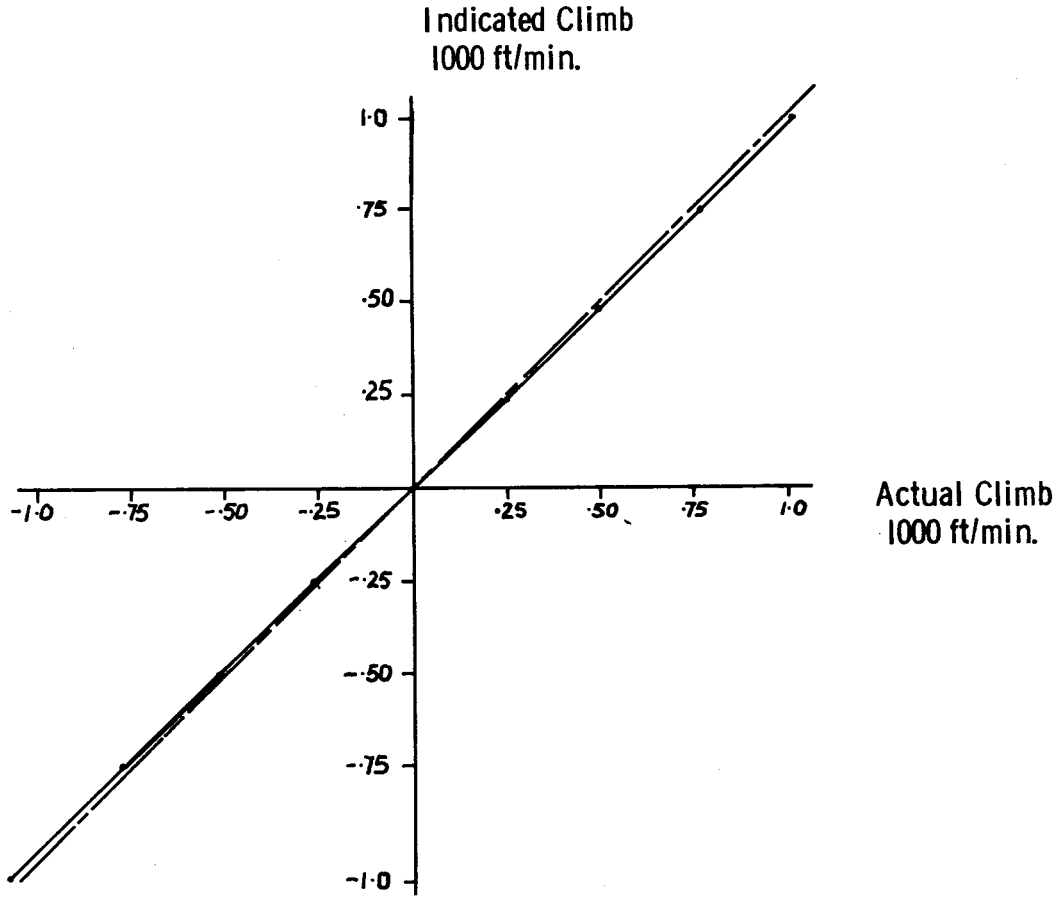


Figure 3. Calibration Plot for Instrument B1.

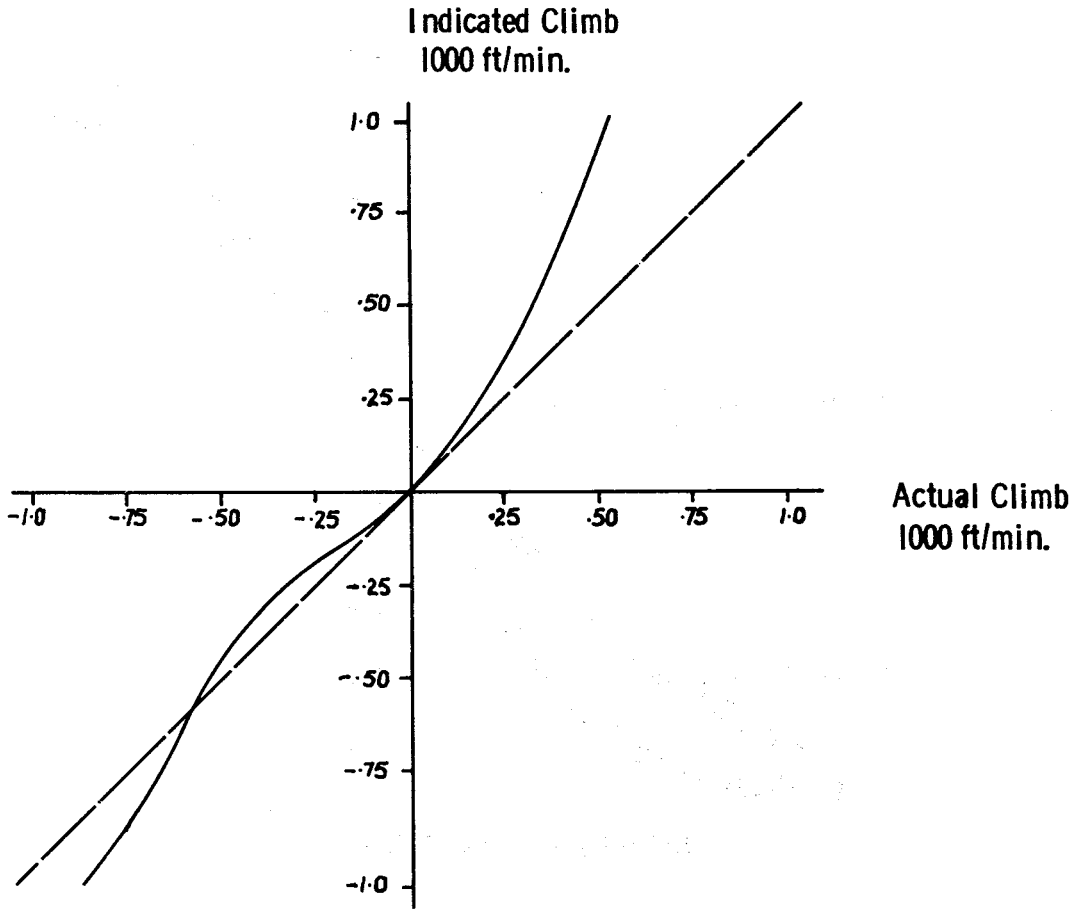


Figure 4. Calibration Plot for Instrument B2.

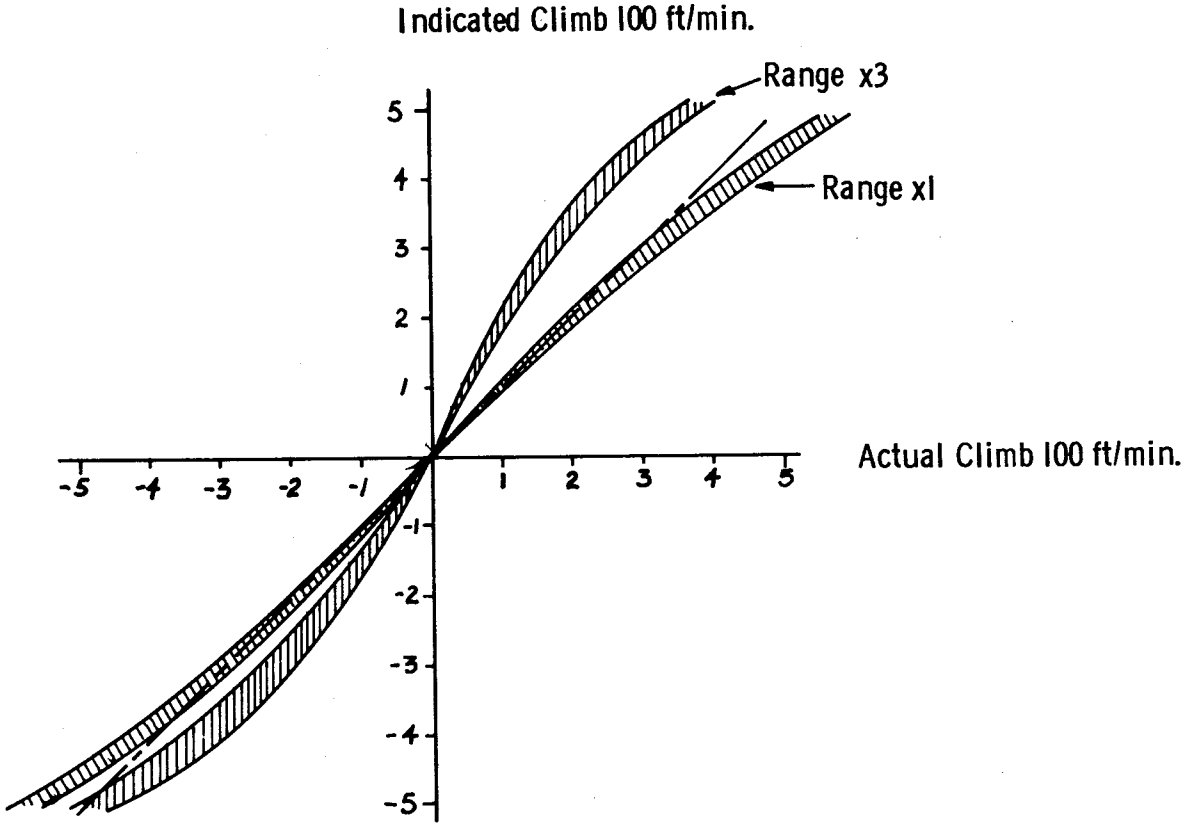


Figure 5. Calibration Plot for Instrument C

Response time check

For instruments with slow response times, such as instrument A, the time delay for registering sudden changes in climb or sink can be obtained using the vacuum chamber.

Most of the time delay effect is not caused by the mechanics of the instruments, but rather by the air conditions (temperature, humidity) in the bottle at the time of the sudden change in climb and sink. For completeness, the thermodynamic problem will be discussed first.

First assume a system with a flow-through variometer and a thermos flask storage bottle. During evacuation of the system (climb) air flows from the bottle while the air remaining in the bottle expands. Over short periods of time the heat exchanged between the air and the walls of the flask is negligible, so the expansion is adiabatic, (no change in heat content, but a change in temperature). As the air cools the pressure in the flask will drop and less air will leave the bottle than would leave if the air remained at constant temperature for the same altitude change.

If the evacuation is suddely stopped, the flask walls are still at the original temperature and the air is at a new lower temperature. Over a time interval of minutes, the flask walls will reheat the air in the bottle. Consequently the air will continue to expand and the variometer will indicate further climb. Almost the reverse will happen under sink conditions.

Addition of a copper heat exchanger to the flask (e.g. three "Chore-Girl" copper wool balls) helps cure this problem. Although this cure has been proposed several times in the literature, there are still many pilots who do not understand the value of this addition to their systems. With the heat exchanger added, more of the air is in contact with material remaining at the original temperature and the expansion of the air during evacuation will be almost isothermal (no change in temperature, but a change in heat content of the air).

Ideally, the air in the static or venturi side of the variometer should also be brought to a constant temperature before it is passed into the bottle during sink. For testing purposes a heat exchanger and an air-drier has been developed which consists basically of a small metal can filled with a mixture of copper wool and silica gel. The addition of the dessicant was made when several ml of condensed water were found in a bottle system without a heat exchanger. In humid climates the bottle acts as a condenser of water vapor during evacuation to 3000 ft. This condensation can cause damage to the variometer system.

After the drier and the heat exchangers had been installed the response time check of the variometer could be carried out. For instruments of Type A, the enclosed-can rate-of-

climb instrument, the air storage could not be equipped with heat exchanger material.

Figure 6 shows a plot of the reponse of a variometer system with heat exchanger and without heat exchanger. During evacuation the instrument without heat exchanger will indicate less climb than the instrument with heat exchanger. The error over the total evacuation time is the cross-hatched area A. This area represents a volume of air which, because of the drop in temperature, was not removed from the flask. After the evacuation is suddenly stopped this air will continue to drain from the flask, the temperature rises causing an error shown as the cross-hatched area B. Area B is equal to area A after equilibrium is re-established.

In order to obtain repeatable Response Time Curves, area A has to be kept constant. The response time check was therefore standardized to evacuation at 500 fpm for six minutes. At that time vacuum line A was suddenly clamped and readings of indicated climb were taken at one second intervals. Characteristic results are represented in the form shown in Figure 6. For instruments with short delay times, the instrument and the stopwatch can be filmed and later analyzed. For electric instruments the output can be recorded on a strip chart recorder.

Temperature sensitivity test

Several types of rate of climb indicators are being used in conjuction with total energy venturis. Such indicators show significant zero errors when subjected to a change in temperature. Also, lightweight plastic bottles have been used instead of thermos bottles in recent times.

Neither type of system will show an error when operated at constant temperature. Figure 7 shows an output trace for a rate of climb indicator subjected to a temperature shock of + 40°F in still air. An indicated climb error which lasts several minutes and has a peak at about one minute is evident.

Another system consisting of a variometer of type B and two lightweight bottles, showed an error exceeding 400 ft/min after 2 minutes when subjected to the + 40°F temperature shock.

The time at which the maximum error occurs is a constant for the system; the maximum reading is proportional to the temperature shock. The error indication for this problem can be expressed as ft/min -°F at a given time. For the second system this represents 10 ft/min -°F at 2 minutes.

The cure for excessive temperature sensitivity is insulation. Both systems were insulated with half-inch foam rubber and an aluminum foil wrap. The error was reduced by a factor of ten to 1.1 ft/min -°F at 30 minutes. For most

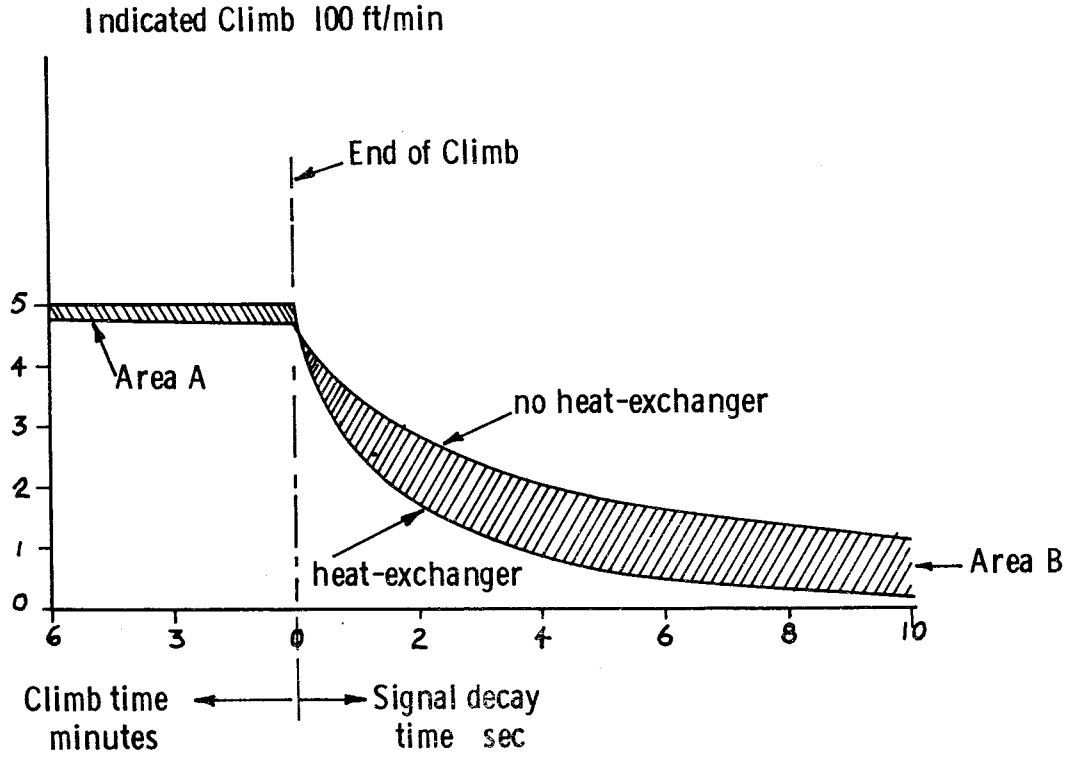


Figure 6. Typical Response Time Curves

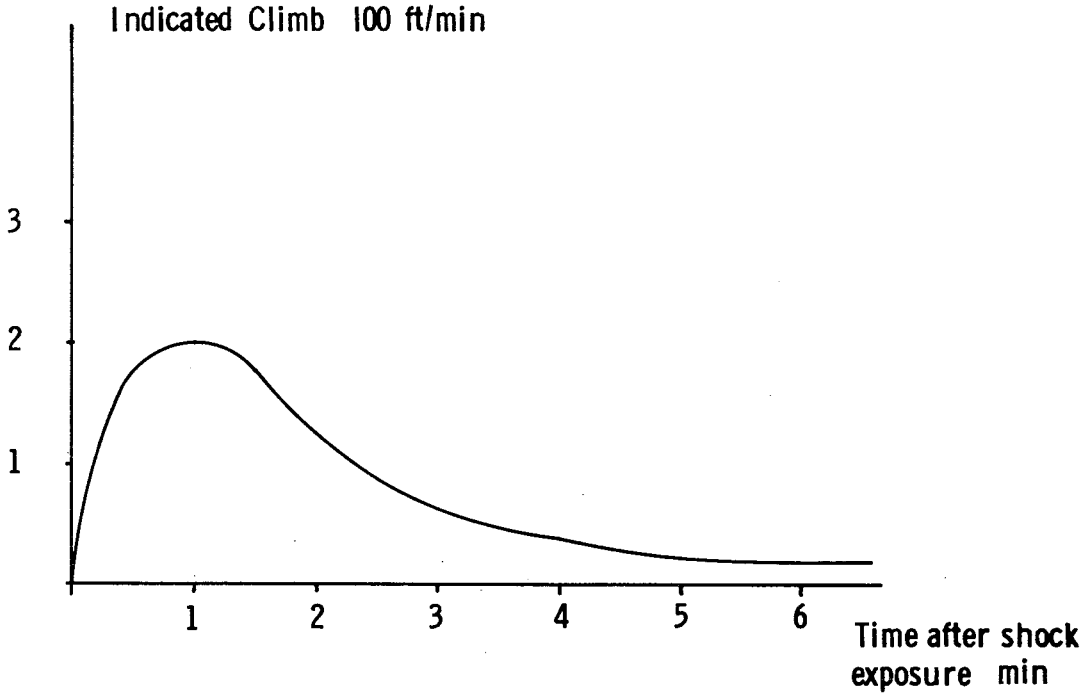


Figure 7. Typical Temperature Sensitivity Plot

thermos flask systems the temperature sensitivity was less than 1 ft/min -°F, but even this could be improved by insulating the instrument case.

The tests were carried out by coldsoaking the instruments for five hours in a refrigerator and then placing them at room temperature while taking readings.

Total energy compensation

Enough has been written in the literature about total energy compensation with membrane compensators. Total energy venturi compensation is superior to membrane compensation in performance, even though it may cause some drag.

In separate tests the author has calibrated a series of commercially available venturis and found that some of these show errors of the order of ± 10%.

When connected to the static port of an airspeed indicator with the pitot port open to static pressure, the venturi should read airspeed. For the tests an automobile speedometer was calibrated for speeds up to 60 mph. An airspeed indicator was calibrated according to the chart by Senn [3]. A total-energy venturi was mounted on the car antenna and connected to the static port of the airspeed indicator. The pitot port was connected to a static line. During several driving tests on windstill nights, indicated airspeed was compared to groundspeed and an average taken over several runs. In all cases over-indication or under-undication agreed with the pilot's claim that his instruments were over or under compensated.

Because the configuration of this venturi is fixed, it cannot be adjusted. Figure 8 shows the configuration of a home-made venturi, copied approximately from a commercially available model. A threaded set-screw at the top is used instead of a fixed-size plug. By varying the gap inside the venturi, the airspeed indication can be varied over a wide range. The indication error could be reduced to almost zero over the test range from zero to 60 mph. When the adjustment was finished, the threads were silver soldered and the screw was ground flush with the outside wall. Installed behind the canopy of a 1-26D, 5 inches above the fuselage, compensation was found to be excellent between stall speed and 90 mph.

Conclusions

This study has shown that variometers can have several types of indication errors. Some of the causes such as leakage, lack of insulation, and lack of heat exchangers occur in the installation and not in the basic instrument. Hence the best instruments may show errors if the system is not in-

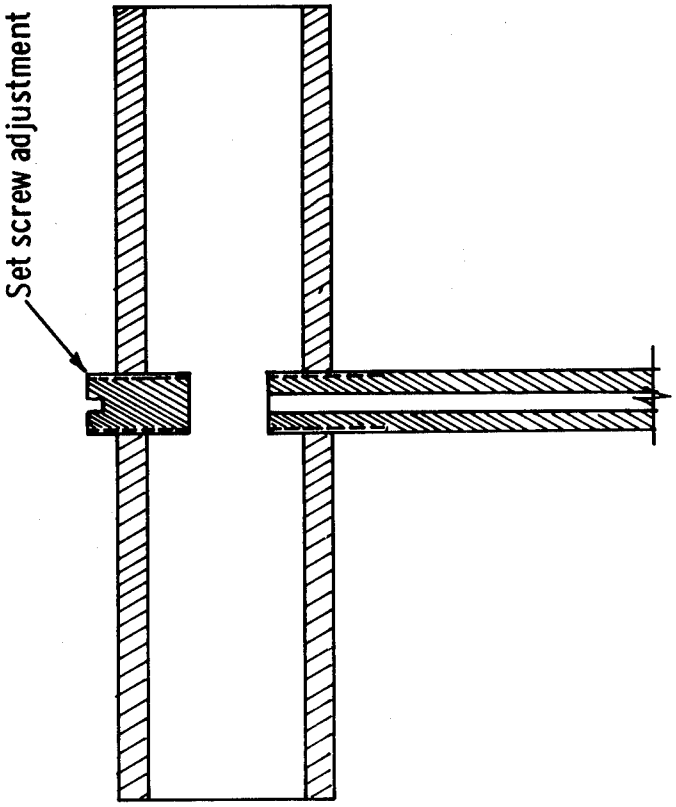


Figure 8. Experimental Adjustable Total Energy Venturi

stalled with some understanding of the problems examined here. Some of the causes of error such as non-linearity may develop during the life of the instrument and may be caused by shock loading.

The instrumentation and methods described are suitable for calibration and performance checking of variometer systems. The checks can be carried out without removing the instruments from the sailplane.

References

1. Moore, Gene; The Electric Variometer System, Proceedings of First Annual Symposium on Competition Soaring 1969, Edited by: Ed Byars and Bill Holbrook, Soaring Symposia, Cumberland, Md., 1970.

2. Byars, Ed, and Holbrook, Bill; Soaring Cross Country, Second Edition, Soaring Symposia, Cumberland, Md., 1970.

3. Senn, Harry; Homebuilt Windtunnel for Instrument Calibration, Soaring, Soaring Society of America, Los Angeles, April 1972.

Session Chairman's
Opening Address

THE STATE OF THE ART, STRUCTURES AND MATERIALS

by

Bernard Paiewonsky
Editor,
Technical Soaring

Summary

The talk included discussions of:

- design objectives
- material properties and a comparison of structural efficiencies for steel, aluminum, composites and wood
- calculations of critical flutter speeds and determination of normal modes
- stiffness measurements
- fatigue - minimum detectable crack and minimum size imperfection that will lead to failure.

Sailplane fuselage mass is small and the whole sailplane (wing plus fuselage plus tail) must be treated as a deformable body.

EXTRUDED LIGHT ALLOY AIRCRAFT STRUCTURES

by

Piero Morelli
Istituto di Costruzioni Aeronautiche
Politecnico di Torino
Italy

Introduction

Extruded light alloy structural elements are widely used in aircraft metal structures (spar flanges, stringers, etc.). Consideration is given here, however, to the possibility of realizing completely extruded structures as a replacement for conventional metal structures (a combination of assembled stringers, panels, and ribs or frames). The main practical advantages of this solution are the following:

1. Reduction of man hours required for construction, once the extruded element or elements are available.
2. Reduction of costs in the case of series production. The cost of the expensive extrusion dies, in this case, can be distributed over a high number of pieces.
3. Accuracy in the reproduction of particular section shapes. This advantage is particularly appreciable when complex section shapes are required, or when the correct profile realization is important, in relation, for instance, to the aerodynamic behavior of a wing or tail (laminar flow airfoils; slotted control surfaces or flaps).

Extruded structures are subject to the following practical limitations, however:

1. The maximum dimension and net area of the profile section are limited by the power of the available extrusion pressing machines. The maximum capacity of the biggest pressing machine now existing in Italy, for instance, is 5000 tons. For such a machine the maximum practicable net section area is 5000 mm^2 for dural; the maximum workable linear dimension of the section is 350 mm. In other countries (U.S.A., U.S.S.R.) much bigger machines exist (up to 25000 tons), with proportionally improved possibilities.
2. Extruded structures typically have constant geometrical and structural sections. Through suitable mechanical and chemical operations, however, it is possible to achieve a certain degree of cross section variation along the structural axis. Either the

over-all linear dimensions of the section, or the dimensions of its elements (wall thickness, for instance) can be tapered, to a certain extent.

3. A minimum value of the wall thickness is imposed by the technological process of extrusion. As a consequence, in the case of small-size sections, such a thickness is excessive in relation to the strength and weight/strength ratio required. A subsequent operation of thickness reduction is necessary in such cases. For this, chemical milling is a particularly interesting process.

Notwithstanding these limitations, a wide field of applications seems to be possible for extruded structures, for powered aircraft as well as for gliders. For gliders, in particular, because of their dimensions and their high wing and tail aspect ratios, the adoption of extruded structures seems to be particularly interesting.

The M-300 sailplane

Some extruded structures have been introduced in the design of a high performance standard class sailplane: the M-300, designed by Alberto Morelli.

Two M-300 prototypes have been built so far by the Centro di Volo a Vela del Politecnico di Torino, CVT. The first of them made her maiden flight in April, 1969. Both have been flown for several hundred hours and have taken part in national and international competitions. An early photo of the first M-300 is shown in Fig. 2, while Fig. 1 shows a three-view drawing. The extruded parts are: 1) the wing spar, 2) the ailerons, 3) the horizontal tail ("all moving" type).

Wing spar: Two-thirds of the wing span is at constant chord. The original intention was an extruded structure for the whole rectangular part of the wing. This idea was abandoned because of the high cost of the dies, the Italian extruding machines being, moreover, inadequate and because a long time would have been needed for experimentation and development.

The wing was thus realized as a composite structure, the skin being made of special preformed thick plywood panels, the ribs milled out of a wooden sandwich. The spar was designed as an I-beam obtained from an extruded ERGAL 55 section (approximately corresponding to 7075 Al-Zn alloy).

The spar section is shown in Fig. 3. Taper of the flanges was achieved by a progressive reduction of their width. The web thickness (3 mm) was excessive in relation to the shear stresses, but necessary for a correct extruding process. Weight was saved, however, by cutting circular holes (60 mm diameter, 105 mm spacing) in the web.

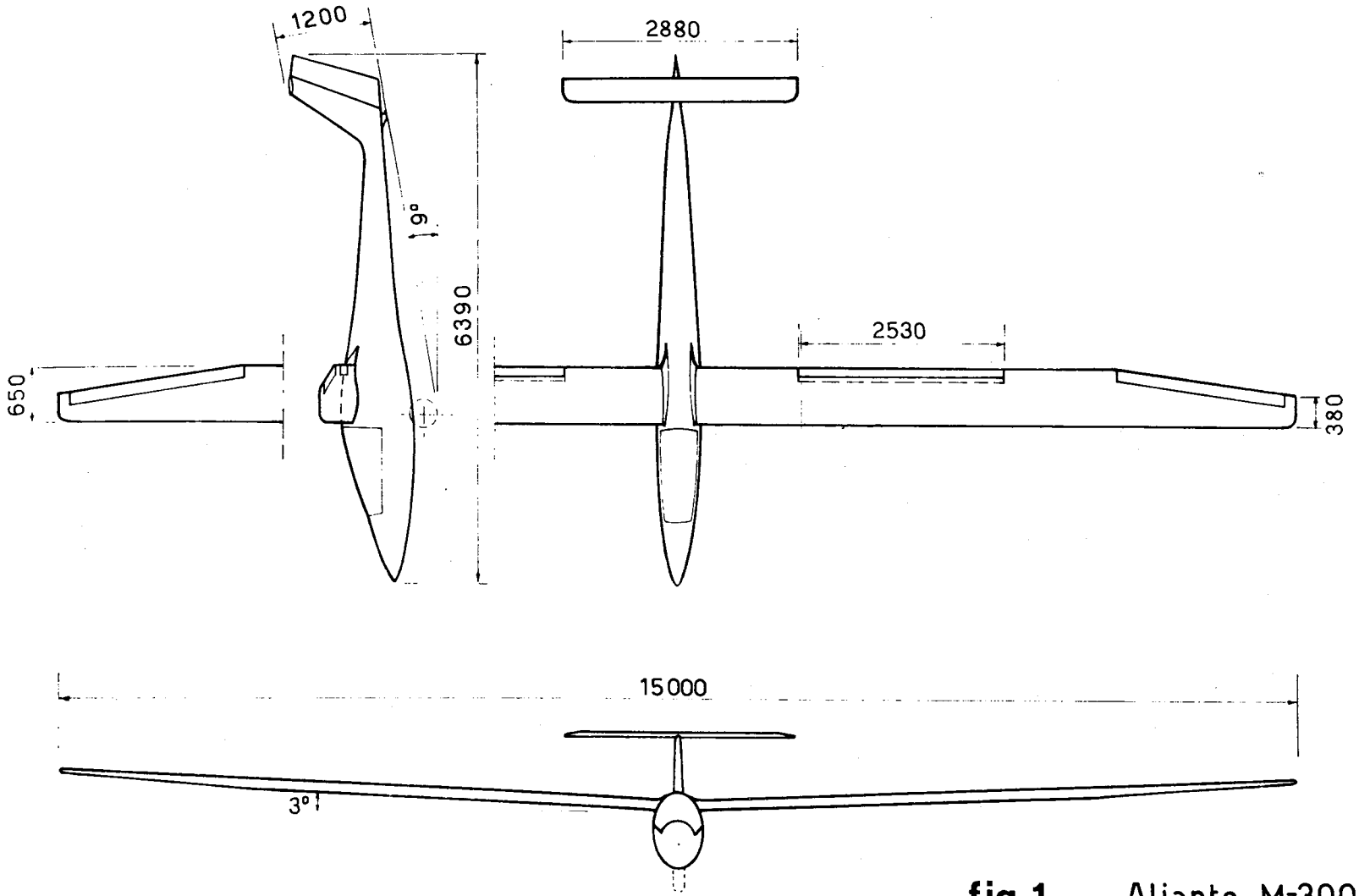


fig.1 - Aliante M-300

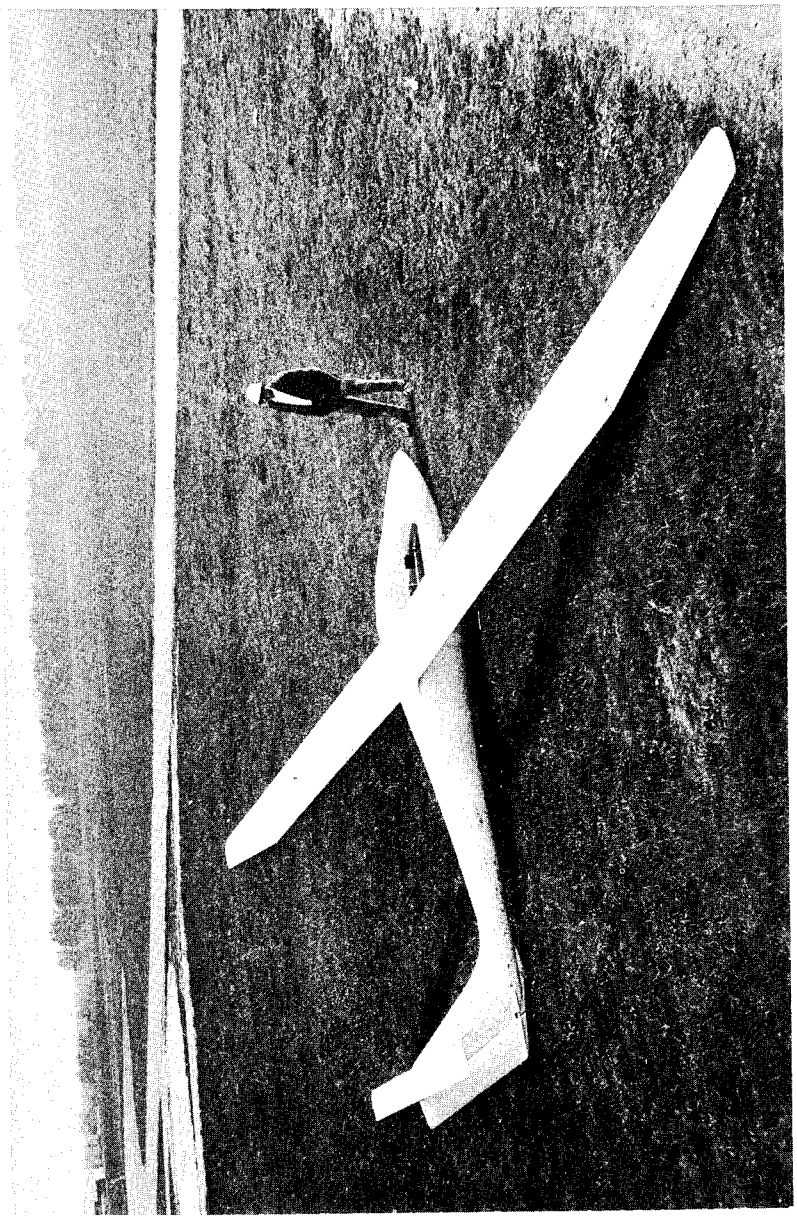


Figure 2.

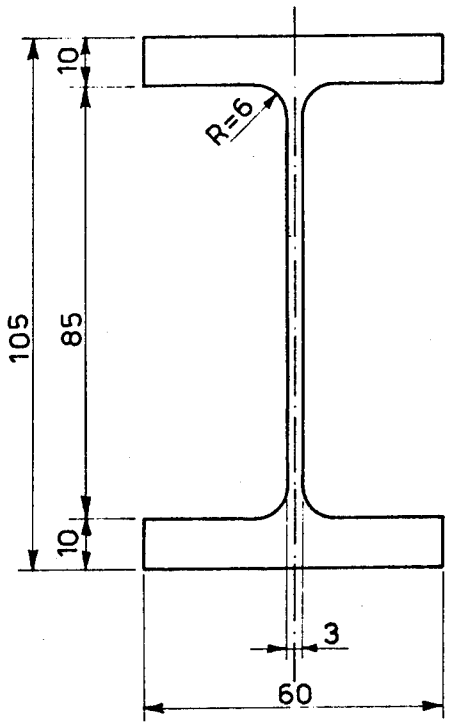


fig. 3

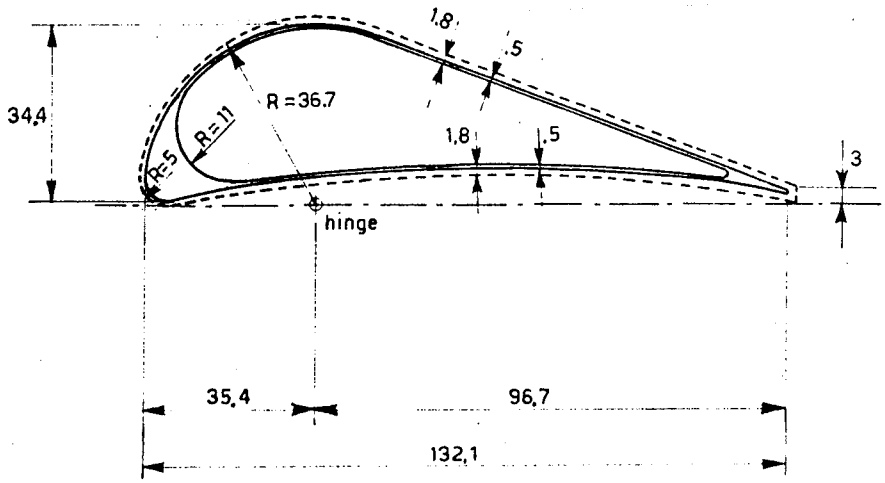


fig. 4

Ailerons: A slotted aileron was envisaged first, in correspondence to the tapered outer parts of the wing. Its section is shown in Fig. 4. It is a pure shell structure made out of a tubular extruded profile. The material employed was an Al-Si-Mg aluminum alloy (ANODAL UNI 3569 TA). The wall thickness was originally 1.8 mm, in order to have a correct extrusion process. The thickness was then reduced to 0.5-0.6 mm through uniform chemical milling of the exterior surface. The bulky leading edge (Fig. 4) was so designed as to fulfil mass-balance requirements.

The structure has no ribs at all except at its ends, where two small ribs, made out of a thin steel plate, are riveted to the skin and carry the two hinges and the control lever (at the aileron inner end).

This type of structure is very light (2.3 kg per aileron) and more than adequate as far as strength and stiffness under the prescribed loading conditions are concerned. The most interesting gain was, however, in the man hours required for the construction: a very remarkable difference with respect to any other conventional construction methods using wood, glass/epoxy, or metal.

During test flights, however, these ailerons proved inadequate from the aerodynamic point of view. They were then replaced by "plain" ailerons, of increased chord and span (section shown in Fig. 5). The construction method was similar to the previous type, the structure being again based on a tubular extruded profile. In this case, an intermediate hinge was added. At the same span station the control lever was located, as required by the increased aerodynamic hinge moments, due to the total absence of aerodynamic balance. Though a little more complicated than the previous solution, the advantages of the construction method were largely maintained. The weight of the new aileron was 2.35 kg.

Although the ailerons are applied to the tapered outer portions of the wing, their cross section is constant along the span. This required a slight modification of the wing profiles in the tapered outer part. How much this modification affects the aerodynamic airfoil behavior, we are not able to say.

Tailplane: The all-flying tailplane was given a rectangular planform for the purpose of employing extruded profiles for its structure. The high aspect ratio (A = 11) was adopted for aerodynamic reasons, the required stability and elevator power being thus achieved with a smaller surface.

Fig. 6 shows the tailplane cross section. The airfoil was designed:

1. for an optimum negative angle of attack;

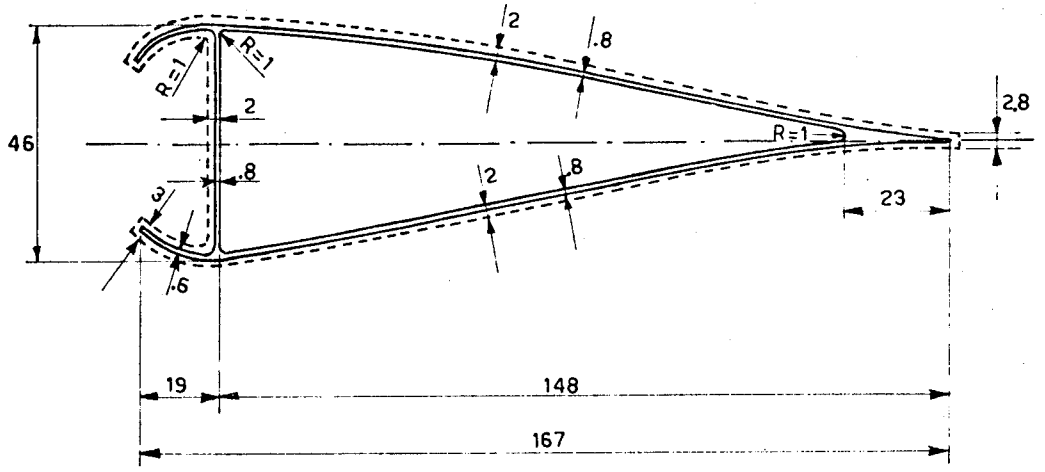


fig.5

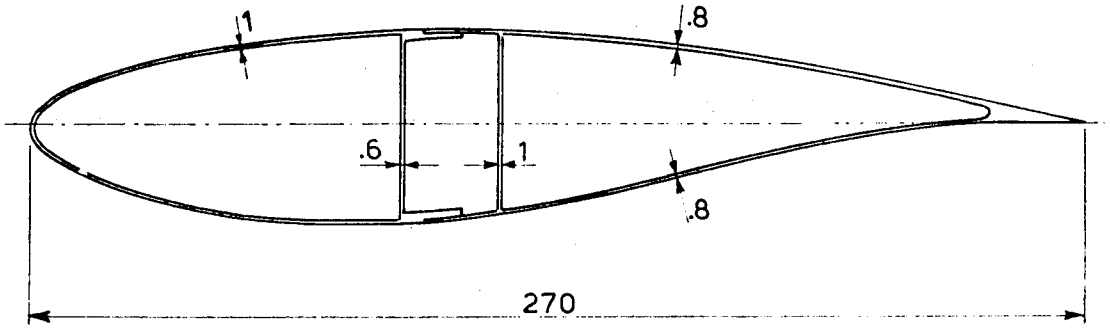


fig. 6

2. for laminar flow within a given range of incidence; and
3. for a fixed value of the pitching moment coefficient in relation to the desired stick force vs. airspeed characteristics.

The structure consists of two aluminum alloy tubular extruded profiles, joined together by rivets along the span. As in the case of ailerons, the original skin thickness was higher than required (2 mm). This value was reduced to 0.8 - 1.0 mm by chemical milling.

The only additions necessary to complete the tailplane were:

1. A T steel tube fitting for the tailplane/fin attachment. This was connected through hinges to the web of the front extruded profile. A cutout (60 x 300 mm) was therefore necessary on the lower skin of the front profile.
2. A faired tip at each tailplane end. These were made of vacuum moulded ABS and directly riveted to the skin.
3. A simple fitting for the control rod connection at the trailing edge of the root section.

The same advantages as claimed for the ailerons were obtained. The reduction of man hours was even more striking, if compared with conventional construction methods. Moreover, less skilled labor is required, as the handwork is practically limited to assembling of already shaped parts.

The load carrying capability and stiffness, as determined through static tests, were far in excess of specified limits. The weight of the tailplane structure, not including the tailplane/fin connection fitting and the tips, was 4.4 kg, corresponding to 6.3 kg/m^2.

Static structural tests

The extruded structures described above were subjected to an extensive static test program. Bending and torsion, which, of course, occur together in the real loading cases of a tailplane, have been studied separately.

In order to give an idea of our test procedures and the results obtained, some peculiarities of the tailplane bending test are illustrated here. The structure was loaded by a simulated span lift distribution, through a single mechanical jack and a system of chain links. The load was distributed along the elastic axis, which was very close to the tailplane aerodynamic center (and hinge) axis.

At increasing load levels, measurements were taken of the vertical displacements at 9 spanwise stations (using 19 mechanical dial extensometers: 2 each at 8 stations, 3 at the center section station) (Fig. 8). Fig. 9 shows the deflection curves at loads of 100, 200, 240, 300, 350, 400 kg (240 kg is the design ultimate load of the tailplane). The dotted lines relate to residual permanent deformations after removal of the 300 and 400 kg loads.

In Fig. 10 each curve shows the vertical displacement at a given station as a function of the load. It can be seen that each curve shows a decreasing slope at low load level followed by a wide quasi-linear portion and then again a decreasing slope at high loads. The first variation is due to progressive buckling of the various skin panels. The linear portion is in the domain of elastic buckling, whereas the last portion corresponds to the appearance of permanent deformations due mainly to local instability.

400 kg was considered as the rupture load of the structure. The corresponding permanent residual displacement, evaluated at the outer end of the structure was approximately 5%. It is important to note, however, that the permanent deformation was mainly due to local instability effects at the edge of the central cutout (Fig. 11).

Fig. 7 shows the structure under the 400 kg load.

The local deformation could be eliminated by an appropriate stiffening of the edge. This was not done, however, as the design ultimate load of the tailplane was exceeded by a considerable margin. Strain-gage measurements were also made of local strains at 27 points located on the outer surface of the skin and on the two webs. The purpose of these measurements was the determination of buckling stresses of various critical panels, the location of buckles, their behavior at increasing loads and the amount of permanent residual deformations. It would be too lengthy to report in detail here the experimental results.

A typical diagram is shown in Fig. 12. It relates to the critical panel at the lower rear surface of the tailplane. This panel is evidently overloaded in compression because of the cutout existing in the corresponding front lower panel.

The strain ($\mu\varepsilon$) distribution is reported at different loads (100, 200, 300 and 400 kg) and after removal of the corresponding load.

The buckling wave length is well in evidence. The residual plastic deformation becomes important at the higher load of 400 kg.

In Fig. 13 the buckling of the lower rear panel and of the rear web is clearly visible (load: 200 kg).

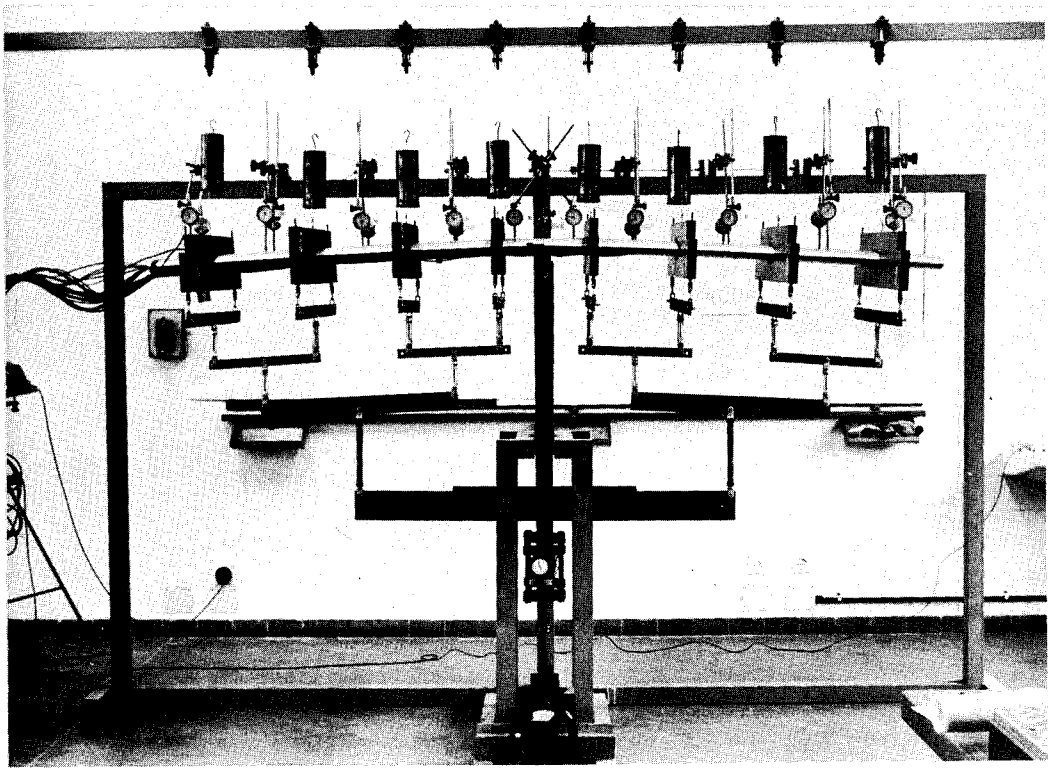


Figure 7.

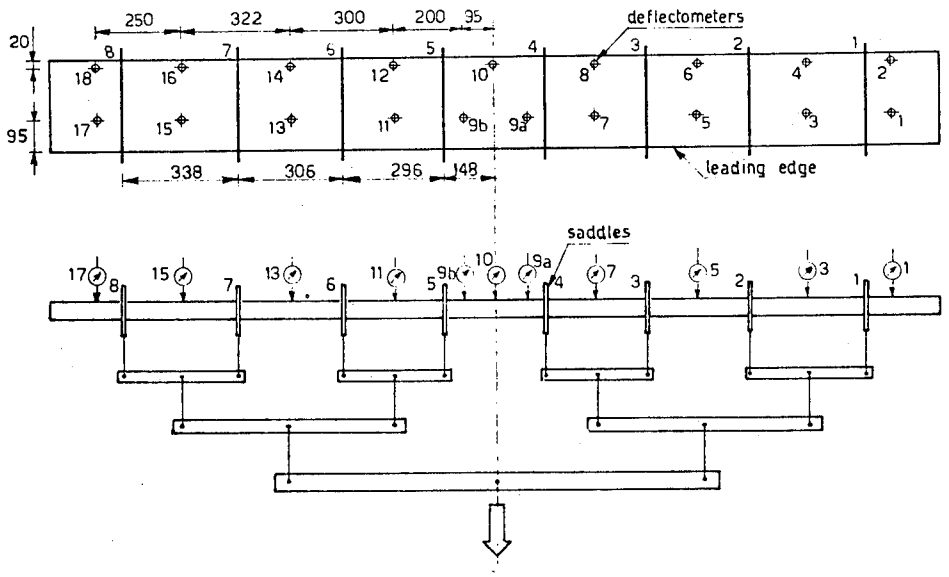


fig.8

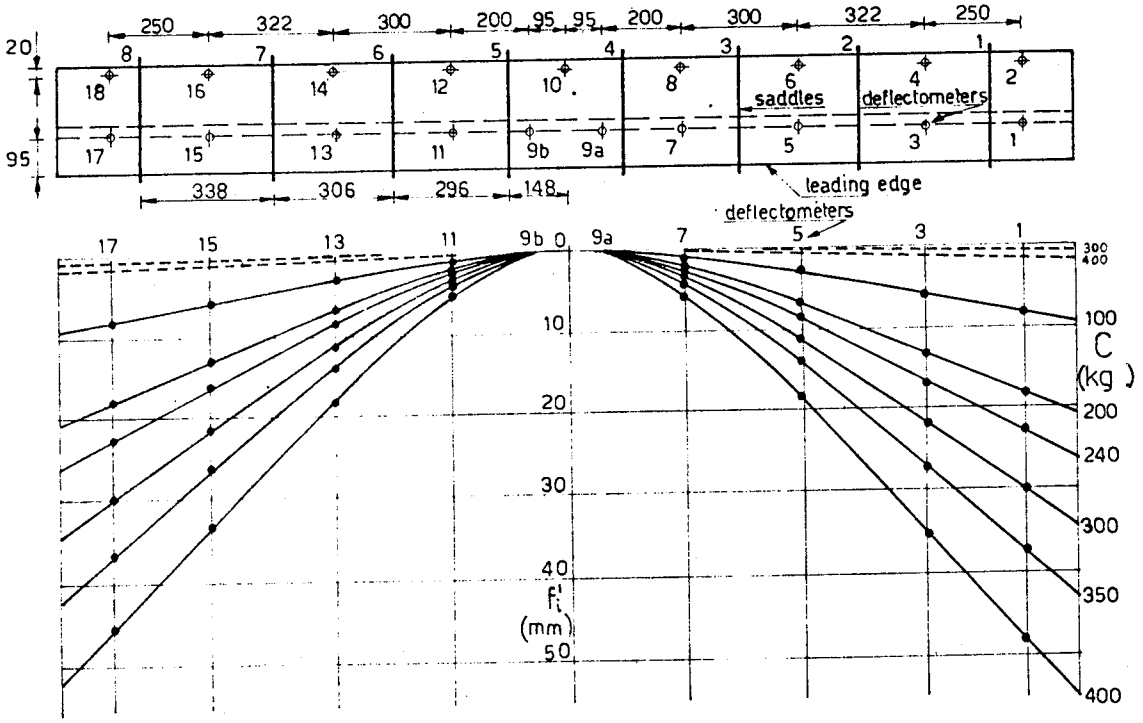

250
322
300
200
95
95
200
300
322
250
20
95
saddles
deflectometers
leading edge
338
306
296
148
17
15
13
11
9b
9a
7
5
3
1
10
20
30
40
f_i' (mm)
50
C (kg)
100
200
240
300
350
400

fig.9

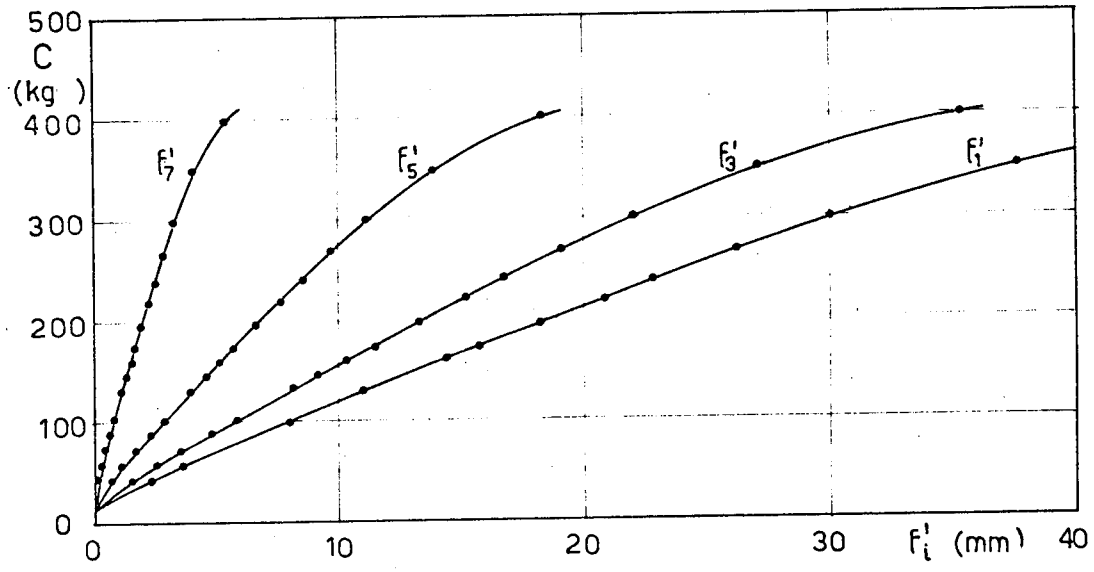

500
C (kg)
400
300
200
100
0
f_7'
f_5'
f_3'
f_1'
0
10
20
30
f_i' (mm)
40

fig.10

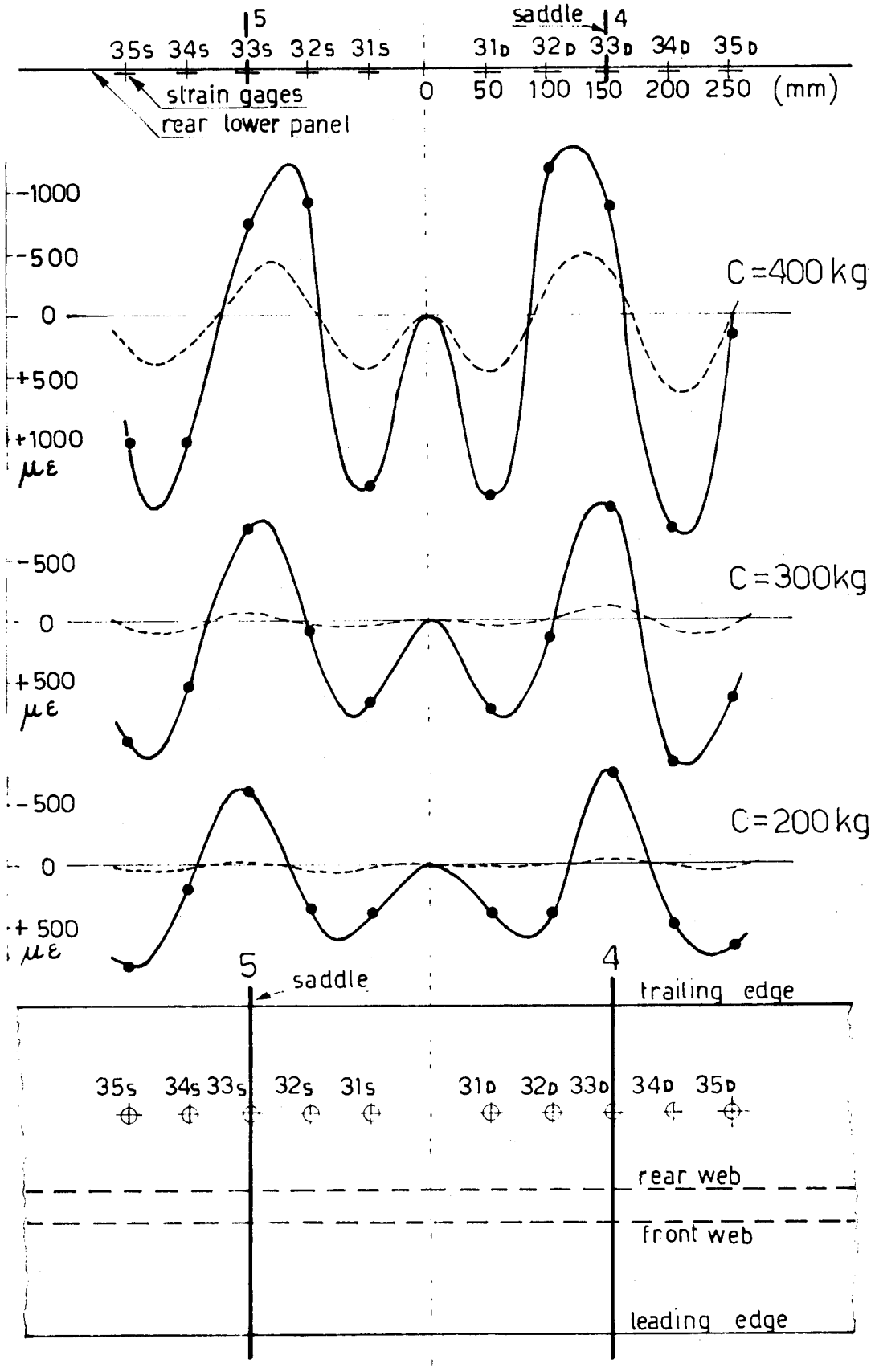

5
saddle
4
35s 34s 33s 32s 31s
31D 32D 33D 34D 35D
strain gages
rear lower panel
0 50 100 150 200 250 (mm)
-1000
-500
0
+500
+1000
με
C=400 kg
-500
0
+500
με
C=300kg
-500
0
+500
με
C=200 kg
5
saddle
4
trailing edge
35s 34s 33s 32s 31s
31D 32D 33D 34D 35D
rear web
front web
leading edge

fig.12

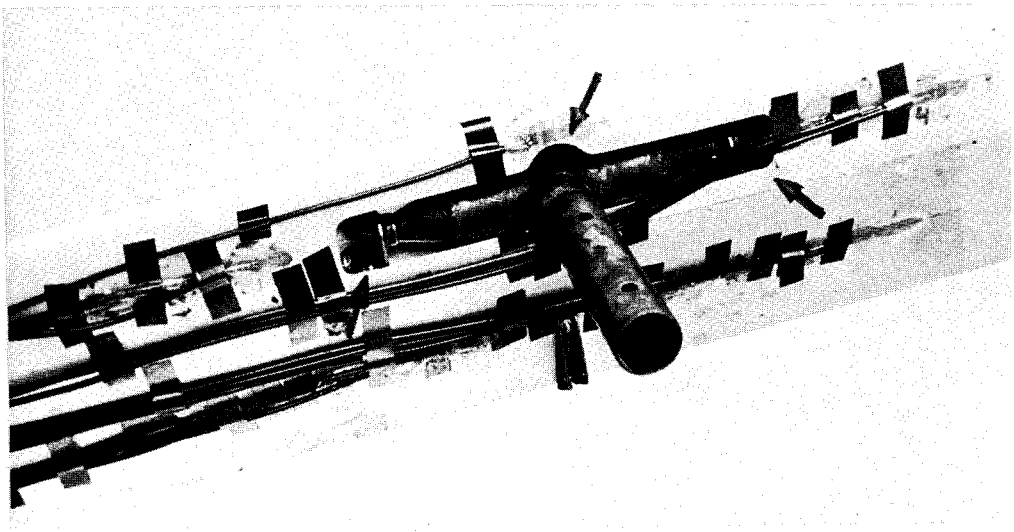


Figure 11.

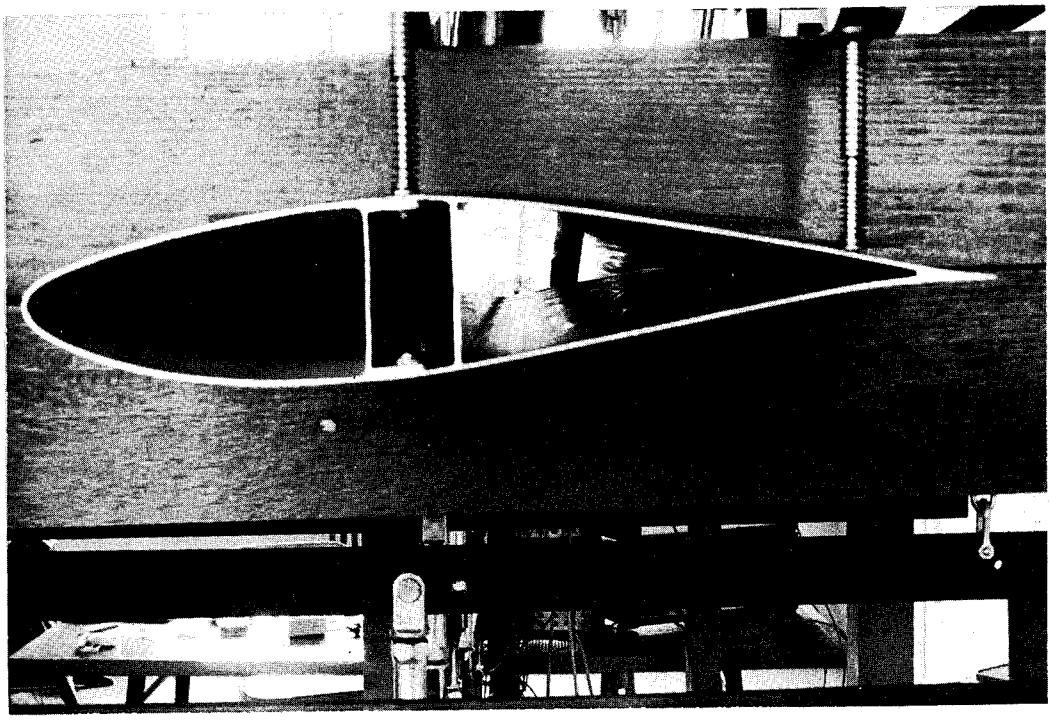


Figure 13.

Conclusions

The application of the structural concept of extruded structures to some parts of the M-300 glider demonstrates the feasibility of this type of construction.

A wider field of application could be attempted: for instance, the construction of a whole wing (or large part of it) through the combination of extruded profiles, longitudinally connected one to the other.

The most attractive advantages of this solution, as already outlined in the introduction, are the reduction of labor costs and the easily obtainable correct reproduction of section profiles.

Structural taper of bending, shear and torsion resisting material could be achieved through the addition of tapered structural elements inside the extruded structures and connected to it, and/or by varying the wall thickness of the extruded profiles spanwise through chemical milling with variable time of immersion.

Of course, buckling problems of panels under compression and shear loads, in such a shell structure without ribs, are delicate. They should be approached using careful location of webs and stiffening flanges. Expansion of resins, as stabilizing material, inside the structure cells might also be worth investigating.

The cost of extrusion dies makes the process interesting, from the economical point of view, only in the case of a series production program.

It is interesting to note, moreover, that this type of construction may be regarded as a possible way of reducing to some extent the need for skilled artisan's work which is typical of current construction methods, using either wood, metal, or reinforced plastics as basic materials.

Acknowledgements

The fundamental idea of realizing the extruded structures illustrated in this paper is due to Alberto Morelli, designer of the M-300 sailplane.

The research and test work at the Politecnico di Torino was carried out by Paolo Piantella, Giuseppe di Grandi and Antonello Cogotti, in close cooperation with the author.

CRACK-TOUGHENED EPOXIES FOR ROOM-TEMPERATURE APPLICATIONS

by

K.J. Strack
Pittsburgh, Pennsylvania

Introduction

Composite materials are favored for the construction of sailplanes because of their great strength-to-weight ratio and the ease with which they can be formed to aerodynamic shapes. Nevertheless, certain weaknesses are inherent to such materials; one notable one in the case of glass-reinforced plastics (GRP) being the development of microcracks in the matrix. The cause has been established as the "strain-expansion" (*dehnungs-vergrosserung*) which exists in the matrix between the glass fibers oriented at 90 degrees to the direction of loading [1]. Because of the differences in modulus between the glass fibers and the resin, strains in the matrix may be 15 to 30 times that of the composite as a whole [2]. As a result a GRP composite subjected to a tensile load experiences microcracking in the direction perpendicular to the load along the fibers. This accounts for the well-known "knee" in the stress-strain diagram for a glass composite having fibers in the direction perpendicular to the tensile load. The "knee" coincides with the strain at which the onset of microcracking may be observed.

Ways of avoiding microcracking have been suggested. The simplest is one offered by Puck [3], dimensioning the structure large enough so that the "knee" strain is not exceeded under the specified service load. This amounts to reducing the maximum allowable stress in the structure to a value far below the actual ultimate tensile strength, thus the superior tensile strength of a glass-fiber laminate when compared to other typical aircraft materials may be illusionary. It may be noted that even if the strain is limited as above, microcracking will still take place after a few thousand cycles of fatigue [4], which would be a small percentage of the fatigue life.

A second method consists of spacing the fibers uniformly, since the microcracking starts more readily in areas where the fibers are most closely packed together [5]. In practice, this method seems virtually unattainable, at least in a hand-layup.

The third method is the one discussed here, that of toughening the matrix against crack propagation by altering

its chemical composition. Polymers may be toughened in various ways, one being the dispersion of a rubber polymer in the glassy matrix. This method has been used quite successfully in thermoplastics like ABS and rubber-reinforced polystyrene, for which fracture surface energies of 10^8 ergs/cm^2 have been reported [6]. The two-phase structure resulting from the rubber additions can be obtained without a great decrease in heat-distortion temperature or modulus, as is ordinarily the case with plasticization. The need for sufficiently high heat-distortion temperature in aircraft construction is self-evident; the influence of matrix modulus on laminate compressive strength has been found to be quite pronounced [7,8].

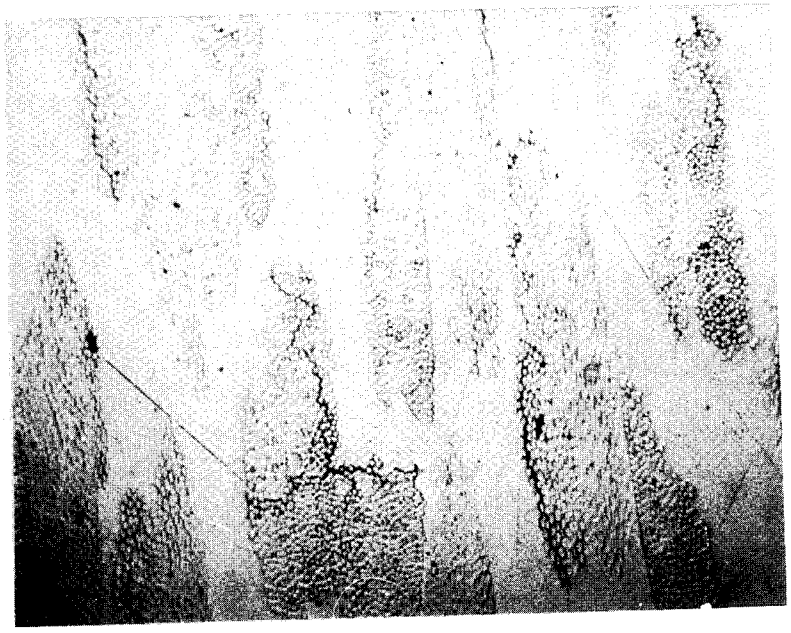
Two phase epoxies

The first actual use of a rubber copolymer to toughen an epoxy was reported in 1968; Ref. 9 describes the pioneering work of MacGarry in the field. It was found that by adding 10 pph of a carboxyl-terminated butadiene/acrylonitrile copolymer, CTBN, to Epon 828, a standard bis-A epoxy, and curing it with 6 pph of DMP-30 (2, 4, 6-tridimethylaminoethylphenol) at 250°F, the surface fracture energy was tripled, and further that if laminates were made with 181 style glass fabric and subjected to a tensile fatigue test, those made with the rubber-modified epoxy showed no microcracking, while those made with the unmodified resin showed appreciable cracking, as shown in Figure 1. Later work at B.F. Goodrich Chemical Company showed that the addition of CTBN caused a 4 to 7-fold reduction in the crack density of composites in flexural fatigue after 10 million cycles.

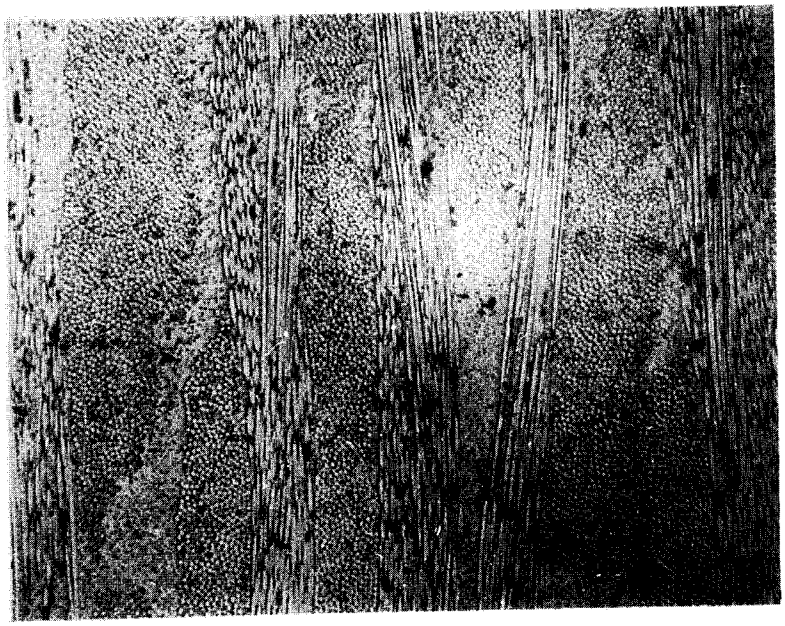
Many factors influence the amount of toughening to be expected from CTBN additions [10,11], and unless the proper microstructure of the cured product is obtained, the modification of the basic epoxy may only degrade the physical properties [12]. A necessary but insufficient condition for toughening is that small (2,000 Å to 30,000 Å) rubbery particles precipitate during the cure. The reaction chemistry involved has been discussed briefly by Drake, Siebert, and Rowe [10]. In addition to the cross-linking of the epoxy, the epoxy-rubber reaction should also be catalyzed. This can be done by using tertiary amines, either alone or in combination with other types of curing agents. Furthermore the epoxy-rubber esterification reaction does not proceed rapidly at room temperature. Formulations published to date have all required the application of elevated temperatures to promote this reaction. This has made it difficult to use these formulations in a large layup.

Room-temperature systems

Since the epoxy-rubber reaction requires heat, but the cross-linking of the epoxy can be accomplished at room temper-



828 / 181 GLASS CLOTH COMPOSITE SUBJECTED TO 75% UTS FOR 100 CYCLES (100X)



828-10% CTBN / 181 GLASS CLOTH COMPOSITE SUBJECTED TO 80% UTS FOR 100 CYCLES (100X)

Figure 1.

ature, it was hoped that the two reactions could be carried out separately, and that the resulting system might still be toughened. Fortunately, this turned out to be the case. Attention was first directed at selecting a room-temperature, low-viscosity laminating resin showing high tensile strength and elongation since these properties were also expected to extend the composite fatigue life. The system chosen was Araldite 6005,[1] a standard bis-A epoxy resin, Araldite RD-4, a cycloaliphatic epoxy, and triethylenetetramine (TETA), in the proportion 84:16:19. In addition to the excellent physical properties for this system, a heat-distortion temperature of 102°C is listed by the manufacturer, as opposed to a value of around 80°C, the value normally expected of low-viscosity laminating resins.

The surface fracture energy for this system was measured and found to be approximately 7.5×10^4 ergs/cm^2; the cure cycle was 12 hours at room temperature plus 12 hours at 50°C. This fracture value is less than the base value MacGarry found for the DMP-30 cured system ($\gamma = 4 \times 10^5$ ergs/cm^2). Thus microcracking would be expected to be more severe for a TETA-based system than one cured with DMP-30, although the cure schedule were not the same. To toughen the system, CTBN[2] was mixed with Araldite 6005 in the proportion 3:1, CTBN/6005, and cooked for 3 hours at 150°C. The mixture was then allowed to cool to room temperature, and more 6005 and RD-4 were mixed in, and finally TETA was added to cure the system, which was cast for testing. The final recipe was 6005/RD-4/TETA/CTBN - 84:16:17:10. The TETA concentration was reduced slightly from stoichiometric (19pph) because published data with heat-cured systems, using Shell Agent-D (which gives higher fracture values than DMP-30 systems) used subnormal concentrations of that curing agent. The specimen blank was cut to shape and cleaved, following the technique described in reference 13; fracture work was approximately 8×10^5 ergs/cm^2, an order of magnitude higher than the value for the straight resin. Thus the method of prereacting the CTBN was found to successfully toughen the resin, although the fracture value was still short of that for heat cured systems.

The next step was to measure the tensile strength of the toughened resin. Here the performance was disappointing. The addition of 10 pph of CTBN dropped the tensile strength from 8.25 kg/mm^2 to 5.32 kg/mm^2, a decrease of 36%. Heat-cured systems normally showed decreases of only 5 to 15%, and a published cycloaliphatic system actually gained 60% in tensile strength [12]; these data seemed to indicate that higher tensile performance than achieved could still be reasonably expected. The elongation with and without rubber was about 3%, although CIBA data shows 10% for the unmodified system when post-cured 8 hours at 100°C.

---

[1] Ciba-Geigy Corporation

[2] Hycar CTBN, B.F. Goodrich Chemical Co., Cleveland, Ohio.

Attention was turned to other curing agents to replace TETA. DMP-30 can be used to obtain room-temperature cures as well as heat cures, so on the basis of its success in toughening at elevated temperatures, it was tried, using the same approach as had been used with TETA. The fracture results were not only inferior to those found when heat curing it, but were actually lower than the TETA values.

A cycloaliphatic amine, aminoethylpiperazine (AEP) was next considered. Several advantages were expected: its Izod impact value was listed as 2-3 times that of TETA, thus it would give naturally tougher cures than TETA. Also it produces sweat-out free castings, which most aliphatic amine systems, like TETA, do not. Other physical properties are very similar to those obtained with TETA. A fracture test of EPON 828 and AEP, (100:22), post cured 12 hours at 50°C gave γ of 10^5 ergs/cm^2. This is 3-4 times the value found for 828-TETA, but still not considered especially high; however AEP's high Izod impact values are obtained only if post cures at 100°C are carried out for at least two hours [14] so the moderate value of fracture work is not surprising. AEP can be used in less than stoichiometric proportions and indeed the experimentally determined optimal mix ratio of 21 pph (based on tensile strength) is less than the calculated ratio, referring now to the 6005-RD-4 blend. The addition of 3 pph Methylon 75108,[3] based on total epoxy weight, is not thought to have significantly affected this result; the Methylon was included in the mix because AEP alone does not provide full RT cures in thin sections.

The first attempt at toughening the AEP system consisted of mixing a 3:1:0.05 batch of CTBN, 6005, and tributyl amine (TBA). The TBA was added to promote the desired epoxy-rubber reaction. This mix was heated to 175°C and then allowed to cool to room temperature. The remaining components were then stirred in; the complete composition was 6005/RD-4/AEP/75108/CTBN/TBA - 84:16:25:3:10:0.16. Fracture work was 17 x 10^5 ergs/cm^2, but tensile strength was only 4.47 kg/mm^2. The fracture work was at a value equal to that of good heat cured systems, but tensile strength was still inferior, although tensile elongation was roughly doubled. Next the AEP concentration was varied. From Table I it may be seen that the tensile values were independent of AEP concentration in the range tested.

Table I

	A	B	C	D
AEP, pph	25	23	21	19
Tensile strength, kg/mm^2	4.47	4.50	4.42	4.40
Elongation at break, %	5.5	4.8	-	-

Lowering the CTBN level to 5 pph, and using AEP at 21 pph raised the tensile value to 5.57 kg/mm^2, while elongation rose to 6.5%. Putting all the 6005 into the premix with the CTBN

[3] Phenolic resin, General Electric Co. Plastics Dept.

instead of mixing at 3:1 as had been done previously, leaving out the TBA, and cooking the premix for 1 hour at 175°C brought the tensile strength up to 6.08 kg/mm^2, a value equal to that of a typical heat cured system. Varying the AEP concentration with the rubber at 5 pph now, and omitting the 75108 gave these results:

Table II

	A	B	C	D
AEP, pph	19	17	15	13
Tensile strength, kg/mm^2	5.87	6.07	6.57	6.42
Elongation at break, %	2.6	3.2	3.8	3.6

Comparing these data with the previous data, two observations may be made. As was the case with 10 pph CTBN, tensile strength is relatively insensitive to the amount of amine in the system, although the variation is stronger at 5 pph (and much stronger with no CTBN). Furthermore the use of Methylon 75108 has a very beneficial effect, since elongation with it was 6.5% and without it around 3%, at least with 19 to 21 pph AEP. Testing the 15 pph system with 3 pph Methylon resin raised the tensile strength to 7.17 kg/mm^2; again the Methylon is seen to be beneficial. Doubling the Methylon level to 6 pph had no appreciable effect on the tensile value; elongation with 3 pph Methylon was 3.8%.

Figures 2 and 3 show the variation of fracture work and tensile strength of the 21 pph AEP system with CTBN content. The best balance of properties is obtained with about 5% rubber. 10 pph seems to overload the system.

Additional tests

In the course of the testing the importance of using Methylon resin together with the CTBN eventually became apparent. An additional variation of the cure cycle was therefore tried: This consisted of including the Methylon in the preheated mix instead of adding it with the AEP for the actual cure of the epoxy. Figure 4 shows the results, now in terms of the stress-strain diagram for the material. There is no decrease in tensile strength, and elongation goes from 3 to 7.6%. Actually the test values for the unmodified resin varied from 5.83 to 8.05 kg/mm^2; this is an unusual amount of variance but is attributed to the flaw sensitivity of the untoughened system. Normally test scatter for straight resins was around 10% and about 4% for toughened resins. From the figure the increase in ductility is obvious. The onset of stress-whitening is easily observable on the toughened test specimen at about 3.5% strain. Fracture work was found to be 15 x 10^5 ergs/cm^2.

Summarizing the mixing procedure: Mix together the following and cook for one hour at 175°C with stirring:

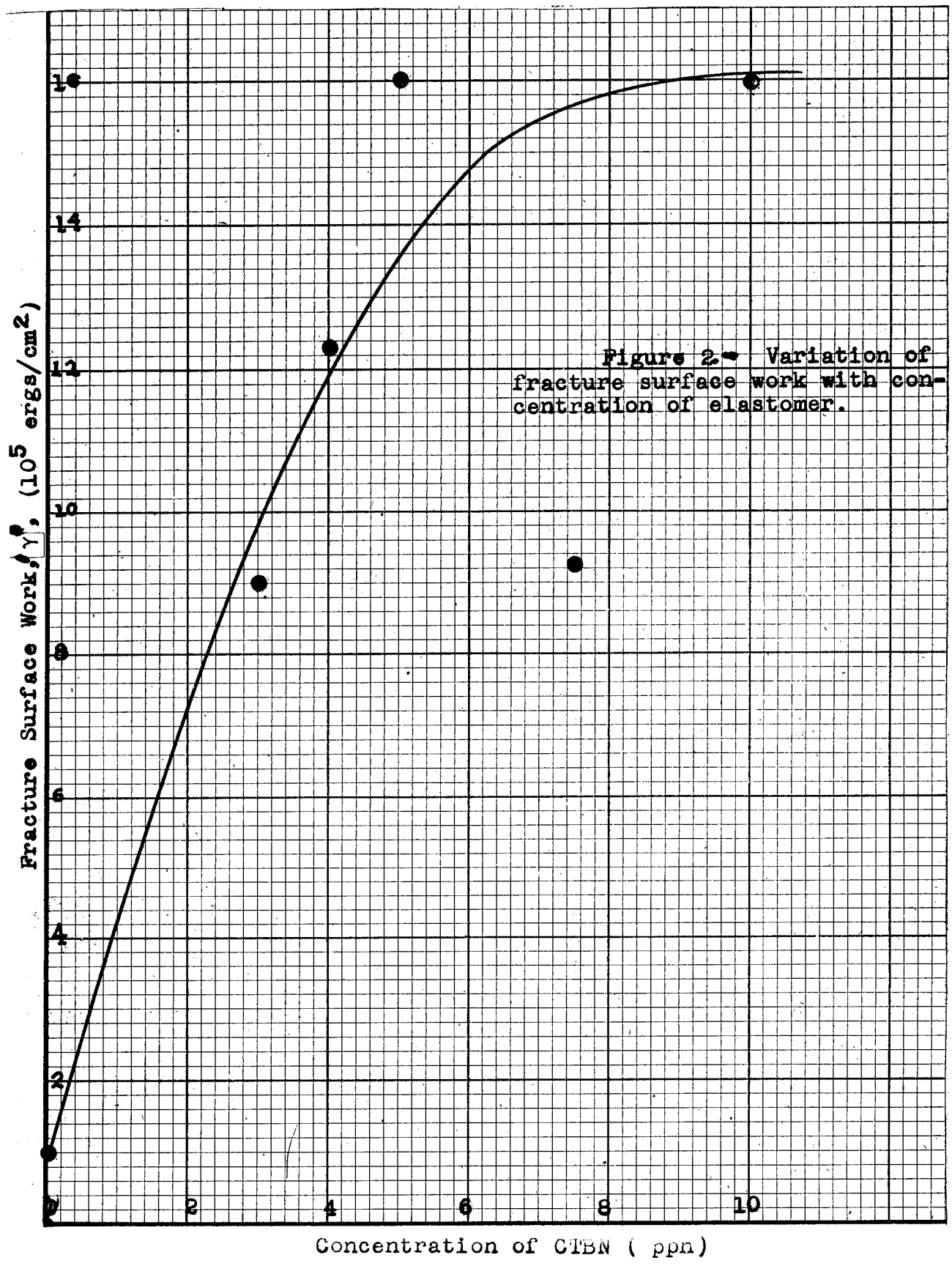


Figure 2.- Variation of fracture surface work with concentration of elastomer.

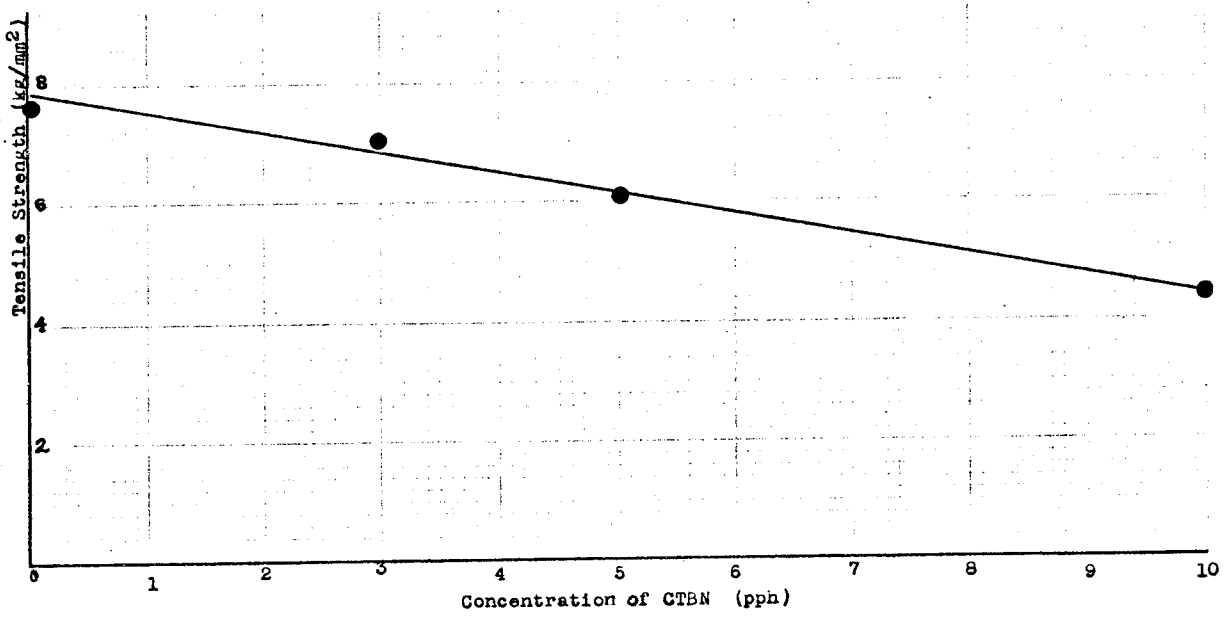


Figure 3 - Variation of resin tensile strength with elastomer concentration

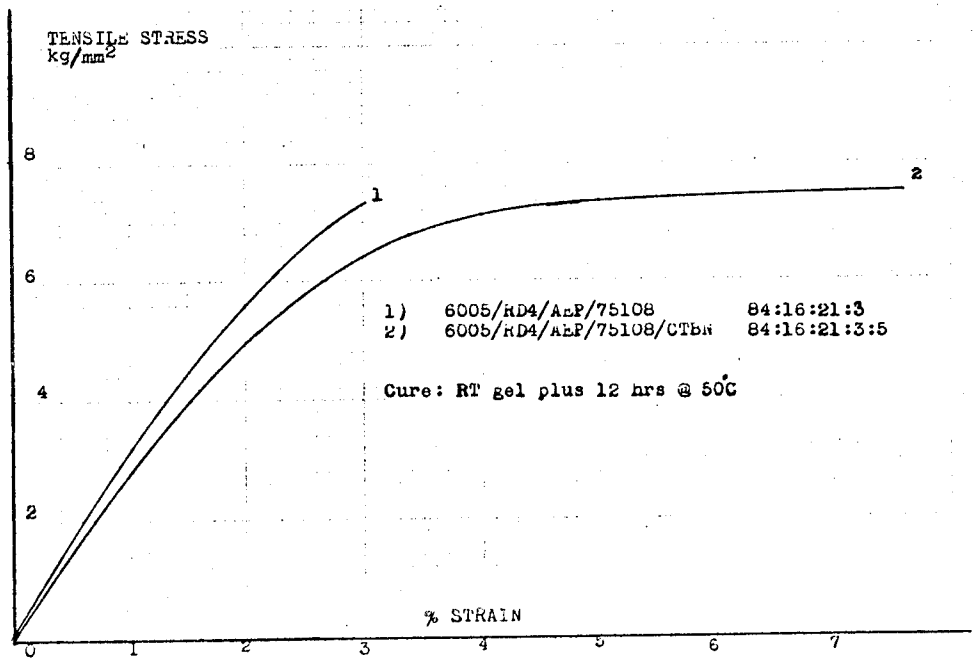


Figure 4 - Cast resin tensile stress-strain curves of CIBA 6005/CTBN systems

Hycar CTBN	5 parts
Ciba 6005	84 parts
Methylon 75108	3 parts

Cool to room temperature and stir in 16 parts Ciba RD-4 (the RD-4 was considered to be too volatile to include in the heated mix). To cure, add 21 parts AEP. Post cure 12 hours at 50°C.

The above procedure gives good toughness with good tensile strength, and it is strongly suspected that the procedure will also toughen systems using a variety of aliphatic and cyclo-aliphatic amine curing agents and epoxies with negligible loss in tensile strength. Single tests with TETA and methane diamine indicated this to be the case, although AEP gives the best toughness and elongation.

Final remarks

Published data by resin manufacturers, as well as by independent laboratories, indicate that the toughness of unmodified, aliphatic amine cured epoxies, is very slow in coming (weeks), even though they gel in a matter of hours, thus it is expected that the systems described herein may well require the 50°C post-cure to obtain the toughness in a reasonable period of time. This is not considered a disadvantage, comparatively, since aircraft manufacturers have found it necessary to use a post-cure with unmodified resins, both for the reason mentioned above, and to increase the heat distortion temperature.

Another factor deserving consideration is the strong dependence of surface fracture energy on temperature. Data obtained with a heat-cured system [5] indicate that at a temperature of 0°C, γ is about one third of its room temperature (20°C) value. At temperatures above 20°C, the slope of the curve is even greater. Since white painted surfaces may experience a 12°C rise in temperature above the air temperature because of solar heating [15], and the air itself can be as high as 38°C on a hot summer day, the fracture values on sunny days would be expected to far exceed those reported in these tests; on the other hand, on wintry days the values would be much less. Fracture energy of unmodified resins does not vary much with temperature in the -40°C to +30°C range.

References

1. Puck, A.; Zum Deformationsverhalten und Bruchmechanismus von unidirectionalem und orthogonalem Glasfaser/ Kunststoff, Kunststoffe 55 (1965) p.914.

2. Kies, J.A.; Maximum Strains in the Resin of Fiberglass Composites, NRL Report 5752, U.S. Naval Research Laboratory, 26 March, 1962.

3. Puck, A.; Das Knie im Spannungs-Dehnungs-Diagram und Rissbildung bei Glasfaser/Kunststoffen, Kunststoffe 58 (1968) p.886.

4. Broutman, L.J., and Sahu, S.; Progressive Damage of a Glass Reinforced Plastic during Fatigue, Proceedings of 24th Annual Technical Conference, SPI, Reinforced Plastics Div. 1969.

5. MacGarry, F.J.; Building Design with Fiber Reinforced Materials, Proc.Roy.Soc.Lond. A 319, 59-68 (1970).

6. MacGarry, F.J., and Selfridge, G.C.; Fracture Surface Work of Modified Polystyrenes and Certain Crosslinked Polymers, Procs.A.C.S. 145th Ann.Mtg. New York September 1963.

7. Puck, A.; Glassfaser/Kunststoff in hochbeanspruchten Leichtbaukonstruktionen, Kunststoffe 53 (1963) p.722.

8. Broutman, L.J., and Krock, R.; Modern Composite Materials, p.387-388, Addison-Wesley (1967).

9. MacGarry, F.J.; Crack Propagation in Fiber Reinforced Plastic Composites, Fundamental Aspects of Fiber Reinforced Plastic Composites, Schwartz, R.T. and Schwartz, H.S. Wiley & Sons, Inc. (1968).

10. Rowe, E.H., Siebert, A.R., and Drake, R.S.; Toughening Thermosets with Liquid Butadiene/Acryonitrile Polymers, Modern Plastics, Aug. 1970.

11. MacGarry, F.J., and Sultan, J.S.; Crack Propagation Studies in Crosslinked Glassy Polymers, 24th Ann.Tech. Conf. S.P.I. 1969, Reinforced Plastics Div.

12. Soldatos, A.C., and Burhans, A.S.; Cycloaliphatic Epoxy Resins with Improved Strength and Impact Coupled with High Heat Distortion Temperature, Ind. Eng. Chem. Prod. Res. Develop. Vol. 9, No. 3, 1970.

13. Broutman, L.J., and MacGarry, F.J.; Fracture Surface Work Measurements on Glassy Polymers by a Cleavage Technique, I and II, J.Applied Polymer Science, 9 (1964), p.589.

14. Lee, H., and Neville, K.; Handbook of Epoxy Resins, McGraw Hill 1967.

15. Semjonow, V., and Wurtinger, H.; Strahlungsaufheizung von Glasfaser/Kunststoffen, Kunststoffe 54 (1964) 1, p.17.

COMPOSITE SYSTEMS FOR AIRCRAFT CONSTRUCTION

by

Stephen T. Bowen
Fiberfil Division,
Dart Industries
Evansville, Indiana

Introduction

Consideration of fiber-reinforced plastic (FRP) aircraft structures requires an understanding of the properties of composite structures. Properties of composite materials are a function of three major factors:

resin

reinforcement

fabrication technique

This paper reviews recent progress in the areas of resin, reinforcement and fabrication. Several new developments may provide improved composite structure for aircraft applications.

Resin

The two major resins used for FRP structures are polyester and epoxy. These resins are similar in many ways. Both are available as low molecular weight, liquid solutions that are easy and convenient to process for a short period of time, after which the resins begin to harden into a rigid, solid condition. Resins, such as polyester and epoxies, which chemically crosslink under specific conditions to form irreversible solid material are called thermosets. The pot life, or working time, for a thermoset resin is a function of the type and concentration of the catalyst or hardner. Pot life can vary from several minutes to several weeks.

Important considerations in resin selection are cost, physical properties, safety (some contain flammable solvents or cause dermititis), ease of fabrication, and convenience.

Polyesters

Polyester laminating resins are solutions of alkyd polymers in reactive monomers. Typical alkyds are solid

polymers with molecular weight 2000 to 3500. When disolved in a low viscosity, low molecular weight, reactive monomer, a syrupy solution results. Commonly used monomers are styrene and vinyl toluene. Monomer concentration may vary from 25% to 50% by weight, with higher monomer levels contributing to lower viscosity in the resultant solution. The addition of a peroxide catalyst to a liquid polyester chemically activates the resin to molecularly crosslink the system into a hard, solid product. The time between catalyst addition and resin hardening is called pot life or working time. Final cured resin properties are determined by the composition and molecular weight of the original alkyd, the concentration and type of monomer, and to a lesser extent by the peroxide catalyst.

The advantages of polyester laminating resins are low cost, low viscosity, good strength and rapid cure at low temperatures. The primary disadvantages are high shrinkage during cure, monomer loss during cure, (which can result in property variation), fire hazard, and stickness or mess, (worse than epoxy), in hand lay-up operations.

Epoxies

Epoxy resins are presently used for all FRP sailplane construction. Epoxies can react through a variety of chemical mechanisms. The type of hardener or coreactant used with the epoxy resin has a definite effect on the properties of the cured system. A given epoxy resin can be cured by many different curing agents. Therefore, the specification of an epoxy resin normally includes the specification of the type and the concentration of hardener. Table 1 illustrates the effect of different curing agents on the mechanical properties of a general-purpose bisphenol-A epoxy resin.

The economic requirements of sailplane manufacture exclude the use of the higher performance, (higher mechanical properties), epoxy systems. The economics of reference are the costs of heated, matched metal dies versus had lay-up in a master mold. Limited production of a single design has restricted, and probably always will limit, the method of fabrication to room-temperature cured, hand lay-up techniques.

The most widely-used epoxy systems for hand lay-up are based on diglycidol ether of bisphenol. The term epoxy is often used indiscriminately for DGEBA based epoxies, although the term epoxy applies equally well to other epoxies that are not derived from bisphenol A. In sailplane construction DGEBA epoxy resins have been used on most European and several U.S. produced FRP sailplanes.

In addition to the selection of epoxy resin and hardener the system is often further modified by the addition of diluents. The addition of a diluent may result in a specific change in viscosity to improve processing or fabrication.

Table 1.

DGBEBA with various hardeners

Hardener Type General Specific	Amine TETA	Modified Polyamine Araldite 956	Amido Amine Araldite 955
Typical Usage, phr	10-12	20-25	35
Pot Life, min.	20-25	35	35
Viscosity, cps. 77F	2500	2500	6400
Properties			
Tensile Str. psi	9000	10,500	8500
Flexural Str. psi	18000	17,500	16000
Tensile Elongation,%	3.8		2.5
Heat Distortion, C	66	100	59
Cure Schedule	7 days R. T.	R.T. gel +2 hrs @ 100C	14 days R.T.

ARALDITE™ manufactured by CIBA PRODUCTS COMPANY

Table 2.

Properties - Fiberous reinforcement

FIBER	MODULUS of ELASTICITY		Sp. Gr.	Tensile Str.
	psi x 10^6	Spec. Mod.		psi x 10^3
Nylon	0.4	1	1.1	100
Carbon	6	11	1.5	120
Glass "E"	10.5	11	2.5	450
Aluminum	10.6	11	2.7	90
Glass "S"	12.5	14	2.5	700
Aromatic Polyimide	18.0	35	1.5	350
Steel	30	11	7.8	600
Graphite HS	40	60	1.8	400
Boron	60	65	2.6	450
Graphite HM	70	97	2.0	325

Table 3.

Physical properties of whiskers*

TYPE	DENSITY gm/cm^3	TENSILE STR. psi x 10^6	MODULUS psi x 10^6	SP. STR. in x 10^6
Aluminum Oxide	3.9	2-4	100-350	14-28
Aluminum Nitride	3.3	2-3	50	13-21
Beryllium Oxide	1.8	2-2.5	100	31-43
Boron Carbide	2.5	1	65	11
Graphite	2.0	3	142	37
Magnesium Oxide	3.6	3.5	45	27
Silicon Carbide	3.2	1-5	70	26-44
Silicon Nitride	3.2	1	55	4-13

*Data published by THERMOKENETIC FIBERS, INC.

Catalysts can also be added to accelerate curing a low temperature. The addition of silanes may improve the bond to fibrous reinforcements.

General

Polyesters and epoxies meet the basic requirements for a matrix for structural composites. They are economical, available as liquids, cure to a rigid, solid condition, harden at room temperature, exhibit good aging characteristics, and they are ideal for hand lay-up fabrication of FRP structures. However, neither polyester nor epoxy resins are very useful in the cured state unless they are filled or reinforced. Reinforcement of these resins provides the strength required for load bearing, structural applications.

Reiforcements

Glass fiber is the most common reinforcement for FRP structures. Fibers such as graphite, boron, aromatic polyamide, polyamide, beryllium, and micro fibers (whiskers), may also be useful. The properties of these reinforcements are listed in Table 2. The dominant factor in fiber selection is cost. Glass fibers cost approximately $.33/lb, the cost of graphite varies from $40.00 to $180.00/lb, while most other high-modulus reinforcements cost over $100.00/lb.

The economics of glass fiber production and the excellent properties of glass fiber at ambient and elevated temperature make it an ideal reinforcing material for composites. Furthermore, glass fiber is available in many forms - roving, chopped strand, woven fabric, woven roving, and chopped strand mat. The selection of the proper glass fiber for a specific application should include consideration of the fiber bundle size, the filament size (diameter), and the type of binder and silane on the glass fiber. The specific aspects of glass fiber selection are throughly discussed in the paper presented at this conference by Elson.

Boron and graphite

Boron and graphite fibers were acclaimed in the 1960's as the fibers of the future. Enormous military expenditures stimulated by the needs of the U.S. space program, resulted in the development of laboratory production of boron and graphite filaments. The initial research data indicated that both graphite and boron could be performance/cost competitive with glass fiber. Costs for these high modulus fibers were projected to be $10.00 - $15.00 per lb when full commercialization was achieved. In the mid 1960's the need for a com-

mercial high modulus fiber was increasing and the research funding was not, so the decision was made to stop funding both boron and graphite development programs on an equal basis and, alternatively, fund the project with the greatest chance for the quickest commercialization, while the other fiber program would be funded at a lower level as a back-up project. The choice at that time was to push boron into commercialization as rapidly as possible and to carry on the graphite fiber work at a lower priority.

The production of boron fiber is based on a technique of electro-deposition of boron on a tungsten filament. The high cost of the tungsten filament excludes low cost boron filament production using this technique. Although methods of manufacturing substrateless boron filament have been proposed, none are known to be commercial. The speculation that an economical manufacturing technique for boron filament would be developed has proven erroneous to date. In the meantime great strides have been made in the commercialization of a variety of graphite fibers.

Graphite fibers are produced by the pyrolysis of rayon fiber, or polyacrylonitrile. Other techniques claim the direct conversion of coal tar pitch to graphite fiber under high temperature conditions. Graphite fibers are available from several major suppliers in the U.S., England, and Japan. Initial work to develop high modulus (760 x 10^6 psi) graphite fibers has succeeded, but such high modulus fibers tend to have lower tensile strength and poorer handling properties than medium modulus fibers (30-50 x 10^6 psi). The present emphasis is to produce a medium modulus with high tensile strength. The medium modulus fibers are also more economical to produce, requiring less heating at elevated temperature. Graphite fibers of 40-50 x 10^6 psi modulus are presently available in continuous strand and tow for $40 - $50/lb.

The handling properties of boron and graphite yarns differ considerably. Boron filament is very stiff and sharp; the filament diameter is approximately .4 mm. The graphite fiber is only 8 microns in diameter. This small fiber is much too delicate to handle alone; graphite filaments are therefore grouped into bundles to form a roving or yarn. The yarn is handled in much the same manner as glass roving. Boron filaments do not ordinarily have a surface treatment or coating. Graphite yarns often have a PVA coating to help retain yarn integrity during handling. When a PVA coating is present on the graphite, it should be removed prior to impregnation.

Polyamide

Although many millions of dollars have been spent by industry and government on high temperature organic fibers very few have reached commercialization. DuPont's Nomex fiber

has been commercial for nearly a decade, but it is not widely used as a fibrous reinforcement for composites. A newer DuPont fiber PRD-49, an aromatic polyamide, is finding good acceptance as a reinforcing fiber. Many other high temperature resistant, high modulus fibers that have been developed, or proposed are simply too costly in small volumes to produce.

Whiskers

The concept of fibrous reinforcement on the molecular scale is theoretically sound, but has yet to be reduced to practice. Small single-crystal fibers have been grown with aspect ratios as high as 10,000 to 1. The efficiency of such reinforcements in composite structures should far exceed that of macro fibers, such as glass and graphite. In practice, however, such whiskers are extremely difficult to wet - out or bound with resin. The resultant efficiency of whisker-reinforced composites is consequently very low. Whiskers may eventually be the ultimate reinforcement, but many problems remain to be solved. Physical properties are shown in Table 3.

General

For the present and in the near future the dominant fibrous reinforcement for structural composites will continue to be glass. Continued improvements in silane technology, glass manufacture, and resin formulation will improve the efficiency of glass/epoxy systems. The more general use of S glass would permit more immediate improvement of existing systems. The decrease in the price of graphite fiber has been dramatic in recent years, and continued cost reduction will allow the range of applications for graphite-reinforced composites to expand.

On a cost/performance basis graphite may close in on glass rapidly as:

1. the cost of graphite fiber is further reduced;
2. the technology of sizings (coupling agents) for graphite fiber is developed; and
3. higher strength yarns are produced.

One should recall that the technology of glass reinforced composites has evolved over the last thirty years. Bare glass fiber is not a very good reinforcement, and it is extremely difficult to work with. The coupling agents, lubricants and binders of glass fiber allow it to be a functional reinforcement; this technology has yet to be perfected for the new high-modulus fibers.

Composite structures

A composite structure offers a means to use the combined properties of materials in applications where the properties of the same materials used individually would be insufficient. The combination of fiber reinforcement and resin matrix allows the designer to use the best characteristics of each component. The fibers are usually oriented to carry the applied load in tension and/or compression, while the resin matrix transfers the applied stress between fibers, maintains fiber orientation and protects the fibers from mechanical and environmental damage. Table 4 gives property data for representative reinforced epoxy composites.

In uni-directional structures, such as spars, it is worthwhile to consider improving the elastic modulus by using fibers with a higher modulus than glass fiber. Table 5 shows property data for uni-directional laminates with incremental substitution of boron fiber for glass fiber. The modulus data in Table 5 was previously published by Langley of Texaco Experiment, Inc. From his data the weight percentage of boron, glass, and resin have been calculated and the composite materials cost has been determined. The data shows that to triple the composite modulus the composite cost must be increased seventeenfold, or stated another way, the modulus to cost ratio would be approximately 1 to 6.

Table 6 shows similar data based on the incremental substitution of high modulus (60×10^6 psi) graphite fiber for glass. It shows a modulus-to-cost ratio of approximately 1 to 5 for graphite when it is substituted for glass. It is interesting to note the difference between the specific gravity of boron and graphite composites. The high specific gravity of boron is largely a result of the tungsten substrate in the boron fiber.

The data presented thusfar indicates that most high-modulus fiber composites are too expensive to be incorporated into sailplane structures without dramatically increasing the cost. A future extrapolation of the data suggests a more encouraging situation.

Assume, for example, that 100 lb of uni-directional composite are incorporated into a sailplane structure. Using E glass/epoxy composites, the cost of the uni-directional materials is approximately \$40, (\$.39 x 100 lb). The typical elastic modulus of such composites is $4 - 5 \times 10^6$ psi. Now, using S-2 glass and 2 - 3% graphite fiber (60×10^6 psi modulus), in plastic of E glass, the modulus will be approximately doubled (10×10^6 psi) and the cost will be approximately \$3/lb, (\$300 for 100 lb). The added cost per aircraft would be \$260.00. Although this would not improve the problem of torsional flexing in the wing, it would substantially improve the wing flutter characteristics induced in high speed flight. It also presents a solution to the problem of bending flex in very high aspect ratio, long-span wings.

Table 4.

Unidiectional epoxy/fiber composite properties*

FIBER TYPE	TENSILE STR. psi x 10^3	TENSILE MOD. psi x 10^6	COMP. STR. psi x 10^3	DENSITY
S Glass	180	7.0	130	0.072
E Glass	60-120	3.8-5.0	90	0.070
HS Graphite	190	20	150	0.057
HM Graphite	110	30	110	0.057
Boron	320	36		0.074
PRD-49**	170	12	50	0.050
Beryllium	97	28		0.058

Table 5.

Boron/glass/epoxy composites

Vol.% Boron	0	10	20	30	40	50	60	70
Vol.% Glass	65	56	47	38	29	20	11	2
Vol.% Resin	35	34	33	32	31	30	29	28
Flexural Modulus* psi x 10^6	5	16	23	28	33	36	38	40
Wt.% Boron	0	13	25	37	49	61	72	84
Wt.% Glass	81	69	57	46	35	24	13	2
Wt.% Resin	19	18	18	17	16	15	15	14
$ Boron @ $50/lb	0	6.50	12.50	18.50	24.50	30.50	36.00	42.00
$ Glass @ 35¢/lb	.28	.24	.20	.16	.12	.08	.05	.01
$ Resin @ 65¢/lb	.11	.11	.11	.10	.09	.09	.09	.08
Materials Cost $/lb	.39	6.85	12.81	18.76	24.71	30.67	36.14	42.09
Specific Gravity	2.04	2.05	2.07	2.10	2.12	2.14	2.16	2.19

* T.W. Langley, Texeco Experiment, Inc.

Table 6.

Graphite/glass/epoxy composites

Vol.% Graphite	0	10	20	30	40	50	60	70
Vol.% Glass	65	56	47	38	29	20	11	2
Vol.% Resin	35	34	33	32	31	30	29	28
Flexural Modulus* psi x 10^6	5	16	23	28	33	36	38	40
Wt.% Graphite	0	10	21	31	43	54	67	80
Wt.% Glass	81	71	61	51	39	28	16	3
Wt.% Resin	19	19	18	18	18	18	17	17
$ Graphite @ $50/lb	0	5.00	10.50	15.50	21.50	27.00	33.50	38.00
$ Glass @ 35¢/lb	.28	.25	.21	.18	.14	.10	.06	.02
$ Resin @ 60¢/lb	.11	.11	.11	.11	.11	.11	.11	.11
Materials Cost $/lb	.39	5.36	10.82	15.79	21.75	27.21	33.67	38.13
Specific Gravity	2.04	1.99	1.95	1.91	1.88	1.84	1.80	1.76

*Theoretical calculations based on graphite fiber modulus of 60 x 10^6.

Table 7.

Graphite/S glass/epoxy composites

Vol.% Graphite	0	10	20	30	40	50	60	70
Vol.% Glass	65	56	47	38	29	20	11	2
Vol.% Resin	35	34	33	32	31	30	29	20
Flexural Modulus* psi x 10^6	7.5	18	24	29	34	36	38	40
Wt.% Graphite	0	10	21	31	43	54	67	80
Wt.% Glass	81	71	61	51	39	28	16	3
Wt.% Resin	19	19	18	18	18	18	17	17
$ Graphite @ $50/lb		5.00	10.50	15.50	21.50	27.00	33.50	38.00
$ Glass @ $2/lb	1.62	1.42	1.22	1.02	.78	.56	.32	.06
$ Resin @ 60¢/lb		.11	.11	.11	.11	.11	.11	.11
Materials Cost $/lb.	1.73	6.53	11.83	16.63	22.39	27.67	33.93	38.17
Specific Gravity	2.04	1.99	1.95	1.91	1.88	1.84	1.80	1.76

*Theoretical calculations based on a graphite fiber modulus of 60 x 10^6.

Table 7 shows the calculations for determining the above-referenced cost of $300/lb for a S-2 glass/graphite/epoxy uni-directional laminate. Figure 1 plots modulus for S-2 and E glass uni-directional laminates, when graphite fiber is incrementally substituted for glass fiber.

The high cost of many "advanced" composite systems may make them impractical for use in sailplane construction at this time and possibly in the near future. In specific cases, however, higher strength composites can also result from the more selective use of existing, low-cost resins and fibers. In a wing spar, for example, the tensile modulus and compressive properties of the uni-directional laminate may be optimized by proper resin and glass selection. Several combinations of glass roving have been tested and found to exhibit the properties shown in Table 8. Several 181 style glass fabric/epoxy laminates have been tested. This data is presented in Table 9.

The design of torsionally stressed skins, impact stress, shear strength, and flexural strength may be more important than tensile or compressive strength. Thus, we should not confine ourselves to one resin system in building a sailplane, but instead we should selectively use different resin/glass systems where they are most ideal.

Fatigue

A difficult, yet essential, consideration in the design of composite systems is structural fatigue. Fatigue strength of FRP structures is probably the least understood characteristic of fiber reinforced composites. Many different theories on fatigue in reinforced plastics have been proposed, but few are acknowledged to be widely accepted.

Fiber reinforced epoxy systems do exhibit fatigue under stress. Structural damage and strength reduction can occur during the initial application of stress. The most common type of failure is delamination of the composite at the resin/fiber interface. If stress is applied to initiate an interfacial crack, the crack will continue to propagate until a cross-ply fiber or resin inclusion is reached, at which point the crack may terminate.

The frequency of interfacial bond failure can be reduced by:

1. increasing the matrix-fiber bond efficiency;
2. using more ductile resin matrices;
3. introducing crack terminating additives into the resin;
4. reducing the applied stress, or increasing the design load of the composite.

Table 8.

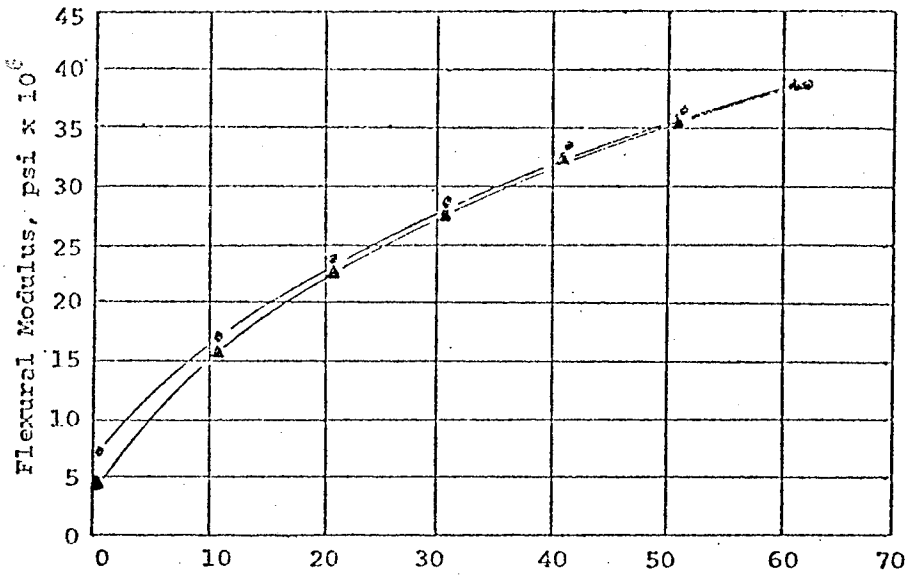
Unidirectional glass/epoxy composites - typical properties

RESIN	Laromin 260 (38) Epikote 162 (100)	Epon 826 (90) BGE (9) A-186 (1) TETA (12.5)	Epon 826 (90) BGE (9) A-186 (1) TETA (12.5)	Epon 826 (90) BGE (9) A-186 (1) TETA (12.5)	Epon 826 (90) BGE (9) A-186 (1) TETA (12.5)
GLASS	OCF 836	OCF 836	OCF 830	OCF 830	OCF 830
% GLASS (wt)	70	70	73	80	91
MECHANICAL PROPERTIES TENSILE STRENGTH psi	93,000	103,229	99,000	110,722	98,200
FLEXURAL STRENGTH psi	89,933	124,000	106,333	115,000	112,900
MODULUS OF ELASTICITY psi x 10^6	3.48	4.76	3.9	4.75	5.3

Care: 7 days at room temperature, (23°), hand lay-up, no pressure.

Figure 1.

Mixed fiber composites



Volume % high modulus fiber

Total fiber volume % constant (70%)

● S Glass fiber

▲ E Glass fiber

Table 9.

Properties - epoxy/181 style fabric laminates

LAMINATE NO.	GLASS wt%	TENSILE psi	FLEX STR psi	FLEX MOD	IMP STR ft-lb/in	HDT @264 psi	POT LIFE min.
L101	57	36,264	46,500	2.55×10^6	12.1	470	30-40
L102	55	35,309	48,000	2.46×10^6	12.4	490	30-40
L103	55	34,650	34,000	1.6×10^6	16.3	510	180-240
L104	51	32,609	43,000	2.05×10^6	11.2	490	30-40
L105	57	35,139	54,000	2.15×10^6	10.1	400	30
L106	60	35,600	38,000	1.9×10^6	11.1	400	180

RESIN COMPOSITION

L101 EPON 826(74) Genamide 2000(26)
L102 EPON 826(75) Genamide 2000(25)
L103 EPON 826(69) VERSAMIDE 140(25) BGE(6)
L104 EPON 826(64) GENAMIDE 2000(30) BGE(6)
L105 EPON 826(100) TETA(13)
L106 EPON 826(100) LANCAST A (30)

A commonly employed technique for improving the resin/fiber bond is to coat the fiber with a silane coupling agent. In theory the silane molecule should be applied in a continuous monomolecular layer to the fiber. The silane molecules are bifunctional and polar. They orient themselves along the fiber in such a manner that one end of the silane molecule is bonded to the fiber and the other end is chemically reacted with the resin. Silane molecules are made with specific reactive functional groups for use with different types of resins. The effect of the silane additive is shown in the data in Table 10. Glass fabrics are commercially available with specific silane agents on them. Further developments in silane technology will undoubtedly increase the strength of FRP composites. Silanes may promote a more continuous interfacial bond, improving the fatigue life of FRP composites because a continuous bond allows an applied stress to be evenly distributed to a reinforcing fiber. Discontinuous bonds promote high local stresses at resin/fiber/void interfaces, and delaminations are easily initiated under such conditions.

The use of matrices of high ductility inhibits the propagation of cracks. Resins which can elongate and deform under load are less susceptible to fatigue than brittle resins. Resin ductility allows high specific strains in the matrix to be dissipated and reduced through matrix deformation. However, high ductility is not desirable in structural aircraft composites because high modulus of elasticity is often the primary design factor.

The use of highly ductile resins is not a satisfatory solution for structural fatigue problems. Ideally, in FRP composites resin elongation should exceed the elongation of the fiber, but once this is achieved, increasing the resin elongation still further will continue to reduce the modulus of the composite.

The incorportaion of fine rubber particles into the resin matrix has been shown to improve effectively the impact strength and the fatigue life of the thermoset FRP composites. Such an approach is especially effective in polyester resin systems, but good results have also been attained in epoxies.

MacGarry has reported substantial improvement in fracture resistance of DGEBA resins cured with DMP-30, (Shell Chemical) 2, 4, 6, -tri (dimethylamino-ethyl)phenol, or the tri(2-ethylhexonic acid) salt of DMP-30, when CTBN rubber is added to the resin. CTBN is a carboxyl terminated butadiene/acrylonitrile copolymer, which is liquid at room temperature. Figure 2 shows the effect of CTBN concentration on resin toughness. The effect of CTBN addition to epoxies is further demonstrated in Figure 3 where the crack density is plotted against flexural cycles in a 50 vol.%, 181 style fabric/epoxy laminate.

Table 10.

Effects of coupling agents on laminate strength

Silane	None	Volan A	Z-6020	Z-6040	Z-8-009
Flexural Strength, psi					
As molded	78,400	85,000	81,000	85,900	98,700
After 2 hour boil	59,000	62,200	64,000	79,500	94,500
Compressive Strength, psi					
As molded	52,600	52,000	46,000	53,200	53,200
After 2 hour boil	26,400	42,000	46,000	49,300	43,300

181 style glass fabric
DGEBA cured with m-PDA

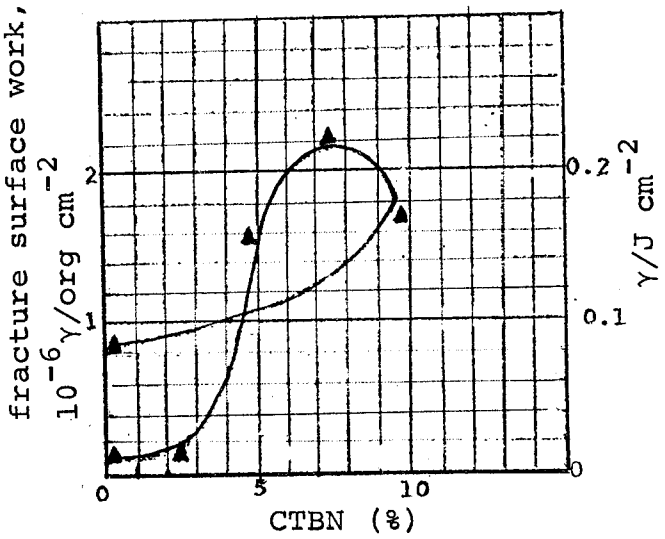
Table 11.

Axial fatigue properties

MATERIAL	DENSITY	ULT TENSILE STR. psi	FLEXURAL MODULUS psix 10^6	FATIGUE STRENGTH psi	SPECIFIC FATIGUE STRENGTH
Epoxy/Glass					
Unidirectional $\pm 5°$	0.065	139,000	5.3	36,000	554,000
Unidirectional	0.065	158,000	5.6	25,000	385,000
Cross-ply (50-50)	0.065	75,000	3.7	22,000	338,000
Woven 181 Fabric	0.065	50,000	3.3	15,500	238,000
Aluminum, 2024-T4	0.100	68,000	10.6	26,000	260,000

Figure 2.

Rubber particle/epoxy blends



Epon 828 epoxy resin cured with
5% curing agent D* DMP-30

*Shell Chemical Company

Figure 3.

Fatigue properties: rubber modified epoxy/glass composite

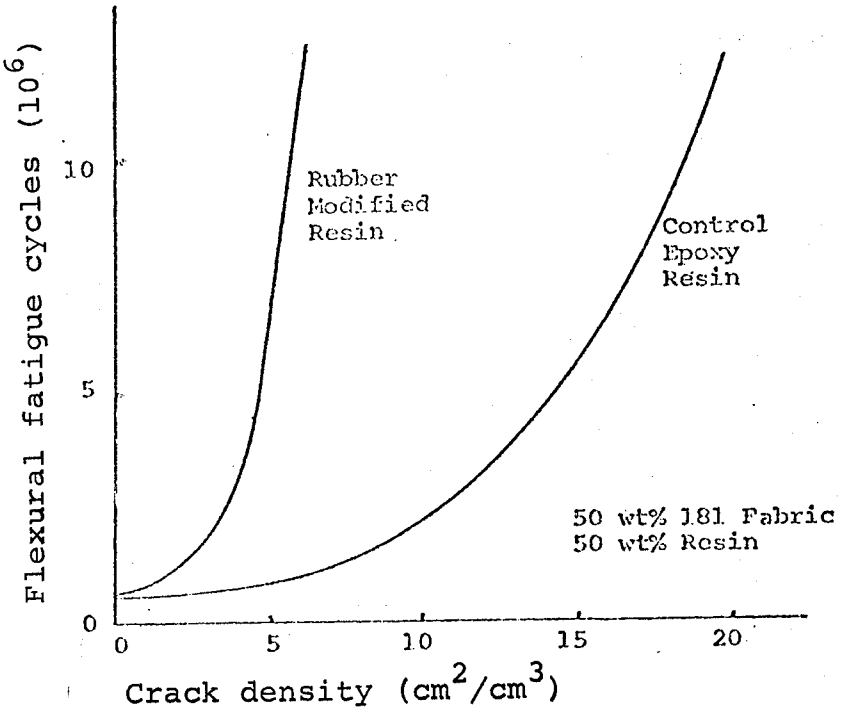


Figure 4.

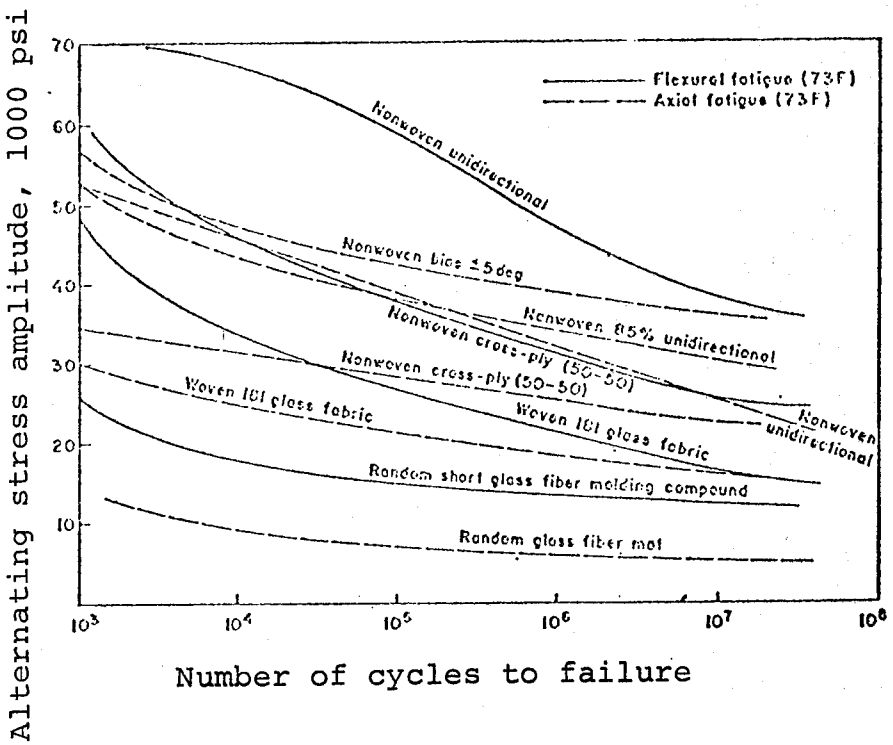


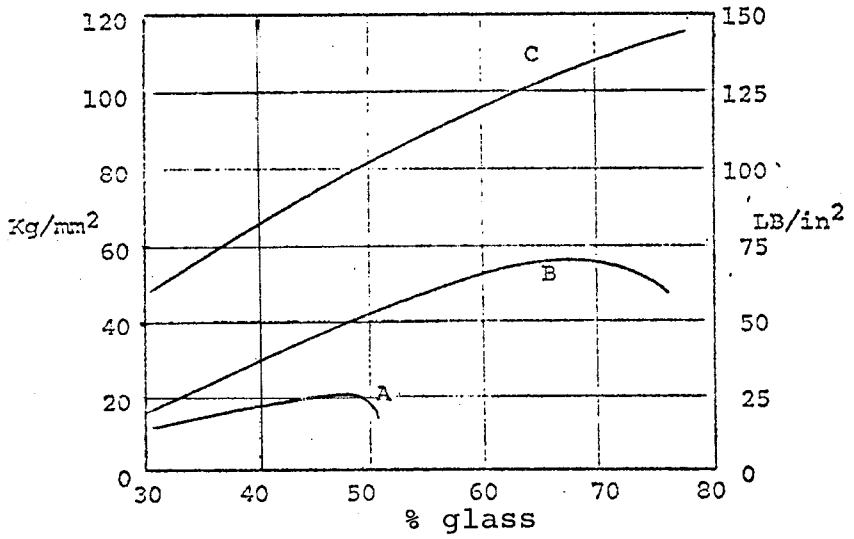
Table 12.

Flexural fatigue properties

MATERIAL	DENSITY lb/cu in	ULT.FLEX. STR psi	FLEXURAL MODULUS 10^6 psi	FATIGUE STRENGTH	SPECIFIC FATIGUE STRENGTH
Epoxy/Glass					
Unidirectional	0.065	165,000	5.3	36,000	554,000
Cross-ply (80-20)	0.065	150,000	5.0	33,000	508,000
Cross-ply (50-50)	0.065	120,000	3.5	25,000	385,000
Woven 181 Fabric	0.065	80,000	3.4	16,500	254,000
Sitka Spruce	0.016	9,000	1.2	2,700	169,000

Figure 5.

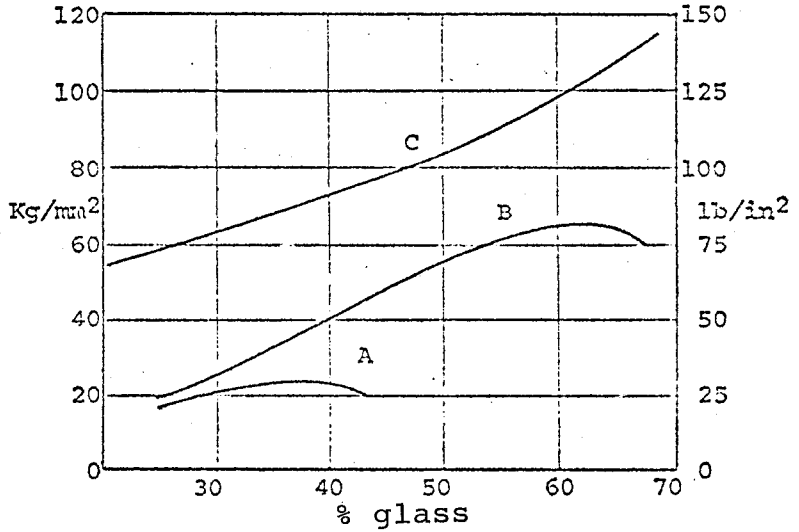
Tensile strength
vs glass content



A mat, B cloth, C roving

Figure 6.

Flexural strength
vs glass content



A mat, B cloth, C roving

Fatigue life data for FRP composites under uniform cyclical stress demonstrate predictable fatigue strength loss. Figure 4 illustrates fatigue strength properties of epoxy/glass laminates. The data was generated from constant amplitude stress cycling. It is much more difficult to predict fatigue strength or fatigue life from non-uniform, random application of stress.

Broutman and Sahu have presented a new theory to predict cumulative fatigue damage in fiber reinforced plastics. Their theory predicts the fatigue life of FRP from measuring the residual strength of a composite after a fractional life at a given stress level. Broutman and Sahu propose a modified Miner's Law to account for residual strength after the application of a two-stress level fatigue test. The results of this study show the cumulative affect of high/low stressing and low/high stressing are not predictable by linear damage theory.

Davis has generated fatigue property data on uni-directional, non-woven epoxy/glass composites, on bi-directional, non-woven composites, and on bi-directional woven composites. Tables 11 and 12 present the results of their study. The flexural fatigue data show that non-woven fiber reinforcement is superior to woven reinforcement when tested for resistance to fatigue. Woven materials are lower in fatigue resistance because the reinforcing fibers are bent in the cured composite and also because the fibers abrade themselves under cyclic loading. Non-woven composites offer fatigue resistance because the fibers are very straight in the cured laminate and because the fibers are surrounded by resin, which helps to protect and insulate them from other fibers. The flexural fatigue data was generated by cycling specimens under three-point loading. The axial fatigue data was derived from alternating cyclic loading in tensile and compression.

Conclusion

The potential applications for FRP composites in aircraft structures will expand as higher modulus reinforcing materials are available at lower cost. Improved composites can be fabricated from blends of glass and higher modulus fibers to yield greater performance at moderate cost. The fatigue properties of FRP, especially with non-woven reinforcement, are superior to most other engineering materials.

References and bibliography

J.H. Alexander et al.; A Study of Low Density High Modulus Filaments and Composites, General Technologies Corp., 1966, NASA CR-523.

Araldite Resins Data; Ciba-Geigy Corp. Ardsley, New York.

P.H. Bishop; An Improved Method for Predicting Properties of Fiber Composite Material, Royal Aircraft Establishment, AD 643-546, 1966.

L. Broutman; Failure Mechanisms for Filament Reinforced Plastics, 19th SPI Conference, 1964.

L. Broutman and S. Sahu; Progressive Damage of a Glass Reinforced Plastic During Fatigue, 24th SPI Conference, 1969.

J.W. Davis et al.; Fatigue Resistance of Reinforced Plastics, Materials in Design Engineering, Dec. 1964.

N.F. Dow; Applications and Optimizations of Structural Composites for Aircraft Wings, GE Missile and Space Div., AD 642-092, 1966.

N.F. Dow; Structural Efficiency of Composite Materials for Aircraft Applications, GE Missile and Space Div., AD 632-492, 1966.

The Engineers of Gibbs & Cox, Inc.; Marine Design Manual, McGraw Hill Book Co. Inc., New York, N.Y. 1960.

K.E. Hofer; An Investigation of the Fatigue and Creep Properties of Glass Reinforced Plastics for Primary Aircraft Structures, ITT Research Institute, AD 652-415, 1967.

P.M. Jenkinson; Compressive and Shear Properties of Polyester and Polymide Film Honeycomb Core, U.S. Forest Service AD 661-107, 1967.

Lee and Neville; Epoxy Resins, Their Applications and Technology, McGraw Hill Book Co. Inc., New York, N.Y. 1957.

McGarry and Fugiwara; Resin - Fiber Load Transfer in Reinforced Plastics, Modern Plastics, July 1968.

W.O. Statton; Recent Advantages in Polymeric Fibers, U. of Utah, 1972.

R.G. Spain; Graphite Reinforced Composites, AMFL TR-66-384, 1967.

Thermoset Reinforced Plastics Formulations, Celanese Resins Corp. Louisville, Kentucky.

FIBERGLASS REINFORCEMENT FOR SAILPLANES

by

Barry R. Elson
Owens-Corning Fiberglas Corporation
Toledo, Ohio

Introduction

This paper discusses glass fibers, how they are manufactured and their properties. The glass fibers of interest are most generally used as the reinforcement component of a composite system.

The composite system is fiberglass reinforced plastics or FRP. This system is a family of engineering materials. The performance of this material is dependent on and achieved by the selection and combinations of three components, resin type, glass reinforcement and processing technique. Resins are categorized into two main types, thermosets and thermoplastics. There are at least eight different thermoset resins in use today for producing FRP parts. For the strength required in sailplanes, epoxies are the usual choice. Thermoplastic resins currently being used in Fiberglas* reinforced plastic applications include polystyrene, nylon, ABS, polycarbonate, SAN, polypropylene, polyethylene, polysulfone and acetal. Versatility is a prime characteristic of plastics. The choice of resin determines such properties as chemical resistance, weatherability, electrical characteristics, thermal properties and, to some extent, appearance.

The second component of the FRP family of materials is the glass fiber. Its function is to increase these properties of the plastic resin:

- mechanical strength,
- resistance to impact,
- stiffness,
- dimensional stability.

The strength properties of FRP parts are a product of the form, arrangement and amount of glass used. Glass fibers reinforce plastics much as steel reinforces concrete and may be directional to resist specific loads or patterned randomly for multi-directional strengths. The usual forms of fiberglas used to reinforce plastics are fabric, roving, woven roving, mat, chopped strands and milled fibers. Within practical limits, the strength properties of FRP composites increase in proportion to the volume of glass used (Figure 1). The lowest glass content is achieved with randomly oriented chopped strands. Increasing glass contents can be achieved

*Trademark of Owens-Corning Fiberglas Corporation.

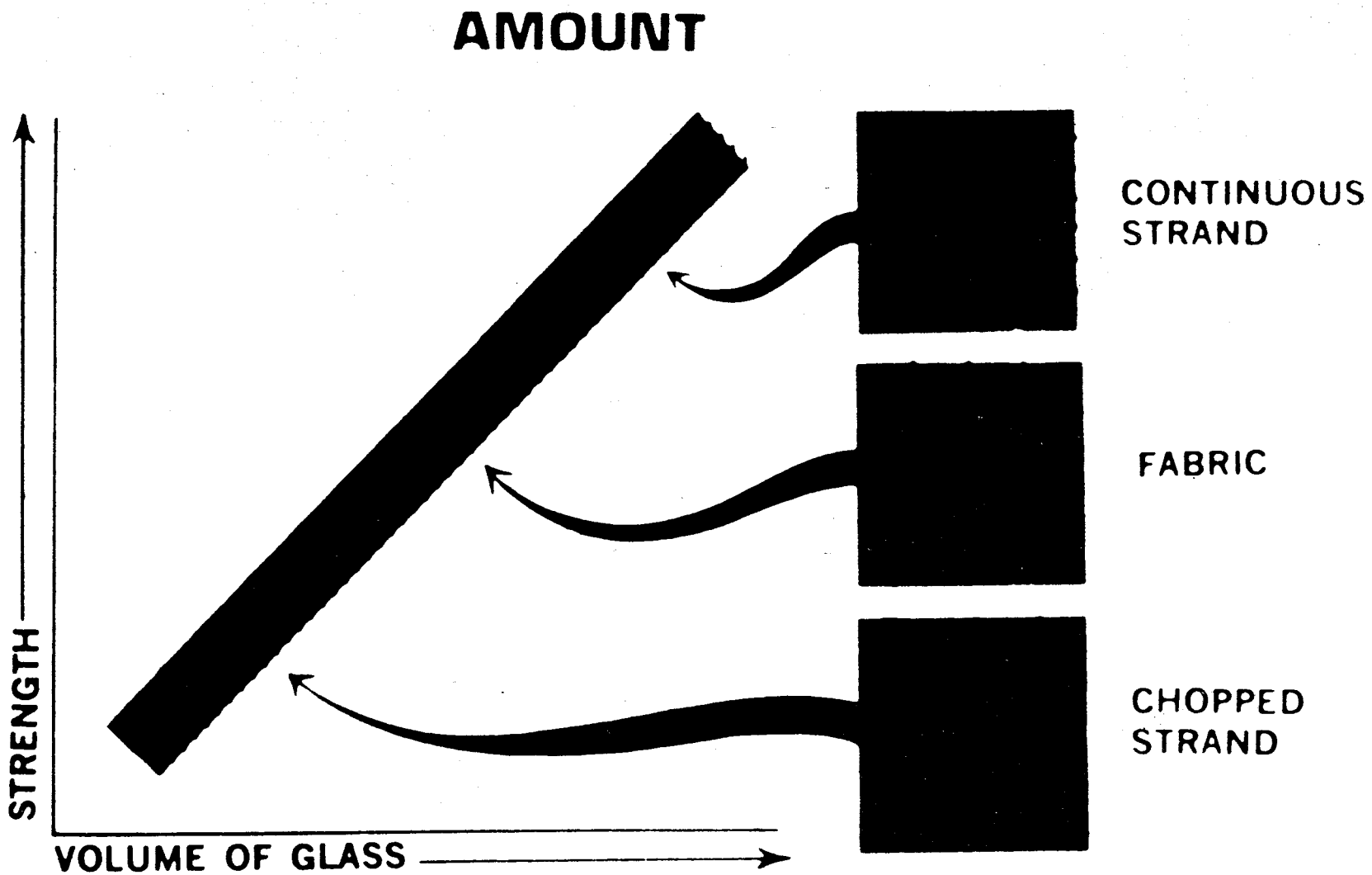

AMOUNT
STRENGTH
VOLUME OF GLASS
CONTINUOUS STRAND
FABRIC
CHOPPED STRAND

Figure 1.

by more orientation from biaxially oriented fabrics to totally unidirectional continuous strand rovings such as those used in the construction of some sailplane spars.

The third component of the FRP family is the manufacturing process. These range from simple hand lay-up methods, through intermediate techniques such as cold molding to fully automated methods such as match metal die molding. The final composite properties are dependent upon all three system components - the resin, the glass and the process.

Glass fibers

Glass is one of the oldest manufactured materials used by man today, dating back as far as 2500 B.C. It is most familiar to the general public in the various forms and shapes of bulk glass - windows, drinking glasses, dishes and lenses. Bulk glass is not thought of as a structural material even though it is very strong in compression because its tensile strength is not as great as other structural materials. It is primarily brittle and subject to easy fracture resulting from minute surface flaws. It does possess extremely high chemical durability and weatherability. Prior to 1938, glass in fiber form was only a laboratory curiosity. Today glass in fiber form is being successfully used as the strength-giving material in many composite structures.

The commonly accepted American definition of glass is that it is an inorganic product of fusion which has cooled to a rigid condition without crystallizing. Chemical, electrical, physical and mechanical properties of glass are controlled largely by composition. It is possible to draw many different glass compositions into fibers. Depending upon the draw media, the resultant fiber will be either a short, non-continuous fiber called a staple fiber, or a long, continuous fiber. This discussion will be concerned only with the continuous type.

The properties of glass fibers can be better appreciated if you have some knowledge of the process by which they are manufactured (Fig. 2). A glass batch is compounded and mixed with great care to ensure consistent glass composition. The incoming ingredients are checked against quality control standards. The composition is important not only from the standpoint of the properties of the glass fibers, but also from the economic efficiency with which they can be produced, which then affects their ultimate price.

Table 1 compares several glass compositions. The standard fiberglas composition is known as E or electrical grade glass. It is an alumina borosilicate glass and is used as the standard reinforcing medium for such diverse products as aircraft wing-to-body fairings, electrical high pressure laminates and

FIBERGLAS MANUFACTURING PROCESS

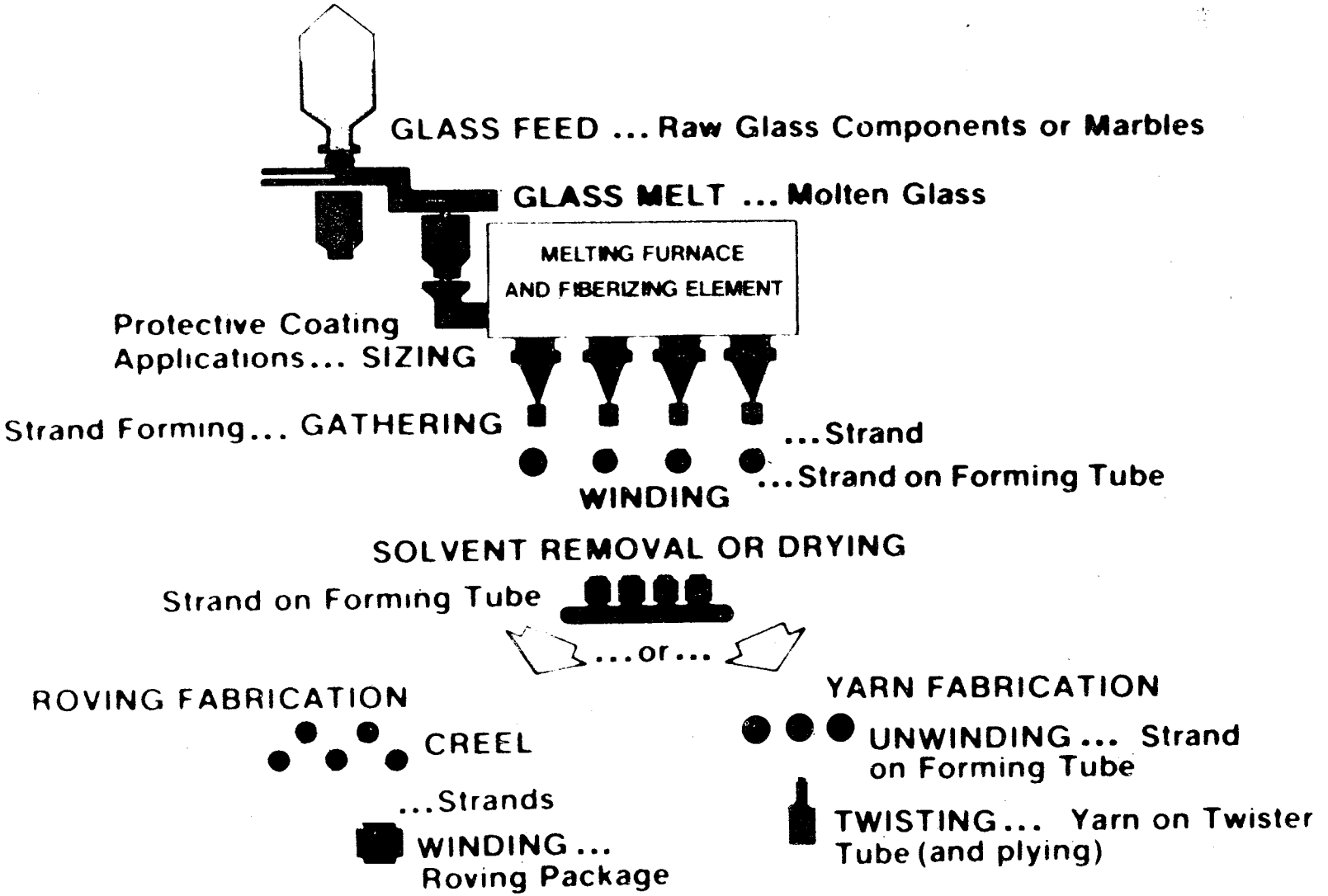


Figure 2.

Table 1.

COMPARATIVE GLASS COMPOSITIONS

(by weight)

	E glass	S & S-2 glass	C glass
SiO_2	53%	64%	65%
Al_2O_3	13%	25%	4%
CaO	19%	-	14%
MgO	3%	10%	3%
B_2O_3	10%	-	6%
Na_2O	-	-	8%
Others	2%	1%	-

Table 2.

PROPERTIES OF GLASS FIBERS

	E	S&S-2	C
Specific Gravity, g/cc	2.54	2.49	2.49
Virgin Tensile Strength, psi	500M	665M	480M
Modulus of Elasticity, psi	10.5M	12.6MM	10.0MM
Elongation, %	4.8	5.4	4.8
Coefficient of Expansion, in/in °F	2.8	3.1	4.0
Dielectric Constant, 1 MHz	6.33	5.34	-

Table 3.

TYPICAL ROVING

FILAMENT DIAMETERS

G	0.00035 - 0.000399 inches
K	0.00050 - 0.000549 inches
M	0.00060 - 0.000649 inches

Table 4.

ROVING STRAND TENSILE AND

SHORT BEAM SHEAR STRENGTHS

(psi)

	E glass	S-2 glass	S glass
Virgin Filament Strength	500M	665M	665M
Roving Strand Strength	280M-350M	530M	550M
Short Beam Shear Strength	6M-8M	8M-10M	10M-12M

various spacecraft components. S glass is a higher tensile strength material that also possesses superior modulus values, higher temperature resistance and a lower density. It is used in high performance applications such as rocket motor cases and other aerospace applications where high strength-to-weight ratios are important. C glass stands for chemical resistant glass. E and S glass are also resistant to most chemicals but C glass is specifically designed for this purpose. Its reinforcing properties are generally lower than E glass or S glass.

Table 2 shows the comparative virgin fiber properties of E glass, S glass, S-2 glass, which is a more economical version of S glass, and C glass. The virgin fiber is that glass tested immediately after leaving the bushing or fiberizing device and before any sizing is applied. The glass composition we saw earlier controls the modulus values but the processing conditions, particularly thermal history, including dwell times at various temperatures, control tensile strength.

The batch is introduced into a melting furnace or tank where it becomes molten glass. The batch can be melted directly or first made into marbles and then remelted. The molten glass then flows from the tank or furnace into the fiberizing device which is called a bushing. This is made out of a platinum alloy to ensure even heat distribution which in turn aids in maintaining uniform filament diameters. The older standard bushings have 204 holes and produce simultaneously 204 individual glass filaments.

The 204 fibers are brought down past a sizing applicator. A size is a three-constituent chemical coating applied to each individual fiber to protect it during further processing, and to couple the glass chemically to the matrix resin. Below the sizing applicator the filaments are gathered together into a bundle called a strand by means of a gathering shoe. The strand then passes down to a winder where it is wound onto a forming tube, which is also referred to as a forming cake. The melting temperature of the E glass bushing is around 2200°F. S glass is higher. A few inches below the bushing the temperature of the filament has dropped to around 500°F. This rapid quenching of the glass, which results from its being wound through still air at speeds over 6,000 feet per minute, is one reason for its high tensile strength.

When the cake has been built up to desired size or weight, the forming tube with the cake is removed from the winder and dried in an oven to remove the solvent associated with the size application. The forming cake is then further processed into roving or yarn.

Roving

A roving consists of a number of "ends" or strands of glass gathered together without purposely induced twist, into

a flat ribbon-like strand. Each strand or end has a number of filaments in it equal to the number of holes in the bushing from which it was pulled. Thus a 20 end roving made from a 204 hole bushing has 20 x 204 or 4080 individual filaments. Conventional rovings normally come in 12, 20, 30, 60 or 120 ends. As forming technology advances, the 204 hole bushing is being replaced by larger bushings with 408 and 816 holes. More recently a new concept in roving, called Type 30, has been introduced. It has only a single end containing in excess of 2,000 filaments. Rovings are primarily used in the filament winding process and for unidirectional laminates. The nomenclature of a roving contains a designation for the glass composition, the type of fiber, the filament diameter, the yards per pound, or yield, of the roving, and a number designating the sizing. Thus, a typical roving might be called out as:

Glass	Type Fiber	Filament	Yield	Sizing
E	C	G 135	225	801

This is an E glass, continuous filament with a G diameter and has 13,500 yards of glass per pound of the basic forming strand and 225 yards of glass per pound of the finished roving. The chemical sizing is designated as 801. The 13,500 yards per pound is arrived at by taking the G 135 strand designation and adding two zeros. The same principle would apply if the basic forming strand were a G 68 with 6,800 yards per pound. The 13,500 is then divided by the 225 yield to determine that you have a 60 end roving. Conversely, if you know you have a 60 end roving you can arrive at the 225 yards per pound figure.

In recent years, economic reasons have forced an increase in filament diameters from the older G filament to larger K and M diameters. Table 3 shows the decimal equivalents of the letter designations.

The sizing of a roving product is a three-constituent chemical composition consisting of a lubricant to help reduce abrasion as the strand is processed over guide eyes and tension bars; a film former to give the fiber additional protection and impart strand integrity; and a coupling agent such as a silane to chemically bond the glass fibers to the matrix resin.

We saw earlier the properties of the virgin fiber before any sizing has been applied and before the strand has been processed into a roving ball (Table 4). In roving form the virgin filament tensile strength of E glass reduces from 500,000 psi to 280,000 - 350,000 psi depending upon the end count and the particular polyester or epoxy sizing used. The virgin tensile of epoxy compatible S glass is reduced only from 665,000 psi to about 550,000 psi. We guarantee a minimum individual package value of 530,000 psi. These values are measured by ASTM 2343-65T.

The shear strengths of epoxy rovings as measured by the NOL short beam shear test generally run around 6,000 - 8,000 psi for commercial E glass sizings and 10,000 - 12,000 psi for S glass. These results are obtained on a 1/4" thick, 1/4" wide, 3/4" chord length ring, wound in air, with about 2% voids and a bisphenol A diepoxide and MMA resins system. Higher values close to the ultimate can be achieved with vacuum winding. Shear values for polyester rings are usually not specified.

Yarn

Another form into which strand from a forming cake is processed is yarn. Yarn may be defined as a twisted strand or an assemblage of twisted and plied strands forming a continuous structure suitable for use in weaving textile materials. The system for identifying fiberglas textile yarns is similar to that of roving. A typical example is ECG 150 2/2, 3.8S, where the letters describe the strand as we saw in roving, (see Table 5). The second number, which looks like a fraction, indicates the number of strands used to construct the yarn. The first digit indicates the number of forming packages or single strands twisted and the second digit the number of twisted strands that are then plied together. The product of the two is the number of ends of yarn on the package or bobbin. The 3.8S refers to 3.8 Turns Per Inch in the S direction. Common yarn filament diameters are B, DE, E and G. Table 6 shows their decimal equivalents.

The sizing on yarn, as opposed to that on roving, usually has no coupling agent. It is merely a starch-oil base to serve as a lubricant during the weaving operation. After weaving, the fabric is usually heat cleaned and a variety of proprietary finishes can be applied by the weaver. Volan A is one usually used. Some yarns do have a direct compatible size applied at the bushing as is done with roving. The fabrics woven from these yarns do not need to be heat cleaned and thus, generally, can have somewhat higher physical properties.

Fabrics

Fabrics and tapes are woven by a weaver from yarns. They are available in a large variety of widths, constructions and weights. The basic weave patterns available commercially are plain, leno and satin. Table 7 describes the construction and properties of some of the common fabrics. The plain weave is the most stable, gives the best cover, and is best suited to flat laminates. It has the lowest strength in a composite. The leno weave has better drape characteristics

Table 5.

YARN NOMENCLATURE

Glass	Type Fiber	Diameter	Strand Yield	Ends	Twist	Sizing
E	C	G	150	2/2	3.85	636

Table 6.

TYPICAL YARN FILAMENT DIAMETERS

B	0.00012 inches
DE	0.00025 inches
E	0.00029 inches
G	0.00037 inches

Table 7.

DOMESTIC FABRIC CHARACTERISTICS

Style	W x F	Yarn W x F	Thickness (inches)	Weight (oz/yd^2)	Tensile W x F (pounds)
120	60x58	D450 1/2 D450 1/2	0.0040	3.16	135 x 125
143	49x30	E225 3/2 D450 1/2	0.0090	8.78	650 x 60
181	57x54	E225 1/3 E225 1/3	0.0090	8.90	350 x 340
1581	57x54	ECG 150 1/2 ECG 150 1/2	0.0090	9.00	375 x 335
7781	57x54	DE75 1/0 DE75 1/0	0.0090	8.95	590 x 396

Table 8.

AVERAGE PROPERTIES OF EPOXY LAMINATES REINFORCED WITH 1581 FABRIC AND VOLAN A FINISH

	Strength (psi)		Modulus (psi x 10^6)	
Property	S glass	E glass	S glass	E glass
Tensile	74,700	55,800	3.29	3.16
Compressive	58,800	59,200	4.67	4.22

and higher composite properties than the plain weave. The satin weave is the most pliable and drapeable and gives the highest strength properties of the three types of basic weaves. Typical fabric styles used in reinforced plastic laminates are 181, 1581 and 7781, which have approximately equal strength in the warp and fill directions; 143, which is essentially a unidirectional fabric with the greatest strength in the warp direction and 34 style fabric with most of its strength in the fill direction. These fabrics have the satin weave.

There are several variables within a glass yarn system which will control the physical and mechanical properties of a glass fiber reinforced plastic fabric laminate other than the type of weave. These variables are the glass composition; the filament diameter; the number of the filaments in a yarn strand; the twist and ply of the yarn; the finish applied to the yarn or fabric.

Table 8 illustrates the effect of composition. These test panels were reinforced with 14 plies of 1581 fabric, woven from ECG 150 1/2 3.8S and SCG 150 1/2 3.8S yarns, and fabricated with an Epon 828 and CL hardener epoxy resin system. The S glass generally shows superior properties. In addition to building up solid fabric laminates, fabrics are also used as skins over various honeycomb materials. This yields a lightweight structure which is thick and thus possesses a higher section modulus. This enables the glass to carry higher tensile loads without buckling before its yield point.

Glass fibers are commercially available in a variety of filament diameters as was previously seen. Generally speaking, the smaller the diameter the more flexible the yarn. Table 9 illustrates the effect of the filament diameter. These yarns have basically the same weight of glass, only the yarn diameters were changed. The yarn which did not require plying reported, generally, the best properties. The twist and ply of a yarn will have an effect on the mechanical properties of a laminate. When a yarn is just twisted, there are economic and property advantages over twisting and plying the yarn. The reason for the property difference has never been fully understood, although the parallel alignment of filaments in the non-plied yarn exposes more surface area for improved glass-to-resin bonding. The effect of each of the variables is very difficult to separate.

To this point, we have illustrated the differences in mechanical properties through the fabric weave, glass composition and yarn construction. There are also certain advantages to be gained through the selection of the finish applied to the fabric. As an example, Table 10 shows S glass with Volan A versus S glass with 901 direct sizing and E glass with Volan A versus E glass with UM 550 finish (Table 11). The finish applied to the fabric has a very definite effect on the properties achievable in the laminate. Most

Table 9.

AVERAGE PROPERTIES OF EPOXY LAMINATES REINFORCED WITH 181 FABRIC VOLAN A FINISH E GLASS

Property	Strength (psi)			Modulus (psi x 10^6)		
	ECE 225 1/3 Yarns	ECG 150 1/3 Yarns	ECDE 75 1/0 Yarns	ECE 225 1/3 Yarns	ECG 150 1/3 Yarns	ECDE 75 1/0 Yarns
Tensile	53,400	51,500	56,100	2.63	2.77	2.70
Compressive	47,500	49,900	44,100	4.25	4.05	4.94
Flexural	80,500	80,800	88,100	3.84	4.15	4.03
Interlaminar Shear	2,770	2,780	2,790	-	-	-

Table 10.

AVERAGE PROPERTIES OF EPOXY LAMINATES

REINFORCED WITH 181 FABRIC S GLASS

	Strength (psi)		Modulus (psi x 10^6)	
Property	Volan A	901	Volan A	901
Tensile	74,700	97,700	3.29	3.15
Compressive	58,800	67,400	4.67	4.60
Interlaminar Shear	2,405	3,040	-	-

Table 11.

AVERAGE PROPERTIES OF EPOXY LAMINATES

REINFORCED WITH 181 FABRIC E GLASS

	Strength (psi)		Modulus (psi x 10^6)	
Property	Volan A	UM 550	Volan A	UM 550
Tensile	56,100	69,800	2.70	2.91
Compressive	44,100	57,600	4.94	5.13
Flexural	88,100	94,800	4.03	4.41
Interlaminar Shear	2,790	2,870	-	-

Table 12.

EUROPEAN INTERGLAS FABRIC STYLES

Style	Use	Warp Yarn	Fill Yarn
91-100	Overlay finish on wings	EC9 68 (ECG 75 1/2)	EC9 136 (ECG 37 1/2)
91-125	Fuselage skin	EC9 34 x 2 (ECG 150 1/2)	EC5 11/2 (ECD 450 1/2)
92-110	Torque shell on wings and fuselage	EC9 68 (ECG 75 1/2)	EC9 68 (ECG 75 1/2)
92-140	Reinforcement of spars and bulkheads	EC9 68 (ECG 75 1/2)	EC9 136 x 4 (ECG 37 1/4)
92-146	Spars	EC9 136 (ECG 37 1/2)	EC9 68 (ECG 75 1/2)

finishes, like most sizings, are based on silane type chemicals, which are compatible with the various resin systems.

The glass fiber sailplane has been developed in European countries, primarily in Germany. The fabric styles used in Europe are shown in Table 12. Unfortunately, with the exception of domestic style number 1557 which corresponds fairly closely to the Interglass number 91-125, there are no standard domestic equivalent fabrics. However, any of the major U.S. weavers have the capability of making equivalent fabrics.

Conclusions

In recent years, the combined efforts of the glass fiber producers and the weavers have led to developments in fabric reinforcements, as well as in roving materials, which have opened new potentials for composite materials. New glass compositions, such as S glass, to improve mechanical, electrical and chemical properties have been developed to advance the state-of-the-art. Improvements in fabric design, weaving technology and finishing technology have increased composite design limitations. It should be remembered that glass fiber reinforced plastics form a family of engineering materials. As such, the key variables to consider are

1. the type of glass with all its associated characteristics such as composition, form, filament diameter and sizing;
2. the resin system; and
3. the process such as lay up, vacuum bagging or matched die molding.

Although there are a number of variables to be considered, their proper choice can pay off in a composite structure with definite performance advantages.

INSTABILITY PATTERNS AT THE HEAD OF A COLD OUTFLOW

by

John E. Simpson
Department of Geophysics
University of Reading
England

Notation

U	Velocity of front of gravity current
ρ	Density of ambient fluid
$\Delta\rho$	Increase of density in gravity current
g	Acceleration due to gravity
d	Height of head of gravity current
H	Total depth of liquid
T	Absolute temperature
$\bar{b}$	Mean width of lobes
ν	Kinematic viscosity (molecular)
h	Height of nose of gravity current front
K_m	Eddy viscosity
H'	Depth of convective layer
s	Spacing between cusps

Introduction

In the sea-breeze convergence zone a front may become progressively sharper during the day. Eventually we may have a gravity current of cool, dense air advancing inland until brought to rest by friction. Similar gravity currents, often much more intense, occur as cold outflows from thunderstorms. Features of such meso-scale cold fronts are of interest to glider pilots.

Gravity currents have been modelled experimentally in the laboratory using gases, but are much more conveniently studied with water flows, using dissolved salt to provide controlled density differences. Useful results can be obtained, even qualitatively, from such hydrodynamical models, as the model may lead to better theoretical methods. Quantitative results can also be obtained, but sometimes only one feature at a time can be paralleled.

Lift

If we create a model gravity current by releasing a lockfull of dyed saline from one end of a perspex tank of

water, we obtain a flow with a clearly marked front. We can see that the surface is irregular and continually changing, but as an overall average the front of the liquid moves forward in a two-dimensional wedge of roughly elliptical cross section. A very similar shape appears in the atmosphere.

In an "ideal fluid", i.e., one with no viscosity, the flow close to a solid half-elliptical body was calculated by Defant [1], and the vertical speeds from the translation of such a cylinder are shown in Fig. 1.

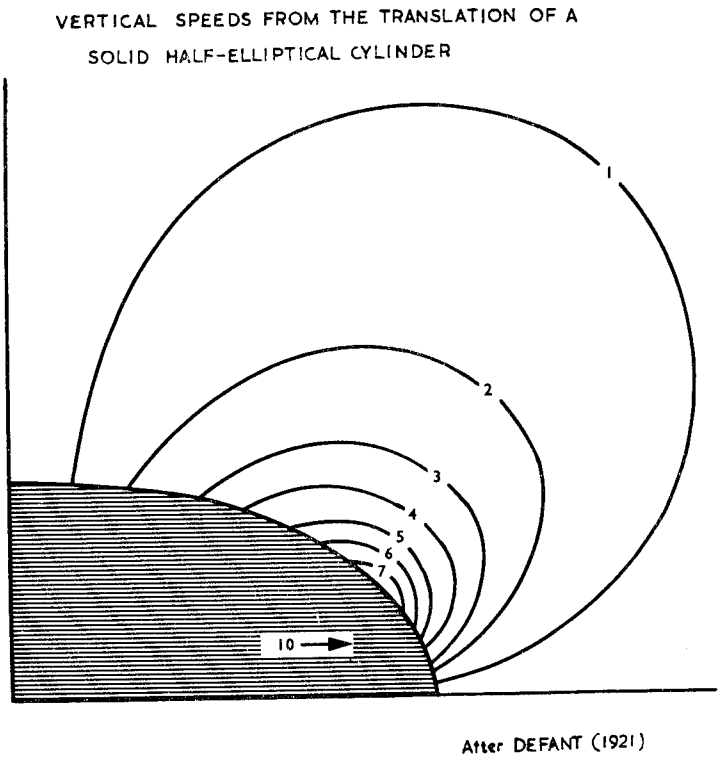


Fig. 1.

Experimental measurements of the upcurrent field were made in water tanks, using streak photography. From a 1/4 s exposure of aluminium particles, an upcurrent field can be plotted, and is very similar to the calculated results.

If we wish to scale this up to the atmosphere; neglecting any effects of either surface tension or viscosity, then the flow pattern is a function of three non-dimensional ratios:

$$\frac{U}{\left[\frac{\Delta\rho}{\rho}\, gd\right]^{1/2}}, \quad \frac{d}{H}, \quad \frac{\Delta\rho}{\rho}.$$

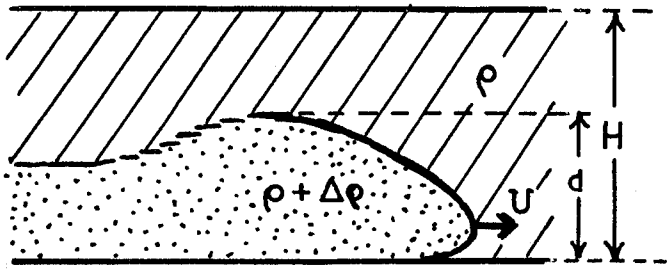


Fig. 2.

Both in the tanks and in sea-breeze fronts, the value of d/H is about 1/2; $\Delta\rho/\rho$ in the tank corresponds to $\Delta T/T$ in the atmosphere, in this case 1% or 3°C.

The important first ratio is the internal Froude number, relating inertia to buoyancy. Its value in the larger and faster tank models, where viscosity effects have become relatively small, approaches a constant value of about 0.7. In sea-breeze fronts at Lasham it has been found to be slightly less, approximately 0.6, (Simpson, [2]) but in thunderstorm outflows in the USA a value of 0.72 applies.

Thus there is good justification for scaling up the upcurrent field model to atmospheric size, and such results have been confirmed by soaring flights at cloudless sea-breeze fronts.

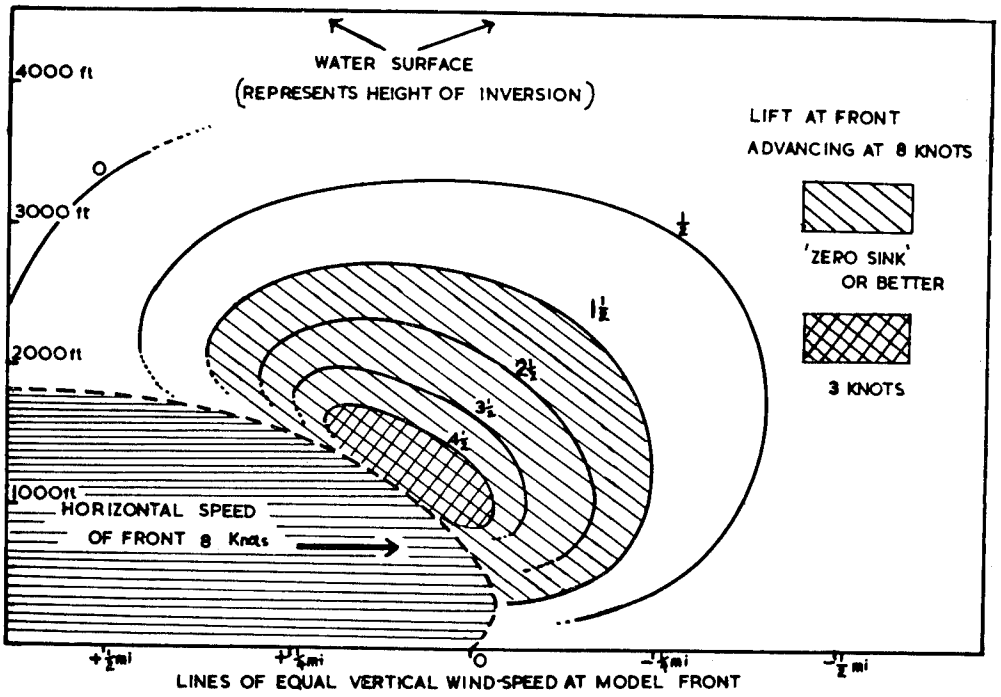


Fig. 3

Profiles of fronts

This "standard profile" is greatly modified when the front moves into an opposing wind. In the tank, as an opposing flow increases, the slope of the front becomes less

steep, until when the opposing wind brings the front to rest, the profile becomes approximately a straight line, with a slope of about 30°. Sea-breeze fronts marked with smoke haze show a similar effect in southern England.

Perturbations of the profile

In practice the profile of the leading edge is by no means smooth and steady. It advances in fits and starts and is divided into a complex shifting pattern of lobes and clefts at an overhanging nose, with billows forming further back above the head.

Three distinct types of perturbation of the smooth flow can be classified as (A) Lobes-and-clefts; (B) Billows; (C) Cusps; as shown in Fig. 4.

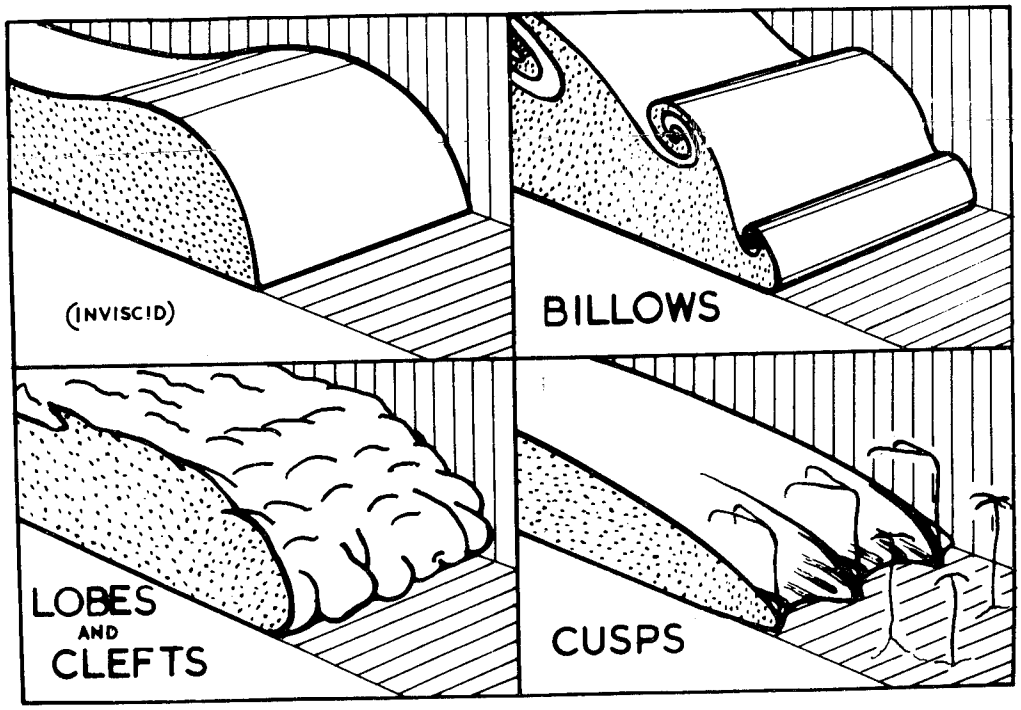
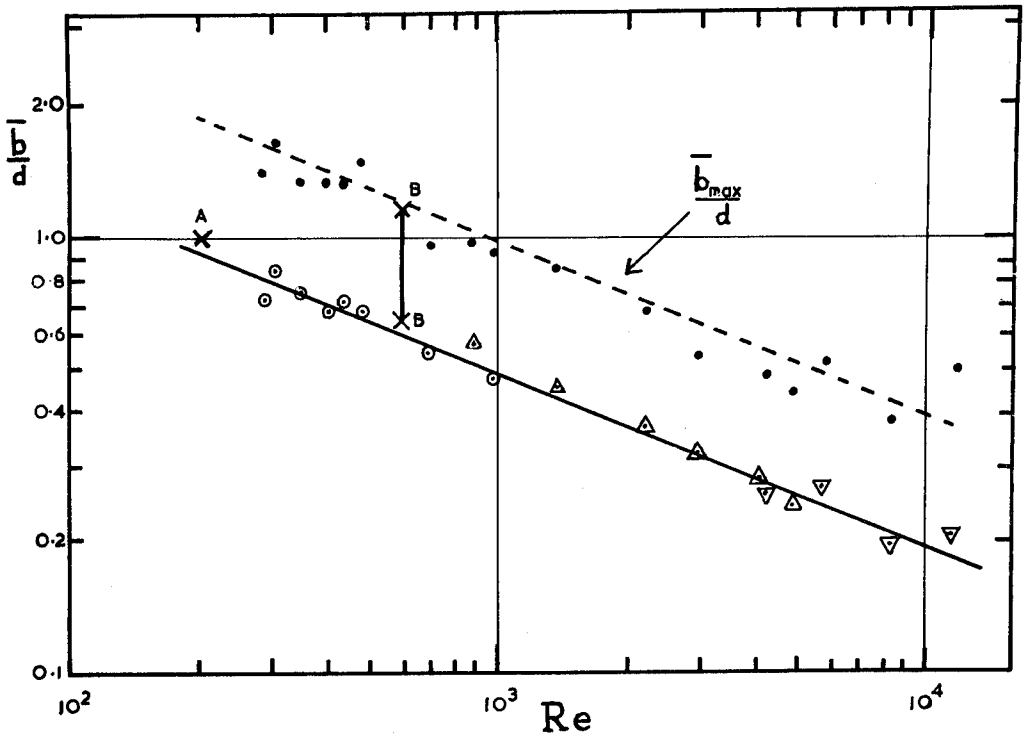


Fig. 4

Lobes and clefts

We have shown in a series of laboratory experiments, (Simpson, [3]) that this pattern is due to over-running of less dense fluid, caused by friction at the floor. In two series of experiments it was found possible to suppress the formation of this lobe-and-cleft pattern. Firstly suppression was achieved by moving the floor in the direction of the flow and thus reducing the stresses at the bottom of the liquid. Secondly when the ambient liquid near the floor was replaced by a heavier liquid, thus preventing any over-running of less dense liquid, the pattern was again suppressed.

By measuring the mean cleft-spacing, $\bar{b}$, through a range of Reynolds number from 300 to 10,000 it was possible to establish an empirical relationship $\bar{b}/d = 7.4 \times (Re)^{-0.4}$. Where $Re = Ud/\nu$. $\bar{b}_{max}$ is the mean breakdown size of the lobes and is about 2 x $\bar{b}$.



Dimensionless lobe-size. Fig. 5.

A relationship was also determined for the dimensionless nose height, $h/d = 0.61\ Re^{-0.23}$, over the same range of Re.

Many photographs have been published of atmospheric gravity currents showing a shape like "folded curtains", but only few actual measurements of such lobes and clefts are available. If we assume the lobe-size relationship found in the tank models applies to the atmosphere, we can use the few actual measurements of atmospheric lobe sizes to examine the value deduced for the viscosity.

However, in these atmospheric flows it is unrealistic to consider Re based on molecular viscosity in the air. We must match the Reynolds number of the laminar flow in the water tank model with that based on K_m, the turbulent eddy viscosity in the atmosphere.

In one example of a sea-breeze front, the lobe width was estimated as 1 km, roughly equal to the depth of the flow, i.e., $b/d = 1$. Here $U = 2\ m\ s^{-1}$, $d = 1000$ m, and if we take the value of Re from the graph corresponding to this size to be 200, $Re_K = 200 = (2 \times 1000)/K_m$, giving $K_m = 10\ m^2\ s^{-1}$. [A].

Lawson [4] measured lobes on a haboob at Khartoum, [B-B], obtaining a value of b/d between 0.66 and 1.16. For this haboob, U = 5 m s^{-1}, d = 1200 m, so from the graph Re is about 600, leading to the same value of 10 m^2 s^{-1} for K_m.

The value of viscosity we are seeking is in the bottom layer, in the over-run fluid through a depth of about d/10. In the atmosphere this is about 100 metres. In these conditions an averaged value of 10 m^2 s^{-1} seems a reasonable one. This was the value used in discussion by the following authors: Abe [5], Faller [6] and Kuettner [7].

Billows

While investigating lobe structure with a narrow slit of light parallel to the direction of the flow in the tank occasional well-marked series of billows were detected. Normally these billows are only detectable by using such special techniques, but in the experiments described above in which the lobe-and-cleft structure had been suppressed similar billows were seen to extend at times right across the tank as in the sketch in Fig. 4.

These have the appearance of Kelvin-Helmholtz billows, and measurements so far suggest that the wavelength is about the expected 3 1/2 times the amplitude. From reports of glider pilots forced to the ground a mile or two behind a sea-breeze front, and from reported accidents to aeroplanes at thunderstorm squall-lines it seems probable that such billows exist in the atmosphere.

Radar echoes from sea-breeze fronts, (Atlas [8]), showed vapour inhomogeneities in sheaths of large radius of curvature, parallel to the front, with spacing 1 km, or 4d/3, similar to that in the tank billows. Further confirmation also comes from pressure oscillations detected on the ground by Donn et al. [9] after the onset of sea-breeze fronts.

As there is Froudian similarity between the tank and atmospheric flows, therefore there must be similarity in the overall Richardson number Ri*, $(\Delta\rho/\rho \cdot gd/U^2)$, which is $1/Fr^2$, and has a value of about 2. Thus it seems likely that if the critical value of 1/4 for the gradient Richardson number is reached in the tank at the interface above the head, it should also be reached in the atmospheric flows.

Cusped pattern

A pattern of cusps, visible in plan form near the nose, has been observed in laboratory experiments when a dense flow advances into an unstable fluid. This seems to be a pattern of organisation of convection in the unstable layer,

and can appear at the same time as the smaller-scale one due to over-run fluid.

The system used of "water over ice", (Myrup et al. [10]), is of value in modelling convective layers, and has a more realistic upper boundary than the "parallel plate model" (Townsend, [11]). A copper base plate in a water tank about 30 cm square is cooled; cold fluid rises up from the floor to the 4°C level, above that the system is gravitationally stable. Thermistors measure the temperature at vertical intervals of about 1 cm.

When a gravity current of dyed saline solution moves slowly across the floor of the tank, it forms a cusped leading edge, with filamentary thermals rising from the cusps. Part of a circulatory system can be seen, with the filaments curving over and downwards.

A rice-grain like pattern is also seen. This appears to be a circulation set up by over-run liquid, corresponding to the clefts seen in the flows at larger Reynolds numbers.

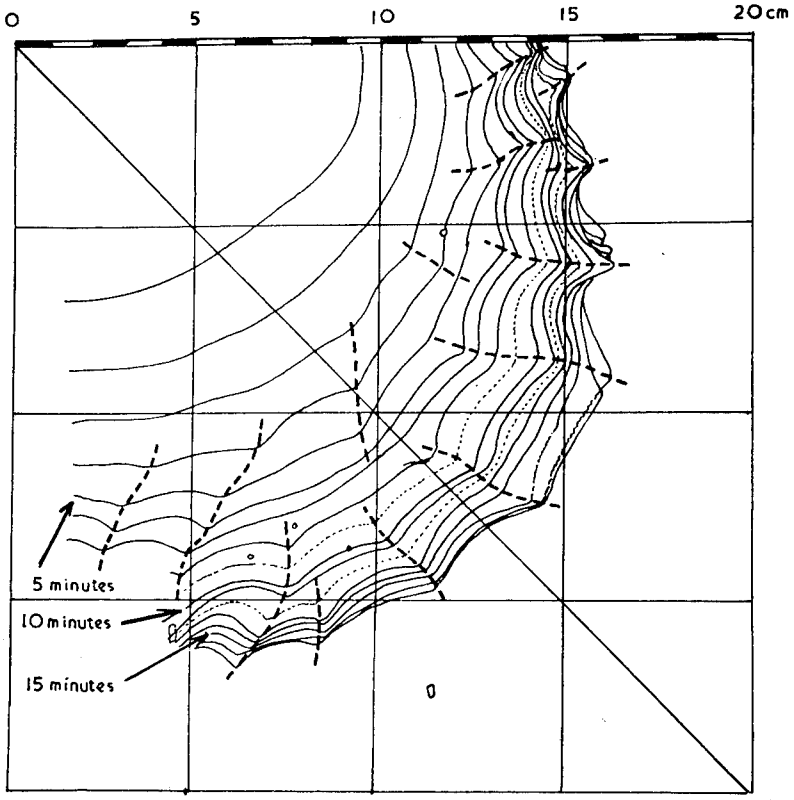


Fig. 6.

In the analysis of a set of experimental measurements shown in Fig. 6, it is noteworthy that the spacing, s, of the cusps remains almost constant at 3 cm. The mean depth H' of the convective layer during the time when the cusps were forming was 1.2 cm, so the value of s/H' is about 2.5. This is about the figure usually found in atmospheric cloud streets.

Atmospheric evidence

From cloud forms: Nielson [12], Corbett [13] and Simpson [14] have noted bars of cloud extending inland from sea-breeze fronts in the south of England. These clouds have been in parallel bands, spaced from 7 to 15 km apart. Typical conditions have been unstable WNW wind, cloudbase 1500 m, with depth of cloud up to 1000 m. In all the cases described, although there was no sign of cloud streets in the convective cloud ahead of the front, at certain periods of the day a clear banded structure appeared in the clouds in or above the sea-breeze.

From radar: Ligda [15], using 10 and 23 cm radar, detected bands with spacing about 6 or 7 km preceding main thunderstorm echoes. Ligda and Bigler [16], following a cloudless cold front with radar, found a thin line with diffuse trailing streamers, having a spacing of 7 or 8 km. This front moved at 15 m s^{-1}.

Atlas and Hardy [17] described radar echoes from a sea-breeze front showing a striated echo pattern in the sea-air, in the actual direction of the sea-breeze. These were claimed to be from waves on an echo layer or inversion at a height of 500 m.

Berson and Lamond [18] observed parallel echo bands at 550 to 950 m height along the wind with superimposed transverse structure. They claim the phenomenon suggested the presence of three-dimensional forced perturbations in the boundary layer (so-called Görtler vortices). Görtler's results were related to the observations by assuming a value of eddy viscosity of 3.8 m^2 s^{-1}.

It seems probable that when the speed of advance of the gravity current is roughly equal to the rate of ascent of the thermals in the unstable section there can be interaction between the two motions.

Conclusions

Dynamical similarity for some of the features deduced from the models is established. Others need further atmospheric observations which could be supplied by glider pilots.

References

1. Defant, A.; Über die Dynamik der Böen, Beitr. frei Atmos., 9, pp. 99-113, 1921.

2. Simpson, J.E.; A Comparison Between Laboratory and Atmospheric Density Currents, Quart.J.R.Met.S., 95, pp. 758-765, 1969.

3. Simpson, J.E.; Effects of the Lower Boundary on the Head of a Gravity Current, J.Fluid Mech., 53, pp. 759-768, 1972.

4. Lawson, T.J.; Haboob Structure at Khartoum, Weather, 26, pp. 105-112, 1971.

5. Abe, M.; Modelling Mountain Cloud Forms, Bull, Centr. Met.Soc.(Japan), 7, p.3, 1941.

6. Faller, A.J.; Large Eddies in the Atmospheric Boundary Layer, J. Atmos.Sci., 22, pp. 176-184, 1965.

7. Kuettner, J.; Cloud Bands in the Earth's Atmosphere, Tellus, 23, pp. 404-426, 1971.

8. Atlas, D.; Radar Detection of the Sea-Breeze. J.Met., 17, pp. 244-258, 1960.

9. Donn, et al.; Gravity Waves and the Tropical Sea-Breeze, J. Met., 13, pp.356-361, 1956.

10. Myrup et al.; Upside Down Convection, Weather, 25, pp.150-158, 1970.

11. Townsend, A.A.; Natural Convection in Water Over An Ice Surface, Quart.J.R.Met.S. 90, pp.248-259, 1964.

12. Neilson, P.; Cambridge to Exeter, Sailplane & Gliding, 7, pp.132-133, 1956.

13. Corbett, J.; Out and Return Using the Sea-Breeze, Sailplane & Gliding, 10, pp.268-269, 1959.

14. Simpson, J.E.; Sea-Breeze Fronts in Hampshire, Weather, 19, pp.208-220, 1964.

15. Ligda, M.G.H.; The Radar Observations of Mature Prefrontal Squall Lines, 6th OSTIV Congress, St.Yan, France, 1956.

16. Ligda, G.H. and Bigler, S.G.; Radar Echoes From a Cloudless Cold Front, J.Met., 15, pp.494-501, 1958.

17. Atlas, D. and Hardy, K.R.; Radar Analysis of the Clear Atmosphere, XV Gen.Assembly Int.Sci.Radio Union, Munich, 31 pp., 1966.

18. Berson, F.A. and Lamond, N.H.; Radar Observations of Wave Perturbations in a Low Level Wind Surge, Austr.Met.Mag., Melbourne, 18, pp.74-93, 1970.

THE MEASUREMENT OF CONVECTION USING A POWERED GLIDER

by

J.R. Milford
Z. Hashmi
P. Purdie
Department of Geophysics
University of Reading (U.K.)

Introduction

For numerical modelling of the atmosphere determination of the values of the heat and water vapour inputs at the lower boundary which should be used remains one of the major problems. To test any scheme of parameterization, local values should be measured in a variety of circumstances, with changes of atmospheric stability, of wind shear, and of topography. The present experiments with a powered glider are one part of a program to explore the use of such an aircraft in meteorological research generally; they are designed to test out the eddy flux method using simple and rather inexpensive equipment. One set of three flights on July 13, 1972 has been partly analysed; on two later days the same flight plan was used. Data from these is being processed at present. The work is notably incomplete, in that the errors in the estimates of the fluxes have not been evaluated. The novelty does not lie in the data processing methods, which have been used on light aircraft [Bunker, 1960] and on larger aircraft with inertial platforms [Warner & Telford, 1965; Lenschow, 1970] as well as on gliders [MacCready, 1962]. However, powered gliders have not been used in this way before and they have considerable advantages over both pure gliders and over conventional powered aircraft.

Instrumentation

The data-gathering system consists of a logger which has already been described elsewhere [Whitfield, 1970; Milford & Whitfield, 1970]. In the present configuration, pressure height, variometer output, airspeed, temperature, wet-bulb temperature, and wet-bulb depression are logged sequentially, with a repetition rate of 1.638 seconds. Speech is recorded on the same tape to relate the data to the flight path, and includes the navigational details; and an accelerometer record taken every 0.1 seconds from an accelerometer close to the center of gravity of the aircraft is available from some of the flights for future comparison.

The equipment is fitted in a Scheibe Falke, (Fig. 1) and, when measurements of vertical air velocity are required, the aircraft is flown at constant power, and constant airspeed. This can be done with any aircraft, but with a powered glider flown at a speed close to that which gives the best glide angle the changes of rate of climb with airspeed are minimised. In addition, it has a good response to changes of vertical air motion, shown in Table 1 as the distance required to adjust to within 1/e of a vertical gust speed.

In order to estimate the range of eddy sizes which can be measured by the system, we consider a ten minute run, flown straight and as nearly level as variations in a throttle setting and in the atmosphere will allow. The data from such a run consists of about 365 points, at 1.638 second intervals, and a spectral analysis, following the methods of Blackman and Tukey [1959], as particularised by Jones [1957] will give estimates of the spectral energy density over the frequency range from about 0.3 Hz to 0.01 Hz. At our operating speed of 30 m s^{-1} this corresponds to wavelengths of 100 m to 3000 m. As the shortest wavelength is over six times the exponential response distance shown in Table 1 the actual response of the aircraft is effectively instantaneous, and indeed the frequency range could be extended slightly by using a higher sample frequency. It is our contention that in convective conditions, and at heights greater than 100 m, a substantial part of the energy is transferred by elements within this size range. Glider pilots are likely to agree to this kind of statement, but our program aims to prove it.

One danger arises from the fact that the wavelength of the phugoid oscillation, according to Duncan [1959], is about 275 m, i.e., within the range of interest. That the contribution from this, and from pilot action, can be small is shown by the sample spectra shown in Fig. 2. In this case the vertical velocity spectrum is derived from the differential of the height record, and this introduces the spurious peak at the high frequency end; the limits of this effect are shown, as are those for the spectrum of vertical velocity from several runs in still air, actually well above a strong inversion. It appears from Fig. 2 that the "noise level" from the aircraft and pilot is small compared to the "signal" from the atmosphere. The "turbulence" in this case was in fact convection. It may be admissable to subtract the still air values from the turbulent ones, but linearity of the spectral densities cannot be guaranteed (see e.g., Zbrozek [1965]): the effect of pilot action is hard to predict quantitatively, but at the 11 sec period of our phugoid it is likely to damp the oscillation.

In addition to the response time of the aircraft itself, those of the sensors must also be sufficiently small. For all the sensors except humidity, this is no problem. The temperature sensors used to date are naked bead thermistors, with a reponse time measured as 0.7 sec, but the best compromise between certainty of wetting and fast response on wet

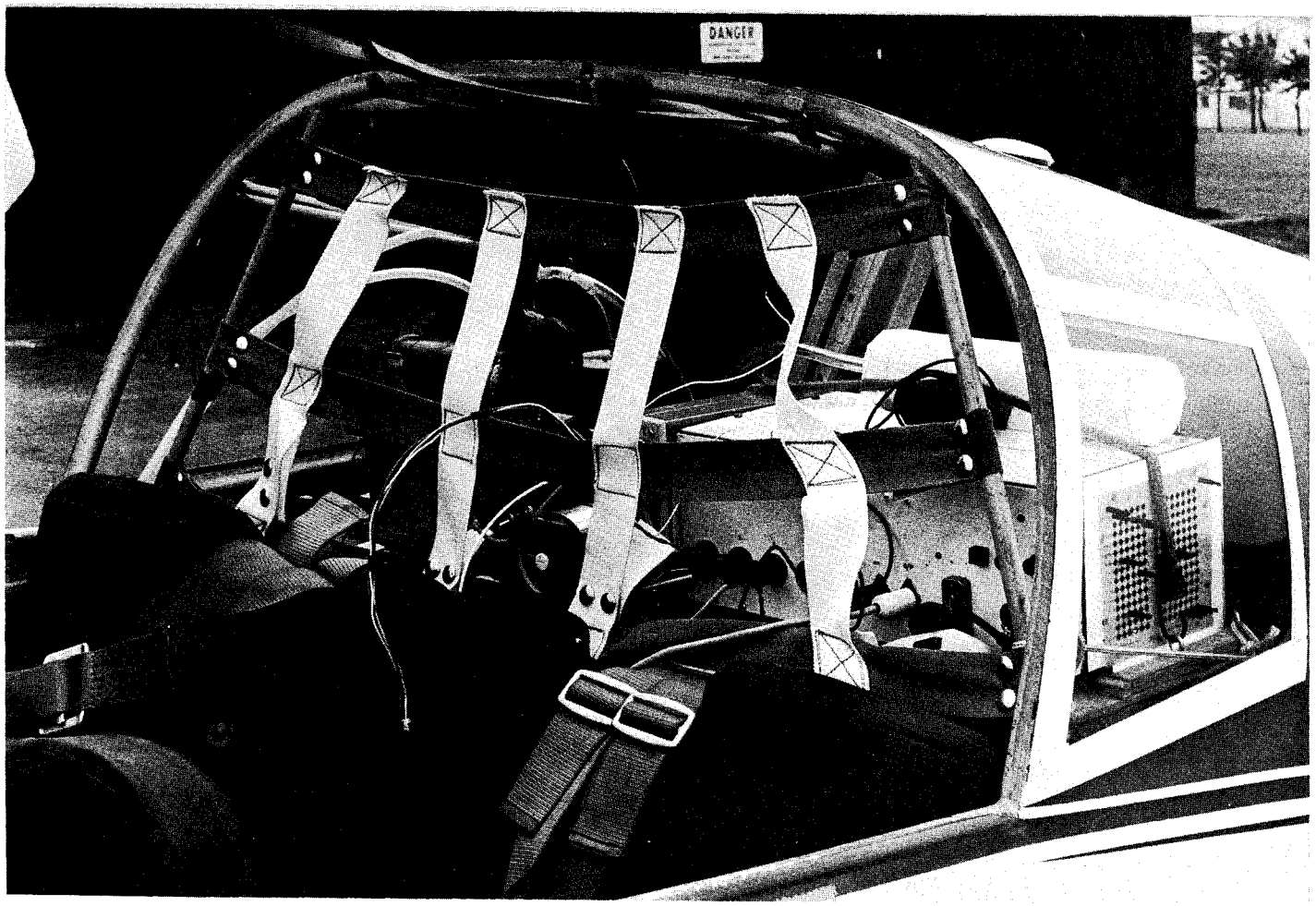


Fig. 1. The data logger installed on the parcel shelf of a Scheibe Motor-Falke. (Crown copyright)

Table 1.

Response to Vertical Gusts

	W	$\frac{\partial C_L}{\partial \alpha}$	V	$\frac{\tau}{\tau_{RQ}}$	L (approx)
	$kg\,m^{-2}$	rad^{-1}	$m\,s^{-1}$		m
Red Queen T 53	30	5·7	20	1·0	10
Falke	35	5	30	0·9	15
Super Cub	60	3	30	2·5	37
Porter	70	3	50	1·8	45
Hercules	370	3	150	3·2	240
Boeing 707	450	3	240	2·4	290

Response time $\tau = \frac{2W}{\frac{\partial C_L}{\partial \alpha} V \rho_{air}}$

Response length $L = V\tau$

W is wing loading

$\frac{\partial C_L}{\partial \alpha}$ is the slope of the lift curve.

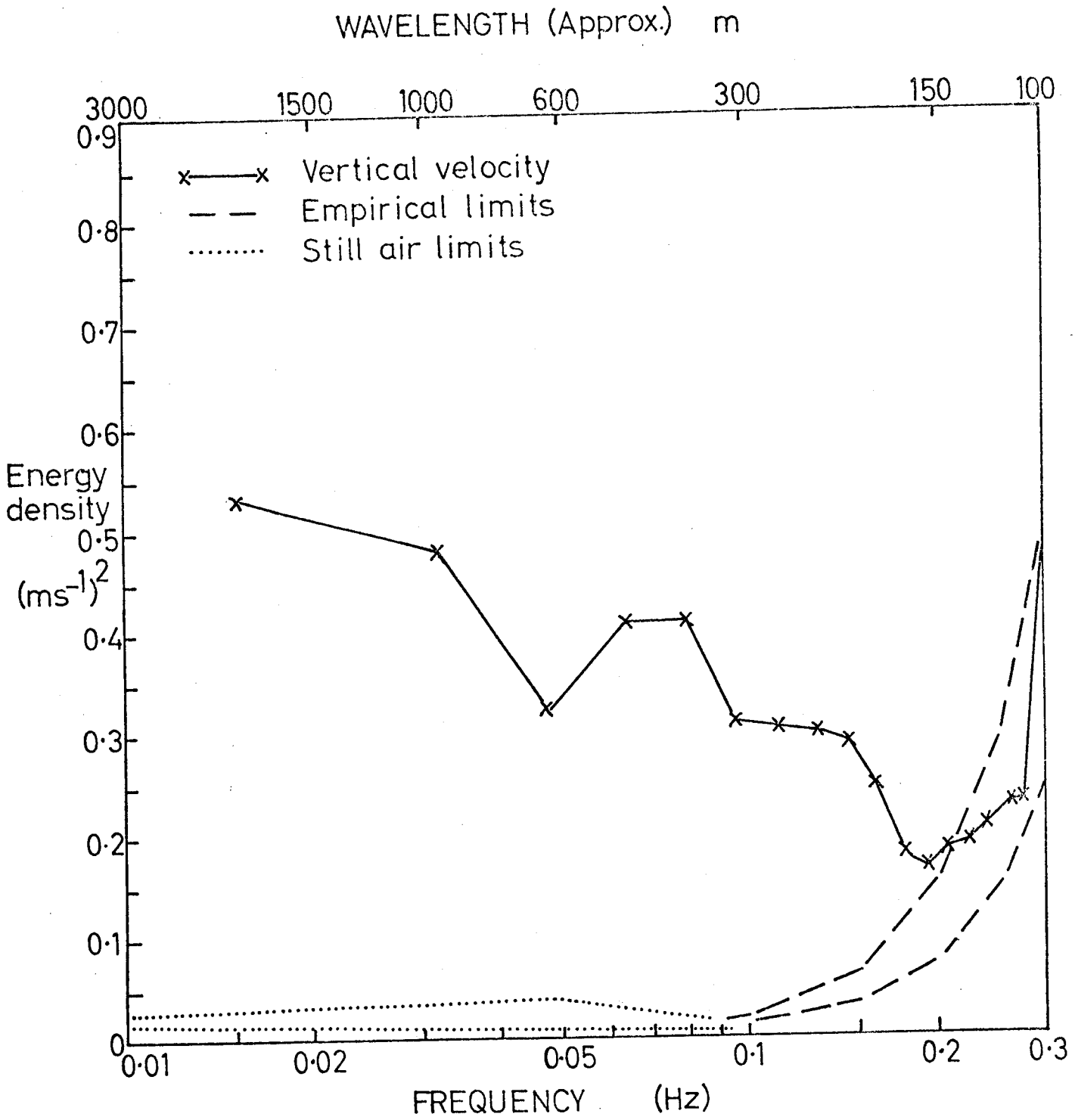


Figure 2. Vertical velocity spectrum for the Falke, in calm and convective air, energy density against frequency. Still air limits from five runs are shown. From 0.1 to 0.3 Hz envelope limits for the system noise are shown; these arise because the vertical velocity is derived from differentiating the height record.

bulbs has been hard to achieve, and the present humidity data suffers from a long lag, between 3 and 4 secs. Future observations will include those from a Lyman-alpha humidiometer or similar device.

Flight plan, July 13, 1972

The flights described took place on July 13, 1972; the general synoptic situation is shown in Fig. 3, with a ridge of high pressure covering Britain, as it had for the previous two days. The occlusion was weak, and gave only light drizzle over a strip of Ireland and N. England. In the South of England it was a good gliding day, with clear sky at first and shallow Cu starting to form around 0900 Z, limited by an inversion. The wind was light NE, and the maximum temperature about 25°C. Winds at Lasham, Hants, were less than 2 m s^{-1} throughout the day, and the surface isotherm chart (Fig. 4) shows that there was slight advection of warmer air at midday. The 850 mb chart (Fig. 5) shows a smaller temperature gradient than at the surface in the opposite sense, and even less possible contribution to the heat budget from the advection. The noon ascent at Crawley showed a deep inversion above 885 mb to limit the convection, and the local inversion is shown clearly from our ascents.

The country upwind of our flight area is typical of Southern England with mixed farming, woods and villages, and gentle relief, all the land lying below 100 m MSL for at least 30 km.

The three flights, starting at 10, 13 and 16 Z respectively, each consisted of a spiral ascent around the centre of a small village up to a height above the cloud top (or the visibly marked inversion) followed by a descent to below cloud base, and four horizontal runs, cross-wind and following the same ground track in each case as accurately as possible. At the end of the fourth run, a further spiral ascent and descent over the same spot completed the flight. Fig. 6 shows the flight plan schematically.

Serial ascents

The first stage of the analysis involves the plotting of the ascents, using means over one minute, or about half a circle of the flight path. Some continuity can be observed between areas of extra lift in successive circles, but positioning is far too inaccurate for any use to be made of this. The temperature profiles are shown in Fig. 7. In each ascent the potential temperature is substantially constant over the heights within which the straight runs took place, and a graph of the variation of this mean temperature against time is shown in Fig. 8. Interpolation from this graph would appear accurate enough for us to apply a reliable "time

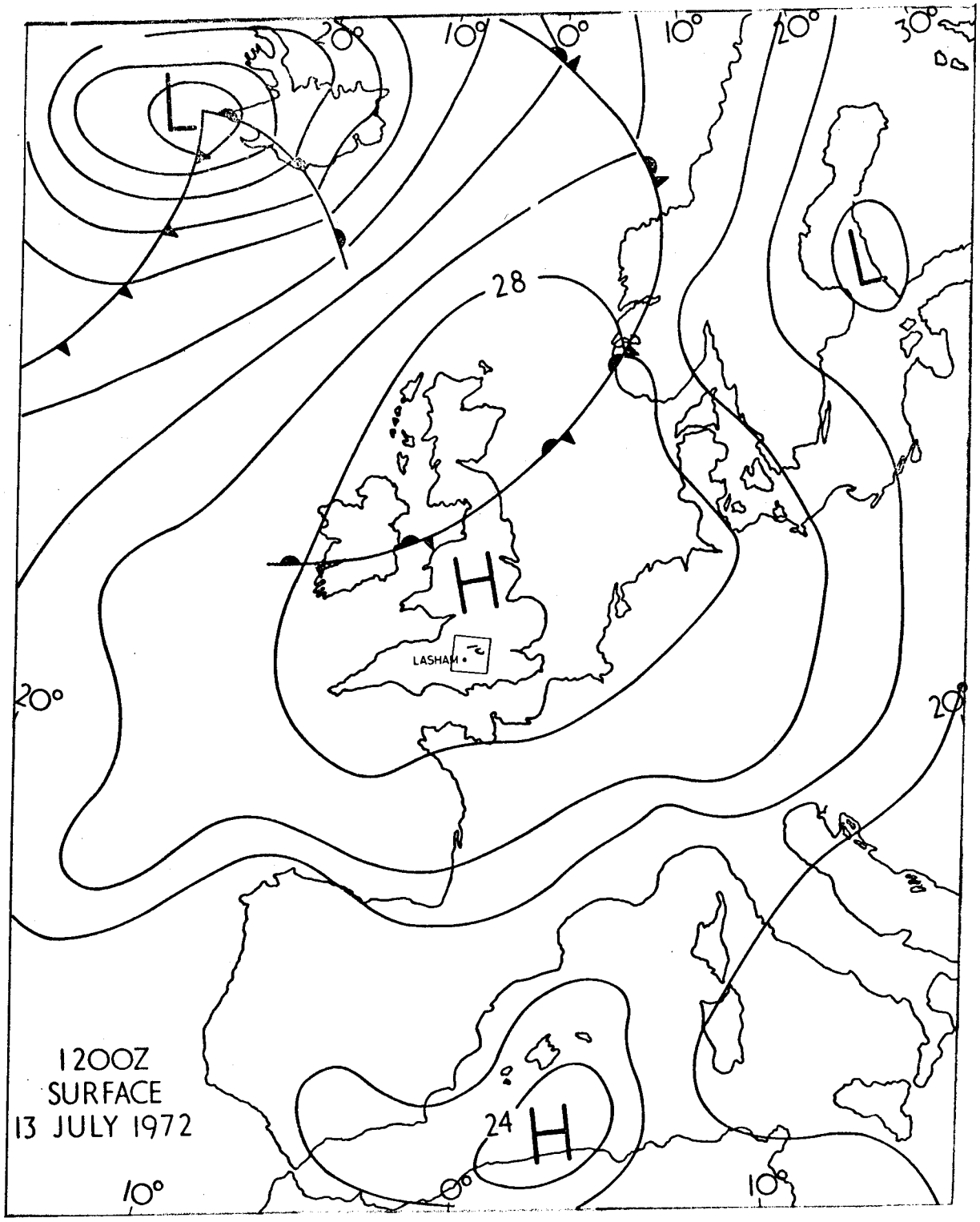


Figure 3. July 13th, 1972: surface pressure, 12 Z.

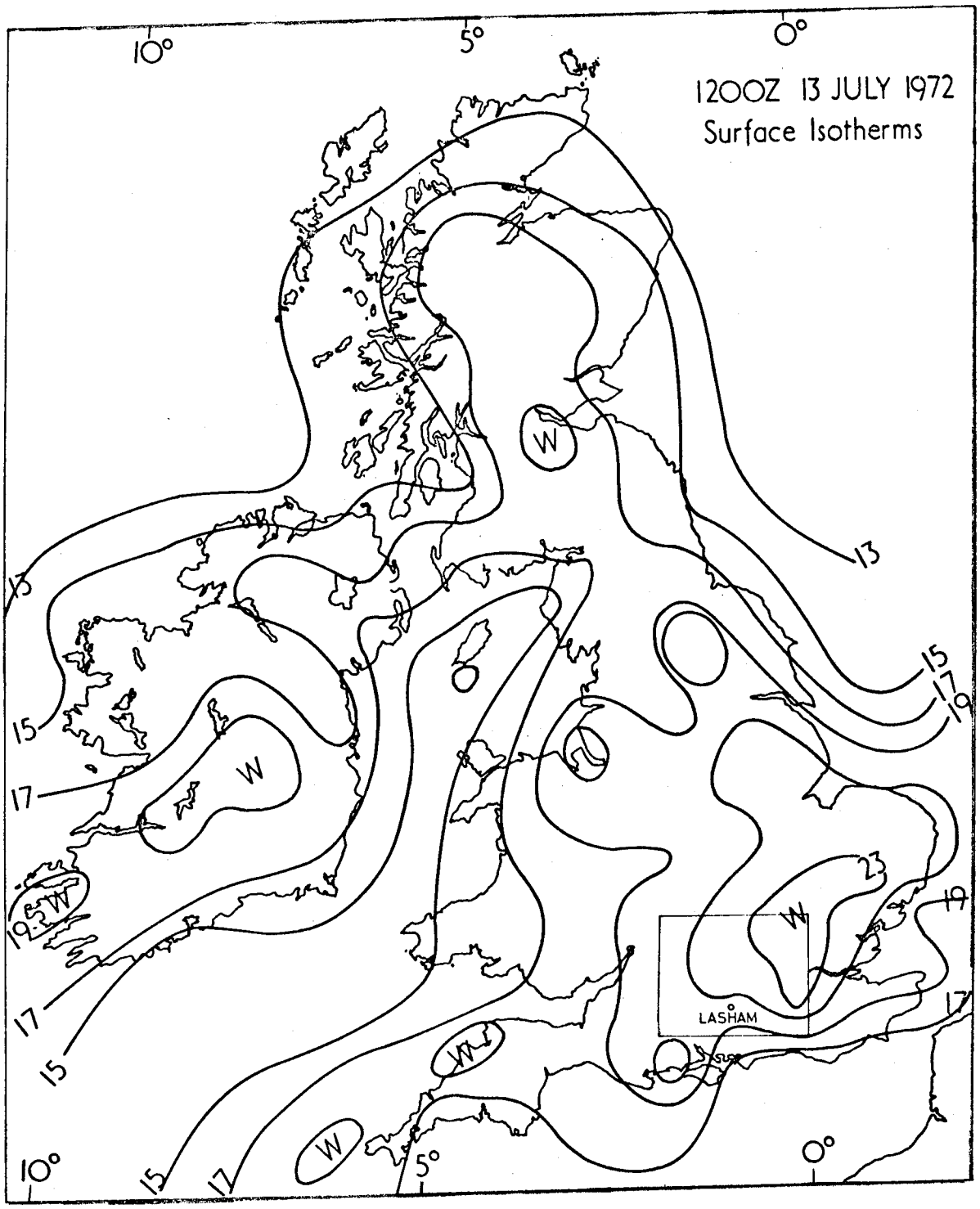


Figure 4. July 13th, 1972: surface isotherms, 12 Z.

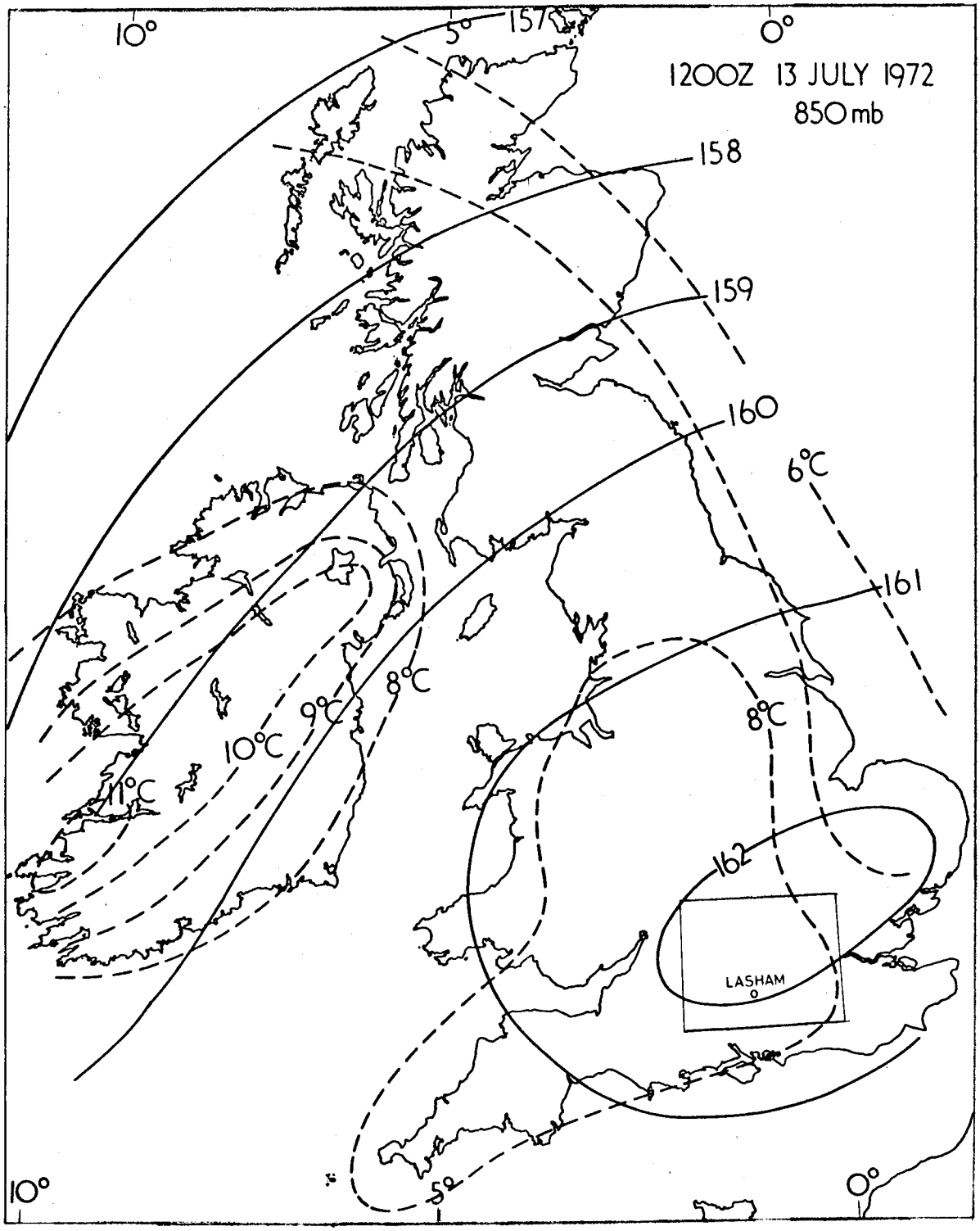


Figure 5. July 13th, 1972: 850 mb contours (in geopotential dekameters) and temperatures, 12 Z

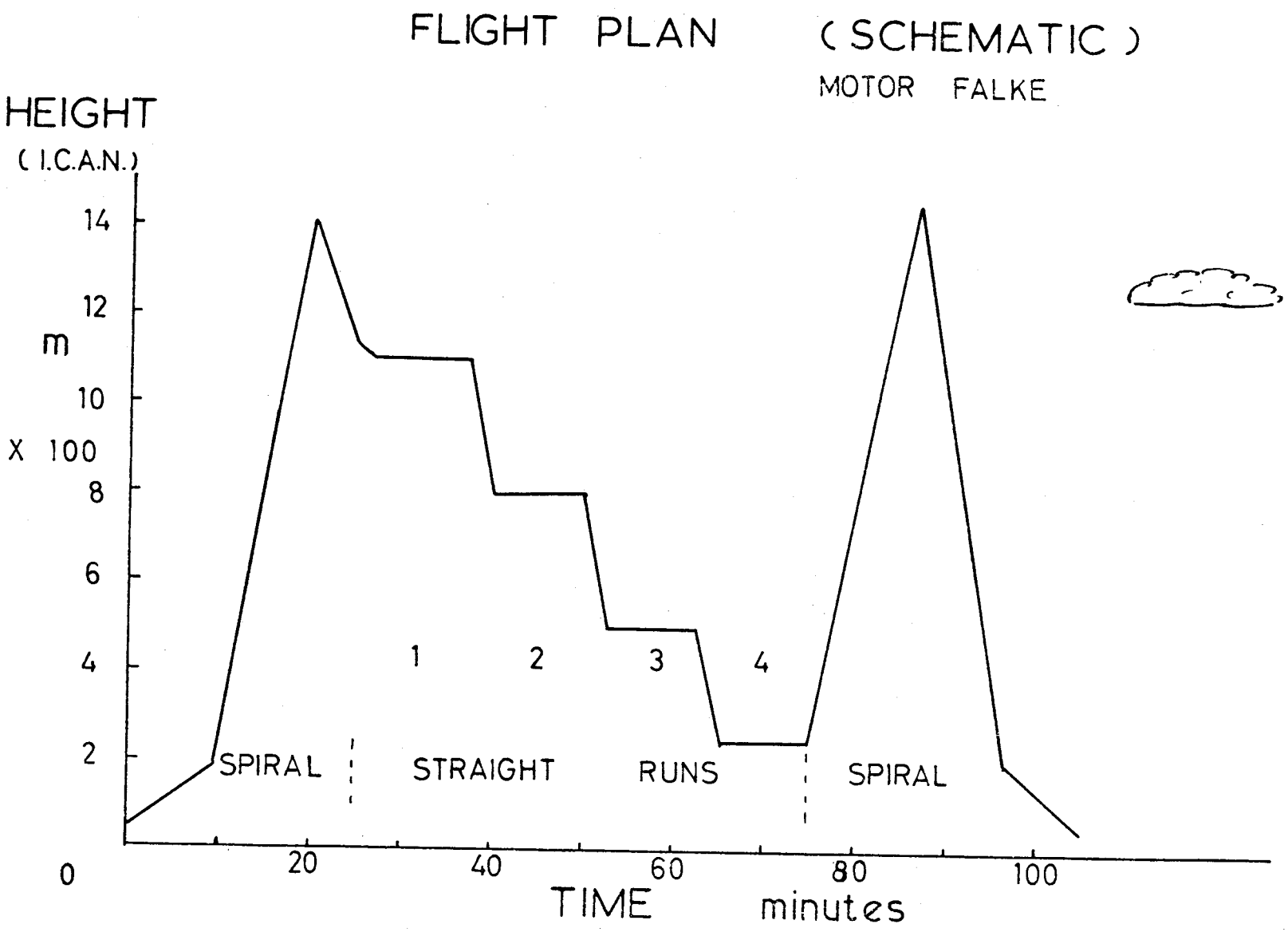


Figure 6. Schematic flight plan.

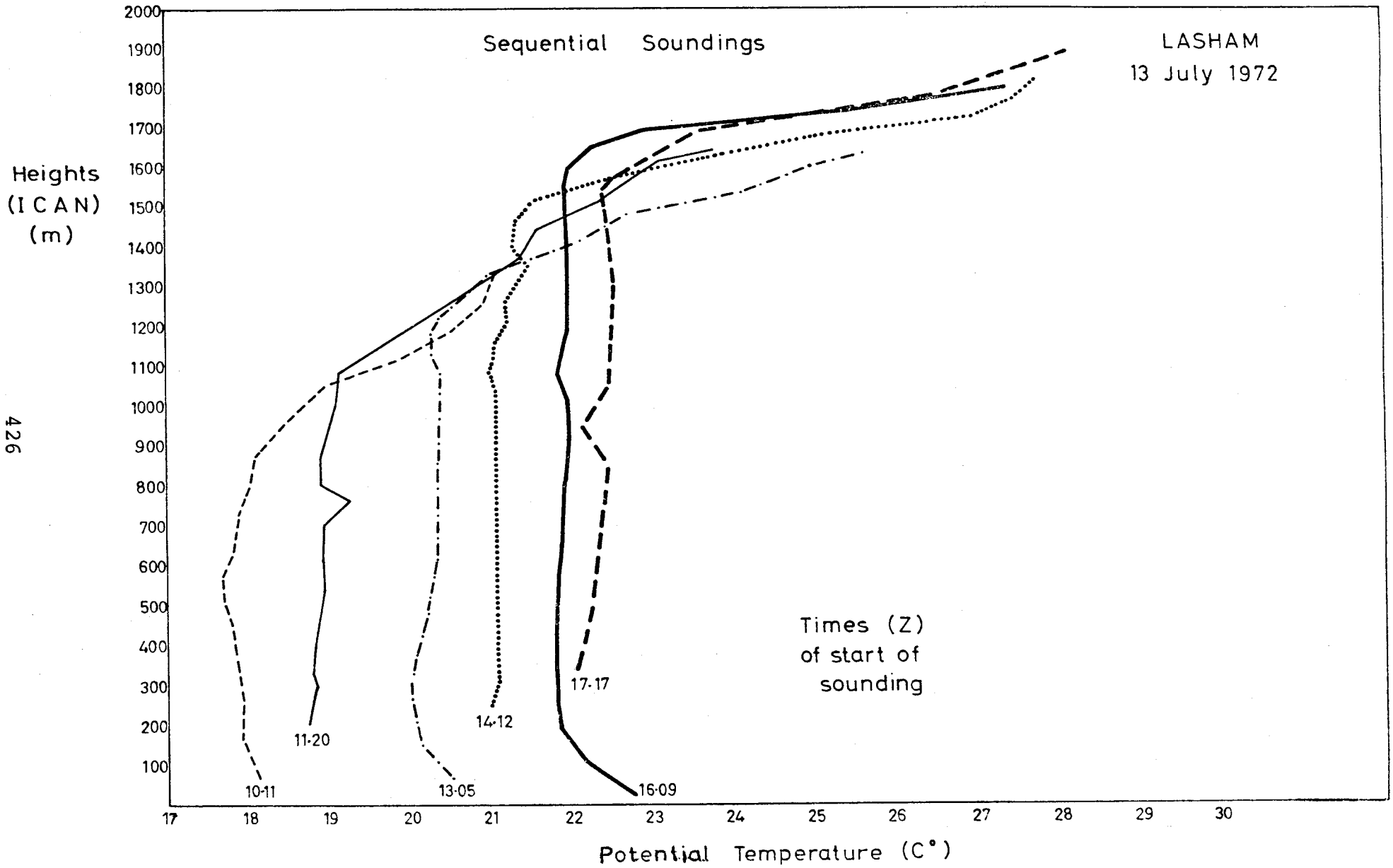


Figure 7. July 13th, 1972: sequential temperature soundings, showing potential temperature against height.

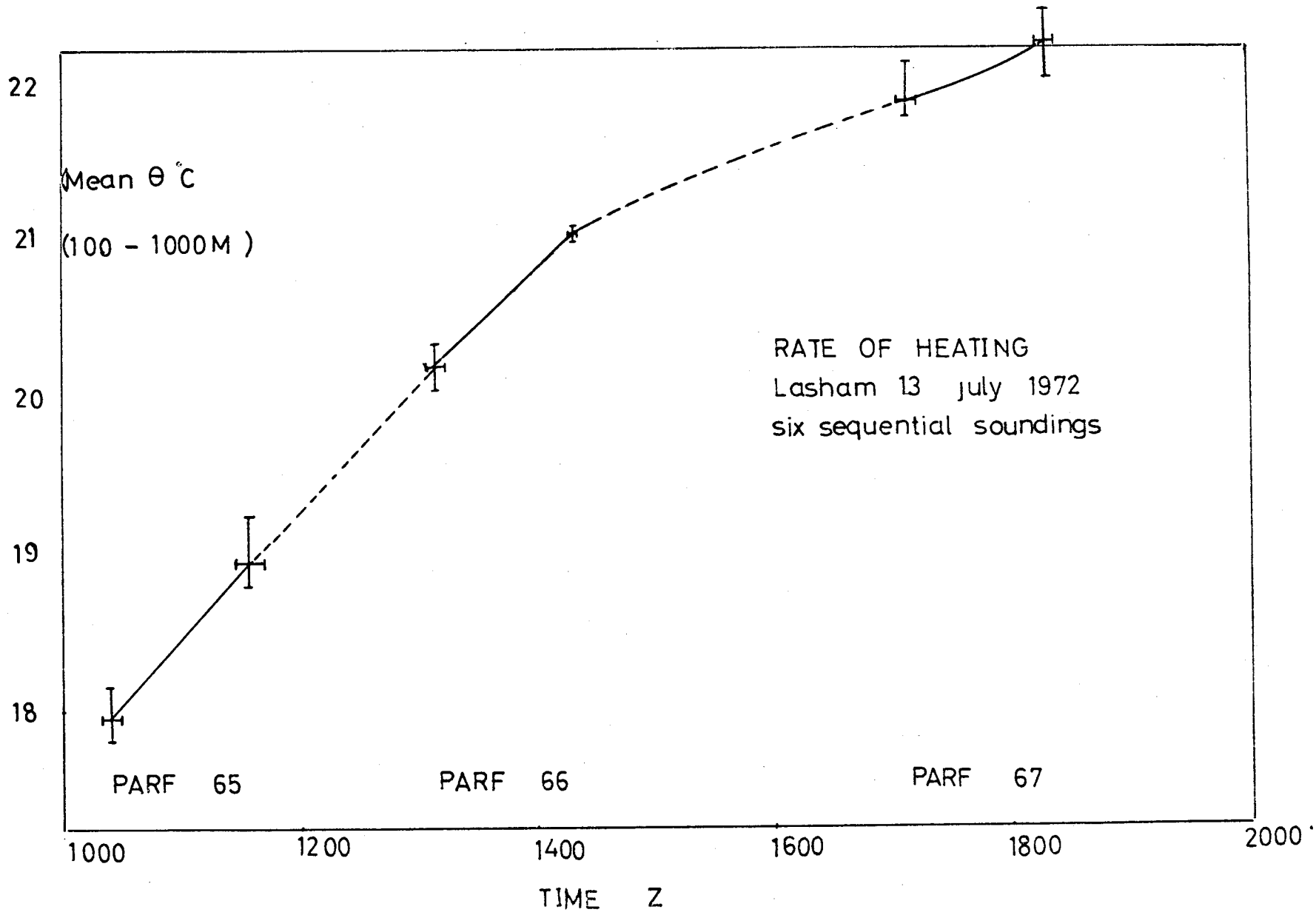


Figure 8. July 13th, 1972: rate of heating, showing mean potential temperature in the well-mixed layer against time.

correction": for example, all temperature data on the straight runs is made effectively simultaneous at the start of the first run by subtracting 0.80°C hr^{-1} from all subsequent readings.

The other main use of the ascents is in the heat budgeting, and the changes in total heat stored below an upper limit, chosen to be above the maximum of the inversion, is calculated.

Heat flux calculation

For each straight run a value of the heat flux

$$H = \rho c_p \overline{w'\theta'}$$

is calculated. To derive the values of the fluctuating quantities, the mean θ for the run is used with the time correction derived for the whole flight. On some occasions, but not here where the potential temperature is sufficiently constant with height, we have applied a height correction to each reading, so that a mean appropriate to that height as well as that time is used. The average value for w is calculated from the overall height change during the run; this assumes that the main cause of the change is an inexact power setting for zero climb, rather than a biased sample of air motions over the run. The calculation can use either the variometer output, or differentiated height for w. The latter gives much less discrimination, but the variometer zero drift can be significant even over a short period, and its calibration has to be checked frequently against overall height changes.

For July 13 the calculated heat fluxes are shown in Fig. 9. The accuracy of the computation has still to be checked by varying the quality control, and by subdividing the runs, but the general form of the variation with height, a linear decrease to zero around 2/3 of the inversion height, is plausible. (See, for example, Lenschow [1970]). It is unlikely that measurements over our limited spectral range will include all the significant eddies even under the most convective conditions, and to estimate the contribution in our range a spectrum is needed. This is in hand, but the programming is not yet completed. If the results of Bean et al. [1972], or Lenschow [private communication] can be applied over land, a maximum of the spectral density would be found at wavelengths around 600 m at our lowest heights of 150 m above ground.

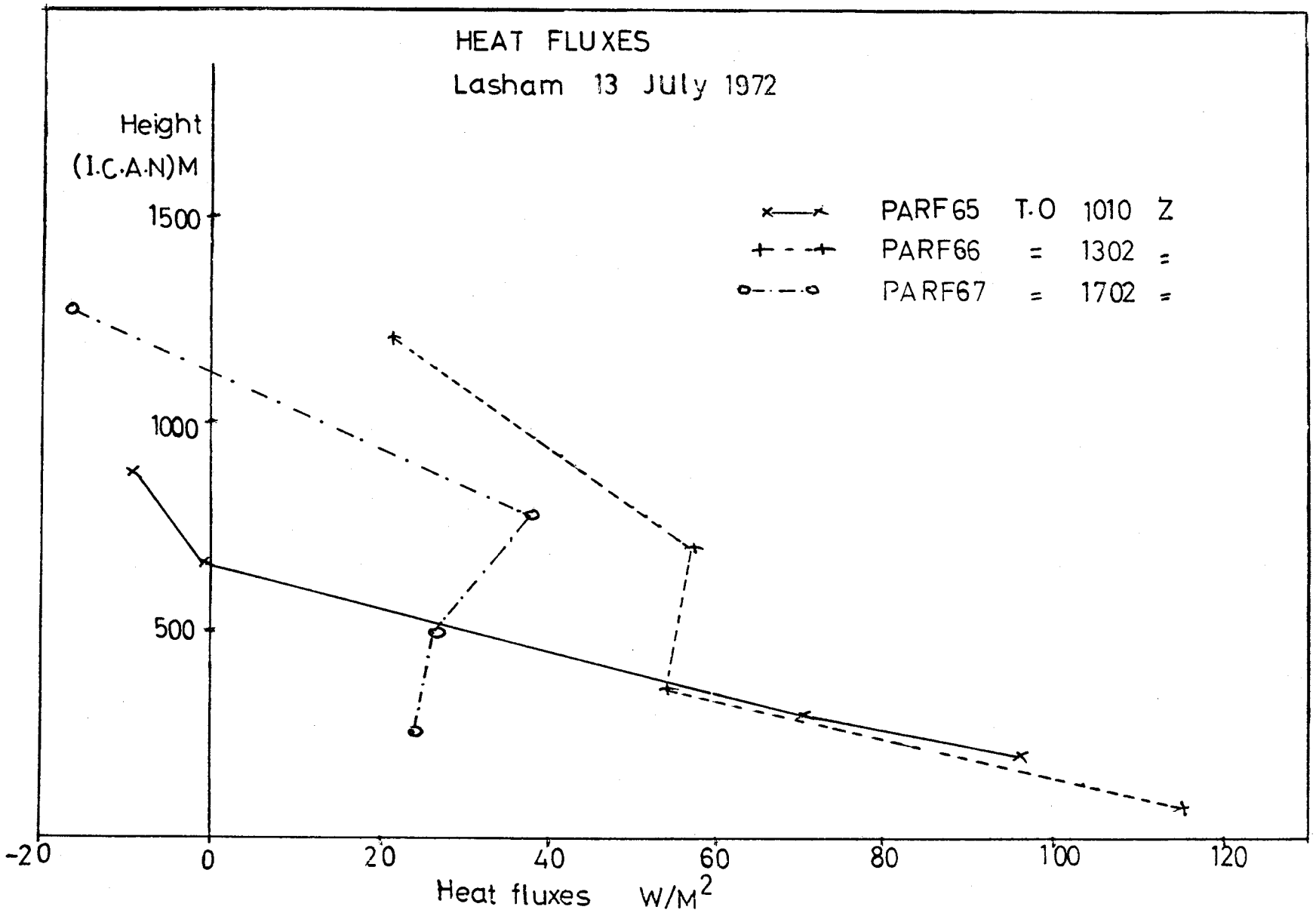


Figure 9. July 13th, 1972: eddy heat fluxes measured from horizontal straight runs at four levels in each flight.

Heat budget

The main independent check on the calculation of the eddy heat fluxes comes from a computation of the heat budget. Taking the value of 115 W m^{-2} for the mean at a height of 200 m during the first two runs, we compare it with the change in heat storage calculated from the changing temperature profiles. These give a value of 220 W m^{-2}. On this particular day winds were less than 2 m s^{-1}, and $\pm$ 10 W m^{-2} are the limits for the advected heat. Radiation, according to an Elsasser chart applied to the Crawley midday ascent, provides a warming of 5 W m^{-2}, assuming a surface temperature of 4°C above air temperature. Overall, from this data set, a discrepancy of a factor of nearly two therefore remains; much of this may be explained when the spectral limits of our measurements are considered.

Structure of the thermals

With measurements only taken every 40 m or so along the flight path, it is not possible to describe the structure of the thermals in any detail. Lenschow [1970] suggests using 10 m resolution. The impression during the flight was that the thermals at lower levels had much sharper boundaries, and a preliminary study of the maximum velocity of the thermals against their size shows a rather uniform size at 200 m, regardless of the lift; at higher levels the larger thermals are associated with higher velocities, and "multiple cores" become more frequent, which corresponds with the findings of Konovalov [1972].

Some other information on the structure of the "average" thermal comes from separating the points within any one run into classes according to the vertical velocity at that point. Because of the uncertainty of the true zero, the air has been described as moving upward or downward if it has a speed greater that 0.5 m s^{-1} in either direction. From the data gathered on the four runs within one flight, mean temperature profiles are computed for each class, and these are shown for the three flights on July 13 in Fig. 10. It is possible to subdivide the data into smaller classes, but no significant difference was found between profiles for air moving upward with velocities greater than 2 m s^{-1}, for example, and those for all upward-moving air. The profiles show the difference in stability between the two temperature profiles in each case to be about 1/3 degree C per km, with the upward moving air having a lapse rate not significantly different from the dry adiabatic.

TABLE 2

HEAT BUDGET

Change in heat storage 995 - 850 mb

Mean 1000 - 1600 z + 220 ± 50 W m^{-2}

Compare:	Measured eddy heat flux at 200m (~ 995 mb)	+ 115*	W m^{-2}
	Advection	0 ± 10	W m^{-2}
	Radiation	+ 5 ± 5	W m^{-2}
	Condensation or evaporation	0 ± 1	W m^{-2}
	TOTAL	120 ± 50	W m^{-2}

* Probable error not known: assume ± 30 W m^{-2}

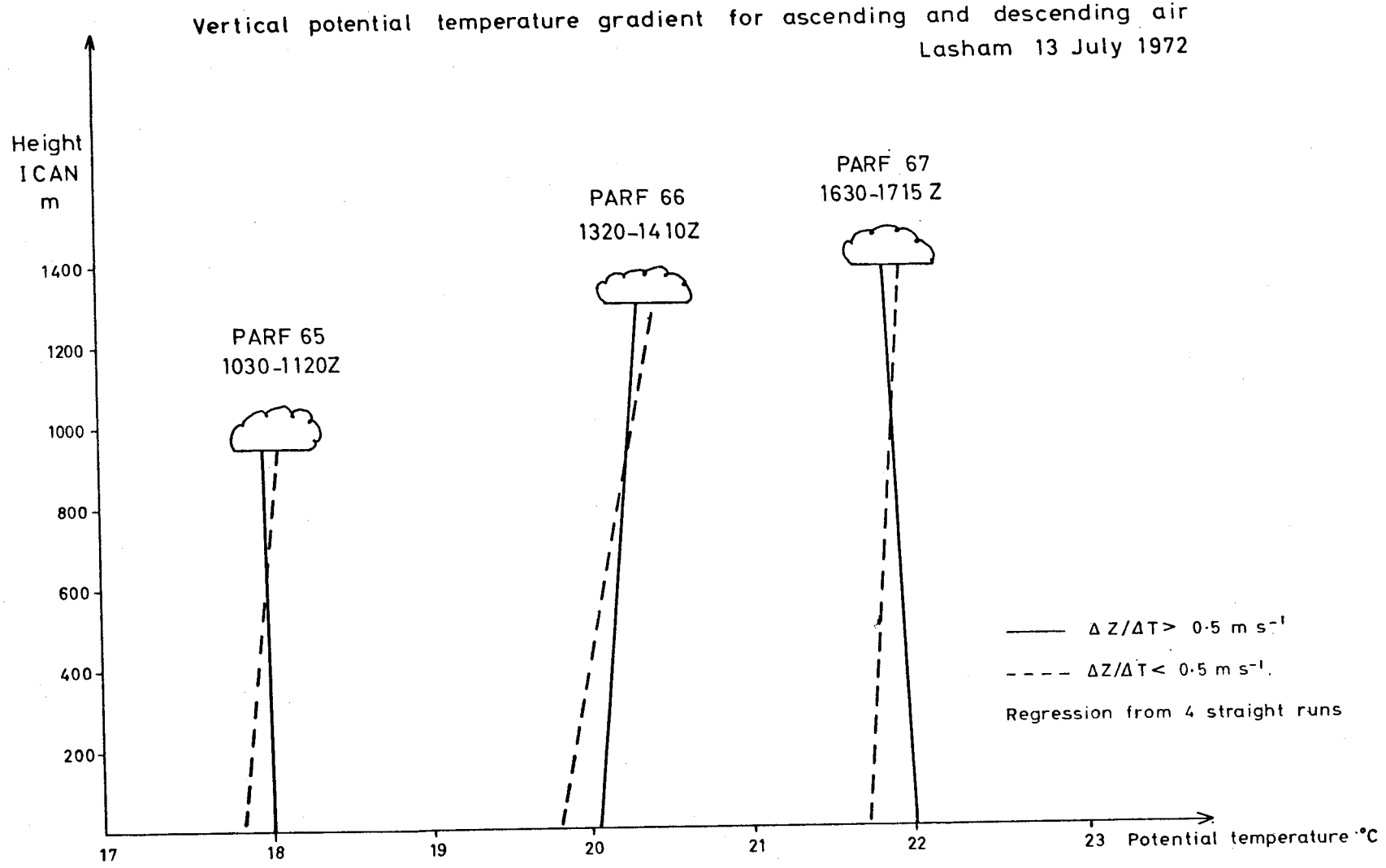


Figure 10. July 13th, 1972: Mean temperature profiles for ascending and descending air. A regression is computed using all points from the straight runs on each flight where the air is ascending or descending with speeds greater than 0.5 m s^{-1}.

Discussion

The analysis of this data has not been completed; that of two later days on which similar programs were flown is to be treated similarly. It is also clear that more detailed information from accelerometer records, and particularly from a rapid humidity sensor such as a Lyman-alpha device, will add interesting information on the convective entities which are acting, and on their variation with height and with the time of day. It is probably not worth while logging more temperature detail because water vapor is more useful as a tracer; upward parcels of air maintain excess humidity mixing ratios all the way through the boundary layer (see e.g., Grant [1965]).

From improved measurements of the distribution of the size of the single thermals with height, of the vertical velocities and of the temperature and humidity lapse rate differences between inside and outside air, we expect to be able to discriminate to a useful extent between theoretical models of thermals. These models have been summarised by Lilly [1965], by Simpson et al. [1965], and implicitly by Turner [1972], among others. Between some models a difference of 25% in the growth size with height will be the most that can be expected, and a considerable amount of data will be needed to discriminate reliably using a statistical approach. We would also stress that the data to be used in any ensemble average must be chosen with care because the distribution of thermals over apparently uniform terrain can be very different in the later parts of different days. These larger patterns of convection, typically on the 3 to 10 km scale, seem to be set by shear and stability patterns on a scale larger than those we can study with the powered glider, but we should not, therefore, ignore their influence on the scale of our investigations. Assuming, however, that we still encourage observers to observe, and to describe the larger scale on which the atmosphere seems to be uniform, it seems probable that the use of the powered glider in the measurement of convection will lead to uniquely useful local measurements of fluxes and studies of boundary layer development, and also to some capability to select between the different thermal models proposed to date.

References

Bean, B.R., Gilmer, R., Grossman, R.L., McGavin, R., Travis, C.R.,; An Analysis of Airborne Measurements of Vertical Water Vapour Flux during BOMEX. J. Atmos. Sci., 29, pp 860-869, 1972.

Blackman, R.B. and Tukey, J.W.; The Measurement of Power Spectra, Dover Publications, New York, 190 pp., 1959.

Bunker, A.F.; Heat and Water-Vapour Fluxes in Air Flowing Southward over the Western North Atlantic Ocean. J. Met. 17, pp 52-63, 1960.

Duncan, W.J.; The Principles of the Control and Stability of Aircraft. Cambridge U.P. 391 pp., 1959.

Grant, D.R.; Some Aspects of Convection as Measured from Aircraft. Q.J.R.Met.Soc. 91, pp 268-281, 1965.

Jones, R.A.; Studies of Eddy Structure in the First Few Thousand Feet of the Atmosphere. M.R.P. 1044, Met. Res. Cttee, London, 1957.

Konovalov, D.A.; On the Structure of Thermals. Swiss Aero Revue, 7, pp 392-394, 1972.

Lenschow, D.H.; Airplane Measurements of Planetary Boundary Layer Structure. J.Appl. Met., 9, pp 874-884, 1970.

Lilly, D.K.; Theoretical Models of Convection Elements; Advances in Num. Weather Prediction. Traveller's Res. Centre Inc., pp 23-24, 1966.

MacCready, P. B.; Turbulence Measurements by Sailplane. J. Geophys Res., 67, pp 1041-1050, 1962.

Milford, J.R. and Whitfield, G.R.; An Instrumented Glider for Meteorological Research. 12th O.S.T.I.V. Congress, Alpine, Texas, 1970.

Simpson, J.S., Simpson, R.H., Andrews, D.A. and Eaton, M.A.; Experimental Cumulus Dynamics. Rev. Geophys, 3, pp 387-431, 1965.

Turner, J.S.; On the Energy Deficiency in Self Preserving Convective Flows. J. Fluid Mech. 53 (2), pp 217-226, 1972.

Warner, J. and Telford, J.W.; A Check of Aircraft Measurements of Vertical Heat Flow. J. Atmos. Sci. 22, pp 463-465, 1965.

Whitfield, G.R.; A Simple Data Recording System with Computer Analysis. The Radio & Electronic Engineer. 40, pp. 255-258, 1970.

Zbrozek, J.K.; Atmospheric Gusts, Present State of the Art and Future Research. J. Roy. Aero. Soc., 69, pp 27-45, 1965.

CONTINUOUS CLOUD PHYSICS DATA OBTAINED IN UPDRAFT SHAFTS OF CONTINENTAL CUMULUS CLOUDS

by

J. Doyne Sartor
Wim Toutenhoofd
National Center for Atmospheric Research*
Boulder, Colorado

Summary

"The Explorer" is an instrumented sailplane belonging to the National Oceanic and Atmospheric Administration and is operated by the National Center for Atmospheric Research. The sailplane is centered in the updrafts of cumulus clouds while circling with a turn radius of $\sim$ 250 m to obtain simultaneous updraft, atmospheric state parameter, and cloud microphysics data.

The sailplane instrumentation includes an electrostatic disdrometer which measures every 0.5 sec a drop size distribution for $\sim$ 1 cm^3 of sampled air, a Cannon cloud particle camera, an impactor slide gun and instruments for obtaining the vertical speed of the air and the ambient temperature. The instrumentation is discussed in more detail by Toutenhoofd, Cannon and Sartor [1].

A one-minute sample of disdrometer and vertical air speed data obtained in a flight on 12 August 1971 is presented in Fig. 1. The sailplane was flown in the updraft through the base of a continental cumulus congestus to an altitude 1900 m above cloud base.

The high resolution of these data makes it possible to derive statistical parameters important for testing certain cloud models.

A summary of the data obtained in the cloud mentioned above is presented in Fig. 2, where σ_r indicates the drop radius standard deviation obtained from an 0.5 sec disdrometer sample. All data are averaged over 100 m intervals of pressure altitude and plotted in solid lines; standard deviations are plotted in dotted lines. Summaries like the one depicted in Fig. 2 are used to plan the application of the data in the testing of theoretical and numerical models

*The National Center for Atmospheric Research is sponsored by the National Science Foundation.

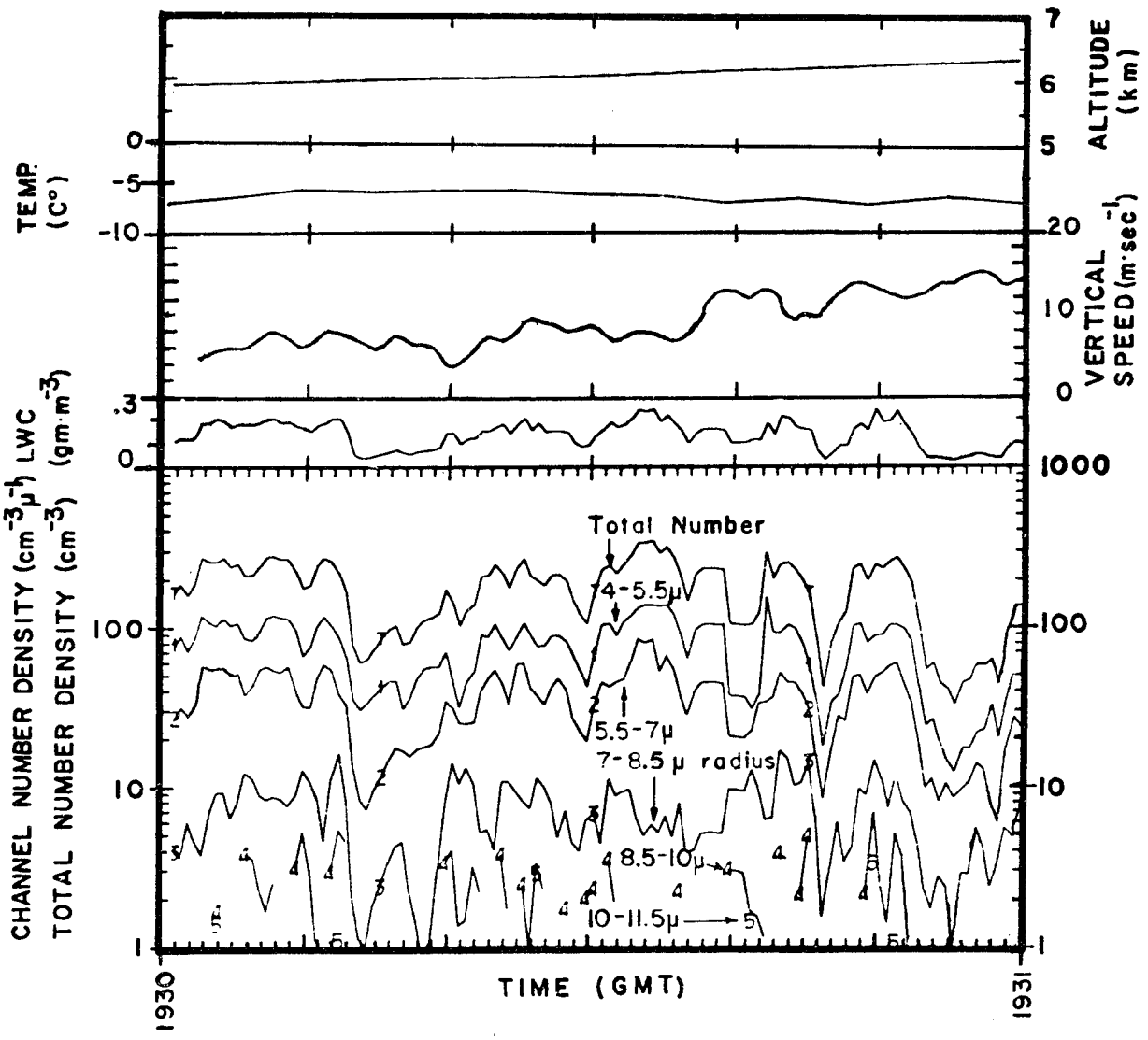


Figure 1. One minute sample of high resolution data from cumulus congestus, August 12, 1971, in Northeast Colorado.

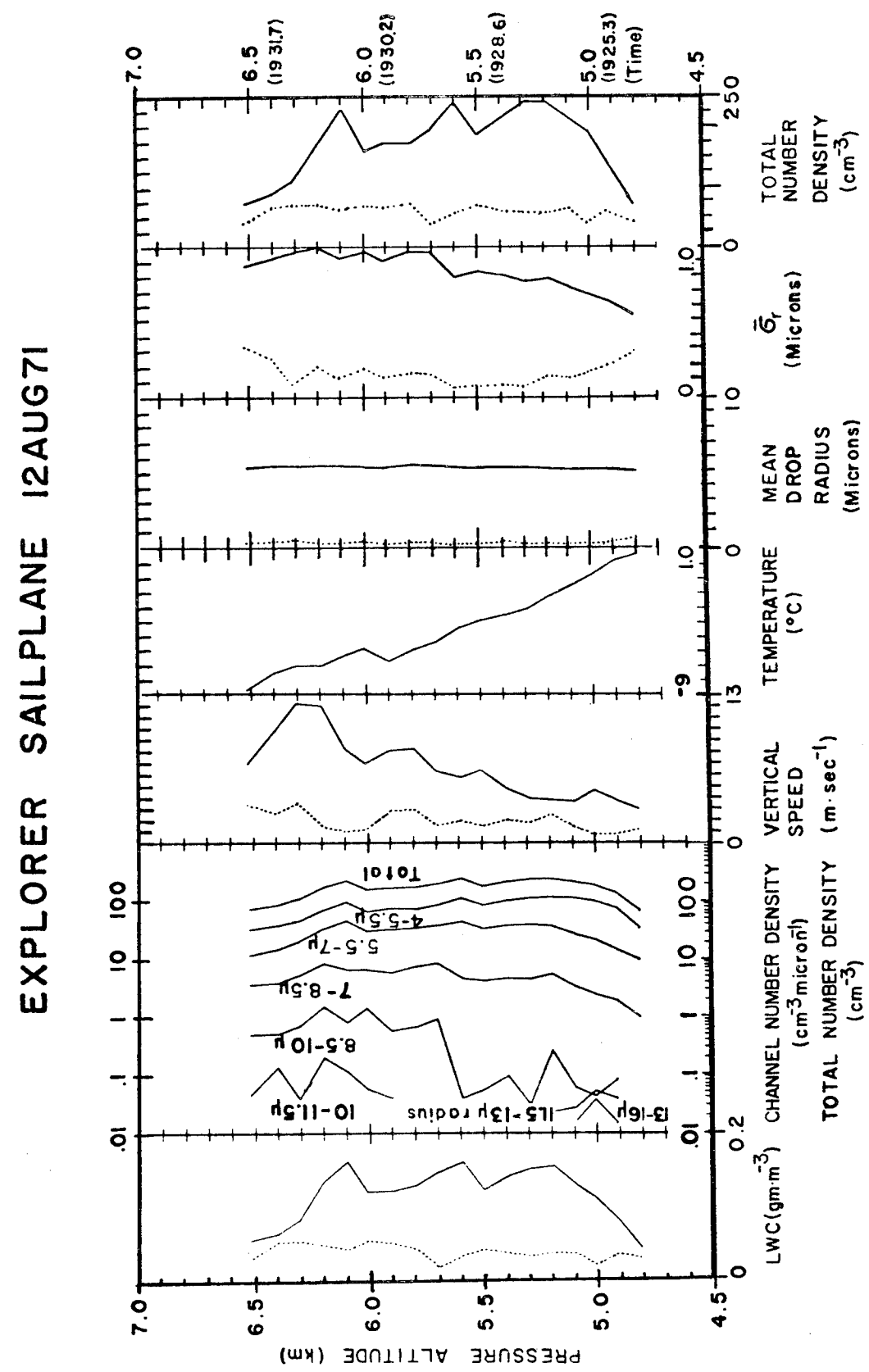


Figure 2. Averaged data obtained August 12, 1971, in the updraft of a cumulus congestus in Northeast Colorado. In each block dotted lines show the standard deviations over 100 meter height intervals of the data depicted by solid lines. $\bar{\sigma}_r$ is the standard deviation of the 1/2 sec samples averaged over altitude intervals of 100 meters.

of cloud convection and precipitation development, in calculations concerning precipitation development and thunderstorm electrification, and in other studies.

References

1. Toutenhoofd,W., Cannon, T.W., and Sartor, J.D.; An Instrumented Sailplane-A Platform for Cloud Physics Research with Continuous Rapid Response Measurements, Symposium on the Technology and Science of Motorless Flight, M.I.T., Cambridge, Mass., October 1972, pp 439-441.

AN INSTRUMENTED SAILPLANE - A PLATFORM FOR CLOUD PHYSICS RESEARCH WITH CONTINUOUS RAPID RESPONSE MEASUREMENTS

by

Wim Toutenhoofd
Theodore W. Cannon
J. Doyne Sartor
National Center for Atmospheric Research*
Boulder, Colorado

Summary

A Schweizer 2-32 sailplane, "The Explorer", has been instrumented as a platform for cloud physics research. The sailplane pilot can center his craft in the core of the updraft of cumulus clouds and in mountain wave clouds he can maneuver to a desired position in the wave. This gives the sailplane pilot the unique capability to investigate the microphysics, kinematics, and dynamics of clouds simultaneously in a steady state or quasi-Lagrangian sense. The relatively slow true air speed and choice of fast response instrumentation allow measurements to be made with a spatial resolution of 15 to 20 meters.

The scientific instrumention mounted on "The Explorer" is summarized in Table I. The electrostatic disdrometer (Abbott, Dye and Sartor [1]) measures and reads out the cloud droplet size distribution each half second during transit through the cloud. Ice crystal concentrations and droplets in the same volume are measured in situ every 1/2 sec using the Cannon particle camera (Cannon[2]). The vertical speed of the sailplane is measured continuously and can be converted to vertical air speed from a simple equation of motion for the aircraft. A diode thermometer mounted at the stagnation point on the nose of the sailplane gives continuous temperature measurements. The measured parameters and voice communications are transmitted to a mobile ground station where the information is received with a nine-channel telemetry receiver and is recorded on magnetic tape. The raw data can be reviewed in real time on strip chart recorders or oscilloscope. The telemetered data is digitized from a playback of the magnetic tape and fed into the NCAR computer so that most of the analysis and reduction of the data can be accomplished with a minimum of effort a short time after local flights.

Results obtained with the sailplane in the updrafts of continental cumuli are discussed elsewhere by Sartor and

*The National Center for atmospheric Research is sponsored by the National Science Foundation.

TABLE I

Instrument	Range*	Accuracy	Sample volume &/or time resolution
Camera-in situ particles, liquid & solid	For concentrations $\geq$1.5μm For sizing $\geq$8μm	±20%	5.0 cm^3 for 10μm droplet, 130 cm^3 for ice; 1/2 sec
Electrostatic cloud droplet disdrometer	4 to 19μm in 1.5μm intervals[1)]	±10%	1.0 cm^3 per 1/2 sec
Cloud droplet impactor slides	$\geq$2μm	±15%	50 cm^3, occasional sample
Variometer, vertical speed of sailplane	-40 to +40 m sec^{-1}	±0.4 m sec^{-1}	<0.5 sec
Pressure altitude	1010 to 120 mb	±0.5 mb	<1 sec (0.5 mb pressure altitude resolution obtained by integrating vertical speed from variometer)
Temperature	-75 to +30°C	unknown	to be determined after computerized analysis
Indicated air speed	0 - 67 m sec^{-1}	±4 m sec^{-1}	<0.5 sec
Vertical accelerometer	-10 to +10 g	±0.3 g	<0.5 sec
Lyman alpha humidiometer	-40 to +20°C dewpoint	±2°C dewpoint	<0.1 sec

*Particle sizes in radius.

1)All droplets with radii >19μm are counted in one channel.

Toutenhoofd [3]. A 16 mm sound movie depicting the sailplane research operations is available for viewing.

References

1. Abbott, C.E., Dye, J.E. and Sartor, J.D.; An Electrostatic Cloud Droplet Probe, to be published in J. Appl. Meteorol., in October 1972.

2. Cannon, T.W.; A Camera for Photographing Airborne Atmospheric Particles, Image Technology, April/May 1970.

3. Sartor, J.D., and Toutenhoofd, W.; Continuous Cloud Physics Data Obtained in Updraft Shafts of Continental Cumulus Clouds, Symposium on the Technology and Science of Motorless Flight, MIT, October 1972.

SOME ASPECTS OF TURBULENCE IN THE ATMOSPHERE

by

Robert R. Long
Department of Mechanics and Materials Science
The Johns Hopkins University

Introduction

The motion of the atmosphere and the turbulence embedded in this motion is of the greatest interest in soaring. The turbulence directly felt by the glider pilot apparently stems from three basic sources. One is the turbulent motion found in clouds, which has its origin in the energy (or heat) supplied to the fluid parcels by the release of the latent heat of condensation. The second has its basic energy supply in the unstable potential energy distribution characteristic of the atmosphere in certain layers and at certain times. These layers are located principally near the ground during the daytime. The third source of energy in atmospheric turbulence is the direct conversion of the kinetic energy in a mean shearing current to the kinetic energy in the turbulent elements. The release of latent heat is a very special circumstance and the associated turbulence requires a separate discussion. Here we will discuss only some aspects of turbulence occurring in the clear air either in stable or unstable situations.

Turbulence near the ground in unstable situations

There is a great body of literature concerning turbulence in the region just above the ground when the ground is heated. In this case, the air above develops an unstable mean potential density gradient. As a result, potential energy can be converted directly into kinetic energy. In addition, if there is shear, an additional source of energy (which may or may not be important) comes from the working of the Reynolds stresses against the mean shear. Two additional terms of importance in the energy equation are the advection of energy by the turbulent elements and the dissipation of energy due to a cascade process in which energy is transferred to smaller and smaller eddies and is finally lost through the action of molecular viscosity.

Theoretical considerations of the unstable case go back to Prandtl [1932]. In general, the buoyancy flux and momentum flux, which we denote by q and τ, are considered to be the

two important parameters of the problem. If we are very close to the ground, it appears indisputable that the thermal instability due to the heated surface may be neglected if there is appreciable wind shear. Then τ alone is the important parameter and the characteristic mean quantities such as mean velocity gradient, mean density gradient, and rms velocities depend only on τ and the distance above the ground z. Dimensional analysis then leads to the form of the dependence of these mean quantities on these two parameters. One is led, for example, to the conclusion that the mean velocity increases with height as the logarithm of z and this has been verified countless times in the atmosphere and the laboratory. If there is no shear, it appears that the molecular coefficient of viscosity and heat diffusion may not be neglected, at least as far as the specification of the buoyancy flux is concerned [Malkus, 1954].

The case of no shear or weak shear is perhaps of limited interest for atmospheric purposes but there is a great body of experimental and theoretical literature related to this case. If the lower boundary is smooth, as it is in experiments, there is a thermal boundary layer just at the surface in which most of the mean temperature difference occurs. Above this is a turbulent situation with rising thermals surrounded by more gently descending motion. Attention has been concentrated on establishing the gradient of mean buoyancy and mean velocity in the layer immediately above the thermal boundary layer. A theory of Malkus, for example, suggests that the buoyancy gradient decreases with height as z^{-2}. On the other hand, the theory of Prandtl predicts a decrease proportional to $z^{-4/3}$. Prandtl obtains this result by assuming essentially that all mean quantities depend only on z and q and not on the molecular coefficients of viscosity and conduction. In a certain sense this is paradoxical because q itself is directly proportional to a power of the molecular coefficient of diffusion. Experimental evidence is contradictory. Townsend [1959] performed experiments in which his measurements of the mean buoyancy gradient were too inaccurate to decide between the two theories. On the other hand, he found a z-dependence of the rms fluctuation which was sufficiently accurate to demonstrate disagreement with Prandtl's similarity theory. We must conclude that the problem is unresolved.

Where there is a wind, an important theory has been given by Monin and Obukhov [1953] in which it is assumed that the molecular coefficients do not enter the analysis at all. The mean quantities such as the buoyancy gradient depend only on z, q and τ. Dimensional analysis then leads to the famous similarity theory of Monin and Obukhov in which all non-dimensional mean quantities depend only on z/ℓ_m were ℓ_m is the Monin-Obukhov length $\tau^{3/2}/q$. If the theory is correct, we deduce therefore that a laboratory model of turbulence in the boundary layer requires only similar values of the ratio z/ℓ_m. The general similarity theory of Monin and Obukhov has been subjected to experimental study by Plate and Arya [1969] who found that a similarity theory seems to work very well for

wind tunnel flow above a cooled plate. Atmospheric observations also indicate that it is a good approximation.

A problem arises with regard to the similarity theory, however, when a special investigation is made for large values of z/ℓ_m. If z/ℓ_m is large, then either z is large or, perhaps, τ is small. An argument dating back to Priestley [1954] then states that in the limit as τ goes to zero such a quantity as the mean buoyancy gradient should become independt of τ. This leads again to the conclusion that the mean buoyancy gradient decreases as $z^{-4/3}$. It was believed for some time that this theory was verified by atmospheric observations [Monin & Yaglom, 1971]. Recently, however, Dyer [1967] and Businger, et al. [1971] have suggested on the basis of their atmospheric data that the dependence for large z/ℓ_m (> 0.1, perhaps) is a $z^{-3/2}$ instead. The data of Businger, et al., in particular, seems especially good and the scatter seems too small to accomodate the possibility of a $z^{-4/3}$ law. In some recent work, I have concluded that the argument leading to the $z^{-4/3}$ is faulty because (neglecting molecular coefficients entirely) it is not possible to allow τ to decrease all the way to zero. The argument will appear in detail in a forthcoming publication.

Turbulence in stable flow

In the case where the atmosphere is stable, for example in the free atmosphere in general or in the atmospheric boundary layer at night, the potential energy distribution is stable and the kinetic energy of the turbulence is lost to potential energy. There is only one source of energy, namely the kinetic energy in the mean shear and, therefore, if there is no shear (no mean motion), there can be no turbulence and the atmosphere comes to rest. If energy is produced by the shear, it is then transferred by the eddy motion or is converted to potential energy or is dissipated by the frictional effects. In the two layers of the atmosphere, the similarity theory of Monin and Obukhov appears to be a good approximation and we have some indication of the velocity and buoyancy gradients, rms velocities, etc.

Turbulence in the upper portions of the atmosphere (commonly called clear air turbulence) may be discussed similarly with respect to energy although the turbulence appears to be triggered by instability processes rather than by the effect of the roughnesses of the ground in the atmospheric boundary layer. Let us discuss the energy equation to some extent. The shear term in the simplest case has the form $-\overline{u'w'}\bar{u}_z$ or $\tau\bar{u}_z$ where $\bar{u}$ is the mean velocity and $\bar{u}'$ and $\bar{w}'$ are the fluctuating components in the direction of the mean wind and vertically. This term tends to be positive, that is to supply turbulent motion. Thus, if the velocity increases with height, $\bar{u}_z$ is positive. Then in the presence of eddy motion, a parcel coming from above ($\bar{w}' < 0$) will presumable have positive mo-

mentum ($\bar{u}' > 0$) when it arrives at its new level. This correlation then yields a negative covariance $\overline{w'u'}$ and this will cause the turbulence to increase. The same argument holds for a decrease of wind with height.

The details of the generation of turbulent energy by shear are currently under investigation in neutral conditions near a wall [Kim, Kline and Reynolds, 1971]. In stratified flow, a possible mechanism involves the creation of a turbulent patch by the breaking of an internal gravity wave. Mixing results, and the local gradient of velocity tends to be destroyed across the patch. The resulting more uniform mean motion has less kinetic energy than before and the excess supports the turbulence [Long, 1970].

The potential energy term in the energy equation has the form $-\overline{w'\rho'} = q$ where ρ is the buoyancy defined by $\rho = (\rho_1 - \rho_o)g/\rho_o$ in which ρ_1 is density and ρ_o is a reference density. In a stable fluid, rising parcel carries the heavier density of its layer of origin; that is, positive $\bar{w}'$ will be associated with positive $\bar{\rho}'$ so that the kinetic energy is decreased as the potential energy is increased. In shear flow in neutral conditions contributions to $-\overline{u'w'}$ are on the scale ℓ_e of the energy-containing eddies and ℓ_e tends to be of the order of the length scale of the mean velocity field [Townsend, 1956]. In stratified flow, it has been suggested that important contributions may arise from smaller eddies.

One of the important aspects of turbulence in stratified shearing flow is the origin and maintenance of the turbulence. Early work by Richardson [1920] looked for a criterion that turbulence could just be maintained. One may imagine an interchange of two parcels of air over a vertical distance. The process yields an increase of potential energy. At the same time the mixing tends to equalize the velocity so that kinetic energy is released from the mean shear. Turbulence can just be maintained when these two processes are in balance. The result, after some assumptions, is that $Ri \leq 1/4$ where Ri is the gradient Richardson number $Ri = \bar{\rho}\tau_z/(\bar{u}_z)^2$.

Another approach to the maintenance of turbulence, which is somewhat more satisfactory and also somewhat less informative, is through the energy equation discussed above. If we neglect the term involving the redistribution of energy, we may be sure that the energy production term must exceed the term involving the loss of kinetic energy to potential energy. The result is that the flux Richardson number $R_f = q/\tau\bar{u}_z$ must be less than 1 for the maintenance of turbulence. It is easy to show, however, that $R_f = Ri\ K_h/K_m$ where K_h and K_m are coefficients of eddy viscosity and eddy diffusion. The latter are unknown so that this approach does not lead to a critical gradient Richardson number.

Studies of instability of small disturbances on laminar stratified shearing flow are also numerous and are on firmer physical and mathematical ground although applications to

real systems are questionable. The basis result is the Miles-Howard theorem [Miles, 1961; Howard, 1961] that flows are stable is Ri > 1/4 *everywhere* in the system. The theorem says nothing about instability but individual cases seem to indicate that instability usually occurs if Ri drops below 1/4 somewhere in the flow field.

Acknowledgment

The research in this paper was supported by the Office of Naval Research under Contract No. N00014-67-A-0163-0013.

References

1. Businger, J.A., Wyngaard, J.C., Izumi, Y. and Bradley, E.F.; Flux-Profile Relationships in the Atmospheric Surface Layer, J.Atmos.Sciences,28, p.181, 1971.

2. Dyer, A.J.; The Flux-Gradient Relation for Turbulent Heat Transfer in the Lower Atmosphere. Quart.J.Roy. Meteor.Soc., 91, p.151, 1965.

3. Howard, L.N.; Heat Transport by Turbulent Convection, J. Fluid Mech., 17, p.405, 1961.

4. Kim, H.T., Kline, S.J. and Reynolds, W.C.; The Production of Turbulence Near a Smooth Wall in a Turbulent Boundary Layer, J.Fluid Mech., 50, p.133, 1971.

5. Long, R.R.; A Theory of Turbulence in Stratified Fluids, J.Fluid Mech., 42, p.349, 1970.

6. Malkus, W.F.R.; Discrete Transitions in Turbulent Convection, Proc.Roy.Soc. A, 225, p.185, 1954.

7. Miles, J.W.; On the Stability of Heterogeneous Shear Flows, J.Fluid Mech., 10, p.496, 1961.

8. Monin, A.S. and Obukhov, A.M.; Dimensionless Characteristics of Turbulence in the Atmospheric Surface Layer, Doklady AN SSSR 93 No. 2, p.223, 1953.

9. Monin, A.S. and Yaglom, A.M.; Statistical Fluid Mechanics: Mechanics of Turbulence, V. 1, MIT Press Cambridge, Mass., 1971.

10. Plate, E.J. and ARYA, S.P.S.; Modeling of the Stably-Stratified Atmospheric Boundary Layer, J.Atmos.Sci., 26, p.656, 1969.

11. Prandtl, L.; Meteorologische Anwendungen der Strömungslehre, Beitr. Phys. Atmos., 19, p.188, 1932.

12. Priestley, C.H.B.; Convection From a Large Horizontal Surface, Aust.J.Phys., 7, p.176, 1954.

13. Richardson, L.F.; The Supply of Energy from and to Atmospheric Eddies, Proc.Roy.Soc., A97, p.354, 1920.

14. Townsend, A.A.; The Structure of Turbulent Shear Flow, Cambridge, Univ. Press, AMR 9, Rev. 4000, 1956.

15. Townsend, A.A.; Temperature Fluctuations over a Heated Horizontal Surface, J.Fluid Mech., 5, p.209, 1959.

Session Chairman's Opening
Adress

STATE OF THE ART OF SELF-LAUNCHING SAILPLANES

by

H.N. Perl

The evolution of the self-launching sailplane began, in the United States, some 40 years ago during the era of the primary glider. Several enterprising enthusiasts installed powerplants in these very basic aircraft with varied degrees of success. The major problem in those days (and in the general sense, even today) was the availability of suitable powerplants. Many of these aircraft employed modified motorcycle engines and a few installed small experimental type aircraft engines. These engines ranged from 25 to 40 horsepower, but, unfortunately, were quite heavy and bulky. In this same time frame there were a few serious attempts to produce a powered trainer. Two such aircraft, the Cycloplane and the Crawford were designed basically as powered gliders to be used as trainers. The depression of the early 1930's took its toll of these and many other aviation activities.

The relevance of this bit of history is to illustrate that even in the early phases of glider activity and development the problems of glider launching and training were recognized and many activities were undertaken in an attempt to provide solutions.

Germany also investigated this problem area. I discovered a photograph, in a 1937 issue of *Soaring* magazine, of a fleet of "Baby Grunau" sailplanes, all with small engines mounted on the fuselage. These engines were developed by Wolf Hirth and had an output of approximately 25 H.P. The present day Hirth engine now being used on many powered sailplanes is undoubtedly an outgrowth of this early development.

The SLS* activity in the U.S. during the late 1930's and during the World War II years was sporadic with no significant developments taking place. However, at the close of the war interest was again renewed. Ted Nelson and the late Wm. Hawley Bowlus began a modest program to explore the feasibility of producing a satisfactory SLS. I had the very good fortune to participate in this early activity.

The initial phase of this program began with the installation of a small two-cylinder target drone engine on the nose of a "Baby Albatross" sailplane. The flight tests were

* SLS - self-launching sailplane

conducted by Bowlus and for the most part were highly successful. A considerable amount of enthusiasm was generated among the group as a result of these tests and opened the way for further exploration. (As in many projects of this nature we had no idea as to where it would eventually lead.)

Nelson and Bowlus then proceeded to form a small company (Nelson Aircraft Corporation) and we were off and running. The chosen aircraft configuration was essentially that of a "Baby Albatross" sailplane and featured a side-by-side seating arrangement in a pod-like fuselage with a fixed engine in the rear. The project eventually culminated in the FAA type certification of a powered sailplane. This aircraft was the first, and to date, the only SLS to receive such an approval. The aircraft was called the Nelson "Dragonfly" and seven were eventually produced. Incidentally, the type certificate was issued in October 1947 -- just twenty-five years ago.

Coincident with the development of the "Dragonfly", Nelson undertook personally the development of the engine for the aircraft. This engine later became the first two-stroke cycle engine to receive an FAA type certificate. (It is certified for use both in conventional aircraft and helicopters.) The "Dragonfly" project was terminated in late 1947 due to adverse national economic conditions; all was not in vain however. The wealth of test data obtained during the type certification process of the "Dragonfly" was invaluable in the later development of the "Hummingbird". This aircraft is a two-place, tandem, retractable engine, high performance (circa 1950), self-launching sailplane. Seven of these aircraft were constructed on an experimental airworthiness certificate. To my knowledge four are still actively flying (including the prototype).

I have used this brief resume of history (with a bit of nostalgia, I might add), to set the stage for a review of the present state-of-the-art regarding self-launching sailplanes. As far as I can determine no other effort of the magnitude of the "Dragonfly" and "Hummingbird" projects has since been undertaken in this country. Current rumors have it that the Ryan Aeronautical Corporation of San Diego, California has a project under development involving a new self-launching sailplane. They are planning to make an announcement of the project in the next few months - at present everything is very hush-hush. I believe Richard Schreder has a project in this category also.

Other present day efforts in this country appear to be individual "one of a kind" projects and on a very small, limited scale, particularly when compared to the European efforts. For instance, the 1971 census for self-launching sailplanes shows only approximately 60 to 70 such aircraft in the U.S. Incidentally, a large fraction of these sailplanes are of European manufacture.

The state of self-launching sailplane activities in this country, as I see it, is still in the very preliminary phase of development. We have yet to optimize the design parameters for this type of aircraft. Factors which will have a major influence and impact on the future of self-launching sailplanes will be those Federal regulations which are now under consideration by the FAA. Proposed regulations include full certification requirements for powerplants, propellers, and ancillary equipment. It is also proposed that airmen's requirements will include a power rating for operation of self-launching sailplanes - this will also apply to flight instructors.

Technically, I feel there exists adequate, or perhaps a better word - sufficient, expertise, (in the general sense), to produce a sound, high performance, reasonably priced, self-launching sailplane. State of the art in such fields as aerodynamics, airfoil sections, structures, materials, powerplant design, etc., together with new, sophisticated analytical techniques are, to my mind, more than adequate to design and build a superior aircraft of this type.

The major problem areas, as I view them, lie basically in:

1. the field of economics,
2. acceptance of the concept by the soaring fraternity (and other related aviation circles),
3. formulation of reasonable, non-restrictive, Federal regulations, and
4. creation of an organization devoted to the promotion and development of self-launching sailplanes.

The big question yet to be answered in the realm of economics are those related to providing sufficient financial resources for development and production, and the creation of an adequate market to justify the investment. Otherwise, supporters of developmental and promotional activities will be forced to seek aid from philanthropic or governmental sources. It should be mentioned in passing that a major reason for the success of the "Hummingbird" project was adequate financial resources.

That the soaring fraternity, in general, has yet to put its stamp of approval on such aircraft is self evident. The "purist" philosophy is still all to prevalent in many areas and cannot be ignored. Certainly much work needs to be done to develop more interest in this field.

One must also be realistic about the ever increasing number of Federal regulations pertaining to such items as airworthiness certification requirements, powerplant certifications, airman's certification requirements, etc., as applied to self-launching sailplanes. These factors can create a significant impact on development and production costs, and on flight training costs.

Indirectly related, and not only confined to self-launching sailplanes, but to all soaring and general aviation activities, are the new airspace limitations now being put into effect. For example, we in the San Francisco Bay Area are just beginning to feel the impact of the new Terminal Control Area (TCA) which goes into effect in December 1972. I feel we must institute more effective liaison with the Federal agencies if we wish to maintain soaring as a viable, on-going sport in this country.

Considering the issues just reviewed it is obvious that some type of formal organization devoted to self-launching sailplanes is in order and long overdue if this facet of the sport of soaring is to succeed. There is a definite need to coordinate the many loose-end activities, formulate standards, and prepare a statement of objectives.

In conclusion, and to repeat my earlier statements, I feel that the technical expertise exists to produce a satisfactory, high performance self-launching sailplane. True, there are many technical fields such as powerplant design, propeller design, materials and fabrication technique improvements, etc., which need further investigation and study to better optimize the aircraft; however, there is no question but that such goals can be achieved. The solutions to the economic and regulatory problems, unfortunately, are not as straightforward as to their solution - but they cannot be ignored if successful self-launching sailplanes are to be built and marketed.

That there is an ever-increasing interest in this field of soaring can be attested to by the fact of this symposium, the recent self-launching sailplane contest held at Rosamond, California this last summer, and also the appearance on the scene of the new magazine *Motorgliding*. This publication is sponsored by the SSA.

That the movement has caught on in Europe is obvious, particularly from the number of new self-launching sailplane models now on the market. Whether the U.S. will step to the forefront in this most interesting and challenging endeavor only the future will tell.

SELF-LAUNCHING SAILPLANE D-39

by

Wilhelm Dirks
Akademische Fliegergruppe,
T.H. Darmstadt, W.Germany

Introduction

A powered glider should fulfil the following demands:

1. Soaring performance should be nearly as good as that of similar sailplanes.
2. Under power it should have a short t.o. distance, a good climbing speed, and a good cruising speed.
3. It should make little noise.
4. It should feature simple handling.

Configuration choice

Some examples already constructed and flying will now be discussed:

1. Engine installed in the front, fitted with a feathering propeller (SFS 31, ASK-14). The cooling air intake is at the nose.
2. Retractable engine and propeller (SF 27 M, D-37).
3. Ducted-fan in the rear fuselage (Sirius).
4. Tailless aircraft with a propeller behind the trailing edge (AV 36, FS 26).

Critical examination of these concepts gives the following results:

1. A front engine installation yields relatively simple construction and handling. The cooling is good and an effective exhaust system can be fitted. The propeller diameter can be as large as necessary when a retractable main wheel is used. Fitting of a drive is possible. Using all these possibilities optimum performance under power and low noise can be obtained. However, having the cooling air intakes and the propeller in front - even when it is feathered- produces so much drag that the gliding performance is unsatisfactory.

2. Retractable engine types guarantee gliding performance as good as those of sailplanes of similar configuration, but performance under power is comparatively poor. The drag increase of the D-37, for instance, is 40% when the engine is swung out. Problems arise for the engine section, which has to be quite small and of very low mass. A propeller of optimum diameter, a drive, and an effective exhaust system can hardly be accomodated in the fuselage of a high-performance sailplane. Because of the complicated mechanism of this configuration the reliability of operation is unsatisfactory.
3. The static thrust of a ducted-fan is too small. The gliding performance is poor because the duct adds drag.
4. Soaring performance of a tail-less glider is always smaller than that of a similar aircraft with a tailplane. Longitudinal stability is often unsatisfactory.

We can see, after this discussion, that a configuration with the engine in front might be optimal for a powered glider, if, during gliding, the propeller is folded away and the cooling air inlets are closed. Thus the D-39 powered glider will have a propeller which folds completely into the fuselage through openings closed by covering flaps. The engine (36 hp Hirth 017 snowmobile engine) has a cooling fan so that it can take the cooling air from the propeller openings, which remain open in powered flight. No further openings are necessary. Thus it is possible to construct a fuselage of high aerodynamic quality as shown in Figure 1.

The D-39 will be of fiberglass construction, with 15 m wing span, aspect ratio 20.5 and Wortmann laminar flow profile sections FX61-184 / FX60-126. Propeller speed is reduced by a cog-belt to half engine speed. The propeller diameter is 1.35 m (Figure 2).

Calculation of gliding performance

Gliding performance of the D-39 has been calculated using a digital computer. The results of this calculation may be compared with that of the high performance sailplane D-38 which has the same wings and tailplane as the D-39:
The drag of the fuselage (Figure 3) will be only 7% larger than that of the smaller D-38 fuselage, if it is possible to have a laminar boundary layer on the front part. However, it is probably not possible to keep laminar flow beyond the spinner. Thus further calculations are done assuming a turbulent boundary layer. The drag is 25% greater than that of the D-38 fuselage. However, the air speed versus sinking speed charts show that the performance of the powered glider is nearly as good as that of the sailplane (Figure 4).

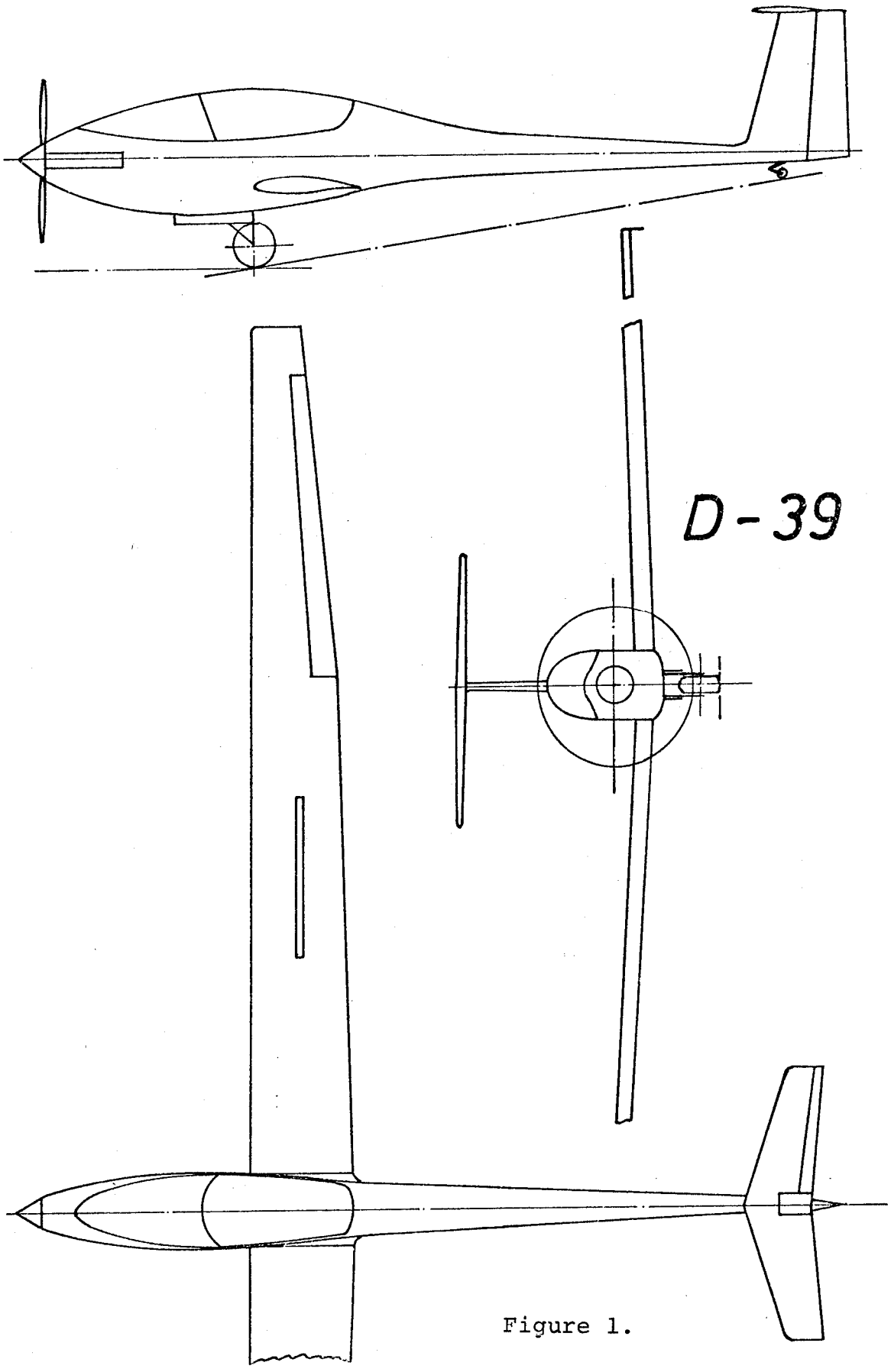


Figure 1.

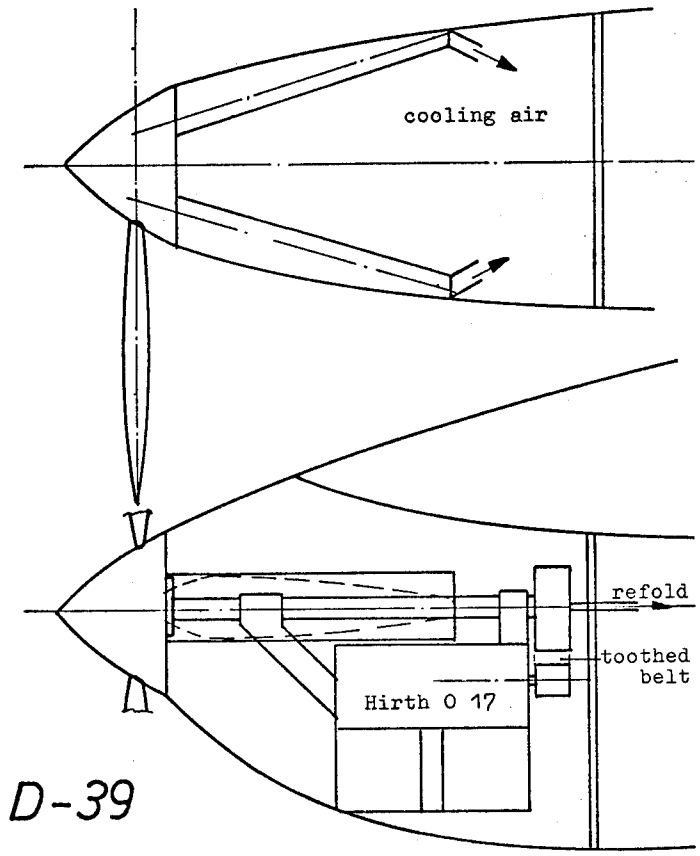


Figure 2.

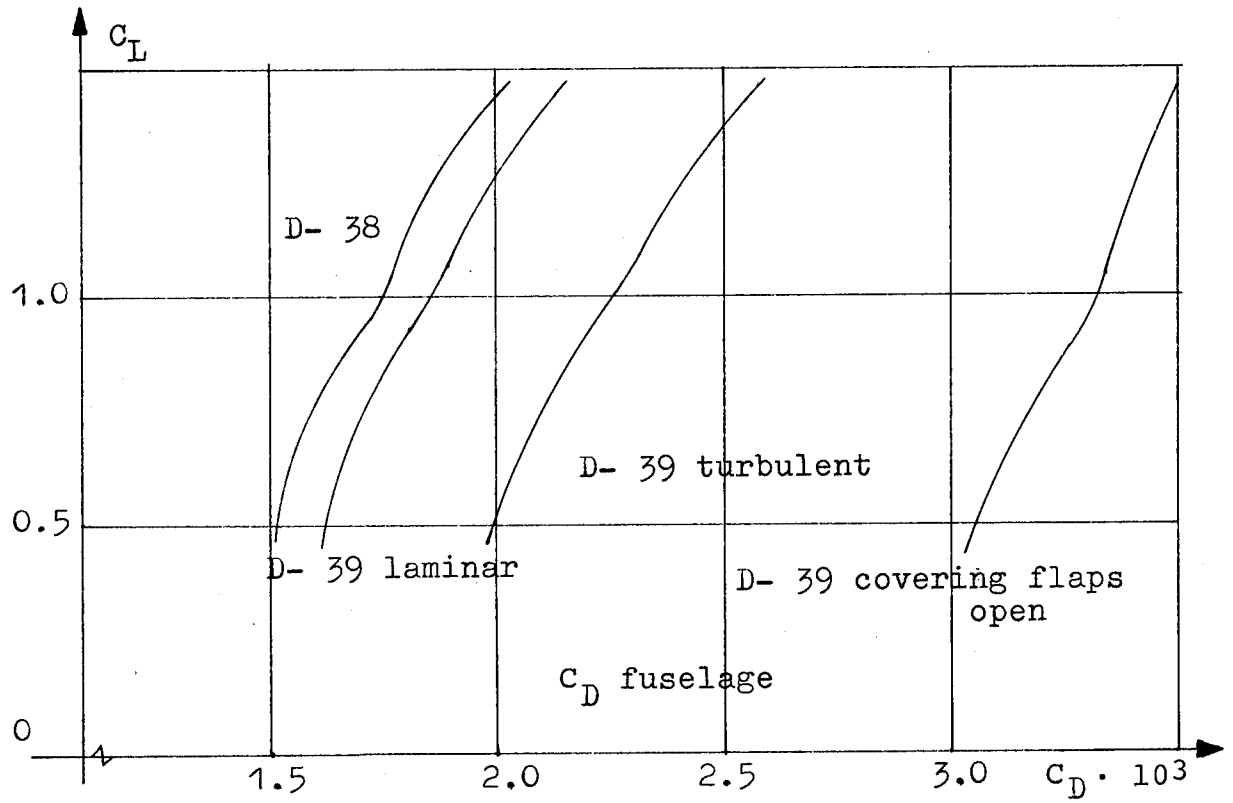


Figure 3.

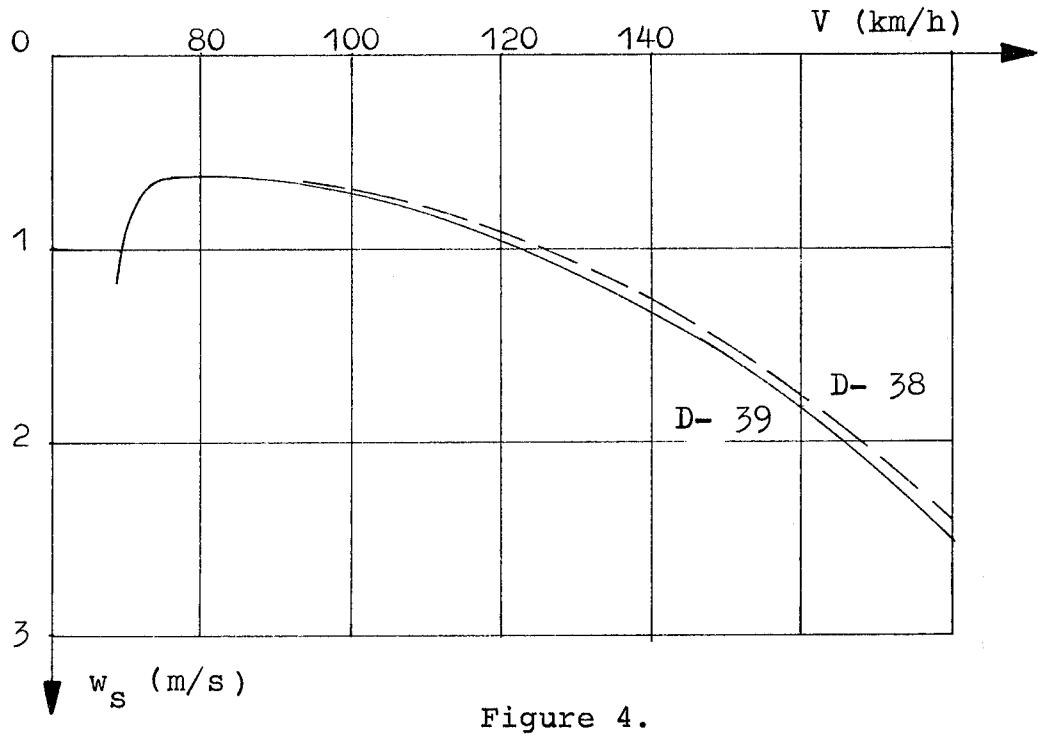


Figure 4.

The best method to compare the performance of sailplanes is to calculate the cross-country cruising speed. This was done using a digital computer. Figure 5 shows the cruising speed calculated for the D-39, the D-38 and the standard class sailplane ASW 15. The cruising speed of the D-39 is only 3% to 5% lower than that of the D-38 and as good as that of the ASW 15. If lift is very weak the D-39 is inferior to the sailplanes because of the minimum wing loading of 29 kg/m^2. (In this case sailplanes normally cannot continue their cross-country flight and have to land. Then the powered glider, of course, is superior.)

Design of an optimum propeller

Using Reference 1 it is possible to choose the optimum propeller diameter, speed, and blade loading for static thrust, climb and cruise. Using these results a propeller for optimum climbing speed was designed using Theodorsen's propeller theory [2]. The result is a C_L vs b distribution, which completes the blade data required. Clark Y profile sections were chosen for the D-39 propeller.

Calculation of performance under power

The calculation of the thrust for various airspeeds was done using the theory of Betz [3,4]. This calculation was also done using a digital computer. The results are plotted in Figure 6. The cruising speed is 51.6 m/s at a propeller speed of n = 2880 rpm. Rate of climb is w_s = 3.60 m/s at an

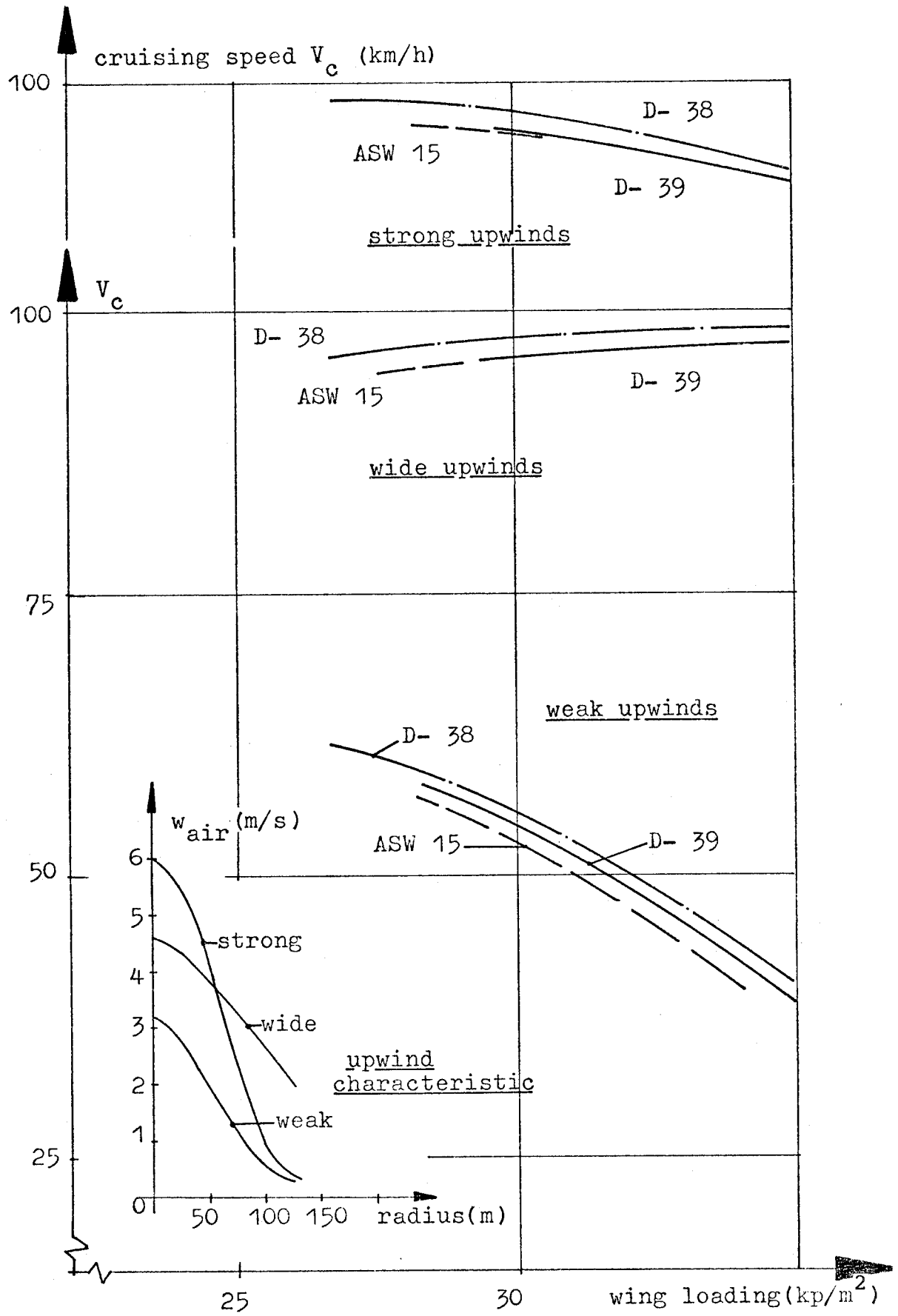

cruising speed V_c (km/h)
100
D- 38
ASW 15
D- 39
strong upwinds
V_c
100
D- 38
ASW 15
D- 39
wide upwinds
75
weak upwinds
D- 38
ASW 15
D- 39
50
w_{air} (m/s)
6
5
4
3
2
1
0
strong
wide
weak
upwind characteristic
50 100 150 radius(m)
25
25
30
wing loading(kp/m^2)

Figure 5.

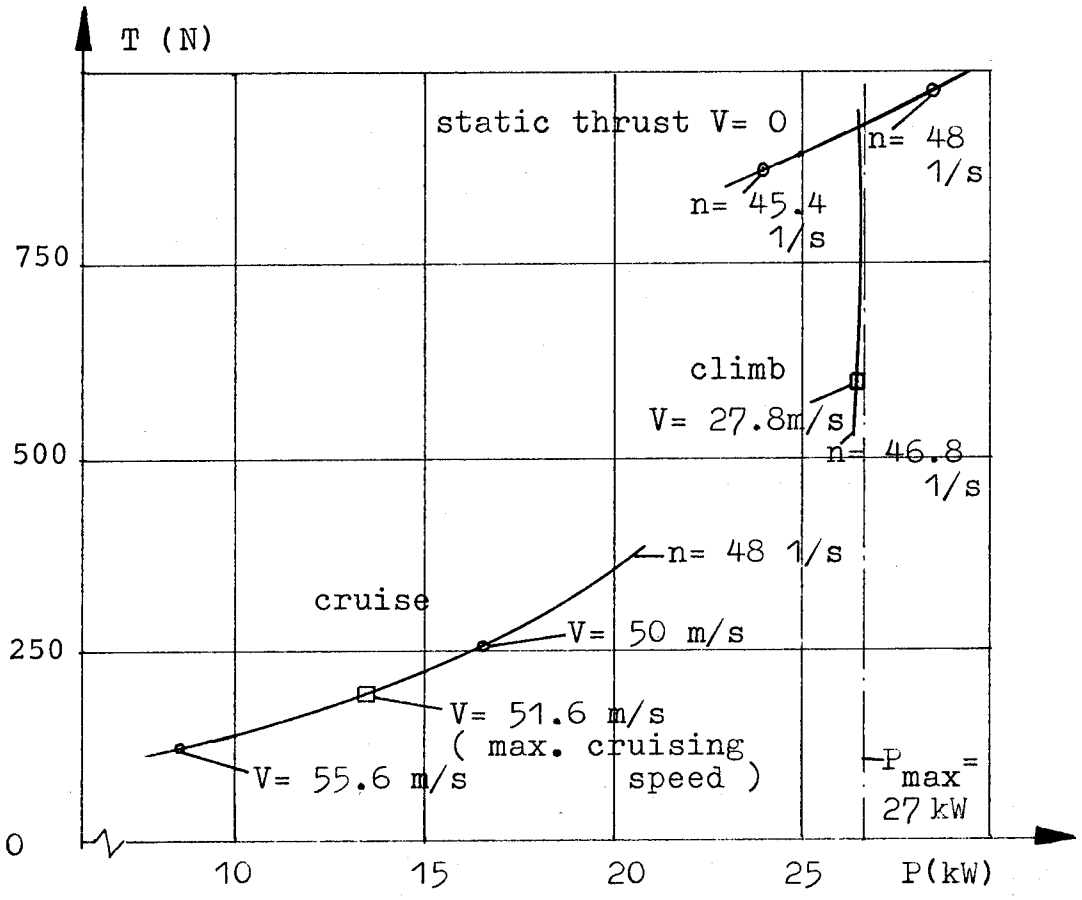


Figure 6. Propeller charts

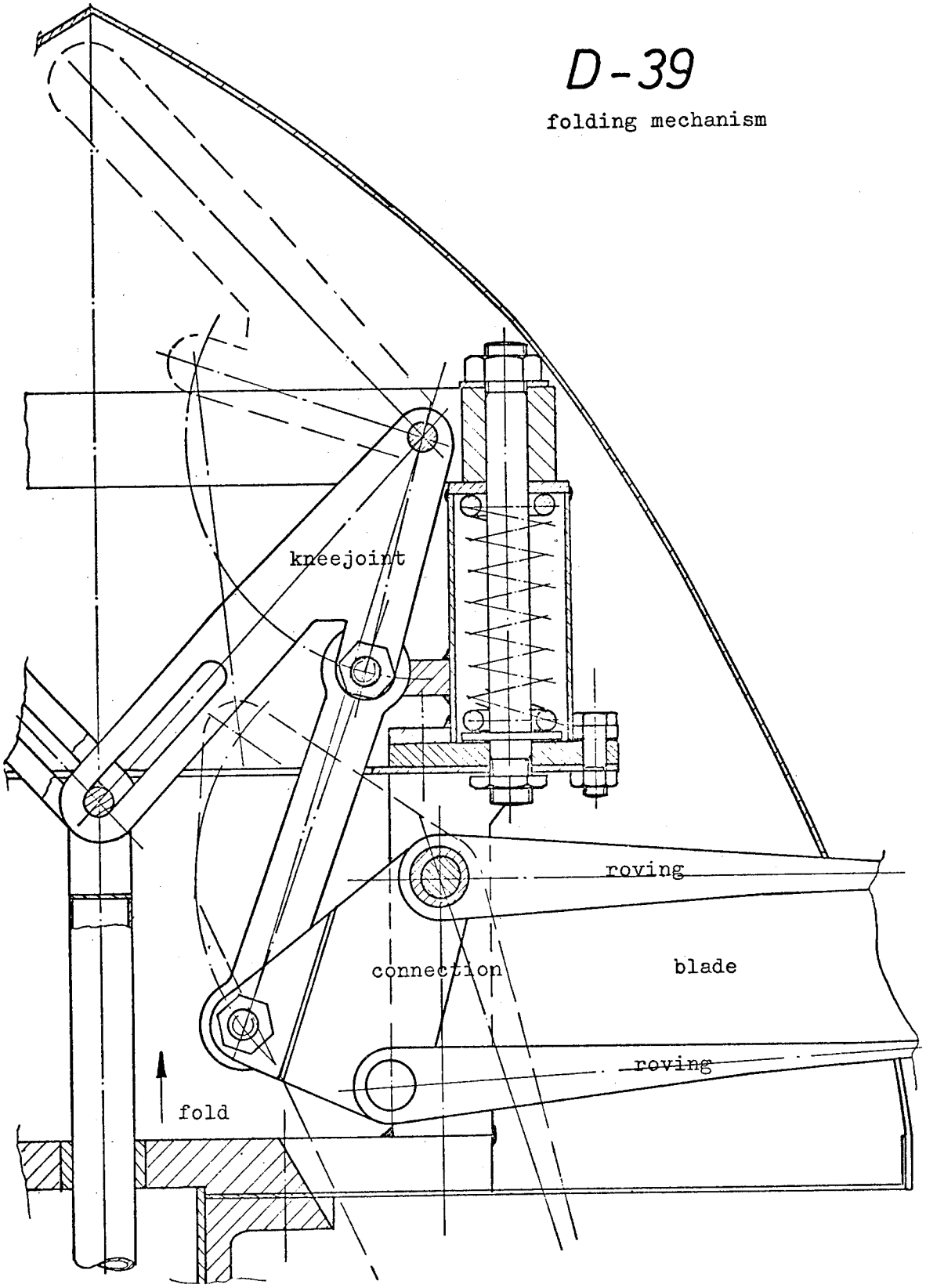

D-39
folding mechanism
kneejoint
roving
connection
blade
roving
fold

Figure 7.

airspeed of V = 27.8 m/s and a propeller speed of n = 2810 rpm. Static thrust is T = 925 N at a propeller speed of n = 2810 rpm. This performance under power is better than that of current powered gliders of similar configuration.

Design of the propeller blades and folding mechanism

The propeller blades will be made of the fiberglass reinforced plastics. The advantage lies in the smaller weight by comparison with wooden blades. The fiberglass rovings of the blade are used for the connection to the hub also, without need for additional material. Figure 7 shows the connection. Figure 8 shows the construction of the blade. Torsion is taken by a fiberglass laminate with the weave directed at 45 degrees to the centerline of the blade.

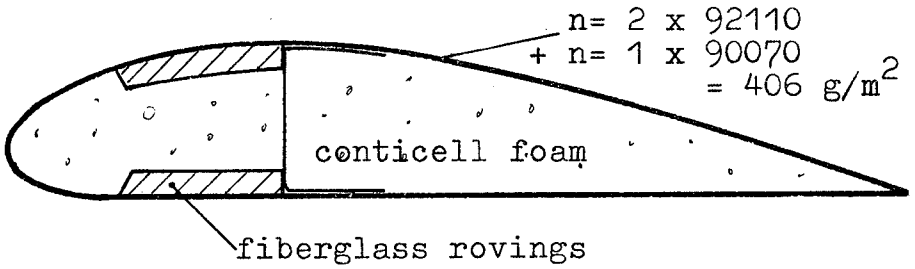


Figure 8.

The blade folding mechanism (Figure 7) is operated by the pilot when the propeller has stopped rotating. In operational position the propeller blades are fixed by a knee joint. Centrifugal forces add to the kneeing action.

References

1. Hartmann, E., Biermann, D.; NACA Report No. 640. The aerodynamic characteristics of full-scale propellers having 2, 3, and 4 blades of CLARK Y and R.A.F. 6 Airfoil sections.

2. Crigler, John L.; NACA Report No. 924. Application of Theodorsen's theory to propeller design.

3. Betz, A.; Schraubenpropeller mit geringstem Engergieverlust, Göttinger Nachrichten 1919 S.193.

4. Just, W., Jaeckel, K.; Bericht 3 Aerodynamik der Hub- und Tragschrauber Teil 2 Berechnung des Rotors, Bericht der Deutschen Studiengemeinschaft Hubschrauber e.V.

THE HIGH PERFORMANCE MOTOR GLIDER AND ITS APPLICATION IN COMPETITION FLYING

by

Ian Strachan
British Gliding Association

Introduction

The pattern of high-performance motor gliding in the future will be set by the next generation of designs reaching the gliding movement. This may in no small measure be influenced by the contest rules approved by the CIVV for the first world Motor Glider championship which will define whether engines will be allowed to be used extensively, or whether they will be regarded simply as aids to prevent field landings. Following this introduction is a design specification for a high performance single seat motor glider (HPMG), a suggested draft for CIVV Motor Glider contest rules, and a list of the additional British Gliding Association (BGA) rules that at present enable motor gliders to take part with gliders in BGA contests. Perhaps the biggest factor which presently holds up HPMG development is the lack of a suitable engine. All motor glider enthusiasts should scan the lists of commercial engines for those will power outputs of 35-50 bhp at high power/wt ratios, and write to their soaring magazines (and the glider manufacturers) with details of likely units.

All glider pilots who find themselves interested in owning the HPMG of the specification described later should make their views known loud and clear to the glider manufacturers. Similarly CIVV should receive as many inputs as possible through national representatives before final decisions are made on contest rules. We must ensure that motor glider contests are won by *soaring* in high performance *sailplanes*, and not be indiscriminate use of engines in "compromise aeroplanes" that do not soar very well but have superb engine-on performance.

Specification for a high performance motor glider

At the recent British Open and Standard Class championships much discussion ensued in the periods of bad weather about the future of our sport. Few pilots denied the place

Note: The views expressed herewith are those of the author and do not necessarily represent British Gliding Association policy.

of the high-performance single seat motor glider (HPMG) in the future, especially in Europe with Air Traffic restrictions becoming more severe, and the pattern of farming making field landings more hazardous. The problem is that a suitable machine does not exist at present. When presented with a really good design specification for the HPMG, many British Championship pilots expressed great interest, several saying "Well, of course I'd buy one like THAT - the trouble at present is that the motor glider has just not been DEVELOPED enough....". Meanwhile the manufacturers try and outdo each other in competing in the same market for bigger and bigger glass gliders and do not seem to be looking to the large international sales which surely must fall to the first of them to come up with a viable HPMG. The most advanced production line MG is still the SF27M, which was flown in German Nationals as long ago as 1968. Its fully retractable engine and K6E soaring performance (except in weak thermals) surely show designers the way to go. Since 1968, Scheibes have added an electric starter and pneumatic strut which compresses on engine retraction, thus aiding the extension of the engine before re-starting. But what is needed now is more span. Most big gliders of the 1970's are carrying water ballast. How much more useful to have "engine ballast" on a congested launch point, or when about to land in a field far from home! So, manufacturers and designers, take an existing advanced glider, put into a suitable engine either mounted on an SF27M type retractable strut or fuselage-mounted driving a ducted fan, and do your best to fulfill the specification below:

Design specification

Points mentioned are in order of importance, 1 - 8 being particularly fundamental.

1. General Philosophy. When soaring with engine switched off, the machine's characteristics should closely correspond to those of existing high-performance gliders. This includes handling qualities, cockpit layout, performance, ancillaries such as airbrakes, flaps etc. The machine should firstly aim to be a viable high performance soaring machine, only secondarily carrying the engine, as an aid to increasing the time spent in soaring.

2. Thermalling Performance, engine-off, should be as good as or better than a Standard Cirrus, with the machine at "Soaring All Up Weight". Soaring AUW is defined as that of a fully equipped machine with a 200 lb pilot and fuel for 150 km of flight in still air. It is essential that any measure or calculation of "thermalling performance" takes account of very weak thermal conditions. The machine's low-speed polar should either be similar to the Standard Cirrus, or if minimum sink were higher it must be achieved at a significantly lower speed.

3. Maximum Glide Ratio, engine-off, should be better than 38 : 1.

4. Restarting the engine whilst airborne should be:

   a. 99.9% reliable, assuming the pilot made correct selections.

   b. Actuated by a single action which should not require any physical effort or mental concentration. It should be possible to thermal the machine down to the same altitude as a normal glider, select a field, make an approach to the field as far as actually using airbrakes. Having ascertained that a safe landing in the field is possible, the engine start circuit should then be actuated. This would automatically extend the engine (if strut mounted) and when extended would make a microswitch which would cut in the starter. When the engine developed power, the airbrakes would be retracted and the throttle opened to climb away. The height loss between engine selection and the development of enough power for level flight should not exceed 100 feet, in the approach configuration and at normal approach speed.

   Notes on restarting.

   a. If a lightweight cartridge starter is used, a breech of at least 6 shots should be designed.

   b. If an electric starter is used, it should work on 12 volts and have a ground power connection fitted for starting from car electrics or portable battery packs. The engine, when running, should recharge the glider batteries.

   c. If the engine is mounted on an extensible strut, a simple manual method of extending the engine should be provided in addition to any automatic (e.g., hydraulic or pneumatic) method.

   d. An emergency starting method should be designed for use on the ground should the main method fail. This could be a method actuated by pulling a cable.

5. Sink at 80 kt should be 3 kt or less (150 km/h, sink 1.6 m/s), engine-off, at soaring AUW.

6. The engine should be designed to be easy to remove, e.g., by use of pip-pins and push-pull connectors. The machine must have a full clearance to fly with engine removed. The designer should ensure that as much weight as possible is removed by this process - for instance it may be possible to remove not only the engine but its mounting strut at the same time. The object should be that, with no specialised tools, it should be possible to remove the engine and make the machine ready for flight as far as the engine ancillaries are concerned, in 10 minutes. For refitting a serviceable engine and making ready for inspection and engine test running, 15 minutes.

7. Take-off run on short grass to 50 feet at speed V2 in still air, ISA + 10°C and at soaring AUW, to be 300 m or less.

8. The normal glider characteristics, mentioned as the over-riding design requirement in number 1 above, to include the following:

a. Full airbrake and/or flap arrangements to make normal short field landings.

b. Normal glider towing hook for launching.

c. Normal stressing and clearance for cloud flying at soaring AUW.

d. Normal rigging, derigging and trailer stowing characteristics.

e. Capability for fitting full glider instruments and oxygen.

9. Engine-on rate of climb to be at least 400 ft/min (2m/s) at climbing power, still air, ISA + 10°C and at soaring AUW.

10. The undercarriage should incorporate shock absorbtion devices and have a powerful wheelbrake.

11. Range on a full tank of fuel should be at least 300 km in still air. It should be possible to use the radio on both transmit and receive whilst running the engine.

12. The engine should be a production line type for which spares are cheap and readily available. Syndicates typically would buy a second engine as a spare.

13. The increase in price over a glider of similar soaring performance should not be greater than £1000 or $3000, the aim being to decrease this differential as numbers of orders increase.

14. Ground handling. Provision should be made for detachable wing supports or wheels, to enable unassisted take-offs to be made. With such supports fitted, the machine should be capable of taxying, directional control being through a steerable tailwheel inter-linked with the rudder.

15. Longe Range Transit. Consideration should be given to the design of over-load fuel tanks and luggage panniers (all detachable). In the "Long Range" configuration, a 500 km minimum range starting at maximum AUW would be required, without assistance from thermals.
Maximum AUW could be cleared for "gentle manoevers only" and must include a generous baggage allowance.

This specification is easily within the state of the art at present. Perhaps the most difficult part is to find a suitable engine. Between 35 - 45 bhp are required, at a high power/weight ratio. So - Manufacturers - Awake, do some research, get the production lines going. There will be plenty

of orders. And more soaring achieved to boot. Our sport may be changed somewhat, and this machine will expand and enrichen it especially in countries which have adverse soaring weather.

Draft CIVV MG rules for contests

Part 1 - Discussion

1. The easiest approach to the problem is to accept that most glider contest rules will apply and all that will be necessary is to specify the extra rules for a motor glider class. The author is in favour of making MG contests as close as possible to glider contests but eliminating the inconvenience of landing out. It is suggested that at this early stage of motor glider development, any departure from the principles of CIVV glider rules should be viewed with suspicion and that rules should encourage soaring and discourage engine running. It follows that:

   a. Penalties should be awarded for <u>any</u> use of engine during the contest performance.

   b. Race tasks only should be set, and no points awarded for failure to complete the race.

2. Point a. is worth discussion. To the author it seems that any completely free use of engine (other than for the launch) is not desirable as it will lead to a glorious "burn-up" of engine time on final glide, aiming to cross the finish line with exactly no free time left. Such calculations seem unnessary and possibly hazardous if engine time is miscalculated and it has to be switched off towards the end of a final glide to avoid penalty. Also the practicality of giving a certain amount of free time and then penalising further use of engine is questionable. Just try writing a suitable formula and rules without incurring anomalies. In particular the machine which has excellent power performance but poor thermalling capabilities will be given a huge advantage on weak thermal days over machines that are far superior soaring gliders. It will be able to run its engine for 1/3 of the time, gain height quickly and glide for the remaining 2/3, repeating the produce over again and achieving an excellent speed without the "inconvenience" of pausing to thermal. Whatever rules are finally agreed, they must not enable pilots of such machines to score well by not soaring and should cater for the case of an aeroplane that can achieve an overall speed of, say, 60 kt (111 km/h) which uses its engine only 1/3 of its total time. If you think this is far-fetched, the RF5b, SF27M and K14 can do this now, and improvements in the next few years should make this a regular feature of motor gliders. After all, it only needs an engine-on rate of climb of twice the numerical sinking speed of the machine at 60 kt to achieve this order of performance without thermals.

3. The alternative of giving all competitors a calibrated amount of fuel to use on the task is a practicable solution but is quite unacceptable because it destroys the flexibility of using only the fuel needed by the soaring conditions found en route. It also commits the pilots to the safety hazard of deliberately running out of fuel just as they finish. And who would decree the basis upon which fuel is issued to each machine? If too little were issued on a day that turned out to be poor, all would land out, so defeating the main advantage of the motor glider.

4. The author considers that the scoring system must cater fairly for three cases:

a. The day of excellent soaring weather where little engine will be used on task by good pilots.

b. The day of poor weather where soaring is hard work but up to, say 5 minutes engine per hour of air time is legitimately used by good pilots to complete the task.

c. The presence of the machine of good aeroplane performance that, without thermals, can achieve 60 kt overall with use of engine for 1/3 of total time.

5. It seems reasonable to base penalties for the use of engine not for set minutes of engine time, but pro rata on engine time used divided by total time on task. Clearly 30 minutes of engine used in 1 hour getting round a 100 km triangle would not be meritorious in the least, whereas 30 minutes in 6 hours getting round a 300 km triangle might be a hard-fought creditable performance.

6. Formulas for engine time penalties should now be considered. It is suggested that a graph be constructed with axes of Scoring Speed (i.e., the devaluation factor to be applied to true speed) against minutes of engine used per hour of flight. It might be thought that the formula derived would be a useful basis for scoring. Unfortunately the formula itself is rather complex and in any case an arbitrary devaluation would have to be applied to pilots achieving a good "soaring speed", but achieving this by bypassing poor soaring weather by running their engines.

7. Figure 1 shows a very simple formula, varying linearly from no devaluation for no use of engine (the only point on which pilots will agree) to complete devaluation at 15 minutes engine per hour. Unfortunately this has a major anomaly. Consider a pilot meeting bad weather en route and running his engine for just over 15 min/h, but when he arrives at the finish line it is still soarable. If he does not cross the finish line, but "holds off" by local soaring, he decreases the proportion of engine time used and so will score. There will then be an optimum time to "hold off" after which his score decreases because his overall speed becomes slower. To impose such calculations on pilots should NOT be the object of the scoring system. It may be shown that with most "straight line" formulas such as this one, if speed is

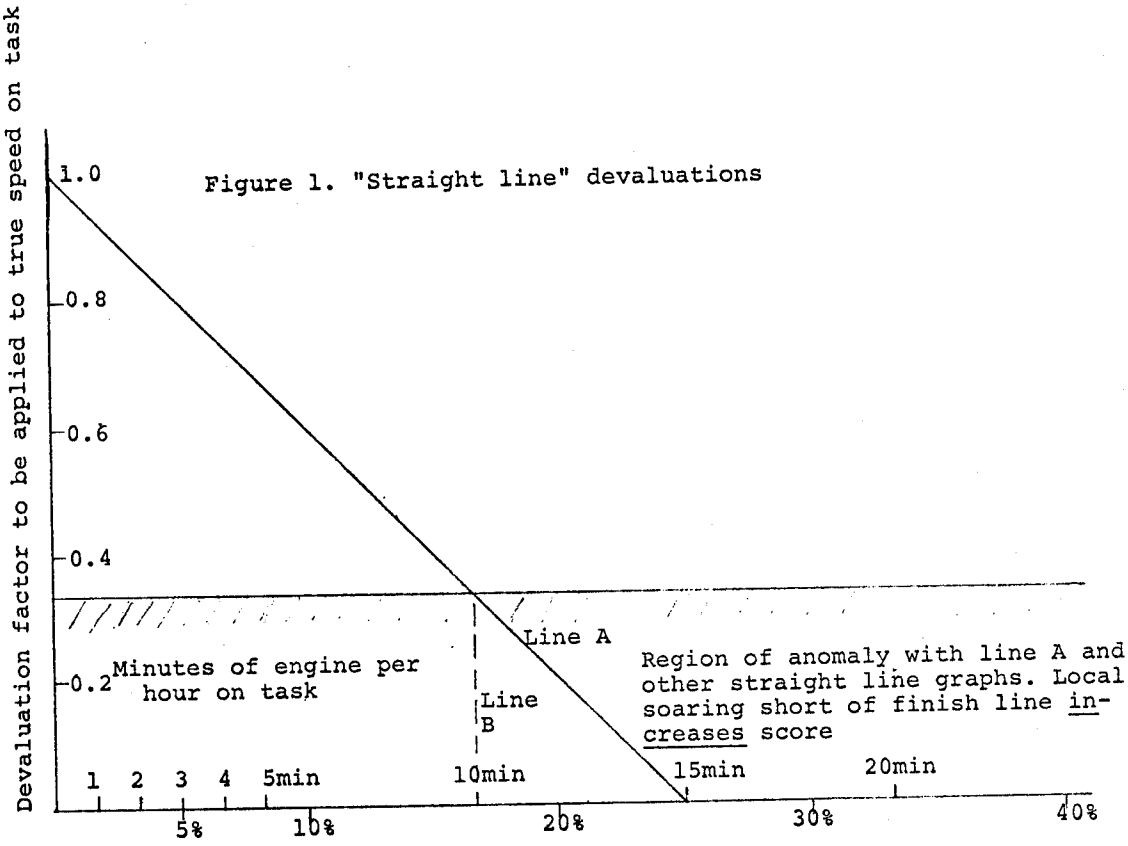


Figure 1. "Straight line" devaluations

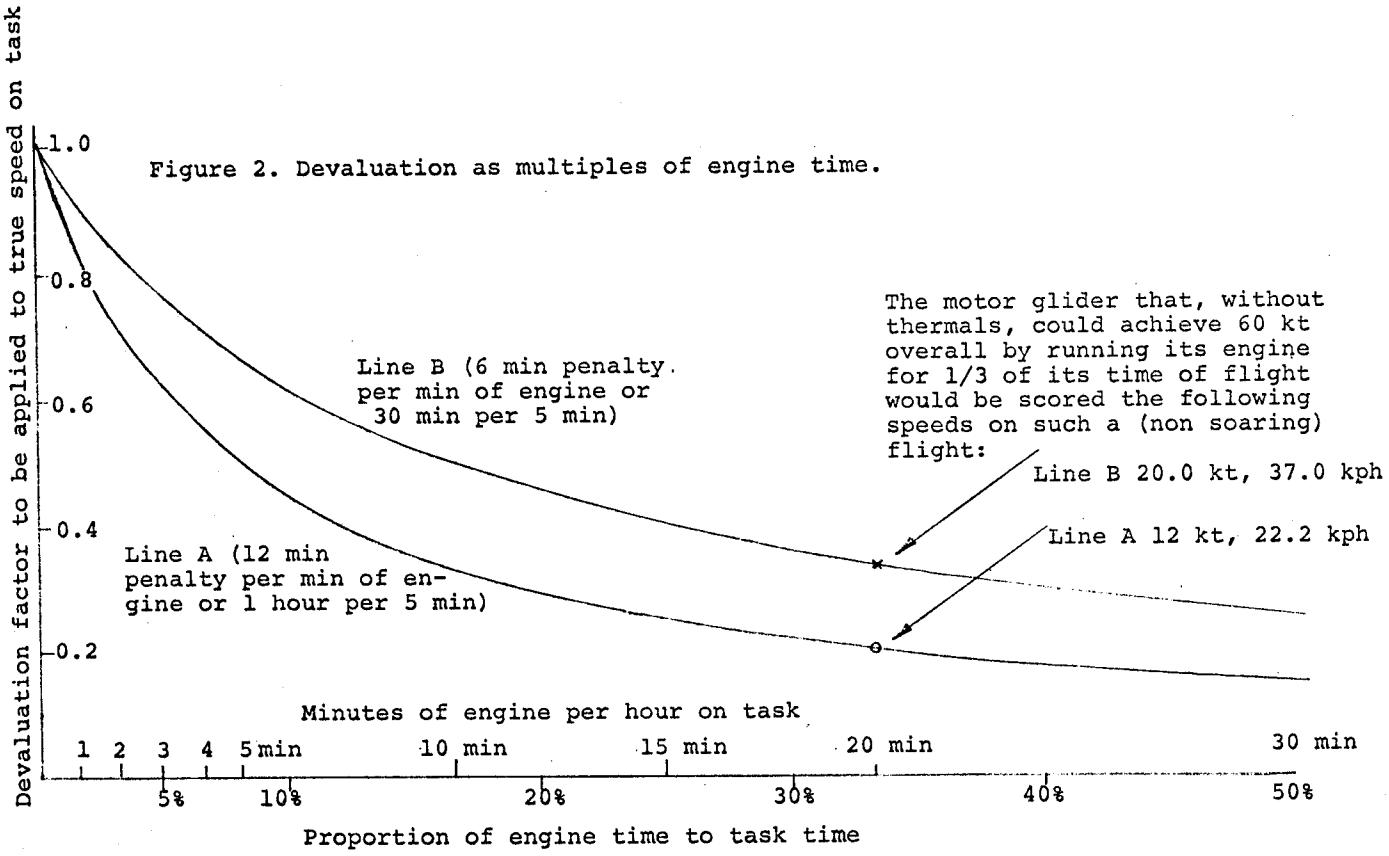


Figure 2. Devaluation as multiples of engine time.

devalued to 1/3 or less of real speed, this anomaly is present and pilots gain from prolonging their flights by local soaring short of the finish line. Line B of Figure 1 is a partial solution to the problem but not a good one.

8. We could also add a set multiple of the engine running time to the real time for instance adding 30 minutes of task time for each 5 minutes of engine. Figure 2 shows the shape of such formulas. The sharp slope at the left hand side prevents indiscriminate use of engine where it isn't necessary. But the small slope later could cause problems on poor soaring days where the machine with good aeroplane performance will tend to win without much soaring. This effect can be reduced in several ways:

a. An efficiency factor could be used, multiplied by the engine time. Such factor should reflect the machine's ability to achieve speed without soaring. A highly efficient "aeroplane" would have a factor of more than 1 and so be pushed further to the right on the curve, thus balancing the faster true speed achieved.

b. As in speed scoring in some glider rules, by having a complete cut-off of marks at, say, half the winner's speed. In this case it would be the speed adjusted for engine time. Motor Gliders achieving poor adjusted speeds due to a lot of engine time would thus score very little.

c. Having a general "day devaluation" for days where most pilots used a lot of engine. It is suggested that if a lot of pilots used engine for, say 1/5 of their total time (12 min/h) then the day would be pretty worthless as a competition. After all, that is the equivalent of 2 "relights" or aero tows per hour of flight!

d. Having a larger, rather than smaller, devaluation for use of engine. Line A in Figure 2 with 1 hour penalty for every 5 minutes of engine would cater for more anomalies in scoring than the shallower line B where only 30 minutes is added for each 5 minutes of engine. It also encourages good, old fashioned, soaring, as opposed to tempting pilots to run their engines when they could stay up in lift if they persisted. Pilots should be given straightforward rules to fly under and should not have to be always calculating if it is better to take a thermal or to use engine. The best rules will make such decisions simple, i.e., that engine should only be used if really desperate. Any deviation from this philosophy will lose credit with the rest of the soaring movement.

9. The advantage of those formulas shown in Fig. 2 is that they are easily intelligible to pilots when airborne A pilot can say to himself: "I am stuck here in a very weak thermal which will take me more than 30 minutes to work up to a decent height and position, so as the penalty for 5 minutes of engine is 30 minutes it will be productive to use the

engine, especially as I can travel along track to a more favourable area in so doing".

10. Other devaluation formulas also exist. Line A of Fig. 3 shows a formula based on a "square law". Five percent of engine time would add 5^2 minutes to task time, 6 percent would add 36 minutes, etc. Line B doubles this so that 5% would add 2 x 5^2 and 6% would add 72 minutes to task time. Line C is a cube law where 5% engine would add 5^3 minutes to task time. The merit of these devaluation laws is the marked reduction in score as engine running increases to a level that implies that not much soaring was done. The cubed law graph is probably too steep but the right hand ends of Lines A and B are entirely practical and better than those shown in Figs. 1 and 2. Note that the point on Line A at 12% use of engine co-incides with the same point on Line A of Graph 2. More of this later.

11. Some motor glider enthusiasts have argued for only a small devaluation for little engine running, steepening with increase in engine time. Lines A and B of Figure 3 might satisfy such pilots who will undoubtedly think that the steep devaluation to the left of Figure 2 is too much. But before agreeing on the best devaluation formula we must carry the argument a stage further.

12. It is no good simply looking at devaluation graphs and selecting the one that "appears" the best. It must be borne in mind that when the engine is running the machine is not only climbing but is progressing along track. If we select the wrong formula we may still allow a pilot to win on a weak day by motoring round. Figure 4 shows the increase in speed round a task assuming the following conditions:
That thermals will allow a 100 km triangle to be completed in 3 hours. This is taken as the datum "weak thermal day". This is a speed of 33 1/3 km/h or 18 kts, using thermals alone. Let us assume also a machine of engine performance as stated in Para 4c and discussed at the end of Para 2. Such a machine achieves 60 kt overall speed by climbing for 1/3 of the time and gliding the rest without soaring. It may be shown by simple calculation that the graph in Fig. 4 is linear between these two points. What we must do now is to combine Fig. 4 with the various devaluations of Figs. 1-3 to see the real effect of such devaluations on the SCORING SPEED of motor gliders. The author suggests as a basic premise that an INCREASE of score should never be possible by deliberately running the engine, for the reasons given in Para 8(d).

13. The convex line at the bottom left of Fig. 5 shows how the "straight line" devaluation of Fig. 1 is translated into scores. It has an anomalous region at its left hand and where more score occurs by engine running. However, the curve drops below its starting point of 18 kts if either the thermal strength increases to allow more speed from soaring, or if the machine in fact cannot achieve the assumed 60 kt with

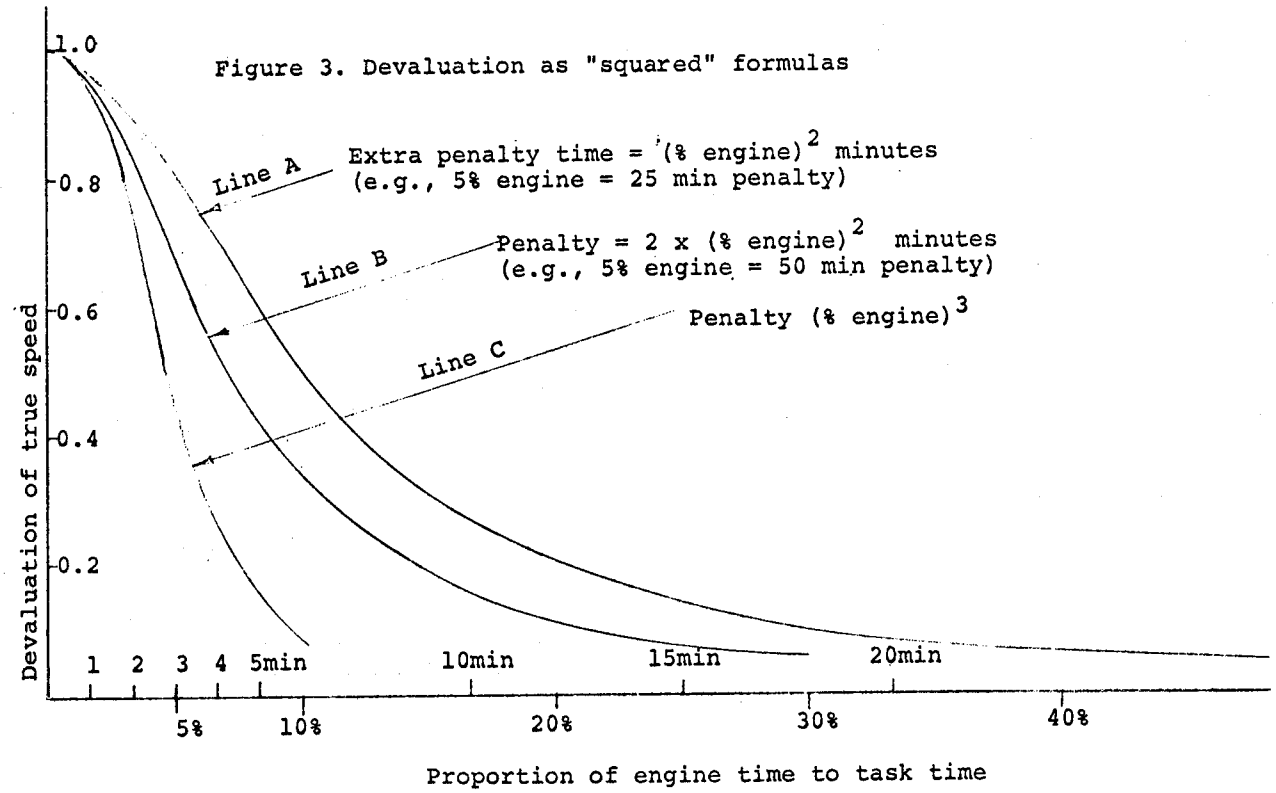


Figure 3. Devaluation as "squared" formulas

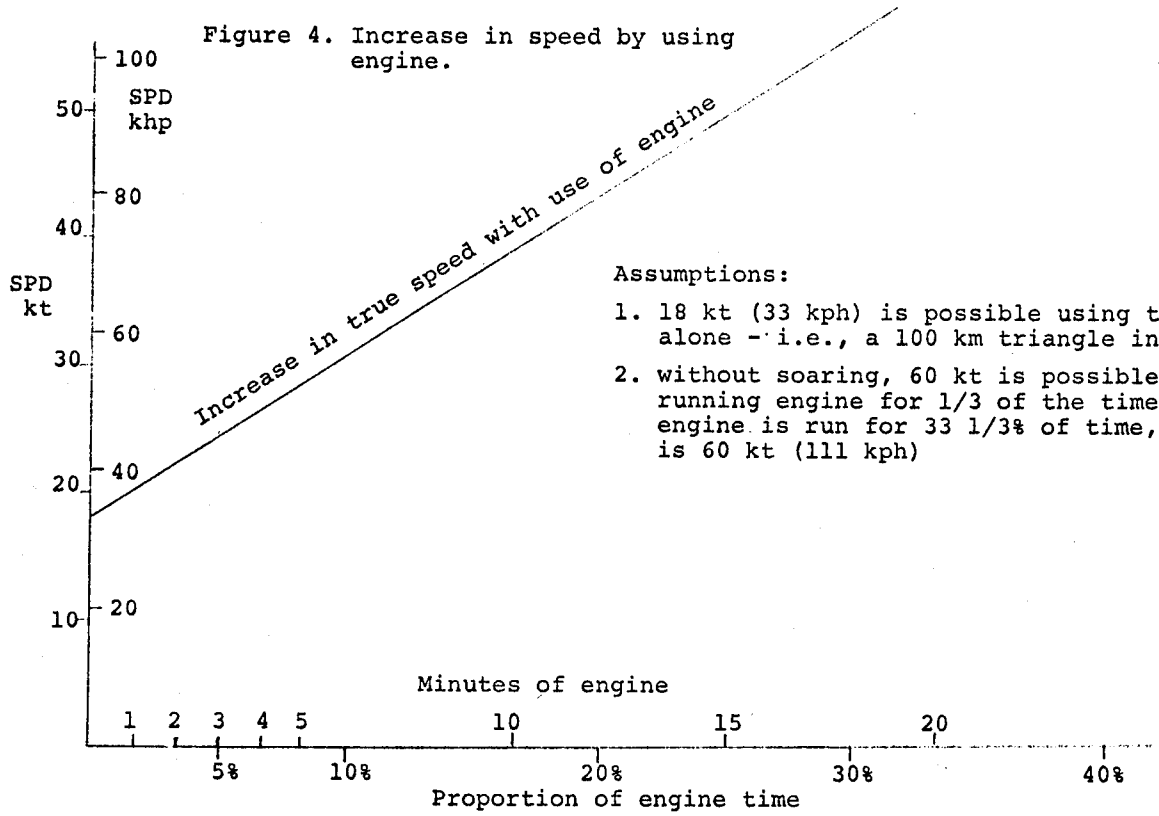


Figure 4. Increase in speed by using engine.

Assumptions:

1. 18 kt (33 kph) is possible using thermals alone - i.e., a 100 km triangle in 3 hr
2. without soaring, 60 kt is possible by running engine for 1/3 of the time. So if engine is run for 33 1/3% of time, speed is 60 kt (111 kph)

Figure 5. Scoring speeds (1)

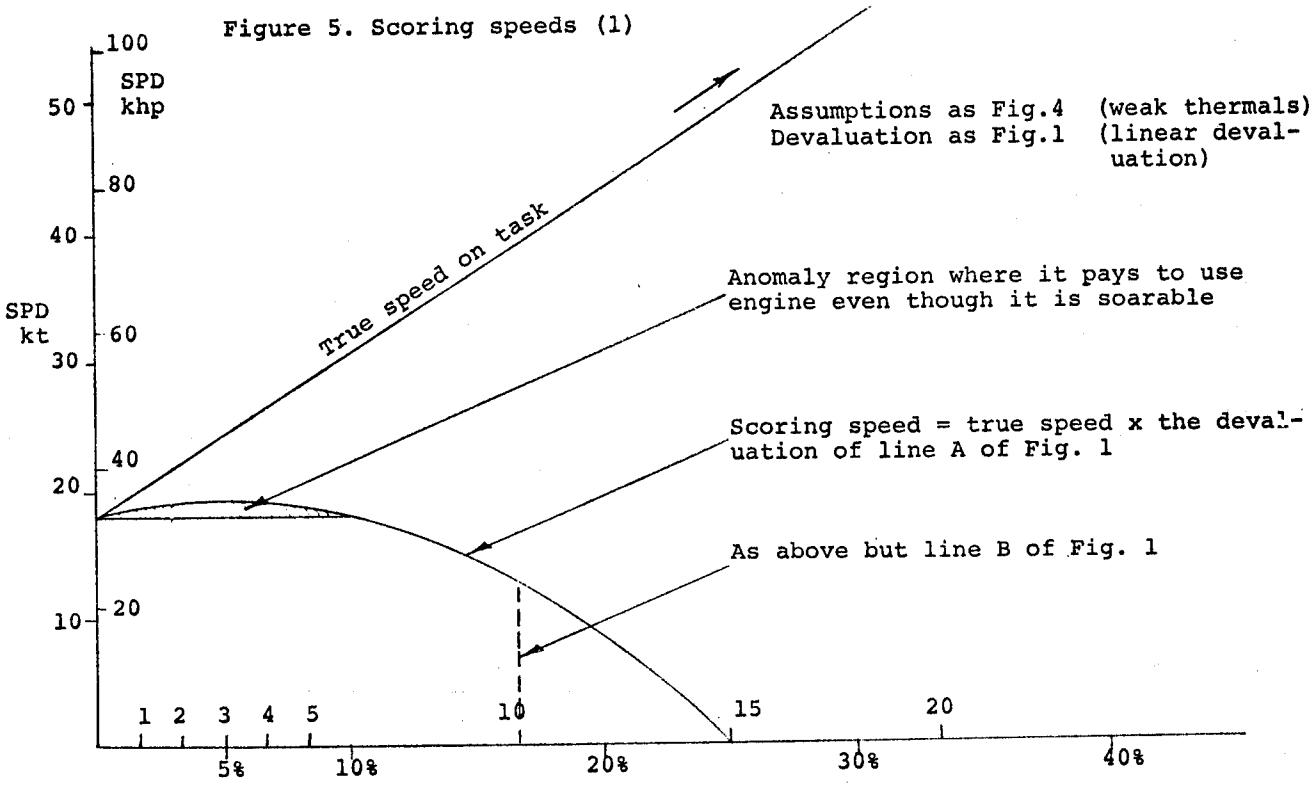
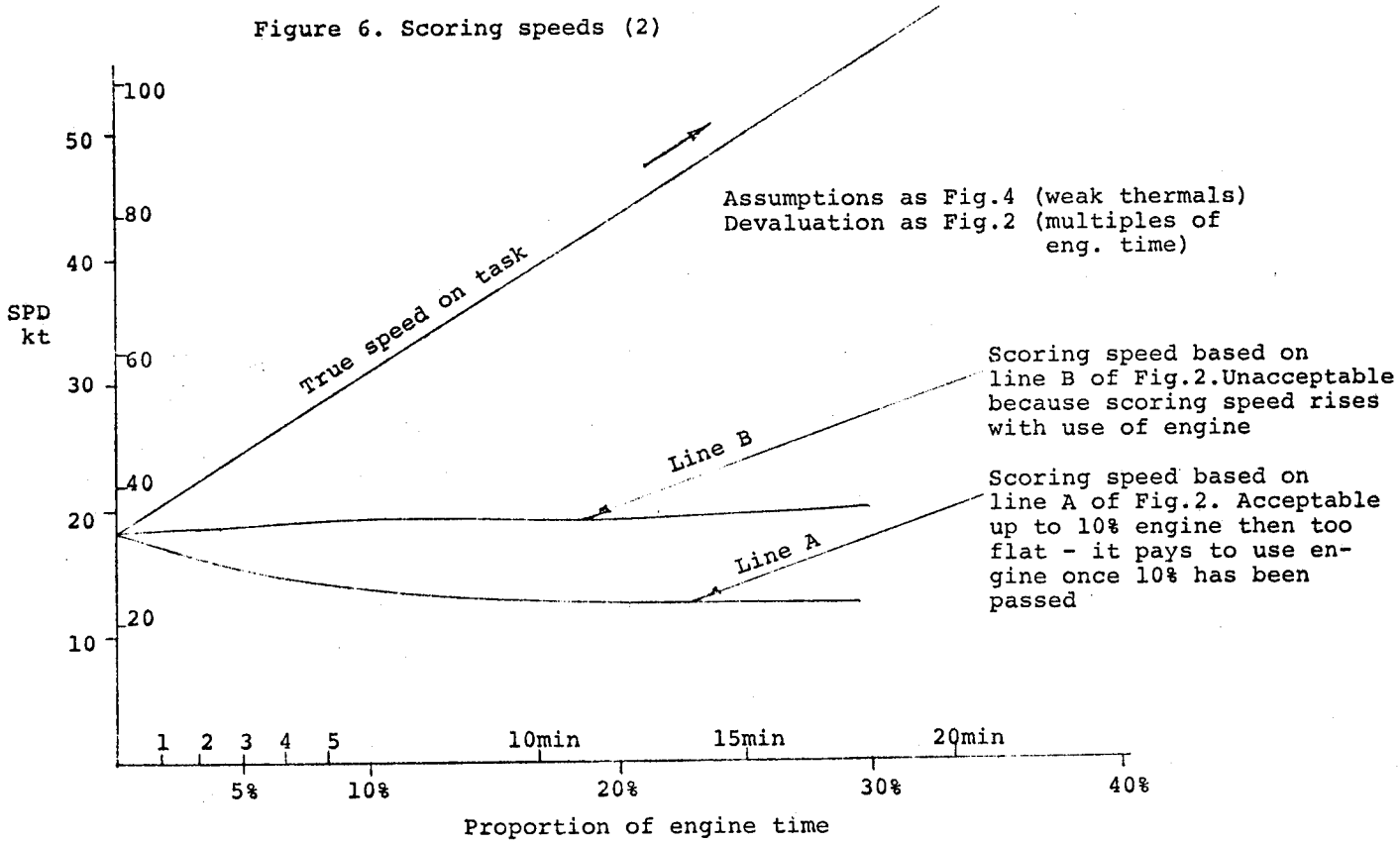


Figure 6. Scoring speeds (2)



1/3 engine. However, it is concluded that the "straight line" graph has not enough advantages to be proposed to CIVV as a practical method.

14. Figure 6 shows how the devaluations of Fig. 2 reflect on scoring speeds. Line B shows a progressive increase in score with further use of engine and shows dangers of selecting too shallow a devaluation graph. The left hand end of Line A shows a practicable slope but the levelling off over 10-15% use of engine is undesirable and the small decrease is score with massive use of the engine at the right hand end of the graph is quite acceptable if a correct soaring philosophy is to be preserved.

15. Figure 7 shows scoring speeds for the "square law" devaluation of Figure 3. Line A shows an improvement in score with use of engine but its slope at the right hand side is favorable. The best single formula for devaluations is probably Line B where penalty time in minutes equals twice the square of the percent engine time. A small anomalous region exists at the left hand side of its curve in Figure 7, but this could probably be tolerated.

16. However, it is concluded that the best overall devaluation formula would result from combining the left hand side of Line A of Figure 2 (1 hour penalty time per 5 minutes engine) with the right hand side of Line A Figure 3 (penalty = the square of percent engine used). These two graphs cross at 12% engine used and are shown in Figure 8.

17. The effect of such a combined formula on scores is shown in Fig. 9 for weak thermal conditions and Fig. 10 for moderate conditions. It is not claimed that such devaluation formulas are ideal but they do represent a reasonable compromise and do not exhibit some of the anomalies in scoring discussed earlier.

18. Even if you do not agree with this conclusion, the graphs and discussion may help to formulate views and to show pitfalls into which a superficial study of the problem may lead. Should you favour a single formula, then the "square law" ones of Figs. 3 and 7 probably contain the least troublesome anomalies. But the author's view is that pilots, when on task, want to know in a straightforward fashion what is the best tactical thing to do. If they know only to use the engine when desperate, then so much the better. Our gliding-purist friends will think the more of us for it.

19. One point worth discussion is the danger, in a motor glider contest, associated with unexpected bad weather en route. In England it is not unknown for a low pressure trough or frontal system to materialise "out of nowhere". In a glider contest this is self-controlling because all the gliders have to land. But in an MG contest, pilots will be tempted to "press on" in the hope of completing the task. As a task setter, this point worries the author considerably.

Figure 7. Scoring speeds (3)

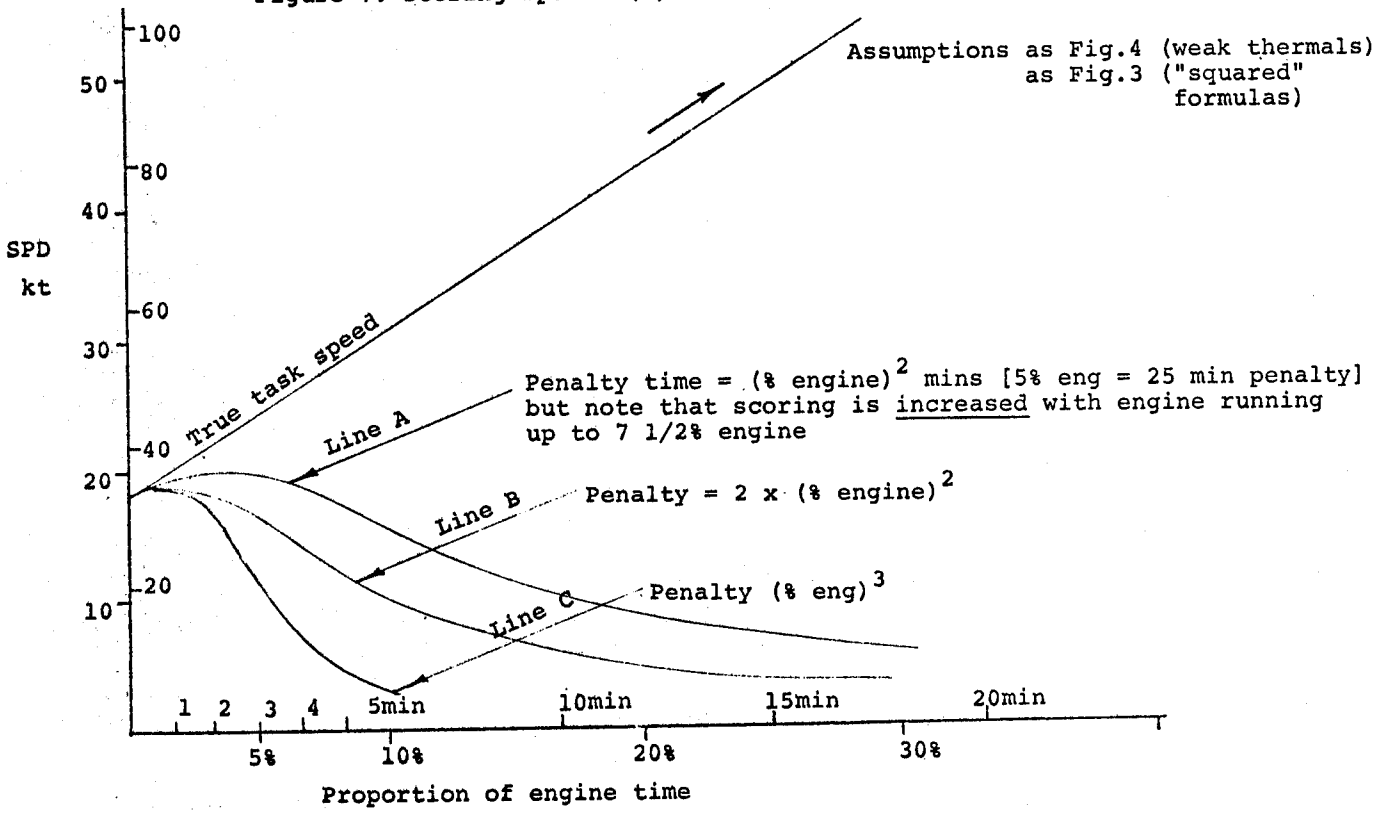
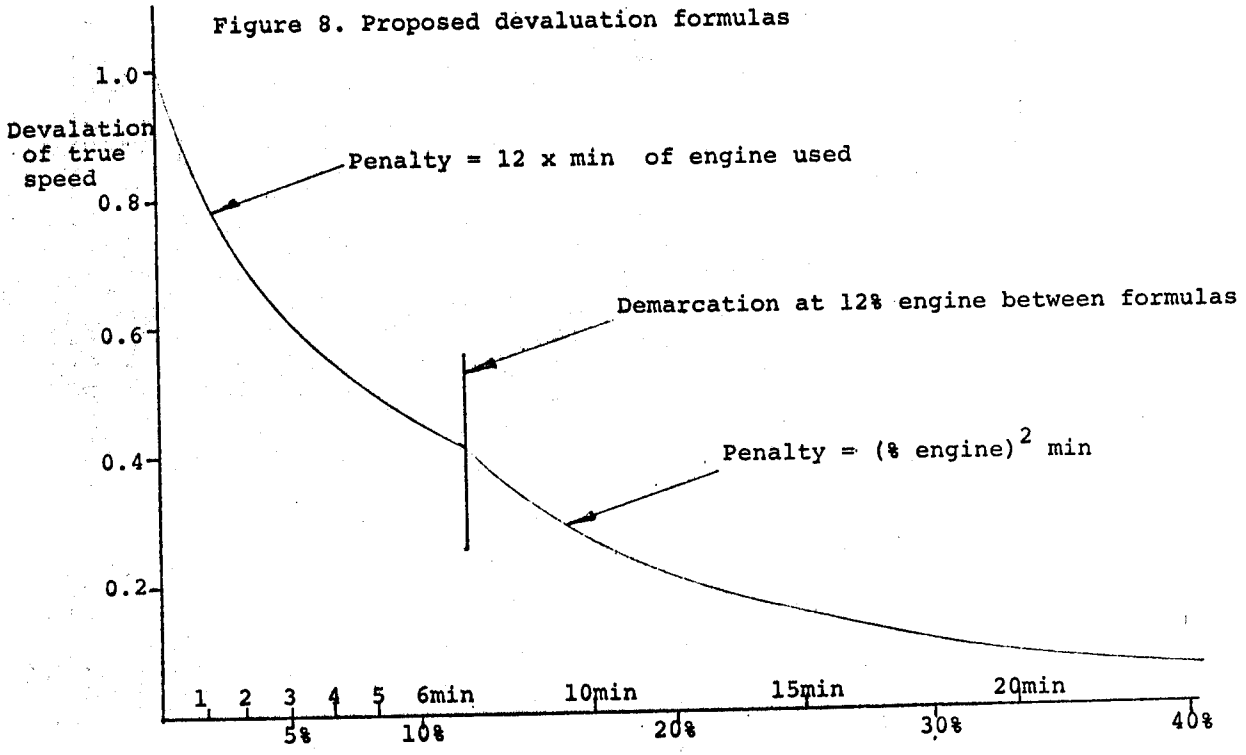


Figure 8. Proposed devaluation formulas



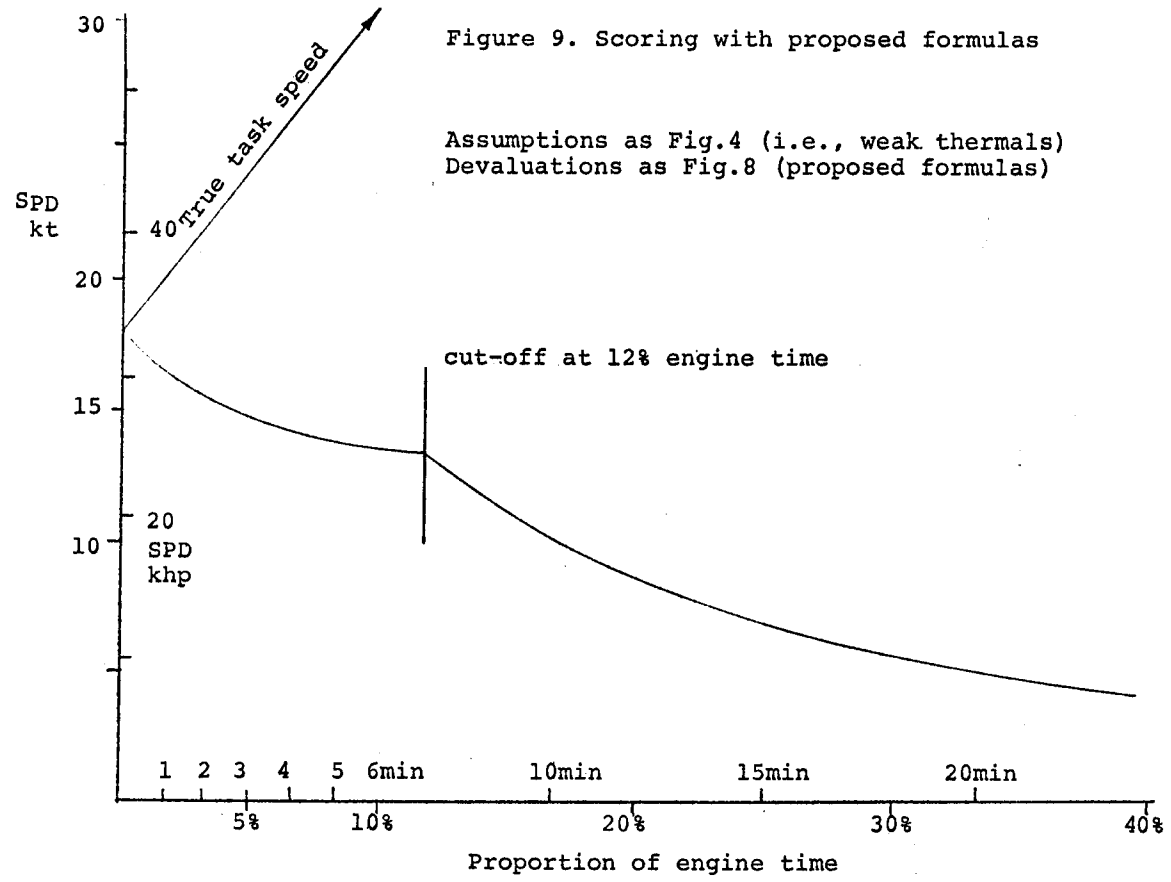


Figure 9. Scoring with proposed formulas

Assumptions as Fig.4 (i.e., weak thermals)
Devaluations as Fig.8 (proposed formulas)

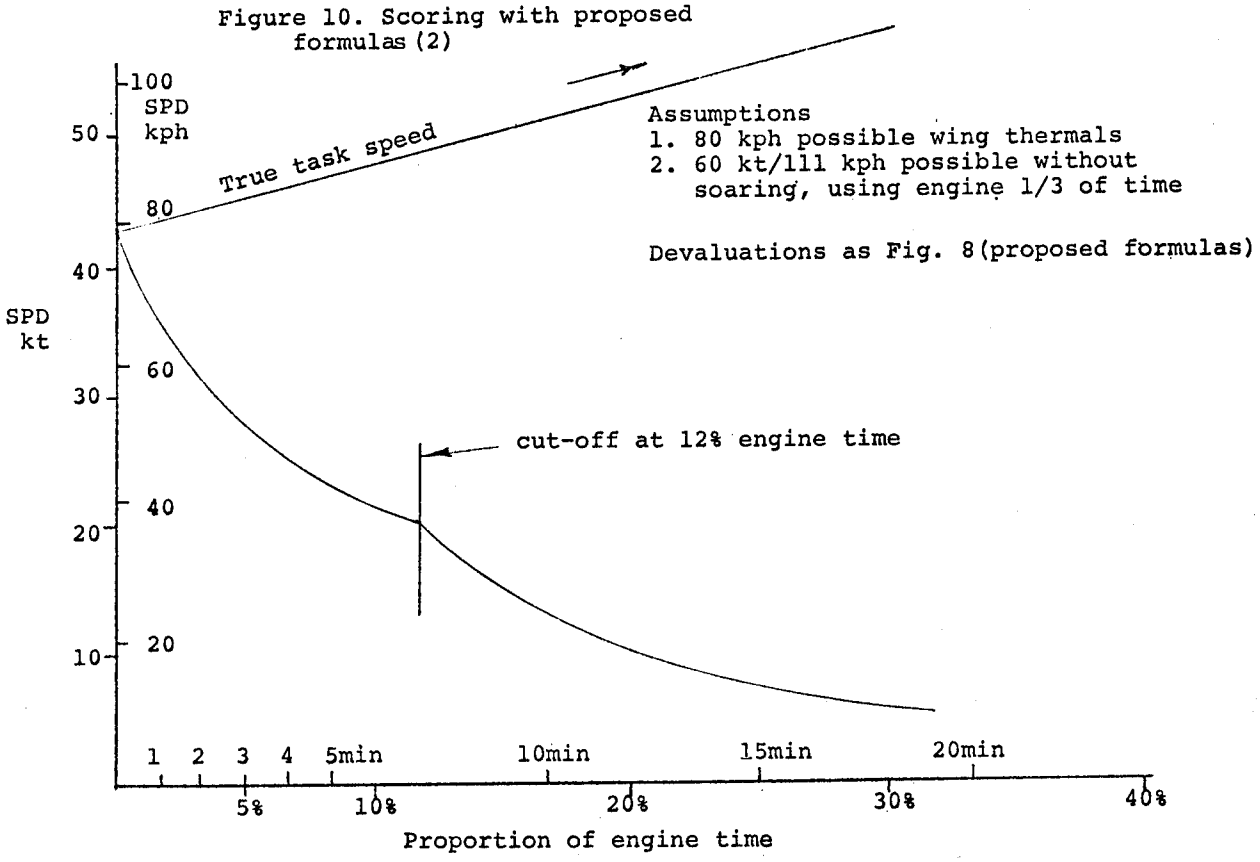


Figure 10. Scoring with proposed formulas (2)

The task setter of the day in a motor glider contest will have to give very careful thought to this problem and pilots need to be firmly instructed to return to base on such days and not hazard their machines. The points in Para 8a-d also cater for this case, since a pilot who finds himself forced to run his engine a lot might just as well return to base anyway instead of pressing on into dangerous weather. It could be said that cloud flying with motor on should be banned, but this is unsatisfactory because there is no way of checking for infringements.

20. Part 2 of this section is a draft complete scoring system for CIVV MG Championships along the lines discussed above. No apology is made for complexity. This is a new branch of our sport, and to retain credibility with the International Gliding Movement the CIVV must encourages advanced motor gliders that are sailplanes first and aeroplanes second. The rules must allow designers no scope for production of light aircraft that do not soar well, and departures from normal gliding practice at this early stage in MG development should be resisted until more experience is gained with the new medium.

Part 2

Supplementary rules for contests involving motor gliders only

MG 1 All glider contest rules, where appropriate, will apply, except as modified by rules in this section.

MG 2 Tasks. Only race tasks will be set.

MG 3 Use of engine. Use of engine is unrestricted except:

3.1 Use of engine during launching is covered in 6.3.

3.2 The engine must be stopped for any crossing of a start line.

3.3 The engine must not be used when thermalling in close proximity to other machines, or when thermalling in cloud.

3.4 The scoring system reduces scores in proportion to the time that engine is used during the contest performance.

MG 4 Contest Number. The last two letters of the motor glider's civil registration will be taken as its contest number.

MG 5 Motor Glider Barographs and Engine Recording Devices.

5.1 A motor glider must be proved with a barograph which has a second needle operated by a solenoid which is actuated by an engine function so that a continuous

permanent record is made of the time for which the engine was "live". Such wiring must not be accessible to the pilot in flight, and any joints, including connections to batteries and to the barograph must be sealed by an Official Observer. The batteries feeding this circuit must not be used for any other purpose and the organisers may check their voltage from time to time during the contest.

5.2 After flights on a contest day, the barograph may only be removed from the machine by an Official Observer, who shall check that the solenoid circuit is working as intended when he unseals and signs the trace.

5.3 Motor glider traces must be handed in to the organisers on every contest day, and should show that the engine was only used in accordance with these rules. Engine "live" indication will be taken as if the engine was running, unless positive proof is shown that no power was obtained (such as by showing a continuous steed descent while the engine was "live", or by showing that a malfunction existed which precluded power being available).

5.4 Barograph failure. In the event of failure of the barograph, the organisers will take notice of any auxiliary device recording the time that the engine was "line". Such device must be wired as in 5.1, must have independent batteries, but need not include a height recording facility.

MG 6 Launching. The launch is defined as that phase between the ground roll and the first subsequent stopping of the engine.

6.1 First launches on a contest day will be by pilot-selected start unless briefed otherwise. The organisers shall regulate the rate of take-offs according to prevailing conditions so that collision hazard is avoided, but shall not allow take-offs more frequently than one every 20 seconds.

6.2 Subsequent Launches. An unlimited number of subsequent launches are allowed unless the task is cancelled or the last launch time is reached. Such launches shall be booked on a "time board" supervised by the organisers.

6.3 Launch height and position. The height above the start line when the engine is stopped shall not exceed cloudbase or such lower height briefed by the organisers. The position at end of launch is unrestricted although for the earlier stages of a congested launch the organisers may indicate a common climbing path to avoid collision.

6.4 Start Line.

6.4.1 A Motor Glider must cross the start line at or below 1000 m AGL with its engine stopped, this being proved by:

6.4.1.1 Direct observation by the organisers either from the ground or from the air.

6.4.1.2 By analysis from the motor glider's barograph trace. The time elapsed between take-off and start will be known to the organisers, and this may be checked against the engine running trace on the barograph, which should show that running time was suitably less than such elapsed time. The height trace should also indicate that the rules were followed.

6.4.2 Number of crossings and use of engine. An unlimited number of start line crossings may be made, and the engine may be used after launch position for starting but only up to the height of cloudbase.

6.4.3 Non observation at start line. Should a motor glider not be observed at the start line, it shall be timed as if starting at take-off time minus 30 minutes and its launch will not be counted as engine time for the purpose of scoring except that in this case the launch will be counted to a height of 1000 m above the start line or 10 minutes engine running, whichever occurs first - subsequent engine time will count in full for penalties.

[Note: 6.4.3. is based on the idea that in the worst case, a pilot might ignore the start line and fly straight down the course. Of course he might also just be unlucky in not being observed at the line, but if we cater for the latter case we must take account also of the former.

The penalty time of take-off minus 30 minutes is based on a comparison of a glider (A) which launches straight to 1000 meters at the start line and then carries on down the course, with a glider (B) which deliberately launches straight to 1000 meters (or 10 mins engine time, see 6.3) flying down the course as it goes. The following assumptions are made:

Climb Rate (A and B) 10 min to 1000 meters.

Climb and glide speeds (A and B) 60 kt.

Glide Ratio (A) 1:30.

Thermal Strength along course (A) 1 kt.

A worked example will show that glider (B) should be given an artificial start time of take-off minus 20 minutes for parity with glider (A). An extra 10 minutes penalty has been added to encourage pilots to use the start line.]

MG 7 Race Scoring

7.1 General Principles.

7.1.1 Motor gliders not completing the course will score zero.

7.1.2 Motor gliders completing the course will be scored at their true speeds of completion only if they do not use power during the contest performance. Others will have their speeds reduced according to the time of engine use and according to an "efficiency factor".

7.1.3 Motor gliders achieving such adjusted speeds of less than half of the winner's shall be scored zero. This allows meritorious performance to score but poor ones involving much use of engine to score zero.

7.1.4 The scoring value of a contest day will be reduced according to the proportion of motor gliders applying power for more than one fifth of their task time plus those not completing the course.

7.2. Times.

"t" = The time in minutes of a motor glider completing the course.

"M" = The time in minutes that a motor glider used its engine under power between the start and finish of the task. Provided that, each separate time that power is applied, the time from zero to five minutes shall be counted as five minutes. After each five minute period true time shall count, being measured by the organisers as accurately as possible from the motor glider's recording device.

"e" = The engine efficiency factor equal to $\frac{\text{ASPECT RATIO} \times \text{ENGINE BHP}}{1.2 \times \text{AUW (kg)}}$ The constant 1.2 is designed to reduce the factor to unity for the datum machines K14 and SF27M. It is intended as an index of the ability to achieve cross-country speed by use of engine alone without thermals. The brake horse power of the engine shall be taken from the manufacturer's specification unless modification has taken place in which case a true value shall be calculated or estimated by the organisers. The AUW taken shall normally be the maximum certified AUW of the motor glider in its Certificate of Airworthiness unless there is evidence (such as by weighing) that this is not a realistic figure for the contest, in which case a true figure shall be taken by the organisers and shall be used for the whole contest. This proviso shall be applied in the use of two seaters flown solo which shall normally be taken as weighing their maximum AUW minus 100 kg.

[Note:

Type of MG	Aspect Ratio	BHP	Max AUW(kg)	"e"
SF27M	18.0	26	386	1.01
K14	16.6	26	360	1.00
Falke	13.4	45	555	0.91
K16	13.5	68	700	1.09
RF5B	15.25	68	650	1.32
SFS 31 "Milan"	18.8	45	421	1.66

The aspect ratio is a measure of glide performance and the rest of the formula is a measure of power-on rate of climb. Combined, they give a measure of cross-country speed that could be achieved without thermals.]

7.3 Speeds. The actual speed achieved by a motor glider completing the course will be reduced to an adjusted speed "S" if power is applied. "S" will be calculated by dividing the course distance by an adjusted time "T". The formula for adjusted time will vary depending on whether the glider being scored ran its engine (corrected time e x M) for more or less than 12% of total task time t.

7.3.1 Engine Running less than 12% (e x M less than 12% t).

Adjusted time T minutes equals task time (t) plus twelve times engine time (eM). Each 5 minutes engine thus carries a penalty of 1 hour.

Definitive Formula: $T = t + 12eM$.

7.3.2 Engine Running more than 12% (e x M more than 12% t).

Adjusted time T minutes equals task time t plus percentage engine square expressed in minutes such that, for instance, 13% engine used equals an additional time penalty of 13^2 minutes or 169 minutes.

Definitive Formula: $T = t + \left(\frac{100eM}{t}\right)^2$.

7.4 Scoring list - merit order for the day.

A list shall be used in descending order of adjusted speeds S. The top of the list shall be the day winner and his adjusted speed shall be called V. Scoring speeds shall be obtained for all gliders by subtracting V/2 from their adjusted speeds, negative values being taken as zero. The list of scoring speeds so produced shall be the merit order for the day, placing those not completing the course at the bottom of the list.

MG 8 Points Scored.

8.1 Definitions

n = The sum of the following motor gliders:

1. Those not completing the course.

2. Those applying power for more than one fifth of their task times, i.e., where "e x M" is more than t/5.

3. Those achieving a scoring speed (as in 7.4) of less than half that of the day's winner.

N = The number of motor gliders having launches on the contest day.

8.2 Maximum Day Points. The winner shall we awarded day points of:

$(\frac{N - n}{N} \times 1000) + 300$. Values over 1000 shall count as 1000, and values under 100 shall count as zero and the day declared a "no contest".

8.3 Points. Other gliders shall be awarded points according to how their scoring speeds compare with the winner's. (See 7.4 for scoring speeds).

MG 9 Place Scoring. If this is to be used instead of points scoring, 8.2 and 8.3 should be ignored.

9.1 Scoring speeds are taken from the merit order produced as in Para 7.4, except that motor gliders achieving a scoring speed of n/N x V, shall also be scored as zero.

9.2 One placing mark is awarded for a "tie", defined as where a given glider has a scoring speed within $\pm$ 1 km/h of another, except that only one glider is taken as scoring zero. This devalues days where there is little differentation between pilots' performances.

9.3 Two placing marks are awarded to the glider being scored for each glider that it beats by more than 2 km/h in the merit order, except that all gliders scoring zero regarded for this purpose as one glider only. This effectively devalues poor soaring days because each glider scoring zero means that two less points are available.

9.4 Similar Performance. The list of placing marks is now examined. Should a glider A score 5 or more placing marks than the glider B immediately below him, the A's score and that of all those above him will be reduced by the same amount so that A scores only 4 placing marks more than B. This ensures that the maximum "step" in the marks is 4, this process being repeated as many times as is necessary.

9.5 Placing Points. After the application of the above rules, the glider's scores are called placing points, which constitute the daily and the running scores for the contest.

9.6 End of Contest "Tie Breaker" Rule. In the event of two or more motor gliders getting the same placing points at the end of a contest, taking the scores of those concerned only, the glider that achieved the highest number of days scoring more placing points than the other(s) will be placed first. The glider that achieved the next highest number of days scoring more placing points than any others concerned will be placed next, and so on.

Motor gliders in gliding contests

1. Until enough motor gliders are available to complete in a "motor glider only" competition, it behoves MG enthusiasts to persuade their National Aero Clubs (NACs) to allow them in normal glider contests. This will enable the soaring fraternity to see the motor glider in a controlled contest environment and to realise that good MG designs will be a credit to the soaring movement.

2. It is also important to get NACs and their CIVV representatives to think seriously about the motor glider in competitions.

3. The author has, over several years, persuaded the British Gliding Association (BGA) to allow MGs in all their contests, under additions to their rules shown below. The conditions comply with the provisors of the CIVV Sporting Code relevant to Motor Gliders breaking Glider records. Self-Launching and Self-Retrieving are allowed, but the engine must be inoperative during the contest performance.

Contest rules applicable to motor gliders flying in BGA contest

RULES: All BGA and Local Rules will apply in toto to motor gliders, with the following additions:

R. 4.6. Contest Number. The last two letters of the Motor Glider's civil registration will be taken as its contest number.

R. 6.1. Motor Glider Barographs. A Motor Glider must be provided with a barograph which has a second needle operated by a solenoid which is actuated by an engine function, so that a record is produced of the time the engine was "live". Such wiring must not be accessible to the pilot in flight, and any joints including connections to the batteries and barograph must be sealed by an official observer. The batteries feeding this circuit must not be used for any other function, and the organisers should check their voltage from time to time during the contest.

After flights on a contest day, the barograph may only be removed from the machine by an Official Observer, who shall check that the solenoid circuit is working as intended when he unseals and signs the barograph trace.

Motor Glider traces must be handed in to the organisers for scrutiny after each contest day, and must show that the engine was not used during the contest performance.

R. 11.1. Add: Launching. Motor Gliders will be placed in the list order in positions to be decided by the organisers. If the organisers desire, all motor gliders may be placed in the list order to assist grouping at the launch point and to ease observations at the DZ.

R. 14. Add: Motor Gliders will be allowed to self launch (But see R. 31). They must be observed at the DZ with engine stopped before starting a contest flight.

R. 3.6. [Note: This is the only completely separate rule pertaining to motor gliders. The above rules are additions to existing rules about such things as Barographs, Launching, etc.]

R. 3.6. Motor Gliders.

3.6.1. A motor glider competing on an equal basis (i.e., not hors concours) with other gliders in BGA contests, must prove by an approved method that between the DZ and Landing on each contest flight, its engine was incapable of starting. Approved methods include:

Removing half of the sparking plug leads and taking a normal glider launch.

Having a mechanical lock to engage when the engine is stopped or retracted, the look to be inaccessible to the pilot in flight.

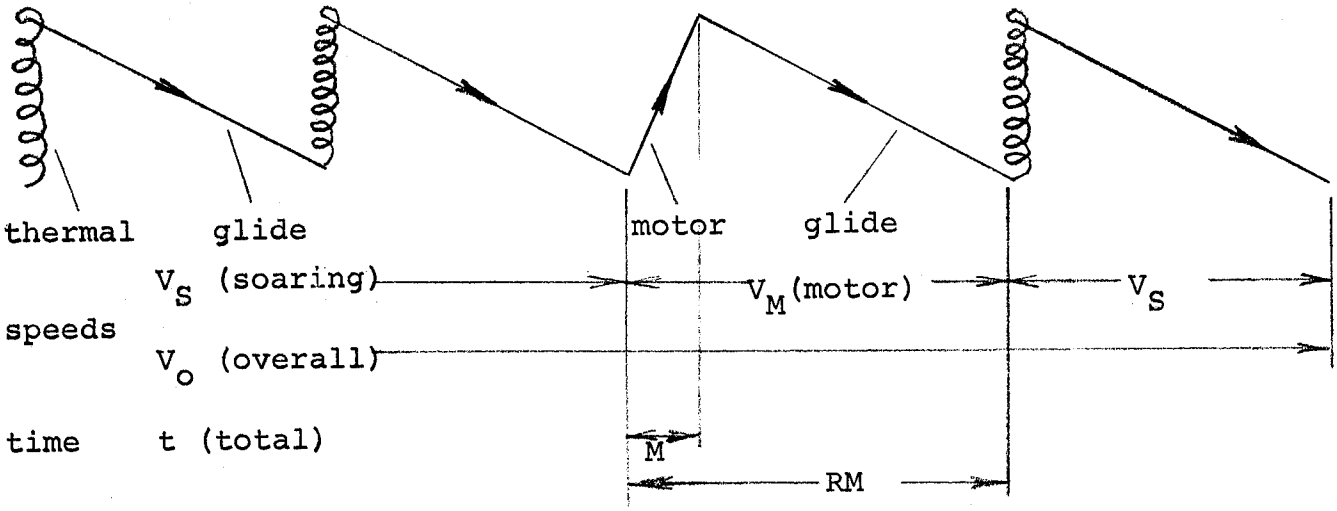
Switching off the engine by pulling on non rigid connection (e.g., cord or wire) attached to a push-pull switch or valve. The normal cockpit ignition and fuel switches must be sealed "ON" by an official observer, and the push-pull device must be inaccessible to the pilot in flight.

3.6.2. Motor Gliders may retrieve themselves back to base using their engines, but after such self retrieves, further contest launches on that day are prohibited.

APPENDIX

Derivation of soaring speed formula

A typical motor glider cross-country flight will include elements of soaring and elements of power-on flight. Distance travelled due to power will include that glided back down to datum height.



V_S is the average soaring speed obtained for the soaring part of the flight from the usual formula

$$V_S = \frac{\text{Gliding Speed x Rate of Climb in Thermal}}{\text{Rate of Climb + Rate of Sink at Glide Speed}}$$

V_o is the average speed of the cross-country flight, a combination of soaring speed and speed due to engine.

V_M is the average speed under power, including the element of gliding back to datum height. It is assumed that the best climbing speed and best glide speed are the same.

M is the number of minutes of motor used on task.

t is the total task time in minutes.

R is the ratio of time due to power, to Motor time M; where time due to power includes the glide back to datum height. This will vary between types and will probably be between 2 and 4. A value of 4 would imply that after 5 minutes of motor, a 15 minute glide would follow before starting height was regained.

We wish to derive a formula separating out V_S, as this is the meritorious element of the flight.

V_o = Proportion of time soaring x V_S + Proportion of time due to engine x V_M = (1 - proportion due to engine) x V_S + + Proportion due to engine x V_M.

And proportion of time due to engine = $\frac{RM}{t}$

So $V_o = V_S \left(1 - \frac{RM}{t}\right) + V_M \left(\frac{RM}{t}\right)$

and $$V_S = \frac{V_o - V_M \left(\frac{RM}{t}\right)}{1 - \frac{RM}{T}}$$

[Note: It might be thought that contest scores should be based on the "Soaring Speed" as above, as it covers the creditable part of the flight and separates out the time due to use of motor. There are two practical problems"

1. A pilot can boost his soaring speed by using motor to bypass the bad soaring areas on route. Hence some arbitrary devaluation would have to be applied, in proportion to engine running time, to reduce scores for this pilot. As an arbitrary factor is being applied, it might just as well be in the form discussed in Paras 6-18 of the second section.
2. The devaluation, being somewhat arbitrary, should be applied in a simple form rather than a complex one. The "Soaring Speed" formula above is much more complex than the suggestions in the second section. So, however elegant any theoretical formula may be, the discussion is still valid.

MIT'S MAN-POWERED AIRCRAFT

by

Paul Hooper and Robert Peterson
Department of Aeronautics and Astronautics
Massachusetts Institute of Technology

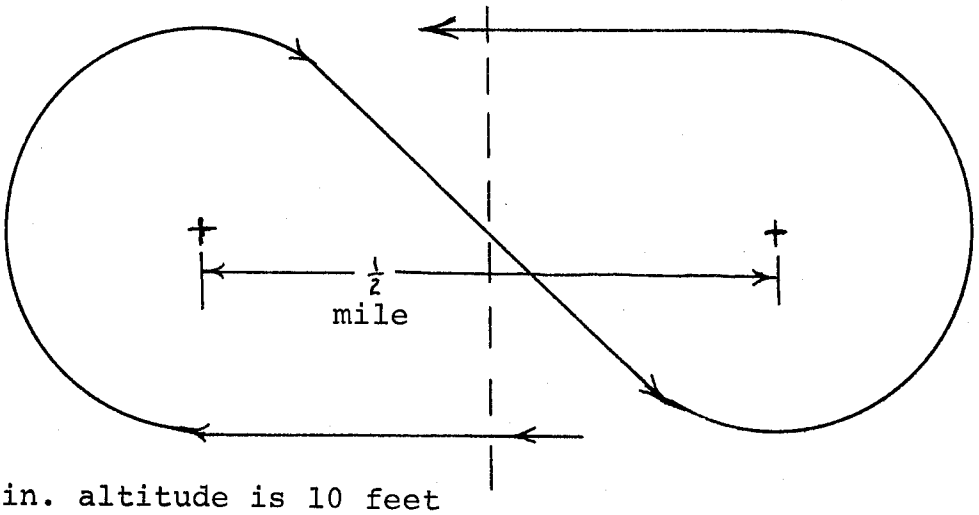
Notation

AR	Aspect Ratio
C_{D_i}	Coefficient of Induced Drag
C_{D_o}	Coefficient of Profile Drag
C_{D_t}	Coefficient of Total Drag
C_l	Coefficient of Lift
D	Drag (lb)
L	Lift (lb)
L_F	Load at Failure (lb)
P	Power Required (HP)
RS	Rib Spacing (in)
S	Wing Area (ft)
V	Flight Velocity (ft/sec)
ρ	Density of air

Introduction

The group of students known as BUMPAS (Biplane Ultralight Man-Powered Aircraft Systems) started its research into man-powered flight in January, 1970. Our goal was to design a man-powered aircraft (MPA) capable of winning the Kremer Competition. This competition, started in 1957, under the auspices of the Royal Aeronautical Society of England, established a £10,000 ($24,000) prize for the first aircraft capable of flying a figure-eight pattern around two poles spaced one-half mile apart, at a minimum altitude of ten feet, entirely under manpower. (See figure 1).

Our first work involved learning the technology of man-powered flight. Today's emphasis on high-speed, high-altitude, high performance aircraft has produced schools of thought on aircraft design quite unsuited to our needs. Our group sensed that there was something wrong with this method of design and we concluded that a "conventional" modern design might not be the best solution to the problem.



Min. altitude is 10 feet
at the start and finish
may be less in between

FIGURE 1

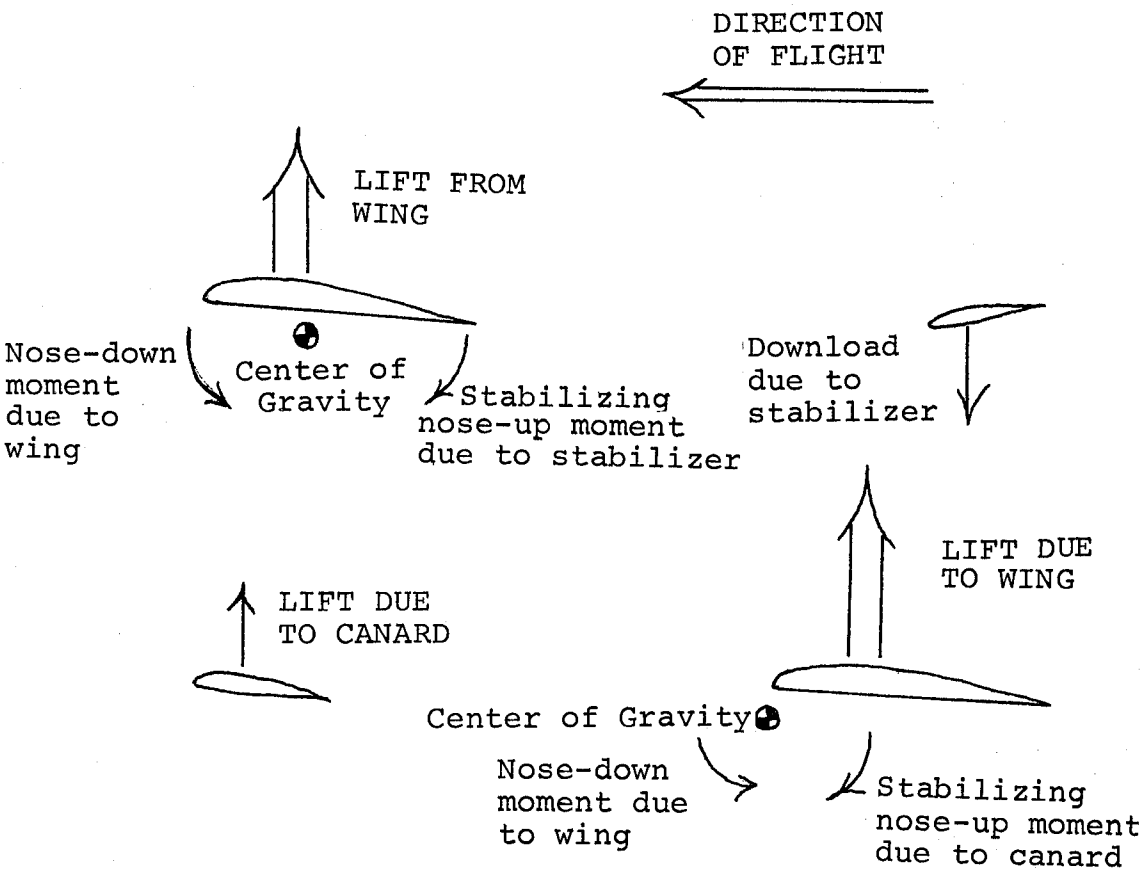


FIGURE 2

We next spent about six months studying low-speed aerodynamics, high-efficiency propulsion systems and low-density materials. Many different configurations were studied. Table 1 presents the specifications of several different man-powered aircraft, including our final design. It can be seen that the conventional design is a high aspect-ratio monoplane with a pusher propeller. Most designs use a crew of one man. The following will present the method by which we arrived at our design and rejected the "conventional" configuration.

Configuration

One of the first decisions to be made was to pick the crew size. The choice of a two-man crew was based on a logical argument rather than any quantitative results. The basic problem of man-powered flight is lack of power. If the power to weight ratio can be significantly increased, the chances for success are much greater. A single man design requires the pilot to not only provide power but to concentrate on flying the aircraft as well. A second crew member will thus add more power than the single man because the second man need not concentrate on matters other than producing power. If the weights of the two crew members are equal and the empty structural weight of a two-man aircraft is only slightly more than that of a single man aircraft, the net result is a greater than 100% increase in power for about a 50% increase in weight. This is a very significant increase in the power to weight ratio. The same argument can be extended to 3, 4 or more man crews. Problems of maintaining the same low structural weight and of coupling the output of large numbers of crew members together, however, lead to diminishing returns. Our design was therefore chosen to have a crew of two men to take maximum advantage of the increased power.

Another early design decision was to use a canard layout. There are several reasons for this choice:

1. A horizontal stabilizer is needed to counteract the downward pitching moment of the wings. If the stabilizer is placed aft of the wing (conventional layout) it produces a down load detracting from the overall lift of the aircraft. If it is placed in front of the wing (canard layout) it produces an up load for additional lift. (Figure 2)

2. Placing the wings and crew at the rear of the aircraft allows a pusher propeller to be used with a very short transmission. This means less weight and less drag since the high velocity air behind the propeller does not impinge on any part of the aircraft.

Table I

Aircraft	First Flight	Wing Span (ft)	Wing Area (ft^2)	Aspect Ratio	Empty Weight (lb)	Loaded Weight (lb)	Wing Loading ($\frac{lb}{ft^2}$)	Cruise Speed ($\frac{ft}{sec}$)
Puffin I[1]	11/1961	84	330	21.4	118	267	0.81	27.5
Puffin II[2]	8/1965	93	390	22.2	140	290	0.75	26.0
SUMPAC	8/1961	80	300	21.3	128	269	0.90	30.0
Weybridge	9/1971	120	485	30.0	130	280	0.58	23.2
Linnet III	3/1970	83	325	21.2	111	225	0.69	23.2
Jupiter[3]	7/1972	80	350	18.0	100	250	0.71	26.0
Ottowa(2-man)	?	90	450	18.0	209	522	1.16	30.0
Toucan(2-man)	1972?	123	600	25.2	145	446	0.74	25.0
MITMPA(2-man)	1972	60	640	13.6	125	400	0.63	26.0

NOTES

1. Flew 993 yards with M.P. $\pm$ T.O. 5/62.
2. Made 180° turns.
3. All values are estimates. Flew 1172 yards 7/72.

3. A major problem in flying an aircraft of this type is the lack of a reference surface on the aircraft. Placing the horizontal canard in front of the pilot gives him a simple and effective reference for bank and pitch indications. This is a vital consideration when making turns at less than 30 feet off the ground!

The major portion of the configuration was a result of the limited available power. For a given weight, the aircraft with less drag will be more successful since it will require less power to fly at a velocity sufficient to provide the needed lift. At the low speeds of man-powered flight, induced drag due to lift is the major concern. The parasite drag of the rest of the airframe is small compared to the induced drag. Drag reduction, therefore, takes the form of reducing induced drag rather than trying to "streamline" the aircraft.

The power curve for a man, for other than very short periods, is fairly steady, declining slowly with increasing time. This steady but low output can be maintained for periods approaching fifteen minutes. The very short period of possible high output is insufficient to complete the course. The comparatively long duration of steady power means that fairly high speeds offer no particular advantages in terms of greater power availability. We therefore designed our aircraft to fly at the speed for least power rather than that for best L/D.

The preliminary design was based on a wing area of 625 square feet, an aspect ratio of 25 and a gross weight of 450 pounds. The following equations were used to obtain approximate power requirements.

$$L = C_L \frac{\rho}{2} V^2 S = 450 \qquad (1)$$

$$C_{D_i} = \frac{C_L^2}{\pi AR(0.8)} \qquad (2)$$

$$C_{D_o} = .006 \quad \text{(constant)} \qquad (2a)$$

$$C_{D_t} = C_{D_o} + C_{D_i} \qquad (3)$$

$$D = C_{D_t} \frac{\rho}{2} V^2 S \quad (4)$$

$$P = DV/550 \quad (5)$$

These equations yield the following

TABLE II

Velocity (fps)	C_L	C_{D_i}	Drag (lb)	Horsepower
15	2.65	.126	22.2	.6
20	1.5	.04	14.0	.51
25	.96	.0162	10.4	.48
30	.62	.006	8.1	.49

The value of the minimum power occurred at a velocity of 25 fps. Note that the best L/D velocity would be 30 fps where the induced drag is equal to the profile drag.

These figures seem to imply it is possible to fly on as little as .48 horsepower. Note, however, that if we assume a 300 lb crew this means we must build a 625 square foot wing for less than .25 lb/ft^2! Any increase in empty weight over this will result in an increase in the power required. The problem now becomes how to build an extremely light aircraft and minimize the induced drag.

The usual methods of reducing drag include selecting a low-drag airfoil section, using a low wing loading and a high aspect ratio. For our aircraft, we chose a Wortmann wing section, FX 61-163, and a wing loading of .66 lb/ft^2. Our original design work resulted in a wing with an aspect ratio of 25 and a span of 125 feet. Building this wing at such a low weight was deemed to be almost impossible.

Our final configuration decision was based on the need to achieve this very low structural weight. Previous designs had not even approached it. The biplane configuration was picked on this basis. By using struts and cables to form a truss between the two wings, the loads on the spars were reduced considerably. These spars constituted a major proportion of the wing weight. Not only does the rigging

permit a light structure, it is also far more rigid. Other designs with cantilever spars have tip deflections of up to 12 feet! Our tips are expected to deflect about 4 inches. The extra drag produced by the rigging of the biplane is more than offset by the drag reduction due to the weight saved. The main disadvantage of the biplane is its low aspect ratio. (Figures 3 and 4 show our final design.) Our design results in an aspect ratio of approximately 13.6. Recalculating the drag and power figures from equations 1 through 5 gives the following results:

TABLE III

V	C_L	C_{D_i}	C_{D_t}	Drag	Power
25	.969	.0238	.0298	13.8	.63
26	.896	.0204	.0264	13.3	.63
27	.831	.0176	.0236	12.8	.63
28	.772	.0152	.0212	12.4	.63
30	.673	.0115	.0175	11.7	.64
35	.494	.0062	.0122	11.0	.70

The result is an increase in drag and in power required. The flight velocity for minimum power has also been increased slightly. In spite of these disadvantages, the biplane configuration was selected. We felt its advantages were sufficiently great to make its use important. Other advantages of our biplane configuration include:

1. The necessary struts at the wing tips have been used as the basis for tip plates which increase the effective aspect ratio. This helps relieve the major disadvantage of this configuration. Since the tips are located behind the center of gravity, the plates also add to the yaw stability of the aircraft.

2. For an equivalent wing area, the span is half that of the monoplane. This is an important consideration close to the ground. The competition requires turns to be made and an extremely long wing span makes this a slow process and increases the distance that must be flown (see figure 5).

The final decision needed to complete the design was to pick a control system. The canard was designed to be all-moving and provide pitch control. This is lighter and produces less drag than having a fixed canard with

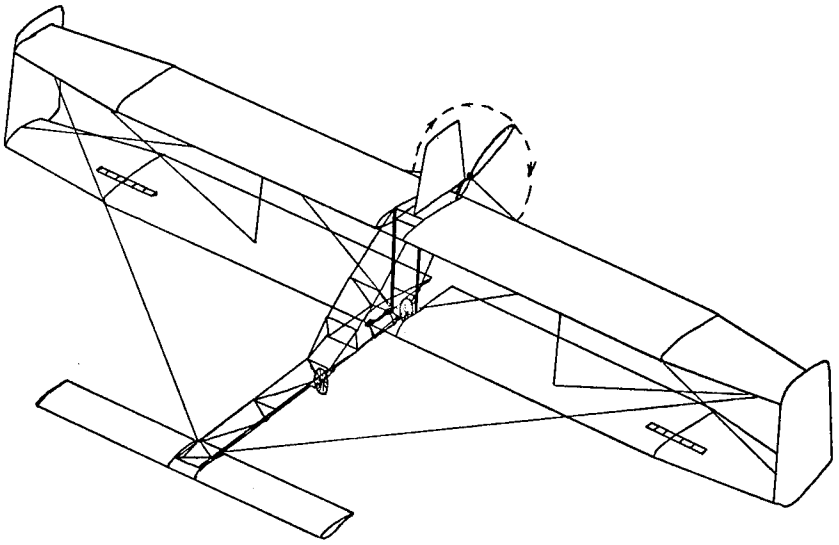


Figure 3a.

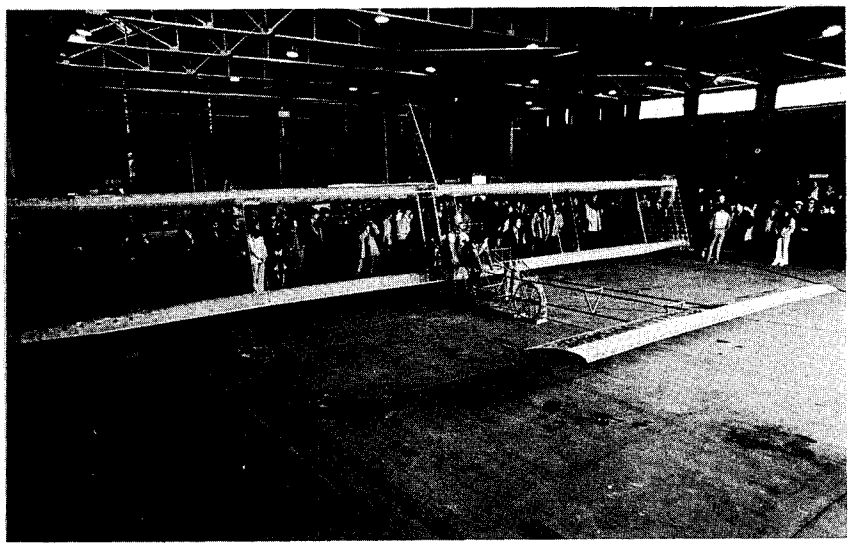


Figure 3b.

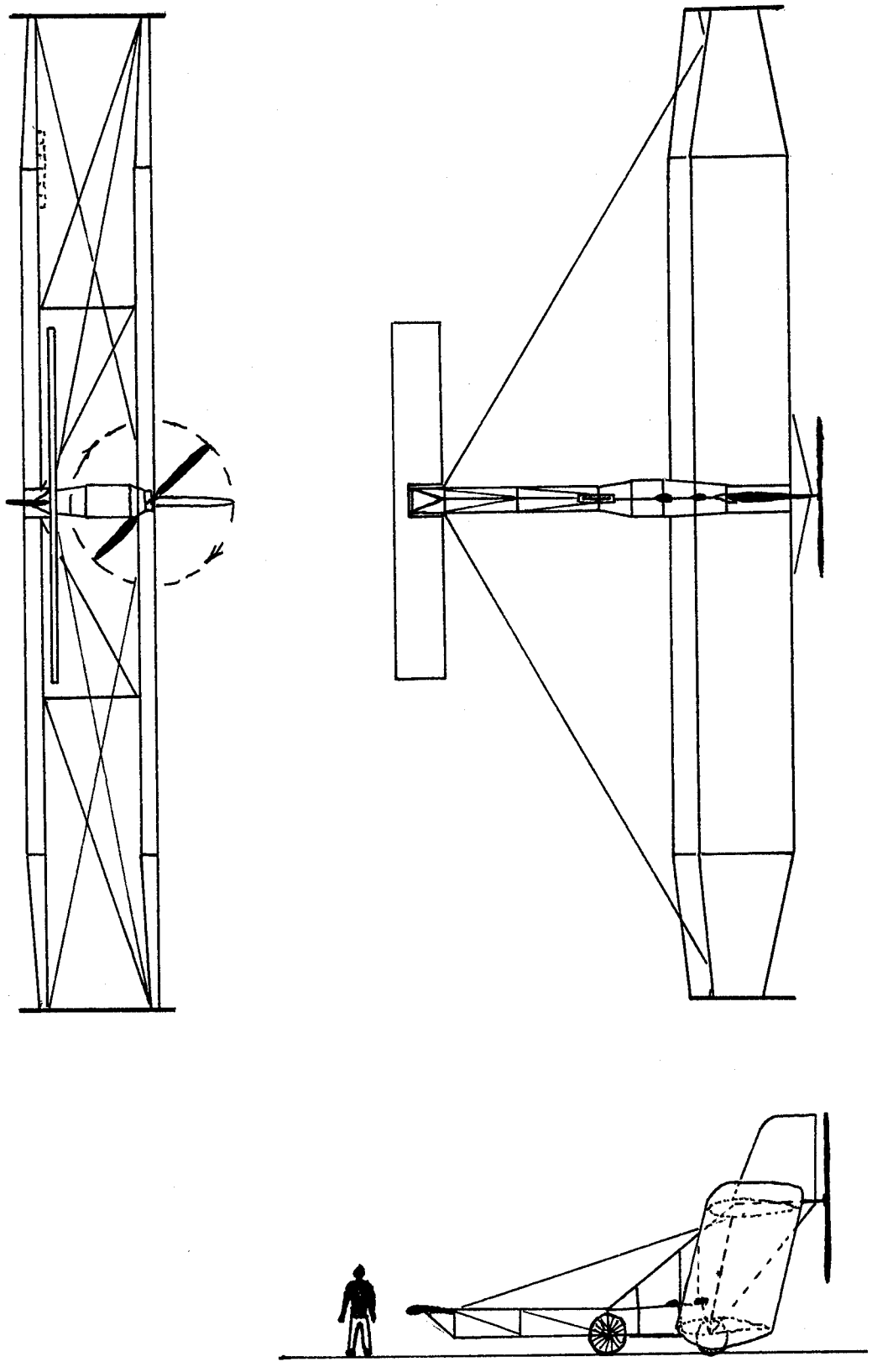


FIGURE 4

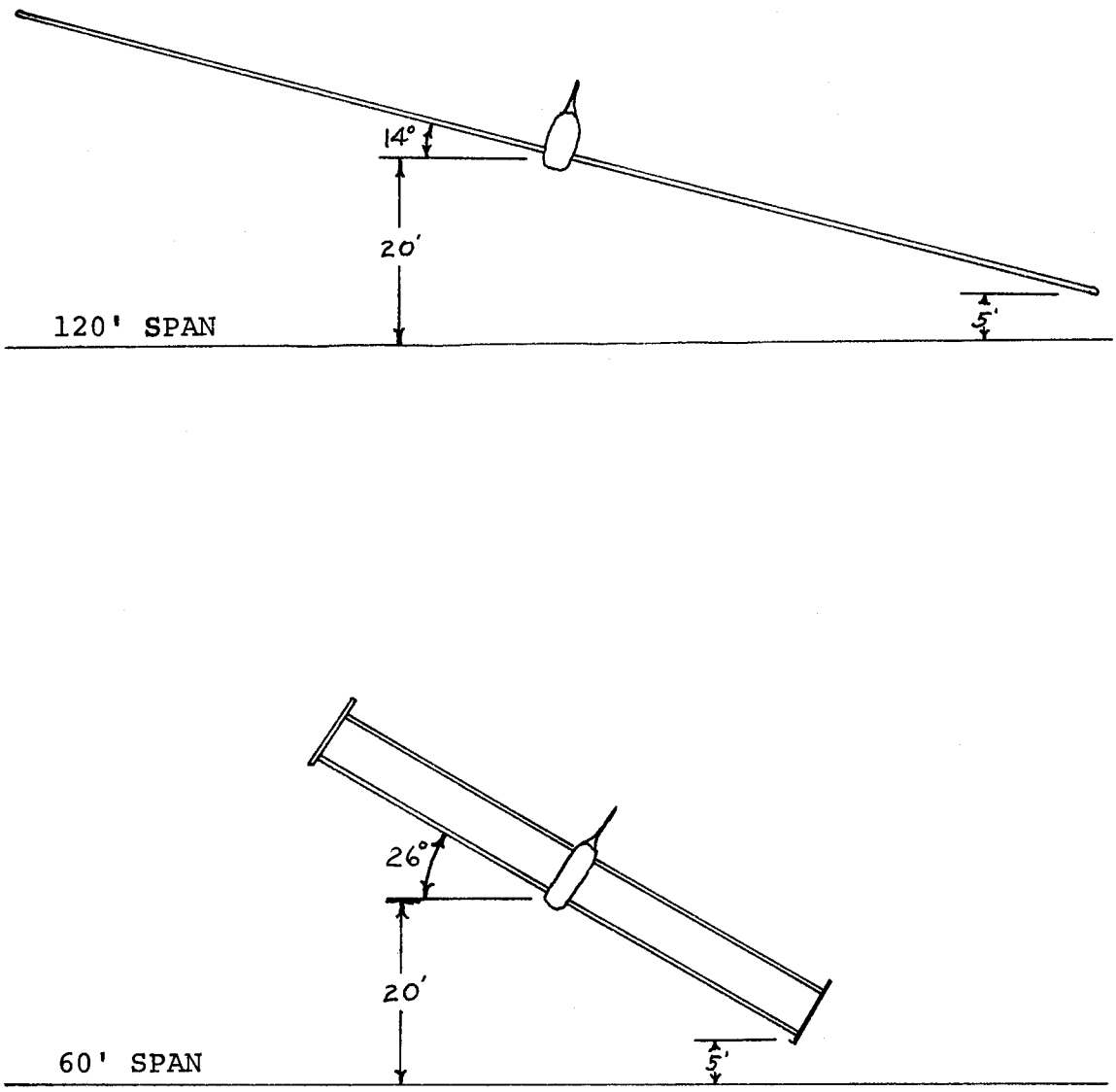


FIGURE 5

hinged control surfaces. Wind tunnel tests, which will be described later, were used to pick a method of roll control. Spoilers on the upper surface of the lower wings were chosen for this purpose. Since they produce a yawing moment in the same direction as the rolling moment, no separate yaw control is needed. They are fastened directly to the spar and thus produce little torsional bending in the wing. Conventional ailerons would have required reinforcement of the wing structure to resist the twisting loads they would have imposed. The net result is the spoilers are lighter, more effective and require a less complicated hook-up than ailerons.

Wind tunnel data

A one-tenth scale model of our aircraft was constructed for testing in the Wright Brothers Wind Tunnel at M.I.T. The model was tested at first just one wing and then succeeding tests were run adding the second wing, fuselage and finally the canard. Test runs on the single wing were run at a speed of 140 mph to closely approximate the full-size aircraft's Reynolds Number. Runs were also made at 100 mph and 60 mph to find the necessary corrections for the slower velocities. All runs with added components were then done at 60 mph. The basic lift, drag and pitching moment results for the aircraft are shown in figures 6, 7 and 8. Test runs were also made to find a method of providing roll control. Methods tested were setting the two halves of the canard at different angles of attack and various size spoilers in various positions on the lower wing. The results of these runs are presented in figure 9.

The basic test data on lift versus angle of attack is shown in figure 6. The results were in agreement with our expectations. The drag versus lift results shown in figure 7, however, were somewhat higher than predicted. The most probable reason for this is the poor surface finish of our model. Laminar flow airfoils are usually very sensitive to imperfections in the surface of the wing. An interesting result is the stall characteristics of the entire airplane. The canard surface stalls first and hence stops increasing the angle of attack of the wing. The drag rises while lift remains fairly constant. If abrupt pitch-ups are avoided during cruise, the stall characteristics of our aircraft should prove extremely gentle. The pitching moment curves shown in figure 8 demonstrate the effectiveness of varying the angle of attack of the canard. Pitch control should offer no problems. The rolling moments generated by the various control systems are shown in figure 9. The measurement system for rolling moment was extremely sensitive and jumpy. For this reason the graph is only approximate. As can be seen, the

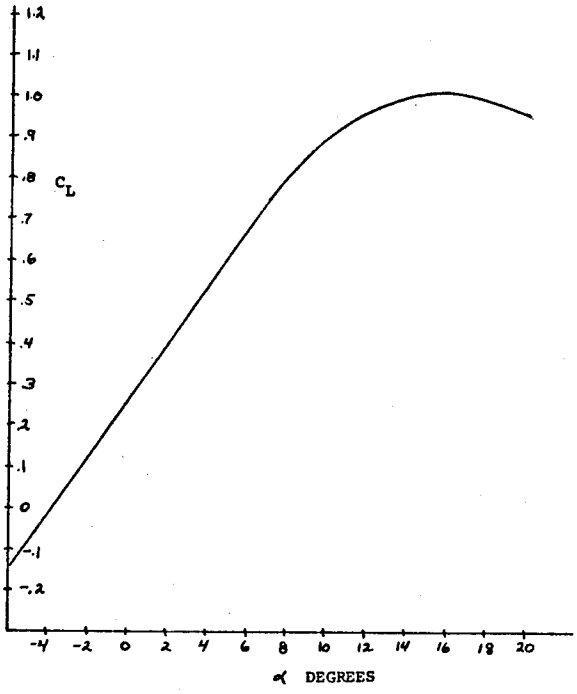


Figure 6

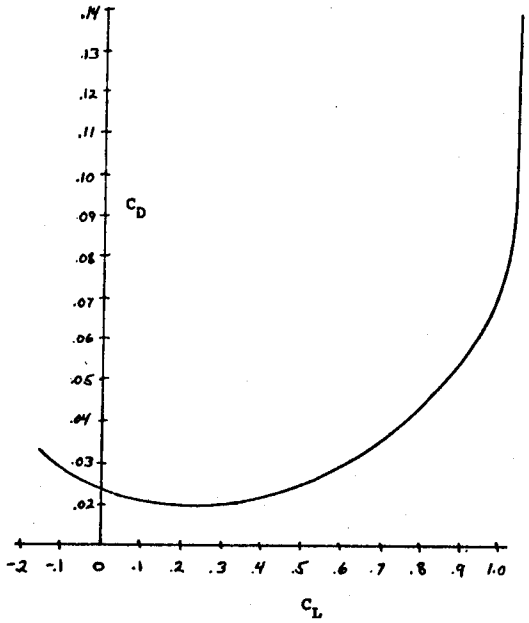


Figure 7

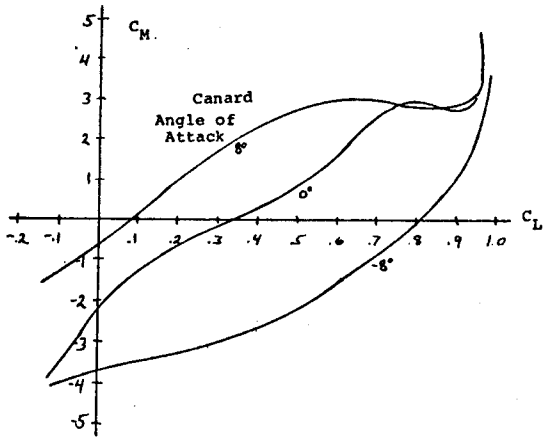


Figure 8

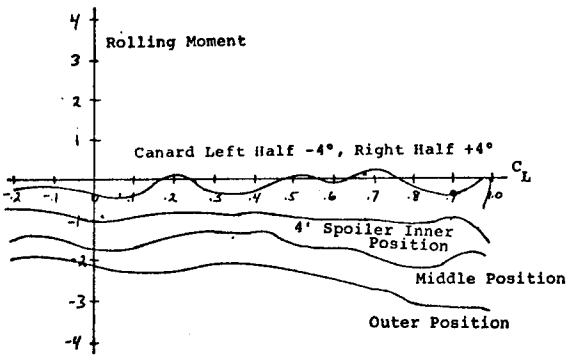


Figure 9

split canard offered very little, if any, rolling moment. The spoilers were much more effective. It was also found that the inner position of the spoilers was affected by the tip vortices of the canard at high angles of attack. Since the outer position was most effective, as would be expected, it was chosen for the actual spoiler location.

Structures

As was pointed out above, weight becomes our primary consideration. Structures design and testing is probably the most important area of work in an MPA. Our design required the lightest weight structure possible which provides the required strength. Our design used a 1.5 safety factor. Every component had to survive at least 1.5 times the maximum load to which that component would be subjected.

Our first major structure was the wing, since this would be the major component of the MPA. We considered several possible methods of construction. These included styrofoam structure, a honeycomb structure, and various spar-rib combinations. We went so far as to even consider the use of the new ultralight-ultrastrong materials, but the problems of handling and joining of these materials made their use difficult for our purpose.

For ease of construction and availability of materials, we chose to go with a conventional spar and rib type construction using balsa wood and a variety of bonding materials. The next step involved the design of the rib and the selection of rib spacing distance. For these purposes, we were required to develop a testing device for the ribs.

The device used to test the ribs is called a "Whiffle Tree". As shown in figure 10, it uses moment arms to distribute a load throughout the rib in accordance with the expected aerodynamic loads. Then, by simply adding weight at one point, the loads can be built up until failure occurs.

Our approach to the design was that of finding a rib strong enough to provide for a minimum rib spacing of nine inches at maximum loading. With a cruise load of about .7 lb/ft^2, our maximum load would be about 1 lb/ft^2. With our 1.5 safety factor, the rib would have to be strong enough to support about 1.5 lb/ft^2. The rib spacing would then be:

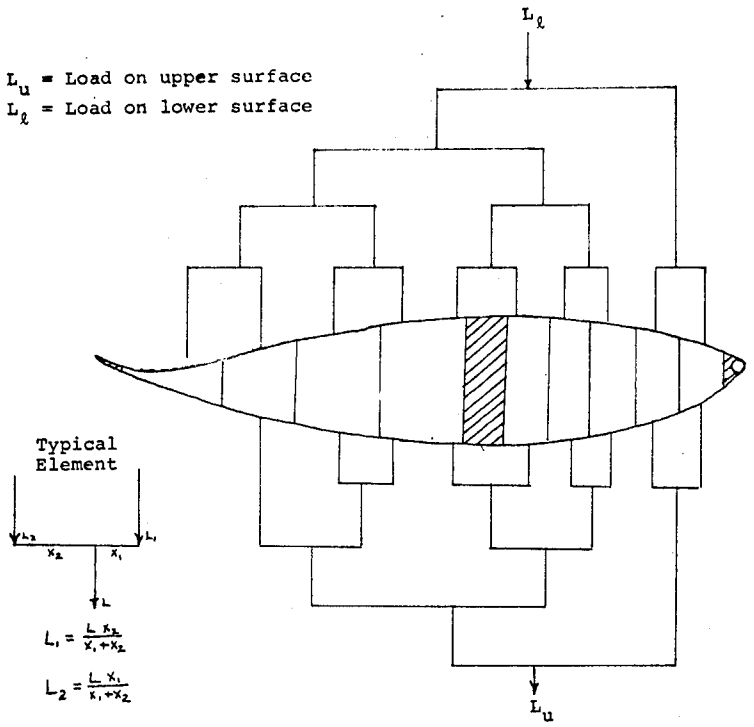
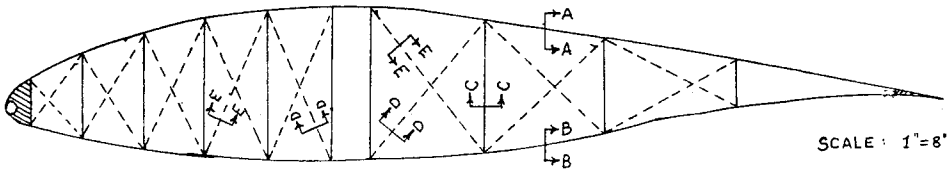


Figure 10



SECTIONS
(FULL SCALE)

	A-A	B-B	C-C	D-D	E-E
TR1	▨	▨	▨	N.I.	▨
TR2	▨	▨	▨	THREAD	THREAD
TR3	▨	▨	▨	▨	N.I.

N.I. - NOT INCLUDED

Figure 11

$$RS = \frac{L_F \cdot 12}{1.5 \cdot C} = 1.45 \cdot L_F \quad (6)$$

which gives:

$$\text{min. } L_F = \frac{RS}{1.45} = 6.2\# \quad (7)$$

Figure 11 illustrates the basic rib design. We analyzed three different versions of this rib before finding a suitable structure for our use. Test Rib #1 (TR1) consisted of 1/8" x 1/8" balsa cap strips with 1/8" x 1/8" balsa verticals, and 1/8" x 1/8" balsa diagonals placed such that they would be in compression under flight loads. This rib weighed .75 ounces and failed at a load of 4.4 pounds.

TR2 included an extra 1/16" x 1/4" balsa strip laminated onto the cap strips. Also, the diagonal members were replaced by a set of bracing threads. This rib weighed about .55 ounces, but failed at 3.99 pounds.

TR3, the actual rib being used, replaced the top cap strip with a 1/16" x 3/8" balsa strip laminated onto a 1/8" x 1/8 balsa strip. The bottom cap strip used a 1/16" x 1/4" laminated balsa strip onto the 1/8" x 1/8" balsa strip. It also incorporated 1/8" x 1/8" diagonal members in a configuration that would load them in tension during flight. This rib weighed approximately .82 ounces and when initially tested it supported 12 pounds without failure. However, in a retest about 4 months later, this same rib failed at about 7.5 pounds, indicating a loss of strength with age. With this in mind, this rib and a nine inch rib spacing were selected for our MPA.

The next major structure to be designed was the wing spar. Our original design was a I-Beam spar with spruce caps and a plywood web. Our computer analysis indicated that it would be strong enough, but due to weight considerations (as designed, the spar would weigh about 65 pounds), we had to undertake a redesign. We opted to use strictly balsa as our construction material, and we resized the I-Beam to provide the necessary strength. Our choice of balsa meant that we would have to manufacture the 3/32" balsa plywood web ourselves, a problem that we were unable to master. This required a second redesign. The final spar design is shown in figure 12.

The canard structure was designed as a smaller wing. The same type of rib structure was used, using 1/16" x 1/4" cap strips, and 3/32" x 3/32" verticals and diagonals. A smaller version of the spar was used with a six inch rib spacing.

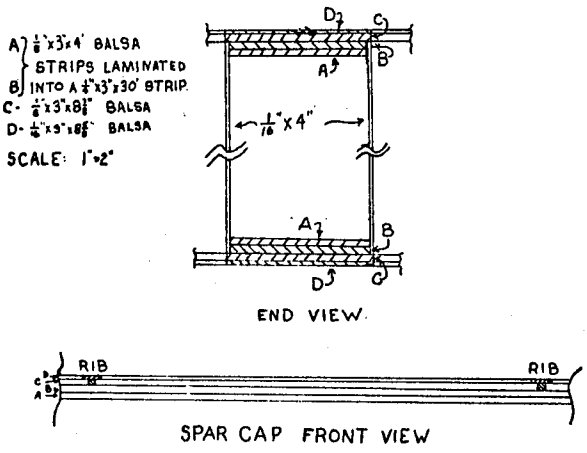


Figure 12

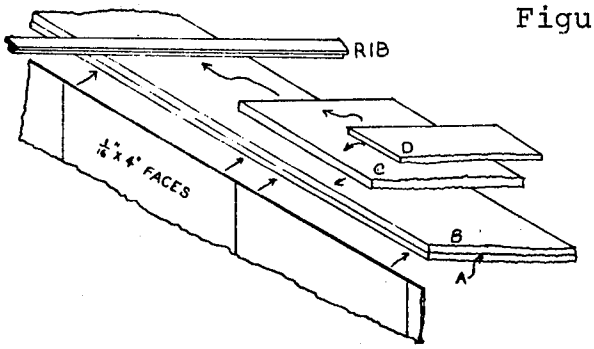
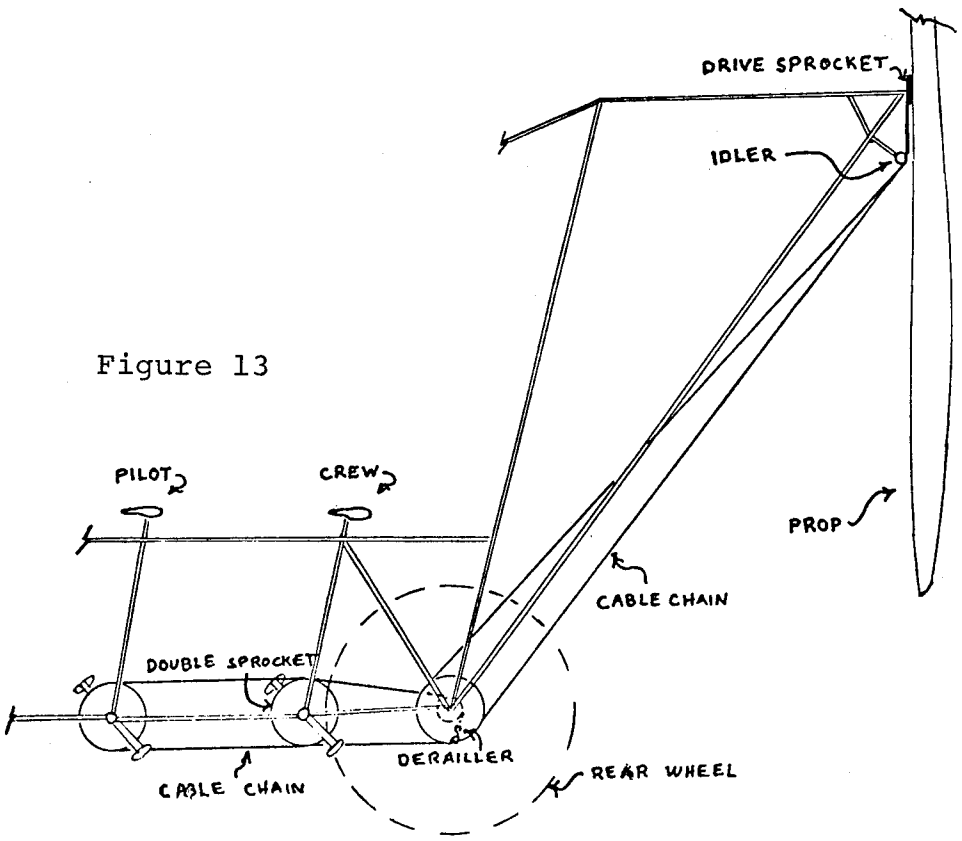


Figure 13



Computer analyses were done on other structures besides the wing spar. The major computer analysis was done on the fuselage truss system. For ease of construction, aluminum tubing was chosen as the main component of the fuselage. Due to the relatively high density of aluminum, the fuselage had to be carefully designed to keep weight to a minimum. Our analysis became quite involved due to the loads at the pedalling positions. However, due to the generosity of the Schwinn Bicycle Company, our problem in this area was solved. Schwinn has designed and provided us with the necessary structure for the support of the two men and the propulsion system.

Other structures, such as the tip plates, leading edge tubes, trailing edges, spoilers, propeller, and vertical stabilizer were designed using similar methods. The major materials of construction in all these components are balsa, spruce, aluminum tubing, aluminum wire, and nylon skin.

The only other major structural test was that of a full scale test section of the canard in a wind tunnel. The results of this test fully supported our previous analyses.

The design and analysis of our aircraft resulted in the weight breakdown shown in Table IV.

Propulsion

The propulsion system was designed to be simple and light. The two crew members are positioned as if on a racing tandem bicycle. The seats are standard light-weight racing bicycle seats and the crew sit in the normal racing crouched posture. The pilot for the prize attempts is an experienced and successful amateur bicycle racer as well as an experienced glider pilot. The other crew member is a professional bicycle racer. This simple cycling position is therefore a natural one for the crew. They are well-trained in putting out large amounts of power while in this position.

The power is transmitted from the two sets of pedals to the rear wheel. This wheel is a standard light-weight racing wheel and is positioned just behind the rear crew member. The axle of the rear wheel is located between the spar ends of the lower wing panels. The chain drives the rear wheel through a modified bicycle derailleur gear set. This gear set is designed to give a low gear ratio to get the aircraft started. Shifting of the gears is done by the rear crew member. The final gear ratio is reached before lift-off and no downshifting is done. One of the modifications to the gear set considered of attaching a large sprocket to provide the drive to the propeller.

Table IV

Weights

WING		
ribs		6.3 lb
spar		32.0
leading edge		2.0
trailing edge		4.0
nylon covering		4.5
controls		2.0
tip plates and struts		6.0
	total	56.8
CANARD		
equivalent weight		5.7
FUSELAGE		
tubing		20.0
bicycle and chains		22.0
wheels		2.0
controls		5.0
skin		1.0
	total	50.0
TRANSMISSION SYSTEM		
chain		0.5
axles, gears, and bearings		0.8
	total	1.3
PROPELLER		5.0
MISCELLANEOUS		
vertical stabilizer		4.0
rigging cables		1.5
	total	5.5
TOTAL EMPTY WEIGHT		124.3

The drive to the propeller has been a stumbling block for many designs. A light-weight, non-slip transmission is needed which has an output rotating on an axis shifted 90° from that of the input. Some designs have used bevel gears, others have used twisted belts. Our design uses a new type of chain. This chain runs on the same sprockets and gears as regular bicycle chain. It is composed of two lengths of aircraft stranded cable sheathed in a plastic coating. This coating serves to bond hard plastic discs to the cables which take the place of the roller cross pieces of conventional chain. The discs do not rotate, but the hardness and self-lubricating properties of the plastic serve to reduce friction and wear. Because cables, rather than individual links, make up the sides of the chain, it is quite flexible. It can easily twist around the 90° needed between the wheel and the propeller. Unlike a twisted belt, the chain has no slippage. It is also much lighter than conventional bicycle chain. For this reason it is also used to connect the two sets of pedals of the crew members. The overall transmission is shown in figure 13.

The propeller itself is carved from a laminated block of balsa wood. It is ten feet in diameter. The maximum chord of the blades is about six inches. The design speed is 240 RPM at a cruise velocity of 26 fps. Tests will be run on the completed propeller to determine the exact RPM for maximum efficiency. Power is transmitted to the propeller by a sprocket mounted directly on the hub. The propeller shaft is only used as a bearing and transmits no power.

It is intended, during early flight tests, to use model airplane engines to provide additional thrust. The engine(s) will be clamped on the fuselage and will drive its own propeller. This added power will enable the pilot to concentrate on handling the airplane and allow longer flights. The pilot and crew will still have to pedal, but at a reduced level.

As a final note on the propulsion system, it should be pointed out that the true power capabilities of man are almost totally unknown. The measured output depends to a large extent on the method being used to perform the measurement. Another factor is whether or not cooling air is supplied to the person being tested. Also important is whether the work is being done at a comfortable pace for the person. The generally used figure of about 1/2 horsepower for extended periods may actually be rather conservative. This is an area that would benefit from more investigation.

References

Czerwinski, W.; Structural Trends in the Development of Man-Powered Aircraft, Journal of the Royal Aeronautical Society, Vol. 71, No. 1, January 1967, pp. 9-13.

McMasters, J.H., C.J.Cole and D.A.Skinner; Man-Powered Flight, AIAA Student Journal, April 1971.

McMasters, J.H., and C.J.Cole; The Prospects for Man-Powered Flight (The Future of an Illusion), Technical Soaring, Vol.1, No. 2, October 1971, pp. 1-16.

McMasters, J.H., and C.J.Cole; Man-Powered Flight - A Review and Status Report, Soaring, Vol. 36, No.2, Febuary 1972, pp. 18-27.

Sherwin, K.; Man-Powered Flight, Model and Allied Publications, Ltd., Hemel, Hempstead, Herts, U.K., 1971.

Wilkie, D.R.; Man as an Aero Engine, Journal of the Royal Aeronautical Society, Vol. 64, No. 596, August 1960, pp. 477-481.

Wortmann, F.X.; in Aero Revue, November, 1963.

Wortmann, F.X.; Some Laminar Profiles for Sailplanes, Soaring, Vol. 28, No. 1, January 1964, pp. 14-18.

ADDENDUM

Performance

A correction to the earlier section of the report is necessary. The original performance calculations used a constant C_{D_o} of .006 based on wing area. This is a very optimistic value, originally chosen as an estimate for a long-chord monoplane configuration. The estimate was made before such things as the aspect ratio and final wing section had been decided upon. The second set of numbers still uses the .006 value, since the purpose of the calculations was to find the performance loss involved in going to the biplane configuration. Everything else (wing area, weight, etc.) was kept the same. The original estimate is even more optimistic for our final configuration than for the monoplane. The actual value of C_{D_o} for the final design will probably be somewhere between .012 and .018. This increases the power required but will not change the cruise speed significantly.

PSEUDO-ORNITHOPTER PROPULSION

by

Grant Smith
Walled Lake, Michigan

Notation

W	aircraft gross weight - pounds
X	maximum vertical center of gravity shift - ft
x	effective center of gravity shift - ft
G	the acceleration factor gross weight must be multiplied by to determine the actual load aero dynamically suported
u,d,r, or x	subscripts used to denote the up, down, or rest stroke, or (x) any stroke in general
a	acceleration of the system center of gravity - ft/sec^2
t	time duration of the subscripted stroke - sec
C_L	coefficient of lift
C_D	coefficient of drag with subscripts p for profile and i for induced drag
AR	aspect ratio
V	velocity - ft/sec
ρ	air density - $pounds/ft^3$
L	lift force - pounds
D	drag - pounds
A	wing area - ft^2
γ	a correction factor to account for cyclic pitch changes
β	the ratio of average vertical speed to average horizontal speed
D_s	specific drag
R	rotation of the lift vector relative to vertical - radians
η_e	overall propulsive efficiency
GST	gross specific thrust
h,v	subscripts used to denote horizontal & vertical components

Introduction

Recent construction of ultralight aircraft and interest in man-powered flight has created a desire for propulsion systems suited to the specific requirements of this type of craft. The Pseudo-Ornithopter (P-0) propulsion principle presented herein is proposed as a suitable method for propelling man-powered aircraft as well as providing auxiliary man-power assist for ultralight gliders. As such, it will be competing against pedal-propeller drives used in virtually all successful man-powered aircraft to date and should rightfully be compared against them.

Objective

P-O propulsion was developed in an attempt to minimize or eliminate the following problems associated with pedal-propeller drives.

1. The pedal to propeller gear ratio and propeller pitch are generally fixed, therefore imposing and off-design penalty for many flight conditions.
2. Effective pedal force is but a fraction of actual pedal force due to crank geometry.
3. Work stroke duration and rest stroke duration are not independent variables.
4. Cyclic torque variation causes off-design propeller operation and high drive-line peak stress.
5. Rest periods and glides impose a large propeller drag penalty.
6. The large propeller diameter requires placement compromises and complicates the drive train, with associated weight penalties.
7. Supplemental arm power is not available with a single crew member.
8. Pedal lever length may not be optimum for a given pilot and flight condition.

In searching for a solution to these problems we naturally consider ornithopters as this is a known alternative. Ornithopters do in fact control or eliminate many of the above problems. The joints, geometry and linkages associated with a typical flapping wing, however, provide many problems of their own.

Investigation into the operating principles of flapping wings indicates that the primary requirement is that there be relative movement between the wing area (up force) and the center of gravity (down force). A bird provides this movement quite naturally by flapping his wings. An ultralight pilot would naturally provide this movement by flexing his

arms and legs. By using this method he can eliminate many of the previously cited problems without suffering the structural disadvantages of flapping wings.

Description

A 150 pound pilot crouches low in a 50 pound ultralight, his feet resting on a foot pad and hands gripping a support. Both may be rigidly attached to the ultralight airframe. Then the operator extends his arms and legs to a semi-standing position. In doing so he raises his center of gravity (CG) 1-1/3 ft and imparts 200 ft-lb work to the system. The system (ultralight plus operator) CG is raised one foot in relation to the wing. No moving structural components are required. The operator's natural joints provide all the required movements. In addition, the hand brace may pivot in any of several modes to provide a means of aircraft control while doubling as a support to aid in balancing the operator.

If the operator squats under the same one gravity acceleration he was experiencing when he stood up, his body will absorb all the energy he expended in the power stroke reducing the cycle efficiency to zero. If, however, the operator could return to the squatting position under a reduced G load, the loss would be reduced proportionally and net work would be imparted to the system.[2]

This may be summarized by the following equations:[3]

$$\text{Gross Work/Cycle} = Wx \cdot Gd \qquad (1.0)$$

$$\text{Net Work/Cycle} = Wx \cdot (G_d - G_u) \qquad (2.0)$$

$$\text{Cycle Efficiency} = \frac{\text{Net Work}}{\text{Gross Work}} = 1 - \left(\frac{G_u}{G_d}\right) \qquad (3.0)$$

Where:

W_x is the product of weight times distance (relative to the wing) of CG movement for the operator or operator plus ultralight system.

G_d is the average G load on the standup (operator pushes down) stroke.

G_u is the average G load on the squat down (operator pulls arms and legs up) stroke.

Notice that optimum cycle efficiency is obtained by squatting down under zero or negative G conditions.

2 This is what happens when a child pumps a swing. He raises his CG at the high G bottom of the arc and lowers his CG at the low G top of the arc.

3 The "UP" stroke is hereby established as the squatting motion to pull arms and legs up while the "DOWN" stroke is the standing movement which involves pushing down on the surrounding structure.

When this cycle is employed on an ultralight, the aircraft reacts to the operator's actions by following a cyclic flight path (Figure 1). We will assume for now that the operator is positioned on the aircraft center of gravity so that pitch trim changes caused by his motion may be ignored. Thus, when the operator pushes down, the aircraft responds by accelerating downward in a constant pitch attitude. The resulting downward wing velocity causes the angle of attack to increase, increasing the lift and providing an upward acceleration to the system CG. The increased lift soon balances the operator's downward push and the wing continues at constant velocity while the operator is accelerated upward.

As the wing lift vector increases in magnitude it also rotates forward (to remain perpendicular to the airflow) providing a horizontal thrust component. The opposite occurs on the up stroke. The lift vector shrinks in size and rotates rearward creating a drag component while the operator accelerates downward. As a result the two strokes combine to either reduce drag or to impart a net thrust to the system (Figure 2).

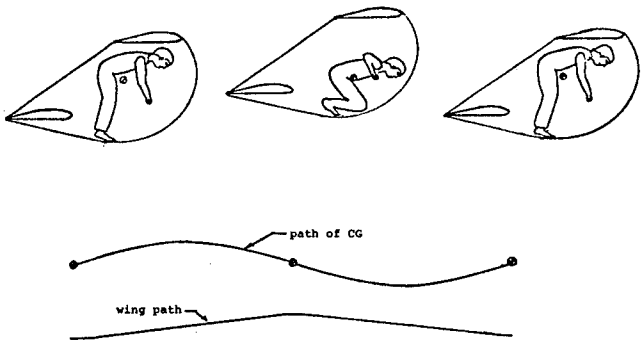


Figure 1.

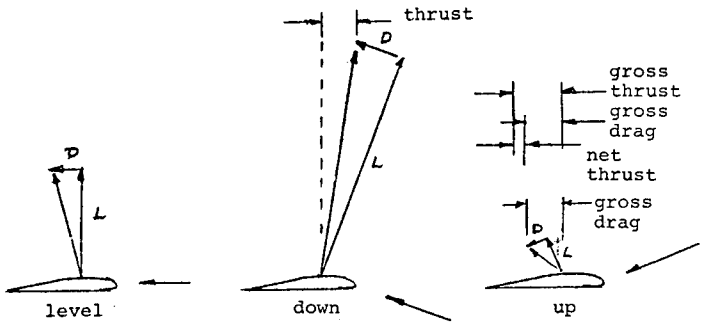


Figure 2.

Cycle analysis

Combining this up and down motion into the saw tooth path of figure 3A allows the performance to be determined by averaging forces on the up and down strokes respectively. In

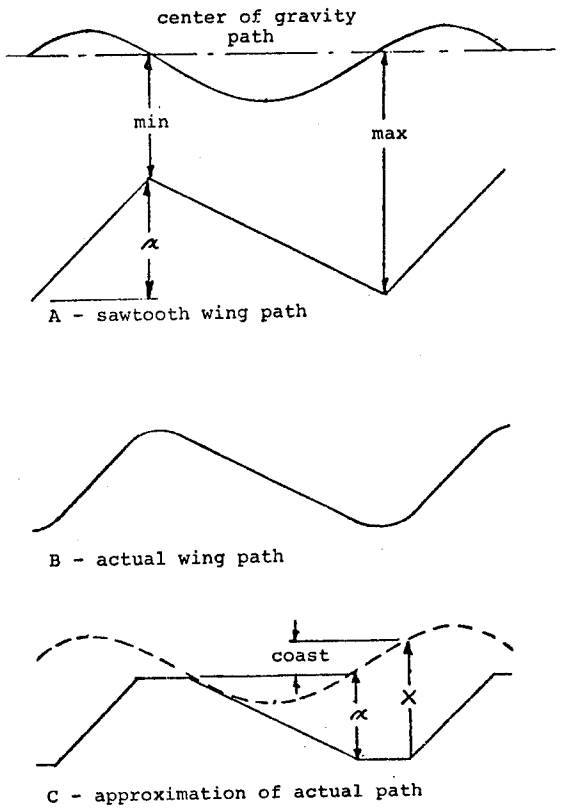


Figure 3 - Wing path profiles

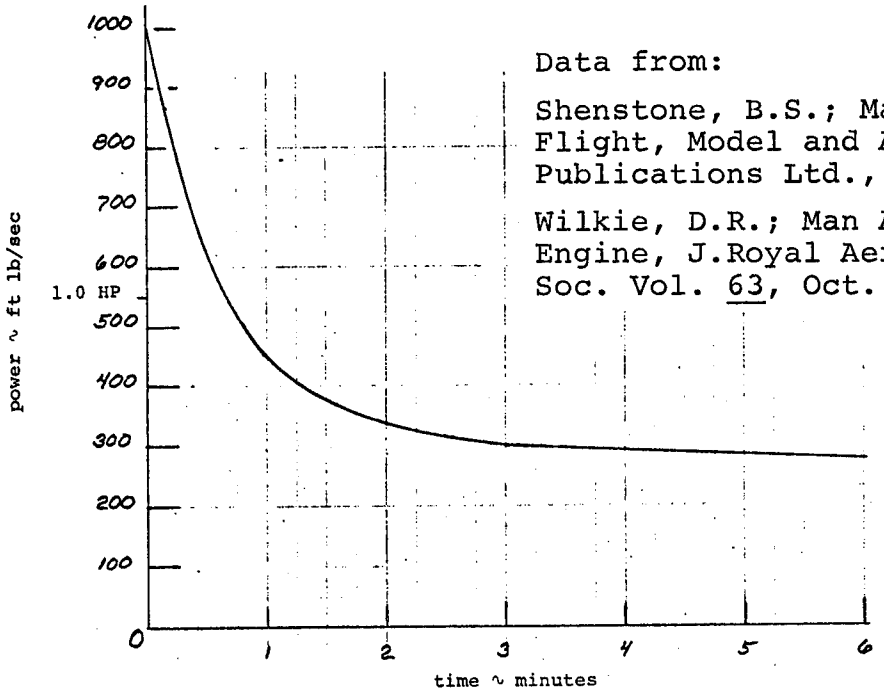


Figure 4 - Pseudo-Ornithopter power output (physically fit pilot)

practice this stroke can never be achieved as it requires infinate wing accelerations at the sharp saw tooth peaks.[4] A more realistic stroke is shown in Figure 3B where the peaks have been rounded to correspond with the finite accelerations. The saw tooth of Figure 3A may be modified to more closely approximate the actual stroke by including a rest period at each peak as shown in Figure 3C. This rest period will cause a performance deterioration due to the work time lost and the reduced effective stroke length.

$$x = X - 1/2\ a_u\ t_u\ t_r \tag{4.0}$$

Where: $a_u\ t_u = a_d\ t_d$ and $a = 32.2(G - 1.0)$

As indicated the up and down stroke need not be of equal time duration. For a given effective stroke length (x) and up stroke G load, the up stroke time duration (t_u) is directly proportional to forward speed (V) and inversely proportional to wing loading (L/A).

$$t_u \propto V \tag{5.0}$$

$$t_u \propto (L/A)^{-1} \tag{5.1}$$

Down stroke time duration is limited by the stalling lift coefficient and is inversely proportional to both speed and wing loading.

$$t_d \propto (V)^{-1} \tag{6.0}$$

$$t_d \propto (L/A)^{-1} \tag{6.1}$$

Therefore, the higher the wing loading the higher the maximum permissable frequency. The smaller the stall margin the higher the ratio of t_d/t_u.

These factors can be noticed in bird flight and we can expect there will be some optimum speed and cycle for each flight requirement. Matching of human factors to aircraft dimensions will also be required.

For these reasons, further analysis will be more meaningful if typical values are indicated. Reference to the tables will be helpful in this regard or the reader may use the following discussion and equations to find his own typical values.

---

[4] An investigation into the force, mass, velocity relationships indicate large vertical accelerations and low vertical terminal velocities. Therefore, a large portion of the stroke is at nearly constant wing vertical velocity and path 3A is a reasonable starting approximation.

Given aspect ratio and profile drag coefficient, lift coefficient for maximum L/D and minimum sink may be determined by equations (7.0) and (8.0) respectively:

$$@ \text{ L/D Max}, C_L = (C_{D_p} \pi AR)^{1/2} \quad ; \quad C_D = 2\, C_{D_p} \tag{7.0}$$

$$@ \text{ Min Sink}, C_L = \sqrt{3}(C_L \text{ @ Max L/D}) \quad ; \quad C_D = 4\, C_{D_p} \tag{8.0}$$

where C_{D_p} is assumed constant.

Appropriate velocities may be determined by equation (9.0):

$$V = \left[\frac{L/A}{1/2 \rho C_L}\right]^{1/2} \simeq 30\left[\frac{L/A}{C_L}\right]^{1/2} \quad \text{ft/sec} \tag{9.0}$$

$$\text{or } C_L = \frac{L/A}{1/2\ V^2} \tag{9.1}$$

Using these values as a guide we may choose an operating C_L or velocity for future calculations. Assuming a profile drag coefficient for the aircraft, lift drag ratio, sinking speed, and power required are determined by equations (10.0), (11.0) and (12.0) respectively:

$$L/D = \frac{C_L}{C_{D_p} + C_{D_i}} \quad \text{where } C_{D_i} = \frac{C_L^2}{\pi AR} \tag{10.0}$$

$$\text{Sink} = \frac{V}{L/D} \quad \text{ft/sec} \tag{11.0}$$

$$\text{Power} = \text{Sink} \cdot \text{Gross Weight} \quad \text{ft-lb/sec} \tag{12.0}$$

The lift/drag ratio represents the angle of glide, while sinking speed is useful to determine soarability. The power requirement indicates the degree of success to expect for a man-powered flight (see Figure 4).

For pumping flight, the average G load (G_R) is related to the up and down G load by equation (13.0). For straight line flight (i.e., no turns or zooms) the average G load must be 1.0 and equation (13.0) reduces to equation (13.1).

$$G_d = G_r + \frac{t_u}{t_d}(G_r - G_u) \tag{13.0}$$

$$G_d = 1 + \frac{t_u}{t_d}(1 - G_u) \tag{13.1}$$

Assuming a constant horizontal velocity component, equations (14.0) and (14.1) may be used to calculate the required up and down stroke lift coefficient.

$$C_{Lu} = C_{Lr} \frac{G_u}{G_r} \tag{14.0}$$

$$C_{Ld} = C_{Lr} \frac{G_d}{G_r} \tag{14.1}$$

Up and down stroke lift vector rotation may be calculated by equations (15.0) and (15.1). A math check is made by use of equation (16.0).

$$R_u = \frac{\gamma(C_{Lr} - C_{Lu})}{2\pi} \tag{15.0}$$

$$R_d = \frac{\gamma(C_{Lr} - C_{Lu})}{2\pi} \tag{15.1}$$

Where radian measure is used and the factor γ is included to allow for any cyclic wing pitch variations.

$$\left|\frac{R_u}{R_d}\right| = \frac{t_d}{t_u} \tag{16.0}$$

Up and down stroke times are calculated by equations (17.0) and (17.1). A math check is obtained by comparing the time ratio with that used in equation (13.0).

$$t_u = \frac{x}{VR_u} \tag{17.0}$$

$$t_d = \frac{x}{VR_d} \tag{17.1}$$

Iterate with equation 4.0 to obtain the appropriate value of x.

The operating cycle is now defined for the speed, steady state lift coefficient and stroke variables chosen. We will do well to pause for a moment and consider the wisdom of our choice. Are the lift coefficients and times reasonable or should new values be chosen?

Performance determination

Lift is defined as the force perpendicular to the airflow and generally has a large vertical and small horizontal component. Drag is an order of magnitude smaller than lift and is parallel to the airflow. Performance may be determined by summing forces in the horizontal direction while the airfoil oscilates about a horizontal flight path and time averaging to determine the net thrust or drag force. This force

may then be compared with other parameters to determine vertical speed and climb/descent angles.

Calculations may be simplified by neglecting the vertical drag components as this small force component combined with low vertical speed minimizes errors. Calculations will be made in terms of specific thrust or specific power, i.e., thrust/pound or power/pound gross weight.

For non-flapping flight, performance may be calculated via the lift/drag ratio.

$$\text{Specific thrust req d.} = \frac{1}{L/D} + \beta \qquad (18.0)$$

where β = Vertical speed/Horizontal speed

$$\text{Specific power req d.} = \frac{V}{L/D} + \text{vertical speed} \qquad (19.0)$$

For powered (flapping) flight, calculations involving the lift/drag ratio should not be used on the up stroke due to the small or negative lift values which may be encountered. Instead, we will calculate the profile and induced drag separately.

If horizontal velocity is assumed constant, profile drag is constant throughout the cycle.[5]

$$\text{Specific profile drag} = \frac{D_p}{W} = \frac{C_{D_p}}{C_L} \qquad (20.0)$$

(constant throughout cycle)

The specific induced drag for each stroke of the cycle may be evaluated in a similar manner and time-averaged.

$$\text{Specific induced drag} = \frac{D_i}{W} + \frac{C_{D_{i(x)}} G_{(x)}}{C_L} = \frac{C_L G^2_{(x)}}{\pi AR} \qquad (21.0)$$

where x indicates the appropriate value for the stroke involved, and the relationships $C_{D_i} = \frac{C_L^2}{\pi AR}$ and $C_{L(x)} = C_L G_{(x)}$ are used in the transformation

$$\text{Average specific induced drag} = \frac{C_L}{\pi AR} \frac{(G_u^2 t_u + G_d^2 t_d + G_r^2 2 t_r)}{t_t} =$$

$$= \frac{C_L \Delta D_i}{\pi AR} \qquad (22.0)$$

[5] In actual practice profile drag is a function of angle of attack and does vary throughout the cycle. This may be corrected for by assuming an appropriate average C_{D_p} or by using a lower than actual aspect ratio to include the profile drag variation with induced drag. For simplicity, we will use the C_{D_p} for steady flight at the chosen velocity and assume this is accurate enough.

The quantity in brackets (ΔD_i) is the factor induced drag is increased by, due to the unsteady flapping flight. Some investigators may argue that induced drag appears to decrease on some ornithopters. If so, this is probably due to the starting and stopping wing vortex, factors not considered in this investigation. Until shown otherwise we will remain conservative and assume that equation (22.0) is valid but admit that induced drag may be lower than calculated.

Combining the profile and induced drag equations yields the total specific drag D_s:

$$D_s = \frac{C_{D_p}}{C_L} + \frac{C_L \quad \Delta D_i}{\pi AR} \tag{23.0}$$

As the pumping G loads approach 1.0 or the pumping time becomes insignificant compared to the rest time this equation reduces to the steady state flight drag and thus may be approximated by $(L/D)^{-1}$.

In addition to the horizontal drag force there is a horizontal lift force component (gross thrust) which must be considered whenever the wing path is not horizontal. This may be calculated by use of the wing path deviation from horizontal which is equivalent to the lift vector rotation.

$$\text{Specific horizontal lift component} = \frac{L_h}{W} = G \tan R$$

where the relationships $W = L_v/G$ and $\tan R = L_h/L_v$ are used in the transformation. (24.0)

Time averaging yields the average gross specific thrust GST:

$$GST = \frac{G_d \; t_d \; \tan R_d - G_u \; t_u \; \tan R_u}{t_t} = \frac{x}{V \; t_t} (G_d - G_u) \tag{25.0}$$

where the negative allows the use of absolute values for angles and the relationship $\tan R_{(x)} = \frac{x}{V \; t_{(x)}}$ is used in the transformation.

Net specific thrust NST is obtained by subtracting the total specific drag from the gross specific thrust:

$$NST = \frac{x}{V \; t_t} (G_d - G_u) - \left[\frac{C_{D_p}}{C_L} + \frac{C_L \Delta D_i}{\pi AR}\right] \tag{26.0}$$

For level unaccelerated flight the net specific thrust must be zero. Otherwise it is equal to the climb or descent angle (β) or an acceleration factor.

Propulsive efficiency η_e is obtained by dividing output by input.

$$\eta_e = \frac{\text{Output}}{\text{Input}} = \frac{\text{Specific Thrust Required}}{\text{Gross Specific Thrust}} \tag{27.0}$$

$$\eta_e = \frac{\frac{1}{L/D} + \beta}{\frac{x}{V\ t_t}(G_d - G_u)} \qquad (27.1)$$

Assuming the net specific thrust equal to β and substituting equations (10.0) and (26.0) we find

$$\eta_e = 1 - \frac{\frac{C_L}{\pi AR}\delta D_i}{\frac{x}{V\ t_t}(G_d - G_u)} \qquad \delta D_i = \Delta D_i - 1 \qquad (28.0)$$

$$\eta_e = 1 - \frac{\text{Induced Drag Increase}}{\text{Gross Thrust}} \qquad (28.1)$$

Overall efficiency may be obtained by multiplying the propulsive efficiency (Eqn 28) by the cycle efficiency (Eqn 3).

Solving equation (27.1) for β we find that the climb/descent angle (β) is equal to the propulsive efficiency times the gross specific thrust minus the non-pumping drag/lift ratio.

$$\beta = \eta_e \frac{x}{V\ t_t}(G_d - G_u) - (L/D)^{-1} \qquad (29.0)$$

where η_e may be evaluated from equation (28.0)

NB: $1/\beta$ is equivalent to the lift/drag ratio while pumping.

For level flight we see that the gross specific thrust must equal the inverse of the lift/drag ratio times propulsive efficiency.

$$GST = \frac{x}{V\ t_t}(G_d - G_u) = \frac{1}{\eta_e (L/D)} \qquad (30.0)$$

Tables 1 through 3 show typical values of performance which may be expected. Table 1 assumes values which are typical of today's ultralight technology. While the performance is not spectacular, it is adequate to gain experience and demonstrate the feasibility of pseudo-ornithopter propulsion. With ground effect and slight refinements, flights comparable to the Wright Brothers 1903 attempt could be expected.

Tables 2 and 3 assume aircraft parameters typical of a second or third generation of ultralights. Even though little optimization has been done, the figures look promising for a true self-launching sailplane or even Kremer competition attempts. The values given are meant as an example only and do not represent a completed design study.

Table 1

SPECIFICATIONS

Span 36 ft Area 200 ft^2 Aspect Ratio Actual 6.5
Effective 12.0

Operator Wt 150 lb
Empty Wt 50 lb Wing loading 1.0 lb/ft
Gross Wt 200 lb Span loading 5.5 lb/ft

Airfoil Clark Y 1.4 C_L Max 0.02 C_{D_p}
Parasite drag 4 ft^2 @ 1.0 $C_{D_p} \div A$ 0.02 C_{D_p}
Total 0.04 C_{D_p}

GLIDING PERFORMANCE

@ Max L/D
$1.23C_L$ 30 ft/sec V 15:1 L/D 1.8 ft/sec Sink 365 ft#/sec Power

@ Operating Conditions
0.8 C_L 33.5 ft/sec V 14:1 L/D 2.39 ft/sec Sink 478 ft#/sec Power

CYCLE PARAMETERS

0.5 t_u/t_d 1.0 γ 1.0 ft x 0.71 ft x t_u 0.1664 sec
0 G_u 1.5 G_d 1.0 G_r t_d 0.3328 sec
0 C_{Lu} 1.2 C_{Ld} 2 t_r 0.2 sec
0.127 R_u 0.0637 R_d t_t 0.6992 sec

$\frac{C_L}{\pi AR} = 0.0212$ $\Delta D_i = 1.3569$

Specific induced drag = 0.0287
Specific profile drag = 0.050
Total specific drag = 0.07876
Gross specific thrust = 0.04546
Net specific thrust =-0.0333

$\eta_e = 83\%$
Glide ratio = 30 : 1

POWERED PERFORMANCE

Vertical speed -1.12 ft/sec Input power 304 ft#/sec.

Table 2

SPECIFICATIONS

Span 42 ft Area 150 ft^2 Aspect Ratio Actual 12, Effective 18

Operator Wt 150 lb
Empty Wt 50 lb
Gross Wt 200 lb

Wing loading 1.333 lb/ft
Span loading 4.76 lb/ft

Airfoil FX - 05191

1.4 C_L Max 0.01 C_{D_p}
$C_{D_p} \div A$ 0.002 C_{D_p}
Total 0.012 C_{D_p}

Parasite drag 4 ft^2 @ 0.1

GLIDING PERFORMANCE

@ Max L/D
0.75 C_L 40 ft/sec V 37.5 L/D 1.06 ft/sec Sink 212 ft#/sec Power

@ Operating Conditions
0.75 C_L 40 ft/sec V 37.5 L/D 1.06 ft/sec Sink 212 ft#/sec Power

CYCLE PARAMETERS

0.5 t_u/t_d 1.0 γ 1.0 ft x 0.75 ft x t_u 0.157 sec
0 G_u 1.5 G_d 1.0 G_r t_d 0.314 sec
0 C_{Lu} 1.12 C_{Ld} 2 t_r 0.2 sec
0.119 R_u 0.597 R_d t_t 0.671 sec

$\frac{C_L}{\pi AR}$ = 0.13127 ΔD_i = 1.3509

Specific induced drag = 0.017734
Specific profile drag = 0.0160
Total specific drag = 0.03373
Gross specific thrust = 0.041915
Net specific thrust = 0.00818

η_e = 89%
Glide ratio = 122 : Climb

POWERED PERFORMANCE

Vertical speed 0.328 ft/sec Input power 335 ft#/sec.

Table 3

SPECIFICATIONS

Span 42 ft Area 150 ft^2 Aspect Ratio Actual 12
Effective 18

Operator Wt 150 lb
Empty Wt 50 lb Wing loading 1.333 lb/ft
Gross Wt 200 lb Span loading 4.76 lb/ft

Airfoil FX - 05191 1.4 C_L Max 0.008 C_{D_p}
Parasite drag 4 ft^2 @ 1.0 C_{D_p} ÷ A 0.002 C_{D_p}
Total 0.01 C_{D_p}

GLIDING PERFORMANCE

@ Max L/D
0.75 C_L 40 ft/sec V 37.5 L/D 1.06 ft/sec Sink 212 ft#/sec Power

@ Operating Conditions
0.75 CL 40 ft/sec V 37.5 L/D 1.06 ft/sec Sink 212 ft#/sec Power

CYCLE PARAMETERS

0.3 t_u/t_d 1.0 γ 1.0 ft x 0.75 ft x t_u 0.157 sec
0 G_u 1.3 G_d 1.0 G_r t_d 0.523 sec
0 C_{Lu} 0.975 C_{Ld} 2 t_r 0.2 sec
0.119 R_u 0.358 R_d t_t 0.8703 sec

$\frac{C_L}{\pi AR}$ = 0.01327 ΔD_i = 1.2459

Specific induced drag = 0.01653
Specific profile drag = 0.01333
Total specific drag = 0.02986
Gross specific thrust = 0.0280
Net specific thrust = -0.00185

η_e = 88%
Glide ratio = 539 : 1

POWERED PERFORMANCE

Vertical speed -0.07 ft/sec Input power 298 ft#/sec.

Conclusions

This brief investigation indicates that Pseudo-Ornithopter propulsion is worth considering. It appears that a worthwhile performance gain is possible with ultralight aircraft. In exchange we must provide

1. sufficient room for the operator to move about
2. a reliable structure
3. considerable muscular output

A four foot vertical height is considered sufficient for most operators. This is slightly larger than the area required for efficient pedal operation.

A reliable structure is required regardless of propulsion system. This is not considered a problem because pumping loads are of the same general magnitude as gust loads.

Muscular output is a problem. My opinion is that if man could fly like a bird 90% of the people would be too lazy to fly. We are talking of that remaining 10% and they are free to work as much as they like. The more ambitious can fly farther and faster and on days when others may not feel it worth the effort. But, like the buzzard, those others will be out when conditions are right and an occasional pump may be made to aid in reaching that next thermal.

Reviewing the pedal-propeller problems listed, we have achieved the following:

1. There is no fixed gear-ratio for flight. However, pumping frequency is limited by forward velocity. More detailed investigation is required in this area.
2. 100% of the leg force is effective for input power. Inertia losses may be greater.
3. Work stroke and rest stroke time duration are independent but limited by flight speed.
4. Cyclic operation requires the wing to operate over a wide range of C_L values.
5. There is no drag increase while resting.
6. Additional structure and drive train requirements are eliminated.
7. Supplimental arm power is available.
8. Stroke length is variable at any time.

Whether this is an improvement remains to be determined. All that is certain is that additional investigation is in order.

Recommendations

Numbers can be chosen to show Kremer competition or better performance, but proof of operation will be in a flight demonstration. Attempts at Pseudo-Ornithopter propulsion whether successful or not will do much to define problem areas and indicate the validity of the assumed values. Very little is known about cycle limitations. How fast can one pump? What is the optimum cycle considering human factors? How does structural flexing affect performance? What percentage of the total arm power is available? Trial flights are recommended as a means to answer these questions.

The cycle chosen for the example was chosen by the best guess method. A thorough investigation of propulsive efficiency for various cycles and speeds is required. This should be run in conjuction with the flight test program as the questions arise: "can the operator perform this cycle", or, "which cycle can the operator perform best?"

References

1. Shenstone, B.S.; Man-Powered Flight, Model and Allied Publications Ltd., 1970.

2. Wilkie, D.R.; Man As An Aero Engine, J. Royal Aeronautical Society, Vol. 63, Oct. 1959.

THE USE OF STORED ENERGY DEVICES IN MAN-POWERED SELF-LAUNCHING SAILPLANES

by

John H. McMasters, Tempe, Arizona
Curtis J. Cole, Marquette, Michigan

Notation

AR	Aspect Ratio = b^2/S
AR_e	Effective Aspect Ratio = AR/K_w
b	Projected Wing Span
BHP	Brake Horse Power
c	Wing Chord
C_D	Total Drag Coefficient
C_{D_p}	Profile Drag Coefficient of Wing
C_{D_π}	Parasite Drag Coefficient
C_{D_i}	Induced Drag Coefficient $C_{D_i} = \frac{K_w C_L^2}{\pi AR}$
C_{D_t}	Trim Drag Coefficient
C_{D_o}	"Zero Lift" Drag Coefficient
C_L	Lift Coefficient
D	Drag Force $D=C_D qS$
K_w	Span Efficiency Factor of a Wing
h	Height of Aerodynamic Center of Wing Mean Aerodynamic Chord Above the Ground.

L	Lift Force	$L=C_L qS$
q	Dynamic Pressure	$q=1/2 \quad \rho V^2$
R	Turn Radius	
R_n	Reynolds Number	$R_n=VC/\nu$
S	Projected Wing Area	
T	Time (Duration)	
V	Speed (Measured along Flight Path)	
W	Gross Weight	
Z	Height (Vertical Coordinate)	
$\dot{Z}$	Climb or Sink Rate (+ for Climb)	
β	Camber Index (See Figure 8)	
η	Propulsive Efficiency	
λ	Power Degradation Factor (See Eqn. A-6)	
ν	Kinematic Viscosity	
θ	Climb (or Glide) Angle (+ for Climb)	
ϕ	Bank Angle	
ρ	Air Density	

Background

The challenge of achieving true man-powered flight has held a special fascination for a few individuals for centuries. Interest in the subject has increased substantially in the last few years as a result of the British £10,000 Kremer Competition. The history of man-powered flight and recent efforts to win the Kremer competions have been chronicled in several recent articles [1,2] and the book by Sherwin [3] in Britain, and need not be repeated here.

The major problem in designing a man-powered aircraft (MPA) is the very low power available and power-to-weight ratio of the human "engine". While it is now relatively easy to design an MPA capable of making relatively long flights (1000 to 2000 yards) in a straight line solely

under human power, the power required to make turns and to climb exceeds even an athlete's capabilities if attempted for more than very short periods of time. This very seriously limits the feasibility of constructing a true "man-powered airplane".

It has long been suggested that the power problem can be partially solved by the use of some sort of stored energy device. By this is meant any device in which energy can be stored to aid in propelling the aircraft when and if such assistance is needed. Such a device can be external to the aircraft (e.g. a catapult) or an integral part of the machine. Examples of this latter category of device are a wound-up rubber band or spring, compressed gas, and a battery.

Little serious attention has been given to the use of stored energy devices in an MPA in recent years, largely because the rules of the Kremer Competitions (which have been the main motive force behind most recent MPA activity) have specifically prohibited the use of such devices. It appears, however, that winning any of the Kremer prizes is a nearly impossible task, at least within the near future. In addition, it appears that any MPA which complies fully with the Kremer Competition rules must be so large and fragile that it can only be flown at heights very close to the ground, under conditions of almost zero wind. A technical discussion of some of the problems associated with the design of a Kremer Competition MPA can be found in References 4 and 5. Even if such a machine could win the Kremer prizes it would be virtually useless for any other than its intended purpose. It would seem, then, that if an MPA is to have any future as a sporting vehicle, the question of use of stored energy devices should be re-evaluated.

Two questions regarding the use of stored energy devices are of importance to the MPA enthusiast:
(1) Does the use of such a device violate the spirit and intent of the goal of achieving man-powered flight?
(2) Does the use of such a device significantly improve the performance of an MPA?

If the ultimate aim of MPA development is to produce a true self-launching sailplane which relies in no way on any external fuel source, then the answer to the first question would seem to be - No, with some qualifications. Our position is that if the stored energy device is carried completely by the airplane and is energized solely by the pilot (and crew members if the vehicle is multi-placed) the use of the device in no serious way violates the purest philosophy of man-powered flight.

The answer to the second question seems to be an obvious - Yes. However, it must be remembered that any energy storage device will have some weight, and this weight must be carried by the MPA. Since weight is the single most important parameter in the design problem [6], some care must be taken in evaluating the real performance improvements to be obtained from the use of such devices.

Some performance estimates

Suppose we have an MPA like the Hatfield "Puffin II" (1) shown in Figure 1. The performance of this machine can be estimated from the formulas in Appendix A. The estimated characteristics of "Puffin II" (without the energy storage device) are:

Loaded Weight 290 lb

Propeller/Transmission Efficiency 83%

Performance: (1) At a height of 10 ft (in ground effect)

L/D_{max} = 35.5 at 18 mph

Cruise power required (level flight) 0.47 BHP

Power required to climb at 10 fpm 0.58 BHP

(2) Free air (outside ground effect)

L/D_{max} = 31 at 19.4 mph

Cruise power required (level flight) 0.58 BHP

Power required to climb at 10 fpm 0.69 BHP

A calculated polar diagram (using rather conservative drag values) for the basic Puffin II operating outside of ground effect is shown in Figure 2 in comparison with Bikle's [7] measured polar for an 1-26. At a loaded weight of 290 lb, the Puffin has a wing loading of 0.745 lb/ft^2. The wing span and aspect ratio are 93 ft and 22.2 respectively.

To demonstrate the performance of the Puffin, consider the following problem: Assuming that the take-off ground run (which ends just as flying speed is reached) required about 30 seconds, what is the maximum height attainable in a 3 minute, maximum effort climb? Suppose that the pilot can produce (while simultaneously controlling the aircraft) between 75 and 100% of the power of the champion cyclist

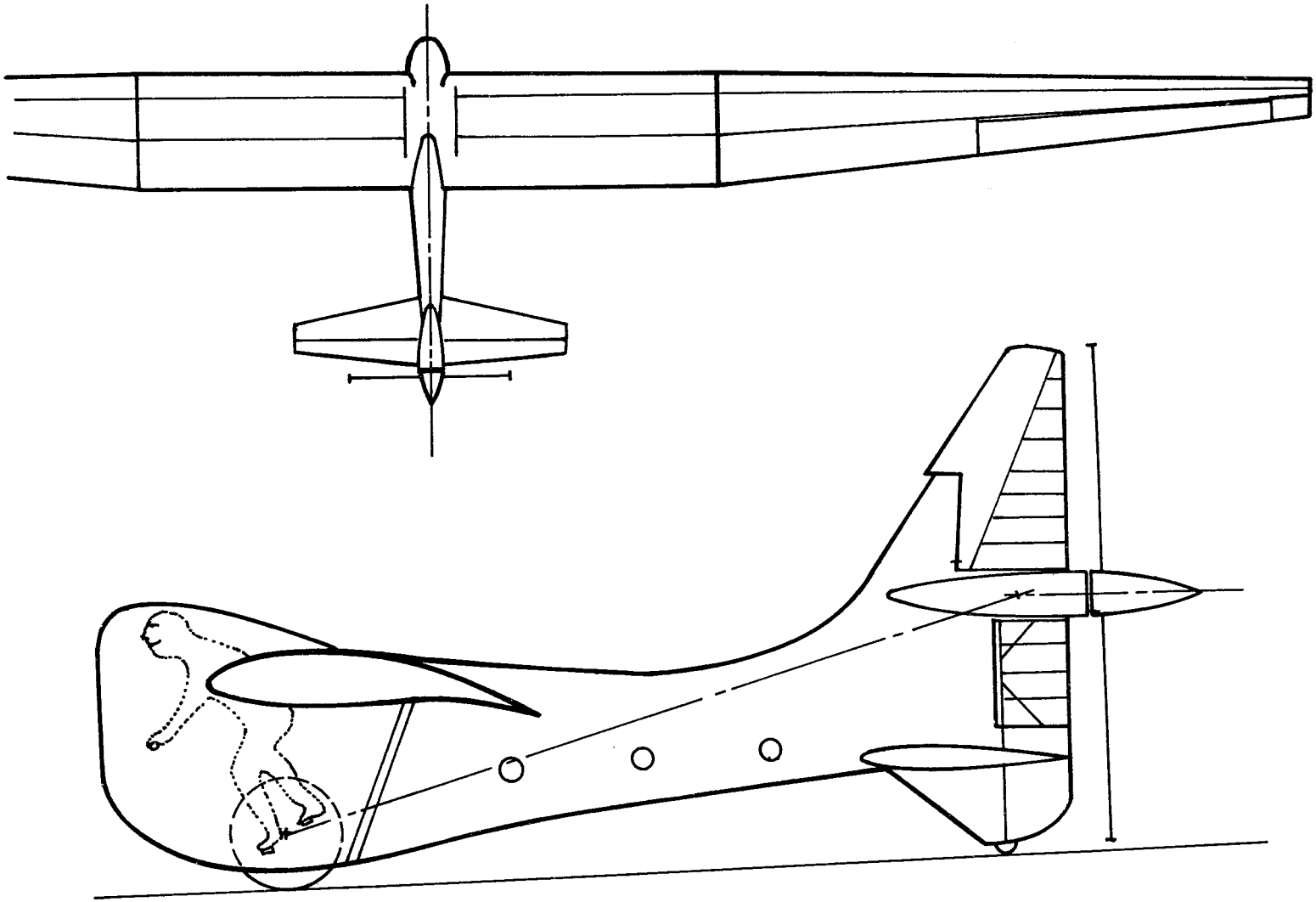


FIGURE 1. HATFIELD "PUFFIN II" MPA

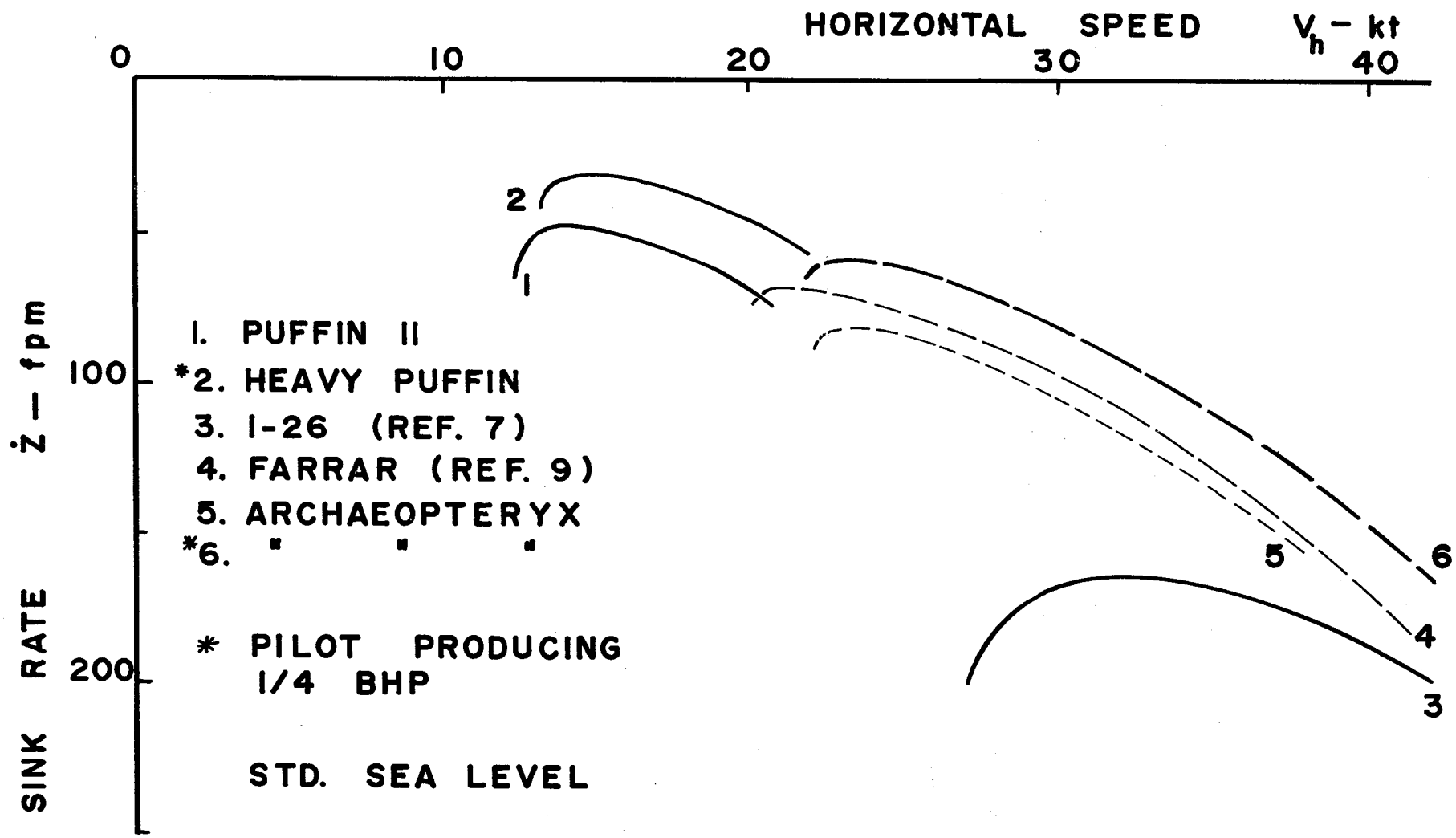


FIGURE 2. ESTIMATED PERFORMANCE POLARS

TABLE I.

Theoretical Climb Performance of the "Puffin II" MPA

Loaded Wt.: 290 lb

Wing Loading: 0.745 lb/ft^2

Minimum BHP Required for Level Flight: 0.35 at h = 0 ft
0.43 at h = 10 ft
0.52 at h outside ground effect.

Time of Climb: 3 minutes

	Champion Athlete	75% Champion Athlete
Maximum BHP Available	0.61	0.46
Maximum Rate of Climb		
h = 0 ft	25 fpm	10.5 fpm
h = 10 ft	17 fpm	3 fpm
h outside ground effect	8.5 fpm	-5.5 fpm
Maximum Height Gained:	40 ft	15 ft
Maximum Horizontal Distance Flown:	1350 yd	1350 yd
Glide Distance from Max. Height:	450 yd	180 yd
Total Flight Distance:	1800 yd	1530 yd

indicated in the human power curve shown in Figure 3. Some simple numerical integrations, accounting for the variations in power required as the aircraft climbs out of ground effect, yield the performances summarized in Table I and shown in Figure 4. These calculations show very clearly the enormous difficulty of flying by unaided human power alone.

Now to show the advantage of the stored energy device, suppose this same machine is fitted with a stored energy device of the type reported by Nonweiler [8]. This device is shown in Figure 5. The device consists of a drum, attached through appropriate gearing, to the propeller shaft. Rubber cord is wrapped around the drum, and may be wound up (thus storing energy) by the pilot prior to takeoff. Nonweiler estimated that 100,000 ft-lb (3 HP-min) of energy could be stored in such a device weighing 10 lb.

It is estimated that the total weight of the device installed in the "Puffin" would be 15 lb, bringing the loaded weight of the aircraft to 305 lb. At this point an additional problem is encountered. The "Puffin" was designed for flight close to the ground under almost ideal atmospheric conditions. Consequently, the design load factor was only + 2 g with factor of safety 1.5. A vehicle designed to fly out of ground effect would have to have a substantially higher load factor. For purposes of this exercise, let us define a "Heavy Puffin" with the same dimension as the original "Puffin" but with a load factor of + 4 g and factor of safety of 1.5. It is estimated that this machine would weigh 320 lb loaded or 335 lb with the stored energy device.

To show the possible gains in performance due to the stored energy device, assume that the device is geared to produce 1 BHP for 3 minutes. As before, it is assumed that the pilot simultaneously produces maximum power until exhausted after 3 minutes of flight. In this example the pilot produces all the power required for the ground run which ends when flying speed is reached and which requires 30 seconds. At lift-off the stored energy device is activated. The anticipated performance in this case is shown in Figure 4.

The performance improvement of the "Heavy Puffin" with the stored energy device can only be considered "spectacular" when compared with the performance of the basic "Puffin" (a 600% increase in maximum height gain!). It should be noted, however, that this example evades entirely the central question: Is it feasible or sensible to go pedalling around at 200 ft AGL, in a machine twice the size and weighing half as much as a 1-26 (with a red line speed of about 22 kt) looking for 30 fpm lift?

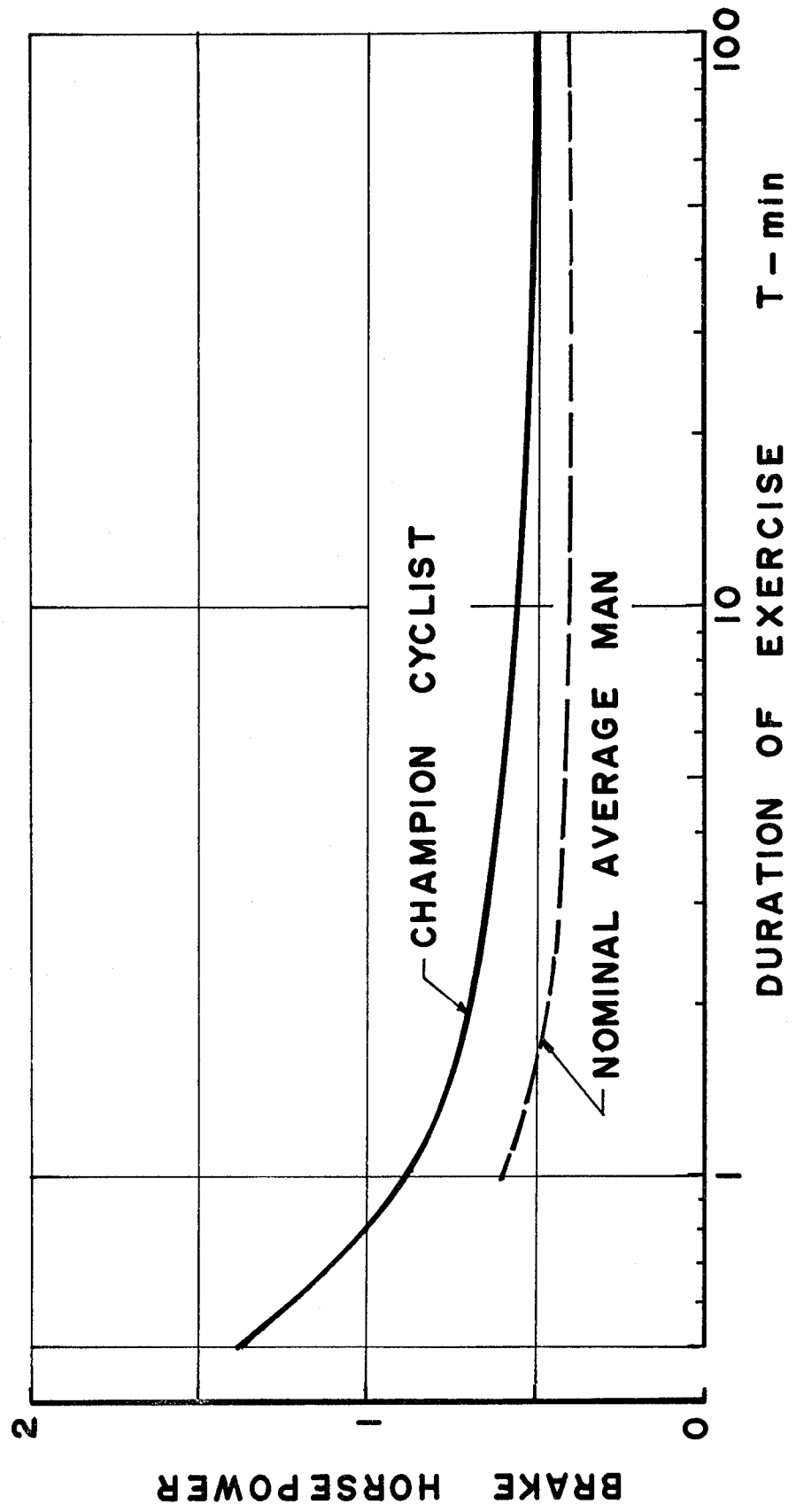


FIGURE 3. HUMAN POWER OUTPUT

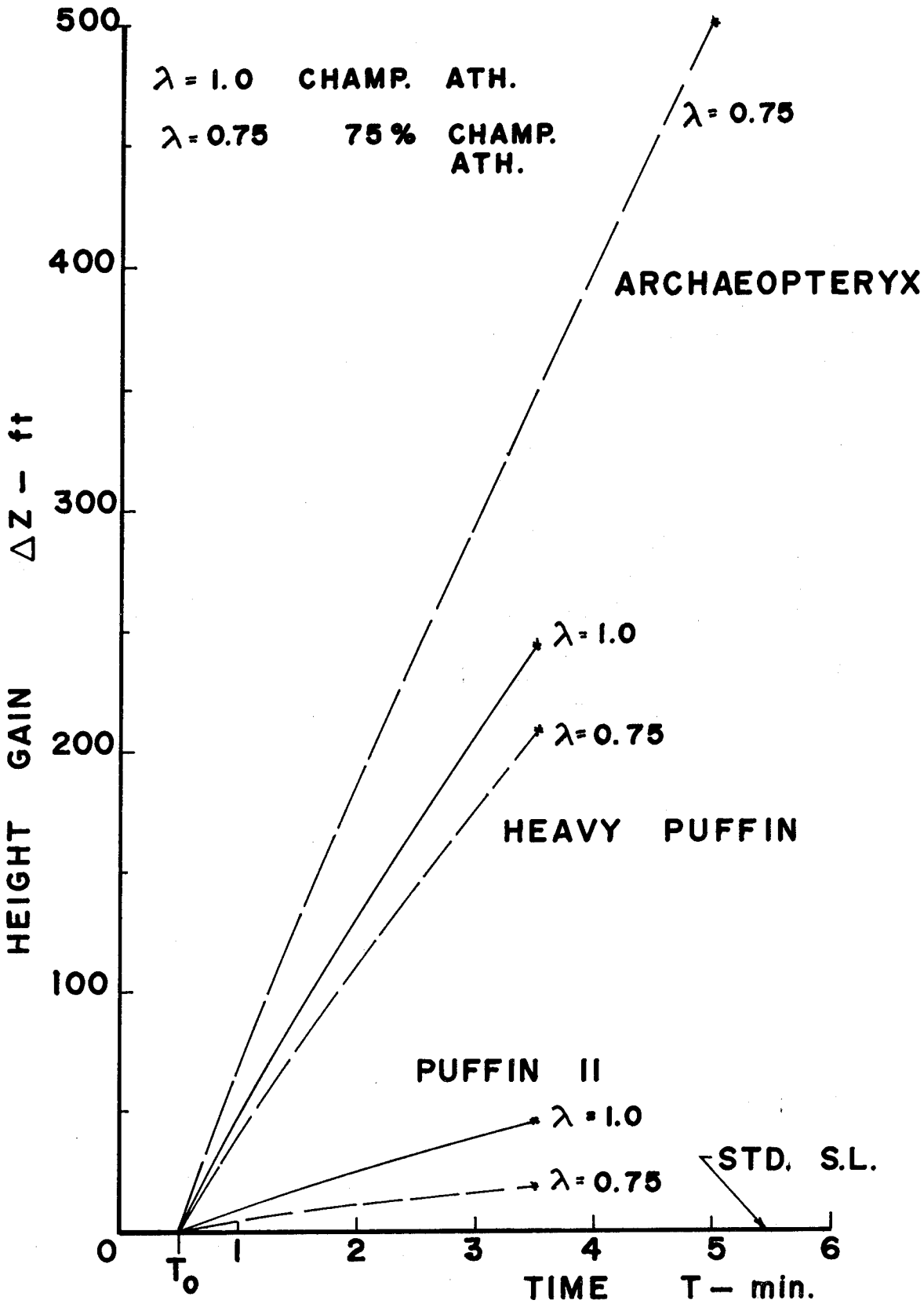


FIGURE 4. ESTIMATED CLIMB PERFORMANCE

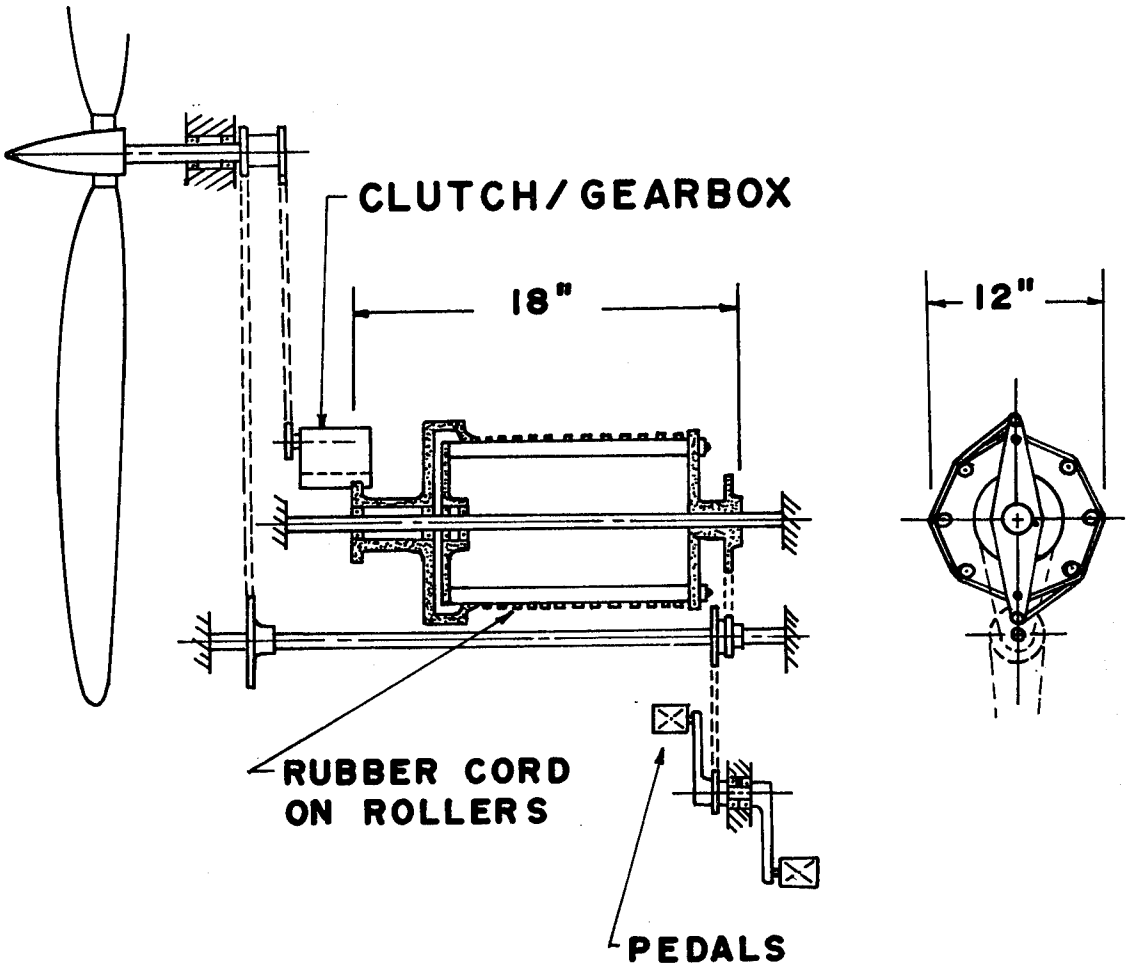


FIGURE 5. TYPICAL STORED ENERGY DEVICE

A proposed design

Before the whole matter of man-powered ultra-light sailplanes is rejected as ridiculous fantasy, consider again the performance polars in Figure 2. There is a substantial area between the "Puffin" (with or without stored energy) and the lowly 1-26. The only recent design that we know of which comes close to flying in this region is Farrar's remarkable low speed research sailplane [9]. One is thus lead to daydream about the possibility of constructing a 15-18 meter span, ultra-light "powered sailplane" with a wing loading of 1.5 to 2 lb/ft^2 and a minimum sink rate of perhaps 70 to 80 fpm. If fitted with two or three stored energy devices, such a machine could serve as a prototype for a true self-launching sailplane (as opposed to motor-glider). A proposed design for this sort of machine, called the "Archaeopteryx" (the first of a new kind of flying device) is shown in Figure 6. No serious attempt has been made to optimize this particular design, and its estimated characteristics were selected mainly on the basis that they result is a "reasonably sized" vehicle with the desired performance. The weights and dimensions of the "Archaeopteryx" are assumed to be:

Wing Span:	59 ft (18 m)
Wing Area:	200 ft^2 (18.6 m^2)
Aspect Ratio:	17.4
Empty Wt.:	225 lb (102 kg)
Flying Wt.:	375 lb (170 kg)
Wing Loading:	1.875 lb /ft^2 (9.15 kg/m^2)

The combination of low weight, wing-loading and speed necessary to minimize the power required by an "Archaeopteryx" type vehicle presents several major problems in both the design and operation of such a machine. The major operational problem is the difficulty of making low speed turns while thermaling. The nature of the problem is briefly described in Appendix B. It is shown in Appendix B and references 4, 5 and 10 that low speed turn problems increase with increasing wing span. This factor, together with the requirement that vehicle weight must be as small as possible and span loading must be as large as possible have a profound effect on the vehicle aerodynamic and structural configuration.

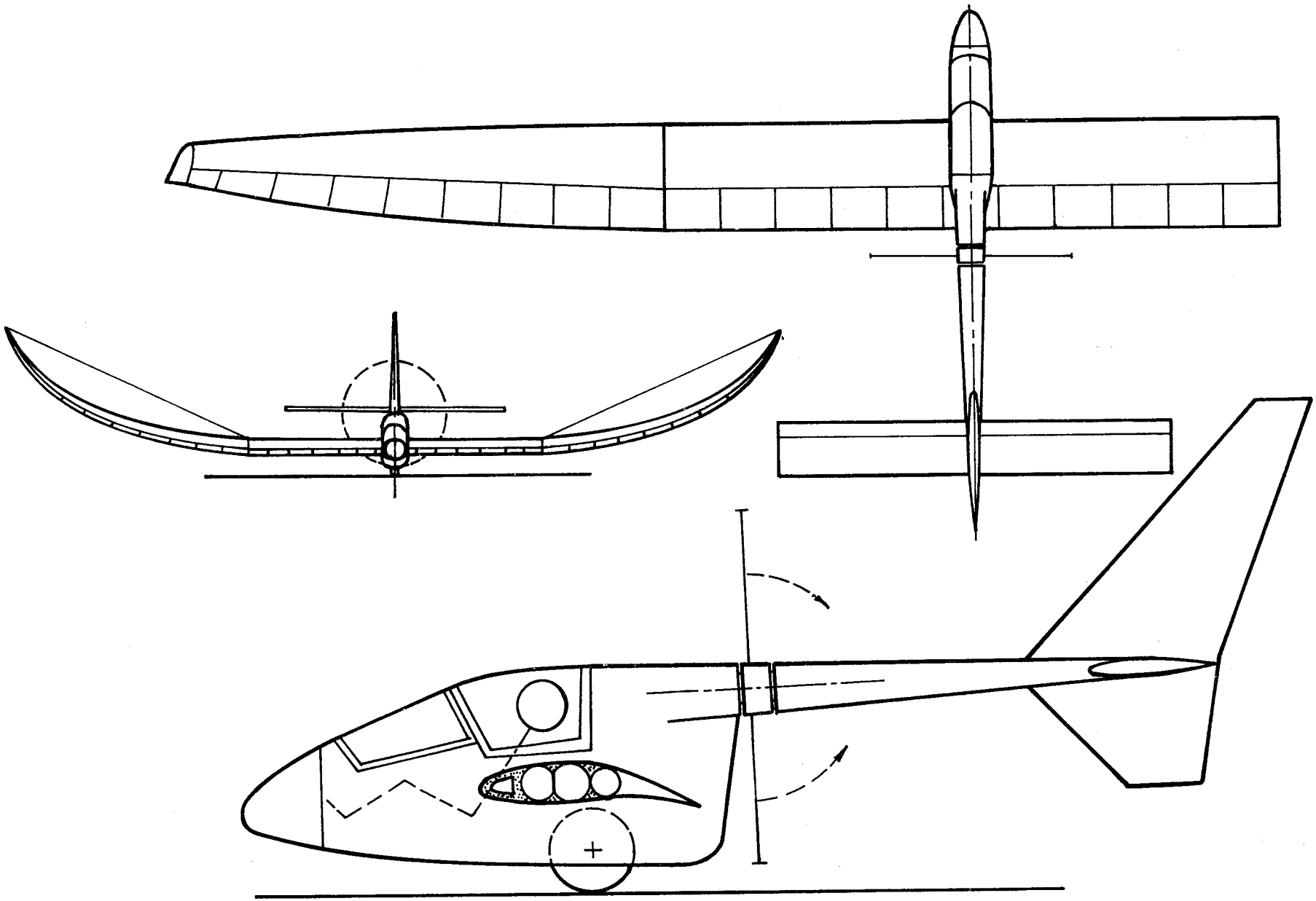


FIGURE 6. ARCHAEOPTERYX

Configuration Selection

Several features of the "Archaeopteryx" configuration require explanation. One of the most obvious peculiarities of the design is the propeller location.* Three main factors influenced the present choice: (1) a desire to keep the propeller slip stream from interfering with the wing's boundary layer, (2) a desire to keep the power transmission system as short and simple as possible to save weight, and (3) the necessity of providing ground clearance for the required large diameter propeller typical of current MPA practice. The propeller selected is 8 ft in diameter, and since this is considerably larger than conventional motor glider propellers, it was decided that the propeller should be folded while not in operation rather than simply stopped and feathered. The simple pod and boom fuselage layout lends itself particularly well to this set of propeller configuration requirements.

The major feature of the proposed design is the wing. Since span and wing weight must be minimized, but span loading (or effective aspect ratio) must be maximized it is proposed to employ a non-planar or span-wise cambered lifting surface for several reasons. Cone [11, 12] has shown that wings with large amounts of span-wise camber should have substantially lower values of induced drag than equal projected span and area flat (planar) wings. A brief discussion of this effect is given in Appendix C. A more complete account is given in Reference 13. Use of the non-planar wing offers the potential for several additionals design advances.

Several existing MPA designs have demonstrated the feasibility of constructing exceedingly large wings with adequate strength and torsional rigidity with extremely low weights using balsa, spruce and mylar. With the possible exception of column efficiency, many materials are superior to balsa and spruce. Specifically, modern fiberglass systems have superior strength/density characteristics. The major problem with the present glass systems is their generally low values of modulus of elasticity. Use of the non-planar wing offers the interesting possibility of capitalizing on, rather than fighting with, the flexibility of glass composite structures, thus producing even lighter weight structures. It is proposed that the wing spar of the "Archaeopteryx" be built up of two or three pressure-stabilized fiberglass tubes arranged chordwise. The tube system should be quite rigid in torsion, particularly if bound together, but relatively flexible in bending. The trick is then to design the tube system

*The authors were unaware of the German C-10 motor glider, circa 1940, when the present design was laid down.

such that it flexes to the correct span-wise cambered shape under airload. The remainder of the wing is to be formed from contoured and hollowed blocks of foam plastic. The whole arrange is then to be covered with a suitable material such as mylar. The major difficulty with this scheme is the problem of negative airloads which could conceivably bend the wing into an unstable configuration. It may therefore be necessary to somehow bind the wing into the correct shape with some sort of external bracing "wire". In place, this wire would resemble a bow-string.

The use of this external bracing leads one to a further interesting possibility--elimination of the need for ailerons for roll control. The use of conventional ailerons on an ultra-light weight wing such as the one proposed presents a real problem because of torsional loads they impose when deflected. Because the wing has been designed to be flexible in bending, it seems possible to let the bracing wires double as control cables. To make a turn, the pilot would (through a suitable leverage system) relax the tension on one cable and increase it on the other--thus creating a wing of un-symmetric planform and, consequently a rolling moment. A strip of boron or carbon filament tape, even at $300/lb, might be suitable for this purpose. The parasite drag penalty of such an arrangement should not be prohibitive and is at least partially off-set by the other problems it solves.

The remainder of the machine would be constructed along conventional man-powered aircraft lines--except that substantially higher load factors would be employed in the structural design. The only other area in which significant advances might be required or expected are in reductions in weight of the energy storage device(s) and increases in the efficiency of the "pedal drive system".

Estimated Performance

Estimated Powered and un-powered polars for the "Archaeopteryx" are shown in Figure 2. It is encouraging to note that a pilot producing only one-quarter horsepower can reduce the sink rate to about 60 fpm. This power level is about 75% of that which can be sustained for periods in excess of an hour by an average pilot in reasonably good physical condition--not necessarily a trained athlete. If the "Archaeopteryx" carries three of the previously described stored energy devices, each geared to produce 2 BHP for 1 1/2 minutes, the machine should be capable of reaching a height of 500 ft if all stored energy is expended during the climb.

A height gain of 500 ft is still not very much, and raises the question: How close to the ground is it possible to fly and still thermal effectively? Most contest pilots have witnessed (and perhaps themselves attempted) ther-

malling below 200 feet. Sometimes it is possible to hang on a few extra minutes by so doing, and once in a great while, to climb on up to cloud base for such a "save", an exhilerating experience indeed. But even those who have done so successfully don't seem inclined to recommend this to others. Flight instructors shudder at the thought of people trying to thermal below, say, pattern altitude of 600 feet. Some are more conservative, a few might set the limit for themselves a bit lower. This concern is rightly placed for conventional sailplanes: the low altitude stall or stall/spin accident continues to take its toll. The source of this problem is briefly discussed in Appendix B.

The key to the question of minimum soaring height seems to be how much time there is between the ship and the ground, rather than some arbitrary altitude figure. Can one recover from a stall and still have time to set up a safe landing? Is there sufficient wing-tip clearance of terrain and obstructions? If these two conditions can be met, it seems feasible to project genuine soaring performance for self-launched man-powered aircraft. This whole matter requires further detailed study.

Conclusions

While still far short of the dream of flying off into the sunrise without assistance from noxious engines, the stored-energy-device-augmented, "powered" ultra-light sailplane does occupy a legitimate place on the fringe of the growing ultra-light movement. The major problem in this line of development is the lack of knowledge on how to use modern materials intelligently to build really efficient ultra-low density aircraft structures with sufficient strength and stiffness. A few possibilities in this area have been indicated, but at present these are merely speculations. In addition, very little serious work has been done in developing really efficient, light-weight stored-energy devices of the type needed for this sort of vehicle. At something on the order of 5 lb /BHP-min installed, the wound-up rubber cord stored energy device is not really adequate.

While it is unlikely that self-launched, man-powered sailplanes will replace either conventional sailplanes or motor gliders, the new vistas opened up by such possibilities are exciting to consider. Perhaps the eventual performance potential of aircraft like the "Archaeopteryx" will encourage some serious hardware development work. At a minimum, this work would be extremely valuable in laying ground work for the coming Golden Age of self-launched soaring - made possible by the development of the solar-powered sailplane.

"... the machine does not isolate man from the great problems of nature but plunges him more deeply into them". (Antoine de Saint Exupèry, Wind, Sand, and Stars)

APPENDIX A: PERFORMANCE ESTIMATES

Power Required: The general formula for the power required by an aircraft executing a steady (constant speed) climbing or gliding turn has been derived in Ref. 6 as:

$$(A\text{-}1) \qquad BHP_{req} = \frac{W\dot{Z}}{550\eta} = \frac{WV\cos\theta}{550\eta(L/D)\cos\phi} \cdot \left[1 + (L/D)\cos\phi\tan\theta\right]$$

For aircraft with sufficiently high values of L/D (small θ) in rectilinear flight, eqn. (A-1) reduces to:

$$(A\text{-}2) \qquad BHP = \frac{WV}{550\eta(L/D)} \cdot \left[1 + (L/D)\theta\right]$$

$$\text{where} \qquad \theta \simeq \dot{Z}/V$$

Drag Estimation: The drag of the complete vehicle is given by (6):

$$(A\text{-}3) \qquad D = \frac{1}{2}\rho V^2 S\left[\frac{C_{D_\pi} S_\pi}{S} + C_{D_p}(R_n, C_L) + \frac{K_w C_L^2}{\pi AR} + C_{D_t}\right]$$

According to the discussion in Ref. 6, for aircraft of fixed weight and known geometry, eqn. (A-3) reduces to:

$$(A\text{-}4) \qquad D \simeq \frac{1}{2}\rho V^2 S\left[C_{D_o} + (K_o AR + K_w)\frac{C_L^2}{\pi AR}\right]$$

If the aircraft is operates in ground effect, simple theory (4,5) shows that the factor K_w in eqn. (A-4) must be treated as a function of the height (h) of the wing m.a.c. above the ground, for height-to-span ratios less than 1/2. Therefore, according to eqn. (A-2), the power required at small values of h is a function of h.

Climb Performance: The instantaneous rate of climb (or sink) can be calculated from:

$$(A\text{-}5) \qquad \dot{Z} = 550\eta \cdot \frac{BHP_{avail.} - BHP_{req.}}{W}$$

From Figure 3, we can approximate the power available as a function of duration of exercise (T) by:

$$(A\text{-}6) \qquad BHP_{avail.} = \lambda\left[\frac{24}{T} + 0.5\right] + BHP_{stored}$$

Where λ is a factor ($0 \leq \lambda \leq 1$) which accounts for less than "Champion athlete" power output.

With the Z given by eqn. (A-5), the total height gained (or lost) can be calculated by simple numerical integration of:

$$(A\text{-}7) \qquad \Delta Z = \int_{T_o}^{T} \dot{Z}\, dt$$

T_o is the time at Lift-off.

APPENDIX B: LOW-SPEED TURNING FLIGHT

Given an aircraft executing a constant altitude, constant speed coordinated turn, refering to Figure 7 we can derive:

(B-1) $$R = V_c^2/g \tan \phi$$ V_c = center-line speed

(B-2) $$V_t = \text{wing tip speed} = V_c \left[1 \pm \frac{b}{2R} \cos \phi\right]$$

or

(B-3) $$V_{t_i}/V_{t_o} = \frac{V_c^2 - \frac{b}{2} g \sin \phi}{V_c^2 + \frac{b}{2} g \sin \phi}$$

If the wing carries an elliptic lift distribution in the un-banked case ($\phi = 0$), then in a turn, the ratio of the un-trimmed lift per unit span (l) at any spanwise station y , to the section lift (l_o) at the center-line is:

(B-4) $$\frac{L(\xi)}{L_o} = (1 - \xi^2)^{1/2} \left[1 + \xi \left(\frac{b}{2R}\right) \cos\phi\right]^2$$

where $$\xi = \frac{y}{b/2}$$

From eqn. (B-4) it can be shown that in a turn, the un-trimmed center of lift shifts outboard by the amount :

(B-5) $$\xi_{c.p.} = + \frac{2\left(\frac{b}{2R}\right) \cos \phi}{4 + \left(\frac{b}{2R}\right)^2 \cos^2\phi}$$

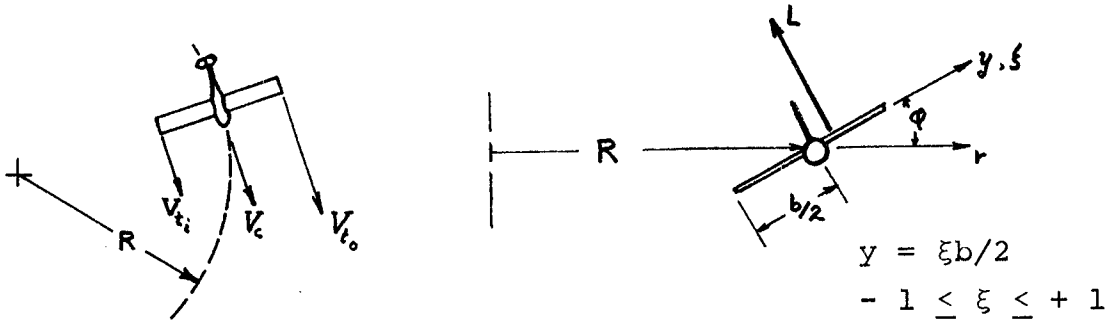


Figure 7. Turn Notation

The simple relations above indicate several important factors in the low speed turn problem:

1. The turn radius decreases rapidly with increasing bank angle and/or decreasing speed. R is independent of the wing span and the minimum value depends, in large part on the maximum wing lift coefficient through the relation (see Ref. 6)

$$(B\text{-}6) \qquad \phi_{max} = \sec^{-1}\left[\frac{1}{2}\rho\frac{V_c^2}{W/S}C_{L_{max}}\right]$$

2. The difference between the speeds of the inboard and outboard wing tips increases with increasing wing span and bank angle, and decreasing centerline speed (V_c). The importance of the wing tip speed ratio can be seen in the following relations for Reynolds number and dynamic pressure:

$$(B\text{-}7) \qquad R_{n_{t_{in}}} / R_{n_{t_{out}}} = V_{t_{in}} / V_{t_{out}} \quad \text{where} \quad R_{n_t} = V_t C_t/\nu$$

$$(B\text{-}8) \qquad q_{t_{in}} / q_{t_{out}} = V_{t_{in}}^2 / V_{t_{out}}^2 \quad \text{where} \quad q_t = \frac{1}{2}\rho V_t^2$$

It should be remembered that, in general, airfoil profile drag coefficients increase and maximum section lift coefficients decrease, with decreasing Reynolds number.

3. The turn induces an out-board shift (away from the turn center) of the center of lift. This shift is approximately proportional to cos ϕ and b and inversely proportional to V_c. This c.p. shift can result in large adverse rolling moments (moments which tend to increase the bank angle) which must somehow be trimmed - conventionally, by the use of ailerons or spoilers. The resulting non-optimum lift distribution results in a trim drag increment due to both induced drag and parasite drag from the aileron deflection. In addition, if the wing is already flying at a high value of lift coefficient, increasing the local lift coefficients in the region of the inboard tip where, as previously noted, the Rn is already diminished, leads to the danger of tip stall-and a spin. There are several ways to circumvent this problem at least partially, but the simplest is to merely limit the bank angle and, if possible, the wing span.

APPENDIX C: SPAN-WISE CAMBERED WINGS

C. D. Cone, Jr. [11,12] has performed an extensive analytical and electrical analog study of a wide variety of "non-planar" lifting surfaces. Many of Cone's results are remarkable, but even more remarkable is the fact that despite the very promising results obtained, very little experimental work has been done in efforts to translate theory into practice. Cone investigated a wide variety of complex camber forms. The discussion here will be limited to simple single-element circular and elliptic arc camber lines.

The usual practice in wing theory is to express the total drag coefficient in the form:

$$(C\text{-}1) \qquad C_{D_W} = C_{D_p} + C_{D_i} = C_{D_p}(R_n, C_L) + K_W C_L^2/\pi AR$$

where C_{D_p} = "profile" drag

C_{D_i} = "induced" drag

Cone's work is basically directed at ways to decrease the induced drag and is not directly concerned with viscosity effects. Refer to Figure 8 for the notation used in the following discussion.

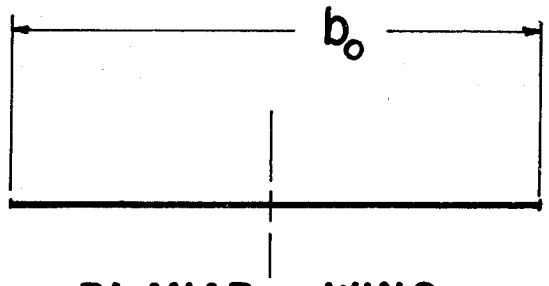
Let S_o be the area of the planar wing or the area of the cambered wing <u>projected</u> onto a horizontal surface. Then

$$(C\text{-}2) \qquad AR = \frac{b^2}{S_o} \rightarrow AR_o = \frac{b_o^2}{S_o} = \frac{\Psi^2 b_\beta^2}{S_o} = \Psi^2 AR_\beta$$

The <u>effective</u> aspect ratio is defined by

$$(C\text{-}3) \qquad AR_e = AR/K_W = AR\ e_W$$

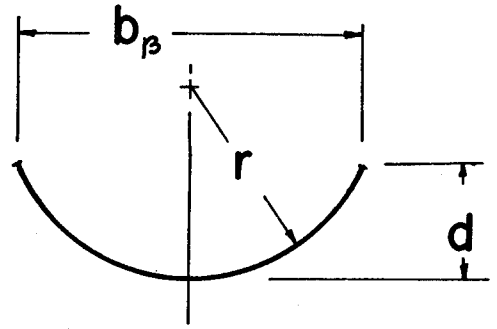
It is well known that for <u>planar wings</u>, the maximum value of e_W is 1.00; this value occurring when the wing carries an <u>elliptic lift distribution</u>. The remarkable thing about Cone's analysis is that it shows that values of e_W substantially in excess of unity can be achieved by optimally loaded, span-wise cambered wings. The usual explanation for this effect is that the "bent up (or down)" wing tip acts as a tip plate. The smooth continuous



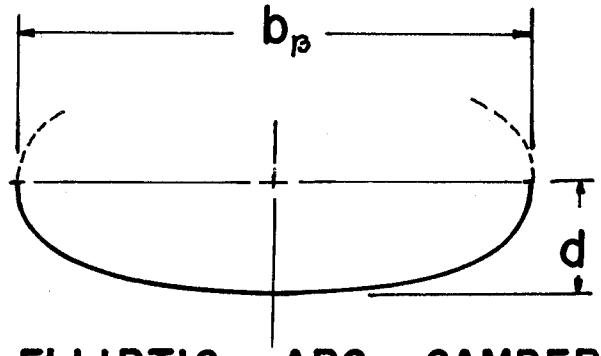
PLANAR WING

β = CAMBER INDEX
= $d / \frac{b_\beta}{2}$

ψ = SPAN RATIO
= b_o / b_β



CIRCULAR ARC CAMBER



ELLIPTIC ARC CAMBER

FRONT VIEWS

FIGURE 8. CAMBERED-SPAN WING NOTATION

camber distribution is, however more efficient in inhibiting the formulation of a strong wing tip vortex than the usual simple "Zulu shield" arrangement customarily used for this purpose. An additional significant factor is is that the smooth contour of the cambered wing should result also in much lower values of parasite drag than those which arise at the juncture of a wing and conventional tip plate. This latter effect partially accounts for the poor performance of conventional unfaired tip plates in practice - parasite drag increase eats up part of the improvement in induced drag.

The results of Cone's analysis for single element circular and elliptic arc wings are shown in Figure 9. Of course, this improvement in induced drag is not entirely free. The penalties are:

1. The cambered wing is longer (for the same projected span) than the planar wing. Realistically wing weight must increase with length rather than projected span. Figure 10 shows the relation between length and projected span for the circular and elliptic are wings. Note that for the β=1.0 circular are wing, the length of the wing is 1.57 times its projected span.

2. For a planar wing, the wetted area is roughly twice the projected area. For the cambered wing this value may be much larger. Skin friction drag depends on wetted area.

The increase in effective aspect ratio may appear magical until one considers the following results:

The geometric aspect ratios of several non-planar wings are calculated from their values of projected span and area. (S_o & b_β). Now suppose we took these wings and "unfolded" them onto a flat surface. The actual spans and areas would be ℓ and S'. Assume the value of K_w for the flattened wing is 1.0. Call the effective aspect ratio of the flattened wing AR'_{e_o} . [Note: S' > S_o]

We then have:

$$\frac{b_\beta}{\ell}\frac{K_{w_o}}{K_{w_\beta}} = \frac{AR_{e_\beta}}{AR'_{e_o}} \qquad \text{(C-4)}$$

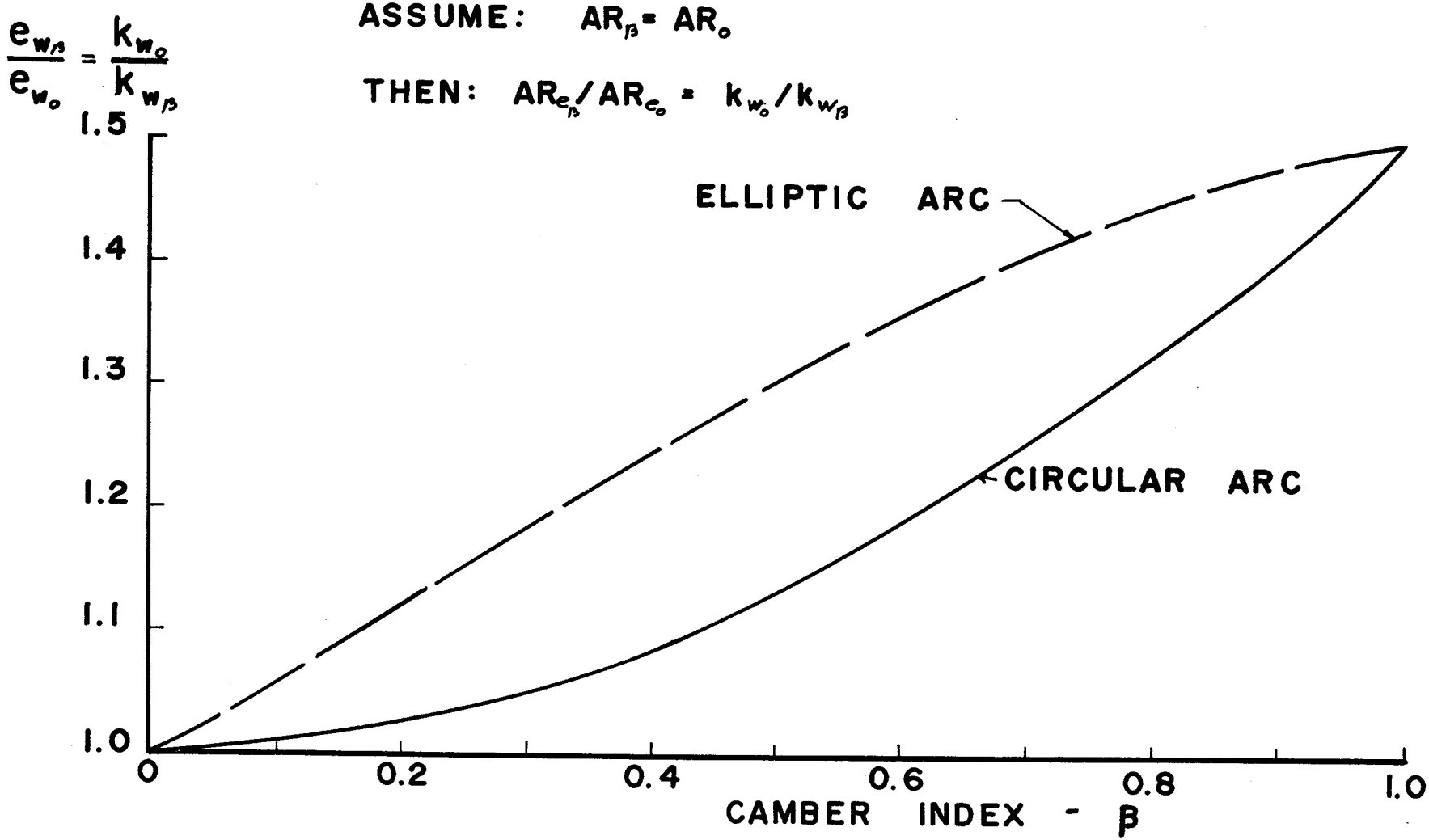


FIGURE 9. COMPARISON OF THE EFFECTIVE ASPECT RATIOS OF CAMBERED SPAN WINGS

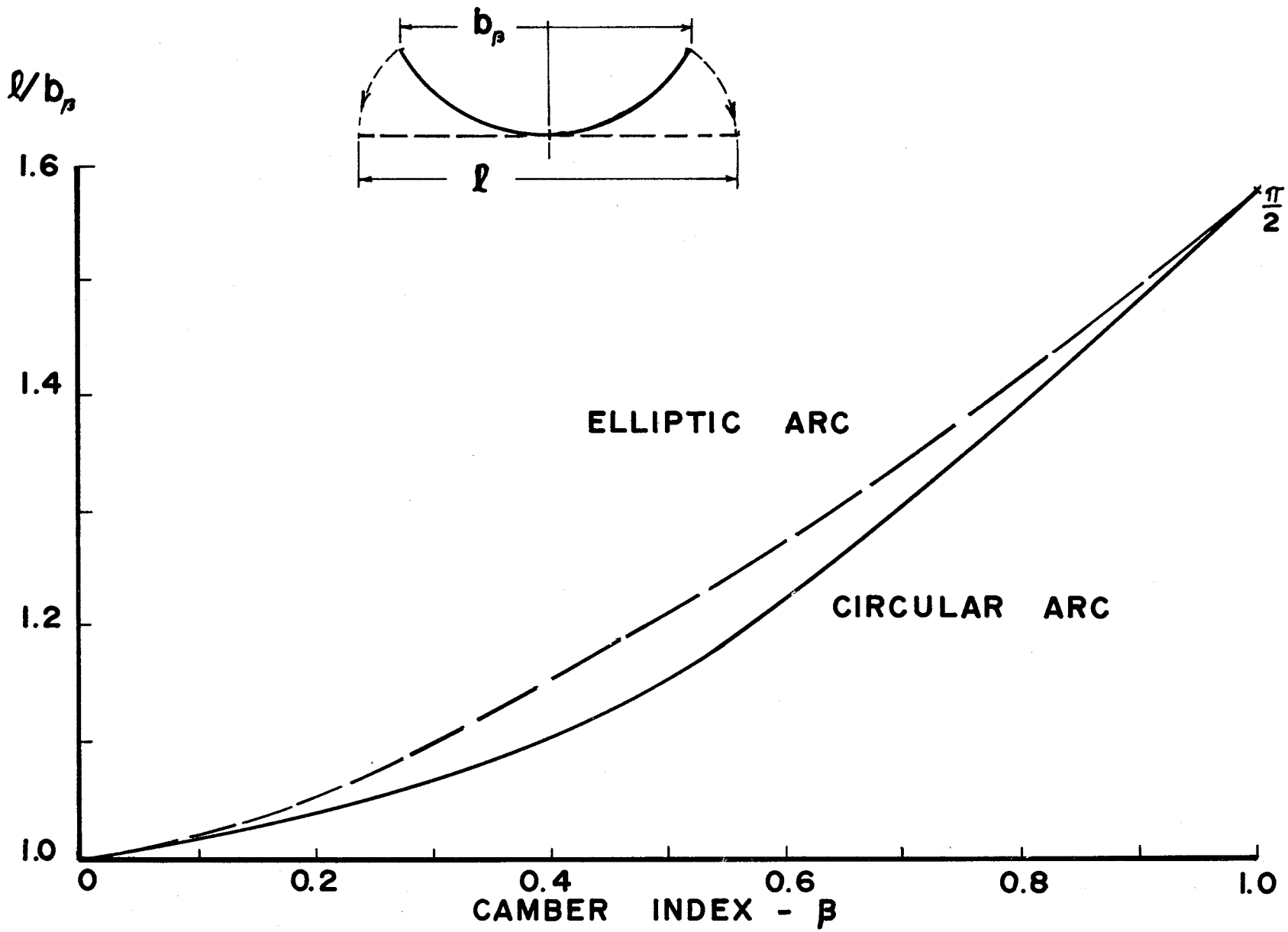


FIGURE 10. RATIO OF CAMBERED-SPAN WING LENGTH TO PROJECTED SPAN

In this case, using Fig. 9 and 10:

	Circular Arc	Elliptic Arc
$\beta = 0.5$	$AR_{e_\beta}/AR'_{e_o} = 0.98$	$AR_{e_\beta}/AR'_{e_o} = 1.07$
$\beta = 0.8$	0.95	1.02
$\beta = 1.0$	0.95	0.95

A much more complete discussion of these results can be found in Ref. 13.

References

1. Cole, C. J. and McMasters, J. H.; Man-Powered Flight - A Review and Status Report , Soaring, February 1972, pp. 18-27.

2. McMasters, J. H.; Cole, C. J. and Skinner, D. A.; Man-Powered Flight , AIAA Student Journal, April 1971. Reprinted in Low and Slow #13.

3. Sherwin, K., Man-Powered Flight, Model and Allied Publications Ltd., Hemel, Hempstead, Herts., U.K., 1971.

4. McMasters, J. H., and Cole, C. J.; The Prospects for Man-Powered Flight , Technical Soaring, Vol. I, No. 2, October 1971, pp. 1-16.

5. McMasters, J. H.; The Optimization of Man-Powered Aircraft , AIAA Pre-print No. 71-798, July 1971. To be published Jour. of Aircraft.

6. McMasters, J. H.; An Introduction to Geometric Programming and Its Application to Sailplane Design, Proceedings of the First International Symposium on the Technology and Science of Motorless Flight, M.I.T., Cambridge, Mass., October 1972, pp 119-146.

7. Bikle, P.; Polars of Eight , Soaring, June 1970.

8. Nonweiler, T. R. F.; The Man-Powered Aircraft - A Design Study , Jour. R. Ae. S., Vol. 62, October 1958, pp. 723-734.

9. Farrar, D. F., Jr.; A Low Speed Sailplane for Research , Tech. Soaring, Vol. 1, No. 2, October 1971, pp. 25-28.

10. Cone, C. D. Jr.; The Design of Sailplanes for Optimum Thermal Soaring Performance", NASA, TN D-2052, January 1964.

11. Cone, C. D. Jr.; The Theory of Induced Lift and Minimum Induced Drag of Nonplanar Lifting Systems , NASA TR-R-139, 1962.

12. Cone, C. D. Jr.; The Aerodynamic Design of Wings with Cambered Span Having Minimum Induced Drag , NASA TR-R-152, 1963.

13. McMasters, J. H.; Some Comments on the Aerodynamic Design of Large Soaring Birds, Ultra-Light Sailplanes, and Man-Powered Aircraft , Unpublished letter to the Editor of Soaring, August 1972. Copies available from the author.

FOOT-LAUNCHED GLIDING

by

Michael A. Markowski
Man-Flight Systems Engineering
Marlboro, Mass.

Notation

AR	aspect ratio, b^2/S
b	wing span, feet
c	wing chord, feet
C_L	aircraft coefficient of lift
L	lift, pounds
p	density of air at standard sea level, slugs/ft^3
Rn	Reynolds number
S	wing area, square feet
W	gross weight

Introduction

It is the intent of this paper to provide an introduction to the new sport of "foot-launched gliding", pointing out its basic problems, potentials and practicality. Hopefully, the motorless aeronautical world will rally to the cause of reviewing this mode of flight, seldom practised since the days of Lilienthal.

Even though Lilienthal was an expert, he nonetheless relied solely upon body movements, or center of gravity changes, to control his craft, thus incurring limitations on his flight envelope. It has been claimed that weight shifting is dangerous, and rightly so, for changes in center of gravity provide controlling moments that are constant, no matter what the relative speed of the craft through the air. This is, of course, a great disadvantage for one who wishes to operate at higher altitudes, greater airspeeds, or in more turbulent conditions, for the disturbing influences increase as the square of the velocity of the relative wind. The way we meet this situation is commonly done by employing conventional aerodynamic controls. Now, this is all well and good, but it leads to complexity. However, all is not lost for those who decide to control their flight by "throwing their weight around" a bit. As long as the weight shifters keep in mind that they should only fly close to the ground (no higher than they are prepared to fall), and operate in winds not exceeding approximately 15 mph, they can learn a great deal about basic flight from simple machines.

As with all self-launched aircraft, the problem of most concern is that of obtaining a good compromise between the ground and air modes of operation. With the conventional hang glider there is a sufficiently large enough overlap in the two modes to permit even a rather crude machine to obtain airborne status. Ultimately, however, the overlap has got to be small, for our main purpose is to remain airborne and in the ground mode as little as possible. Therefore, our only recourse is to strive for the maximum aerodynamic efficiency possible consistent with the lightest practical structure. Let us illustrate:

In the ground mode, our would-be aeronaut needs a machine with as light a frame as possible with small moments of inertia to facilitate his handling of the craft in transport to a site and in performing his run to take-off speed. Our intrepid bird-man would also like a craft that is not easily upset in a light breeze, thus he would also like his machine to be as compact as possible. However, if he expects to fly, his glider must possess an appropriate surface area consistent with the gross weight of his body and the machine. In fact, it would be nice to have as large a wing area as possible so that he can launch himself into the air with a minimum of airspeed. A compromise is clearly indicated.

As a first pass, let us consider an average man and his ability to run. If I can recall, the average high school kid could run a hundred yard dash in around 14 seconds, or at 14.6 mph. Add to this the fact that he will be running downhill, partially supported by his flying machine it is reasonable to assume that he can attain a speed of 20 mph. This, of course, is a ground speed calculation and assumes no benefit from an up-hill breeze, which would make an airspeed of 20 mph all the easier to obtain.

Assume further, that our man weighs 165 pounds clothed and ready for flight and that his airframe weighs 35 pounds with all fittings. This will hopefully put us in the ballpark and allow us to begin our proposed design. Using the above numbers as a starting point, we can calculate the following basic factors:

$$\text{For level flight we have, } W = L = (1/2)\rho V^2 S C_L \qquad (1)$$

Thus we can solve for the quantity, SC_L:

$$SC_L = 2W/\rho V^2 = 400/(2.378 \times 10^{-3})(29.3)^2 \qquad (2)$$
$$= 196$$

Now we can solve for the required wing area for flight:

$$S = 196/C_L \qquad (3)$$

From this simple exercise, we can easily see that if $C_L = 1$ (which is a reasonable assumption), we would need 196 square feet of wing area to maintain flight at a 200 pound

gross weight at 20 mph. These numbers do indeed sound very feasible, but how do we arrange those 196 square feet? Let us try a couple of examples.

First off, considering that a C_L of 1 is attainable, we will assume that our wing has an aspect ratio of 6. This is as good a place as any to begin with and we can expect a reasonably efficient wing.

$$\text{Since } AR = b^2/S \tag{4}$$

we can calculate, $b = \sqrt{(AR)S} = 34.3$ feet of wing span, with a chord, $c = 5.71$ feet for a rectangular planform. This, at first, does not seem too bad. But 34.3 feet? It might be difficult to handle. Suppose we try a wing with an aspect ratio of 3:

Calculating, as before, we obtain the following:

$b = 24.2$ feet,

$c = 8.07$ feet.

Let us assume further, that we chose a highly tapered planform for our second wing. Why not a delta configuration? Assuming a leading edge sweep of 40 degrees, we find that by using leading edge spars of 17.45 feet and a keel of equal length, we have required surface area. The average chord is now 8.725 feet, the span 22.5 feet, and the aspect ratio around 3. This sounds more compact than our first attempt, but what about that aspect of ratio 3? It sounds awfully inefficient. Let us compare:

If we examine the aerodynamics of the situation, we realize the following: the Reynolds number of the AR = 6 wing is about 1 million, while the delta wing has a Reynolds number of 1.75 million. This is a particularly significant increase, and the gains will in some degree offset the loss in span efficiency of the delta, but some mathematical optimization and an experience factor will be necessary before we can determine just how this compromise can be most effective. The weight savings and smaller size of the lower aspect ratio machine indeed make it an alternative of more than just passing interest. But what can we expect in the way of stability?

The problem here is not as critical as might at first be anticipated. By using a highly tapered delta wing, a Rogallo type for instance, with its consequently long root chord, and an underslung position for the pilot, we find that we can achieve a reasonable degree of stability with a minimum of effort. The low center of gravity position is of prime importance, as it gives us a sort of "pendulum stability". Aside from this fact, the sweep angle and the addition of an "apex cover" (a taut sail located at the apex of the wing, on the underside), gives us a wing with inherent stability with quite reasonable flight characteristics.

As a final consideration, we have skill. As with all athletic sports, and hang-gliding can indeed be considered as such, some degree of skill is going to be required of the pilot. Even with the best equipment, a sufficiently graded slope, and the proper relative wind in his face, a certain amount of skill must be demonstrated in order that our bird-man may take-off and fly. It is not hard to think of several ways in which an attempted flight might fail. At any rate, a successful flight might be considered as one of the following:

Case 1. Here, insufficient airspeed, or inadequate efficiency would prevent true flight from occurring. In this instance, the man-wing is no more than a projectile, with stability arising purely from the inertial forces generated in the trajectory.

Case 2. A condition where the required relative airspeed is attained and maintained in a stable flight path consisting of a ground skimming take-off where the airspeed is increased to the point where the glide ratio is optimized, followed by a gradual sink and increase in angle of attack as the ground is approached.

Case 3. This would be a combination of cases 1 and 2. In this instance, the pilot would have sufficient airspeed for a good take-off only to stall in flight and end his flight prematurely in a semi-controlled, mushy crash landing. This would probably be common until our man-bird gained sufficient skill and "feel" for case two.

As a final analysis then, it would appear that due to a somewhat small speed margin, the success of a flight would depend upon the skill and self-confidence of the operator. It appears that he must not only learn the limitations of his craft, but he must also master its particular requirements, no matter what its degree of efficiency may be.

Aside from this, it would seem that the idea of foot-launched gliding is ready to be developed and used as a sport that can be enjoyed by all. At long last, mankind's age-old dream of flying like a bird is at hand. This concept, as no other in aviation, can bring flying to the masses. It certainly deserves a chance.

Session Chairman's Opening Address

STATE OF THE ART REVIEW - PERFORMANCE TESTING

by

William M. Foley
United Aircraft Research Labs.
E. Hartford, Conn.

Good afternoon ladies and gentlemen. Welcome to the Performance Testing session. Several recent articles have been written about performance testing [e.g., see Refs. 1-3]. Consequently, I don't expect to take up my allotted time summarizing the state of the art. Instead, I will only give a very short overview and will then use some of the additional time at the end of this session to report on a recent test program in which I have been involved and which may be of greater interest than repetition of readily available material.

By the time of World War I, rudimentary performance testing techniques were developed for airplanes. Immediately after the war, the techniques were rapidly refined. The major impetus for this work was from the military to ensure that contracted-for performance was met in new aircraft. Later, similar techniques were applied to commercial airplanes to ensure that they met specified performance goals. The NACA in this country was a major contributor in this work. All of the emphasis was on airplane performance testing with no attention being given to sailplane testing. In fact, most of the test techniques developed at this time period were not directly applicable to sailplane performance testing. However, many of the special instruments and the techniques for instrument calibration which were worked out were directly applicable to sailplanes and were, consequently, applied in succeeding years. In the late 1930's, performance testing procedures specifically for sailplanes were developed in Germany. Professor Zacher, who is with us here today, was one of the individuals who was involved in this development. After World War II, Professor Zacher and his collaborators continued making performance measurements in Germany [see Refs. 4 and 5]. In this same time period, Dr. August Raspet of Mississippi State College introduced systematic sailplane performance testing techniques into this country [Ref. 6]. The procedures which he used were based on the earlier German work and continue to be used even today in this country (and in most other countries, for that matter).

Before we discuss techniques of performance testing, it is probably appropriate to consider why we need to make performance measurements. Most of you have undoubtedly constructed MacCready ring scales from sailplane polars and used them to optimize your cross-country speed. Thus, we need to know the performance of a sailplane in order to fly it properly. More important, however, performance testing can serve as a tool during the development process. The group at Mississippi State demonstrated how useful testing could be in improving the performance of the RJ-5 (see Ref. 7 and Fig. 1, which is reproduced from that Ref.) and other sailplanes. I understand that considerable testing has also been done by Slingsbys during development of the Kestrel. Quite honestly, I don't understand why performance testing is not used more by present manufacturers in the development of their aircraft.

A number of methods has been considered for making performance measurements. One method is to measure the rate of deceleration of the aircraft while it is flown at constant altitude. Another is to tow the aircraft at various speeds and directly measure the drag by use of a load cell in the tow line. Rate of sink testing in which the sailplane is flown at constant air speed for a sufficiently long period of time to measure its rate of sink is by far the most common method used today. This method requires a very still, stable air mass and consequently is restricted to very few days of the year. A related technique which is not quite so dependent upon weather is to make a number of comparison glides at several air speeds with an already calibrated sailplane and measure the relative performance. Both Professor Zacher and Paul Bikle [Ref. 8] have used this comparison glide method quite effectively. The test techniques which are employed today have changed little since the 1930's. Improved instrumentation -- which can make the job either easier, faster, or both -- is getting the major attention at the present time, and it is in this area that we will hear the most recent results today.

The instrumentation for performance measurements does not need to be elaborate. Basically, it consists primarily of the basic sailplane instruments, properly calibrated, plus a stop-watch. Special equipment is required, however, to perform the calibration of the airspeed measuring system. A Kiel probe is temporarily installed on the sailplane to obtain the true total pressure (see Fig. 2). This is then compared with the sailplane pitot pressure to obtain pitot source error. A trailing static source is also required to calibrate the sailplane's static pressure sensing system. The most conventional system is a trailing bomb -- so called because of its shape (see Fig. 3) -- which is towed on a long tube away from the influence of the sailplane. More recently the towed cone (Fig. 4) has been used and has the advantage that it can be deployed before take-off, rather than during the flight as is done with the trailing bomb. The static pressure measured from one of these towed static

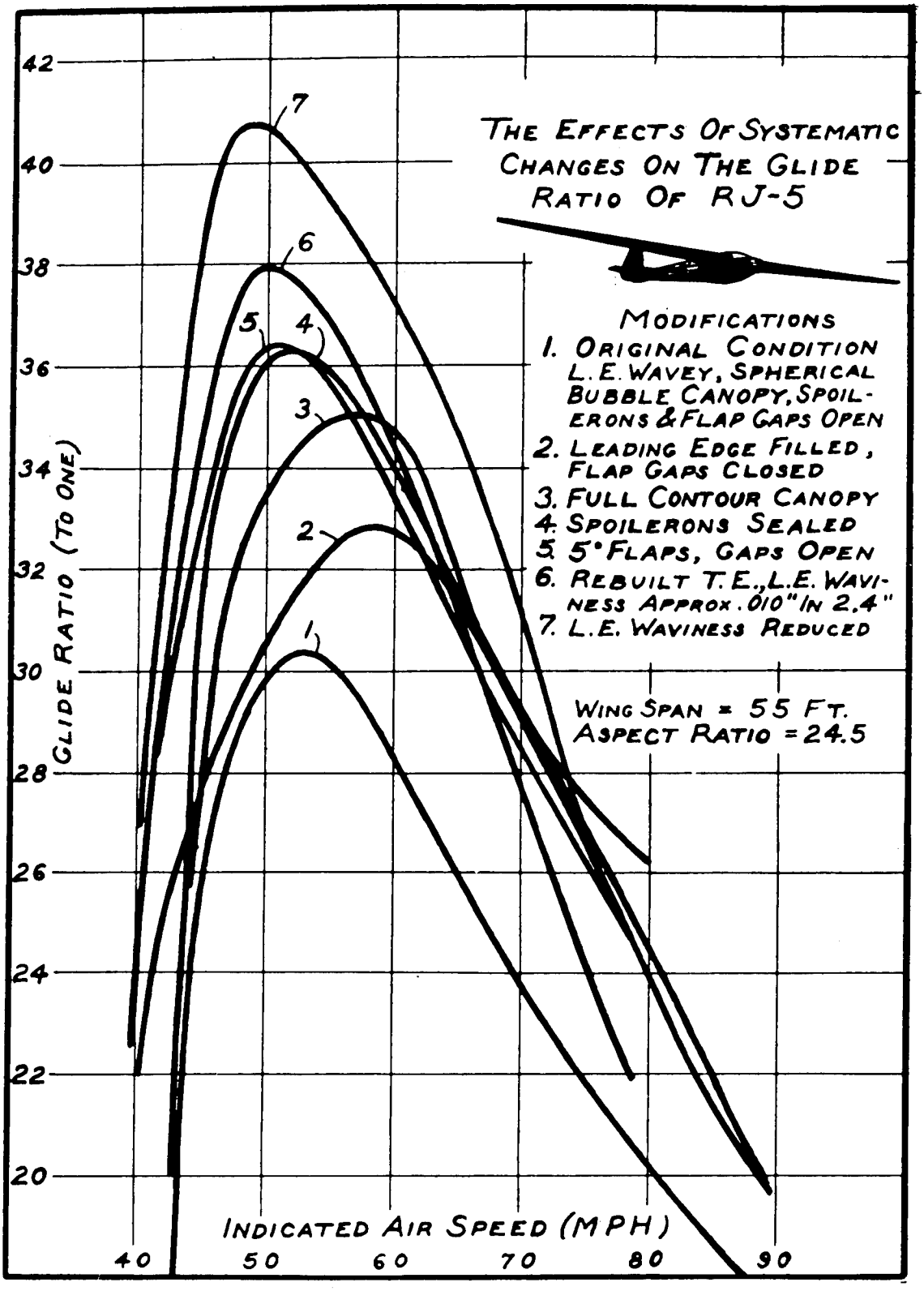

THE EFFECTS OF SYSTEMATIC CHANGES ON THE GLIDE RATIO OF RJ-5
MODIFICATIONS
1. ORIGINAL CONDITION L.E. WAVEY, SPHERICAL BUBBLE CANOPY, SPOILERONS & FLAP GAPS OPEN
2. LEADING EDGE FILLED, FLAP GAPS CLOSED
3. FULL CONTOUR CANOPY
4. SPOILERONS SEALED
5. 5° FLAPS, GAPS OPEN
6. REBUILT T.E., L.E. WAVINESS APPROX. .010" IN 2.4"
7. L.E. WAVINESS REDUCED
WING SPAN = 55 FT.
ASPECT RATIO = 24.5
GLIDE RATIO (TO ONE)
INDICATED AIR SPEED (MPH)
42
40
38
36
34
32
30
28
26
24
22
20
40
50
60
70
80
90
1
2
3
4
5
6
7

Figure 1.

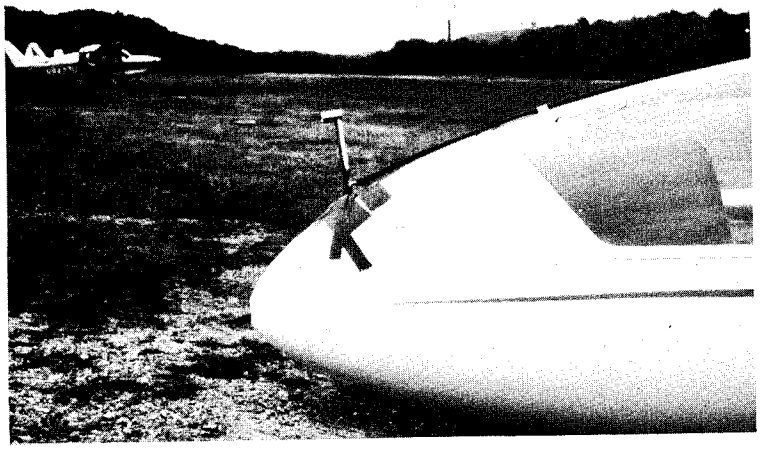


Figure 2.

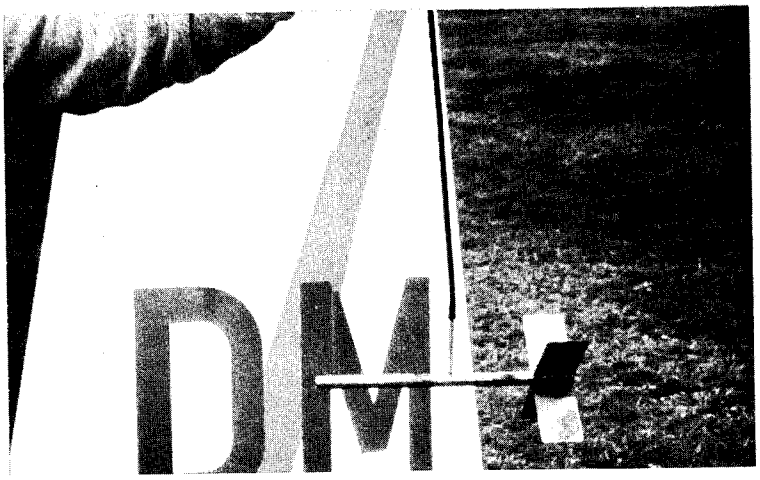


Figure 3.

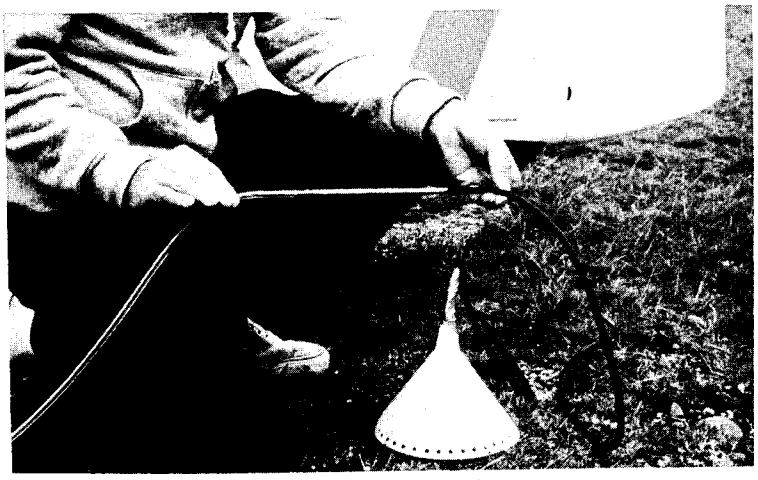


Figure 4.

sources is then compared with the pressure sensed with sailplane static pressure source to obtain static source correction. Calibrations of the pitot and static sources and direct calibration of the instrument permit the true indicated airspeed to be determined from measurements read from the sailplane airspeed indicator.

To measure accurately the rate of sink at a given airspeed, an altimeter which has been appropriately calibrated is required and also a good stop-watch. Performance measurements are then made by holding constant airspeeds for periods of time exceeding two or three minutes and measuring the altitude change and the time lapse. From these measurements the rate of sink at a given airspeed is determined. More information on this subject is given in Refs. 1 and 3.

There are perhaps eight or nine groups making performance measurements. These groups are located in Germany, England, Poland, and the USA. Today you will have an opportunity to hear of some of the work which is being done in Germany, England, and the USA.

References

1. Johnson, R.; Sailplane Flight Performance Measurement, Soaring, April 1968.

2. Bikle, P.; Gear Up, Sun Up. Soaring, July 1970.

3. Bikle, P.; Sailplane Performance Measured in Flight. Technical Soaring, Vol. 1, No. 3, January 1972.

4. Zacher, H.; Flugeigenschaftuntersuchungen an 14 Segelflugzeugen, Bericht Nr. 40 der Flugwissenschaftlichen Forschungsanstalt E.V., Munich, December 1960.

5. Zacher, H.; Flugmessungen mit Segelflugzeugen von 12-13 m Spannweite, Aero Revue, October 1966.

6. Raspet, A.; Sailplane Performance Evaluation, Soaring, May-June 1947.

7. Raspet, A.; Systematic Improvement of the Drag Polar of the Sailplane RJ-5, Soaring, September-October 1951.

8. Bikle, P.; Polars of Eight 1971, Soaring, June 1971.

RECENT STANDARD CIRRUS PERFORMANCE MEASUREMENTS

by

William M. Foley
United Aircraft Research Labs
E. Hartford, Conn.

Recently, several members of the New England Soaring Association have been developing the capability for making performance measurements of sailplanes. To date, they have gained a significant body of data on the performance of a Standard Cirrus, which is destined to be the standard sailplane for performance comparison, and a Blanik L-13. Test flying during the Summer and Fall of 1972 has been seriously restricted because of the particularly bad weather in New England during that time period. Had it not been for this, a substantially greater body of data would be available. Particular credit for the work which has been accomplished is due Mr. Frank Martin, Jr., who built all of the special instruments and assisted in flight tests, and Dr. Douglas East, who also assisted in the flight tests. Mr. Stephen Grady, who did all of the towing during these tests, should also be acknowledged. This report is only a progress report since the work is still ongoing.

At the time Bikle published his flight test results on a Standard Cirrus sailplane [Ref. 1], an aircraft with current production static ports was not available. The aircraft employed in the present test has the standard arrangement -- a set of static ports forward of the canopy and another set below the wings on each side of the fuselage. Calibration curves for the forward and aft statics determined by use of a Kiel probe and a towed cone static source identical with that used by Bikle are shown in Figs. 1 and 2. Note that both static sources give nearly correct airspeed indication at thermaling and approach speeds but yield very optimistic results at high speeds. Stall speeds agree with those of Bikle within one-half mile per hour when the results are corrected for differences in flight weight.

The measured polar curve for the Standard Cirrus is shown in Fig. 3. All data points were obtained in calm, early morning air before convection started with glides of at least 1000 feet or five minutes, whichever was longer. The measurements were made on four different days -- numbers on the data points indicate flight number to illustrate repeatability of the results. The aircraft was in the condition received from the factory with the exception that the canopy had been sealed and an Althaus compensator had been installed. As can be seen, the tests repeat Bikle's result corrected for weight

STANDARD CIRRUS AIRSPEED CORRECTIONS - AFT STATIC

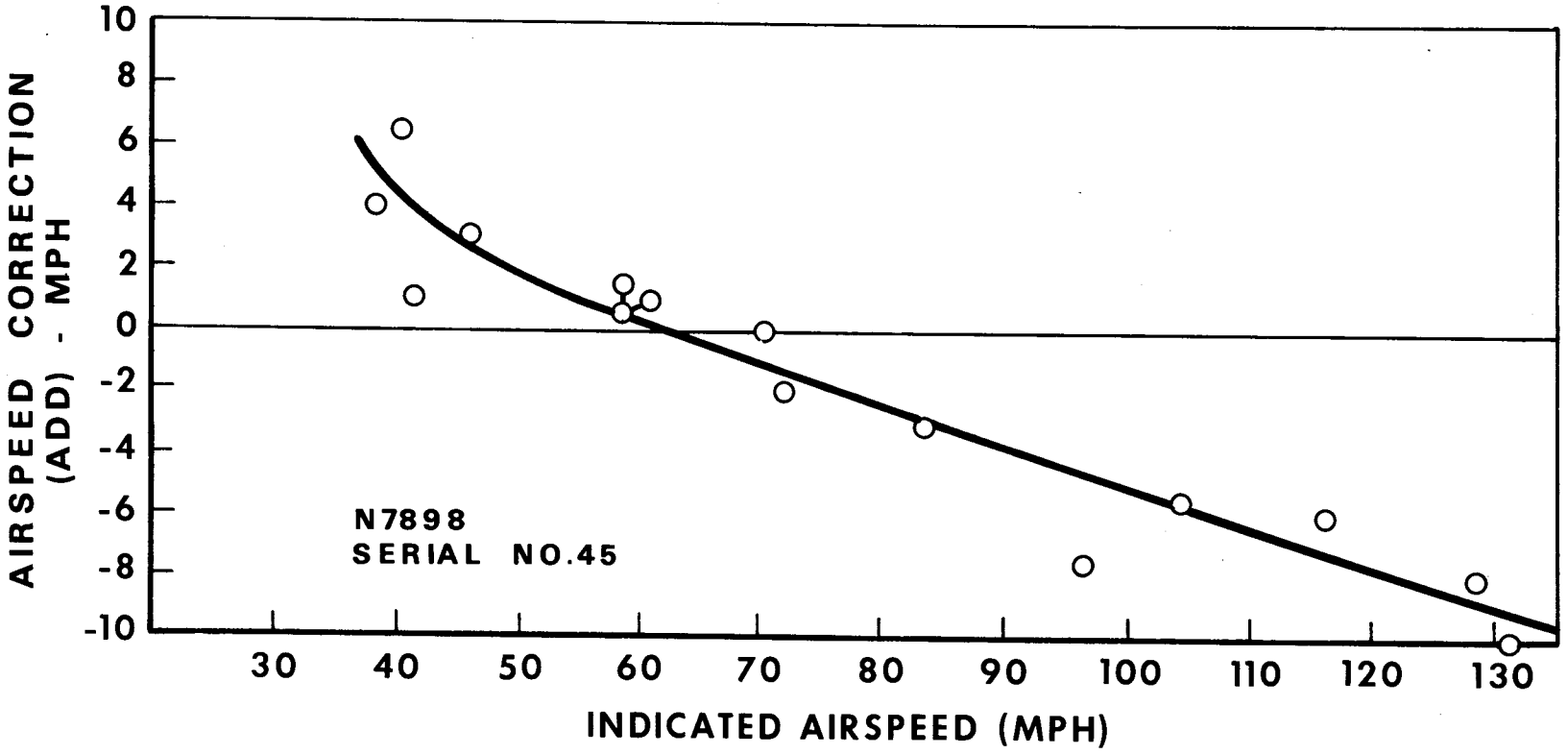


Figure 1.

STANDARD CIRRUS AIRSPEED CORRECTIONS - FWD STATIC PORTS

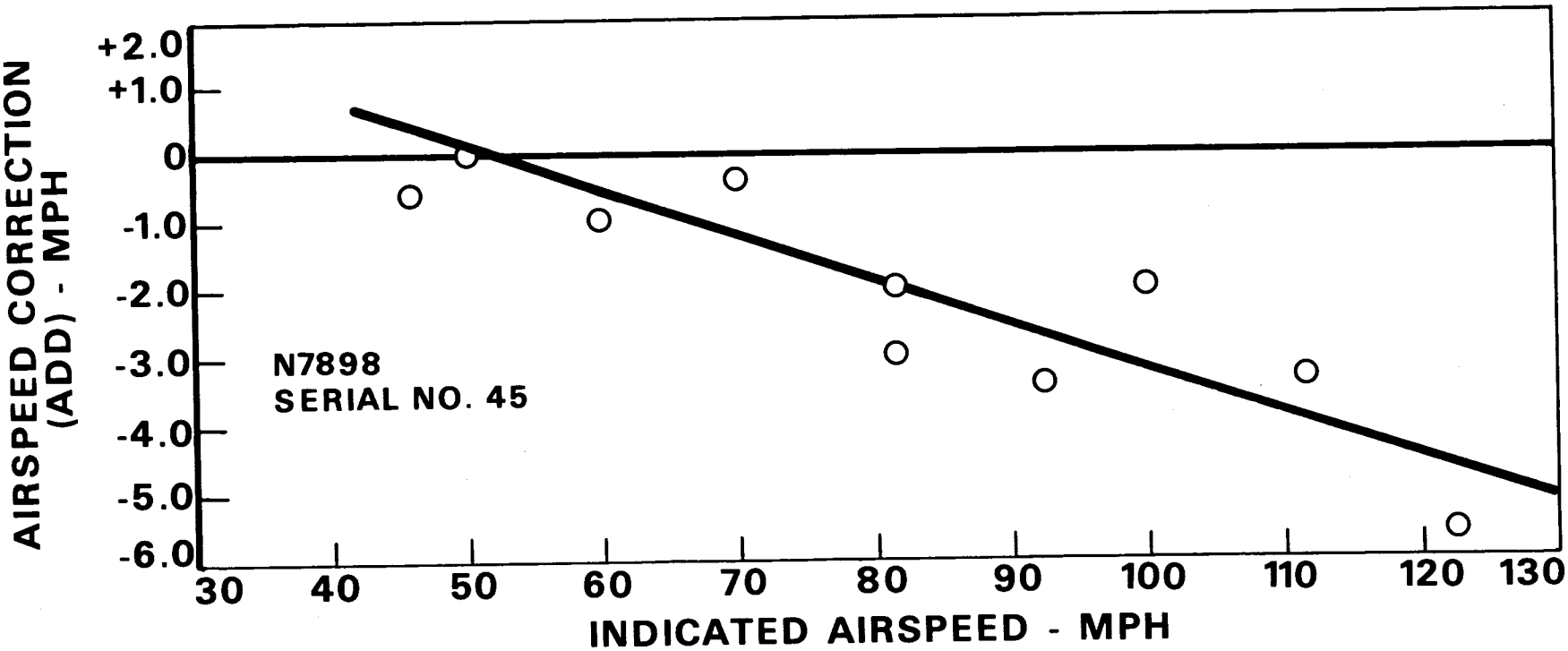


Figure 2.

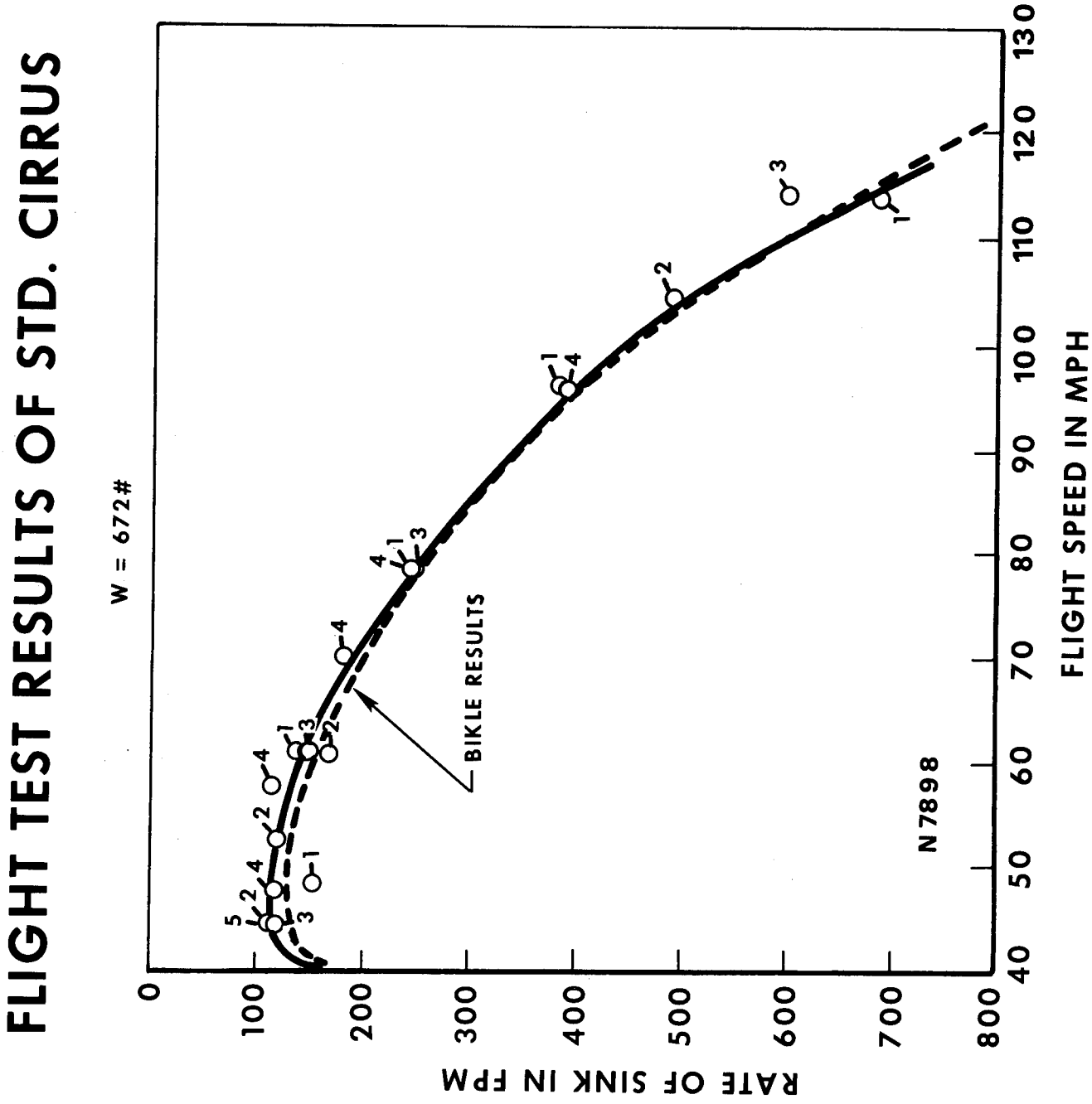

FLIGHT TEST RESULTS OF STD. CIRRUS
W = 672#
BIKLE RESULTS
N7898
RATE OF SINK IN FPM
FLIGHT SPEED IN MPH
0
100
200
300
400
500
600
700
800
40
50
60
70
80
90
100
110
120
130

Figure 3.

differences at high speed and at stall. The rate of sink from slightly above stall speed to eighty miles per hour is, however, noticeably lower than Bikle's result. At present, no explanation for this is available but it can be seen that the low minimum sink results were repeated on all days at which flight tests were conducted.

It is interesting to try to understand the results of these tests. Hence, the performance to be expected has been calculated based upon the following assumptions:

1. Wind tunnel test data for FX 61-183 airfoils applies, corrected for Reynolds number effects.
2. Fuselage drag can be calculated based upon the product of wetted area and the local skin friction coefficient (from Schoenherr equation). Transition Reynolds number is 10^5.
3. Symmetrical airfoil data applies to vertical fin and stabilizer.
4. Althaus compensator and tail skid are only protuberances which must be corrected for.
5. Induced drag coefficient is based upon a span efficiency factor of 0.98.
6. No trim, interference or leakage drag.

The solid line in Fig. 4 shows the results of the calculated Standard Cirrus performance compared with the flight test results. Note that the calculated result correctly predicts the low speed performance, but the measured results are inferior at speeds above 95 miles per hour. The dashed lines show the performance to be expected if the wings were completely laminar or completely turbulent. Above 95 miles per hour, the test results are nearly half way between the calculated performance curve and the fully turbulent wing curve and indicate that transition may be occuring at smaller length Reynolds numbers than in the wind tunnel.

A more convincing way to look at discrepancies is to compare the difference between the actual and predicted performance at high speed with the magnitude of the drag components. Figure 5 illustrates the performance in nondimensional form as lift coefficient squared versus drag coefficient. The high speed results occur near lift coefficients of zero. It can be seen that the difference in drag coefficient between the straight line fit to the data and the theoretical drag coefficient at zero lift coefficient is about 0.001, or ten percent of the total drag. At this lift, any error in the tail drag, C_{D_t}, fuselage drag, C_{D_f}, or wing induced drag, C_{D_i}, would have to be unexpectedly large to account for the discrepancy and can be discounted. The wing profile drag $C_{D_{ow}}$, dominates the drag sources and, hence, is the parameter which most likely is in error. This is consistent with the impression obtained from Fig. 4. To check this conjecture, an integrating survey rake to measure

COMPARISON OF FLIGHT TEST RESULTS WITH THEORY

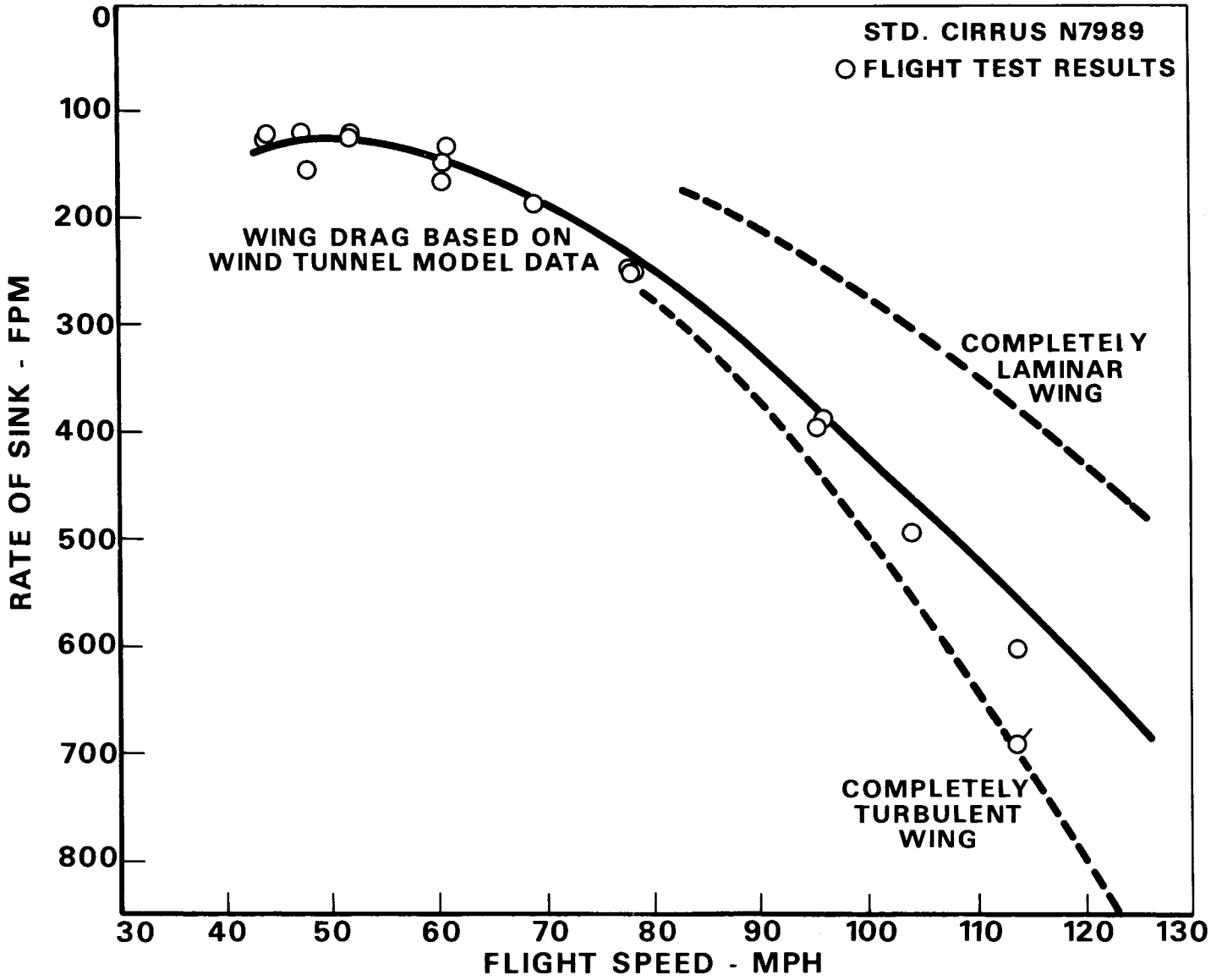


Figure 4.

POLAR COMPONENTS - STD. CIRRUS

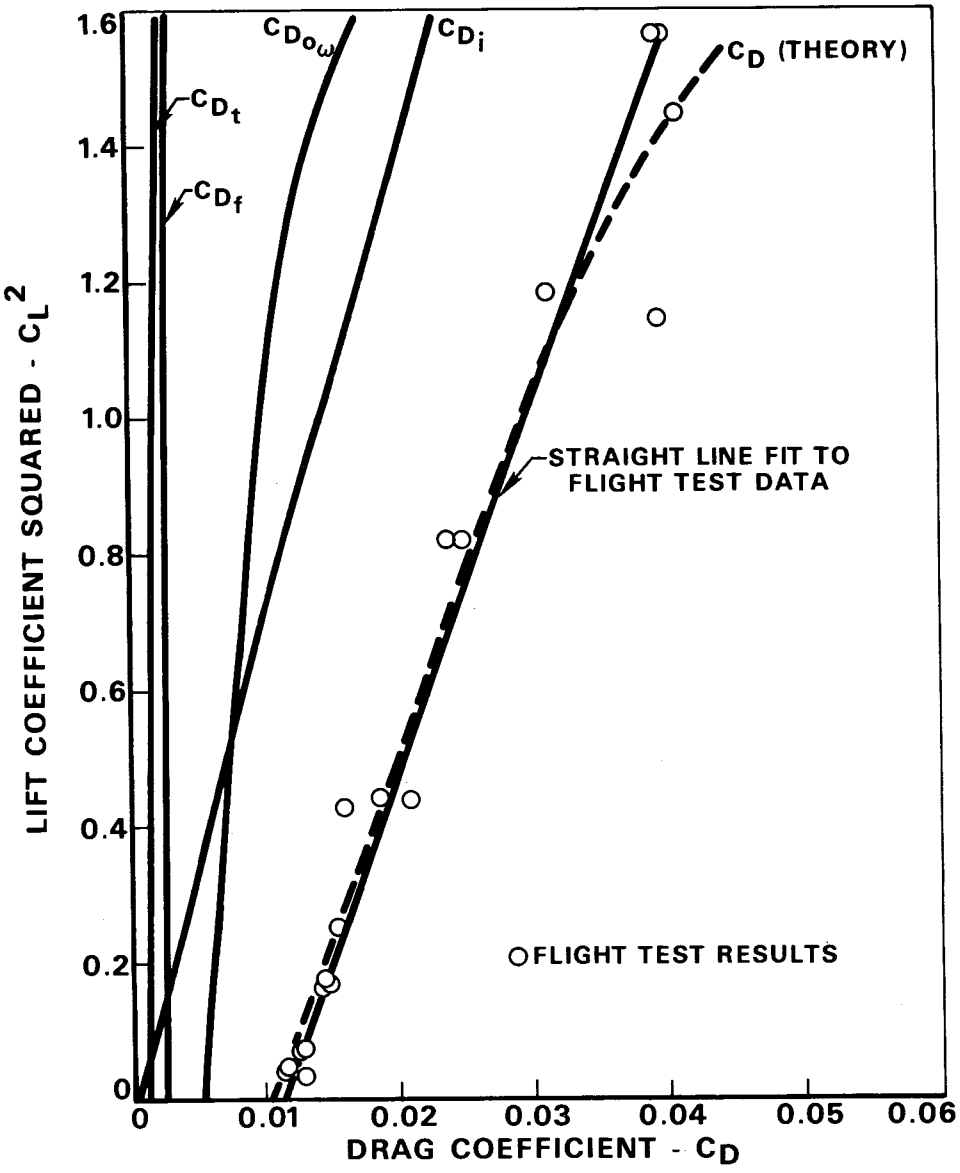


Figure 5.

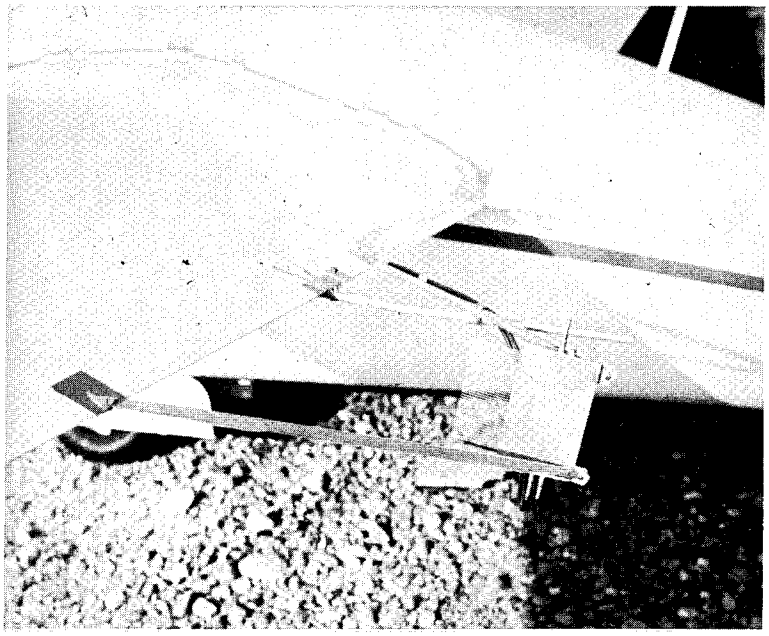


Figure 6.

profile drag has been constructed -- see Fig. 6. It is planned that data will be taken at several stations behind the wing, including an aileron, to determine the actual wing profile drag in flight. Because of poor Fall weather, the wake survey tests have not yet been completed and must await a future occasion for presentation.

Reference

1. Bikle, P.; Polars of Eight, 1971, Soaring, June 1971.

FLIGHT EVALUATION OF AEROELASTIC DISTORTION EFFECTS ON PERFORMANCE, STABILITY AND CONTROL OF A SAILPLANE

by

H.A. Torode
The College of Aeronautics
Cranfield Institute of Technology
Cranfield, England

Introduction

The College of Aeronautics, C.I.T. Cranfield, is carrying out, under Ministry of Defence sponsorship, a program of flight research into the effects of aeroelastic distortion on performance and handling of sailplanes. The program is broad-based in layout and further to its primary research aim is providing independent, accurately measured flight data for comparison with existing theories in the fields of sailplane performance and stability and control. The vehicle in use is a current generation glass fiber sailplane of West German origin.

To date testing of sailplane performance and longitudinal static stability have been completed. A longitudinal maneuvering stability phase has recently completed its flight trials and for the future it is hoped to carry out dynamic response trials for comparison with an already completed resonance test and to conclude with a series of trials to evaluate longitudinal stability derivatives from unsteady symmetric flight maneuvers.

Part I Performance aspects

Performance testing

Performance test instrumentation was obtained from G.R. Whitfield for use on this test series. The instrumentation was operated without modification and data analysis techniques were essentially similar [Refs.1 and 5]. Due to the extremely variable nature of the British weather and our inability to tow high to smoother upper altitude, our testing was limited to early morning operations except in periods of heavy anti-cyclonic conditions. Fortunately our basic testing coincided with one such period and basic testing (some 90 test runs) was completed in two days. This intensive test period resulted in an extremely good set of data by "British weather" standards. A second series with the aircraft loaded with 220 lb of water ballast was carried out under more typical weather conditions over a period of some six weeks, during early morning, with a

significantly reduced accuracy. On occasions when conditions became unsuitable for normal testing, other trial runs were carried out in "high drag" configurations such as wheel extended, airbrake extended etc. in order to evaluate the effect of these changes and the power of approach control devices.

Pressure error testing

This was carried out using basic flight test methods, with two airspeed indicators, one connected to the aircraft system and the other to a reference static source. The sailplane's nose duct mounted pitot source was common to both systems and reference static was taken from a trailing cone drogue. This was the first occasion that such a drogue had been used in England and it was found to produce results in good agreement with other evaluations (Fig. 1) and has since been calibrated to show zero error above 45 knots T.A.S.

Performance data analysis

Data analysis was carried out using the full facilities of the Whitfield test system. A curve fit using raw data points was used in preference to the normal $C_D \sim C_L^2$ fit for the reasons outlined by Whitfield [ref. 5]. The curve fit and 5 knot means are shown in Figs. 1 and 3. The data used for this analysis included the ballasted trials points since as a result of a separated analysis, these were discovered to be statistically identical to the basic data, after application of the normal first-order weight correction. No second-order Reynolds Number effects were observed from the tests and indeed after a series of performance simulations on the College computer (using the program developed by Goodhart) it was concluded that these were unlikely to be measurable in flight.

A statistical analysis of the data is shown in Fig. 4. This shows a histogram of error sink rate and a graph of these, shown on error probability scales. The near straight line graph shows that these are samples from a normal distribution whose standard deviation is $\pm$ 0.3 knots. This compares with other evaluations of airmass movements in Britain under performance test conditions of 0.23 by Machin and 0.5 by Whitfield.

Evaluation of drag constants

Drag constants in the form of a zero lift profile drag and a lift dependent drag factor may be extracted from the polar curve fit. Experience with these and other results show that zero lift profile drag is easily obtained to reasonable accuracy (i.e., about 4%). This is due to the ease of accurate

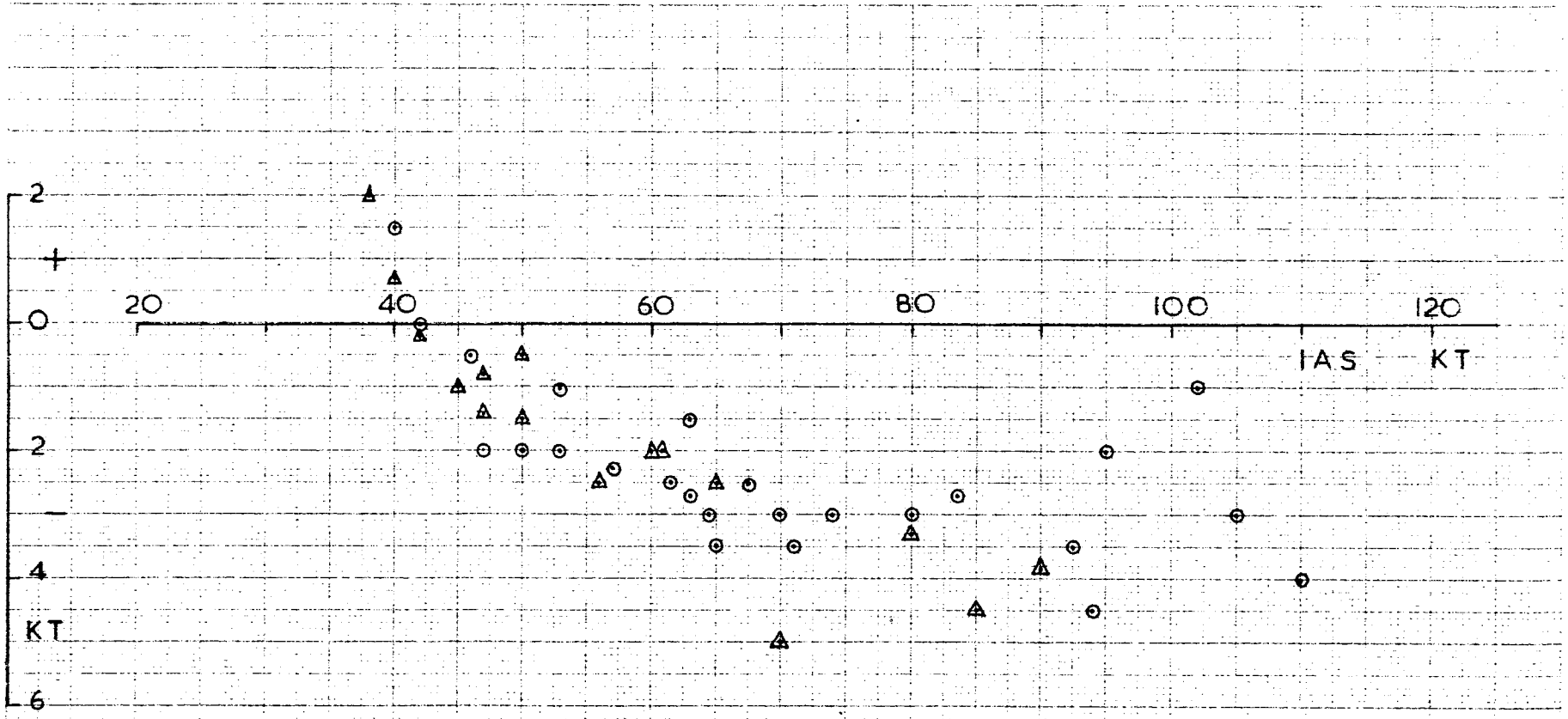


Figure 1.
Pressure error correction data points.

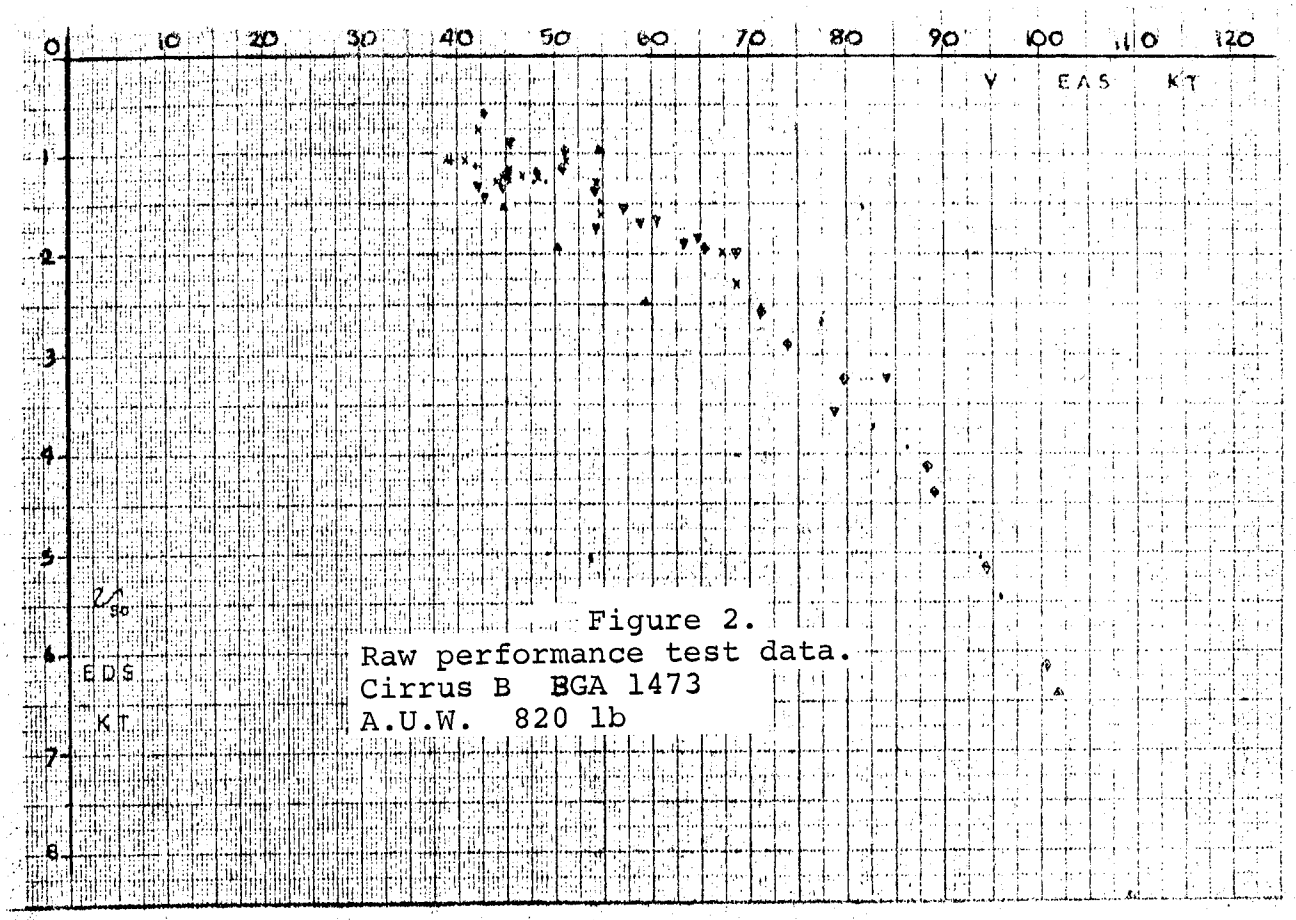


Figure 2.
Raw performance test data.
Cirrus B BGA 1473
A.U.W. 820 lb

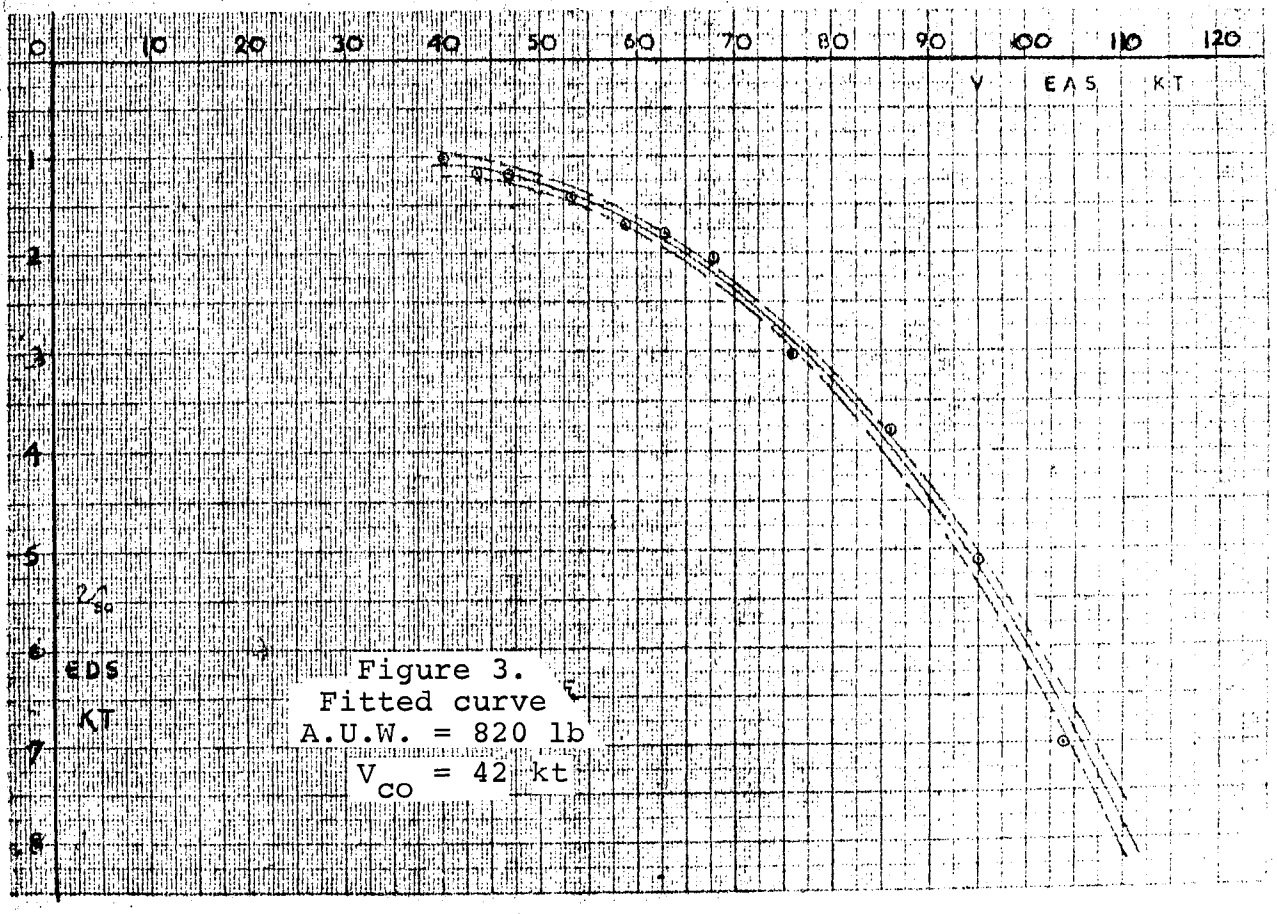


Figure 3.
Fitted curve
A.U.W. = 820 lb
V_{co} = 42 kt

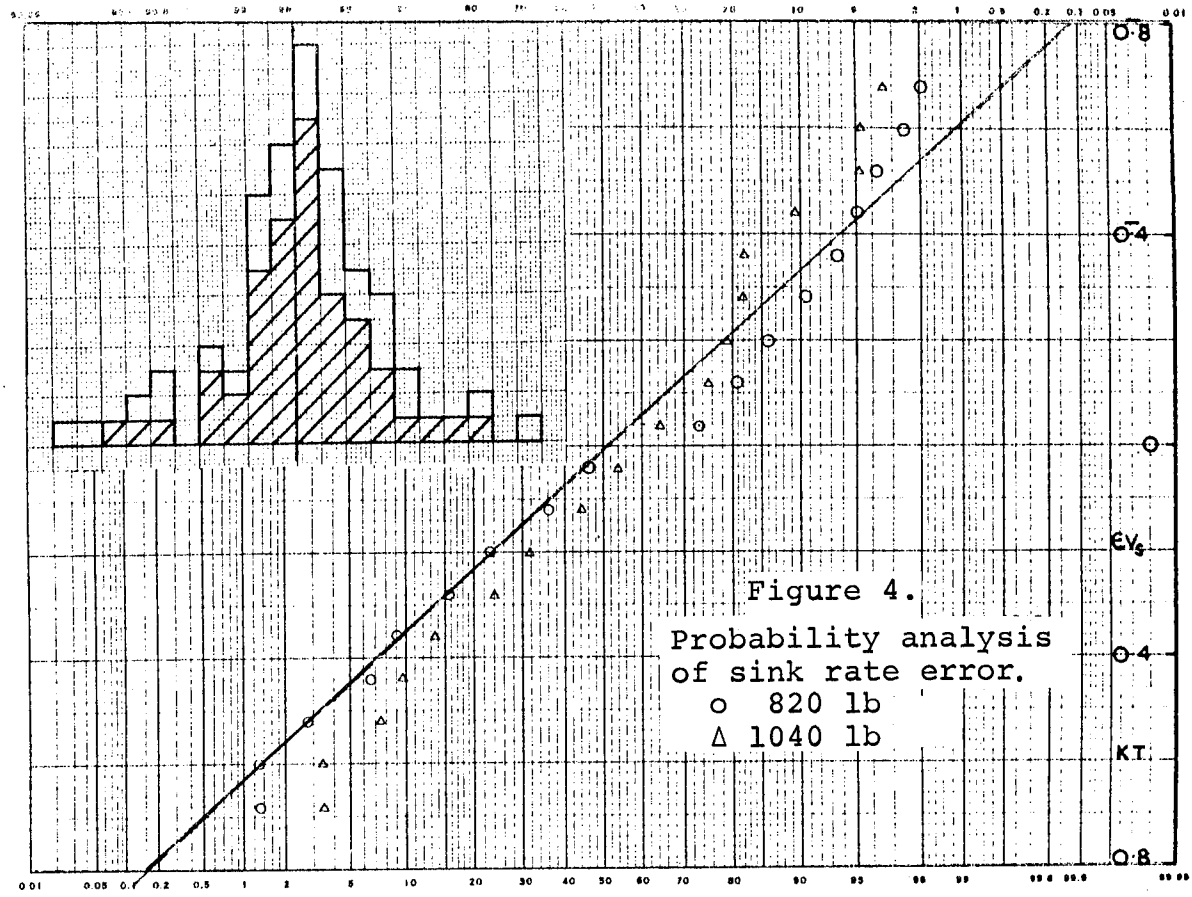


Figure 4.
Probability analysis of sink rate error.
o 820 lb
Δ 1040 lb

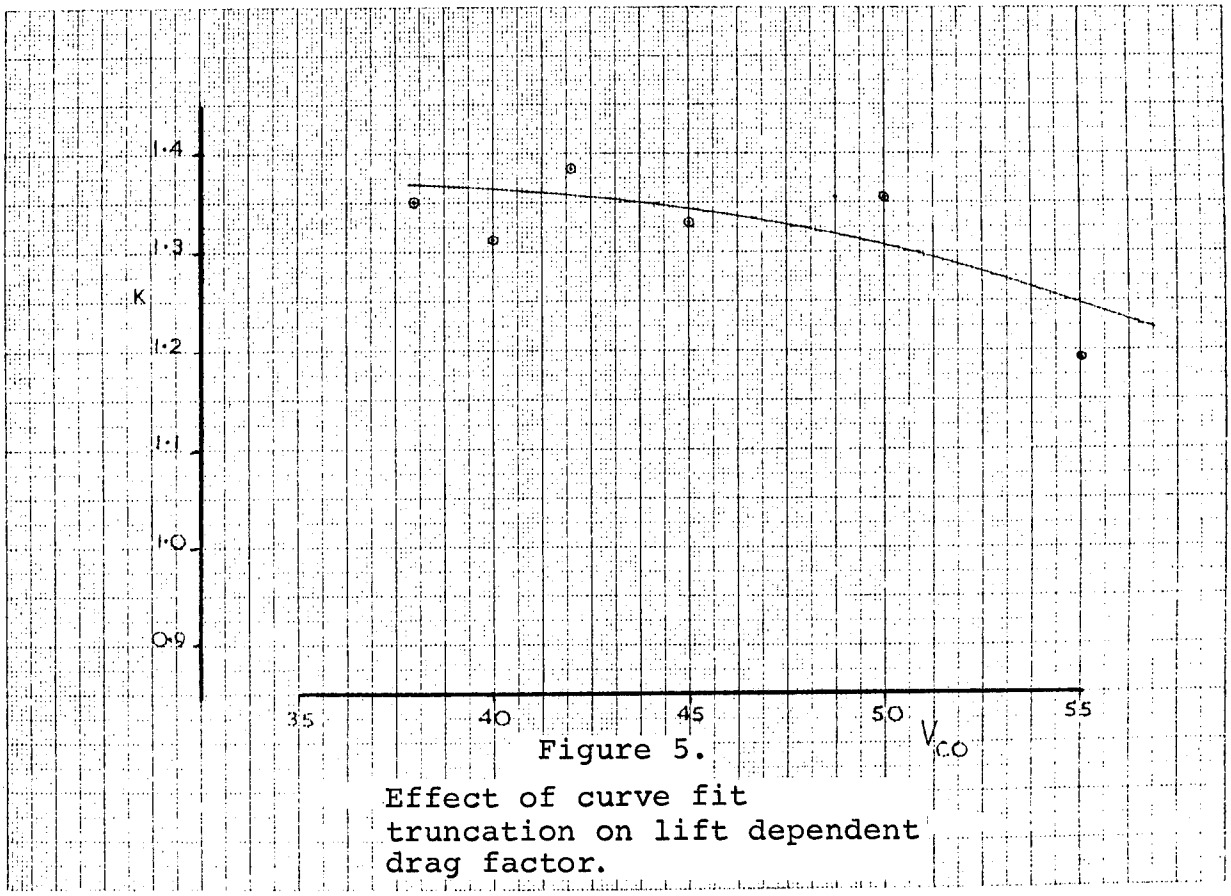


Figure 5.
Effect of curve fit truncation on lift dependent drag factor.

measurement at high speeds were profile drag is dominant. Unfortunately, the same cannot be said for lift dependent drag factors. This, when deduced from the slope of a $C_D \sim C_L^2$ type curve fit, is extremely sensitive to low speed, low accuracy data close to the non-linear stall boundary.

In order to assess the sensitivity of K to isolated data points or points in the run linear region, analysis of data was carried out neglecting all data below a specified speed V_{C_o}. V_{C_o} was varied from 38 knots (all parts) to 55 knots. Clearly, as V_{C_o} is increased, the drag contribution from lift dependent drag will decrease and the value of K may be expected to lose accuracy and to converge on the theoretical ideal of 1. This can be seen to be generally the case (Fig. 5). It should be noted that each value of K is equally valid dependent on the operator's interpretation of extent of non-linear deviations in the polar. Also, the same exercises carried out with the badly weighted direct C_D vs C_L^2 curve, gives more varied results. However at the conclusion of these experiments the basic aircraft lift dependent drag factor was taken to be 1.34, with a zero lift profile drag of 0.0099.

Drag coefficients attributed to the approach devices and wheel are shown in Fig. 6, and Table 1. In the case of brake parachute and extended wheel, these have been deduced on the assumption that the effect contributes only to profile drag. The high profile drag of the extended wheel is 0.0045, about one third that of the complete aircraft (this figure becomes 1.1 based on its own frontal area). The non-dimensional polar complete with all experimental points is also shown (Fig. 7).

Theoretical estimates

Following the conclusion of the data analysis, careful comparison with theory was carried out in order to establish any unexplained phenomena. The following contributions to the drag have been considered, values being taken from the stated references.

a. Wing profile drag for the wing section FX 66-S-196 was taken from the published data, gathered in the laminar wind tunnel at Stuttgart. These data were re-corrected for the variation of Reynolds number during flight condition. This correction brought about an addition of 0.235 to the lift dependent drag factor, even though this drag is basically attributable to skin friction and pressure drag (Fig. 8).

b. Wing induced drag was estimated using the data given in the article "Drag Reduction in Sailplanes" [F.X. Wortmann, Ref. 6]. These were corrected for aspect ratio, giving a contribution of 1.025 to lift dependent drag.

Table 1.
Cirrus drag parameters.

(A) Complete aircraft.

	CDO	K
C.I.T. TESTS	0·0099	1·34
BIKLE (REF 3)	0·0102	1·356

(B) Component breakdown.

	ΔCDO	ΔK
WING SECTION DRAG	0·0066	0·235
INDUCED DRAG		1·025
FUSELAGE DRAG	0·0021	0·034
TAIL UNIT PROFILE DRAG	0·0008	
TRIM DRAG		0·015
TOTAL c.f. (A)	0·0096	1·309

(C) Drag producing devices.

	ΔCDO	ΔK
WHEEL	0·003	
PARACHUTE	0·065	
AIRBRAKES	0·048	4·09

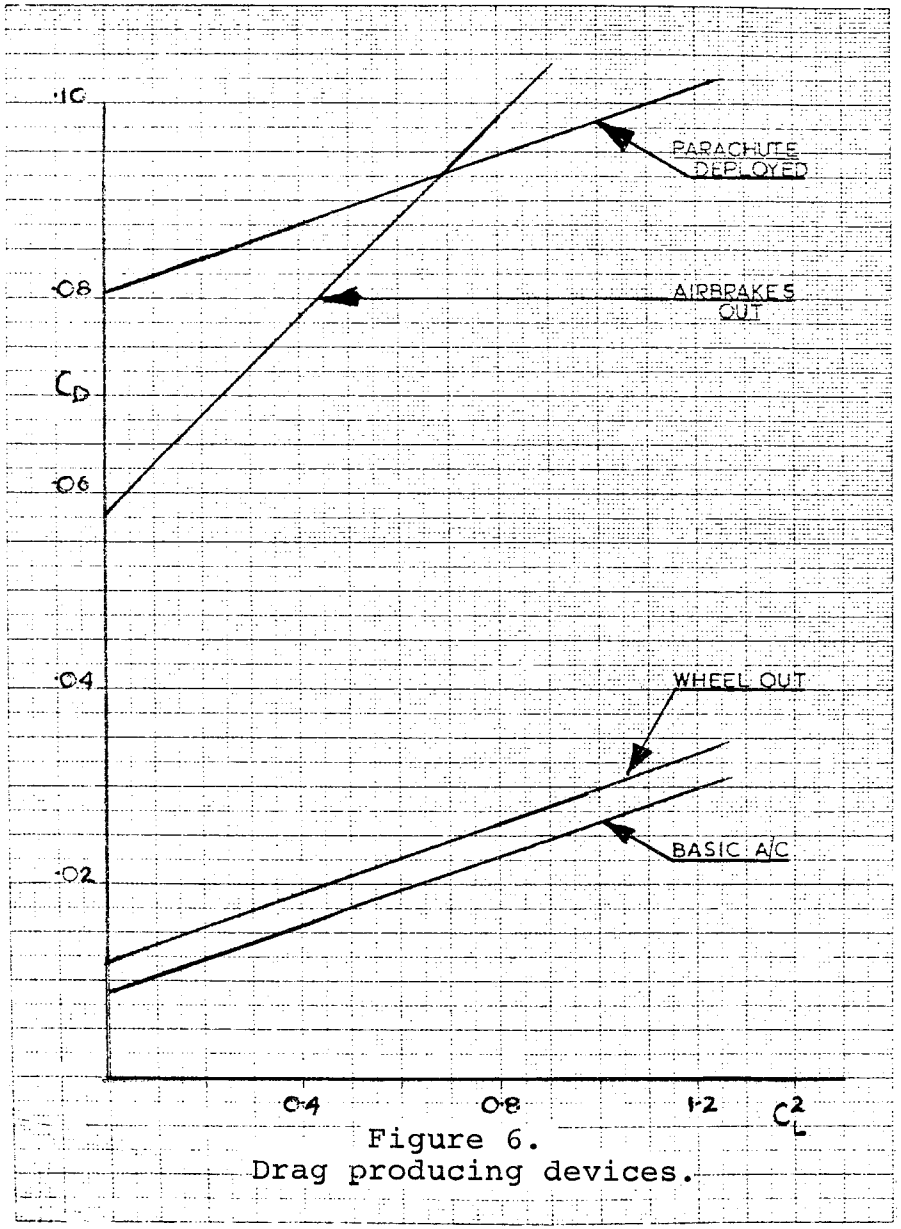


Figure 6.
Drag producing devices.

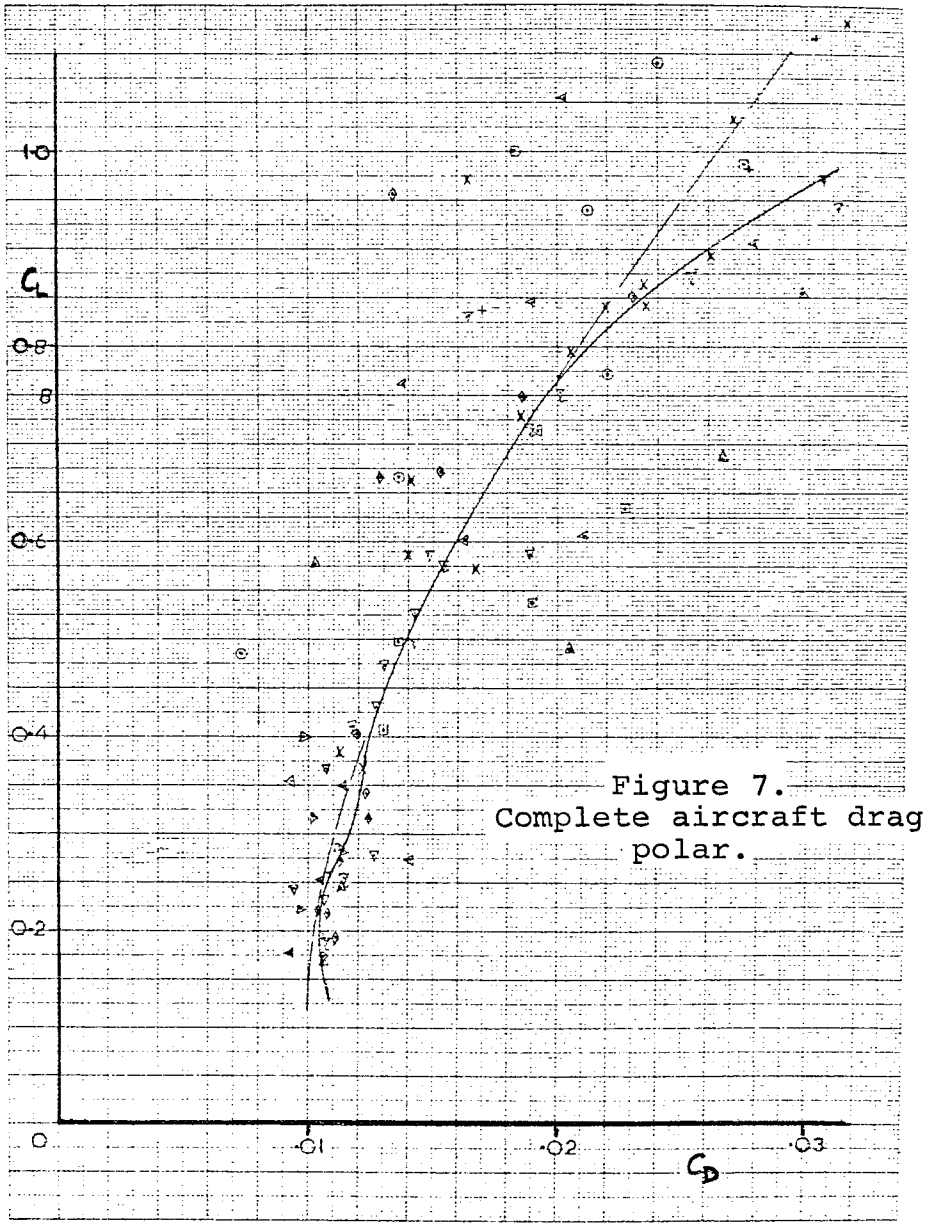
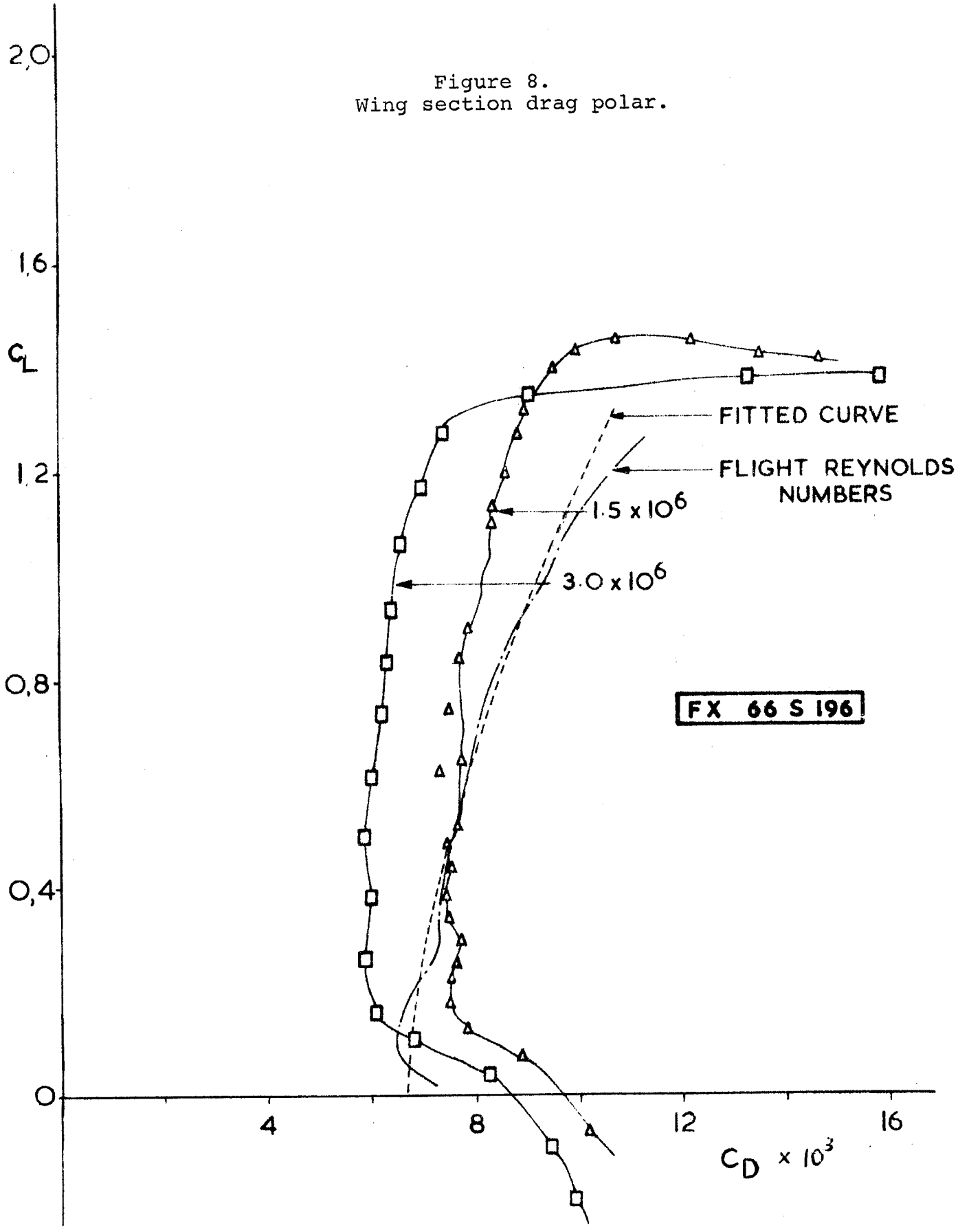


Figure 7.
Complete aircraft drag polar.

Figure 8.
Wing section drag polar.



c. Fuselage drag was estimated from a publication of Stuttgart University [Ref. 7] describing tests on two sailplane-like bodies of resolution one of which alone marked similarity to the Cirrus' waisted fuselage. This, as shown in Fig. 9, was corrected for premature separation and also for the wing-fuselage setting angle, (Fig. 10).

d. Tail unit drag was split into two sources. A longitudinal stability analysis was carried out and following establishment of the tailplane lift coefficients, a tail profile drag was calculated using the characteristics of the tailplane and fin sections [Ref. 10]. Trim drag was considered from the induced drag of the tailplane due to the pre-determined tail lift coefficients.

Comparison with theory

Following the consideration of all these "classical" contributions to the sailplane's drag (see Fig. 11), the sums were compared with the flight test results. In many cases a curve fit of the type used on the overall aircraft was used to idealise the drag contribution (see Table 1). This technique was particularly successful in the case of wing and fuselage profile drag contribution, and would thus indicate that the original assumption made in the use of the curve fitting routine was justified.

This exercise has shown that the zero lift profile drag coefficient found from test produces a high speed performance (within the laminar range of the aerofoil) that agrees well with that established in theory. This would indicate that performance is generally unaffected by aeroelastic distortions in this particular case, within the speed range considered. Observation of the wing twisting in flight and static evaluations of wing torsional stiffness show that although there is twisting distortion of the wing at high speed, which will doubtless distort the lift distribution, this will only effect induced (lift dependent) drags which are insignificant at high speed (low lift coefficient). The performance of the sailplane only becomes significantly affected when the tip section is distorted sufficiently to move its operating C_L outside the laminar bucket region. On the Cirrus, this situation occurs at 115 knots, $C_L = 0.2$. Several performance points above this speed have shown a non-linear increase in sink rate. The basic (rigid) wing should remain "laminar" i.e., with the drag bucket down to a C_L of 0.08 ($\simeq$ 145 knots). In view of the high cruise speed used by today's top cross-country pilots, this effect is clearly becoming significant and should be considered when laying out a new design.

The other disagreements with theory were discovered in the low speed regime. Even considering the large contribution

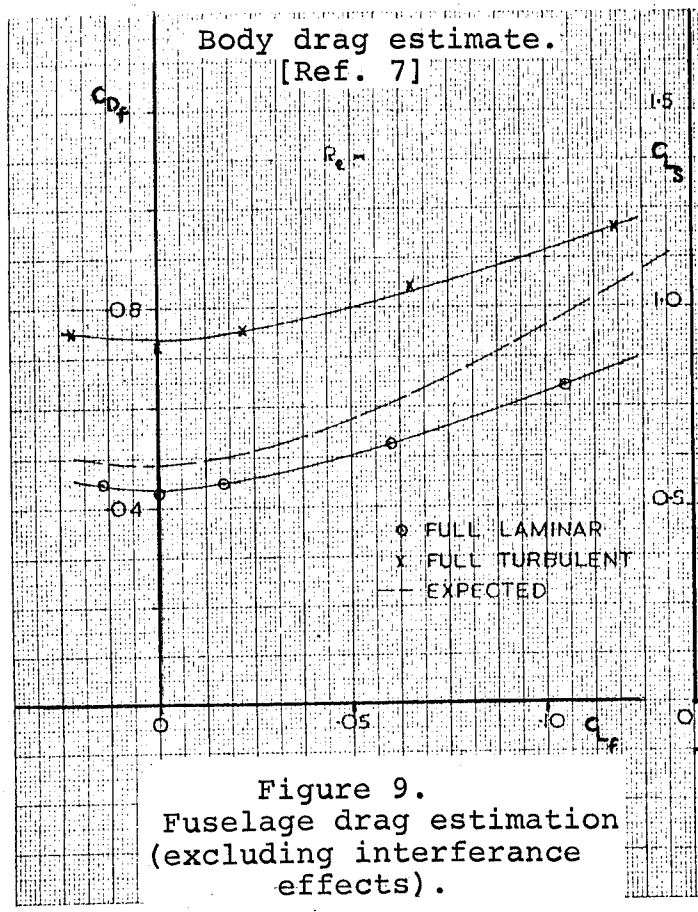


Figure 9.
Fuselage drag estimation (excluding interferance effects).

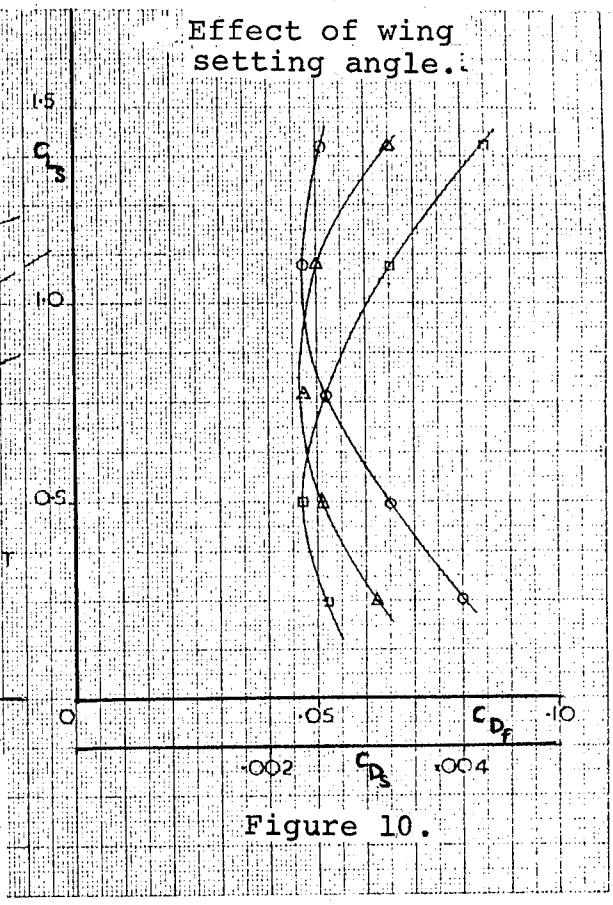


Figure 10.

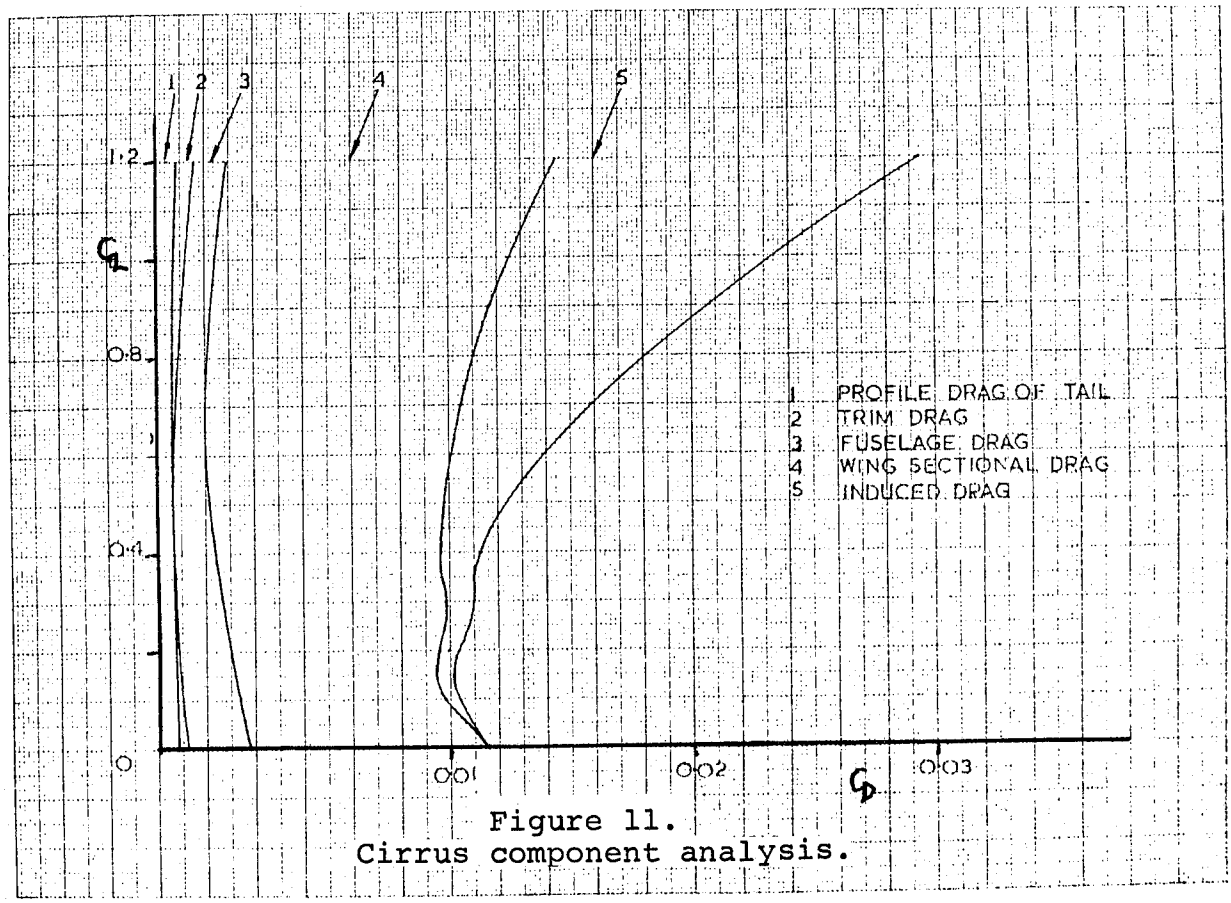


Figure 11.
Cirrus component analysis.

to lift dependent drag from the wing section characteristics, there still remained a further unexplained increment of lift dependent drag, ($\Delta K = 0.10$). This may be attributed to one of two sources:

a. Losses in the wing/fuselage junction.

b. Loss of predicted section performance at the wing tip due to highly reduced Reynolds numbers.

The functional flow was investigated in flight using tufting (Figs. 12 and 13) which shows some separated flow existing at high and moderate lift coefficients. However, the flow would appear to be highly sensitive to detailed conditions as may be seen by the marked asymmetry of the flow.

It is also considered that the flow in this area is extremely local and unlikely to significantly effect the overall performance of the sailplane. Source b. is considered to be the primary cause of this apparent deficit in low speed performance.

Part II Stability and control aspects

Instrumentation

The instrumentation for the stability and control phase was developed "in-house". It is an 8 channel, a-c carrier system powered by sealed lead-acid accumulators, and outputting into either:

a. a Hussenot A22 trace recorder, or

b. a specially-developed 8 track portable tape recorder.

The carrier frequency is 3 kHz, exciting a programmable set of up to 10 transducers. Battery current drain without recorder varies between 0.6 to 1.4 amps, dependent on the transducers in use.

The instrumentation system is basically housed in the centre-section of the sailplane, and is split into:

a. a signal conditioning module which generates the required a-c frequencies and a set of phase sensitive demodulators to condition the transducer output signal for use in the recorder, and

b. a power module housing battery voltage stabilizers and power amplifiers to produce transducer drives.

The system is laid out with high power signals restricted to the power module in order to minimise problems of a-c pick up and interference. The functions at present embodied in the system are:

Airspeed, vane incidence, pitch attitude, stick force, elevator position, C.G. acceleration, wing tip acceleration, pitch rate and outside air temperature.

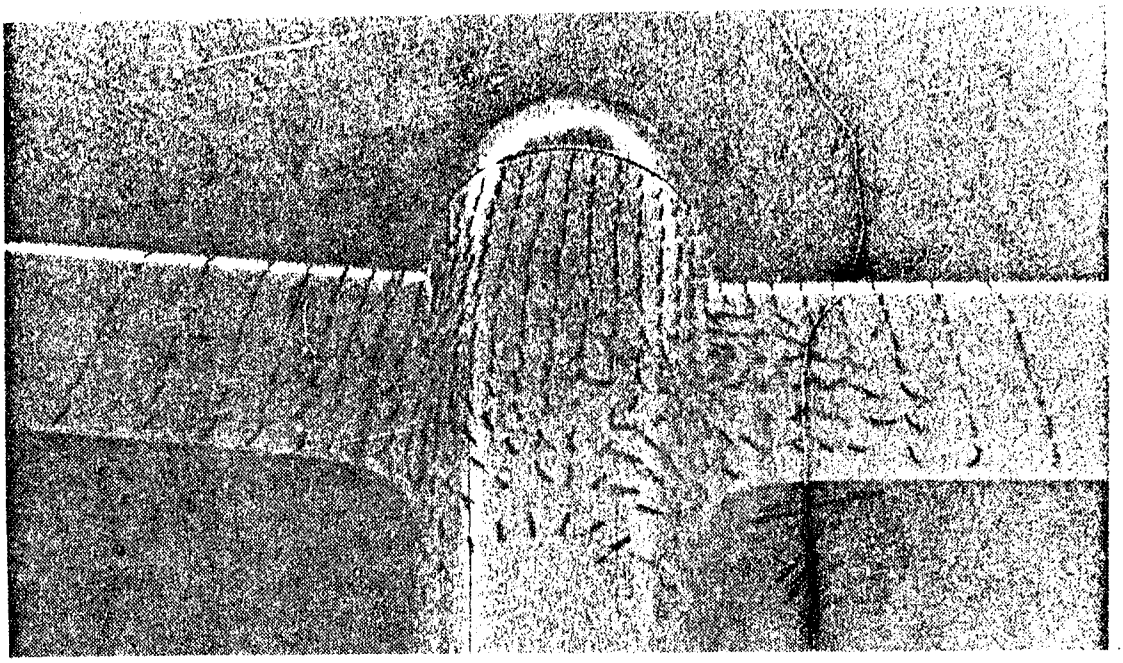


Figure 12. Junction flow at 45 kt ; C_L = 0.92.

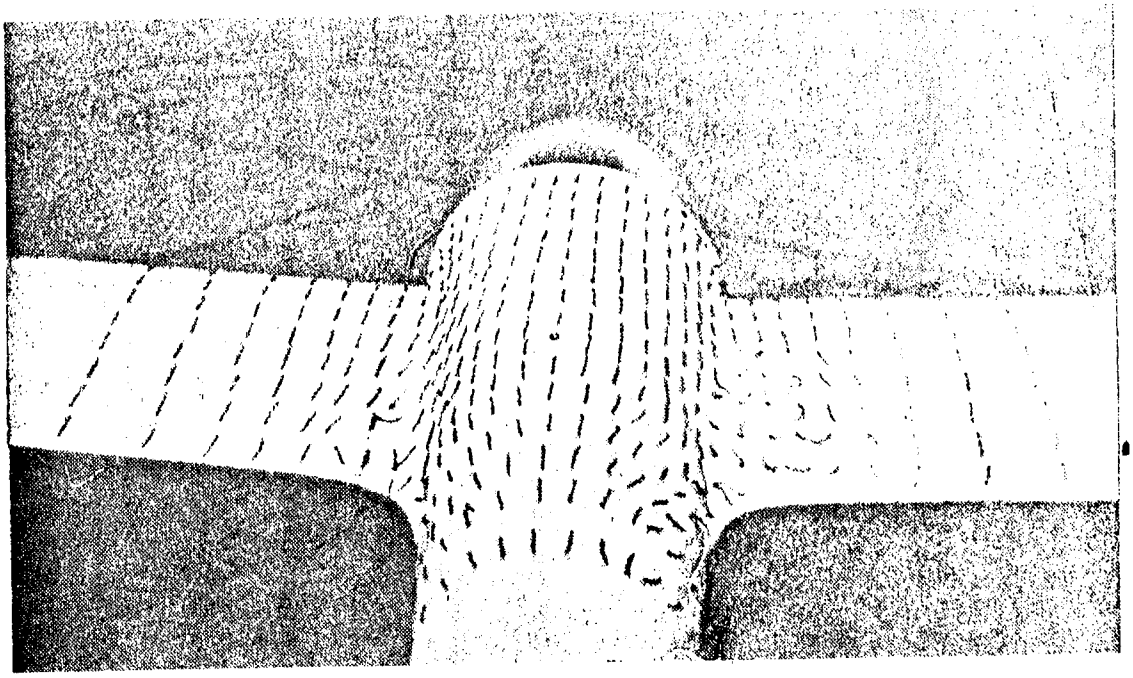


Figure 13. Junction flow at 50 kt ; C_L = 0.71.

Lift curve evaluation

This was carried out in steady glides monitoring airspeed, incidence, and pitch attitude. Airspeed and pitch attitude were used together with the sink rates deduced from the tested polar to calculate true incidence. From this a $C_L \sim \alpha$ curve was plotted (Fig. 14), and also a vane incidence calibration curve. It is worthy of note that this exercise is extremely simple using a sailplane of known performance since the true sink rate of the vehicle with respect to the surrounding air is always known to very good accuracy.

The sailplane's maximum lift coefficient was found to be 1.37 which compares favourably with a tunnel section value of 1.45 at very similar Reynolds number.

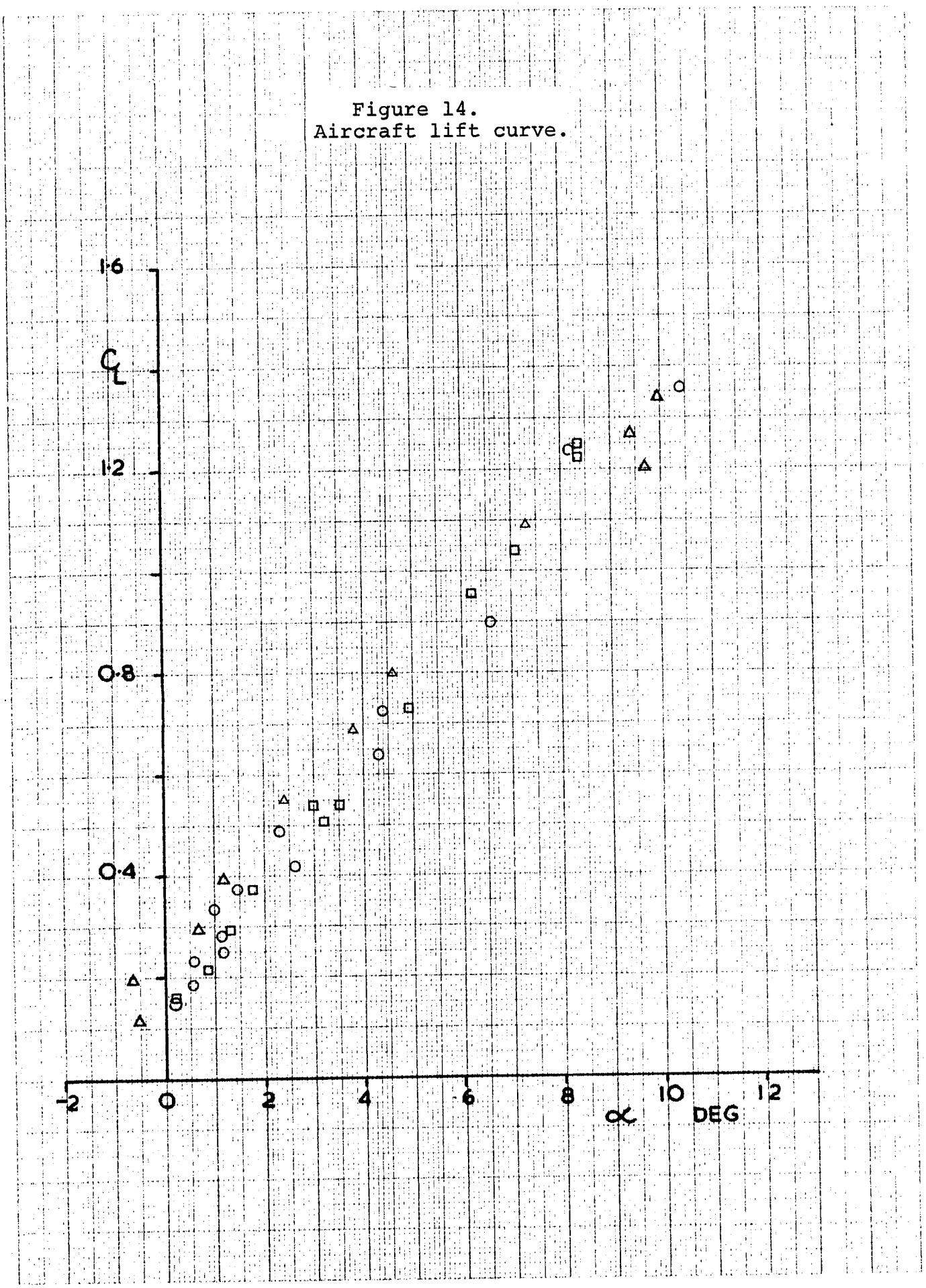
The lift curve data was clearly linear and a least squares fit produced a best estimated lift curve slope of 6.93/rad. This is notably in excess of the thin aerofoil value of 2π but the Royal Aeronautical Society Data Sheet would indicate that this is not an unreasonable value for a section of 19.6% thickness. However, the tunnel results, when corrected for aspect ratio and tailplane load, suggest a figure of 5.98/rad.

Assuming the tunnel results to be more trustworthy, this anomaly could be explained by continuous elastic twisting of the wing throughout the speed range causing a correction to be necessary to the pitch attitude as measured, in this case, at the fuselage. The order of this correction would appear to be similar to that amount of twisting required to cause the outer wing panels to leave the laminar regions at high speed, as outlined in the performance test section.

Longitudinal static stability

These tests were carried out in the conventional manner, by flying at a series of steady speeds throughout the operating range, measuring stick force and elevator angle. This procedure was repeated in this case at four different C.G. positions from the forward limit of 32.2% $\bar{C}$ to the aft limit of 44.0% $\bar{C}$. In each case the spring type trim was maintained set in a specially reworked detent. Trials were also repeated with the trim springs disconnected. It was found that due to the marginal stability of the sailplane and the high gains required within the instrumentation, that no less than "performance test" standard conditions were sufficient for these tests and thus the customary early morning operations were required.

Figure 14.
Aircraft lift curve.



Stick-fixed trends

The results of the elevator angles to trim measurements are shown in Fig. 15 and plotted non-dimensionally in Fig. 16. It can be seen that the elevator angles curves steepen non-linearly at low speed due to non-linear downwash effects on the tailplane, and furthermore, flatten significantly, tending to neutral stability, and in the case of the aft C.G.'s instability at moderate and high speeds. Plotting non-dimensionally and continuing the normal processes of plotting slopes to find the stick-fixed neutral point, [Refs.11 and 12], the aircraft's behaviour at various C.G.'s was found to agree very closely with linear theory in the mid speed ranges, leading to a stick-fixed neutral point at 5% $\bar{C}$. However, in the higher speed ranges the analysis shows a marked forward movement of the stick-fixed neutral point until at aft C.G. it has passed well into the normal C.G. range. This non-linear behavior is well in accordance with the prediction of Refs. 14 and 13 and is thus considered to be due to aero-elastic wing twisting.

This phenomenon is further highlighted when estimations of elevator and tailplane lift curves are deduced. Unfortunately, the sailplane used does not have an all-moving tail so deductions of A_1 (the tailplane lift curve slope) are purely from estimation and not directly deduced from flight tests. The elevator lift curve slope A_2, however, can be directly estimated throughout the speed range (Fig. 18), and can be seen to increase markedly from its first order theory value of 1.68/rad at high speed.

This value of 1.68/rad establishes, with the assumption of the basic aircraft pitching moment, that the tailplane lift curve slope is of the order of 2.85/rad. Both these figures are well below the estimates previously made from Ref. 15, which is universally accepted for deduction of stability parameters for sailplanes. The reasons for these discrepancies are considered to lie in the nature of the vehicle under examination. Study of Ref. 15 shows that derivative estimation is generally carried out by factoring the over-all aircraft lift curve slope. This, as we have previously established, is quite large in the case of a sailplane, owing to its high aspect ratio, and usually very thick wing. This layout does not necessarily affect tailplanes and elevator lift curve estimates which have been devised in the sheets for aircraft with over-all aircraft lift curve slopes in the region of 4.0 to 5.0/rad. There would seem to be a case, were the information available, to devise a new data sheet for future use by the sailplane movement.

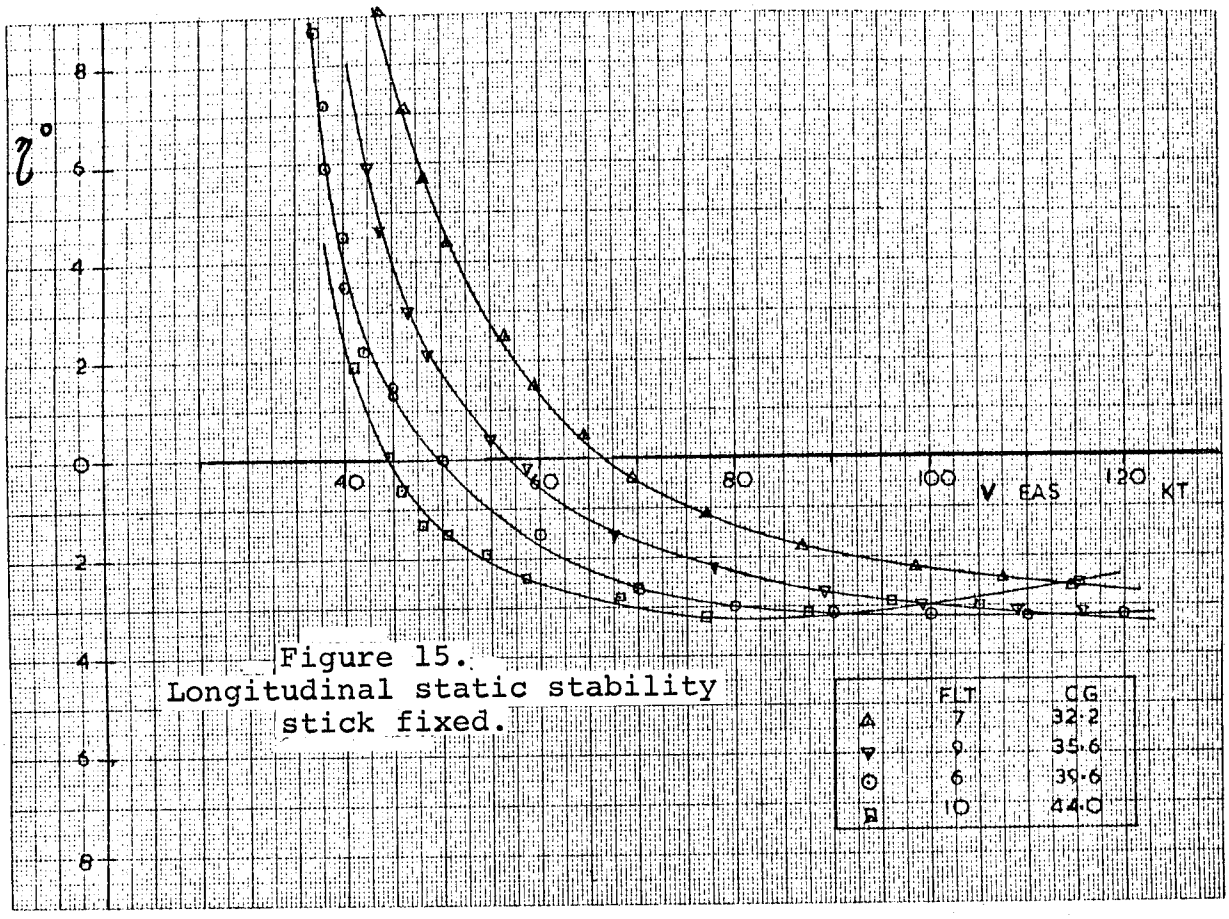


Figure 15.
Longitudinal static stability
stick fixed.

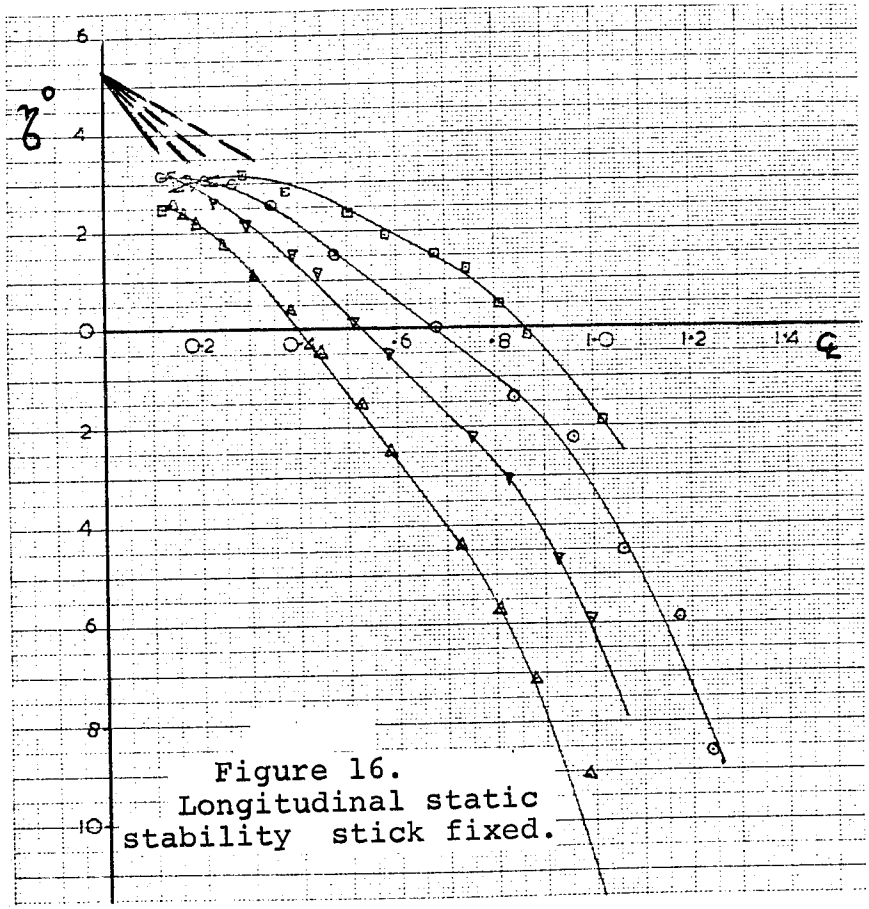


Figure 16.
Longitudinal static
stability stick fixed.

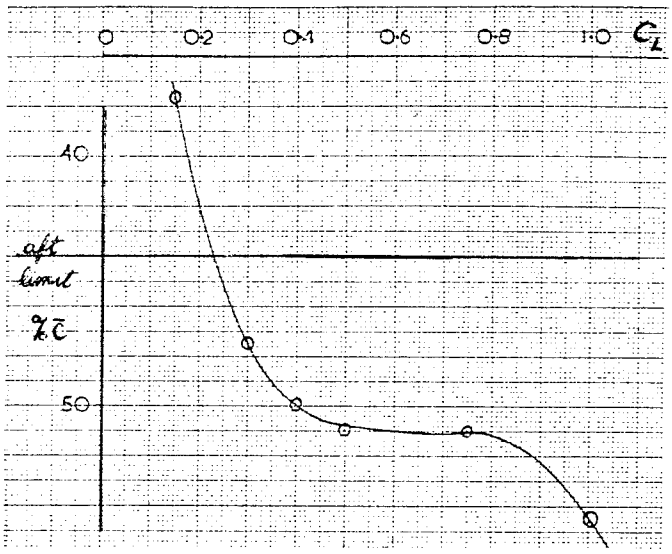


Figure 17. Movement of stick fixed N.R. with C_L.

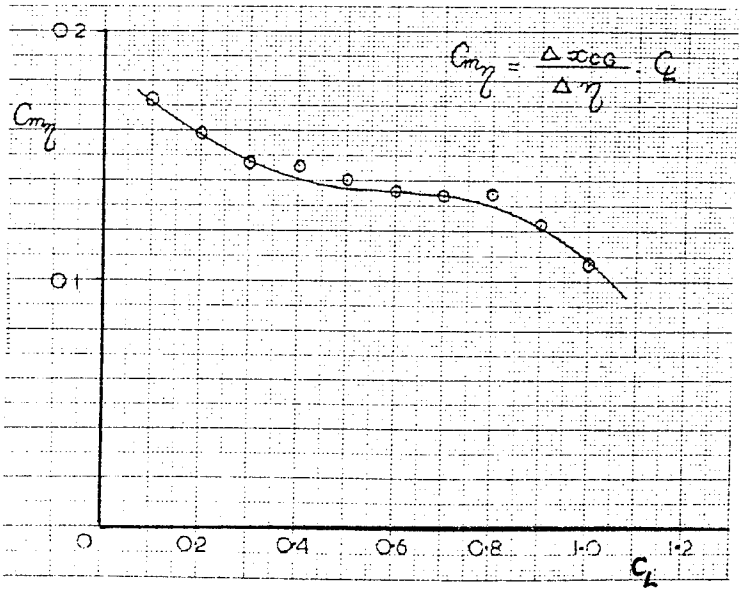
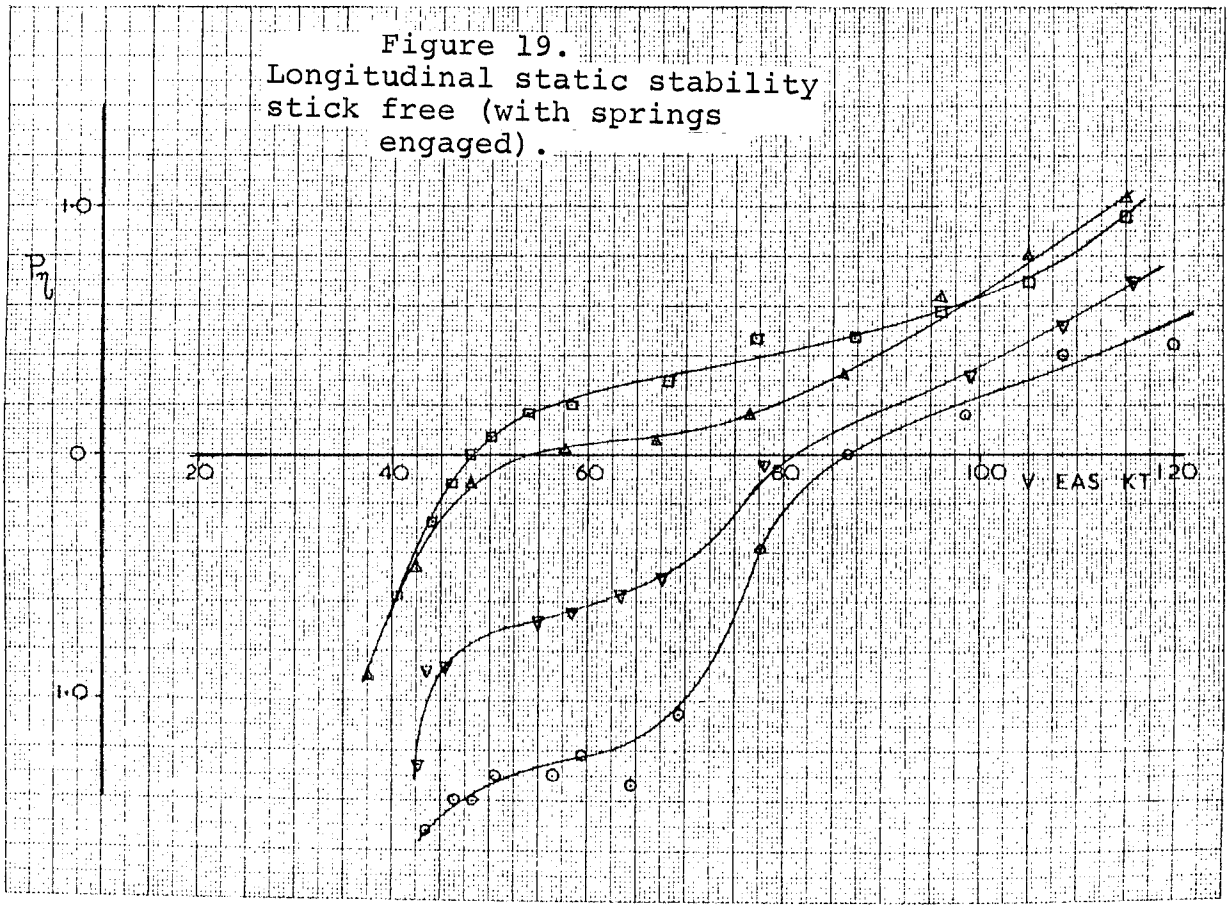


Figure 18. Elevator power coef.



Stick-free trends

Whilst the stick-fixed information has shown much of the behavior of the over-all aircraft, the stick-free (control force stability) data will be more relevant to the control system itself. From the ouset, this operation has been much more delicate. Fig. 19 demonstrates that elevator forces are of such a low absolute value that acquisition of stick force information has been a problem. Indeed "performance test" meteorological conditions were, in the main, necessary in order to minimise pilot hand shake on this data channel, but even so, remarkable resolution has been demonstrated by the good quality and small scatter of these tests.

In the light of the elevator force values achieved during these tests, the possibility of elevator circuit friction interfering with the test result was considered of significance. A special flight was conducted using differing techniques of entry to the flight condition. This repeated flight was in excellent agreement with the original and showed little scatter of points between techniques.

Unfortunately the stick force gradients deduced are markedly non-linear both in respect of airspeed and with C.G. position, and no meaningful deduction of a stick-free neutral point has yet been possible. All that can be said at the present time is that the aircraft is statically stable stick-free, to a greater or lesser extent, throughout the speed range. About half of the present stick force stability is provided by the trim springing layout and the remainder of the hinge moment must be supplied in a non-linear way by the very narrow-chord elevator which features a slightly hooked trailing edge; this may well contribute a non-linear tailplane pitching moment.

Conclusions

These tests, when viewed as a whole, have shown that in many aspects the aerodynamic qualities of a sailplane may easily deviate from existing theories and that, particularly at high speeds (above 70 kt), aeroelastic phenomena, whilst not in themselves rendering the aircraft structurally unsafe, may well detract from its aerodynamic performance and stability. In view of the trends towards larger, more flexible sailplanes retaining the existing very low stability margins and being flown at much higher cross-country speeds, these effects must be considered, preferably in the light of data gathered using the existing sailplane types rather than, as in the past, from data sheets created for conventional aircraft which are rapidly becoming less and less applicable to the needs of the sailplane design movement.

References

1. Whitfield, G.R.; A Simple Data Recording System with Computer Analysis, Published in Radio & Electronic Engineer.

2. Torode, H.; Performance Testing of Sailplanes, College of Aeronautics Report.

3. Bikle, P.; Polars of Eight, Soaring, June 1970.

4. Ikthara and Marth; Trailing Cone Static Pressure Measurement Device, J. of Aircraft, Vol. 1, No. 2 1964.

5. Whitfield, G.R.; Automatic Recording & Analysis for Glider Performance Testing, 12th OSTIV Congress Marfa, Texas 1970.

6. Wortmann, F.X.; Drag Reduction in Sailplanes, Soaring, June 1966 or Sailplane & Gliding 1966 (Translated from original German).

7. Fix, A., Jahn, H. and Stellbrink; Messungen an zwei Rotationsymmetrischen Rumpfen, Technische Hochschule Stuttgart 1966.

8. Hoerner; Fluid Dynamic Drag, (Priv. Pub.)

9. Power Jet Co. of America; N.A.S.A Contractor's Report ASN-TR-61-579 429971.

10. Abbott & Van Doenhoff; Theory of Wing Sections Dover.

11. Irving, F.G.; Introduction to Longitudinal Static Stability of Low Speed Aircraft, Pergamon Press.

12. Gates, S.B. and Lyon, H.M.; A Continuation of Longitudinal Stability and Control Analysis. Part II Interpretation of Flight Tests. R & M 2028, 1944.

13. Jakubov, V.K.; Influence of Elastic Wing Twisting on Certain Characteristics of Longitudinal Stability and Controllability of a Glider. 10th OSTIV Congress S.Cerney, June 1965.

14. Kaprzyk, J. and Nowak, M.; The Influence of Wing Flexibility on Elevator Angle to Trim for a Sailplane in a Steady Glide, 11th OSTIV Congress Leszno, Poland.

15. Royal Aeronautical Society Data Sheets.

GLIDER PERFORMANCE TESTING WITH AN AUTOMATIC RECORDING SYSTEM

by

G.R. Whitfield
Dept. of Applied Physical Sciences
University of Reading, England

Introduction

The only current practical method of measuring the performance of a glider is to measure the rate of sink at a series of constant airspeeds with clock and altimeter. Because of the random vertical motion of the air, many such "partial glides" - typically more than 100 - have to be measured to establish the polar with reasonable accuracy. The recording methods used so far include pencil and knee-pad [1], radio to an observer on the ground and photography of the instrument panel [2]. These all require manual analysis on the ground after flight. The present research began with a resolution to avoid this manual labor, by using a recording system in the glider that could be played back directly into a digital computer on the ground. All subsequent calculations can be done by the computer. Such a system greatly reduces the time and labour required to measure each glider's polar.

The flying program

The flying program is very similar to that used by previous observers. The glider is towed to a convenient height, usually 9,000 ft, and is flown in a series of straight runs at constant speed. The pilot is given a flight plan consisting of a list of the desired speeds for the runs with the height to be lost at each speed. A significant improvement on earlier work is the high sensitivity ($\pm$ 3 ft) of the height measurement, which allows the use of very short runs. As many as 25 runs, over the entire speed range from 30 to 100 kts, can be obtained from one flight. Six flights, giving between 100 and 150 runs, are sufficient to establish a polar.

The weather must, of course, be carefully chosen to minimise the vertical air movements which are the most serious source of error [2]. All the flights took place in the early morning, before convection started: but standing waves were troublesome, and perhaps only days with little or no wind are really suitable.

Apart from these flights, at least one flight is needed to measure the position error of the pitot and static pressure sources in the glider.

The recording system [3]

The system, Fig. 1, measures height and indicated airspeed (I.A.S.) at intervals of about 1.6 sec. The transducers convert the input quantity into frequency, variable from 4 to 10 kHz, by using standard altimeter or A.S.I. capsules to move the plates of a variable capacitor, which controls the frequency of an R-C oscillator. Fig. 2 shows the height transducer, and a block diagram of its oscillator (which is contained in the same case). A crystal oscillator and counting chain is used to generate sampling pulses, which gate samples from the transducers alternately, with gaps between, to the recorder. The samples are of defined duration, so the number of cycles in each sample is a measure of the appropriate quantity.

On the ground, the record is played into a computer, which counts the cycles in each sample. Using a calibration table, the computer converts each count to a reading of height or I.A.S.

In addition to the data a filtered speech channel (up to 3.5 kHz) is fed to the summing amplifier and recorded. It does not affect the data, which occupies the band 4 to 10 kHz, and is filtered off before feeding the data to the computer; but it allows the pilot to mark the recording, and make comments which the computer operator can use to guide him when playing it back.

The whole airborne system occupies about 1 ft^3 and weighs 25 lb with batteries. It records height from 0 to 10,000 ft ICAN with a reading accuracy of $\pm$ 3 ft and long term accuracy of about $\pm$ 300 ft, and I.A.S. from 0 to 120 kts, with a reading accuracy of $\pm$ 0.1 kt and a long term accuracy of $\pm$ 0.5 kt. The time intervals, controlled by a crystal oscillator, are so accurate that their errors are negligible.

Analysis

The magnetic tape is played back into a PDP-8 computer, which is programmed to count and store the number of cycles in each sample, together with a run number allocated by the operator. All these counts are punched out on paper tape for later analysis on a larger computer.

This reads the data one run at a time, converts each count to ICAN height or I.A.S. (there is no ambiguity, since the height count is greater than 3000 and the speed count is

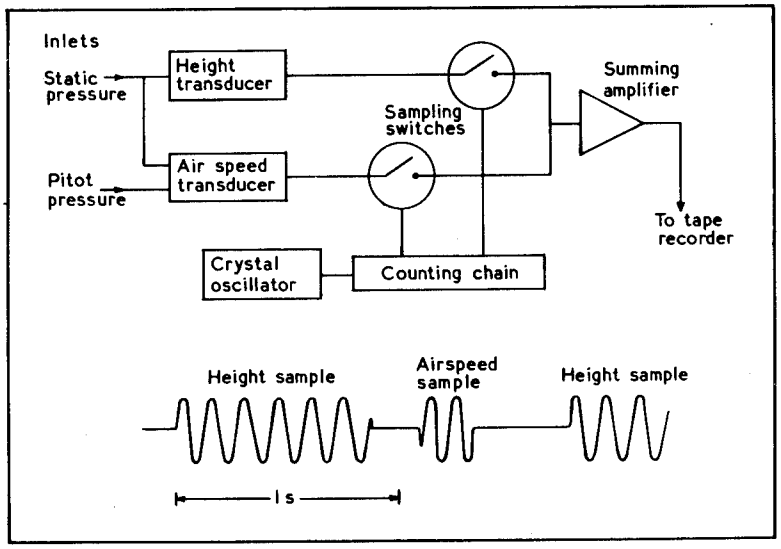


Fig. 1. The Recording System and the Recorded Waveform

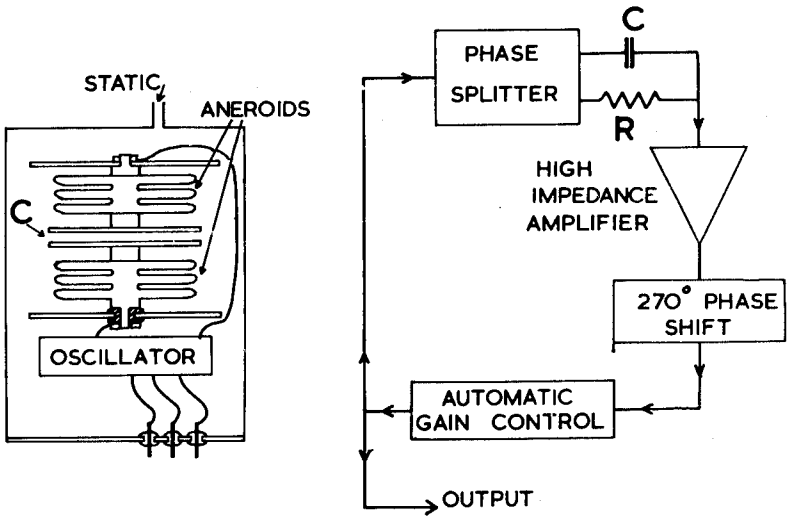


Fig. 2. Height Transducer.

less than 2500) and performs a least squares fit of a straight line to the height vs time graph. It also averages the I.A.S., inserts all the corrections to reduce the measurements to mean sea level, and computes the measurement errors. The normal output of this program is a table giving, for each run, the average values of equivalent air speed (V) and equivalent rate of sink (S_o), with their errors. The operator can also call for a plot of height and speed vs time on the computer's graph plotter (Fig. 3), but this is only used as an occasional check as it takes 4 minutes per run to plot the graphs. When all the runs have been analysed, these tables are examined and a new tape is made listing pairs of V and S_o for each run. Occasionally runs have such large errors as to be meaningless, and are omitted, or are split in two (by a recording fault, interpreted by the computer as ending the run) and have to be combined. So manual intervention at this stage is useful. This tape of V vs S_o is used in all subsequent analysis. The process is illustrated by the measurements obtained for the BG135.

First, every point is plotted (by the computer) (Fig. 4). This shows the general shape of the polar and the amount of scatter. It allows the operator to estimate the speed, V_{min}, at which the glider starts to stall and the polar departs from the theoretical curve

$$S_o = AV^3 + B/V \qquad (1)$$

Next, this theoretical curve is fitted, by a least-squares technique, to all the points faster than V_{min}. This gives a fitted polar, with lines at 2 standard deviations above and below it (Fig. 5).

Then, using a table of defining speeds (usually every 5 kts, but closer around V_{min}), the centre of gravity of all the points in each interval is plotted, with the standard deviation S_o for each (Fig. 6).

From the values of A and B, the computer calculates C_{D_o} and k in the drag equation

$$C_D = C_{D_o} + k\, C_L^2/(\pi AR) \qquad (2)$$

and their standard deviations.

Calibrations and corrections

The height transducer is calibrated every few weeks against a mercury barometer. The airspeed transducer is

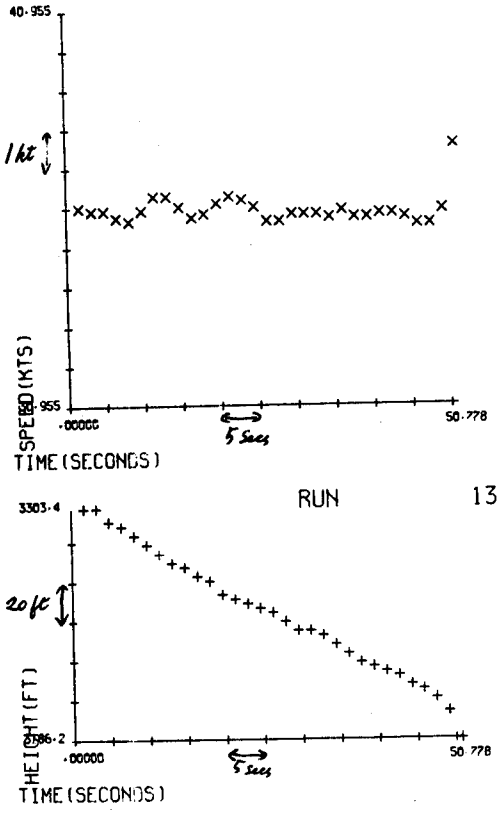


Fig. 3. Height and Speed Graphs from One Run

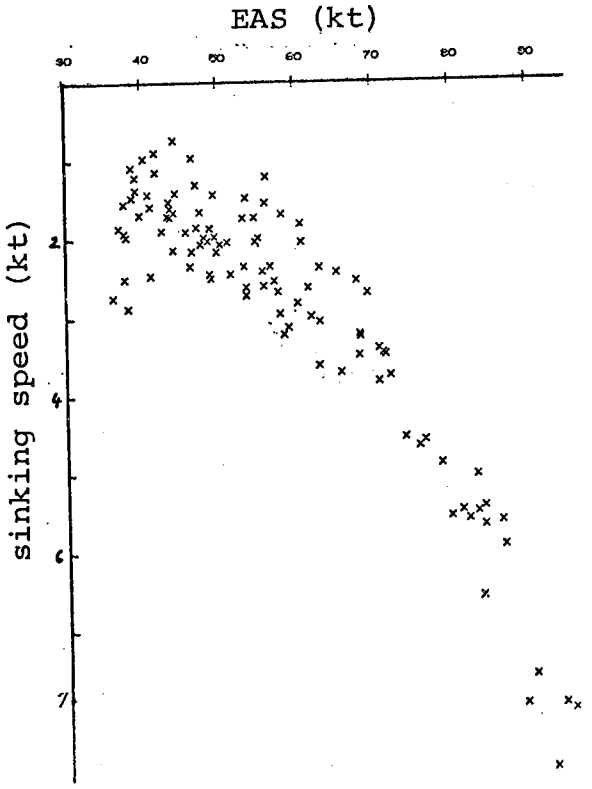


Fig. 4. All Measured Points for the BG 135

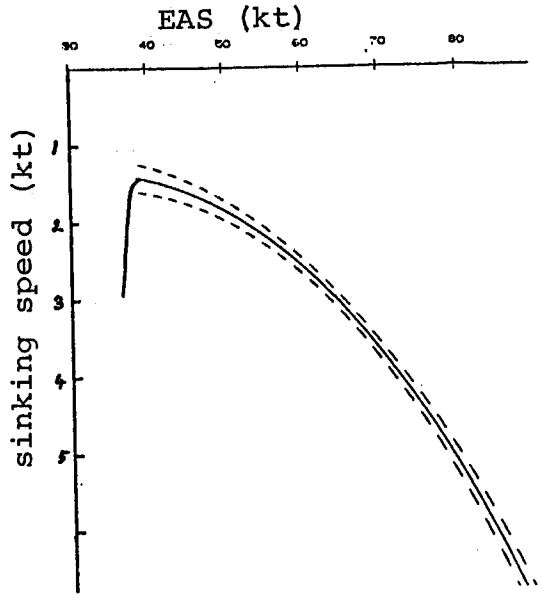


Fig. 5. Fitted Polar of BG 135 With 2-sigma Limits

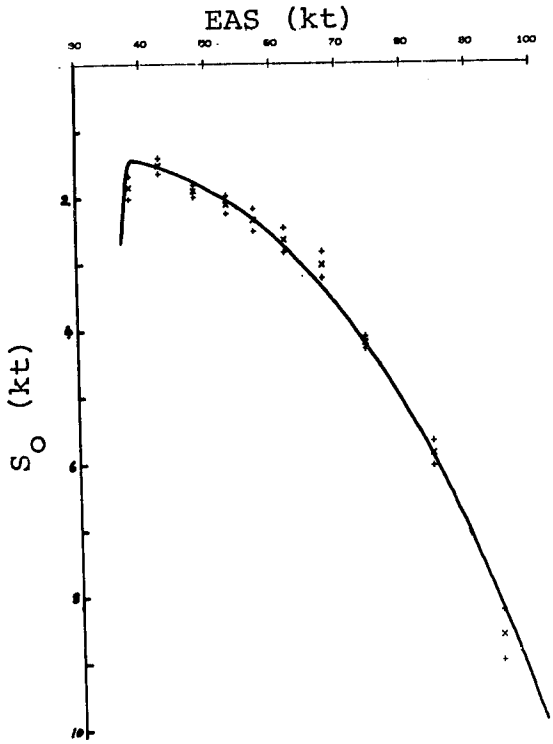


Fig. 6. Five Knot Means cf. Fitted Polar of Fig. 5 (BG 135, AUW=613 lb)

calibrated daily against a water manometer. Air temperature is measured with a mercury thermometer during the climb.

The position error of the glider is measured, on a separate flight, using a trailing static head and an auxiliary pitot head (an open ended tube, usually mounted through the clear vision panel on the canopy). Two A.S.I.'s are used, read manually; one is permanently connected to the aircraft system and the other is switched manually between the aircraft and external pitot and static. Since the glider is sinking, air is flowing from the static head up the long tube to the A.S.I. case; this causes a small error in the measured airspeed, depending on the rate of sink of the glider [4]. This error, typically, 1%, has been allowed for.

All the calibrations, and corrections for air density, are applied by the computer.

Results

Measurements on four gliders, Dart 15R, Skylark 4, Bocian and T53B have already been published [5]. More recently, the SF 25B Falke and the BG 135 have been tested. These are presented below. All the results are corrected to mean sea level, at the A.U.W. given in Table 2.

The BG 135

The BG 135 (Fig. 7) is a small general purpose sailplane built mainly of metal with G.R.P. cockpit shell and wing tips [6,7]. It has a parallel-chord wing, a V tail and a relatively large unfaired fixed wheel.

The sample tested was the prototype; it was in good condition and clean but was not specially polished. The canopy frame at the back was bent, and did not fit very well.

The results are summarised in Table 1, and the polar is shown in Fig. 5. In Fig. 8 the polar of the BG 135 is compared with those of the Dart and the Skylark 4.

The SF 25B Falke

The Falke (Fig. 9) is a two seater motor-glider powered by a 45 H.P STAMO engine.

The main purpose of the tests [8] was to measure the drag of the propeller and engine cooling ducts; thus the performance was measured with the propeller windmilling, stationary and removed, and with the cooling ducts sealed.

Table 1. Summary of Results

Type	Minimum sinking Speed (kts)	at (kts)	Best Gliding Angle	at (kts)	C_{D_o}	k
Dart 15R	1.47 ± 0.07	46.5	31.7 ± 1.2	50	.0113 ± .0006	1.25 ± .09
Skylark 4	1.27 ± 0.07	40	31.5 ± 1.5	40	.0142 ± .0006	1.14 ± .1
Bocian	1.76 ± 0.09	40	24.8 ± .8	50	.0131 ± .001	1.58 ± .13
T53B	1.91 ± 0.06	40	22.6 ± .5	50	.0167 ± .001	1.465 ± .08
BG 135	1.42 ± 0.1	39	28.1 ± 1.4	44	.0165 ± .0003	1.165 ± .13
SF 25B Falke Configuration						
a) Engine idling	2.08 ± 0.12	34	18.6 ± 0.6	44	0.0261 ± 0.0009	1.177 ± 0.100
b) Prop.horizontal	2.07 ± 0.08	34	18.3 ± 0.4	43	0.0273 ± 0.0008	1.151 ± 0.070
c) Prop. vertical	2.04 ± 0.09	34	18.1 ± 0.4	43	0.0295 ± 0.0010	1.087 ± 0.080
d) Prop. off					0.0224 ± 0.0008	1.199 ± 0.070
e) Prop. off & cooling sealed					0.0231 ± 0.0010	1.238 ± 0.087
d) and e)	2.06 ± 0.06	35	19.6 ± 0.3	47	0.0227 ± 0.0006	1.218 ± 0.050
b), c), d) and e)	2.06 ± 0.04	34				1.169 ± 0.030

Type	Wing Area (ft^2)	AUW (lb)	Aspect Ratio
Dart 15R	134.8	780	18.0
Skylark 4	173	840	20.5
Bocian	215.3	1160	16.2
T53B	194	1190	15.9
BG 135	101	613	19.3
SF 25B Falke	188	1190	13.4

Table 2. Leading Particulars of the Aircraft Tested

Configuration	From C_{D_o}	From C_D at 50 Kts	Calculated Value
Engine idling	0.0034 $^{+0.0010}_{-}$	0.0028 $^{+0.0012}_{-}$	
Prop. horizontal	0.0046 $^{+0.0010}_{-}$	0.0040 $^{+0.0009}_{-}$	0.0061
Prop. vertical	0.0068 $^{+0.0012}_{-}$	0.0053 $^{+0.0009}_{-}$	0.0084
Prop. windmilling at 50 kts (600 rpm)		0.0089 $^{+0.0015}_{-}$	0.0098
Internal cooling drag	< 0.0010		0.0008

Table 3. Propeller Drag Coefficient

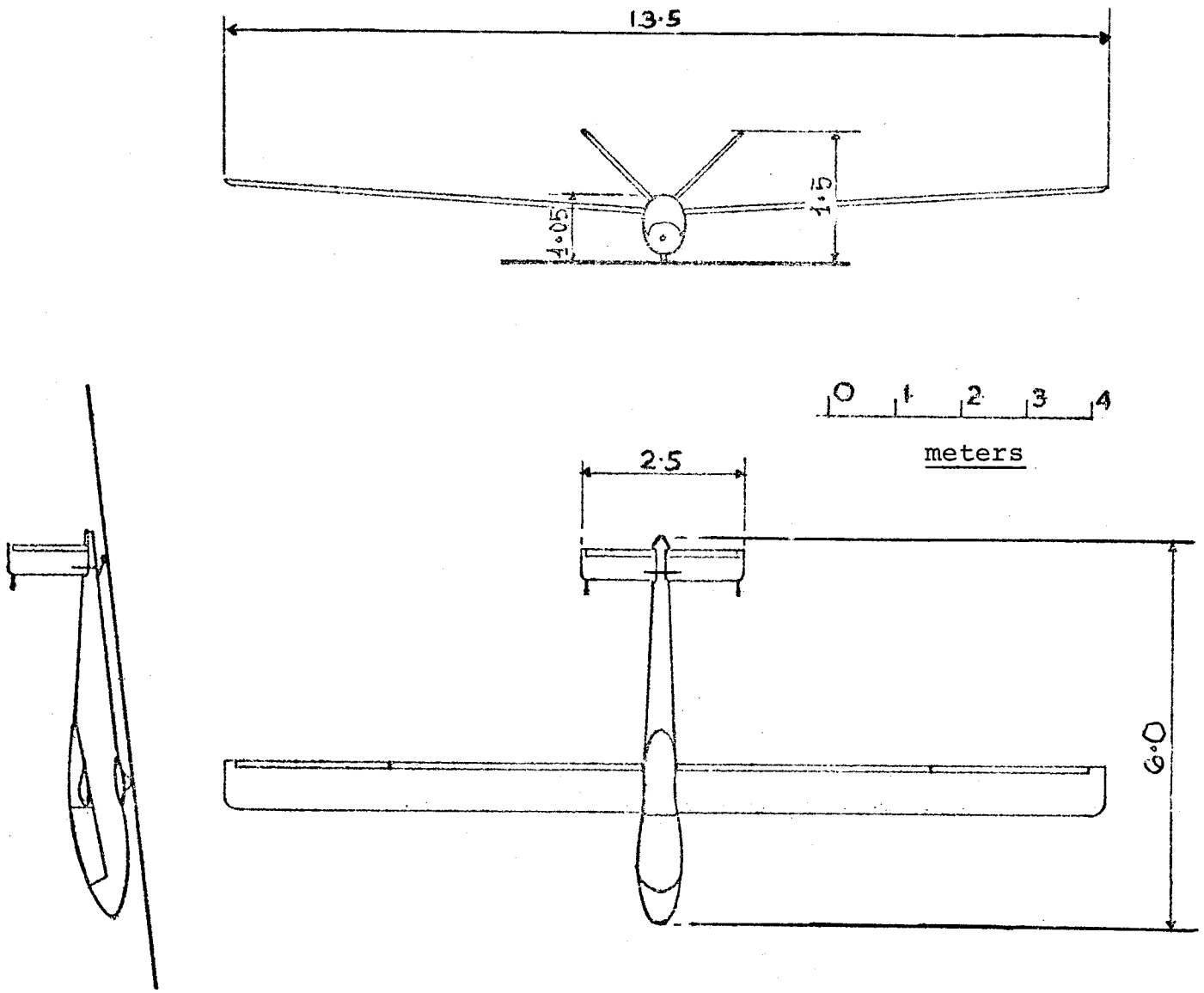


Fig. 7. G.A. of the BG.135

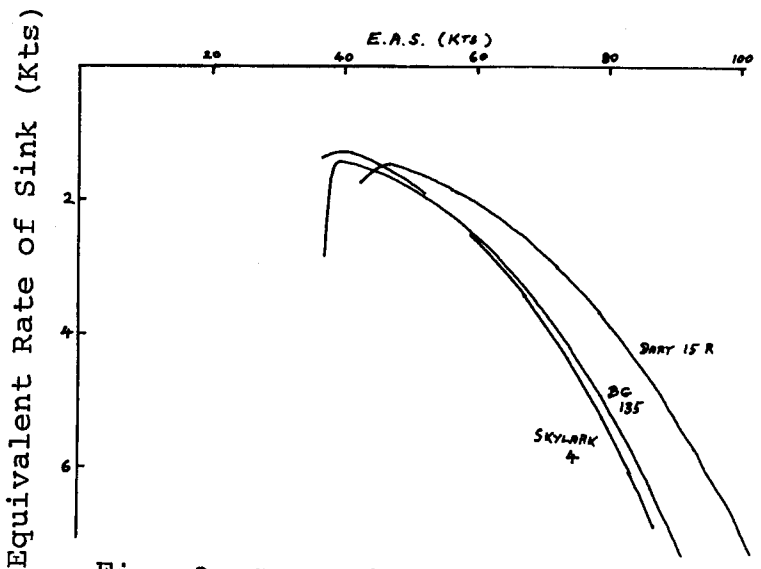


Fig. 8 Comparison of Polars

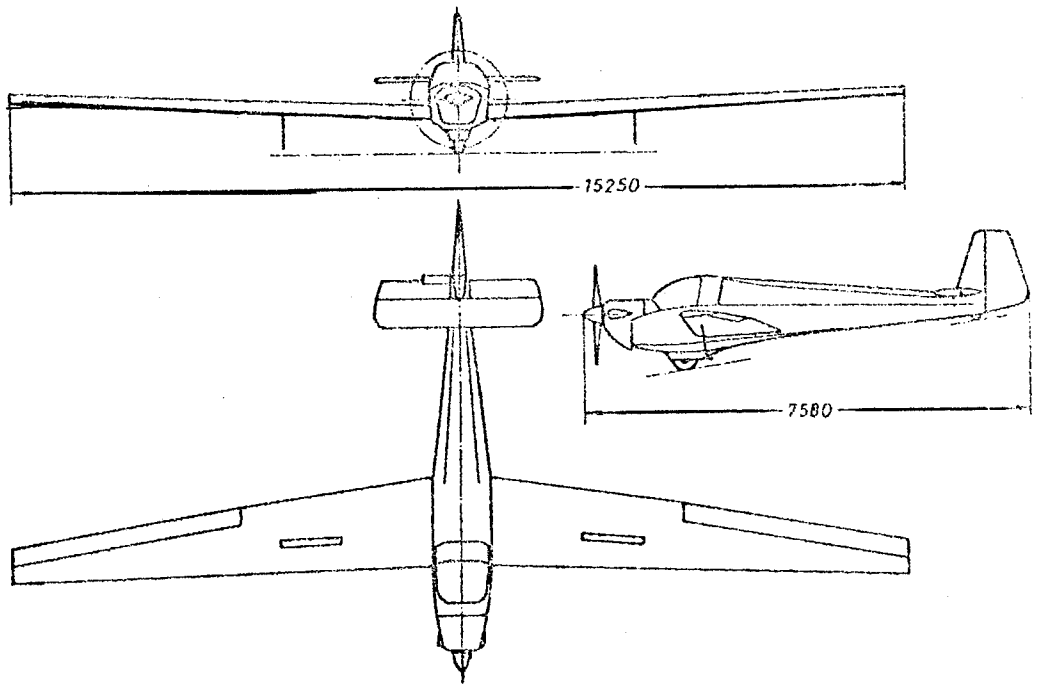


Fig. 9. G.A. of the Scheibe SF25B Falke

The polars are shown in Fig. 10, and summarised in Table 1. The propeller drag derived from these measurements is given in Table 3, and compared with that calculated from Hoerner [9].

Clearly the Falke is not a very good glider, as one would expect from its low aspect ratio and lack of aerodynamic refinement. Performance has been sacrified for convenience, and the result is an excellent trainer.

The drag of the propeller is surprisingly high, considering its small size (a 5 ft propeller on a 50 ft span aircraft). At high speeds it contributes 10% of the drag of the whole aircraft. The cooling drag was much lower, and was not detectable in the tests. Clearly a feathering or folding propeller is necessary on a high performance motor-glider, but blanking of the cooling ducts is less important.

Hysteresis in glider performance

During a discussion of glider performance at Oberwolfach in 1971, Walter Stender recalled that, when measuring the top speed of powered aircraft in 1935, a higher speed could be maintained if the aircraft were first dived and then allowed to slow down to the level maximum speed. He suggested that I should examine my results to see whether the performance of a glider at a given speed depended on the direction from which the speed was approached.

My normal test of a glider consists of about 100 partial glides at different speeds, taken in a random order. I sorted them into two groups; "increasing speed", where the previous partial glide was slower than the one considered; and "decreasing speed" where the previous run was faster. These two groups were then used separately to derive the polar of the glider. Fig. 11 shows the two polars of the Bocian 1D, with error limits at two standard deviations. It is apparent that at high speed the best performance is obtained by increasing the speed to the test speed, while at low speed it is better to slow down to the test speed. A similar effect was observed with the Skylark 4 and SF 25B Falke (without propeller), but not with the Dart 15R, T53B or BG 135 sailplanes (Fig. 12). Whenever the effect is observed it is always in the same direction, and the crossover speed is about 55 kts (30 m/s).

It is possible that the effect is due to systematic errors, either in the flying techniques, or the measuring system, since the "increasing speed" group contains many more high speed points than the "decreasing speed" group (Fig. 13). But it is difficult to imagine such an error affecting only half the gliders tested. The effect is small, typically 5% in rate of sink, which is comparable with the accuracy of the measurements; so it cannot be considered as proven. More measurements are needed.

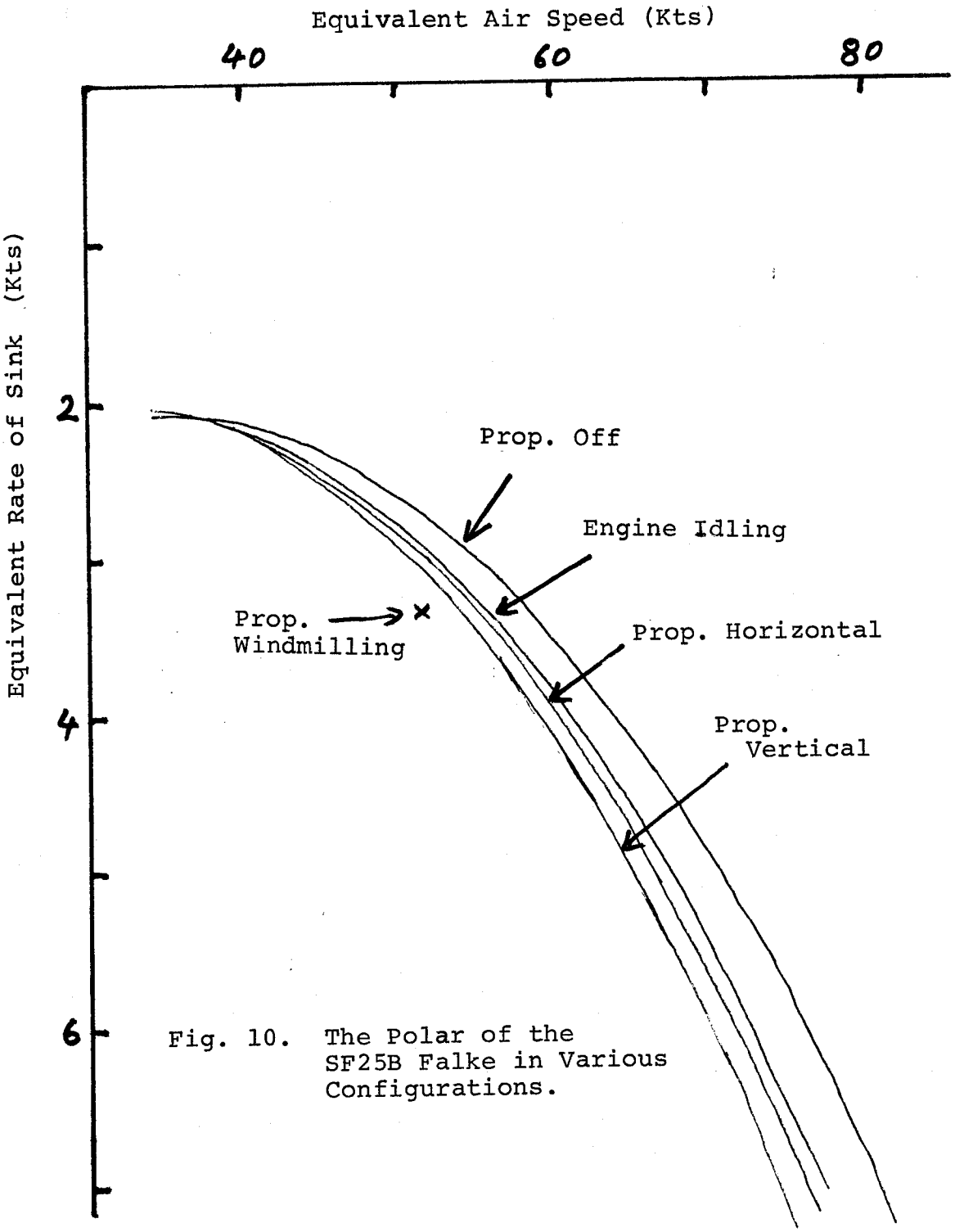


Fig. 10. The Polar of the SF25B Falke in Various Configurations.

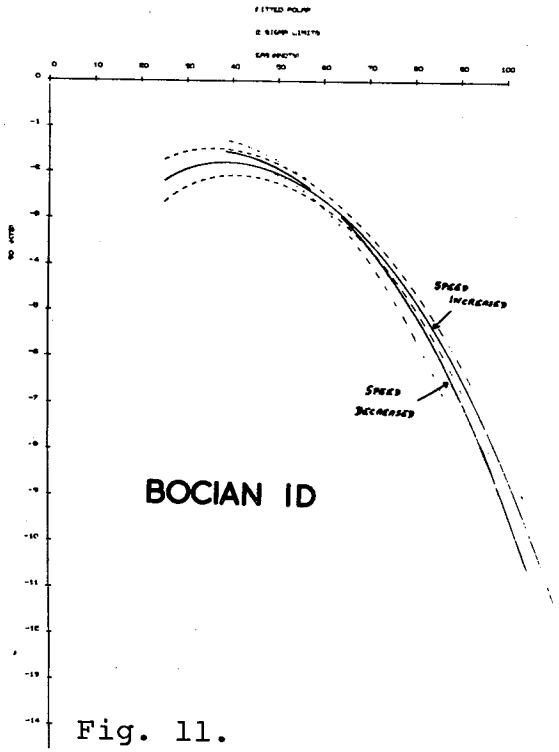


Fig. 11.

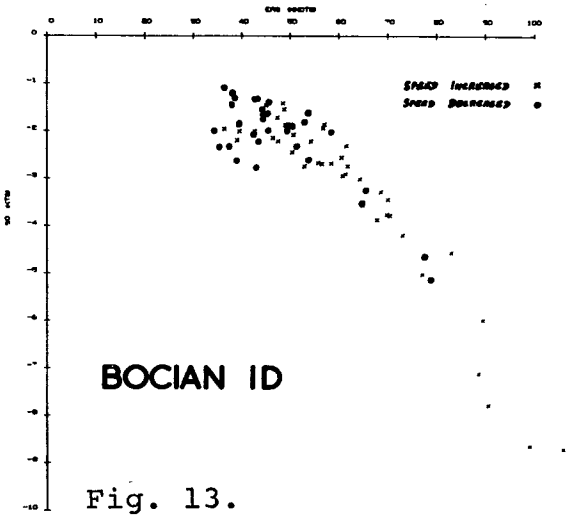


Fig. 13.

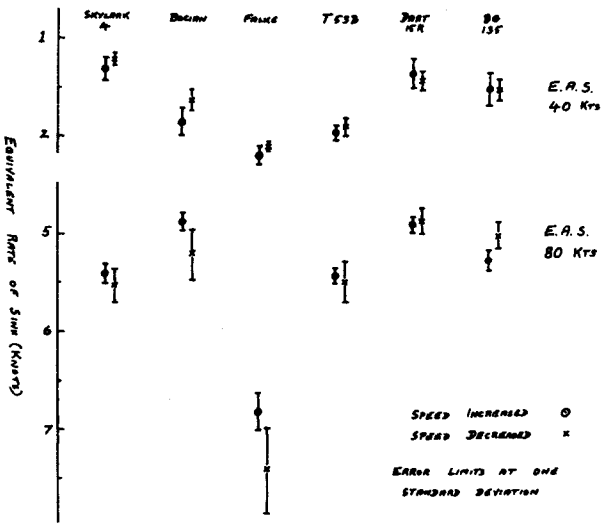


Fig. 12.

Hysteresis in Performance

Fig. 11. The Two Polars of the Bocian ID.

Fig. 12. Rates of Sink of Six Aircraft at 40 Kts and 80 Kts.

Fig. 13. The Points used to Derive the Polars of Fig. 11.

References

1. Irving, F.G.; Performance Tests By BGA Flight Test Groups, Gliding Vol. 2, p.7, Spring 1951.

2. Machin, K.E.; The Performance Testing of the Slingsby Sky, J.Roy. Aero. Soc., Vol. 58, p.470, July 1954.

3. Whitfield, G.R.; A Simple Data Recording System with Computer Analysis, Radio and Electronic Engineer, Vol. 40, pp. 255-258, November 1970.

4. Machin, K.E.; The Effect of Lag in Pitot-Static System, BGA No. 2 Flt.Test Gp., Rep. No. 5, British Gliding Assoc., London, 1954.

5. Whitfield, G.R.; Automatic Recording and Analysis for Glider Performance Testing, 12th OSTIV Congress, Alpine, 1970. Also Aero Revue, April 1972, pp. 203-206.

6. Procter, R.G.; Flying the BG 135, Sailplane and Gliding, Vol. 23, pp. 235-237, June-July 1972.

7. Moore, L.P.; Completion of the Programme, Sailplane and Gliding, Vol. 23, pp. 237-238, June-July 1972.

8. Whitfield, G.R.; Performance Testing the SF 25B Falke, 13th OSTIV Congress, Vrsac, 1972.

9. Hoerner, S.F.; Fluid Dynamic Drag, 2nd Ed. Published by the author, Midland Park, New Jersey, 1964, pp. 13-22 and 13-27.

SOME FLIGHT TESTS ON SELF-LAUNCHING SAILPLANES

by

Hans Zacher
DFVLR, München-Riem, Germany

Introduction

Self-launching sailplanes (SLS's) have proved themselves; there are 500 training and high performance machines flying in Germany. The increase is due mainly to the availability of usable powerplants, but also to the acknowledgement that SLS's are used abroad. The author has reported on the philosophy and purpose of SLS's at the OSTIV Congres in Junin, Argentina (1963) [2] as well as technical characteristics; this report was updated and published in Holland [3]. Table 5, taken from that publication, lists almost all the SLS's which have been developed and flown in Germany.

There has been a lengthy preoccupation in several places with the question of what a SLS is. Table 1 presents a selection of different requirements, (corresponding to "definitions") set by particular organizations, which have been brought to the attention of the FAI [4]. The official requirements, which are primarily concerned with flight safety, depart understandably from competition requirements in many ways. One can nevertheless be thankfull that the Luftfahrt-Bundesamt (Federal Aviation Office) in Braunschweig left plenty of room in its "Guidelines" [1] for technical development, and so encouraged SLS's in this manner. Unfortunately the Sporting Commissions have all too often wished for a very strict definition of SLS's; if this definition were applied to gliders themselves, nearly all training machines would lose their licenses.

The technical development of SLS's has been accomplished without government support, and even working against the resistance of aero clubs and/or soaring associations. The industry, some groups, and certain individuals have succeeded, nonetheless, in creating a new aircraft at a time when a reduction in airspace is desired, even though not strictly necessary.

Work is still in progress on specifications and requirements. The requirements should be based on the "Guidelines". Since it is important that the performance and characteristics of SLS's be measured and verified, the DFVLR section for sailplanes and light aircraft has assumed responsibility for SLS's (since 1962). Measurements have been made of performance, flight characteristics, propeller thrust, fuel consumption,

	maximum weight (kg)	climbing speed (m/sec)	minimum speed (km/h)	glide ratio	sinking speed (m/s)
ARB England	750	1.25	75	1:20	-
FAA USA	-	1.00	-	1:20	1.0
FAI CIVV	750	1.25	75	1:20	-
LBA Germany	700	1.25	(65)	-	1.5
L+A Switzerland	600	1.25	60-65	1:20	1.0
ČSSR	600	1.50	65	1:17	1.5

Table 1.

Powered glider "Definitions" of different organizations. (January 1970)

noise, and so on at SLS meets and trials; evaluation formulas have been investigated. Over and above this, precise flight tests have been carried out on individual aircraft. Fortunately other establishments have concerned themselves with similar investigations, (see, for example, Whitfield at Reading University (England) [5]).

Flight tests

In connection with the flight tests of the D 36 glider and other aircraft [6] (further bibliography in the cited reference) it should be mentioned that partial glide sinking speed as well as climbing speed tests were made for SLS's. The climbing speed curves are limited to full throttle or maximum permissible engine speed limits, the sinking speed curves to locked propeller or covered propeller operation. Performance with idling propellers was only determined in certain cases because the results show more scatter than usual (possibly because of the idling rotation speed change with cooling down of the engine). Comprehensive tests and calculations, such as those carried out by Whitfield [5] on one machine in a praiseworthy manner, were rejected by us in favor of tests on many machines. All climbing speed polars are presented with altitude as a parameter. The measured points are corrected to a payload of 90 kg(or 180 kg for two seaters). The sinking speed polars are also corrected for 90 kg (or 180 kg, correspondingly), but only for sea level air density.

Description and data

The aircraft selected for test purposes were not specially chosen; the examples which were tested were those which were available. In this way SLS's were proven in the fullest sense of the word. Concerning these aircraft, the following points should be noted:

RF-3

Built in 1964, with more than 1200 hours, not especially good condition. Wood construction - measured ceiling ≃ 4900 m, measured cruising speed ≃ 175 km/h.

RF-5

Built in 1970. Two examples existed, both in good condition. Measured ceiling over 5000 m, measured cruising speed ≃ 185 km/h.

SF 25 B Falke (Falcon)

Built in 1969. Apparently well repaired after an accident. Wooden wing, steel-tube fuselage. Measured ceiling ≃ 4900 m, measured cruising speed ≃ 145 km/h.

SF 27 M

Built in 1969. Good condition. Wooden wing, steel tube fuselage. The minimum climbing flight conditions were not available. The sinking speed polar was evaluated by correcting tests on the SF 27 A for the new wing loading.

Krähe (Crow)

For data see Table 5, and the pictures in refs. [2], [3].

Motorspatz (Motorsparrow)

For data see Table 5, and the pictures in ref. [2].

ASK-14

For data see Table 5.

SF 25 A. Motorfalke (Motorfalcon)

Predecessor of SF 25 B. Data in Table 5. Shoulderwing, different powerplant than the B model.

Results

Figs. 5-8 and Table 2 present the essential results from the performance tests. Fig. 5 gives the climbing speed as a function of flight speed with altitude as a parameter. The figure serves as an example of the scatter of the data points. Figs. 6 and 7 contain the sinking speed and climbing speed for the four aircrafts. In Fig. 3 the sinking speed polars of the four SLS's are compared with those of two sailplanes, the SF 27 A and the well-known Ka 6CR (all machines at 90 kg, or correspondingly, 180 kg loading and at sea-level air density). Air brakes are indicated by BK (Bremsklappen).

Table 3 presents a collation of the important flying qualities. Table 4 shows take-off and performance measurements which were obtained from SLS tests held at Leutkirch and Feuerstein from 1962 through 1970. Average and extreme values are included; these show that the current guidelines may be met, at contests, either with high weight or without special skill (the practical case). The stated climb and sinking speeds correspond rougly to those which were measured in precise altitude step interval flights; they correspond to the average values for different examples of one type at altitudes between 500 and 1500 m.

Conclusions

From a great number of measurements at contests, comparative flight trials, and altitude step test flights the most important results have been extracted. They present a picture of a broad region between high performance sailplanes (SF 27 M) on down to training and school aircraft (RF 5). The "Guidelines" laid down by the Luftfahrt-Bundesamt and also by the sport organizations as minimum performance definitions may be regarded as fulfilled.

References

1. LBA-Mitteilung 10.05: Vorläufige Richtlinien für die Prüfung und Zulassung von Motorseglern (14.4.1967).

2. Zacher, H.; Die Entwicklung von Motorseglern in Deutschland. Vortrag Junin (Argentinien) 1963. OSTIV-Publication VII.

3. Zacher, H.; Ueber die Entwicklung des Motorseglers. Lucht- en Ruimtevaarttechniek 3 (Holland, Dec. 1971).

4. FAI-CIVV: Sporting Code, Sect. 3, Class D: Gliders (1971).

5. Whitfield, G.; Glider Performance Testing with Results of Tests of the Motorglider Scheibe SF 25 Falke. Noch nicht veröffentlicher Vortrag beim Euromech 26, Oberwolfach 1971.

6. Laurson, H. and Zacher, H.; Fluguntersuchungen mit den Segelflugzeugen D 36, BS 1 und ASW-12. Vortrag Leszno (Poland) 1968. OSTIV-Publication X (more references in this publication).

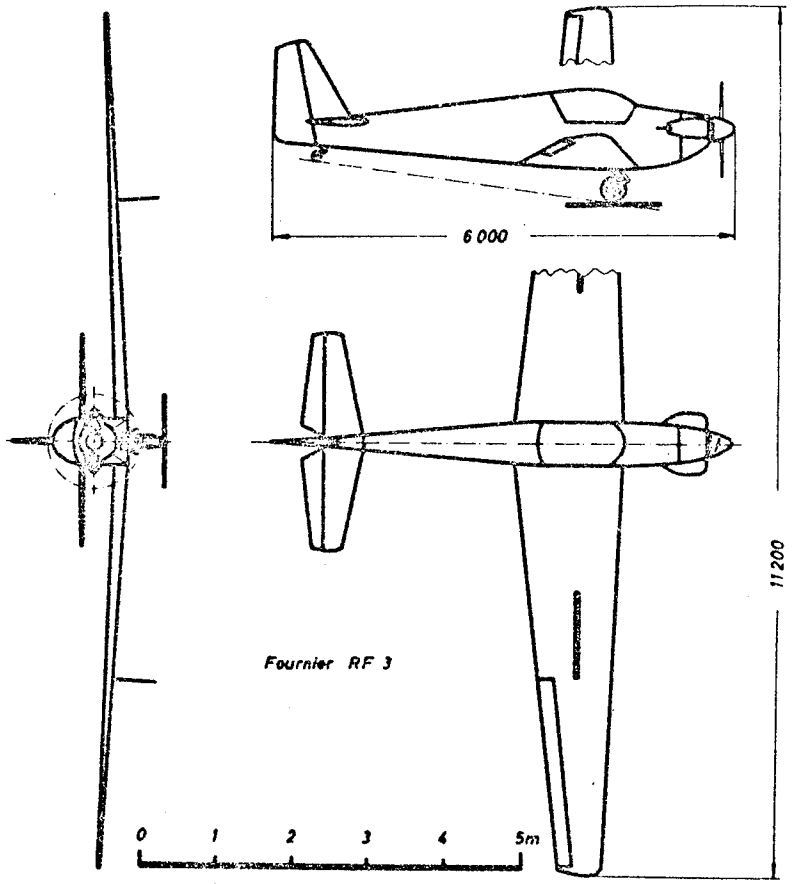


Fig. 1. Single seater SLS RF 3.

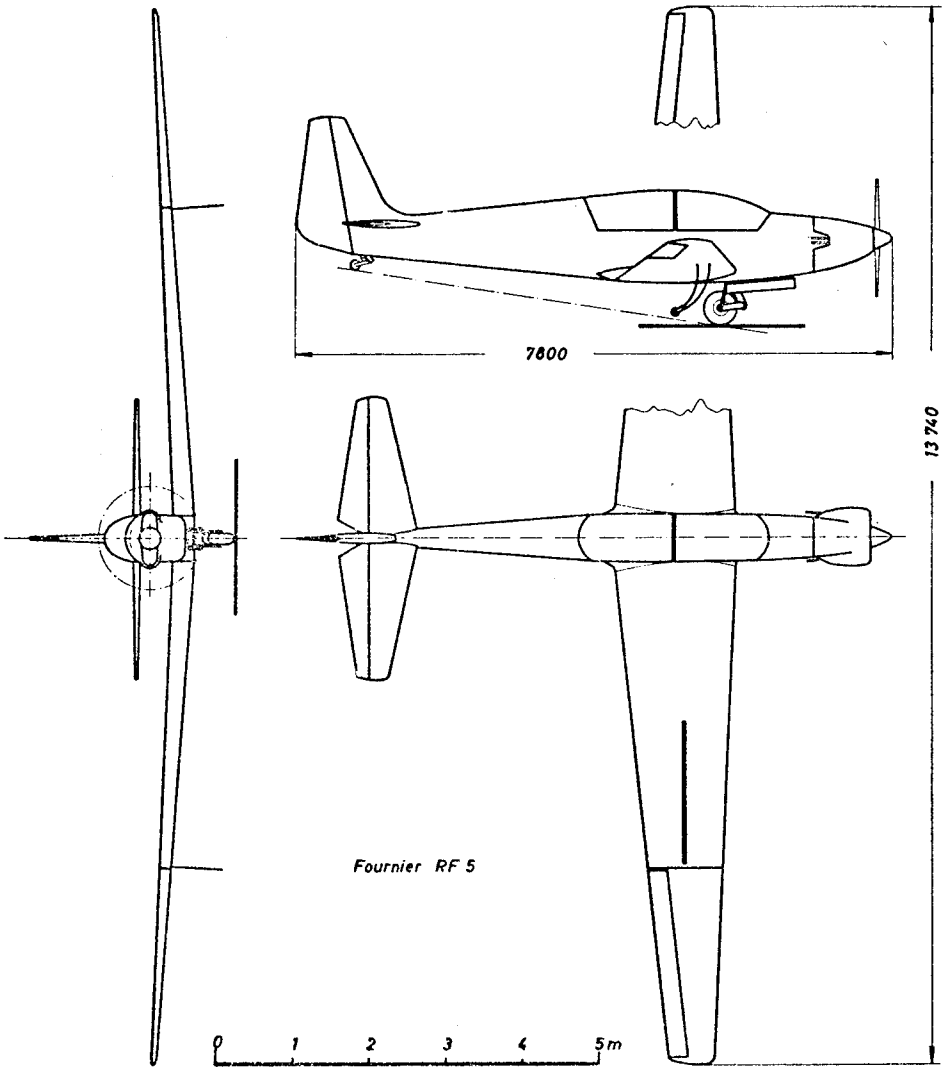


Fig. 2. Two seater SLS RF 5.

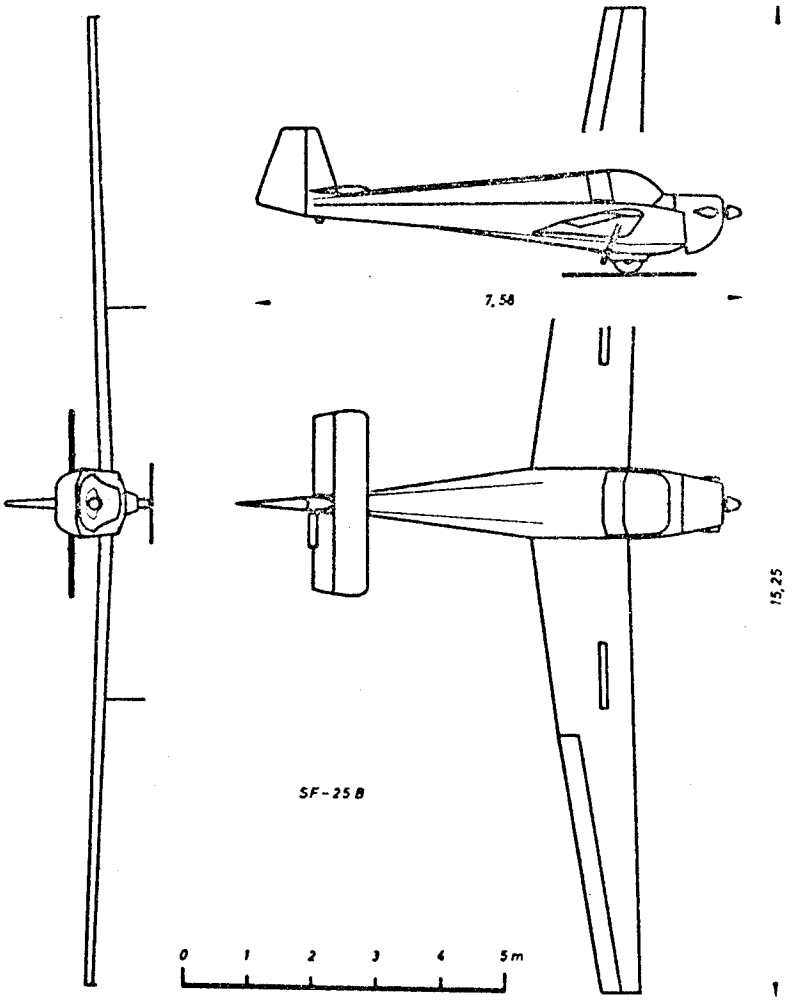


Fig. 3. Two seater SLS SF 25 B.

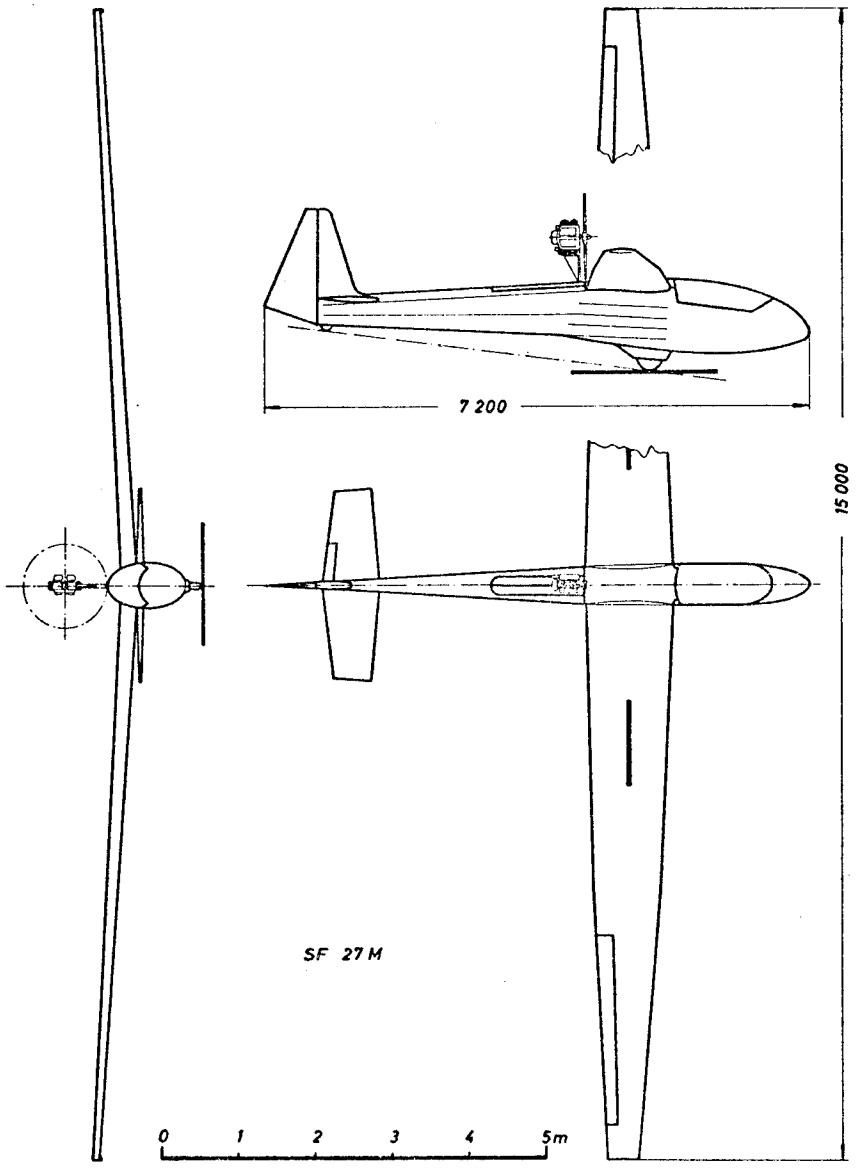


Fig. 4. Single seater SLS SF 27 M.

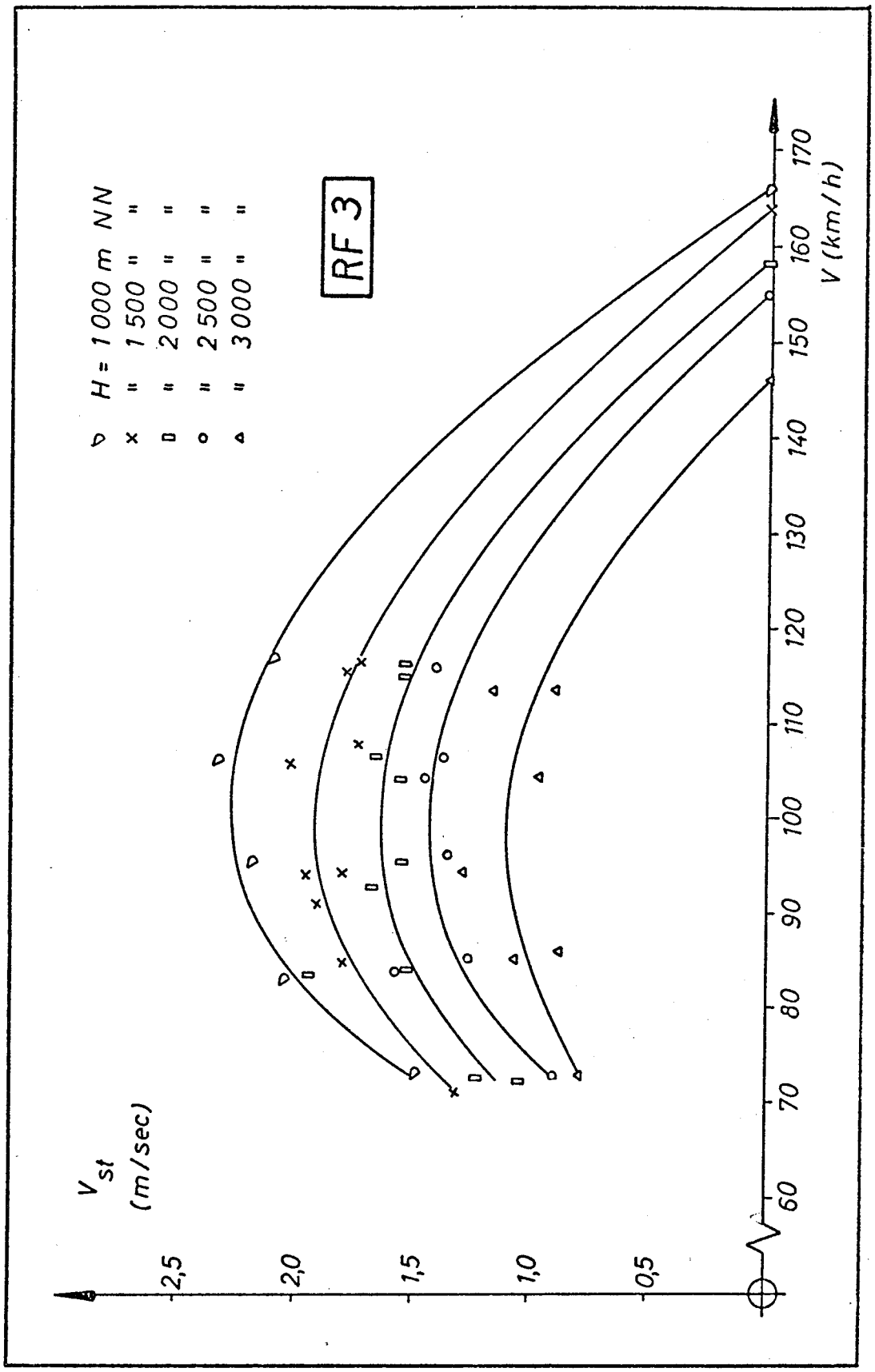


Fig. 5. Climbing speed polars of the RF 3 with data points at different altitudes (example).

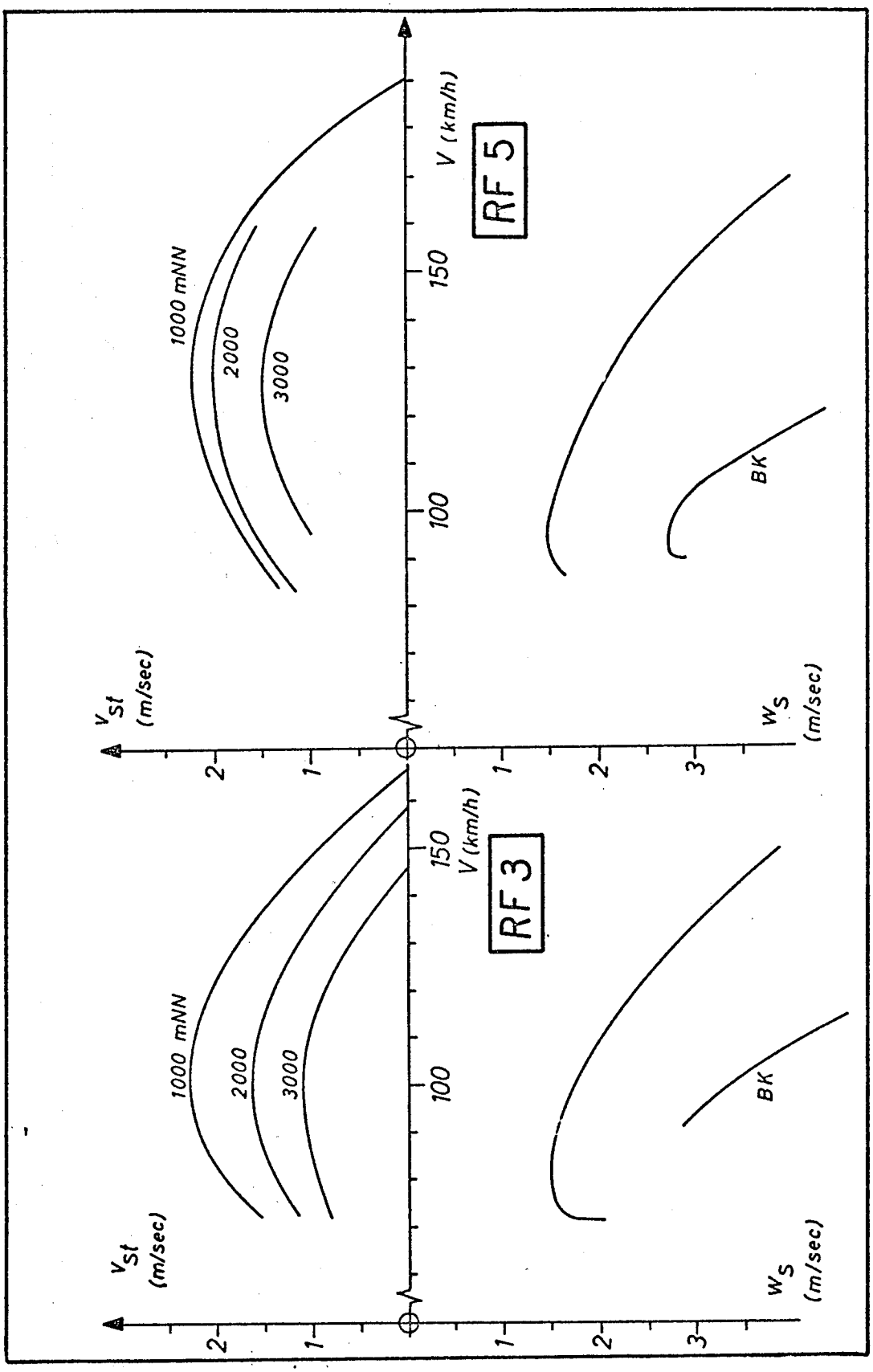


Fig. 6. Climb and sinking speed polars of the RF 3 and RF 5.

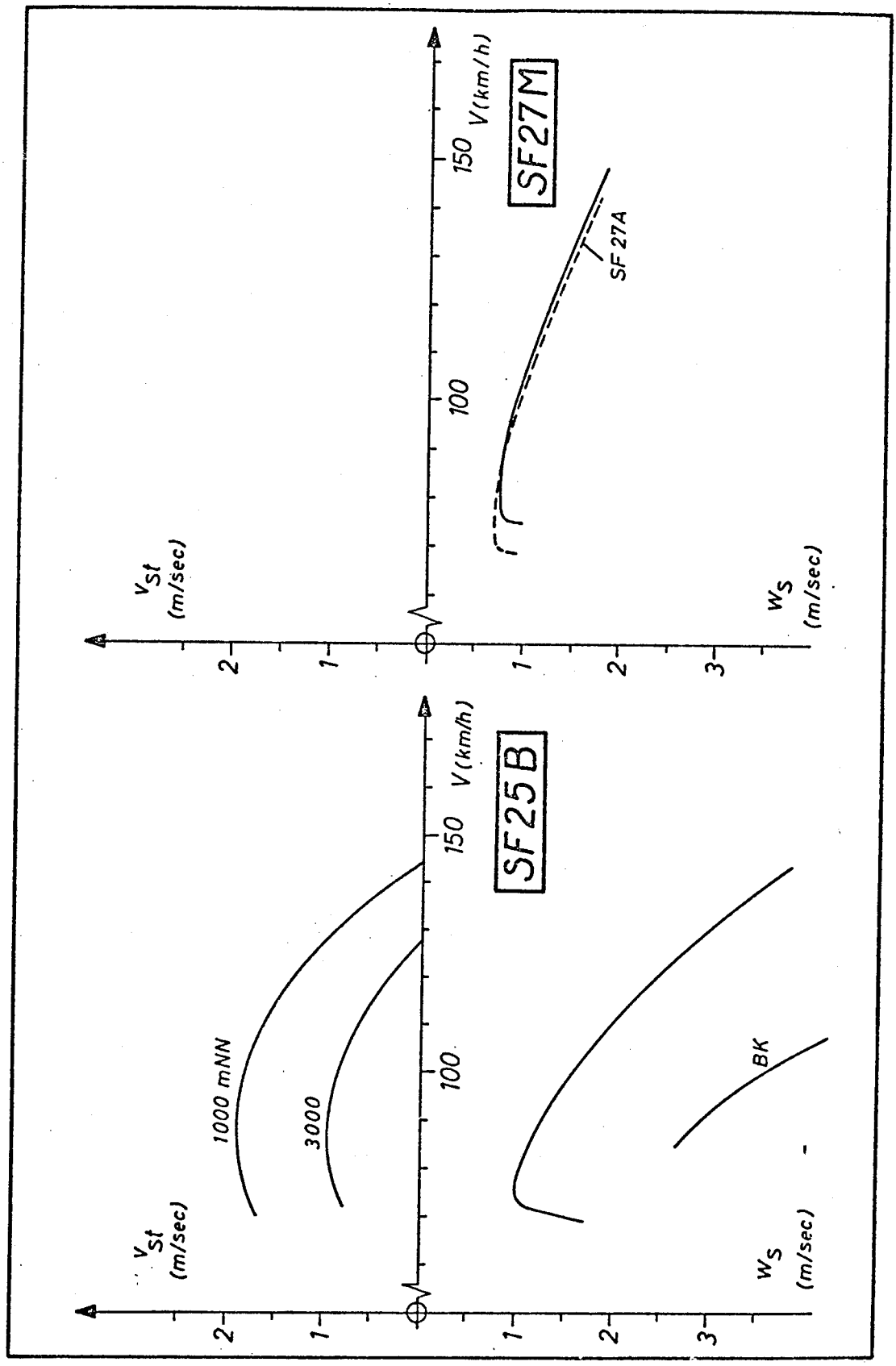


Fig. 7. Climb and sinking speed polars of the SF 25 B and SF 27 M.

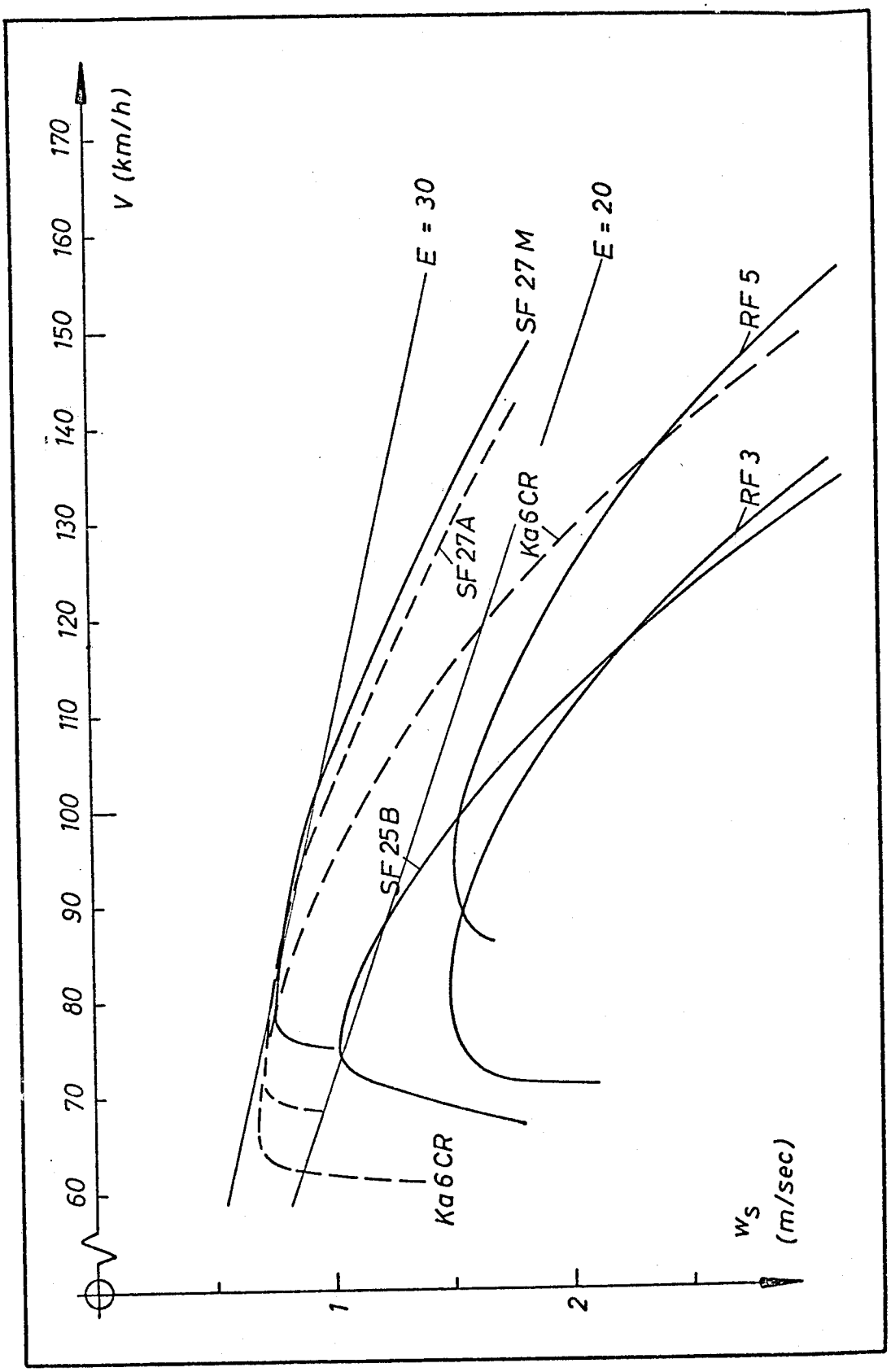


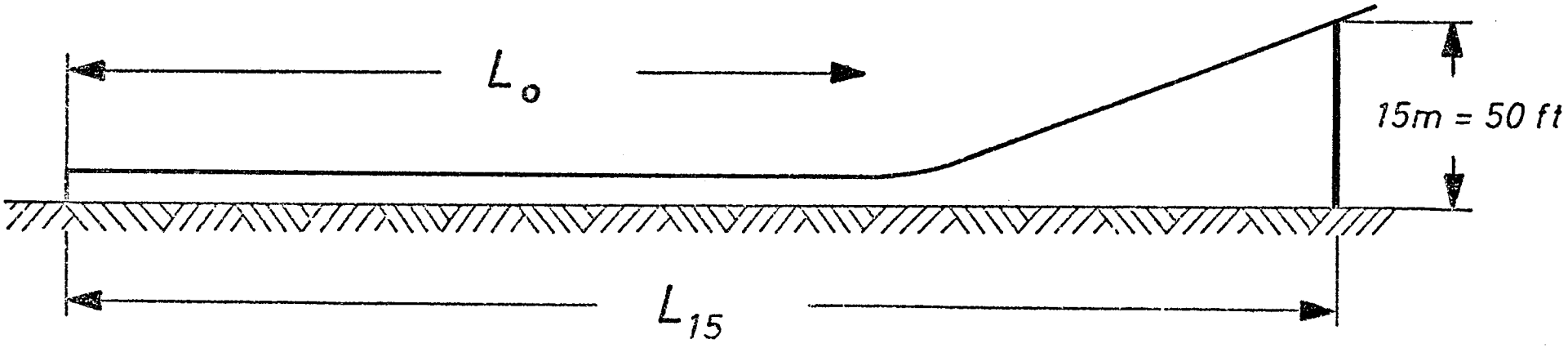
Fig. 8. Sinking speed polars of four SLS's compared to two sailplanes.

Type	Profile	Span m	wing area m^2	aspect ratio (no units)	empty weight kg	flying weight kg	wing loading kg/m^2	minimum speed km/h	minimum sinking speed at V (m/sec)	(km/h)	best glide ratio at V (no units)	(km/h)	sinking speed at V (sinking speed in m/sec) V = 100 km/h	120 km/h	150 km/h	engine	climbing speed in m/sec at V(km/h) at altitude H(m)
RF 3	NACA 23015 23012	11.2	11.0	11.4	280	370	33.7	71.3	1.49	80.5	16.1	94.0	1.74	2.37	4.0	Rectimo 4AR1200 39 PS	2.3 100 in 1000 m
RF 5	NACA 23015 23012	13.7	15.1	12.5	470	650	43.0	86	1.52	95	18.0	105	1.56	1.92	2.9	LimBach SL1700E 68 PS	2.3 125 in 1000 m
SF25B	Mü 14%	15.3	17.5	13.4	360	540	31.0	67.2	1.02	75	21.1	81	1.65	2.55	-	Stamo MS 1500 45 PS	1.9 88 in 1000 m
SF27M	FX 61-184 60-126	15.0	12.1	18.6	280	370	30.5	75	0.77	83	31	95	0.92	1.28	(1,9)	Hirth F10A1a 26 PS	(1.6) 105 in 1000 m
for comparison																	
SF27A	FX 61-184 60-126	15.0	12.1	18.6	222	312	25.8	68	0.70	75	31	87	0.95	1.33	(2.0)	-	-
Ka6CR	NACA 63_3-618	15.0	12.4	18.1	185	275	22.2	61	0.68	67	29	78	1.13	1.70	3.05	-	-

Table 2. Data and performance values for SLS's (with comparative values for two sailplanes) at 90 or 180 kg loadings.

	RF 3	RF 5	SF 25 B	SF 27 M	for comparison Ka 6 CR
Cockpit	good, good visibility	fairly good, good visibility	average, (tight for 2 people), very good visibility	very good, good visibility	average, somewhat uncomfortable, fairly visibility
Stalling behavior	abrupt wing down, but controllable	wing down, controllable	wallowing without pitching	gentle wing down	mushes, controllable
Maneuverability in normal flight	very good, good response, fairly airbrakes	very good good response moderate airbrakes	good moderate response fairly airbrakes	good good response good flaps	good good response fairly airbrakes
Slip	not useful	moderately useful	moderately useful	useful	useful
Air starting	through diving with compression release	electrical starter	mechanical pull cord or diving at 140 km/h	mechanical pull cord	-
Turn reversal time +45°roll to -45°roll at 1.4 V_{min}	3.2 sec	3.7 sec	5.2 sec	3.8 sec	4 sec

Table 3. Flying qualities of powered gliders.



(Requirement, 600 m = 2000 ft)

Type	Weight kg	Output hp	Take-off L_o (m)	Take-off L_{15} (m)	climbing speed m/s	sinking speed m/s
Krähe	340	23.0		440...750		
Motorspatz	345	25.0		300...850		
SF 27 M	370	26.0	210...260	410	1.60	0.70
ASK 14	360	26.0				
RF 3	350	39.0	200	340	2.30	1.50
RF 4	390	39.0	160...200	300...410	1.75	1.40
Motorfalke SF 25 A	490	25.0	120...200	320...480	1.25	1.20
Falke SF 25 B	540	45.0	120...240	300...430	1.80	1.00

Table 4. Measurements at SLS contests 1962-1970.
Field height = 600 m.

type	supplier	year	wing span (m)	wing area (m2)	aspect ratio	empty weight (kg)	flying weight (kg)	powerplant	nominal power	wing loading kg/m2	power loading kg/hp	self-launching	seats
Mü 13	Akaflieg München	1937	16	17	15.3	175	285	Kroeber M4	18.0	16.8	15.8	yes	1
C 10	Akaflieg Chemnitz	1940	12.5	12.0	13.0	170	300	Kroeber M4	18.0	25.0	16.7	yes	1
Hi 20 "Mose"	Hirth, Nabern	1942	14.8	18.7	11.7				20.0			yes	1
LK 10 A	Eilers, Bremen	1956	15.2	15.7	14.8	310	395	Lloyd 400 cm^3	12.0	25.2	33.0	no	1
AV 36 CM	Bölkow, München	1958	12.0	14.3	10.0	158	240	Solo	12.0	16.9	20.0	no	1
Dohle I	Pützer, Bonn	1956	13.2	18.0	9.7	300	420	Lloyd LP 400	13.5	23.4	31.0	no	1
Dohle II	Pützer, Bonn	1957	13.2	18.0	9.7	325	450	Ilo F2 376	24.0	25.0	18.0	yes	1
Illerfalke I	Obermeier, Illertissen	1956	19.0	21.2	17.1	310	500	AVA 4A	25.0	23.6	20.0	no	2
Illerfalke II	Obermeier, Illertissen	1962	19.0	21.2	17.1	370	550	Brändl ZB 700	30.0	26.0	18.4	yes	2
Motorraab B	Neulen, Oberhausen	1957	13.7	18.6	10.0	405	625	STAMO 1400 B	42.0	33.7	14.9	yes	2
P 77	Sterz, Augsburg	1956	14.4	16.8	12.2	250	350	AVA 4A	25.0	20.8	14.0	yes	1
Mü 23	Akaflieg München	1960	20.0	24.0	16.7	475	600	various types	(30.0)	25.0	(20.0)	yes	2
SP 1 - WM	Wezel, Reutlingen	1959	10,0	9.3	10.8	190	300	Wezel WR 3 G	25.0	32.2	12.0	yes	1
Krähe I	Raab, München	1957	12.0	14.4	10.0	230	340	Brändl ZB 300 S	18.0	23.6	14.2	yes	1
Krähe II	Raab, München	1961	12.0	14.4	10.0	230	340	Brändl ZB 300 SG	23.0	24.0	14.8	yes	1
Krähe V6	Raab-Blessing, Hamburg	1960	11.8	14.0	10.0	246	340	Pollmann HEPU 40/3500	40.0	24.3	8.5	yes	1
Motorspatz A	Scheibe, Dachau	1957	14.1	11.8	16.7	220	340	Brändl ZB 300 S	18.0	28.8	18.9	yes	1
Motorspatz B	Scheibe, Dachau	1962	14.1	11.8	16.7	225	345	Solo 560	25.0	29.2	13.8	yes	1
La 16	Landmann, Dresden	1961	12.5	12.5	12.5	170	275	Kroeber M 4	18.0	22.0	16.3	yes	1
La 17	Landmann, Dresden	1961	13.0	20.4	8.3	228	420	Zschopau BK 350	15.0	20.6	28.0	no	1
MS 60	Pützer, Bonn	1961	15.5	16.0	15.0	410	520	Ilo F2 376	30.0	32.6	17.3	yes	1
H 30 TS	Hütter-Kensche-Allgeier, Uhingen	1961	15.0	9.5	23.5	240	370	BMW 8026 turb.	(45 kp)	39.0	(8.2 kp/kp)	yes	1
SF25A Motorfalke	Scheibe, Dachau	1963	16.6	17.7	15.5	300	(460)	Sole 560 A	25.0	(26.0)	(18.4)	yes	2
SF25B Falke	Scheibe, Dachau	1967	15.3	17.5	13.4	335	530	STAMO 1400 C	45.0	30.3	11.8	yes	2
SF 27 M "Illerschwalbe"	Scheibe, Dachau and Obermeier, Illertissen	1966	15.0	12.0	18.7	250	380	Solo-Hirth F 10	26.0	31.7	14.6	yes	1
K11 Lückenbüsser	Kaiser, Poppenhausen	1964	12.8	12.6	13.1	200	310	Solo	25.0	24.6	12.4	yes	1
K12 - ASK 14	Schleicher, Poppenhausen	1967	14.3	12.6	16.2	230	360	Solo-Hirth F 10 A	26.0	28.6	13.9	yes	1
MS 65	Blessing-Gomolzig, Wuppertal	1965	15.5	16.0	15.0	420	520	STAMO 1400 S	45.0	32.5	11.6	yes	1
K 8 B Stihl	Bruns, Münster	1965	15.0	14.2	15.9	205	310	Stihl SK 120	7.0	21.9	44.2	no	1
K 8 B Wankel	Fichtel & Sachs, Schweinfurt	1967	15.0	14.2	15.9	200	310	KM 48 Wankel	10.0	21.9	31.0	no	1
K 8 B - 2 M'	Hennigs, LSV-Detmold	1968	15.0	14.2	15.9	220	310	Stihl SK 120/137 Fi	2x7	21.9	22.0	yes	1
Ka 6 Stihl	Bruns, Münster	1969	15.0	12.4	18.1	210	310	Stihl SK 120/137 Fi	8.5			no	1
RF 3	Pützer, Dahlemer Binz	1963	11.2	11.0	11.4	240	350	Rectimo 4 AR 1200	39.0	31.8	9.0	yes	1
RF 4	Pützer, Dahlemer Binz	1966	11.2	11.0	11.4	265	390	Rectimo 4 AR 1200	39.0	35.4	10.0	yes	1
RF 5	Pützer, Dahlemer Binz	1968	13.8	15.1	12.3	380	650	Rectimo AR 1600	68.0	43.0	9.6	yes	2
K 7 Stihl	Auweiler, Köln	1968	16.0	17.5	14.6	320	480	Stihl SK 120	2x10.0	27.4	24.0	no	2
Gleitermax	Blessing, Hamburg	1968	15.3	18.5	12.7	490	690	Porsche	52	36.0	13.0	yes	1
SFS 31	Pützer, Scheibe	1969	15.0	12.0	18.7	310	420	Rectimo 4 AR 1200	39.0	35.0	10.8	yes	1
D 37	Akaflieg Darmstadt	1969	18.0	13.0	24.8	329	445	Wankel KM 914	18.0	34.0	24.7	no	1
Sirius	Rhein-Flugzeugbau	1969	17.5	13.8	22.0	290	400	Nelson	43.0	29.0	9.3	yes	1
fs 26	Eppler-Akaflieg Stutt.	1971	12.6	13.2	12.1	250	360	Solo-Hirth F 10 A	26.0	27.2	13.8	yes	1

Table 5. A compilation of data on German SLS's.

A COMPARISON OF CLASSICAL DRAG ESTIMATION TECHNIQUES WITH SAILPLANE FLIGHT TEST RESULTS

by

William E. Brown
Beech Aircraft Corporation
Wichita, Kansas

Notation

A	aspect ratio $A = \frac{b^2}{S}$
b	wing span (ft)
B	constant in Brown equation for e (5)
C_D	drag coefficient $C_D = \frac{D}{qS}$
C_{D_f}	fuselage frontal area drag coefficient
C_{D_i}	induced or lift-varying drag coefficient
C_{D_o}	profile or non-lift-varying drag coefficient
C_{D_t}	tail drag coefficient
C_{D_w}	wing profile drag coefficient
C_f	wetted area drag coefficient
C_L	lift coefficient $C_L = \frac{L}{qS}$
D	drag (lb)
e	span efficiency factor
f	equivalent flat plate area (ft^2)
K	constant in Brown equation for e (5)
L	lift (lb)
q	dynamic pressure $q = 1/2\ \rho V^2$ (lb/ft^2)
ρ	air density ($lb\ sec^2/ft^4$)
R	Reynolds number
S	wing area (ft^2)
S_f	fuselage frontal area (ft^2)
S_t	combined tail planform area (ft^2)
V	flight vehicle velocity (ft/sec unless noted)
V_s	sink speed
W	flight weight (lb)

Introduction

Recent flight testing of modern, high performance sailplanes by Bikle [References 1, 2, and 3] has provided accurate experimental data whereby the classical methods of estimating aerodynamic drag can be compared with actual flight test measurements. A study of drag polars generated by conventional methods and compared to Bikle's test data indicates that excellent results can be obtained by the traditional techniques, if a realistic means of estimating the span efficiency factor, "e", is used.

Overly optimistic performance polars are obtained unless the relationship is understood between the span efficiency factor, e, in the rigorously derived drag equation and the span efficiency factor, e, in the equation as it is actually applied.

The drag equations

In the classical drag equation [4], the drag coefficient is broken into two components:

$$C_D = C_{D_o} + C_{D_i} \tag{1}$$

The first component, C_{D_o} accounts for the so-called profile drag. The second component, C_{D_i} represents the induced drag, or drag due to lift. This drag is the result of the lift vector being tilted aft. For wings of elliptical lift distribution this component of drag can be shown to be:

$$C_{D_i} = \frac{C_L^2}{\pi A} \tag{2}$$

For wings of non-elliptical lift distributions, a so-called span efficiency factor [5], e, is applied to account for the added induced drag due to the non-elliptical lift distribution. The induced drag equation then becomes:

$$C_{D_i} = \frac{C_L^2}{\pi e A} \tag{3}$$

The complete drag equation is then:

$$C_D = C_{D_o} + \frac{C_L^2}{\pi e A} \tag{4}$$

Application of the drag equations

In conventional practice there are very important modifications applied to the equations. In any flight vehicle the profile (or parasite) drag also increases with increasing

angle of attack (and lift coefficient). There are many contributions to this increase, notably fuselage drag, trim drag due to the elevator down-load, the wing's increase in profile drag as it comes out of the drag bucket, changing Reynolds number, etc. It is generally more convenient to account for the increase in profile drag with increasing C_L in the induced term, C_{D_i}, than it is in the profile drag term, C_{D_o}, where in properly belongs. We then speak of the first term, C_{D_o}, as representing the non-lift-varying drag and the second term, C_{D_i}, as representing the lift-varying drag. This is a subtle, but profound modification. Indeed it would be sufficient to completely shatter the illusion that the equations have any rigorous theoretical validity if it were not for the fact that they give such excellent results.

The upshot of this modification to the drag equations is that the e values used in them must be lower than would be the case if they were rigorously followed, because e must now account for such things as the airfoil drag bucket, trim drag, induced fuselage drag and all the other lift-varying drag factors. This is why those not intimately familiar with the modifications are shocked when they find that a sailplane which should have nearly perfect elliptical lift distribution has an e value of 0.7 rather than 0.95.

The state-of-the-art for the span efficiency factor

The term, "e", as applied in the modified drag equations, can be shown to be a function of both aspect ratio, and the relative cleanliness of the aircraft. When something is added to "dirty" the aerodynamics, both the non-lift-varying *and* the lift-varying drag are increased. This is shown graphically in Figure 1. The achieved *vehicle* e values vary with aspect ratio in a fairly linear fashion. It can be seen that the curve is displaced as the configuration changes from the super-clean sailplane, to the clean jet airplane, and finally to the relatively dirty propeller airplane.

A state-of-the-art e curve was developed from a study of Bikle's test data [1, 2, and 3], which represents the sailplane e factor in a simple linear relationship with the wing aspect ratio:

$$e = B - K(A) \qquad (5)$$

It is recognized that there are not very many strictly linear relationships in the real world, but for the aspect ratios of interest, in general from 10 to 25, a value of $B = 1.1$ and a K value of 0.016 correlate fairly well with test data. Test derived values for e are shown compared with the curve from equation (5) in Figure 2.

The test points were obtained by measurement of the slope of the test data C_L^2 vs C_D curves taken from Bikle's data. It should be noted that some sailplanes exhibit a nearly linear relationship between C_L^2 and C_D, while others

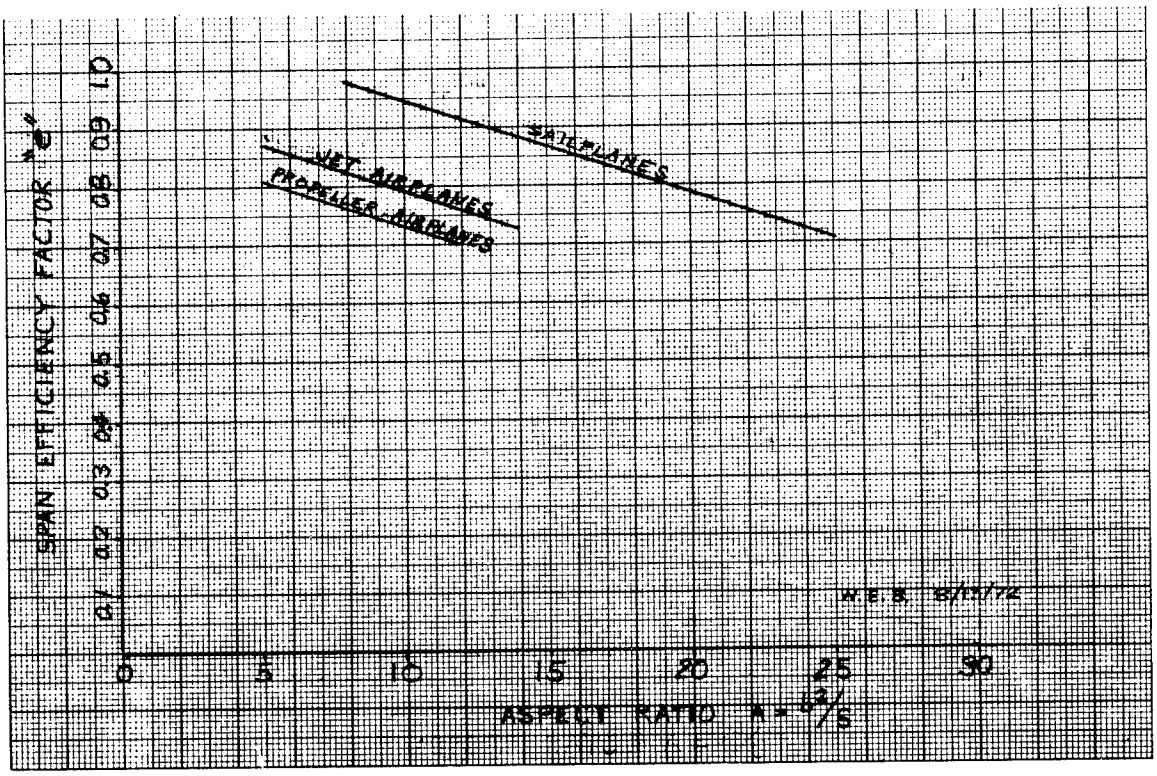


Figure 1. The character of the span efficiency factor.

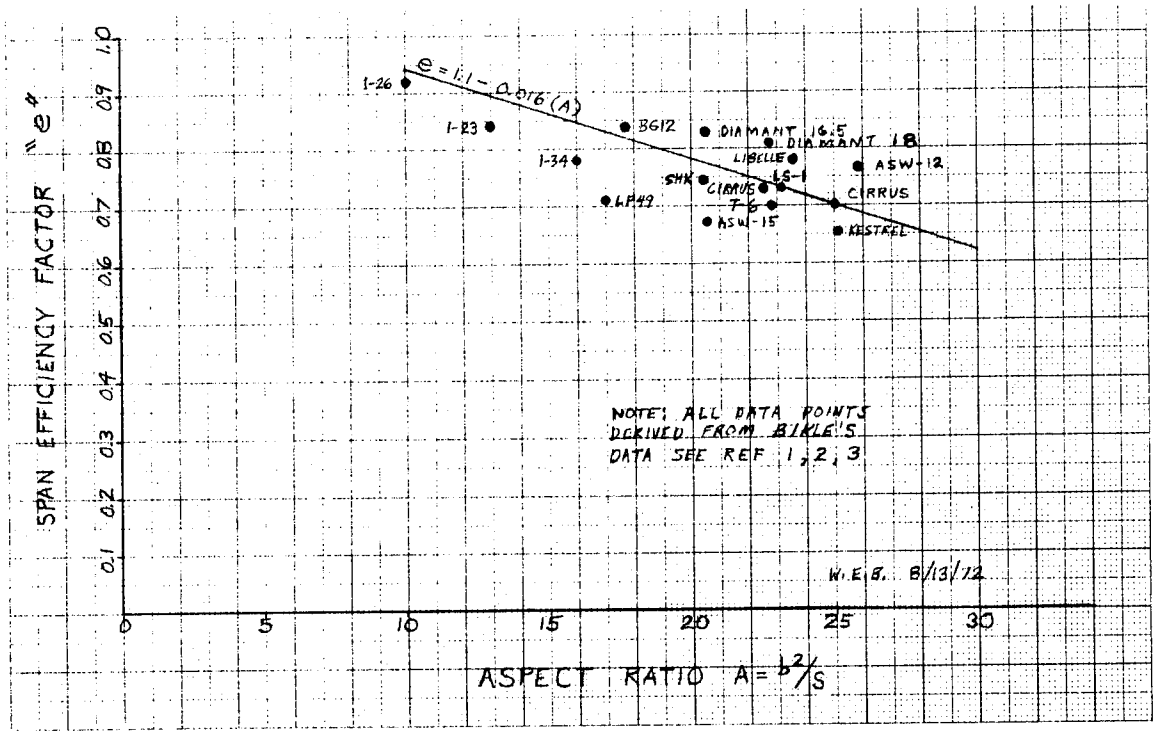


Figure 2. The state of the art for the sailplane "e".

have a break in the curve. This can be seen in the curves for the Phoebus sailplanes in Figure 3, which has been reproduced from Bikle's test results [1]. For such a curve e can only have meaning as an *average* value.

Similarly, the BG-12 does not show a linear C_L^2 vs C_D relationship. This is the weakness of the whole concept of a span efficiency. It should also be remembered that the e values in Figure 2 represent sailplanes of similar configuration. Many sailplanes do not achieve e values this high because of basic design deficiencies. There is also some preliminary evidence that the e values of the super sailplanes are better than would be predicted by the curve in Figure 2. It may be that the state-of-the-art e curve has a shallower slope than K = 0.016. Some judgment should be used in selecting constants for equation 5. If the configuration is extremely efficient (Nimbus, ASW-17) a slope as shallow as K = 0.01 might be achieved. The Diamant curve in Figure 3 shows another common characteristic, namely that at high lift coefficients, the C_L^2 curve becomes non-linear, especially in flapped sailplanes. This results in actual sink speeds being greater than calculated at the low speed end of the polar if a constant value for e is assumed.

It should also be noted that there is a large scatter factor in the e values shown in Figure 2. Since C_L^2 is a function of V^4 this is not surprising. However, it also seems probable that the newer sailplanes are achieving higher span efficiencies. The curve shown in Figure 2 represents a sort of average value of what can be expected. We may expect that in a few years another curve can be added in Figure 1 which we can label "super-sailplanes". It will not be surprising if it is nearly parallel to other curves, but with possibly a slightly shallower slope.

A simple drag build-up method

It is not the purpose of this paper to detract in any way from the more rigorous drag analysis methods. It is hoped that these simple methods, which have been around for nearly 50 years, can be applied in calculating glide performance estimates which can be used in developing pilot glide calculators, instrument speed-to-fly indicators, competition handicapping factors and for other purposes where a more rigorous approach would be impossible. It is recognized throughout the soaring community that achieved flight performance is nearly always less than advertised. As will be seen, calculated polars can be generated which correlate well with test data if realism is used in the drag build-up.

A build-up of non-lift-varying drag is achieved through use of the equivalent flat plate factor, "f". This factor is defined as follows:

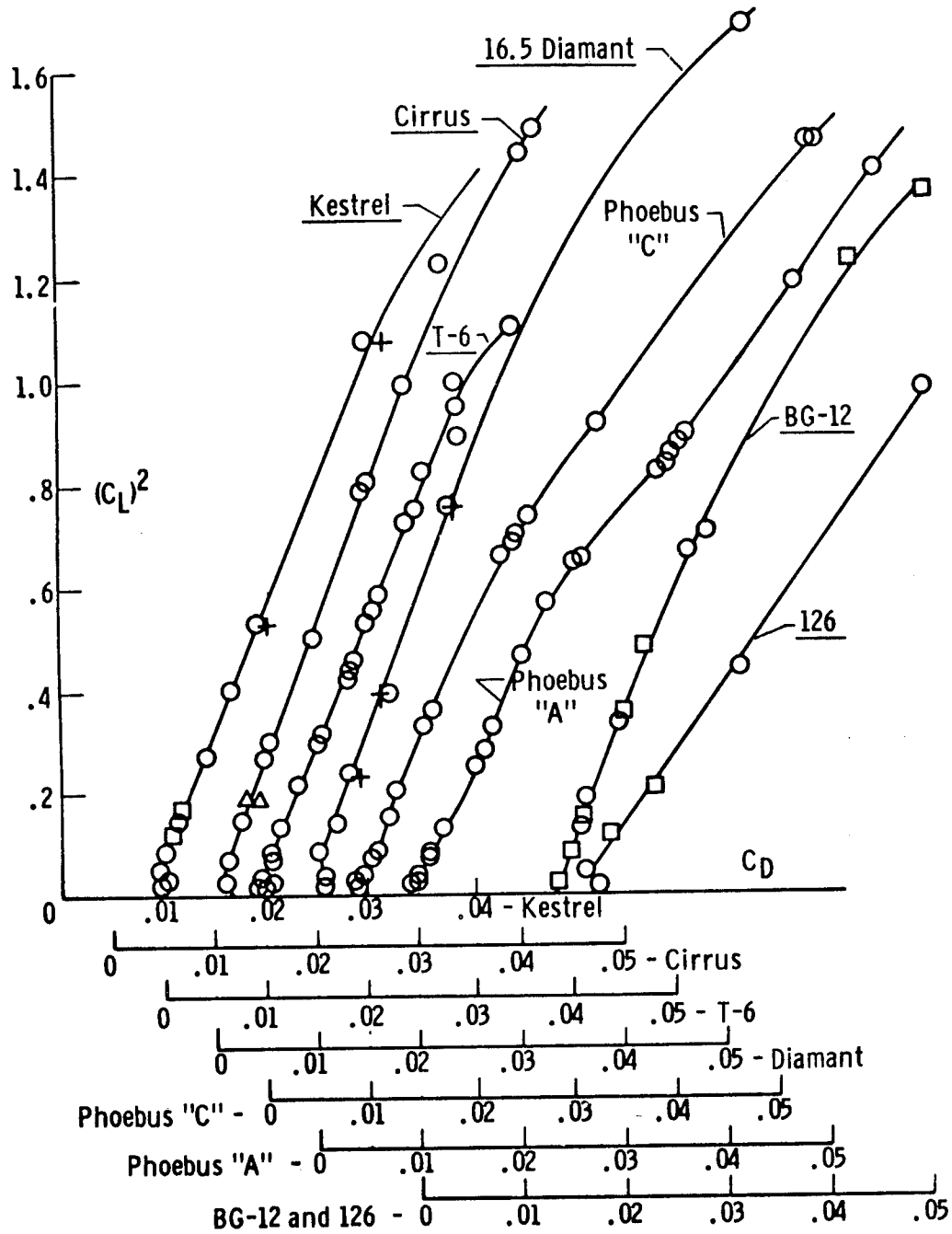


Figure 3. Measured sailplane drag data. Extracted from Bikle, Reference 1.

Figure 3.

$$\Delta f = S_{component} \times C_{D_{component}} \quad (6)$$

Due to the interference of airframe components, the total equivalent flat plate area, f, is equal to more than the sum of the component Δf's. Since sailplanes are highly efficient vehicles, a 5% factor for interference is adequate. The following relationship can be applied:

$$f = 1.05 \times \Sigma \Delta f_{component} \quad (7)$$

A sailplane non-lift-varying drag coefficient, C_{D_o}, is then:

$$C_{D_o} = \frac{f}{S} \quad (8)$$

The component drag coefficients are arrived at as follows:

Wing

$$\Delta f_{wing} = S \times C_{D_w}$$

For the state-of-the-art fiberglass sailplanes using modern sections, C_{D_w} can be as low as 0.005 [6] and as high as 0.006 [7] depending on airfoil section, surface fineness, and Reynolds number. Figure 4, extracted from Reference [8] shows what can be expected from some of the current low drag airfoil sections. This is further borne out in the calculated polars for the Kestrel and Phoebus sailplanes where C_{D_w} = 0.005 was used for the calculated polar with good results. For metal wing construction with careful smoothing Bikle has achieved a C_{D_w} = 0.0055 on the T-6 [1]. The calculated polar for the T-6 based on a C_{D_w} = 0.0055 correlates very well with the test results. The polar for the Cirrus indicates C_{D_w} = 0.006 is being achieved while the Diamant value is slightly higher than this. These are more nearly the values that would be expected for the earlier Wortmann sections [7]. The wing sections for these sailplanes are not known by the author. For the earlier sailplanes with wood or fabric surfaces and older airfoils, the wing C_{D_w} can be based on turbulent flow conditions. The BG-12 NACA 4415/4406 section could be expected to duplicate the best turbulent section properties for the 44 series section seen in Figure 5 which was extracted from Reference [9]. A value of C_{D_w} = = 0.0078 taken from this curve resulted in good correlation between the calculated and measured polars. For the 1-26 C_{D_w} = 0.008, taken from the section data in Reference [10] for the 43012 section, gave good results.

Fuselage

In the simplified approach the fuselage drag estimation is based on frontal area. This is not, perhaps, as accurate as one based on wetted area, but it can be readily calculated

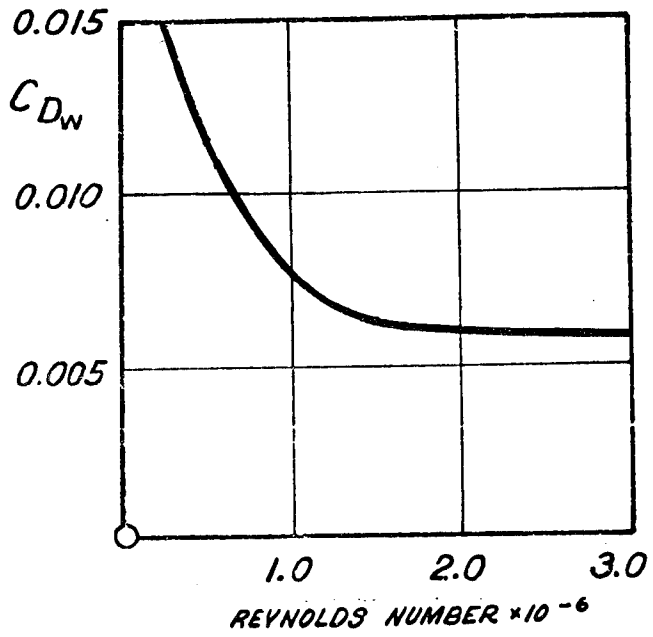


Figure 4. Modern laminar section properties. Extracted from Reference 8.

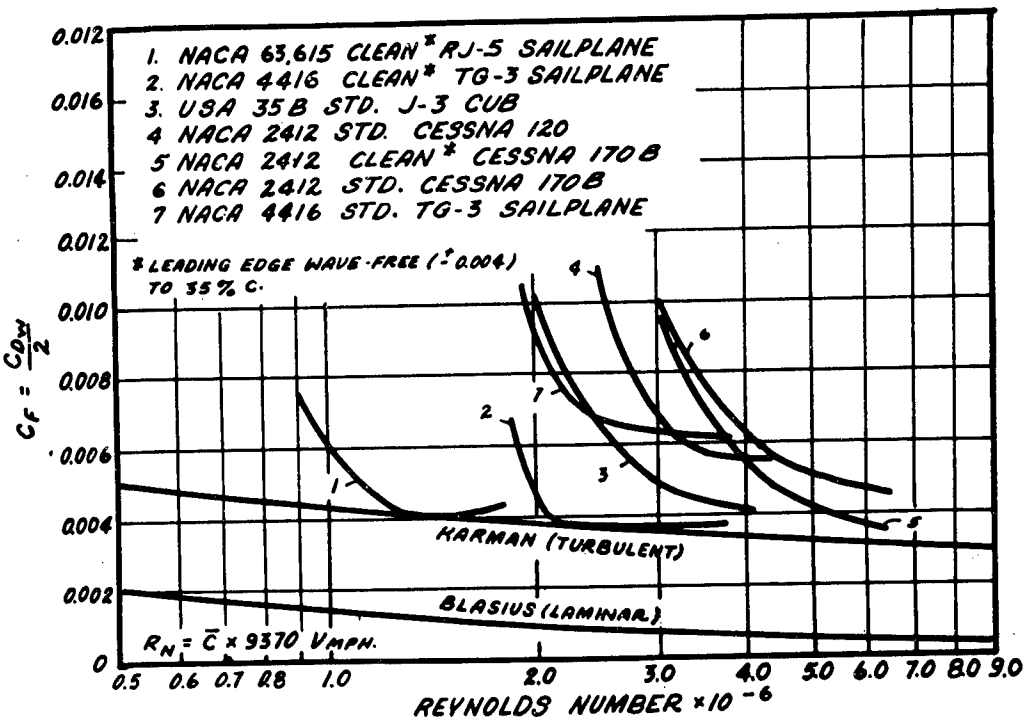


Figure 5. Turbulent section properties. Extracted from Reference 9.

from the three-view drawing. The following applies:

$$\Delta f_{fuselage} = S_f \times C_{D_f}$$

For area calculation the tire should be included if it is not retracted. The following values were used with good results:

Simple construction fuselage, unfaired, non retracting gear	$C_{D_f} = 0.100$
Refined form, retracting or well faired gear	$C_{D_f} = 0.080$
Refined form, retracted gear extreme attention for details	$C_{D_f} = 0.070$

Probably the ultimate fuselage might be able to achieve a $C_{D_f} = 0.060$ but the practical aspects of building canopies, ventilation, landing gear doors, etc., would make this value too optimistic to be applied without good justification.

Tail

For the tail drag build-up the tail planform area is used rather than the wetted area. The following applies:

$$\Delta f_{tail} = S_t \times C_{D_t}$$

A value of $C_{D_t} = 0.006$ correlates well for nearly all types of tail construction. Since the tail drag is a small part of the total drag, further refinement of this value is probably not justified.

Example drag build-up of T-6 sailplane

Component	Area	C_D	Δf
Wing	142.5 ft^2	0.0055	0.784
Fuselage	4.3 ft^2	0.08	0.344
Tail	20.7 ft^2	0.006	0.124
		$\Sigma\Delta f$ =	1.252

$$f = 1.05 \times \Sigma\Delta f = 1.31 \quad (7)$$

$$C_{D_o} = \frac{f}{S} = \frac{1.31}{142.5\ ft^2} = 0.0092 \quad (8)$$

$$A = 22.8$$

$$e = 1.1 - 0.016(A) = 0.73 \quad (5)$$

$$C_D = C_{D_o} + \frac{C_L^2}{\pi e A} \quad (4)$$

For the T-6, the calculated drag curve is:

$$C_D = 0.0092 + 0.019\ C_L^2$$

The calculated polars are then generated using the following relationships:

$$q = 1/2\ \rho V^2 \quad (9)$$

$$C_L = \frac{L}{qS} \quad (10)$$

$$L/D = \frac{C_L}{C_D} \quad (11)$$

$$V_s = \frac{V}{(L/D)} \quad * \quad (12)$$

*With proper attention to units.

To speed the calculations, a simple program was developed for the IBM 1130 computer which permitted the rapid generation of a complete drag polar.

Calculated polars of eight

In addition to the T-6, polars were generated for the other sailplanes measured in Reference [1]. The values applied in the drag build-up are shown in Table 1.

The calculated polars with test points from Reference [1] plotted are found as follows:

1-26	Figure 6
BG-12	Figure 7
Phoebus A	Figure 8
Phoebus C	Figure 9
Cirrus	Figure 10
Cirrus with ballast	Figure 11
T-6	Figure 12
Kestrel	Figure 13
Diamant 16.5	Figure 14

The curves were only plotted to a $C_L = 1.2$ at the low speed end as experience has indicated the actual sink above this C_L is higher than the curve predicts so that the curve no longer represents the sailplane to any useful degree.

TABLE 1 INPUT PARAMETERS FOR CALCULATED DRAG POLARS

Sailplane	(1) SPAN ft	(1) A	(1) S ft^2	(3) S_f ft^2	S_t ft^2	(1) W lb	C_{D_w}	C_{D_f}	C_{D_t}	Remarks
1-26	40.0	10.0	160	6.56	32.5 (3)	593	.008	.10	.006	43012 Section Properties from Ref. 10
BG-12	50.0	17.7	141	4.50	25.95 (2)	828	.0078	.08	.006	Section Properties from Ref. 9
Phoebus A	49.2	17.3	139.7	4.70	30.86 (2)	711	.005	.08	.006	E403 Section
Phoebus C	55.8	20.6	151.2	4.40	30.86 (2)	769	.005	.07	.006	E403 Section
Cirrus	58.2	25.0	135.6	4.37	23.7 (2)	878	.006	.08	.006	Section assumed early Wortmann
Cirrus with Ballast	58.2	25.0	135.6	4.37	23.7 (2)	1093	.006	.08	.006	"
T-6	57.0	22.8	142.5	4.29	20.7 (1)	810	.0055	.08	.006	FX 61-163 (Mod) data from Ref. 1
Kestrel	55.7	25.1	123.7	3.70	25.7 (3)	803	.005	.07	.006	Section assumed late Wortmann
Diamant 16.5	54.2	20.54	143	3.48	20.5 (3)	864	.006	.08	.006	Section assumed early Wortmann

DATA SOURCE CODE: (1) Ref. 1 (2) Ref. 11 (3) Scaled from Drawings

TABLE 2 CALCULATED VS MEASURED MAXIMUM GLIDE PERFORMANCE

Sailplane Type	Calculated Max. L/D	Measured Max. L/D
1-26	22.9 @ 41.5K	21.5 @ 42K
BG-12	30.6 @ 47.5K	31.0 @ 50K
Phoebus A	34.3 @ 48K	34.0 @ 48K
Phoebus C	37.9 @ 48K	37.5 @ 49K
Cirrus	36.7 @ 50K	37.0 @ 50K
Cirrus with Ballast	36.7 @ 56K	37.0 @ 55K
T-6	37.7 @ 48K	36.3 @ 48K
Kestrel	39.6 @ 52K	38.0 @ 52K
Diamant 16.5	36.6 @ 51K	38.5 @ 51K

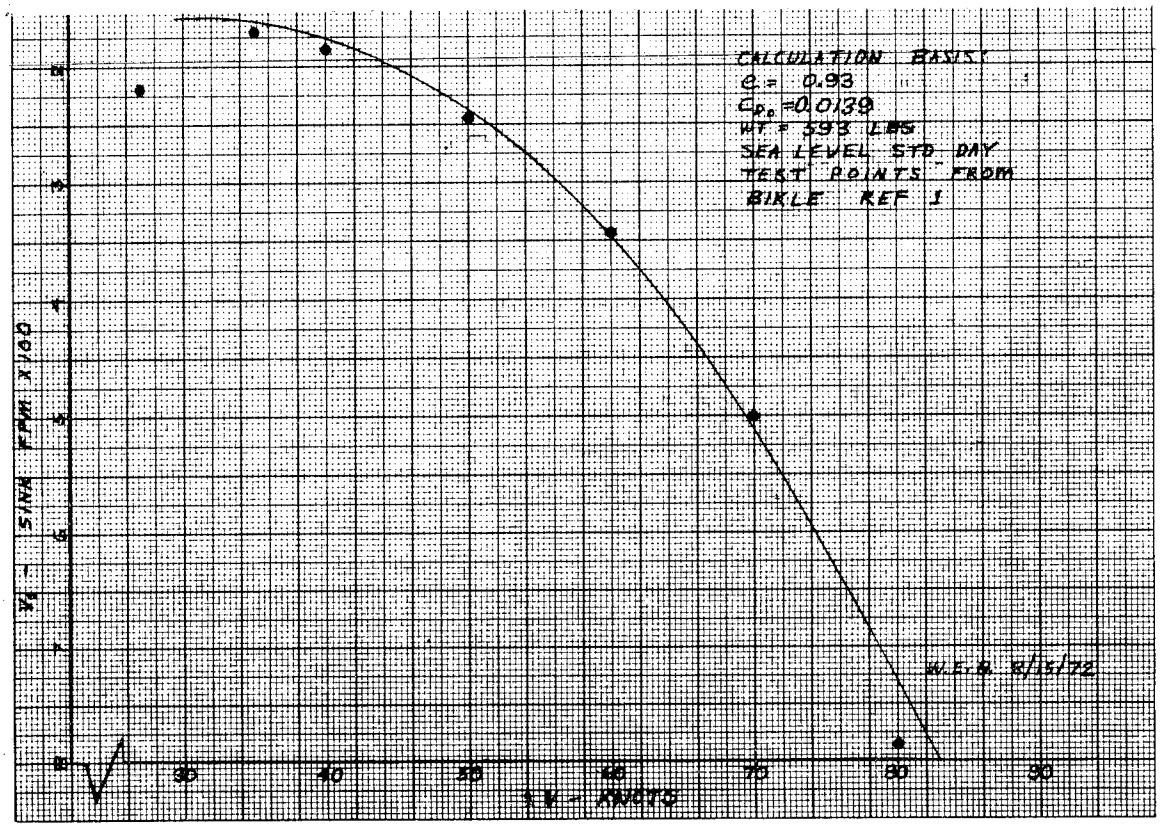


Figure 6. Calculated glide polar 1-26 sailplane.

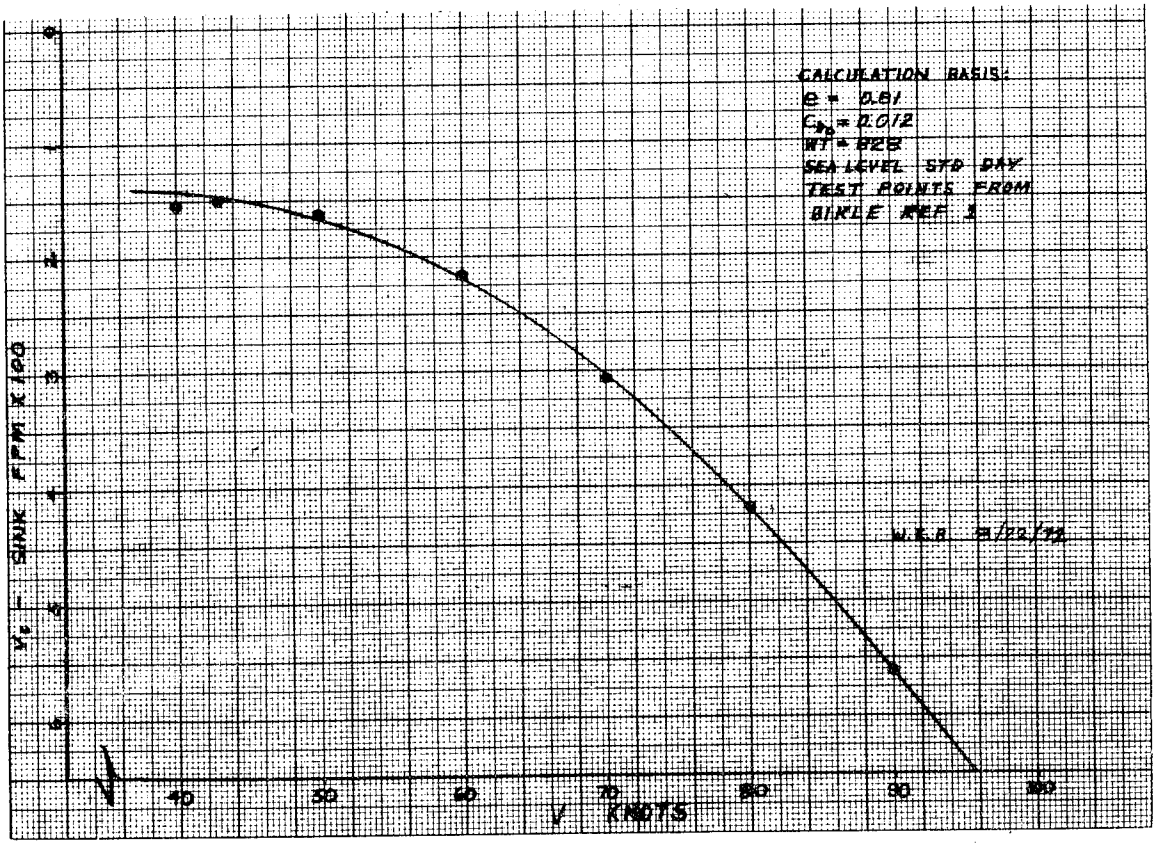


Figure 7. Calculated glide polar BG-12 sailplane.

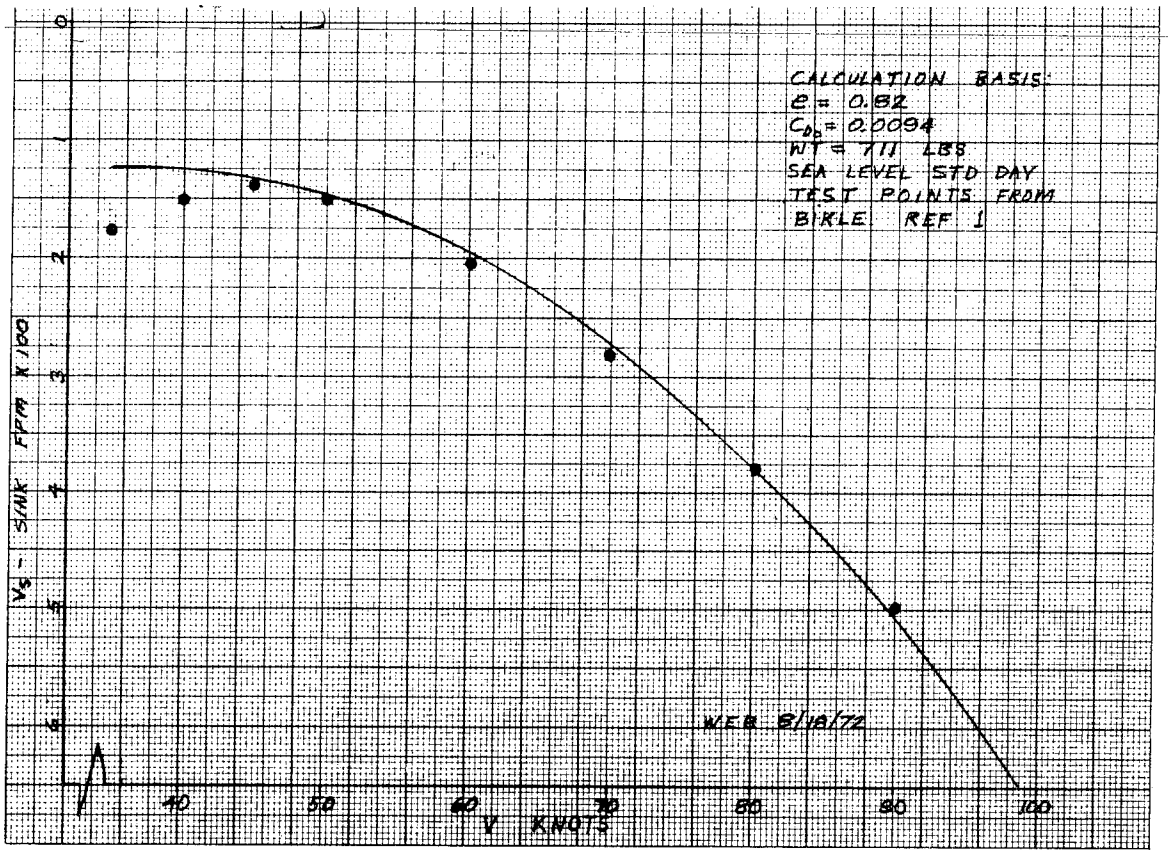


Figure 8. Calculated glide polar Phoebus A sailplane.

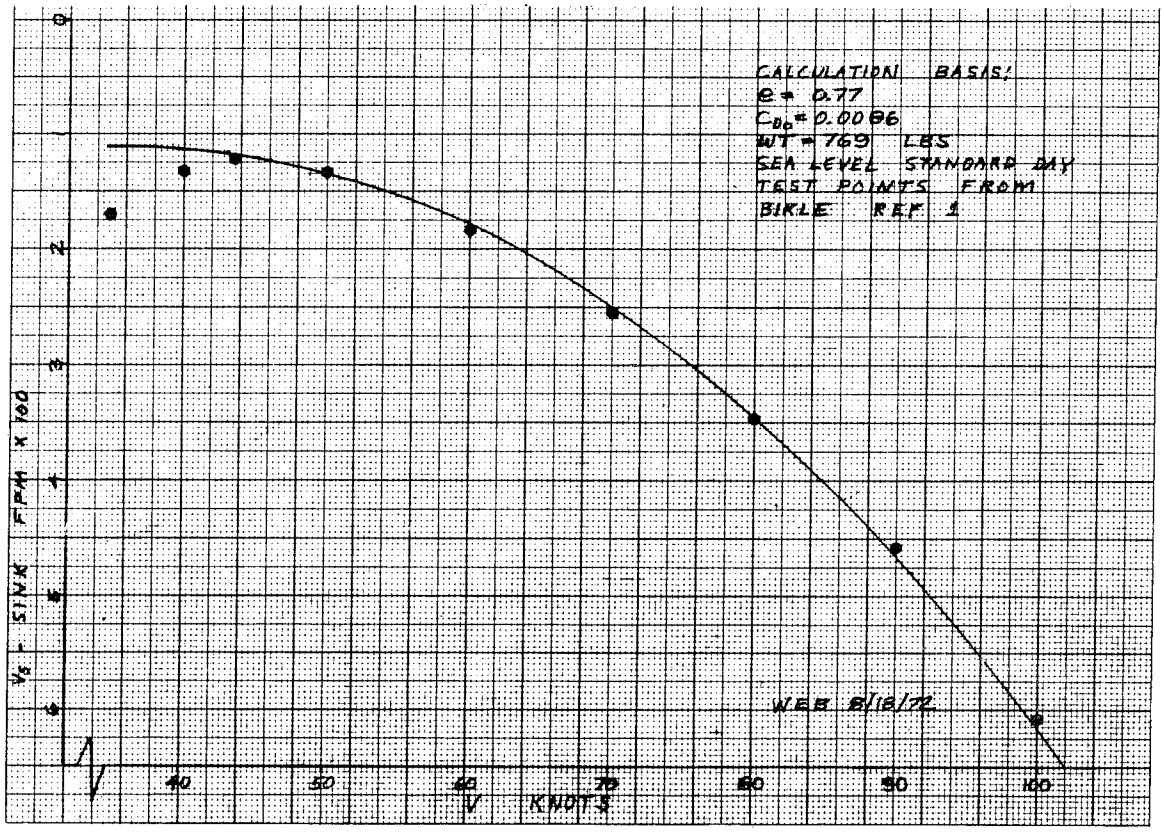


Figure 9. Calculated glide polar Phoebus B sailplane.

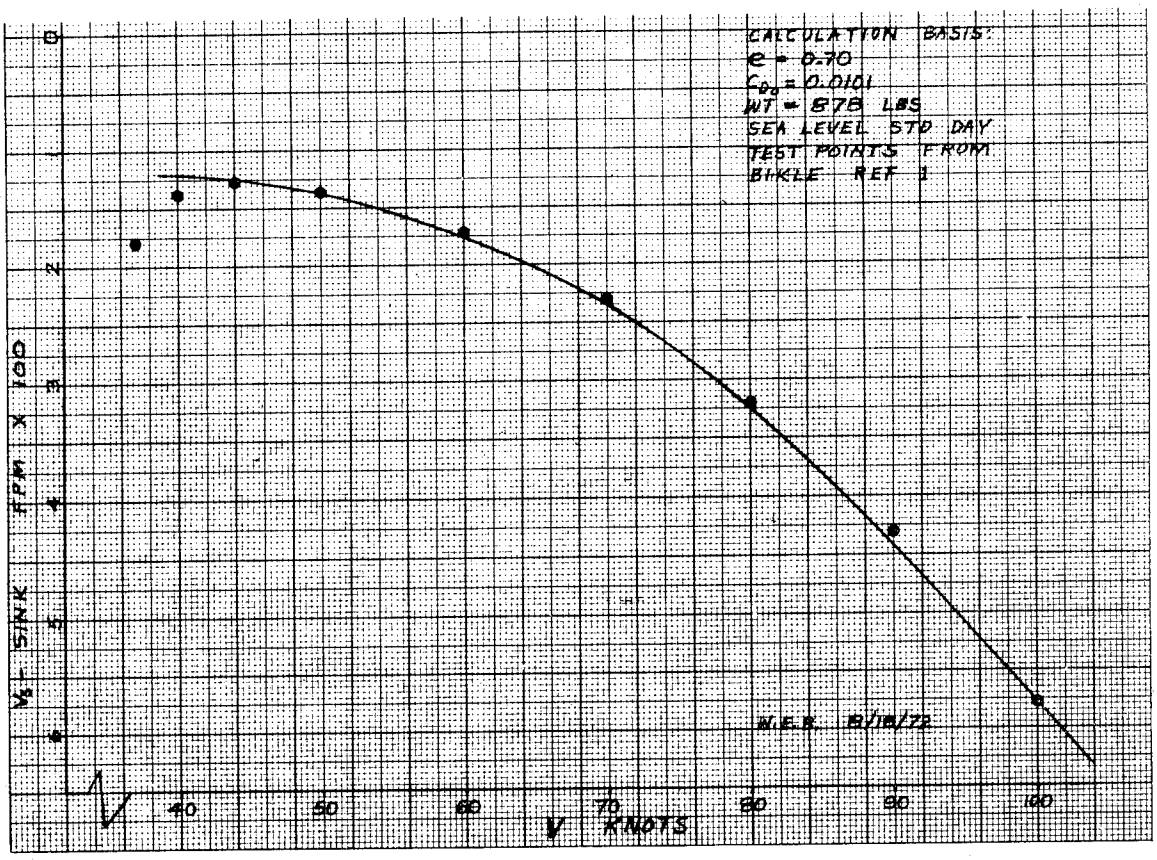


Figure 10. Calculated glide polar Cirrus sailplane.

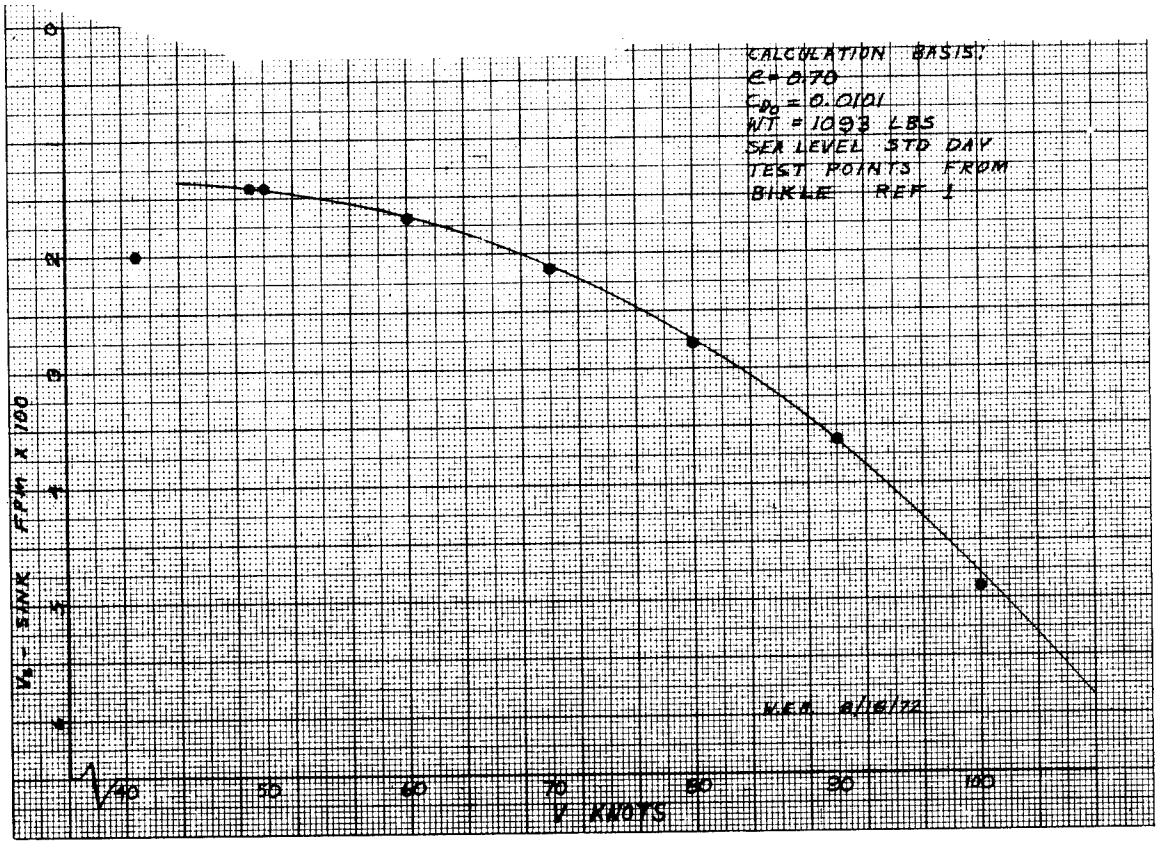


Figure 11. Calculated glide polar Cirrus sailplane with water ballast.

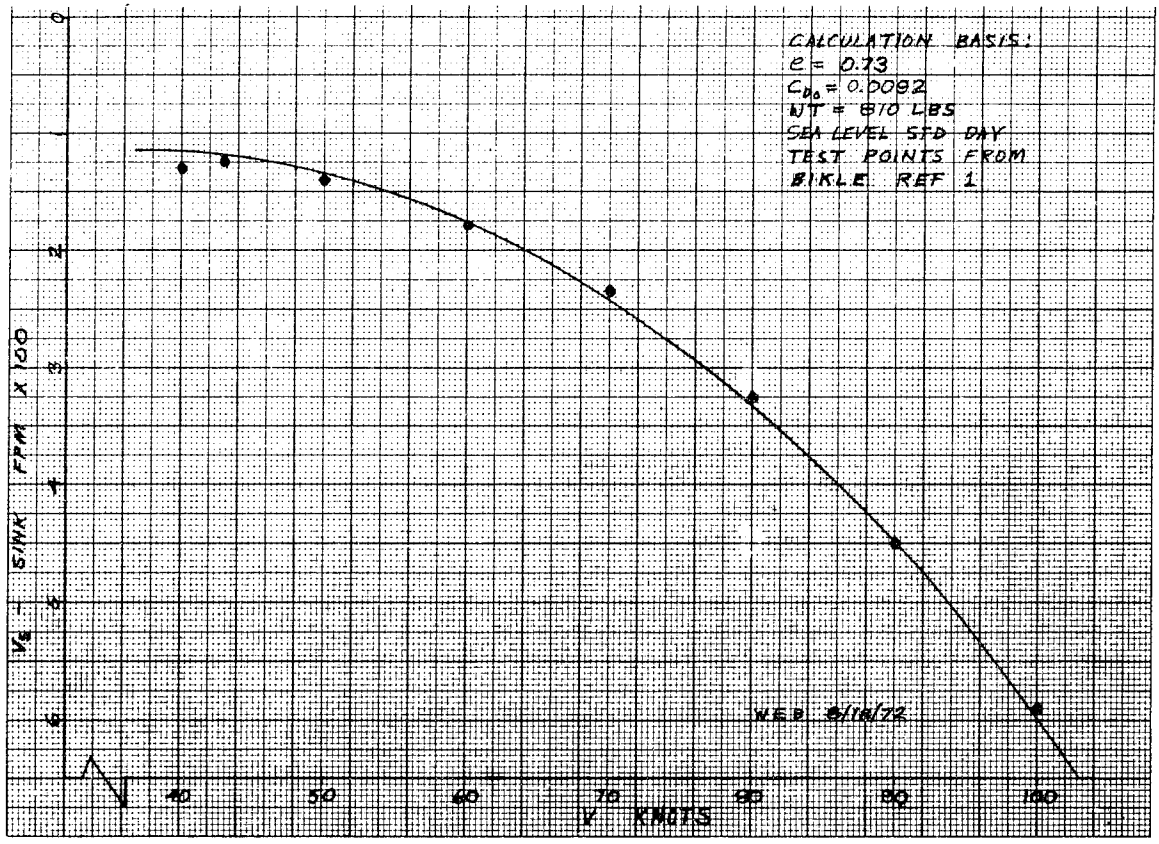


Figure 12. Calculated glide polar T-6 sailplane.

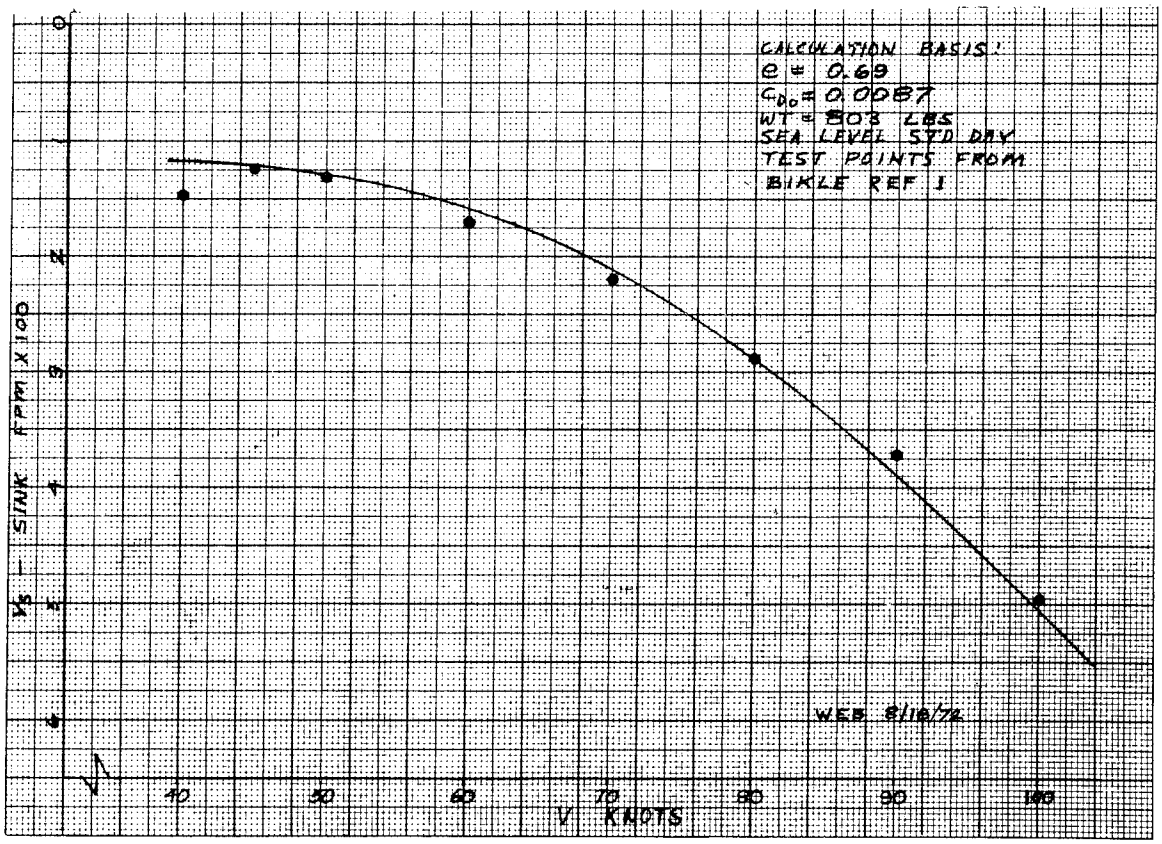


Figure 13. Calculated glide polar Kestrel sailplane.

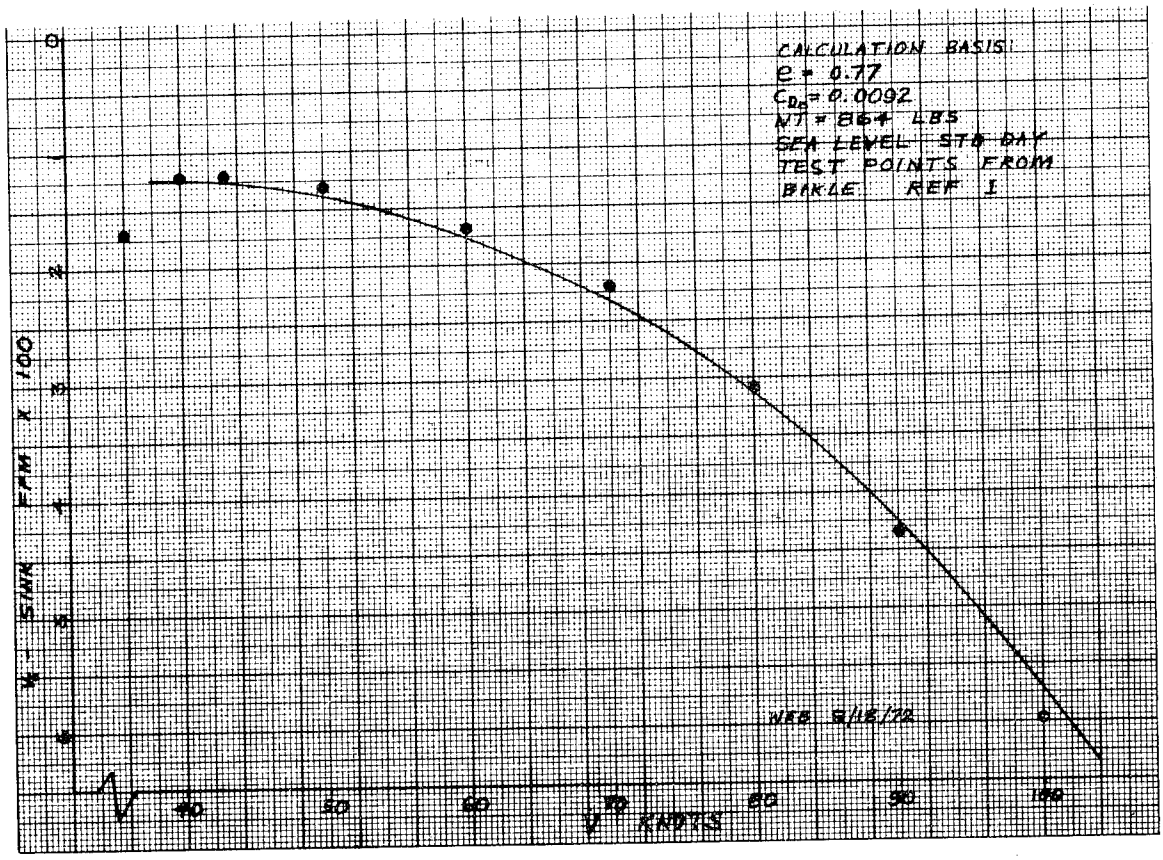


Figure 14. Calculated glide polar Diamant 16.5 sailplane.

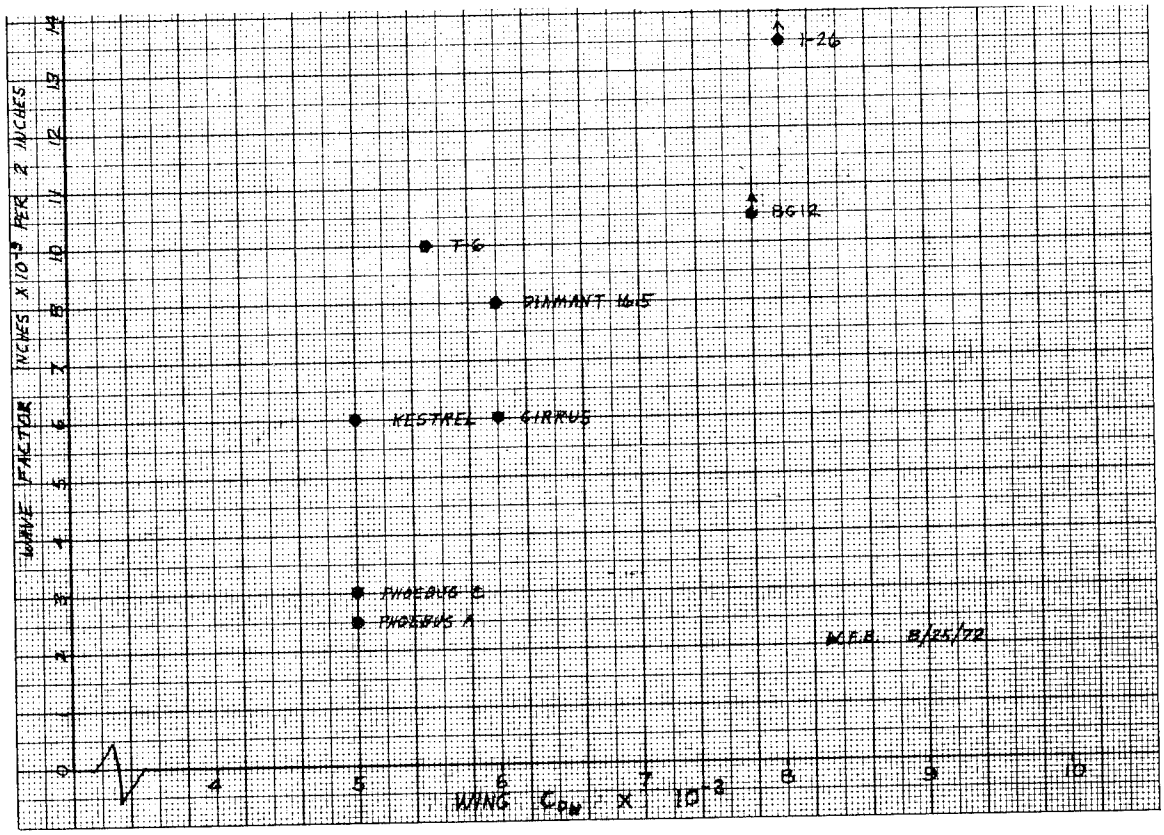


Figure 15. Comparison wave factor vs wing C_{D_W}.

Discussion

The general procedure followed was to generate a polar and to compare results with the Bikle test data. In some cases the first try resulted in good correlation. In other cases, adjustments were made where they could be justified on a rational basis; the program was re-run and the comparison repeated. The polars shown in Figures 6-14 could be further refined; however, as plotted, they represent the results which could be obtained had they been made without the benefit of the test data using the methods described, and had the drag coefficients listed in Table 1 been chosen in the initial estimates.

As would be expected those sailplanes with non-linear C_L^2 vs C_D curves show more variation between the calculated curves and the test points than do the others. This includes both of the Phoebus sailplanes (Figures 8 & 9) and the Diamant (Figure 14). In the case of the Phoebus, equation 5 gives an e value which is a fair expression of the average e achieved by these sailplanes; however, the break in the actual C_L^2 vs C_D curve results in some non-correlation in the middle of the curve. This is not a serious difference, and the calculated curves still give a fairly good estimate of the performance which could be expected.

The Diamant polar was based on $C_{D_w} = 0.006$. In this case, the actual e is greater than that calculated by equation 5, while C_{D_w} is apparently higher than $C_{D_w} = 0.006$. This results in the actual performance being better at the low speed end and poorer at the high speed end than was calculated. This curve showed the greatest variation between calculated performance and test results of the eight sailplanes studied.

Of special interest are the polars of the Kestrel (Figure 13) and the Phoebus C (Figure 9). In these two cases, the lowest wing and fuselage drag coefficients were used to obtain the calculated polars, $C_{D_w} = 0.005$ and $C_{D_f} = 0.07$. Since the curves correlate well with the test points, it would indicate that these two sailplanes have achieved the lowest drag coefficient values of the eight sailplanes tested in Reference 1. The Phoebus A polar was also based on $C_{D_w} = 0.005$ while $C_{D_f} = 0.08$ was used, the higher value being justified by the non-retracting landing wheel.

The Cirrus polars (Figure 10 & 11) are based on $C_{D_w} = 0.006$ and $C_{D_f} = 0.08$. If the wing section is of the earlier Wortmann type, the wing estimate would be justified. The calculated curve shows good agreement with the test data.

An item of interest is the difference between the ballasted and unballasted Cirrus polars (Figures 10 & 11). While the test points for the unballasted Cirrus are just above the calculated curve, the ballasted points lie just below the calculated curve for the higher weight. Difference is not

enough to be conclusive but suggests that the ballast may have adversely effected wing twist by some small amount. The Reynolds number effect should have had the opposite effect and we would have expected the ballasted performance to be slightly better on this basis.

The calculated polar for the T-6 was based on C_{D_w} = = 0.0055 and C_{D_f} = 0.08 with excellent correlation with the test points. This would indicate that a lower C_{D_w} was obtained with the T-6 than was achieved on the tested Cirrus, if both calculated polars are based on a fuselage C_{D_f} = 0.08.

It is of interest to examine the C_{D_w} used in the calculations in the light of the wave factor measured in Reference [1]. This is shown in Figure 15. Here, again, the data is not sufficient to be conclusive but it is noteworthy that the three sailplanes which correlated with C_{D_w} = 0.005 (Kestrel, Phoebus A and C), all have very low wave factors. Perhaps when this sort of comparison is made over a larger number of cases a more definitive correlation of drag with wing wave factor will be achieved.

At the low speed end of all of the calculated polars, the actual sink is greater than calculated. In general, the simplified method does not account for the large increase in drag near the stall which is brought about by the basic airfoil characteristics and by local separation on components of the sailplane at high lift coefficients. For this reason the calculated polars are not shown above C_L = 1.2. In general, the method does not predict accurately the minimum sink speed or the speed for minimum sink. However, at the maximum L/D, the curves are in much better agreement with the test data. A comparison of predicted vs measured L/D is shown in Table 2.

Conclusions

When good judgement is applied to the drag coefficient estimates and a realistic span efficiency factor is applied, calculated polars can be generated which will accurately represent what the actual sailplane will achieve in flight, at least over that portion of the flight speed envelope where it will be operated most.

The achievement of an accurate prediction does hinge upon accurate airfoil section data.

These simple methods, which are almost as old as aviation itself, can also be a useful tool in the analysis of test results.

It would seem that with further refinement, the methods developed in this paper could be used to develop a sailplane

competition handicapping formula which would only require a three-view drawing and basic data on the airfoil, weight and method of construction.

It should be recognized that unless the theory is subjected to test measurement and correlation, it ceases to relate to what is happening in the real world. The soaring community, as a whole, owes a tremendous debt to Paul Bikle for his meticulous test measurements, without which an analytical study such as this would have been impossible.

References

1. Bikle, Paul; Sailplane Performance Measured in Flight, Technical Soaring, Vol. 1, No. 3, January 1972, based on "Polars of Eight", Soaring, June 1970. (Both published by The Soaring Society of America.)

2. Bikle, Paul; Flight Test Performance Summary, Soaring, February 1971.

3. Bikle, Paul; Polars of Eight, Soaring, June 1971.

4. Dommasch, Sherby and Connolly, Chapter 5; Wing Theory, Airplane Aerodynamics, Pitman Publishing Corporation New York.

5. Oswald, W.; General Formulas and Charts for the Calculation of Airplane Performance, NACA TR 408, 1932.

6. Wortmann, F.X.; On the Optimization of Airfoils with Flaps, Soaring, May 1970.

7. Wortmann, F.X.; Some Laminar Profiles for Sailplanes, Soaring, January 1964.

8. Holighaus, K.; Designing for Competition, Proceedings of the 1971 Symposium on Competitive Soaring (Published by Soaring Symposia, 408 Washington St., Cumberland, Md. 21502.)

9. Backstrom, A.A.; Some Considerations in the Design of Light Airplane Wings, EAA Design File No. 3, Vol. 2. (Published by the Experimental Aircraft Association P.O. Box 229, Hales Corners, Wisconsin 53130.)

10. Airfoil Section Data, NACA Report 669, 1939.

11. Jane's All the World's Aircraft, Mc Graw Hill.

*U.S. GOVERNMENT PRINTING OFFICE: 1973-739-153/51

NATIONAL AERONAUTICS AND SPACE ADMINISTRATION
WASHINGTON, D.C. 20546

OFFICIAL BUSINESS
PENALTY FOR PRIVATE USE $300

SPECIAL FOURTH-CLASS RATE
BOOK

POSTAGE AND FEES PAID
NATIONAL AERONAUTICS AND
SPACE ADMINISTRATION
451

U.S.MAIL

National Aeronautics and Space Administration
WASHINGTON, D. C. 20546

OFFICIAL BUSINESS
Penalty For Private Use, $300.00
Special Fourth Class Mail

POSTAGE AND FEES PAID
NATIONAL AERONAUTICS AND
SPACE ADMINISTRATION

131 001 C1 U 02 731116 S00942DS
DEPT OF THE ARMY
PICATINNY ARSENAL
PLASTICS TECHNICAL EVALUATION CENTER
ATTN: SMUPA-VP3
DOVER NJ 07801

verable (Section 158
nual) Do Not Return

"The aeronautical and space activities of the United States shall be conducted so as to contribute . . . to the expansion of human knowledge of phenomena in the atmosphere and space. The Administration shall provide for the widest practicable and appropriate dissemination of information concerning its activities and the results thereof."

—NATIONAL AERONAUTICS AND SPACE ACT OF 1958

NASA SCIENTIFIC AND TECHNICAL PUBLICATIONS

TECHNICAL REPORTS: Scientific and technical information considered important, complete, and a lasting contribution to existing knowledge.

TECHNICAL NOTES: Information less broad in scope but nevertheless of importance as a contribution to existing knowledge.

TECHNICAL MEMORANDUMS: Information receiving limited distribution because of preliminary data, security classification, or other reasons. Also includes conference proceedings with either limited or unlimited distribution.

CONTRACTOR REPORTS: Scientific and technical information generated under a NASA contract or grant and considered an important contribution to existing knowledge.

TECHNICAL TRANSLATIONS: Information published in a foreign language considered to merit NASA distribution in English.

SPECIAL PUBLICATIONS: Information derived from or of value to NASA activities. Publications include final reports of major projects, monographs, data compilations, handbooks, sourcebooks, and special bibliographies.

TECHNOLOGY UTILIZATION PUBLICATIONS: Information on technology used by NASA that may be of particular interest in commercial and other non-aerospace applications. Publications include Tech Briefs, Technology Utilization Reports and Technology Surveys.

Details on the availability of these publications may be obtained from:

SCIENTIFIC AND TECHNICAL INFORMATION OFFICE

NATIONAL AERONAUTICS AND SPACE ADMINISTRATION

Washington, D.C. 20546